The synthesis and characterization of diphenylacetylene containing ion channels

by

Joanne Marie Moszynski
Master of Science, The University of Western Ontario, 2006
Bachelor of Science, The University of Toronto, 2004

A Dissertation Submitted in Partial Fulfillment
of the Requirements for the Degree of

DOCTOR OF PHILOSOPHY

in the Department of Chemistry

Supervisory Committee

The synthesis and characterization of diphenylacetylene containing ion channels

by

Joanne Marie Moszynski
Master of Science, The University of Western Ontario, 2006
Bachelor of Science, The University of Toronto, 2004

Supervisory Committee

Dr. Thomas Fyles, Department of Chemistry
Supervisor

Dr. Cornelia Bohne, Department of Chemistry
Departmental Member

Dr. Lisa Rosenberg, Department of Chemistry
Departmental Member

Dr. Terry Pearson, Department of Biochemistry
Outside Member

Abstract

Supervisory Committee

Dr. Thomas Fyles, Department of Chemistry
Supervisor
Dr. Cornelia Bohne, Department of Chemistry
Departmental Member
Dr. Lisa Rosenberg, Department of Chemistry
Departmental Member
Dr. Terry Pearson, Department of Biochemistry
Outside Member

This Thesis presents the synthesis, characterization and mechanistic explorations into a series of diphenylacetylene-containing oligoester ion channels. Eighteen final compounds were synthesized and tested for ion transport activity utilizing both vesicle and planar bilayer assays. The oligomers varied in length, hydrophobicity and the nature of the aromatic moiety. Compounds incorporating a modified diphenylacetylene ('Dip'), or a novel phenyl-extended fluorophore ('Trip') were made using a reliable, modular synthesis. The final compounds were prepared in a total of 5 to 11 steps from commercial materials in yields ranging from 10 to 40%.

The compounds' activity varied considerably; both highly active and completely inactive compounds were discovered. The differences in activity are controlled by structure *via* the influence of structural variables on the aqueous phase aggregation and the ability of the compound to insert into the bilayer membrane. These structure-activity studies uncovered two highly-active ion transporters, HO_2C-Hex-Dip-Hex-Hex-OH and $–OPO_3^{2-}$ (Hex = 6-hydroxyhexanoyl) which exhibited activity almost 10-fold higher than the fully-saturated oligoesters developed in previous work. In some cases, the transport activity is initially high but declines over a period of 20-30 minutes following compound addition. This suggests that the compound slowly transitions to an environment where it cannot form active channels.

In the bilayer clamp, a variety of behaviours including highly-conducting openings were observed. An apparent voltage-gated response was exhibited by one of the Trip compounds (HO_2C-Trip-G(E3)-OH), a property rarely seen for synthetic ion channels.

The Dip and Trip molecules exhibited environment-sensitive fluorescence. The observed Dip excimer-like emission is the second reported instance of this in solution. The Trip compounds are solvatochromic; this property was used to infer their location in the membrane. Partitioning into the membrane was followed by a blue-shifting and increased intensity of the fluorescence emission for both series of compounds. For the Trip isomers, which are significantly more emissive than the Dip molecules, this enhancement in intensity could be visualized by eye.

For the Dip oligomers, the excimer emission is a broad band with variable shape and intensity; it is time-dependent under some conditions. The excimer emission has a sub-nanosecond lifetime in homogenous solution that is significantly prolonged in the presence of vesicle bilayers, in which a number of lifetimes could be detected. Both monomer and excimer emissions can be quenched by aqueous copper, the excimer emission is more efficiently quenched than is the monomer.

The photophysical characteristics of these molecules allowed for a variety of experiments designed to probe their membrane partitioning and localization behaviours. The results indicate the formation of a complex mixture of interconverting monomeric and aggregate species as the compounds move from water to the bilayer. The slow evolution of the mixture is consistent with the times noted for loss of membrane activity in transport assays. From these data a new model that describes the transport process is proposed. The key feature of this model is that transport must occur *via* a species that forms quickly upon the mixing of the components. Possible structures of the intermediates formed are discussed.

Table of Contents

Supervisory Committee ii
Abstract iii
Table of Contents v
List of Tables vii
List of Figures ix
List of Schemes xix
List of Abbreviations xx
List of Numbered Compounds xxii
Acknowledgements xxxi
Chapter 1 : Introduction 1
1.1: Factors driving synthetic ion channel research 1
1.2: Synthetic ion channels 5
1.2.1: Overview & classification 5
1.2.2: Characterization of ion channel activity 7
1.2.3: Planar bilayer experiments 9
1.2.4: Vesicle-based assays 11
1.3: Synthetic ion channels studied in the Fyles lab 17
1.4: Project goals 22
1.5: Thesis overview 24
Chapter 2 : Diphenylacetylene-containing synthetic ion channels 26
2.1: Rationale & design 26
2.2: Synthesis 27
2.2.1: Attempted solid-phase synthesis 27
2.2.2: Solution phase syntheses 30
2.3: Ion transport activity; vesicle assays 42
2.4: Ion transport activity; bilayer clamp assay 51
2.5: Photophysical characteristics 58
2.5.1: Fluorescence in solution 58
2.5.2: Fluorescence with vesicles 63
2.5.3: Quenching studies 66
2.6: Mechanistic implications 74
2.7: Conclusions & future work 76
Chapter 3 : Synthetic ion channels based on an extended chromophore 78
3.1: Rationale 78
3.2: Initial tetra-aromatic design & attempted synthesis 78
3.3: Modified design & synthesis: the ‘Trip’ scaffold 83
3.4: Ion transport activity 89
3.4.1: Vesicle assays 89
3.4.2: Bilayer clamp assay 92
3.4.3: Non-linear current-voltage response 97

3.5: Photophysical characterization 100
3.5.1: Fluorescence in solution 100
3.5.2: Fluorescence with vesicles; pre-incorporation 108
3.5.3: Fluorescence with vesicles; partitioning from aqueous solution 110
3.6: Conclusions & future work 117
Chapter 4 : Second-generation Dip containing compounds 120
4.1: Rationale & design 120
4.2: Synthesis 122
4.3: Ion transport activity; HPTS assay 127
4.3.1: Structure-activity correlations 128
4.4: Ion-transport activity; bilayer clamp assay 137
4.5: Photophysical characteristics 144
4.5.1: Fluorescence in solution 144
4.5.2: Fluorescence with vesicles; membrane partitioning studies 151
4.5.3: Quenching in vesicles 155
4.5.4: Quantifying partitioning 159
4.6: Conclusions & future work 164
Chapter 5 : Time-resolved studies and mechanistic implications 169
5.1: Rationale 169
5.2: Time-dependent ion transport activity 171
5.3: Fluorescence lifetime studies 177
5.4: Mechanistic implications 186
5.5: New model 192
5.6: Conclusions 195
Chapter 6 : Conclusions, future directions & significance 196
Bibliography 201
Appendix 1: Synthetic experimental details 208
Appendix 2: Supporting Information; Synthesis 255
Appendix 3: Transport assay & fluorescence experimental details 444
Appendix 4: Supporting information; fluorescence 452

List of Tables

Table 2.1: Standard solid-phase synthesis conditions developed for the saturated oligoesters [41]. 28

Table 2.2: Standard reaction conditions utilized in the Dip oligomer syntheses. Compare with Table 2.1 for the SPS reactions. 37

Table 2.3: Name, number, structure and overall yields from commercially-available starting materials of the first-generation of Dip oligomers. Full experimental details and characterization available in Appendices 1 and 2. 40

Table 2.4: Summary of HPTS activity for first generation Dip oligomers, comparison with parent compound (HO_2C-Oct-Dod-Oct-G(10)-OH). a= number in parentheses is rate achieved at highest tested concentration. b= number in parentheses is highest concentration assayed before visible precipitation occurred. Details of HPTS assay available in Appendix 3. 44

Table 2.5: Summary of quenching data obtained for Dip-containing compounds in MeOH 68

Table 2.6: Experimentally-derived Stern-Volmer constants in aqueous solution or in methanol for selected first-generation Dip isomers quenched by $CuSO_4$. Constants in methanol had linear fits, while aqueous-derived constants sometimes deviated from linearity, due to changing emission over time. 70

Table 3.1: Summary of HPTS activity for Trip isomers, comparison with Dip compound (HO_2C-Hex-Dip-Hex-G(12)-OH). *a*= number in brackets is highest concentration assayed before visible precipitation occurred. Details of HPTS assay available in Appendix 3. ... 89

Table 3.2: Summary comparison of representative photophysical parameters of the Dip and Trip fluorophores in methanolic solution. a= The reported values are for 16 μM HO_2C-Trip-G(E3)-OH compared with the same concentration of HO_2C-Dip-6-6-(G12)-OH with same slit widths (3nm); the CPS are above the instrument limit for the Trip compound. 102

LEFT:Figure 3.15: Solvent effects for HO_2C-Trip-Hex-G(12)-OH. Fluorescence emission spectra (λEx~325 nm) for 17 μM compound in selected solvents, and pre-loaded into vesicles at 0.5 mol%, or approximately 3.5 μM. INSET: λMax as a function of solvent polarity. Open circles= tested solvents, black circles= fit of vesicle wavelengths onto linear relationship. RIGHT: **Table 3.3:** E_T values and emission maxima as shown in Fig. 3.15. a= inferred from fit of data. 109

Table 4.1: Names, structures and yields of second-generation Dip containing compounds from 4-ethynylbenzyl alcohol (**2-5**)..... 126

Table 4.2: Summary of HPTS activity for head-group modified Dip isomers, comparison with parent compound (HO_2C-Hex-Dip-Hex-G(12)-OH). *a*= number in brackets is rate achieved at highest tested concentration. *b*= number in brackets is highest concentration assayed before visible precipitation occurred. Details of HPTS assay available in Appendix 3. 129

Table 4.3: Summary of fluorescence emission properties for 2^{nd}-generation Dip isomers. For quenching studies, the extent of quenching (with $CuSO_4$) was measured at the maximum emission wavelengths determined in CH_3OH (~320 nm) or aqueous (AQ) solution (~380 nm). Extent of quenching at both wavelengths in the presence (VES) or absence (AQ) of lipid vesicles was then compared. Excitation wavelengths varied minimally around 305 nm (301-305 nm). Emission intensity in aqueous solution was found to vary over time for some compounds. Experimental details available in Appendix 3. 159

Table 4.4: Partitioning data for various membrane probes. a= value corresponds to lipid concentration needed to incorporate 50% of the probe molecule. b= determined by Haugland and Huang [123], c= determined by Gokel *et al*. [98]. 163

Table 5.1: TCSPC fitting results for HO_2C-Dec-Dip-Hex-G(12)-OH..... 179

Table 5.2: Initial, intermediate and final lifetimes and proportions of each species obtained from the TCSPC experiment for 20 µM HO_2C-Hex-Dip-Hex-C6 and 20 µM HO_2C-Hex-Dip-Hex-C12..... 182

List of Figures

Figure 1.1: 1,2-dipalmitoyl-sn-glycero-3-phosphocholine (DPPC): **A**: Chemical structure, **B**: approximate dimensions of regions and tilt from the bilayer normal, based on X-ray structures obtained for actual bilayers; adapted from Ref [2]. Two of these lipids stack end to end to produce the lipid bilayer, schematically depicted in **C**: to-scale drawing with molecular dimensions and **D**: simplified 'cartoon' representation; the grey spheres are the headgroups. 2

Figure 1.2: Synthetic ion channel classification. **A**: Unimolecular channels. **B**: Aggregate channels in which the individual monomers (rectangles) laterally diffuse in the membrane to form the channel. 6

Figure 1.3: Chemical structures of synthetic channels exemplifying the classes shown in Fig. 1.2. **A**: unimolecular 'hydraphile' channel developed by Gokel *et al*. [28] (**1-1**), **B**: a 'simple' channel-former synthesized by Fyles *et al*.,(**1-2**) several of these monomers are assumed to form the active aggregate structure [29]. 7

Figure 1.4: The bilayer clamp experiment. **A**: the electrolyte-filled chambers (black circles) are separated by a cup containing a small aperture (blue lines), over which a bilayer membrane is formed. **B:** In the absence of a transporter, no current (I) is observed as the bilayer acts as a resistor. **C:** With the addition of an active channel, ions flow and a current is detected as a step-up from the baseline. 10

Figure 1.5: The HPTS experiment. **A**: The dye is loaded into vesicles, to which the putative transporter (blue cylinder) is added. **B**: 'Raw' data from the experiment; once the pulse of NaOH is added, the emission of the base form of the dye (EX 460, red line) increases as the pH gradient is collapsed. The maximal response is obtained by lysing the vesicles with a commercial surfactant. **C**: Rate constants can then be derived by plotting the extent of transport over time (N, for equation see text) for varying concentrations of tested compound. Full experimental details available in Appendix 3. 13

Figure 1.6: The carboxyfluorescein (CF) assay. **A**: the dye is loaded into vesicles; its fluorescence is minimal due to concentration-quenching. **B**: the tested compound ('surfactant') is added, and if pores large enough for CF to escape the vesicle are formed, the fluorescence intensity increases. **C:** 'raw' data: solid lines represent increasing amounts of added compound, the dashed line is the maximal response; **D:** the data are used to obtain a percent CF efflux using the equation in the INSET. Full experimental details in Appendix 3. 14

Figure 1.7: Schematic diagram illustrating the formation of vesicles pre-loaded with compound. After co-evaporation of a solution of compound and vesicles, sonication in

aqueous buffer and extrusion through a membrane filter, a suspension of free compound, vesicles and compound-containing vesicles results, **A**. This suspension is then loaded onto a size-exclusion column, which separates components, **B**. The desired compound-containing vesicles are then collected, **C**. 16

Figure 1.8: Structure of **1-3**, the first Na^+-transporting synthetic ion channel developed in the Fyles lab [45]. The dashed line represents the bilayer midplane. 17

Figure 1.9: Progressive iterations of 'bola' (2-headed)-amphiphile aggregate channels developed in the Fyles lab. From compound **1-3** in Fig. 1.8, the compounds lost the central crown ether (**A**) and were de-macrolized (**B**), eventually leading to the 'fully saturated' oligoester HO_2C-Oct-Dod-Oct-G(12)-OH (**C**). 20

Figure 1.10: Proposed working model based on extensive structure-active relationship studies carried out on the saturated oligoesters [40]. **A**: the compounds aggregate in aqueous solution, and can potentially partition *via* an aqueous monomer (**B**) into the membrane; **C**. The monomers then re-aggregate in the membrane to form the active channel; **D**. 22

Figure 1.11: Structure and naming scheme of substituent parts of the target oligomer HO_2C-Hex-Dip-Hex-G(12)-OH, **1-7**. *****Once the initial numbers of final oligomers are given, the compounds will be referred to by their trivial names, starting from the carboxylic acid terminus. 23

Figure 2.1: Structure of the target oligomer HO_2C-Hex-Dip-Hex-G(12)-OH (**1-7**), compared to the fully saturated precursor compound HO_2C-Oct-Dod-Oct-G(12)-OH (**1-6**). 27

Figure 2.2: Structures of products resulting from reaction of THP-protected Dip subunit **2-1** with the ester coupling conditions developed in previous work [41]. The desired methyl ester **2-3** was formed in equal or lesser proportion to the undesired N-acyl urea side product **2-2** under these conditions. THP= tetrahydropyran, DIC= *N, N*-diisopropyl carbodiimide, DMAP= *N, N*-dimethylaminopyridine. 29

Figure 2.3: ^1H NMR spectrum of **2-6**, run in $CDCl_3$ at 300 MHz. Key signals indicating successful ester coupling are indicated. 33

Figure 2.4: NMR spectra of HO_2C-Dec-Dip-Hex-G(12)-OH (**2-15**) taken in $CDCl_3$ **A**: ^1H, 500 MHz, the letters correspond to assigned signals on the structure. The large unassigned peaks at ~1.2 and 1.5 ppm are due to the alkyl regions. **B**: ^{13}C spectrum, 125 MHz. Key peaks are assigned, with the brackets indicating regions of similar carbon types. 39

Figure 2.5: Plot of apparent rate constant versus concentration for a selection of first-generation Dip isomers. See Table 2.4 for full dataset. Details of HPTS assay available in Appendix 3. 43

Figure 2.6: The pyrene aggregation assay. **A**: fluorescence emission spectra of pyrene (structure shown in INSET) in aqueous solution in the presence of low (black line) or high (grey line) concentration of an aggregate-forming compound. **B**: ratio of pyrene vibronic band intensities (I1/I3) as a function of the concentration of HO_2C-Hex-Dip-Hex-G(12)-OH (10 mM Na_3PO_4 aqueous buffer, 100 mM NaCl, pH 6.4, 2 µM pyrene). Further details of the assay available in Appendix 3. 45

Figure 2.7: Schematic illustration of presumed method of membrane insertion for HO_2C-Hex-Dip-Hex-G(12)-OH 47

Figure 2.8: Bilayer clamp analysis for 'regular' behaviour observed for HO_2C-Hex-Dip-Hex-G(12)-OH preloaded into a diPhyPC bilayer in 1 M CsCl. **A**: 'raw' bilayer trace displaying current (I) as a function of applied potential (arrows, -175, -150 and -100 mV) over time. **B**: all-points histogram of the trace shown in **A**, displaying the average current observed at each potential; **C**: these values are plotted as an I-V trace, from which the conductance (g) is obtained. **D**: expansion of **A**. 52

Figure 2.9: Examples of types of behaviours seen in the bilayer clamp for HO_2C-Dip-G(12)-OH, 0=closed (no current) state, 1, 2, 3= open (conducting) states, multiple levels correspond to multiple open channels. **A**: 1 M CsCl , +175 mV, **B**: 1 M CsCl, +75 mV, red arrows refer to area of multiple irregular openings, further discussion in text. **C:** 1 M CsCl, +150mV, **D:** 1 M KCl, +50 mV. DiPhyPC was the lipid used in all cases. Further experimental details available in Appendix 3. 56

Figure 2.10: Examples of diphenylacetylene (DPA) containing environment-sensitive compounds. **A**: PPE-SO_3^-, a conjugated polyelectrolyte ('CPE') [87]. **B**: DNA-DPA system developed by Letsinger *et al*. [58]; a red-shifting of the emission by ~100 nm was observed when the individual DNA strands base-pair to each other. 60

Figure 2.11: Fluorescence excitation (grey lines) and emission (black lines) spectra of 20 µM HO_2C-Dip-Hex-Hex-G(12)-OH in **A**: THF and **B**: aqueous buffer (10 mM Na_3PO_4, 100 mM NaCl, pH 6.4). The scale of the y-axis is the same in both panels. Other Dip isomers exhibit nearly identical behaviour. 61

Figure 2.12: Fluorescence emission spectra of 20 µM CO_2H-Dip-Hex-Hex-G(12)-OH in **A:** mixed THF/aqueous buffer solution (10 mM Na_3PO_4, 100 mM NaCl, pH=6.4) 10% THF= grey line, 20% THF= black solid line, 30% THF= black dashed line, **B**: 100% aqueous buffer immediately after mixing (black line) or after 10 mins (grey line), **C**: 100% aqueous buffer, concentration ranges from 16 µM to 0.1 µM. **INSET**: dependence of fluorescence intensity on concentration. λ_{EX} = 305 nm for all panels. 62

Figure 2.13: Chromophores that exhibit significant spectral changes (blue-shifting, emission enhancement) upon vesicle introduction. **2-27**: Tryptophan, **2-28:** Indole derivative from Ladokhin *et al*., **2-29:** NBD, **2-30**: PRODAN, **2-31:** 'MFL', a flavone derivative. 63

Figure 2.14: Fluorescence emission spectra in aqueous buffer (grey lines) (10 mM Na_3PO_4, 100 mM NaCl, pH 6.4) or after 10 minutes incubation time with lipid vesicles (black lines) for selected 1st-generation Dip isomers. **A**: 22 µM HO_2C-Dip-Hex-Hex-G(12)-OH, **B**: 20 µM HO_2C-Hex-Hex-Dip-G(12)-OH, **C**: 20.5 µM HO_2C-Hex-Dip-Hex-G(12)-OH, **D**: 25 µM HO_2C-Dec-Dip-Hex-G(12)-OH. λ_{EX} = 305 nm for all compounds. 64

Figure 2.15: A: Fluorescence emission ratio at 320 nm (black line) versus 380 nm (grey line) as a function of time of 22 µM HO_2C-Dip-Hex-Hex-G(12)-OH in aqueous buffer (10 mM Na_3PO_4, 100 mM NaCl, pH 6.4) into which a suspension of lipid vesicles was injected at the specified time. **B:** analogous experiments for 25 µM HO_2C-Dec-Dip-Hex-G(12)-OH. λEx= 305 nm for both compounds..... 65

Figure 2.16: Fluorescence quenching in **A**: methanol and **B**: aqueous solution (100 mM NaCl) for 30 µM HO_2C-Dec-Dip-Hex-G(12)-OH. From top to bottom, [$CuSO_4$] = 0, 0.125, 0.25, 0.49, 0.74, 0.98 and 1.23 mM in methanol and 0, 0.0625, 0.125, 0.5 and 1.0 µM in water. **INSET:** Stern-Volmer analysis of quenching data. Constants in methanol had linear fits, while some aqueous-derived constants deviated from linearity, due to changing emission over time. λEx= 305 nm in both panels. 70

Figure 2.17: TOP PANEL: Fluorescence emission spectra of 16 µM HO_2C-Dip-Hex-Hex-G(12)OH in aqueous solution (0.1 mM NaCl) (grey lines) or after incubation with lipid vesicles (black lines) in the absence (solid lines) or presence (dashed lines) of 1 µM $CuSO_4$. **BOTTOM PANEL**: Time-based emission ratio at 320 nm (black line) or 380 nm (grey line) of 16 µM HO_2C-Dip-Hex-Hex-G(12)OH in aqueous solution (0.1 mM NaCl), to which vesicles and 1 µM $CuSO_4$ were added at the indicated times. λEx= 305 nm. 72

Figure 2.18: TOP PANEL: Fluorescence emission spectra of 20 µM HO_2C-Dec-Dip-Hex-G(12)OH in aqueous solution (0.1 mM NaCl) (grey lines) or after incubation with lipid vesicles (black lines) in the absence (solid lines) or presence (dashed lines) of 1 µM $CuSO_4$. **BOTTOM PANEL**: Time-based emission at 320 nm (black line) or 380 nm (grey line) of 20 µM HO_2C-Dec-Dip-Hex-G(12)OH in aqueous solution (0.1 mM NaCl), to which vesicles and 1 µM $CuSO_4$ were added at the indicated times. λEx= 305 nm..... 73

Figure 2.19: Schematic diagram illustrating the results of the in-vesicle quenching assays. **A**: active compounds are inserted into the membrane; 380nm emitting aggregates are protected from quencher. **B**: inactive compound; aggregate remains in aqueous solution and is not protected from quenching. 74

Figure 2.20: Schematic illustration of proposed mechanism of action of Dip-containing aggregate channels. The compounds exist mainly as 380 nm– emitting aggregates in aqueous solution (red rectangle), the active compounds can partition via a presumed aqueous monomer into an in-membrane monomer which emits primarily at 320 nm (blue rectangle). These monomers aggregate in the membrane, forming the active structure (red cylinder). 75

Figure 3.1: Proposed tetra-aromatic 'Bi(Dip)' structure: HO_2C-Bi(Dip)-OH (**3-1**)..... 79

Figure 3.2: Early examples of the octiphenyl class of ion channels developed by Matile *et al*. **A**: **3-11**, a highly-insoluble intermediate in the synthesis of the octiphenyl rod **3-12** shown in **B**..... 83

Figure 3.3: NMR spectra of $PREO_2C$-Trip-OH (**3-17**), taken in $CDCl_3$. **A**: ^1H, 300 MHz, **B**: ^{13}C, 75 MHz. 87

Figure 3.4: HPTS results for HO_2C-Trip-G(E3)-OH. **A**: raw data, **B**: plot of rate as a function of concentration. 90

Figure 3.5: Carboxyfluorescein assay for HO_2C-Trip-G(E3)-OH. **A**: raw data, **B**: fraction CF release as calculated in Figure 1.6. 91

Figure 3.6: Triton and 'Triton-like' channel-forming molecules. **3-27** Triton-X-100 , **3-28** and **3-29**, calixarenes reported by Cragg *et al*. [112,113], **3-30**; aromatic polyethers from Schafer *et al*. [78]; x=4,5, y= 6,8,10,12. 92

Figure 3.7: Bilayer clamp data for HO_2C-Trip-G(E3)-OH. Conditions; **A**: 1 M KCl, +90 mV, **B:** 1 M CsCl, +175 mV; 0= closed, 1= open. **C**: 1 M NMe_4Cl, (i) 50 mV, (ii) 75 mV, (iii) 100 mV, (iv) 150 mV **D**: expansion of **B** (150 mV region); red arrow indicates spontaneous channel closure, potential is still being applied. **E:** expansion of **C**. **F**: 1 M KCl, +10 mV. 95

Figure 3.8: Voltage-gated behaviour of HO_2C-Trip-G(E3)-OH, 1 M NMe_4Cl, diPhyPC lipid. **A**: 'raw data trace indicating the potential steps applied over each time period. **B**: IV trace of average obtained current at each time period as a function of voltage. **C**: gV trace of data. The lines in **B** and **C** are to guide the eye. 98

Figure 3.9: Voltage-gating and rectification behaviour of HO_2C-Trip-G(E3)-OH. **A:** 1 M NMe_4Cl, **B**: 1 M KCl, IV response of trace 'A' in Figure 3.7. DiPhyPC was the lipid used for both examples. The line in **B** is to guide the eye. 99

Figure 3.10: HO_2C-Trip-G(E3)-OH fluorescence in methanol or aqueous solution. **A**: Excitation (dashed lines) or emission (solid lines) spectra of 14 µM compound in CH_3OH (black line) and aqueous buffer (10 mM Na_3PO_4, 100 mM NaCl, pH=6.4) (grey line). INSET: photograph under UV light of the same solutions as in the graph. **B**: Fluorescence emission intensity as a function of compound concentration in CH_3OH, **C**: in aqueous. Lines in **B** and **C** are to guide the eye..... 101

Figure 3.11: Structure of anthroyl-PC (**3-31**). 104

Figure 3.12: Aqueous aggregation of $PREO_2C$-Trip-OH. **A**: Fluorescence emission spectra (Ex~325 nm) for 14 µM compound in aqueous/MeOH mixtures, concentrations of water as marked. **B**: fluorescence intensity as a function of water concentration, fit to a logistic function, $r^2 > 0.99$. 105

Figure 3.13: Solvatochromism of HO_2C-Trip-G(E3)-OH. Fluorescence emission spectra (λEx~325 nm) of 16 μM compound in selected solvents. INSET: λMax as a function of solvent polarity for all solvents tested. 107

Figure 3.14: Solvatochromic dansyl-containing peptidic ion channel **3-32** developed by Gokel *et al*. 107

LEFT:**Figure 3.15:** Solvent effects for HO_2C-Trip-Hex-G(12)-OH. Fluorescence emission spectra (λEx~325 nm) for 17 μM compound in selected solvents, and pre-loaded into vesicles at 0.5 mol%, or approximately 3.5 μM. INSET: λMax as a function of solvent polarity. Open circles= tested solvents, black circles= fit of vesicle wavelengths onto linear relationship. RIGHT: Table 3.3: E_T values and emission maxima as shown in Fig. 3.15. a= inferred from fit of data. 109

Figure 3.16: Fluorescence emission spectra of 15 μM HO_2C-Trip-G(E3)-OH in aqueous buffer (10 mM BisTris, 100 mM NaCl, pH 6.4) in the presence (black) or absence (grey) of lipid vesicles, with the addition of 200 μM $CuSO_4$ (dashed lines). λEx= 325 nm..... 111

Figure 3.17: Fluorescence emission spectra of 25 μM HO_2C-Trip-Hex-G(12)-OH after 10 minutes incubation time with lipid vesicles in aqueous buffer (10 mM Na_3PO_4, 100 mM NaCl, pH 6.4) in the presence (black) or absence (grey) of Triton X-100. INSET: Emission over time of 25 μM HO_2C-Trip-Hex-G(12)-OH with vesicles, showing response to Triton addition. λEx= 325 nm. 113

Figure 3.18: Partitioning of 16 μM HO_2C-Trip-G(E3)-OH from aqueous solution into lipid vesicles. **A**: From i to vi, lipid concentrations= 0, 0.25, 0.5, 1, 2.5, 5 mM. INSET: Plot of CPS versus lipid concentration, saturation was not reached, Kp not determined. **B**: comparison of maximal fluorescence in vesicles (curve vi as marked in **A**) compared with that in MeOH (dashed black line) and aqueous (curve i). 114

Figure 4.1: Planned sites of modification leading to 2nd-generation Dip isomers. 121

Figure 4.2: Plot of apparent rate constant versus concentration for a selection of 2nd-generation Dip isomers. The lines shown are fits of the data to either logistic or linear functions. See Table 4.2 for full dataset. Details of HPTS assay available in Appendix 3. 128

Figure 4.3: Structure of **4-23**, one of the 'aplosspan'-type synthetic ion channels developed by Gokel *et al*. [62,63] 130

Figure 4.4: Schematic illustration of proposed transmembrane orientation of first-generation Dip isomer HO_2C-Hex-Dip-Hex-G(12)-OH (**A**) compared with the most active second-generation Dip compound HO_2C-Hex-Dip-Hex-Hex-OH (**B**). The lipid pair (in grey) is shown for scale..... 131

Figure 4.5: An expansion of Figure 4.2, showing the HPTS concentration-rate response of HO_2C-Hex-Dip-Hex-Hex-OH in detail. The line shown is a fit of the data to a logistic function. 132

Figure 4.6: Proposed transmembrane orientations of **A**: HO_2C-Hex-Dip-Hex-Hex-OSucc, **B**: HO_2C-Hex-Dip-Hex-Hex-OPhos, **C**: HO_2C-Hex-Dip-Hex-Hex-OH. 136

Figure 4.7: Bilayer clamp results for HO_2C-Hex-Dip-Hex-Hex-OH. Conditions: **A**: 1 M CsCl, +40 mV, **B**: 1 M NMe_4Cl, red dashed line marks switch from +150 mV to +100 mV, **C**: 1 M CsCl, +100 mV. DiPhyPC was the lipid in all cases. 139

Figure 4.8: Bilayer clamp results for HO_2C-Hex-Dip-Hex-Hex-OPhos. Conditions; diPhyPC lipid, **A**: 1 M KCl, +50 mV, **B**: 1 M CsCl, +25 mV, **C**: 1 M KCl, +40 mV. 141

Figure 4.9: Fluorescence emission spectra in CH_3OH (black lines) or aqueous buffer (grey lines) (10 mM BisTris, 100 mM NaCl, pH 6.4) for head-group modified Dip isomers. **A**: 25 µM HO_2C-Hex-Dip-Hex-C6, **B**: 25 µM HO_2C-Hex-Dip-Hex-C12, **C**: 16 µM HO_2C-Hex-Dip-Hex-OH, **D**: 17 µM HO_2C-Hex-Dip-Hex-Hex-OH, **E**: 15 µM HO_2C-Hex-Dip-Hex-Hex-OPhos, **F**: 18 µM HO_2C-Hex-Dip-Hex-Hex-OSucc. Excitation wavelengths varied minimally around 305 nm (302-305) for all compounds in both solvents. Fluorescence intensity varied over time in aqueous solution. 145

Figure 4.10: Fluorescence quenching in CH_3OH for 17 µM HO_2C-Hex-Dip-Hex-Hex-OH. From top to bottom, $[CuSO_4]$ = 0, 0.25, 0.5, 1, 1.5 mM. INSET: Stern-Volmer analysis of quenching data, $K_{SV} = 1.19 \pm 0.08 \times 10^3\ M^{-1}$. 146

Figure 4.11: Fluorescence emission spectra in aqueous buffer (10 mM BisTris, 100 mM NaCl, pH 6.4) immediately after mixing (black lines) or after 10 minutes stirring time (grey lines) for **A**: HO_2C-Hex-Dip-Hex-Hex-OH and **B**: HO_2C-Hex-Dip-Hex-Hex-OAc. 148

Figure 4.12: Fluorescence quenching in aqueous buffer (10 mM BisTris, 100 mM NaCl, pH 6.4) for 17 µM HO_2C-Hex-Dip-Hex-Hex-OH. From top to bottom, $[CuSO_4]$ = 0, 0.1, 0.2, and 0.5 mM. λEX= 305 nm. INSET: Stern-Volmer analysis of quenching data at 320nm, $K_{SV} = 3.28 \pm 0.07 \times 10^3\ M^{-1}$. The fluorescence at ~400 nm did not follow a linear Stern-Volmer relationship. 150

Figure 4.13: Fluorescence emission spectra in aqueous buffer (grey lines) (10 mM Na_3PO_4, 100 mM NaCl, pH 6.4) or after 10 minutes incubation time with lipid vesicles (black lines) for selected head-group modified Dip isomers. **A**: 16 µM HO_2C-Hex-Dip-Hex-OH, **B**: 17 µM HO_2C-Hex-Dip-Hex-Hex-OH, **C**: 18.5 µM HO_2C-Hex-Dip-Hex-OAc, **D**: 15 µM HO_2C-Hex-Dip-Hex-Hex-OPhos, **E**: 18 µM HO_2C-Hex-Dip-Hex-Hex-OSucc. Excitation wavelengths varied minimally around 305 nm (302-305) for all compounds. Data for HO_2C-Hex-Dip-Hex-C6 and HO_2C-Hex-Dip-Hex-C12 available in Fig. 4.14. 152

Figure 4.14: TOP PANEL: **A**: Fluorescence emission ratio at 320 nm (solid line) versus 380 nm (dashed line) as a function of time of 25 µM HO_2C-Hex-Dip-Hex-C6 injected at the specified time into an aqueous suspension of lipid vesicles (10 mM Na_3PO_4, 100 mM NaCl, pH 6.4). λEx= 305 nm. **B**: fluorescence emission spectra of the same solution before (grey line) and after (black line) vesicle incubation. **BOTTOM PANEL**: analogous experiments for 25 µM HO_2C-Hex-Dip-Hex-C12..... 154

Figure 4.15: TOP PANEL: Fluorescence emission spectra of 25 µM HO_2C-Hex-Dip-Hex-C6 (λEx= 305 nm) in aqueous solution (10 mM BisTris, 100 mM NaCl, pH 6.4) in the absence (grey) or presence (black) of lipid vesicles with the addition of 0.1 mM $CuSO_4$ (dashed lines). The bar graph shows the extent of quenching at both 320 and 380 nm, in the presence and absence of vesicles, as marked. **BOTTOM PANEL**: analogous experiments for 25 µM HO_2C-Hex-Dip-Hex-C12..... 155

Figure 4.16: Fluorescence emission summary for selected head-group modified Dip isomers. **A**: 16 µM HO_2C-Hex-Dip-Hex-OH, **B**: 17 µM HO_2C-Hex-Dip-Hex-Hex-OH, **C**: 18.5 µM HO_2C-Hex-Dip-Hex-Hex-OAc, **D**: 15 µM HO_2C-Hex-Dip-Hex-Hex-OPhos, **E**: 18 µM HO_2C-Hex-Dip-Hex-Hex-OSucc. Conditions as marked. [$CuSO_4$] = 0.1 mM for all compounds except HO_2C-Hex-Dip-Hex-Hex-OPhos, for which it was 0.2 mM. Excitation wavelengths varied minimally around 305 nm (302-305) for all compounds. 157

Figure 4.17: Fluorescence partition assay for HO_2C-Hex-Dip-Hex-C6. **A**: Fluorescence emission spectra of 17 µM compound (λEx= 305 nm) titrated against increasing concentration of lipid vesicles. From i to vi, lipid concentrations= 0.0625, 0.125, 0.25, 0.5, 1.5, 2.5 mM. **B**: Plot of CPS at 320 nm (closed circles) and 380 nm (open circles) as a function of lipid concentration, double reciprocal plot (INSET) used to determine Kp using Eqn 3. 1, r^2= 0.99. 160

Figure 4.18: Fluorescence partition assay for HO_2C-Hex-Dip-Hex-Hex-OH. **A**: Fluorescence emission spectra of 17 µM compound (λEx= 305 nm) titrated against increasing concentration of lipid vesicles. From i to vi, lipid concentrations= 0.0625, 0.125, 0.25, 0.375, 0.5, 1.5, 2.5 mM. **B**: Plot of CPS at 320 nm as a function of lipid concentration, double reciprocal plot (INSET) used to determine Kp using Eqn 3.1, r^2= 0.99. 162

Figure 5.1: Copy of Figure 2.20, working hypothesis to explain the activity of the Dip oligomers. 171

Figure 5.2: Fluorescence emission at 320 nm (black lines) and 380 nm (grey lines) (λEx= 305 nm) for an aqueous suspension of vesicles pre-loaded with **A**: 0.3% HO_2C-Hex-Dip-Hex-C6, or **B**: 0.3% HO_2C-Hex-Dip-Hex-C12. The arrow indicates the addition of 15 µM HO_2C-Hex-Dip-Hex-C6 in **A**, and 20 µM HO_2C-Hex-Dip-Hex-C12 in **B**. The vertical scale is the same for both panels. 173

Figure 5.3: Results of long time-scale HPTS activity assay for 22 μM HO_2C-Hex-Dip-Hex-C6. **A**: Decreasing HPTS activity over time; from initial scan at t= 0 minutes, to 10, 20 and 30 minutes. **B**: Rates of HPTS activity (Black circles) compared with increase in emission at 380 nm (grey circles). **C**: Fluorescence emission (λEx= 305 nm) at t= 0 minutes (black line) and t= 40 minutes (grey line). **D**: Bar graph illustrating the same data as in **B** (black bars), indicating the effect of an additional 22 μM of compound (grey bar). 175

Figure 5.4: Results of long time-scale HPTS activity assay for 10 μM HO_2C-Hex-Dip-Hex-Hex-OH. **A**: Fluorescence emission spectra (λEx= 305 nm) of compound incubated with an aqueous solution of vesicles taken at t= 1 min (black line), and t= 40 min (grey line). **B**: HPTS rates over time (black circles), compared with emission at 390 nm (grey circles). HO_2C-Hex-Dip-Hex-Hex-OPhos exhibited identical behavior. 176

Figure 5.5: TCSPC results for HO_2C-Dec-Dip-Hex-G(12)-OH. **A**: 20 μM compound in methanol, **B**: 20 μM compound in phosphate buffer (10 mM Na_3PO_4, 100 mM NaCl, pH=6.4), **C**: 1 mol% compound pre-loaded into vesicles. λEx= 276 nm, λEm= 380 nm. Blue line= IRF, black line= experimental decay curve, red line= calculated fit of the data. Further experimental details are available in Appendix 3. 178

Figure 5.6: Change in fluorescence decay profiles over time for 20 μM HO_2C-Hex-Dip-Hex-C6 incubated with a suspension of lipid vesicles in aqueous phosphate buffer (10 mM Na_3PO_4, 100 mM NaCl, pH 6.4). Scans were taken after **A**: 1 min, **B**: 20 mins, **C**: 70 mins of mixing time. 182

Figure 5.7: Change in relative proportions of each lifetime component over time. LEFT PANEL: 20 μM HO_2C-Hex-Dip-Hex-C6, RIGHT PANEL: 20 μM HO_2C-Hex-Dip-Hex-C12. Black = τ1 (shortest-lived component), Grey = τ2 (mid lifetime component), Red = τ3 (longest lived component). 183

Figure 5.8: Change in fluorescence decay profiles over time for 20 μM HO_2C-Hex-Dip-Hex-C12 incubated with a suspension of lipid vesicles in aqueous phosphate buffer (10 mM Na_3PO_4, 100 mM NaCl, pH 6.4). Scans were taken after **A**: 1 min, **B**: 20 mins, **C**: 70 mins of mixing time. 183

Figure 5.9: Proportion of longest lived species (τ3) (black circles)(LEFT AXIS) as a function of time for 20 μM HO_2C-Hex-Dip-Hex-C6, compared with growth of 380 nm emitting species over time for 15 μM of HO_2C-Hex-Dip-Hex-C6 added to an aqueous suspension of vesicles to which 0.3 mol% of the compound had already been pre-loaded (grey line) (RIGHT AXIS). 185

Figure 5.10: Proposed structures of 320 nm-emitting species initially inserted into bilayer. **A**: "U"-shaped monomer. **B**: linear transmembrane-inserted monomer. The compounds and lipids are drawn to scale. 188

Figure 5.11: Initially-formed dimers. **A**: rapidly-formed U-homodimer, a potential active structure, **B**: mixed linear-U dimer formed either from slower linear insertion of monomer, or slow opening of U-monomer (red arrow). **C**: linear homodimer, presumed to be the slowest forming of the initial species. The lipid pair is omitted for clarity.... 189

Figure 5.12: Examples of some of the processes that can occur in a phospholipid bilayer, including flip-flop, the crossing of a lipid from one bilayer leaflet to the other. Adapted from Ref. [2]. 191

Figure 5.13: Potentially slow structural reorganizations. **A**: initial U-monomer undergoes slow flip-flop to monomer in other bilayer leaflet (**B**). Once formed, this monomer aggregates to a transmembrane linear monomer (**C**); rearrangement to form the stable, final transmembrane linear 'sink' aggregate (**D**) with carboxylates on both sides of the bilayer finally occurs. 192

Figure 5.14: Schematic illustration of the proposed new model. **A**: the compounds aggregate when initially introduced into aqueous solution, from which the active compounds partition *via* an aqueous monomer into the bilayer (**B**). Once partitioned, the initially formed U-monomers (blue rectangle in **B**), laterally diffuse to form the U-aggregate, opening an ion conducting pathway (red cylinder) (**C**). Slower rearrangement (to form **D**) and eventual flip-flop (to form **E**, the final 'sink' aggregate) then occurs, forming the transmembrane species (red rectangle in **D** and **E**), which are transport inactive. Other intermediates are also possible. 193

List of Schemes

Scheme 2.1: Successful solution-phase synthesis of the first Dip isomer; HO_2C-Hex-Dip-Hex-G(12)-OH. Full experimental details and characterization available in Appendices 1 and 2. TBDMS= *tert*-butyl dimethylsilane, TMSOTf= trimethylsilyl triflate, DiPEA= diisopropyl ethylamine, pTsOH= *para*-toluenesulfonic acid. 31

Scheme 2.2: Synthesis of HO_2C-Dec-Dip-Hex-G(12)-OH. Full experimental details and characterization available in Appendices 1 and 2. 38

Scheme 3.1: Attempted synthesis of the tetra-aromatic trimer HO_2C-Hex-Bi(Dip)-G(12)-OH (**3-10**). The solid arrows indicate successful reactions, while the identity of the final compound could not be satisfactorily assessed, due to poor solubility. Full experimental details and characterization available in Appendices 1 and 2..... 81

Scheme 3.2: Synthesis of the Trip scaffold and Trip-containing molecules..... 85

Scheme 4.1: Synthesis summary, compound naming, numbering and structures for 2^{nd}-generation Dip isomers. Full experimental details and characterization available in Appendices 1 and 2..... 123

List of Abbreviations

ACN: acetonitrile

CF: 5(6)-carboxyfluorescein

Chol: cholesterol

cmc: critical micellar concentration

CPE: conjugated polyelectrolyte

DCM: dichloromethane

Dec: 10-carbon piece

DHP: 3,4-dihydro-2H-pyran

DIC: *N,N*-diisopropyl carbodiimide

DiPEA: diisopropyl ethylamine

DiPhyPC: diphytanoyl phosphatidylcholine

DIU: N,N-diisopropyl urea

DLS: dynamic light scattering

DMAP: 4-dimethylaminopyridine

DMF: dimethylformamide

Dod: 12-carbon piece

DPA: diphenylacetylene

DPH: 1,6-diphenylhexatriene

EC_{50}: effective concentration; concentration at half-maximal response

FDQ: fluorescence depth quenching

g: conductance

GUV: giant unilamellar vesicle

Hex: 6-carbon piece

HOBt: hydroxybenzotriazole

HPLC: high performance liquid chromatography

HPTS: 8-hydroxy-l,3,6-pyrene trisulfonate

IRF: instrument response function

Kp: partitioning constant

LUV: large unilamellar vesicle

MeOH: methanol

NBD: nitrobenzodioxazole

NMR: nuclear magnetic resonance

Oct: 8-carbon piece

PA: phosphatidic acidic

pA: picoAmpere

PC: phosphatidylcholine

PRE: prenyl

pS: picoSiemen

pTsOH: *para*-toluenesulfonic acid

REES: red-edge excitation spectra

R_f: retention factor

SPS: solid phase synthesis

TBDMS: *tert*-butyl dimethylsilane

tBu: *tert*-butyl

TCSPC: time correlated single-photon counting

TES: trimethylsilyl ethanol

TFA: trifluoroacetic acid

THF: tetrahydrofuran

THP: tetrahydropyran

TLC: thin-layer chromatography

TMS: trimethylsilyl

TMSOTf: trimethylsilyl triflate

TRES: time-resolved emission spectra

List of Numbered Compounds

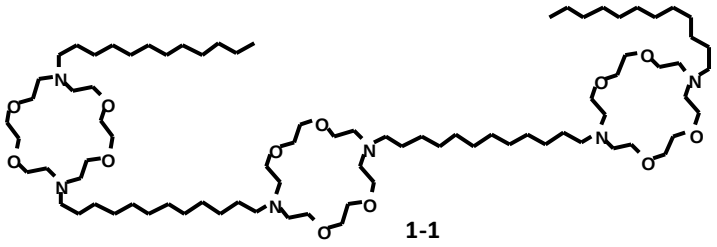

1-1

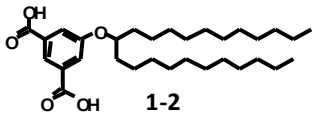

1-2

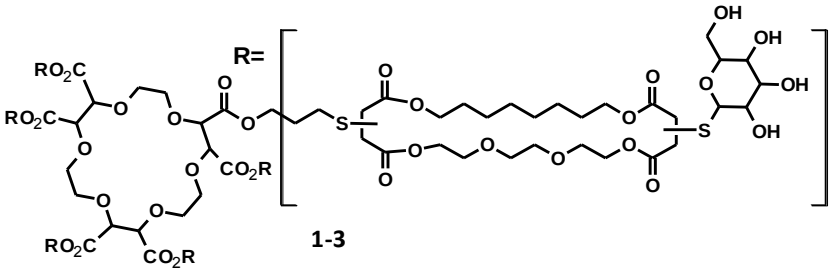

1-3

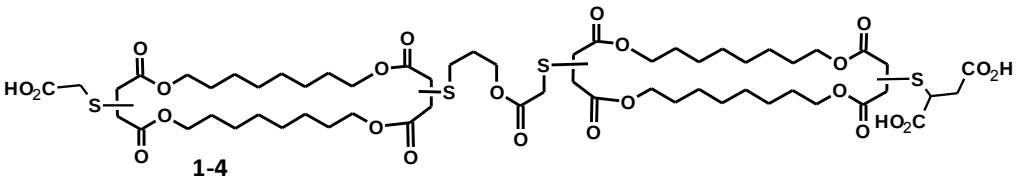

1-4

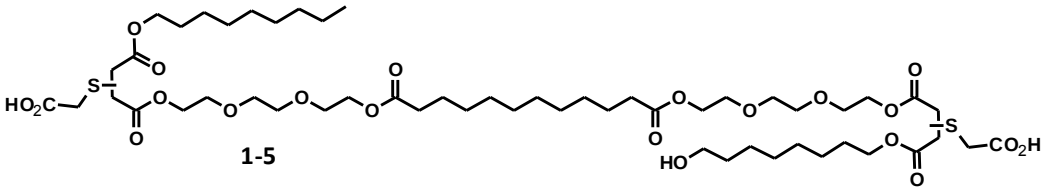

1-5

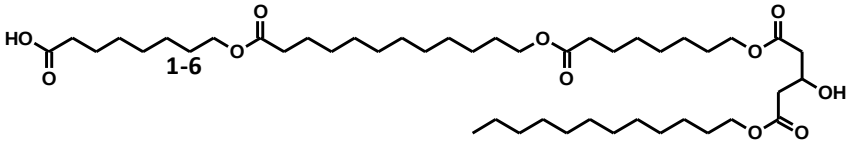

1-6

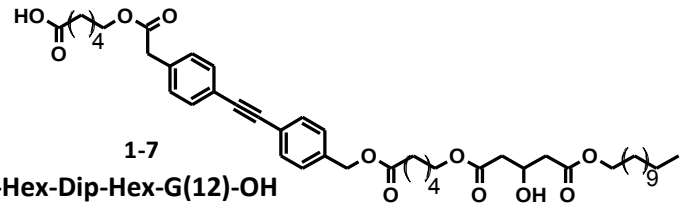

1-7

HO_2C-Hex-Dip-Hex-G(12)-OH

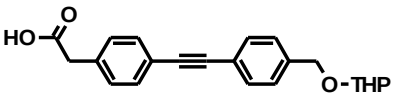

2-1

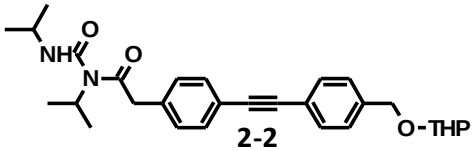

2-2

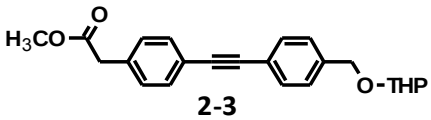

2-3

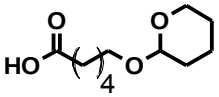

2-4

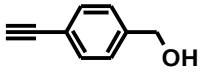

2-5

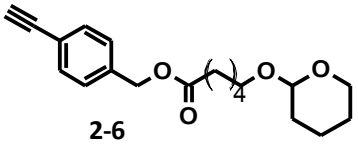

2-6

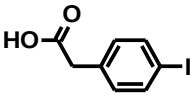

2-7

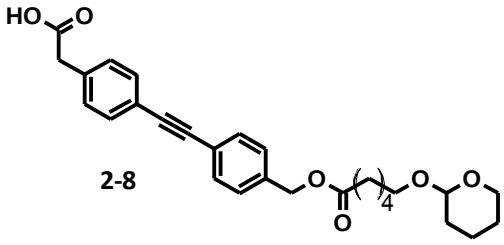

2-8

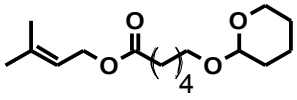

2-9

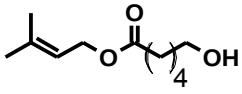

2-10

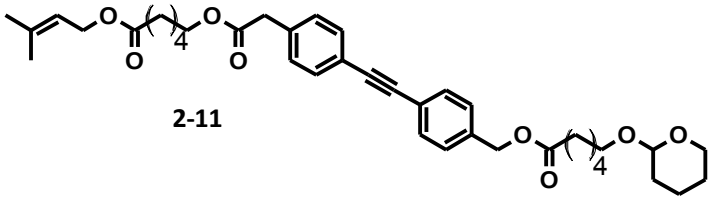

2-11

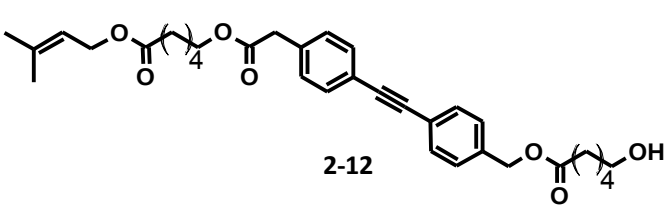

2-12

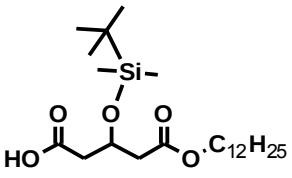

2-13

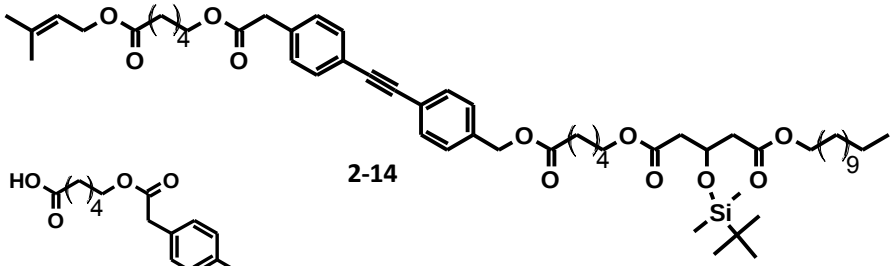

2-14

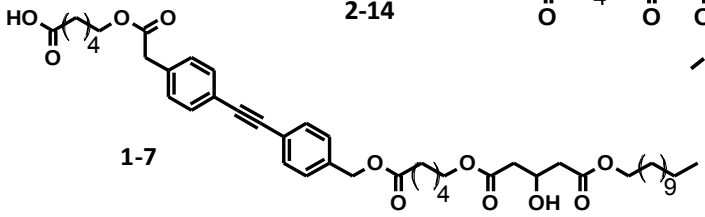

1-7

HO_2C-Hex-Dip-Hex-G(12)-OH

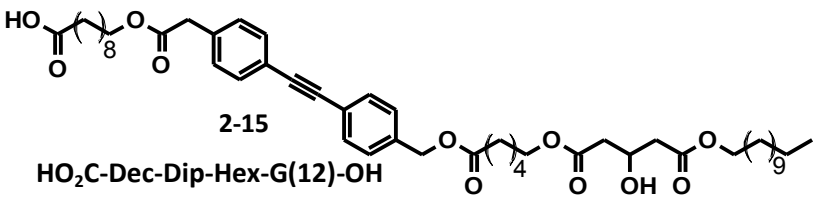

2-15

HO_2C-Dec-Dip-Hex-G(12)-OH

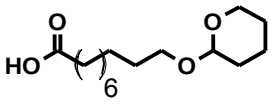

2-16

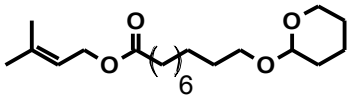

2-17

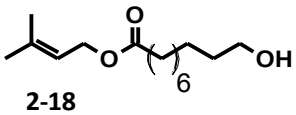

2-18

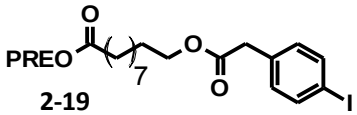

2-19

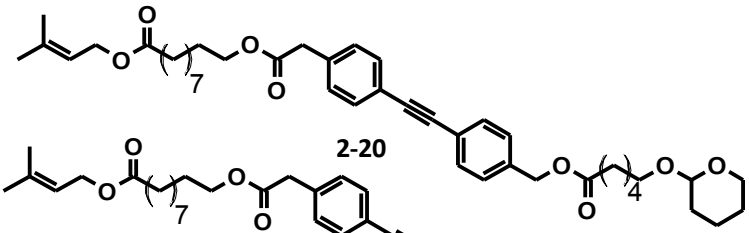

2-20

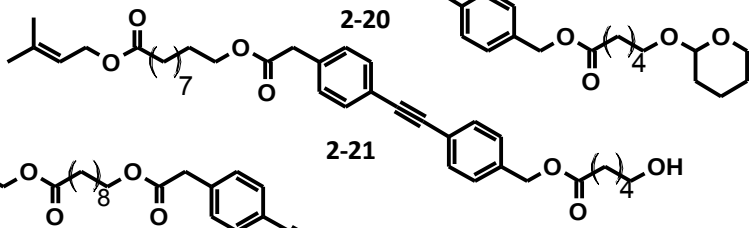

2-21

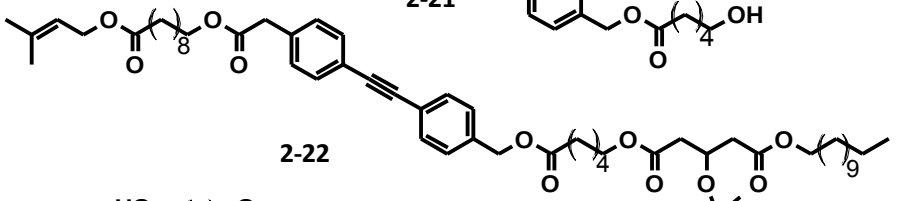

2-22

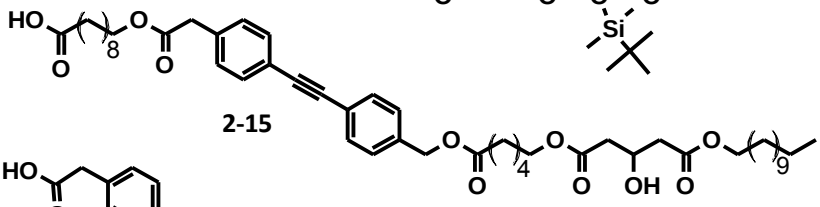

2-15

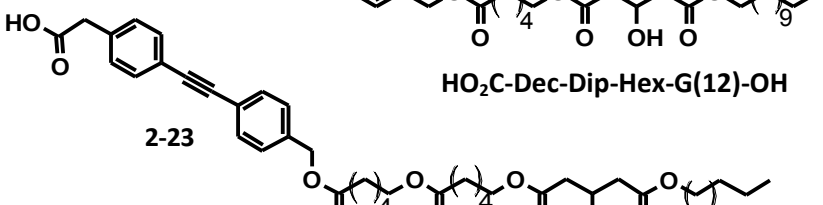

HO_2C-Dec-Dip-Hex-G(12)-OH

2-23

HO_2C-Dip-Hex-Hex-G(12)-OH

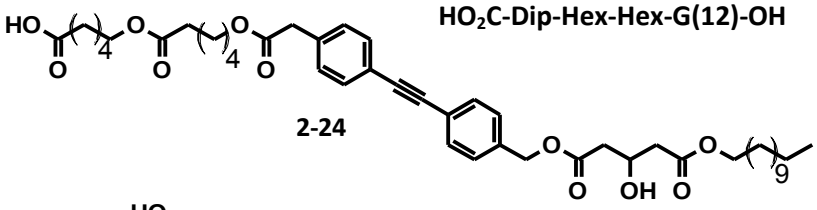

2-24

HO_2C- Hex-Hex-Dip-G(12)-OH

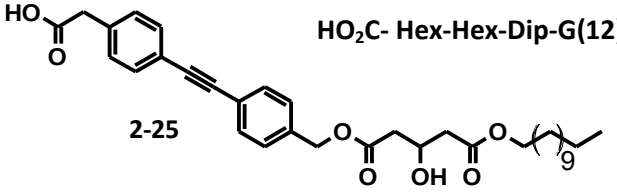

2-25

HO_2C-Dip-G(12)-OH

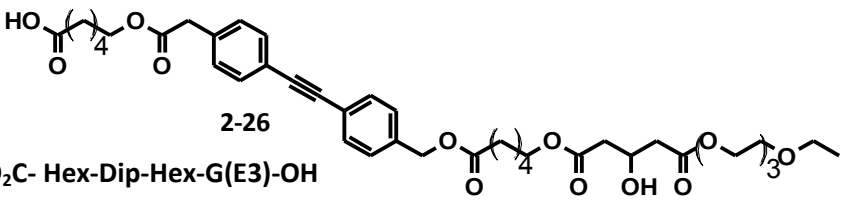

2-26

HO_2C- Hex-Dip-Hex-G(E3)-OH

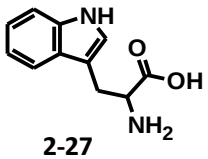

2-27

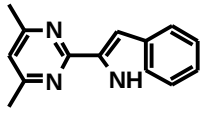

2-28

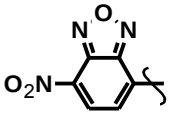

2-29

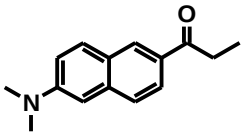

2-30

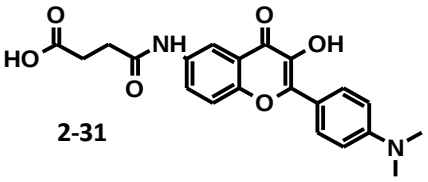

2-31

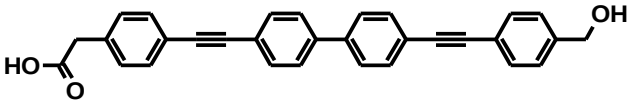

3-1

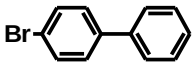

3-2

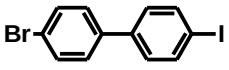

3-3

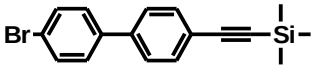

3-4

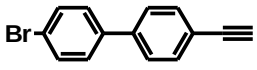

3-5

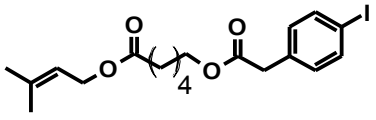

3-6

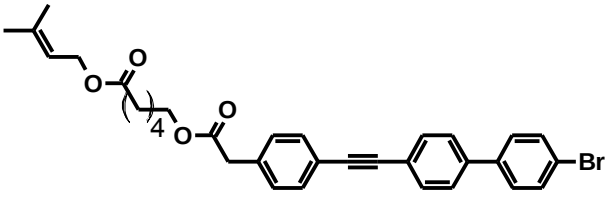

3-7

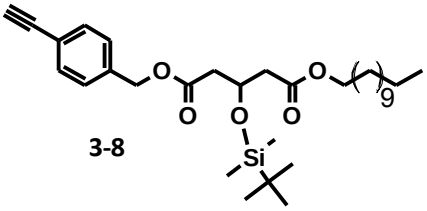

3-8

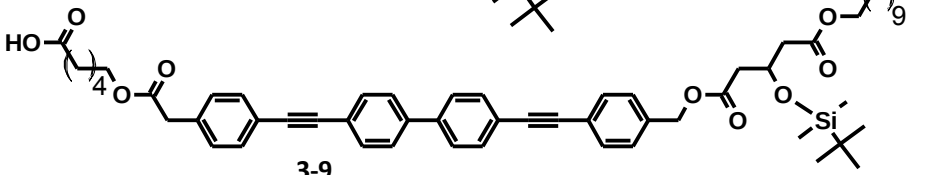

3-9

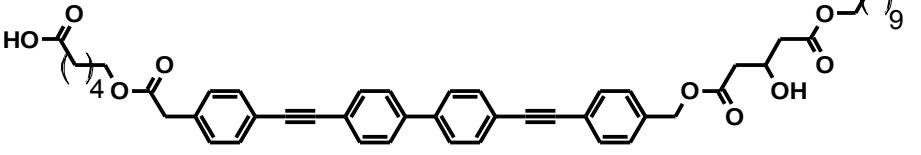

3-10 HO_2C-Hex-Bi(Dip)-G(12)-OH

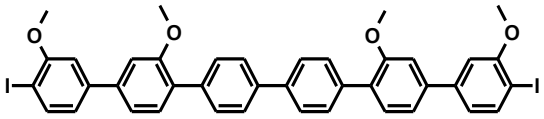

3-11

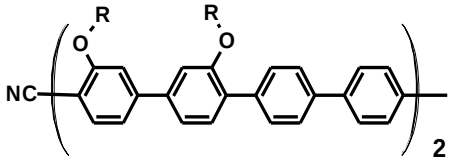

3-12

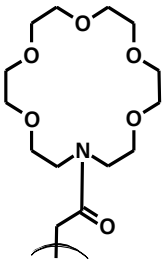

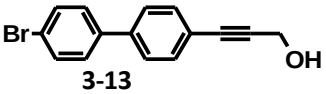

3-13

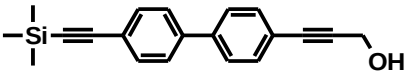

3-14

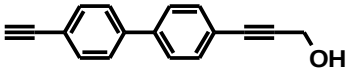

3-15

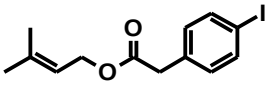

3-16

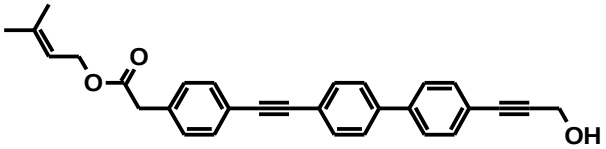

3-17

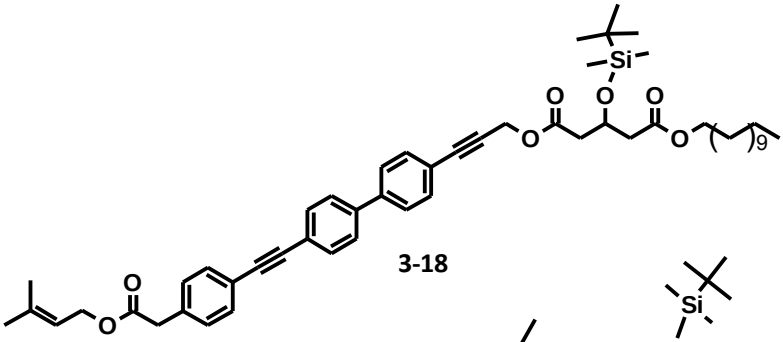

3-18

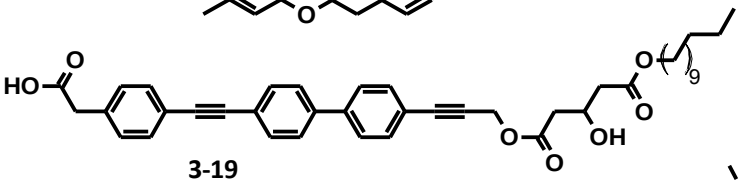

3-19

HO_2C-Trip-G(12)-OH

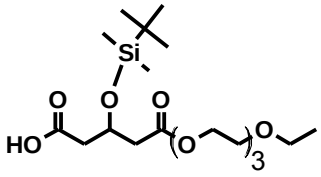

3-20

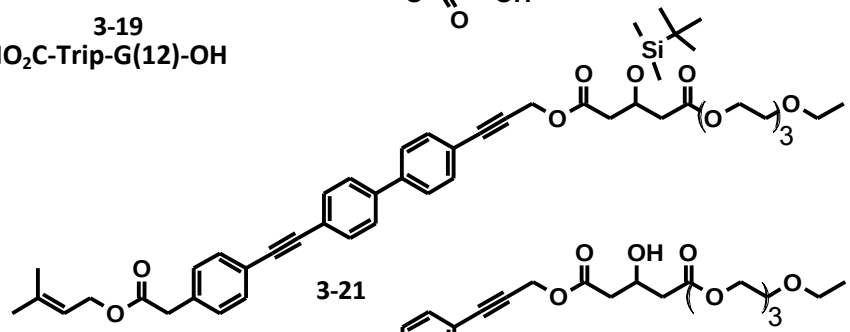

3-21

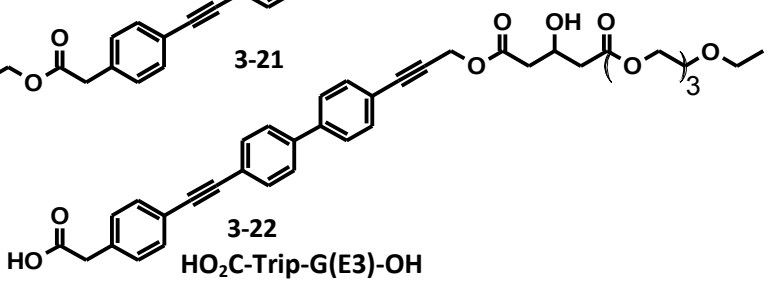

3-22

HO_2C-Trip-G(E3)-OH

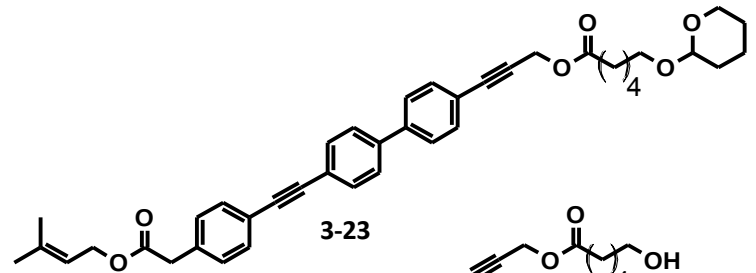

3-23

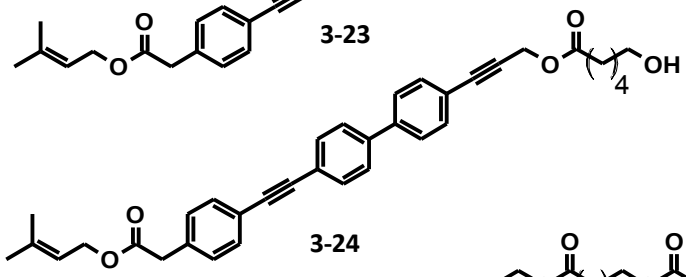

3-24

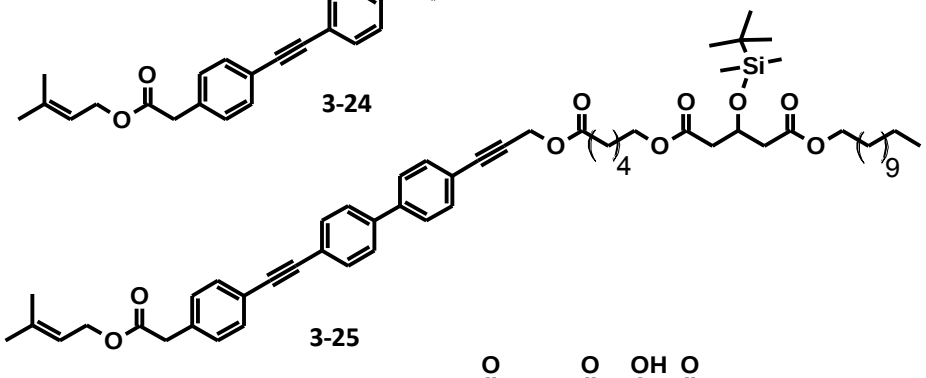

3-25

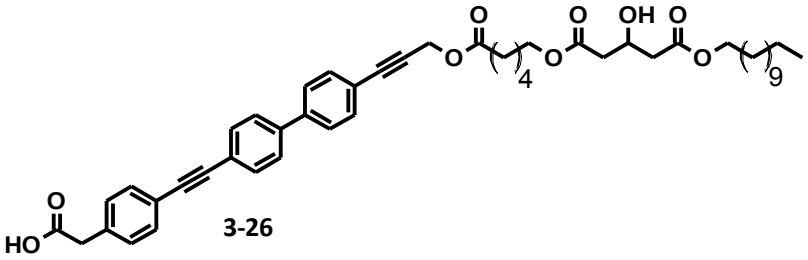

3-26

HO_2C-Trip-Hex-G(12)-OH

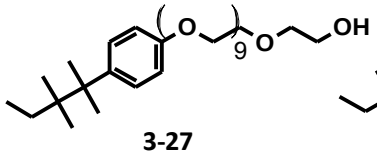

3-27

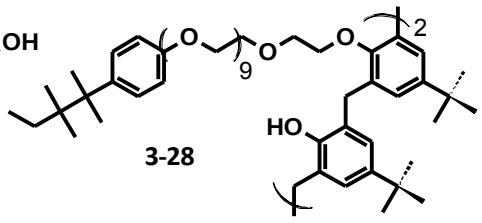

3-28

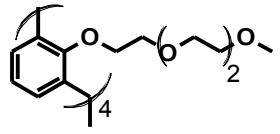

3-29

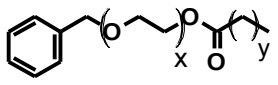

3-30:
x= 4, 5, y= 6,8,10,12

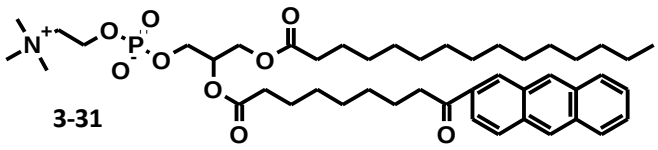

3-31

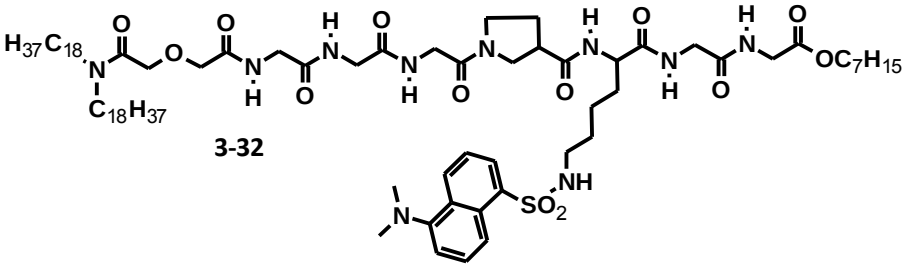

3-32

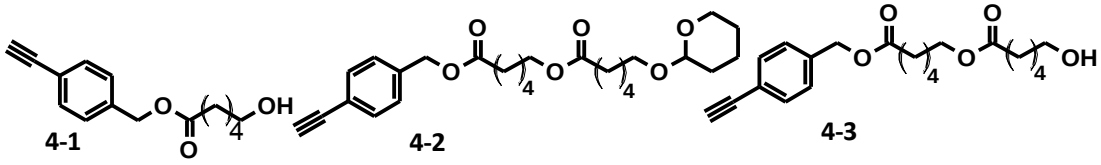

4-1 4-2 4-3

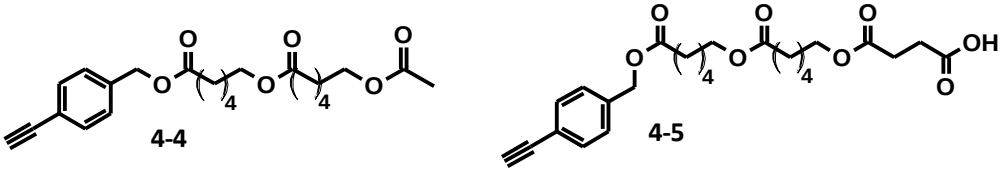

4-4 4-5

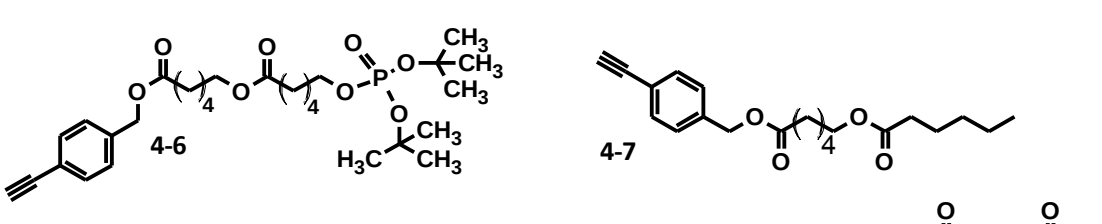

4-6 4-7

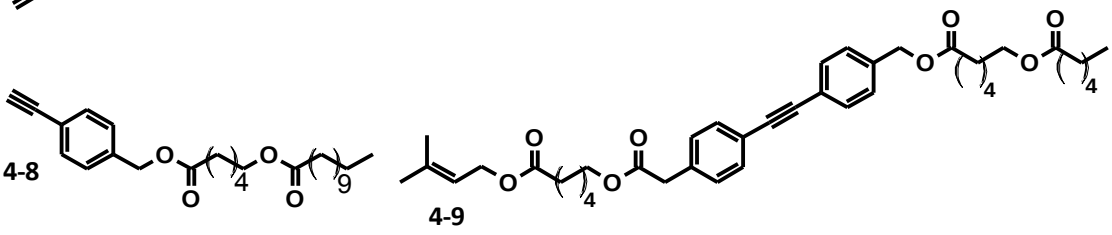

4-8 4-9

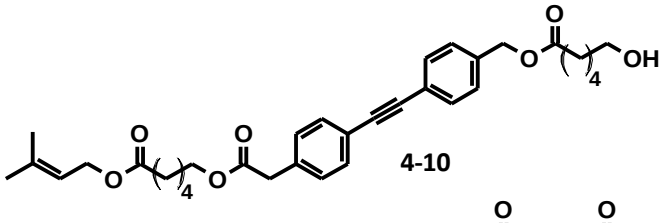

4-10

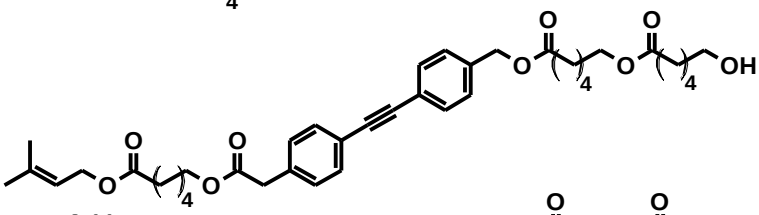

4-11

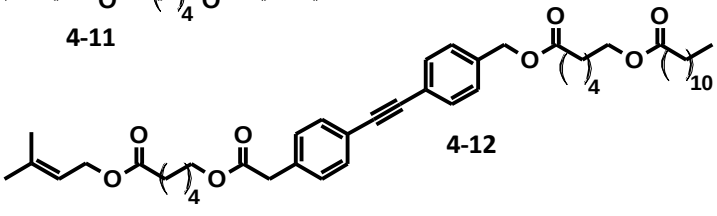

4-12

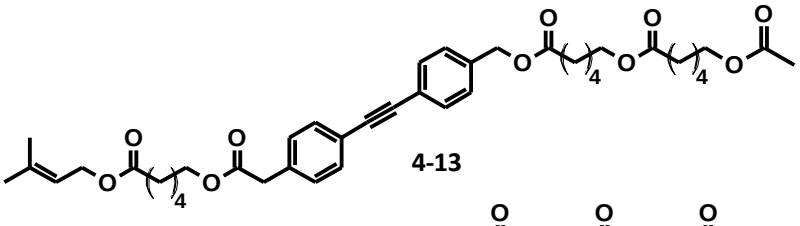

4-13

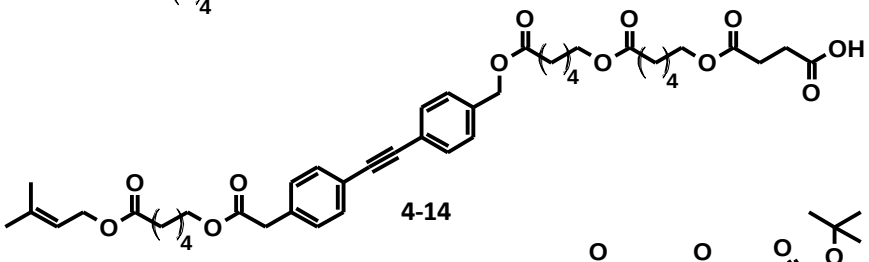

4-14

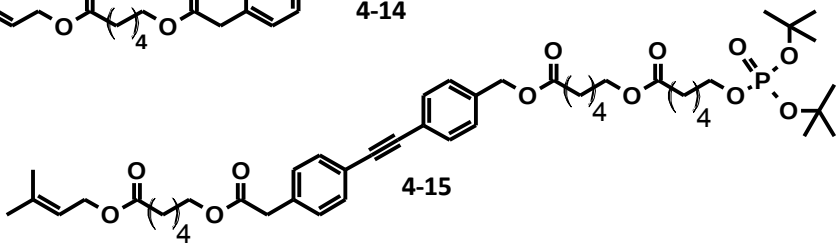

4-15

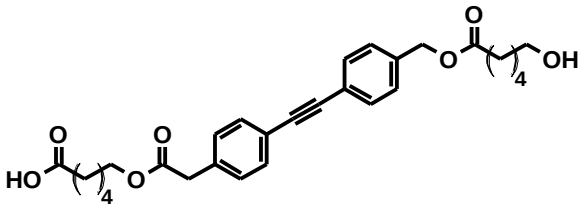

4-16

HO_2C-Hex-Dip-Hex-OH

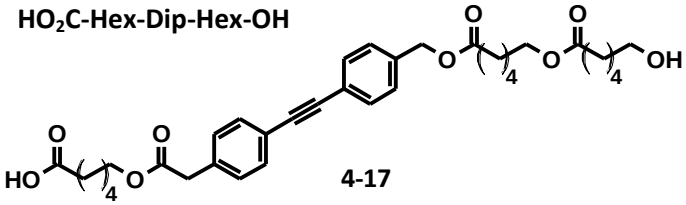

4-17

HO_2C-Hex-Dip-Hex-Hex-OH

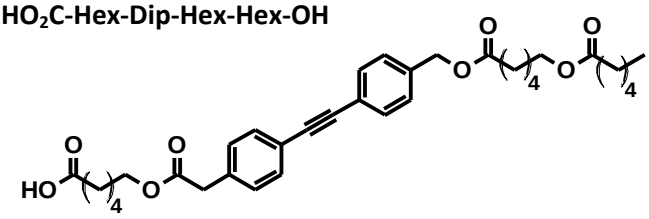

4-18

HO_2C-Hex-Dip-Hex-C6

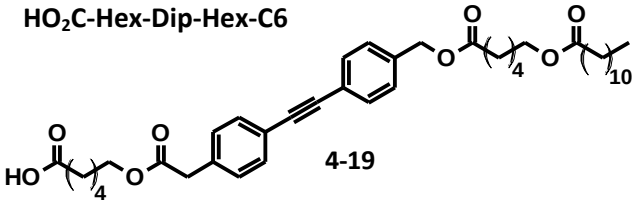

4-19

HO_2C-Hex-Dip-Hex-C12

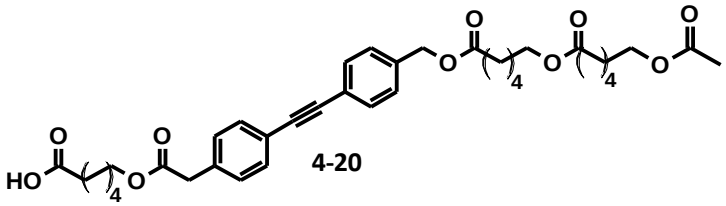

4-20

HO_2C-Hex-Dip-Hex-Hex-OAc

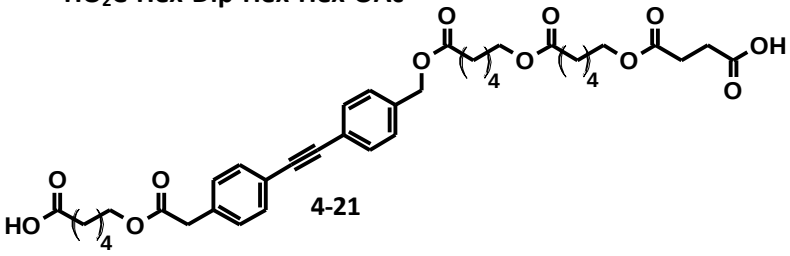

4-21

HO_2C-Hex-Dip-Hex-Hex-OSucc

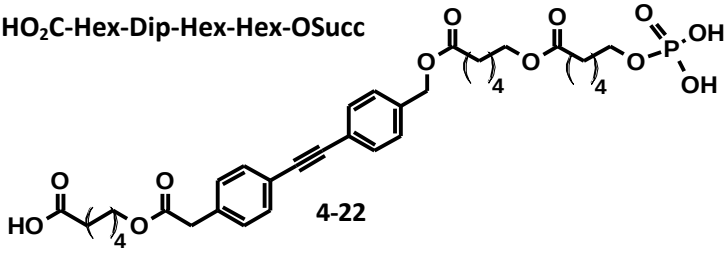

4-22

HO_2C-Hex-Dip-Hex-Hex-OPhos

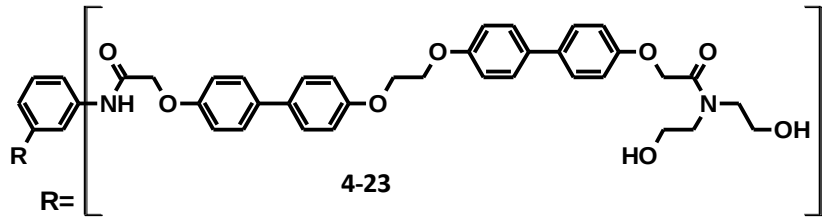

4-23

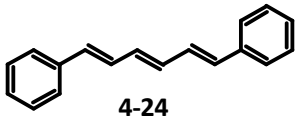

4-24

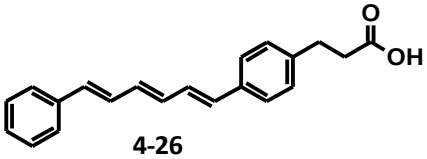

4-26

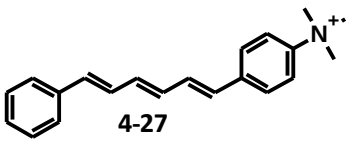

4-27

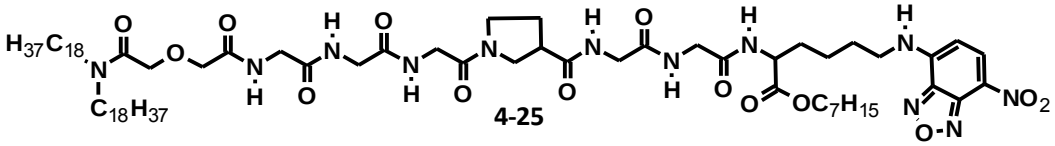

4-25

Acknowledgements

I would like to acknowledge my supervisor, Dr. Tom Fyles, for providing me with such an interesting project which I have thoroughly enjoyed and for the guidance, great ideas and suggestions over the years.

Members of the Fyles lab both past and present should also be acknowledged for their helpful discussions and good company; Dr. Horace Luong deserves special mention for laying the groundwork for this project. Andrew, Jonathan, Paria, Kathleen, Matt – thanks as well! I also extend my thanks to Dr. Cornelia Bohne and the Bohne lab members for helpful discussion, experiment suggestions and fluorescence assistance, especially TCSPC, as this was new to me. The University of Victoria Chemistry Department, faculty and staff, the Mark and Nora DeGoutiere Memorial foundation are also acknowledged. I also thank my Committee for reading this Thesis.

Finally, I would like to acknowledge my parents Christine and Ted, my sister Dorothy, my boyfriend Andrew Dambenieks and the rest of my family and friends for their support over the years.

Thank you all for your part in this Thesis.

Chapter 1 : Introduction

1.1: Factors driving synthetic ion channel research

All cells are surrounded by membranes, which act as semi-permeable barriers between the cell and its environment [1]. While certain non-polar molecules and gases may freely diffuse across this barrier, charged species such as ions, and polar substances such as peptides and sugars cannot [1]. The structure of the cellular membrane is responsible for many of these unique properties. It is comprised of two layers ('leaflets') of phospholipids arranged in an end to end stack, Figure 1.1. The phospholipids consist of a polar phosphate-containing headgroup which is in contact with the aqueous environment inside and outside the cell. The headgroups are connected *via* ester bonds (the 'midpolar region') to long alkyl fatty acid 'tails'; usually two such tails are present per headgroup and these make up the hydrophobic 'core' of the membrane. The identity of the headgroups depends on the nature of the lipid; most commonly, charged species such as choline are appended to the phosphate as esters; DPPC (1,2-dipalmitoyl-*sn*-glycero-3-phosphocholine) a major constituent of cellular membranes is shown in Figure 1.1A and B [2]. The length of each component of the phospholipid can vary, however, the overall thickness of a bilayer membrane is approximately 5nm, of which 3.5nm make up the hydrophobic core, Figure 1.1C, D [3,4]. It is this hydrophobic core that prevents the free passage of ions across the membrane, as transferring an ion from aqueous solution where it is well-solvated to the non-polar interior of the membrane in which it is highly destabilized is a very energetically unfavourable process [1]. It is therefore the role of ion channels to make this more favourable by replacing some of the stabilizing solvent interactions present in aqueous solution [5].

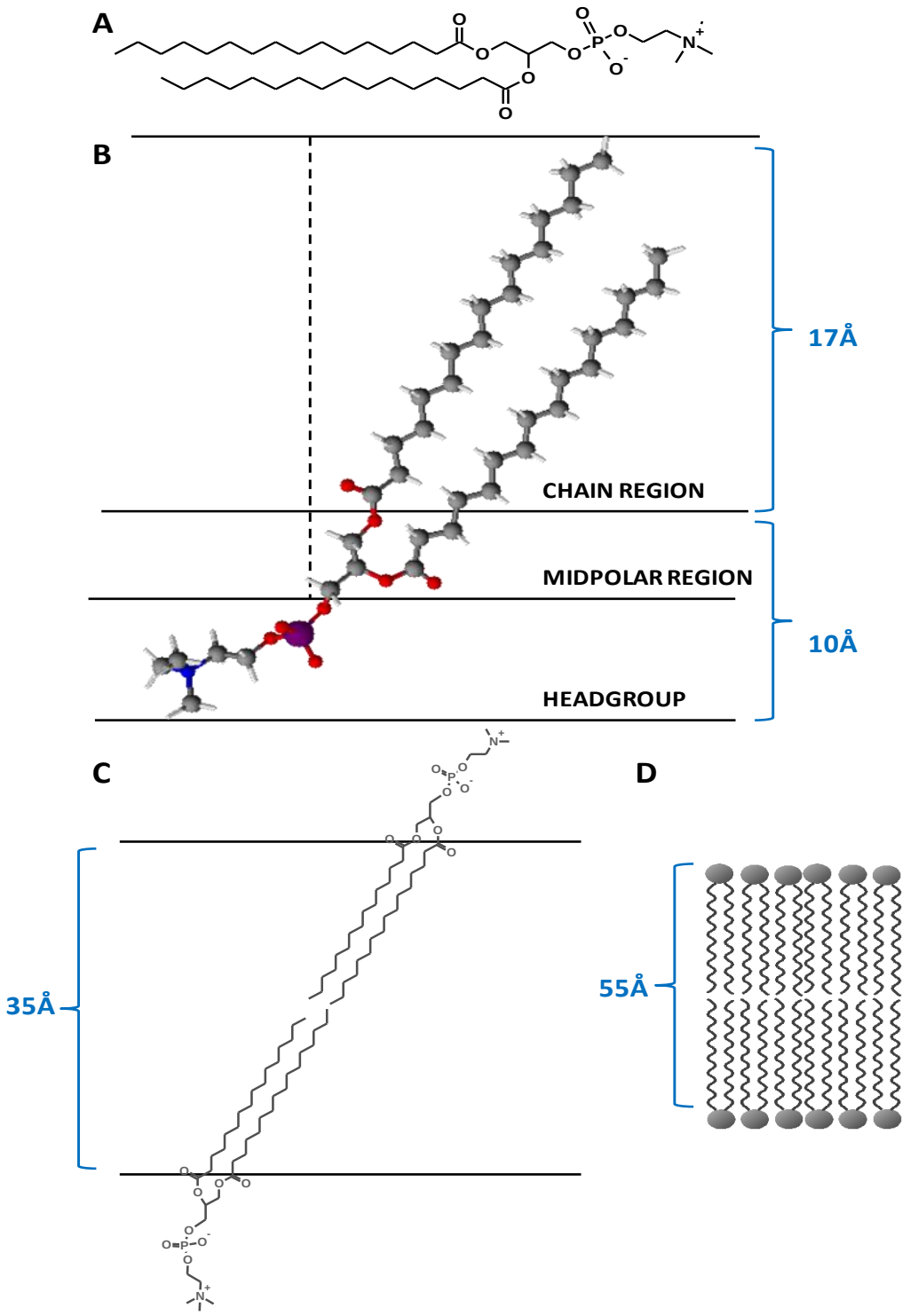

Figure 1.1: 1,2-dipalmitoyl-sn-glycero-3-phosphocholine (DPPC): **A**: Chemical structure, **B**: approximate dimensions of regions and tilt from the bilayer normal, based on X-ray structures obtained for actual bilayers; adapted from Ref [2]. Two of these lipids stack end to end to produce the lipid bilayer, schematically depicted in **C**: to-scale drawing with molecular dimensions and **D**: simplified 'cartoon' representation; the grey spheres are the headgroups.

It is important to note that the bilayer membrane is not a static environment; rather, it is highly dynamic and chaotic, the structure of the alkyl tails in particular is highly disordered, especially when moving towards the bilayer midplane [6, 2, 7]. The tails undergo very fast processes such as cis-trans bond isomerizations, while the entire lipids themselves laterally diffuse through each leaflet of the membrane, and even 'flip-flop' (translocate) from one bilayer leaflet to the other [2]. In addition, the entire membrane can 'undulate'. Considering these factors, accurate depictions of a bilayer membrane are therefore difficult to represent in a schematic way; any such depictions will necessarily be only 'snapshots' of a highly variable environment. Nevertheless, such representations are needed; with this in mind, Figure 1.1 demonstrates both a 'structurally-accurate' depiction in which the lipids and the spacing between them is drawn to-scale (C); this will be used when discussing structural characteristics of molecules in the membrane, as well as a highly simplified version (D) which will be used to illustrate concepts when molecular scales are not needed for the discussion.

The regulated transport of ions by ion channels across cell membranes is a fundamental process essential to all cells [1, 8]. Cellular signalling in the nervous system, muscle contraction, maintaining cellular volume and pH, removing waste products and delivering needed metabolites are all tasks relying on the barrier properties of the cell membrane coupled with the regulated activity of ion channels and pores. Serious deficiencies in any of these processes would quickly render the cell inviable; ion channel disorders have been linked to cystic fibrosis, epilepsy and hearing loss, amongst others [9, 10, 11]. In addition, the unregulated transport of ions across bacterial membranes is believed to be the mechanism by which certain antibiotics act [5, 11], further demonstration of the importance of ion channels in maintaining proper ionic gradients across membranes.

Natural ion channels are remarkable molecules, not only are they able to transport up to 10^8 ions per second, they accomplish this in an extremely selective way; a potassium channel almost exclusively transports potassium ions at the expense of others such as sodium [12]. In addition, natural ion channels utilize a variety of

mechanisms to open and close their pores in response to stimuli such as membrane potential and pH; these multiple forms of 'gating' and ion selectivity are what allow the channels to perform their necessary functions so effectively. Clearly, natural ion channels are worthy of study; however, this is complicated by the fact that they are large, complex proteins which can reach molecular weights well over 10^4 grams per mole; methods to extract, characterize and study them are therefore challenging. This is well illustrated by the fact that the first high-resolution X-ray crystal structure of a natural ion channel (the bacterial potassium-selective 'KcsA' channel) obtained by MacKinnon *et al.* earned the Nobel Prize [13]. While this is an extremely significant achievement that has led to much insight into how channels function, and will certainly have an impact on channel research for many years, this was a very difficult task, and the majority of natural ion channel structures will most likely remain unknown for some time.

The impetus to develop structurally simpler synthetic analogs of the natural channels is therefore clearly evident. Synthetic ion channels can act both as model systems to aid in understanding how the natural channels function, as well as potentially achieving interesting and important functions of their own. The potential biological applications of synthetic ion channels have already been mentioned; both to develop channel-based therapeutics to possibly treat diseases such as cystic fibrosis, as well as to produce novel antibacterial agents [5]. In addition, ion channels are sensors; they detect and interact with analytes in their environment which therefore elicits a response [14]; this too is a very important property that can be targeted with synthetic ion channels.

Synthetic ion channel research is therefore driven by several important goals: to design and synthesize molecules that are ion transport-active and have regulatory properties such as gating which are similar to natural channels; such molecules can therefore function as model systems of natural channels, potential therapeutic agents, and sensors. However, while the potential applications of synthetic ion channels are significant, before these applications can be realized much more information must be

gained as to how these molecules actually function as ion transporters. Therefore, in addition to designing and synthesizing active compounds, research into their mechanism of action in the membrane should be a key component of synthetic ion channel studies.

1.2: Synthetic ion channels

1.2.1: Overview & classification

For the past several decades, synthetic ion channel research has been extensively pursued by many groups worldwide, and a large number of not only individual compounds but entire classes of transport-active molecules have been made over this time. A number of these developed compounds have indeed achieved interesting properties in addition to ion transport; they have been used as anti-bacterial agents [5, 15, 16] and sensors for various analytes such as sugars [17]. These synthetic systems are also becoming increasingly sophisticated; examples in which the ion transport activity can be turned on and off in response to voltage [18, 19, 20], light [21] and the binding of certain ligands [22] exist. The ability to regulate the activity of these synthetic ion channels is a much sought-after property, as this is one of the key features of natural ion channels [9]. Progress is being made on this and many other fronts in synthetic ion channel research, and will certainly continue in the future.

While the successful synthesis and characterization of such a vast number of synthetic ion channels is certainly an achievement, this fact renders a discussion of the specific structures beyond the scope of this Introduction. Instead, a selection of those which are particularly pertinent to the current work will be discussed throughout this report. A more detailed discussion will be focused on previous studies carried out in the Fyles lab which have led to the current work. The field has been extensively and

recently reviewed, and for further information the interested Reader is directed towards these reviews [1, 8, 23, 24, 25, 26].

Attempts to classify and organize the vast number of known transport-active molecules have centred mainly on the type of active structure the synthesized component molecules are expected to form in the membrane. A variety of 'motifs' are known [27], but the two most general classes distinguish between compounds which are meant to act as unimolecular channels, and those which are comprised of a number of monomers which arrange themselves together into an aggregate-type channel ('barrel-

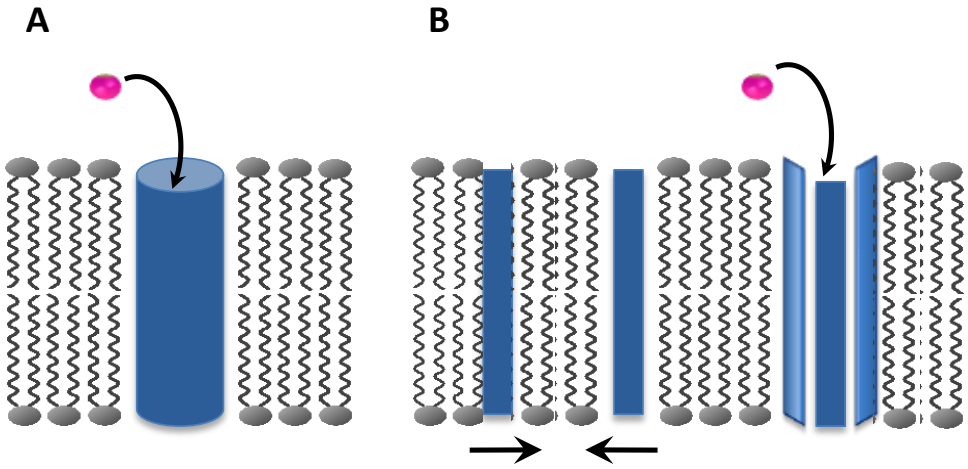

Figure 1.2: Synthetic ion channel classification. **A**: Unimolecular channels. **B**: Aggregate channels in which the individual monomers (rectangles) laterally diffuse in the membrane to form the channel.

stave' architectures are one such example) [27]. Both classes have advantages and disadvantages associated with them. As illustrated in Figure 1.2A, the unimolecular type of channel adopts an explicitly tubular structure; these compounds are large and of high (greater than 500 g/mol) molecular weight, as they must span the membrane and fully enclose a pore through which an ion can transit [1]. These molecules, an early example of which is shown as compound **1-1** in Figure 1.3A [28] are pre-organized to a certain extent, and therefore their conformation in the membrane is expected to be similar to that of the synthesized compound. While this is certainly an advantage, the synthetic effort involved in these types of molecules is significant, and if the obtained compound is inactive a great deal of time must be invested to make other analogs. In contrast, aggregate channels, depicted in Figure 1.3B, are comprised of

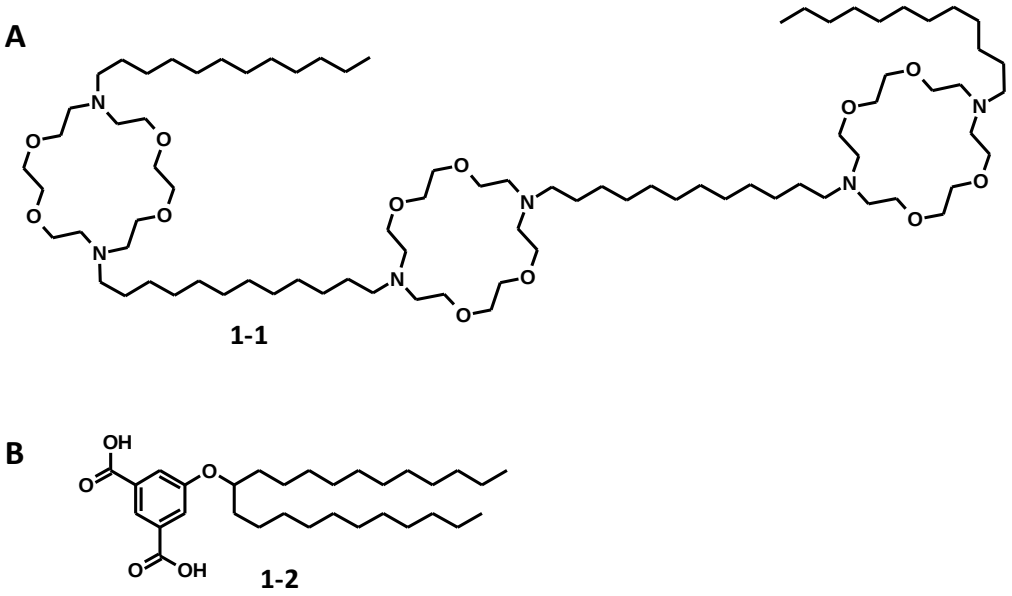

Figure 1.3: Chemical structures of synthetic channels exemplifying the classes shown in Fig. 1.2. **A**: unimolecular 'hydraphile' channel developed by Gokel *et al*. [28] (**1-1**), **B**: a 'simple' channel-former synthesized by Fyles *et al*.,(**1-2**) several of these monomers are assumed to form the active aggregate structure [29].

monomers which can be individually rather simple; compound **1-2** is highly transport-active in planar bilayers, despite its structural simplicity [29]. The synthesis and characterization of these monomers is much more straightforward than that of the unimolecular systems, however, the structures assumed when these monomers enter the bilayer are usually very difficult to assess. These compounds can therefore display a variety of behaviours when assayed, and developing mechanisms to explain their observed activities is a challenging task.

1.2.2: Characterization of ion channel activity

Once the potential channel-forming molecule is synthesized, the first step is to assess its activity. Is it transport-active, if so, how active and can this activity be regulated are all questions that need to be addressed, as synthetic ion channels are foremost judged on their function. This type of functional characterization is most important for synthetic ion channels, and therefore makes up the majority of studies carried out on these molecules [27]. The *structural* characterization of synthetic ion

channels, however, provides an interesting challenge. While the structural characterization of the individual components that comprise the putative channel can be accomplished easily using well-known spectroscopic and analytical methods, the structural characterization of the active channels themselves is more difficult. This is especially true for the aggregate-type channels discussed mainly in this report. This is due to a number of reasons: firstly, the active structures are transient in nature, as the aggregate channels form and open in response to random 'collisonal activation' of the component monomers in the bilayer; regulation of such openings has not yet been extensively achieved for aggregate-type channels [18]. Secondly, the active structures usually exist only in the bilayer itself [25], so the structures of individual monomers can only suggest how the active channel actually looks. Furthermore, the active channel is usually a minor species present in the mixture and may not be the most thermodynamically stable structure; therefore it is detectible for only a short period of time [1,27].

Considering these factors, it is not surprising that the vast majority of active structures of synthetic ion channels are unknown. However, while *proof* of a particular structure, such as that obtained for the natural KcsA channel, is currently unavailable for synthetic channels, many methods exist that can be used to infer active structures. These methods can potentially report many structural characteristics of a synthetic ion channel such as its diameter and how many monomers comprise it, as well as a number of functional properties such as ion selectivity, gating ability, concentration and pH dependence, stability (lifetime) and other characteristics [27]. A combination of these techniques including extensive functional characterization, structural characterization of the individual monomers and a variety of structure-activity relationship studies are therefore necessary to gain as much information about the synthesized channel as possible. From these studies, mechanisms to explain the observed activities are proposed, from which active structures are inferred; this has led to the description of a number of synthetic ion channel active structures which are highly plausible [30]. An overview of a selection of these techniques is presented here; other techniques are

known and widely-used [27], but will not be mentioned as they have not been utilized in this research.

1.2.3: Planar bilayer experiments

The techniques used for synthetic ion channel characterization are usually categorized as those utilizing planar lipid bilayers, such as the 'bilayer clamp' experiment [31,27,32,33], or those carried out with spherical bilayers called liposomes or vesicles [34,35,27]. In the bilayer clamp experiment, a set voltage is applied across a planar lipid bilayer that has been 'painted' (applied by brushing of a lipid solution) over a small (typically 250 µm) aperture in a plastic cup, Figure 1.4A. This cup is placed into one of two chambers which are immersed in a bathing solution of electrolyte; the lipid bilayer is therefore at the interface between the two chambers, in contact with aqueous solution on either side. When intact, the lipid bilayer is a good resistor; this is due to the insulating properties of the hydrophobic membrane interior, and forms the basis of the membrane's barrier properties, as discussed. The quality of the formed bilayer can be judged by comparison to known 'ideal' values of resistivity and capacitance [31]. In general, bilayer formation is quite reproducible and the membranes themselves are stable if formed correctly, lasting several hours without significantly varying properties. Once a satisfactory membrane is formed and duly monitored to ensure no extraneous activity occurs (Figure 1.4B), the compound of interest is introduced into the solution (Figure 1.4C). If the molecule successfully partitions into the membrane and is transport-competent, the ion channel that subsequently forms allows ions to pass from one electrolyte chamber to the other. This completes the circuit and generates a current; the applied voltages are of milliVolts (mV) and the observed currents are usually in the 1-100 picoAmpere (pA) range.

What does ion channel activity look like in this technique? In an ideally behaved ion channel, the observed current is recorded as a discrete step-up 'square-top' opening as shown in Figure 1.4C. This opening then remains at this higher level for a specific

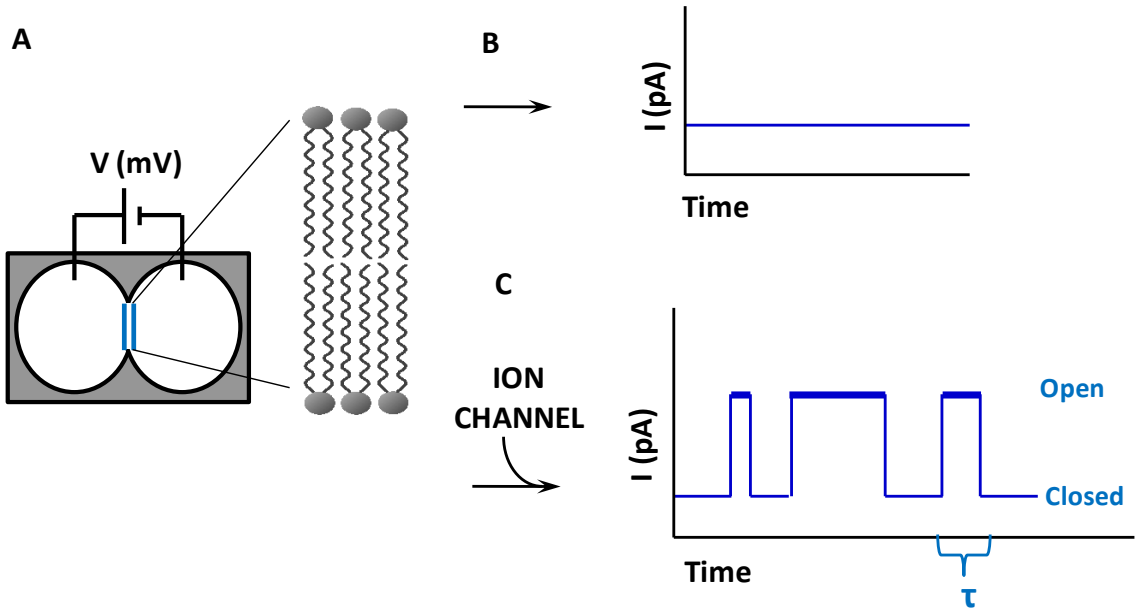

Figure 1.4: The bilayer clamp experiment. **A**: the electrolyte-filled chambers (black circles) are separated by a cup containing a small aperture (blue lines), over which a bilayer membrane is formed. **B:** In the absence of a transporter, no current (I) is observed as the bilayer acts as a resistor. **C:** With the addition of an active channel, ions flow and a current is detected as a step-up from the baseline.

time, (its lifetime, τ) ranging from a few milliseconds to minutes and even longer; indeed, synthetic ion channels that 'never' close have been reported [36]. The vertical axis represents current; a single-step up is indicative of a single ion channel active in the membrane, while multiple step-ups of the same magnitude indicate the opening of multiple channels [27]. The current (I) is then converted to conductance (g) using Ohm's law: I=gV, where V is the applied potential. However, not all channels are 'Ohmic' and have their current linearly respond to the applied potential; non-Ohmic behaviour occurs in cases such as voltage-gating, in which a certain 'gating potential' must be applied in order for the channel to open [1]. The conductance value, measured in Siemens (S), is a measure of the ability of an ion channel to pass ions across the membrane, and can be used to determine a variety of useful properties such as channel diameter [37]. Conductance depends on the counterion present in the electrolyte used, however, typical conductance values for natural channels are usually in the picoSiemen (pS) range, corresponding to channel diameters of several Angstroms (Å). Once again,

however, over-generalization is to be avoided, as examples of synthetic ion channels exhibiting 'huge' pore sizes of up to several nanometers exist, such as in a recent report by Davis *et al*., in which conductances of over 20 nS were occasionally observed for the studied compounds [38,39].

By varying the experimental parameters such as the counterions or pH of the electrolytes, the applied potential or identity of the lipids comprising the bilayer, detailed characterization of the synthetic channel can occur. As the formation of these ion channel openings is a random process, the observed activities are analysed using well-developed statistical methods to obtain average values of the lifetime, conductance and open probability (the amount of time the channel is expected to be open) [27]. Further discussion will be deferred to Chapter 2, in which actual data are presented. However, it should be mentioned that as the bilayer clamp is a single-molecule technique, it is highly sensitive to background noise and artefacts; this necessitates repeated experiments to ensure the behaviours observed are indeed due to the introduced molecule. In addition, the activity represented in Figure 1.4 is indeed for an 'ideal' channel, it should be appreciated that such activity is by no means the only, or even the majority, or observed behaviours. As alluded to, examples of synthetic ion channels with extremely long lifetimes and 'giant' pore sizes exist, as do compounds exhibiting exclusively very short lifetime, high conducting 'spikes' or 'flickers' and a variety of other 'irregular' types of activity. As will be further discussed, these types of activities are no less important or information-rich than the more regular variety; however, the methods used to analyze this type of activity remain less developed.

1.2.4: Vesicle-based assays

The other main type of technique utilized in synthetic ion channel research involves vesicles; spherical lipid capsules in which the lipid bilayer has sealed itself to enclose an aqueous internal volume. The preparation of these structures follows well-

known procedures and is quite facile [34,35]. It usually involves the re-hydration of a dried-down solution of lipids with aqueous buffer, followed by a freeze-thaw cycle and sonication to form the unilamellar vesicles, extrusion through a sub-micron track-etched membrane filter to ensure they are of uniform size, and size-exclusion chromatography to remove extraneous components that are not of this uniform size [40]. The vesicles thus formed can then be analyzed for concentration using known assays [35], and size by dynamic light scattering (DLS). They are stable structures that have remarkably similar characteristics from 'batch to batch', and can last for several days when properly stored. Vesicles can be made in a variety of sizes from many different lipid components; the ones utilized in this report are made primarily of phosphatidylcholine and are typically 200 nm in diameter.

Perhaps the most important characteristic of vesicles thus prepared is that molecules such as fluorescent dyes, labelled phospholipids or even putative channel forming compounds can be incorporated into either the aqueous internal volume of the vesicle, or into the membrane itself, depending on the polarity and solubility of the target molecules. The entrapment of fluorescent dyes within the aqueous internal volume forms the basis of several extremely important assays utilized in synthetic ion channel research. The first of these, the HPTS assay, involves incorporating the pH-sensitive dye HPTS (hydroxypyrene trisulfonate) into the vesicle [27], Figure 1.5. HPTS has two excitation wavelengths; one for the hydroxyl form at 403 nm, and another for the conjugate base at 460 nm; both forms emit at 510 nm. In the assay, the HPTS-vesicles are suspended in an aqueous buffer and the putative transporter molecule is then introduced (Figure 1.5A). After a period of equilibration in the fluorimeter, a pulse of sodium hydroxide is added; if the compound is transport-competent, ions will begin to flow across the membrane under the driving force of the established pH gradient. This increases the intra-vesicular pH, and leads to a concomitant increase in the intensity of emission due to the base form of the dye. After a period of time, the assay is terminated by the addition of a commercial surfactant (Triton X-100), which lyses the vesicles to give the maximal response (Figure 1.5B). This also ensures that the response seen from

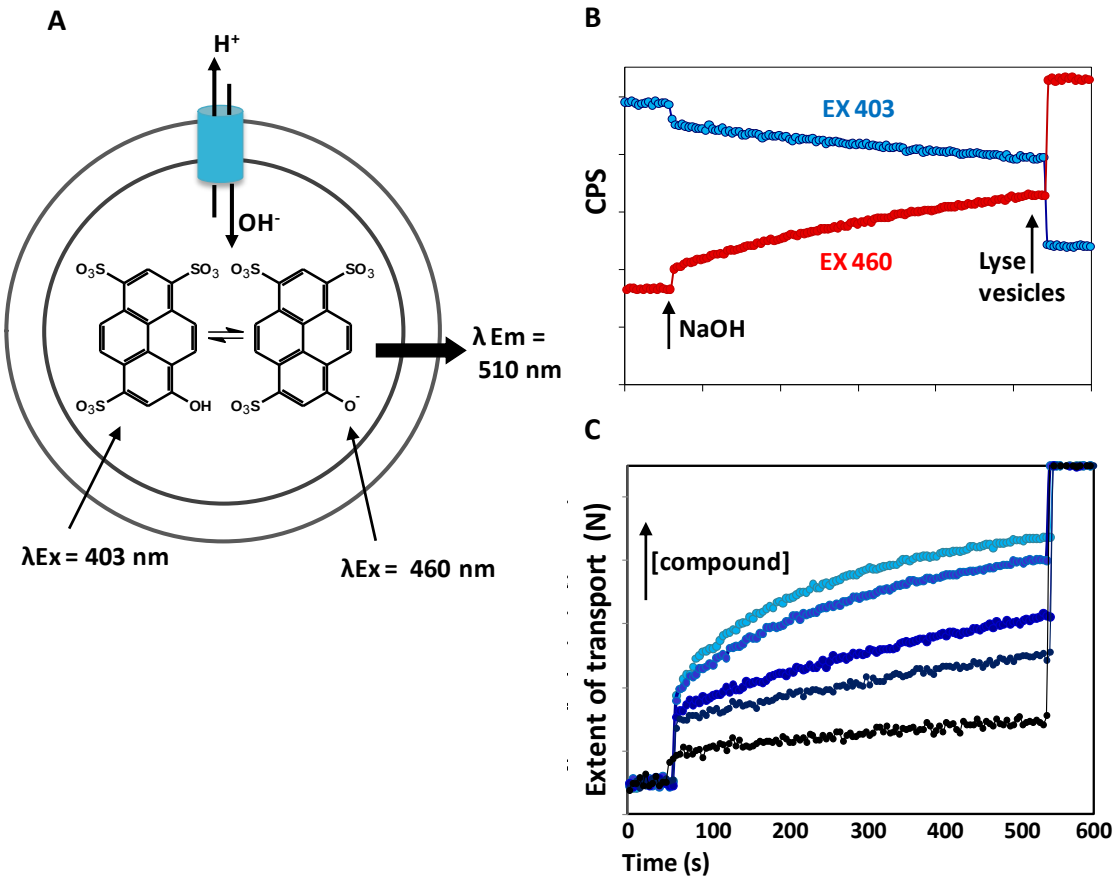

Figure 1.5: The HPTS experiment. **A**: The dye is loaded into vesicles, to which the putative transporter (blue cylinder) is added. **B**: 'Raw' data from the experiment; once the pulse of NaOH is added, the emission of the base form of the dye (EX 460, red line) increases as the pH gradient is collapsed. The maximal response is obtained by lysing the vesicles with a commercial surfactant. **C**: Rate constants can then be derived by plotting the extent of transport over time (N, for equation see text) for varying concentrations of tested compound. Full experimental details available in Appendix 3.

the transporter was not due to membrane disruption. The 'raw' data of such an assay therefore consists of an excitation ratio followed over a set period of time. Utilizing previously-developed procedures [40,41], this excitation ratio is converted to a normalized extent of transport (N) using Equation 1.1, (Figure 1.5C) in which the intensity

$$N = \frac{(I_{403}/I_{460})_t - (I_{403}/I_{460})_0}{(I_{403}/I_{460})_f - (I_{403}/I_{460})_0} \qquad \text{Eqn. 1.1}$$

(I) at each wavelength is compared between that of the sample at any particular time t, the initial response without transporter (o), and the final response after vesicle lysis (f). Apparent rate constants (k) can then be obtained by fitting the extent of transport data

to either a linear or logarithmic function. By plotting the observed rate constants as a function of the concentration of added transporter, the relative activities of a series of compounds can be compared. Further discussion will be deferred to Chapter 2, in which actual data are presented. In contrast to the bilayer clamp, the HPTS assay is an 'ensemble' technique, however, many of the same properties determined in planar lipid bilayers such as ion selectivity, pH and concentration dependence and inferred size can be obtained by the HPTS assay as well [27].

Another widely-used vesicle based fluorescence assay utilizes carboxyfluorescein (CF) [27], another dye that can be easily entrapped within the vesicle interior. CF is loaded

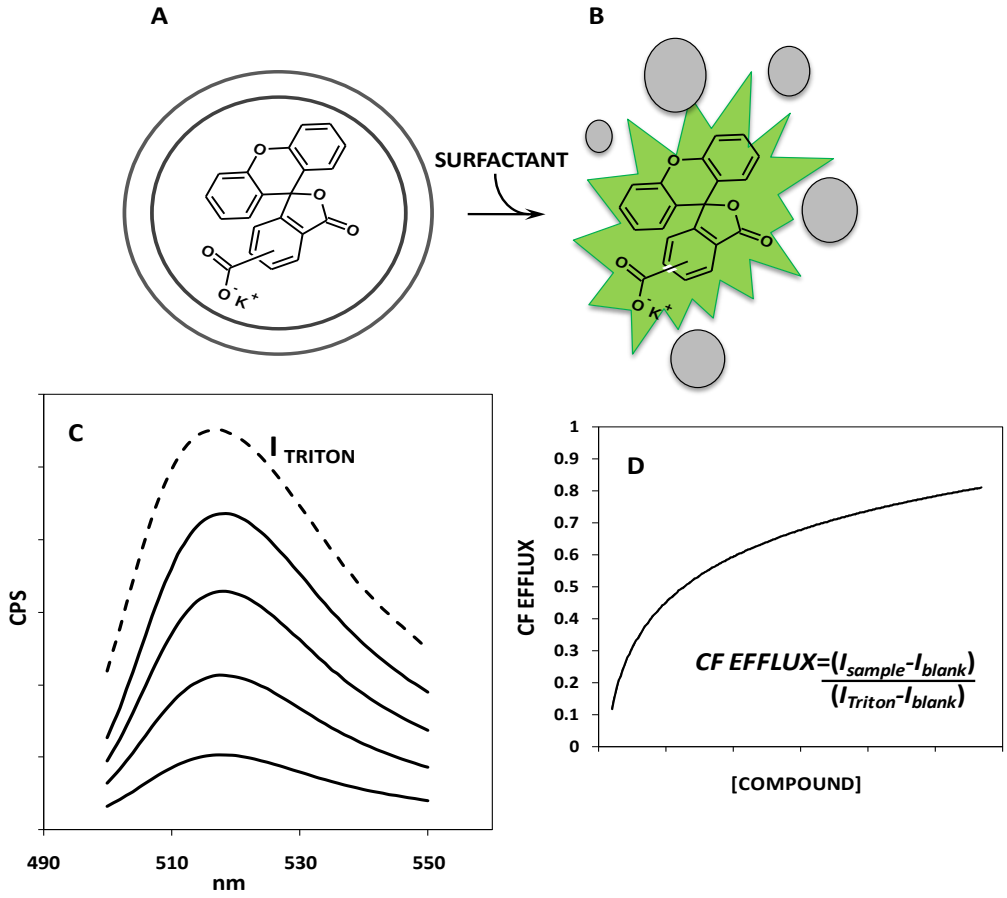

Figure 1.6: The carboxyfluorescein (CF) assay. **A**: the dye is loaded into vesicles; its fluorescence is minimal due to concentration-quenching. **B**: the tested compound ('surfactant') is added, and if pores large enough for CF to escape the vesicle are formed, the fluorescence intensity increases. **C:** 'raw' data: solid lines represent increasing amounts of added compound, the dashed line is the maximal response; **D:** the data are used to obtain a percent CF efflux using the equation in the INSET. Full experimental details in Appendix 3.

into vesicles at a concentration high enough to cause its fluorescence to self-quench (Figure 1.6A), and the test molecule is then introduced; if it can make pores large enough for the CF to escape the vesicle, the fluorescence at 515 nm increases dramatically due to dilution of the fluorophore in the external aqueous volume [8] (Figure 1.6B). As the size of CF is approximately 1 nm, this assay is used to detect the presence of quite large pores, or membrane-disrupting, surfactant-type behaviour. The 'raw' data can then be converted to a proportional 'extent of CF release' by comparison with both a blank (no added compound) and a maximal value (added Triton), Figure 1.6C,D [42].

As mentioned, in addition to entrapping molecules within the internal volume of the vesicle, non-polar, lipid-soluble compounds can also be introduced into the bilayer membrane itself by co-evaporating the molecule of interest with the lipid solution. After vesicle preparation in the usual way, size-exclusion chromatography removes excess compound, ensuring that the molecule is indeed present within the bilayer (Figure 1.7). This technique is also utilized in the present work, and is most useful in a number of cases. As the majority of the vesicle-based assays involve the injection of a solution of compound into an aqueous suspension of vesicles, the activity of the compounds is therefore controlled by their ability to partition into the membrane from the aqueous solution. Bypassing this partitioning step by placing the compound directly into the membrane allows the activity of such compounds to be tested. This technique is also utilized in other applications, as will be discussed during this report.

In terms of comparing these two main techniques, both have advantages and disadvantages; vesicle assays are certainly faster to carry out than the bilayer clamp, and the results are in general easier to analyse. In contrast, the observation of single 'step-up' conductances are generally considered to be the best proof that the introduced molecule is indeed acting as a ion channel, instead of as a detergent or carrier [29]. The data obtained from both techniques are directly comparable [27], and the majority of properties can be detected using either method; therefore, it is not uncommon to see reports where one technique is omitted at the expense of the other.

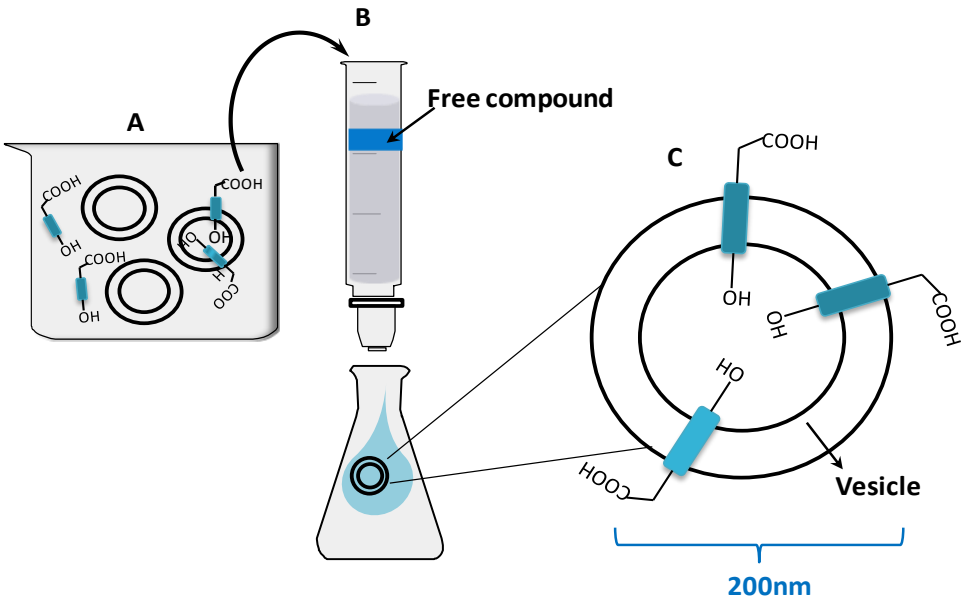

Figure 1.7: Schematic diagram illustrating the formation of vesicles pre-loaded with compound. After co-evaporation of a solution of compound and vesicles, sonication in aqueous buffer and extrusion through a membrane filter, a suspension of free compound, vesicles and compound-containing vesicles results, **A**. This suspension is then loaded onto a size-exclusion column, which separates components, **B**. The desired compound-containing vesicles are then collected, **C**.

While certainly acceptable, the opportunity to carry out both techniques is of value, as occasionally interesting, contradictory results can be obtained; for example, a compound could show bilayer activity while being HPTS-inactive [29]. Therefore, both techniques were utilized in the characterization of the compounds discussed in this work.

It is worth mentioning that the bilayer clamp technique, while appearing highly specialized, was in fact originally developed to study natural ion channels using methods such as 'patch-clamping' of pieces of natural membranes or in fact whole cells [37], and is widely used today in a number of applications outside of synthetic ion channel research such as electrophysiology. Vesicle-based techniques are also very well-developed and numerous dyes sensitive to parameters such as voltage and pH have been incorporated into vesicles [27] ranging in size from less than 100 nm to 'Giant Unilamellar Vesicles' (GUVs), which approach the size of actual cells [43]. The fact that synthetic ion channels can be studied and characterized by the same methods as their natural counterparts indicates that if interesting or potentially useful activities are

observed for synthetic ion channels in such an assay utilizing 'artificial' model membranes, these characteristics should be well transferrable to natural membranes and possibly whole cells. Indeed, although the incorporation of synthetic ion channels into whole or live cells is still an emerging field, recent examples indicate that results from model membrane experiments can in fact be a good prediction of activities observed in such systems [44].

1.3: Synthetic ion channels studied in the Fyles lab

The first synthetic ion channels which were shown to successfully transport sodium ions across a membrane were developed in 1989, almost simultaneously by the Fyles [45] and Gokel [28] groups. The Fyles compound, designed to be a 'bio-mimetic', unimolecular channel (Figure 1.2), is worth mentioning as it exhibits some key design characteristics which are quite similar to those seen for the natural KcsA channel studied by MacKinnon *et al*., despite being synthesized before the structure of the natural channel was solved. It also was the starting point on which further simplifications and iterations of channel molecules were based, eventually leading to the compounds synthesized for the current work.

The structure itself (compound **1-3**), shown in Figure 1.8 illustrates several important design criteria that have been, and still are, extensively used in the design

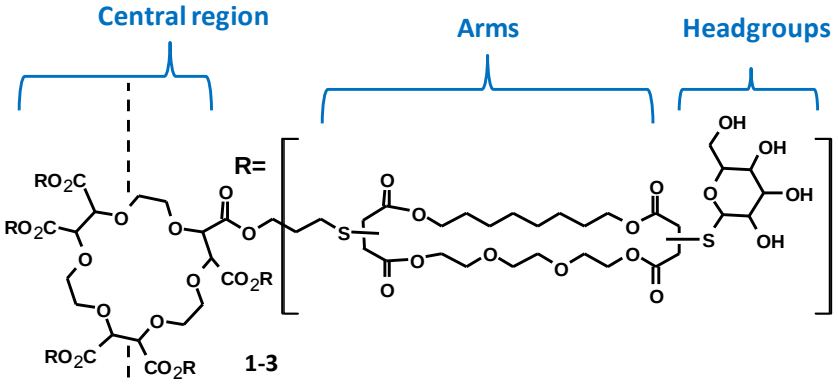

Figure 1.8: Structure of **1-3**, the first Na^+-transporting synthetic ion channel developed in the Fyles lab [45]. The dashed line represents the bilayer midplane.

and synthesis of novel ion transporting molecules. The long macrocyclic 'arms' emanating from the central crown ether are meant to align themselves parallel to the bilayer lipids and form the walls of the channel. Each arm is approximately the length of one leaflet of the bilayer, making the overall structure membrane-spanning. The arms themselves are relatively hydrophobic, while still containing some polar functionality to aid in stabilizing the ion in the channel. A similar analog, in which the arms consisted only of alkyl chains was also synthesized and found to be similarly active. In the natural channel, the peptidic residues that make up the walls of the pore are also mainly hydrophobic in nature [12]. This demonstrates the important principle of hydrophobic matching, in which the length of the transmembrane portion of the designed molecule should correspond to the non-polar core of the bilayer, approximately 3.5 nm. This allows a relatively 'inert surface' [5] to be presented to the ion as it traverses the membrane, increasing ionic flux, as if the ion was overly attracted to the lining of the pore, transport rates would be decreased. In addition, the overall appearance of the molecule should resemble that of a column or tube, depending whether it is made up of individual monomers that laterally diffuse together to form the walls (aggregate channel), or of an explicitly tubular structure (unimolecular channel). This minimizes bilayer disruption as the compound inserts into the membrane [1]. In the Fyles channel, the length of each arm is such that it positions the central crown ether, which is lined with electron-donating oxygens, at the bilayer midplane, this allows it to stabilize the ion as it passes through this region of the membrane, another important design feature. Finally, the polar headgroups are expected to be in contact with the aqueous environment at the water-membrane interface, matching the polarity of this region and again stabilizing the ion by the multiple donor oxygens present. This also occurs for the natural channel, and it is interesting to mention that the positioning of these polar headgroups is what allows for the highly selective transport of potassium over sodium. The donor atoms in this 'selectivity filter' bind the incoming K^+ ion and help to desolvate it by replacing the ion-water interactions with ion-donor interactions. The cavity formed by these polar residues perfectly accommodates the ionic diameter of

potassium, while being too large for sodium [12]. Therefore, the desolvation energy of Na^+ cannot be compensated for by the specific donor-atom interactions, and its transport is disfavoured.

For the Fyles channels, the design features certainly worked; in vesicle-based studies, both compound **1-3** and its more hydrophobic analog exhibited ion transport activity almost equivalent of that of gramicidin, a well-studied, highly active natural channel-forming molecule [46]. This clearly indicates that a rational design based on the principles of molecular recognition, hydrophobic matching and a knowledge of the structure of the bilayer itself can lead to highly-active synthetic ion channels which are significantly less complex than their natural inspiration. However, it should be emphasized that there exists no direct structural evidence of the aforementioned molecules in the bilayer, so their active structures in the membrane remain a hypothesis [45].

The significance of these early compounds is evident; however, what is also clear is that while simpler than their natural counterparts, these molecules are still very large (compound **1-3** has a molecular weight of approximately 4800 g/mol), and their synthesis, purification and characterization were all extremely challenging. High activity is important, but a long, difficult synthesis was a serious limitation for these molecules. By simplifying these compounds, and their synthesis, a large number of related species could be accessed in a time-efficient manner. This would allow structure-activity studies to be carried out more effectively, and if compounds were found to have interesting properties, the ability to make them quickly and easily would be very desirable. This was fully appreciated by the Fyles lab (as well as by others), and further iterations of the original compound transitioned through molecules which lost the central crown ether, such as compound **1-4** (Figure 1.9A) [18]. This molecule was in fact shown to exhibit voltage-gating; this remains one of the very few synthetic ion channels for which this highly important property was achieved. From here, several compounds were made in which the 'arms' were opened up into linear chains instead of macrocycles [47] (compound **1-5** in Figure 1.9B) and a variety of spacers including more rigid aromatic

rings [33] as well as flexible alkyl chains were explored [48]. Recently, in work directly precedent to the current project, structures such as **1-6**, (shown in Figure 1.9C) were designed and synthesized [40,41]. This particular molecule; HO_2C-Oct-Dod-Oct-G(12)-OH, based on a linear oligoester backbone, was one of the most highly active of a large library of similar analogs. These compounds were easily and efficiently synthesized using a solid-phase synthesis (SPS) approach, and were found to have reasonable activity in both vesicle-based [40] and planar lipid bilayer [49] assays. A thorough structure-activity study encompassing approximately 20 potential channel-forming compounds was therefore

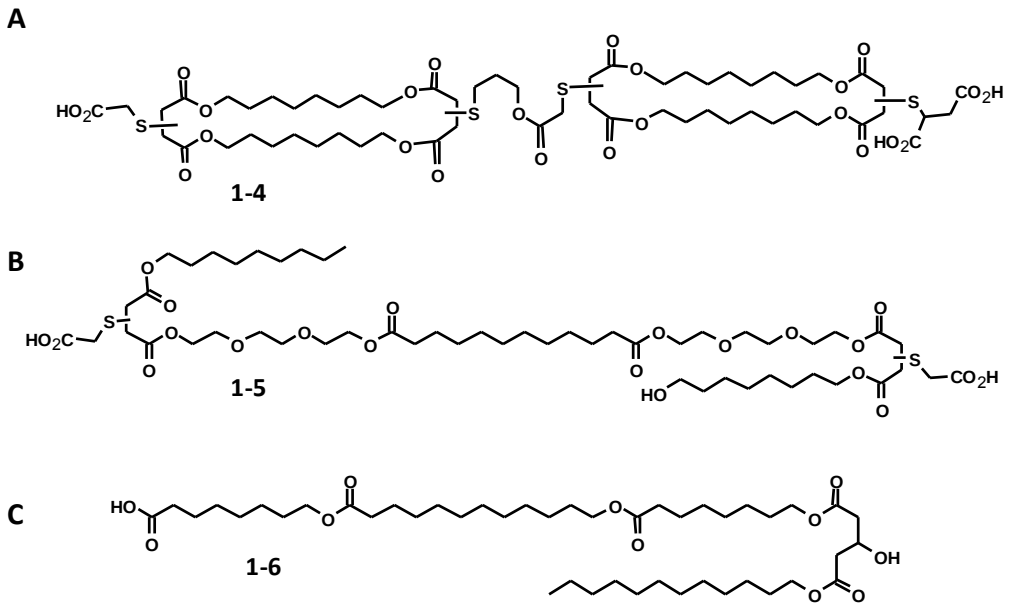

Figure 1.9: Progressive iterations of 'bola' (2-headed)-amphiphile aggregate channels developed in the Fyles lab. From compound **1-3** in Fig. 1.8, the compounds lost the central crown ether (**A**) and were de-macrolized (**B**), eventually leading to the 'fully saturated' oligoester HO_2C-Oct-Dod-Oct-G(12)-OH (**C**).

accomplished in a short period of time. In terms of structure, the compounds varied in properties such as the length of the internal alkyl units (Oct for example refers to an 8-carbon chain, Dod signifies 12 carbons), the number of esters (dimers, trimers and tetramers were all made), and the identity of the hydroxyl terminus (the glutaric-anhydride derived 'G'-headgroup was not present in all cases). These compounds are structurally simple, synthetically accessible and yet remain transport active; evidently, the goals set out for simplification have been met, and the fact that activity was

observed for such 'simple' compounds, which now barely resemble their far-off 'grandparent' compound **1-3** is indeed quite remarkable. A large number of such 'simple' compounds that exhibit ion transport activity are now known in the literature [1,24]; and will be mentioned throughout this dissertation.

While retaining key structural features such as overall length sufficient to span the bilayer, polar headgroups at both termini and hydrophobic alkyl chains connecting them, the 'saturated' oligoesters shown in Figure 1.9C are clearly now no longer tubular unimolecular channels. Instead, they have transitioned to the aggregate type in which multiple monomers are expected to join together to form the active channel. For this to occur, the compound must first be able to partition into the membrane from the aqueous solution into which it is initially introduced. As mentioned, the activity of the saturated oligoesters was found to be rather low; further investigation indicated that the compounds were indeed aggregating to a large extent (at concentrations around 15 μM) in aqueous solution [40]. This would certainly limit the activity of these compounds, as the aggregates would first have to break up in order to effectively partition into the vesicle; partitioning of the aggregates themselves is believed to be unfavourable due to the extent of membrane disruption necessary for this to occur. In addition, the aggregates could precipitate from solution, thereby decreasing the effective concentration of compound available to form channels. Consideration of the data indicated that the low activity of these compounds could therefore be well explained by the proposed working model shown in Figure 1.10. In aqueous solution the compounds are present as aggregates (Figure 1.10A). When vesicles are introduced, the partitioning of monomers into the vesicle occurs for those compounds which are hydrophobic enough to partition, but hydrophilic enough to leave the aqueous aggregate (Figure 1.10B-C). Eventually, these monomers assemble in the membrane to form an active channel with a presumed tubular structure, Figure 1.10D. The accumulated data support this model, however, none of these proposed intermediates could be directly observed, both due to the lack of any sort of spectroscopic tag present on the oligoesters, as well as to the inherent difficulties of characterizing the structures

of active ion channels, as discussed previously. Nevertheless, a very important conclusion resulted from these studies; in order to achieve highly-active compounds, either the extent of aqueous aggregation of the individual monomers that are meant to comprise the channel must be minimized, or the partitioning step must be enhanced in some way.

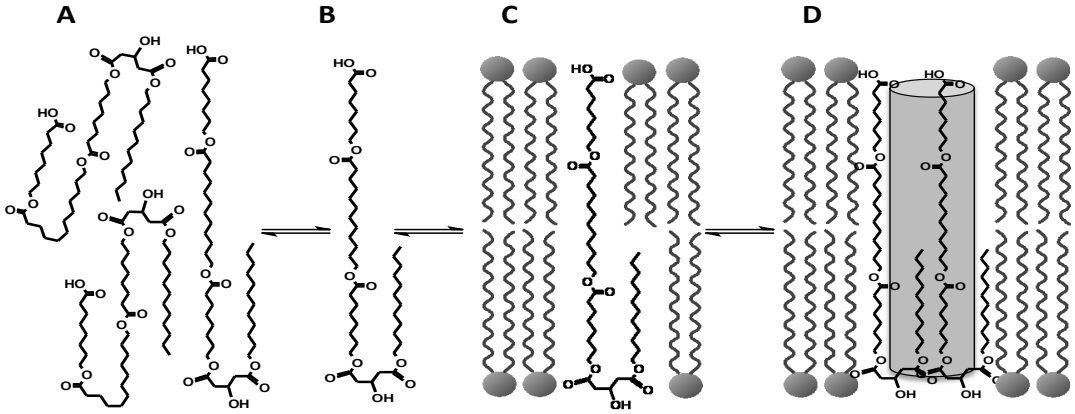

Figure 1.10: Proposed working model based on extensive structure-active relationship studies carried out on the saturated oligoesters [40]. **A**: the compounds aggregate in aqueous solution, and can potentially partition *via* an aqueous monomer (**B**) into the membrane; **C**. The monomers then re-aggregate in the membrane to form the active channel; **D**.

1.4: Project goals

Considering these options, it was decided that for the next iteration of the oligoester aggregate channels, the partitioning step would be targeted by increasing the rigidity of the monomers, resulting in structures such as that shown in Figure 1.11. In this molecule (compound **1-7**), the central alkyl chain present in the fully-saturated precursor compound has been replaced by a modified diphenylacetylene, or 'Dip' moiety. The carboxyl and hydroxyl ('G') headgroups are retained, however, the alkyl chains have been shortened to 6-carbon 'Hex' pieces to retain a similar length to the parent HO_2C-Oct-Dod-Oct-G(12)-OH. The new compound is also named analogously to the precursor oligoesters; HO_2C-Hex-Dip-Hex-G(12)-OH. Overall, this molecule, and other analogs based upon it, is meant to test the hypothesis that increased rigidity will

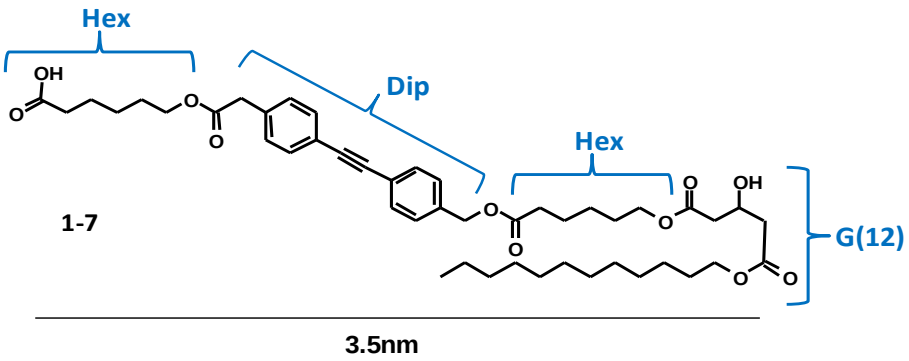

Figure 1.11: Structure and naming scheme of substituent parts of the target oligomer HO_2C-Hex-Dip-Hex-G(12)-OH, **1-7**. *Once the initial numbers of final oligomers are given, the compounds will be referred to by their trivial names, starting from the carboxylic acid terminus.

lead to enhanced ion transport activity *via* increased membrane partitioning.

Introducing rigid units such as steroids [50,51], cholates [20] and multiple aromatic rings [52,53,54] is a widely-used technique in synthetic ion channel research, and many structures incorporating such units are known [25]. Rigid units are expected to be beneficial in stabilizing the channel structure within the membrane, possibly leading to a more defined channel. For this work, the diphenylacetylene group in particular was chosen for several reasons. In terms of synthesis, it was believed that the 'Dip' subunit could be easily made and incorporated as a building block into the previously-developed solid phase synthesis conditions used to access the saturated precursors, thereby a large library of Dip-containing oligoesters could be quickly achieved. The Dip chromophore would also be beneficial for purification, as methods such as HPLC (high performance liquid chromatography), which require a UV-active molecule for detection, could be accomplished [55]. This would guarantee high purity of the final compounds, which is important for sensitive assays such as the bilayer clamp.

Finally, and perhaps most importantly, diphenylacetylene is a known environment-sensitive fluorophore [56] which has exhibited excimer-type emission in a few cases [57,58]. An excimer is an excited-state dimer which can be formed between fluorophore monomers in close proximity (usually within 0.5 nm) to each other, and has certain characteristics such as a broad, red-shifted emission spectrum which can be used to distinguish it from the fluorescence of the monomer [59,60,61]. The Dip molecules could therefore lead to increased mechanistic understanding as now the species formed

in solution and perhaps in the membrane itself could be spectroscopically observed, and if excimer emission is present, these species could be separately probed and identified. As both the active structures of synthetic ion channels and mechanisms to explain their activity are not well known or understood, the experimental observation of putative intermediates along a mechanistic pathway such as that proposed in Figure 1.10 would be a significant achievement.

This therefore leads to the goals of this Thesis; firstly, to synthesize and characterize a series of diphenylacetylene-containing oligoester ion channels to study the effect of rigidity on ion transport activity. Secondly, to use the inherent fluorescence of the Dip chromophore as a membrane probe in order to test and refine the working hypothesis proposed in Figure 1.10.

1.5: Thesis overview

Chapter 2 discusses the synthesis and activity of the 'first-generation' of the Dip-containing oligoesters, while Chapter 3 focuses on a series of molecules based upon an extended, multi-aromatic core which shows red-shifted fluorescence emission as well as increased fluorescence intensity. These molecules were made to improve upon the relatively low fluorescence intensity of the Dip fluorophore. Chapter 4 returns to the Dip scaffold for the second generation of these compounds, in which further refinements and structure-activity relationships were obtained from a larger suite of compounds. Chapter 5 involves a series of studies including time-resolved fluorescence assays to further probe and refine the proposed mechanism. Chapter 6 is a short summary of the presented work, and overall conclusions gained from these studies.

Supplementary materials are presented in the Appendices. Appendix 1 outlines the synthetic details and schemes for all synthesized molecules. Appendix 2 consists of full structural characterization of all novel compounds including ^{1}H and ^{13}C NMR, HPLC and Mass Spectrometry. Appendix 3 outlines the experimental details for the transport

and fluorescence assays, while Appendix 4 contains supplementary fluorescence data. Due to their length, the Appendices will appear in the electronic version of the manuscript, but will not be printed.

Chapter 2 : Diphenylacetylene-containing synthetic ion channels

2.1: Rationale & design

The main impetus behind the current work was to study the effect of rigidity on ion transport activity. The desired structures, incorporating the diphenylacetylene-based 'Dip' chromophore as the rigidifying element, were expected to retain the key features of the previous set of fully saturated oligoesters developed by Fyles *et al*. [40, 41], which had demonstrated fairly high activity as ion transporters. However, as the activity of the saturated oligoesters was thought to be limited by their aggregation in aqueous solution, as well as poor partitioning into the membrane, the Dip compounds were meant to address this by increasing membrane partitioning due to their rigid structure. Their increased rigidity could enhance insertion by being able to more effectively 'push aside' the individual lipid molecules in the membrane. The increased rigidity could also stabilize the pore formed in the membrane, leading to enhanced activity. This reasoning was in fact recently used to explain the high activity of the most rigid compound in a set of the 'aplosspan'-type synthetic ion channels of Gokel *et al*., which will be discussed in more detail in Chapter 4 (an example structure of which is shown in Figure 4.3) [62,63].

In addition to enhanced activity, another key feature to explore with the Dip molecules is their fluorescence properties. The fluorescence of the diphenylacetylene chromophore, and in particular its previously-noted environment-sensitive excimer emission [57] could act as a spectroscopic probe, potentially leading to mechanistic insights into the compounds' activity. Finally, the incorporation of the Dip chromophore would allow efficient purification by HPLC, guaranteeing high compound purity which is most important in spectroscopic studies and highly sensitive assays such as the bilayer clamp. As shown in Figure 2.1, the planned Dip-containing oligomers were therefore designed to be of a similar length (~3.5 nm), hydrophobicity and overall

charge as the fully-saturated precursors, in order to best judge the effect of the Dip substituent.

Before discussing these 'first-generation' Dip oligomers in detail, it should be noted that some of the contents of this chapter have been published [64]. The note about naming will be re-iterated as well; after the initial numbering, the 'final' oligomers will be referred to by their trivial names (i.e. HO_2C-Hex-Dip-Hex-G(12)-OH).

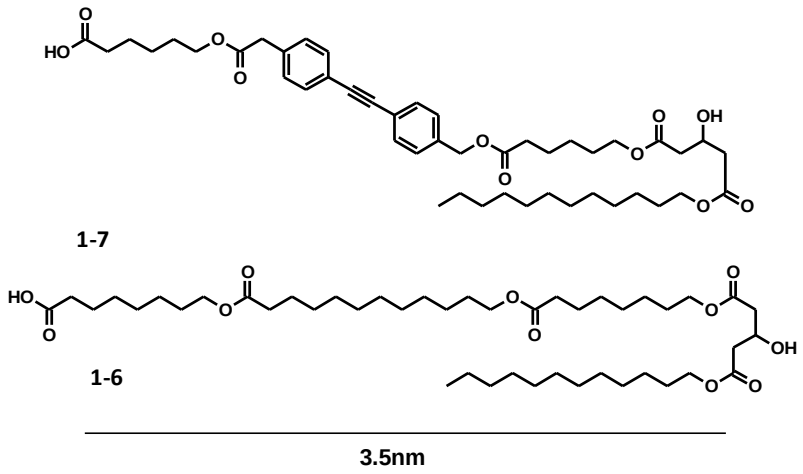

Figure 2.1: Structure of the target oligomer HO_2C-Hex-Dip-Hex-G(12)-OH (**1-7**), compared to the fully saturated precursor compound HO_2C-Oct-Dod-Oct-G(12)-OH (**1-6**).

2.2: Synthesis

2.2.1: Attempted solid-phase synthesis

In work directly preceding this project a solid-phase synthesis (SPS) [65] approach was utilized to access a large number of oligoester ion-channel compounds [48,41]. SPS has been extensively used for the synthesis of polynucleotides and peptides as well as oligoesters [66], and the benefits of SPS are well-known [67]. These are centered on the ease of purification between each synthetic step; as the growing polymer remains bound to a solid support, a simple washing of the resin between reaction cycles removes unreacted materials from the desired compound. The SPS cycle of protection, coupling and deprotection can be optimized and then applied to a wide variety of

compounds, leading quickly to a large library of oligomeric molecules, as seen in previous studies. With this precedent, it was decided that the current work would involve similar SPS protocols, a summary of which is shown in Table 2.1, to access the desired Dip-containing oligoesters.

REACTION	STANDARD CONDITIONS
Ester coupling	1:0.1 DIC:DMAP, THF, rt
Carboxylic acid group protection	Resin: Wang resin + ester coupling conditions
Hydroxyl group protection	THP group: 1.2 equivalents DHP, 0.1 equivalents pTsOH, DCM
Hydroxyl group deprotection	5mg pTsOH, 10mL 3% MeOH/DCM
tBDMS deprotection	1%AcOH/1M TBAF in THF, rinse resin with aq NaI in acetone
Carboxylic acid deprotection	Resin cleavage: 5M HCl in dioxane

Table 2.1: Standard solid-phase synthesis conditions developed for the saturated oligoesters [41].

In the initial synthetic plan, similar building blocks, protecting groups and identical reaction conditions as those used for the fully-saturated precursors were applied to the attempted synthesis of the desired Dip oligoesters, the only exception being the Dip subunit itself. This proved to be a notable exception indeed, as despite repeated attempts, the Dip oligoesters were not successfully synthesized using the previously-developed SPS protocols. In most cases, the substance isolated at the end of the attempted synthesis was a mixture of UV-absorbing and fluorescent products, as evidenced by HPLC (multiple peaks present). Mass spectral analysis of the most abundant peaks confirmed that the desired molecular weights were not obtained. Unfortunately, it did not suggest what types of compounds had been made, as the fragments obtained did not correlate to any reasonable 'deletion' sequences. As the Dip subunit was clearly not coupling efficiently under the standard conditions, efforts were then turned to optimizing the reaction conditions in an attempt to correct this. In an extensive set of solution-phase test reactions, in which a total of approximately 25

different combinations of coupling agents, bases, additives and solvents were tested, conditions that led to successful, high yielding Dip-incorporation with minimal side products were eventually developed. The developed conditions, which used a 1:2:1 stoichiometry of DIC: DiPEA: HOBt, were not dramatically different from the previously-employed set of coupling conditions, however, the key difference was the use of HOBt (Hydroxybenzotriazole) as a coupling agent. In the test reactions, it was found that a major side reaction occurring with the THP-protected Dip subunit **2-1** under the standard conditions with methanol as the test alcohol was the formation of a rearrangement product, the N-acyl urea compound **2-2** (Figure 2.2). In peptide synthesis, HOBt is known to suppress this reaction [67], and it was fortunately seen to have this effect in this instance as well. This led to efficient ester coupling of the Dip subunit in reasonable yields; crucially, minimal side product was formed, and the unreacted starting material could be easily recovered and re-reacted if necessary.

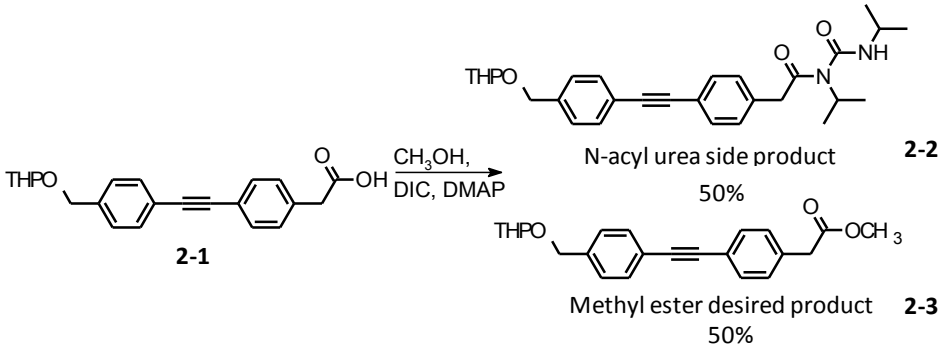

Figure 2.2: Structures of products resulting from reaction of THP-protected Dip subunit **2-1** with the ester coupling conditions developed in previous work [41]. The desired methyl ester **2-3** was formed in equal or lesser proportion to the undesired N-acyl urea side product **2-2** under these conditions. THP= tetrahydropyran, DIC= *N, N*-diisopropyl carbodiimide, DMAP= *N, N*-dimethylaminopyridine.

While the discovery of these conditions was a significant advancement, they still did not lead to an overall successful synthesis of the desired oligomers when applied to the SPS protocol. After further investigation, it was concluded that the problem lay with the final acidic cleavage of the synthesized oligomers from the resin. In the saturated oligoester work, a solution of 5 M HCl in dioxane was used to effect deprotection (Table 2.1); however, this was not effective for the Dip oligoesters, as these conditions led to

complex UV-absorbing mixtures observed by HPLC, while lower HCl concentrations did not remove the oligoester from the resin. Another common deprotection strategy is to use trifluoroacetic acid (TFA) [66]; this was attempted both in the saturated oligoester work as well as with the Dip oligomers, and was unsuccessful in both cases. For the saturated oligoesters, the main problem stemmed from the production of a trifluoroacetate ester of the desired alcohols [41], while the Dip compounds appeared simply to decompose under these conditions, again evidenced by HPLC. The acid-mediated decomposition of the Dip-containing oligomers thus proved to be an insurmountable hurdle in the attempted SPS of these compounds, as the resultant product mixtures were too complex to efficiently purify. Therefore, it was evident that solid-phase synthesis was not feasible, and a solution-phase approach was pursued.

2.2.2: Solution phase syntheses

The developed solution phase synthesis also follows a modular approach, with a few key reaction conditions and building blocks being utilized to obtain a variety of oligomers. Therefore, only two representative syntheses will be discussed in detail; that of the first successful synthesis (HO_2C-Hex-Dip-Hex-G(12)-OH), and that of the longest, 10 carbon ('Dec')-containing isomer HO_2C-Dec-Dip-Hex-G(12)-OH (**2-15**), as the latter illustrates the most efficient combination of the standard reactions. Full experimental details for the remainder of the obtained compounds are available in Appendix 1, while supporting information such as NMR spectra are available in Appendix 2.

The first successful solution phase synthesis of a Dip-containing oligomer is shown in Scheme 2.1. In many respects, this synthesis retains similarities to the unsuccessful SPS approach; the building blocks such as **2-4** and the glutaric-anhydride derived 'G' headgroup (**2-13**) were known from previous work [48], and the coupling conditions (DIC, DiPEA, HOBt) were those mentioned above. In fact, as dissymmetric compounds were desired to access possible voltage-gated activity, the key considerations for the synthesis turned out to be the choice of protecting groups,

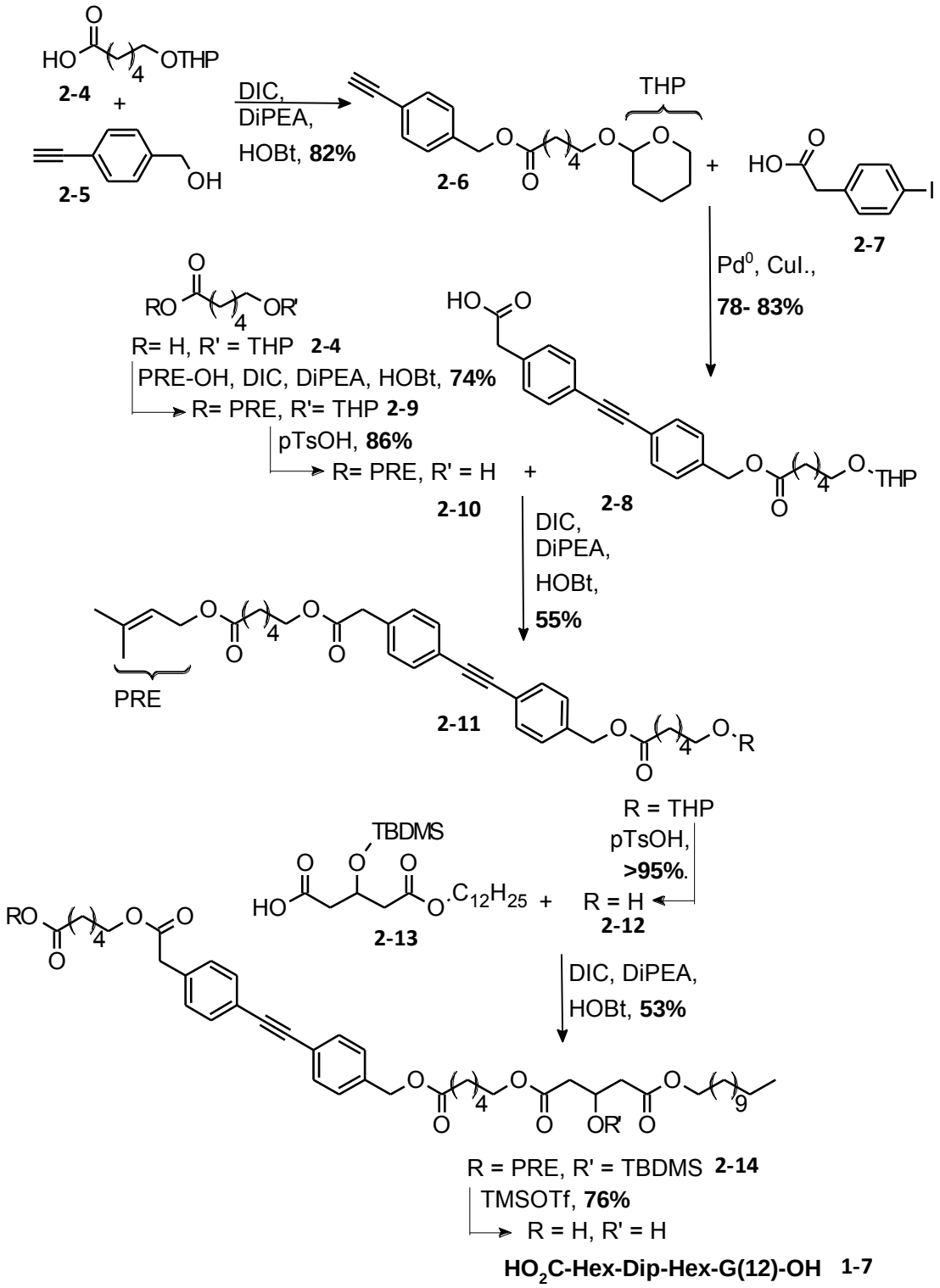

Scheme 2.1: Successful solution-phase synthesis of the first Dip isomer; HO_2C-Hex-Dip-Hex-G(12)-OH. Full experimental details and characterization available in Appendices 1 and 2. TBDMS= *tert*-butyl dimethylsilane, TMSOTf= trimethylsilyl triflate, DiPEA= diisopropyl ethylamine, pTsOH= *para*-toluenesulfonic acid.

especially for the carboxylic acid terminus as the resin, which had provided this function in the SPS protocol, was no longer present. As the tetrahydropyran (THP) group was already present on one of the key building blocks **2-4**, a carboxylic acid protecting group with removal conditions orthogonal to THP was desired. The Prenyl moiety ($CH_2CHC(CH_3)_2$) was thereby chosen as it is stable to mild acid (p-toluenesulfonic acid), which removes THP [68]. The deprotection conditions for both the Prenyl and THP moiety were expected to be compatible with the presence of esters, and THP had indeed been successfully used in the previous saturated oligoester work [41], Table 2.1.

The first step of the synthesis involves the ester coupling between the previously known [41] THP protected 6-carbon containing 'Hex' building block **2-4** and the commercially available *p*-ethynylbenzyl alcohol **2-5**. The coupling was extremely efficient, leading to the coupled product **2-6** in overall 82% yield after purification, clearly indicating the utility of the developed set of ester coupling conditions.

The success of the coupling reaction can be judged in several ways: firstly, TLC analysis clearly indicated that only one major aromatic species had been formed, with an R_f (retention factor) much higher than that of the starting material. This was observed in the majority of ester couplings for the various compounds; in most cases, if any other aromatic-containing species was present, it was unreacted starting material and not some other byproduct. Most compounds then underwent column chromatography and were found to be of fairly high purity by NMR by the observance of certain key features. In the ^{1}H NMR spectrum of **2-6** for example (Figure 2.3), in addition to the fairly obvious addition of the THP signals, in particular that of the methine proton between the two oxygens (Hb), the benzyl methylene protons (Hc) experience a downfield shift from approximately 4.5 ppm in the free alcohol to 5.0ppm in the ester. This is a key signal, as the integration of these 2 protons in comparison to those on the carbon adjacent to the ester carbonyl (Ha, 2.3 ppm, triplet, 2H) indicates if any extra, UV-invisible **2-4** is present in the mixture. For the majority of the obtained compounds, the proton signals around the newly-formed ester bond were in general found to be most useful when assessing coupling efficiency.

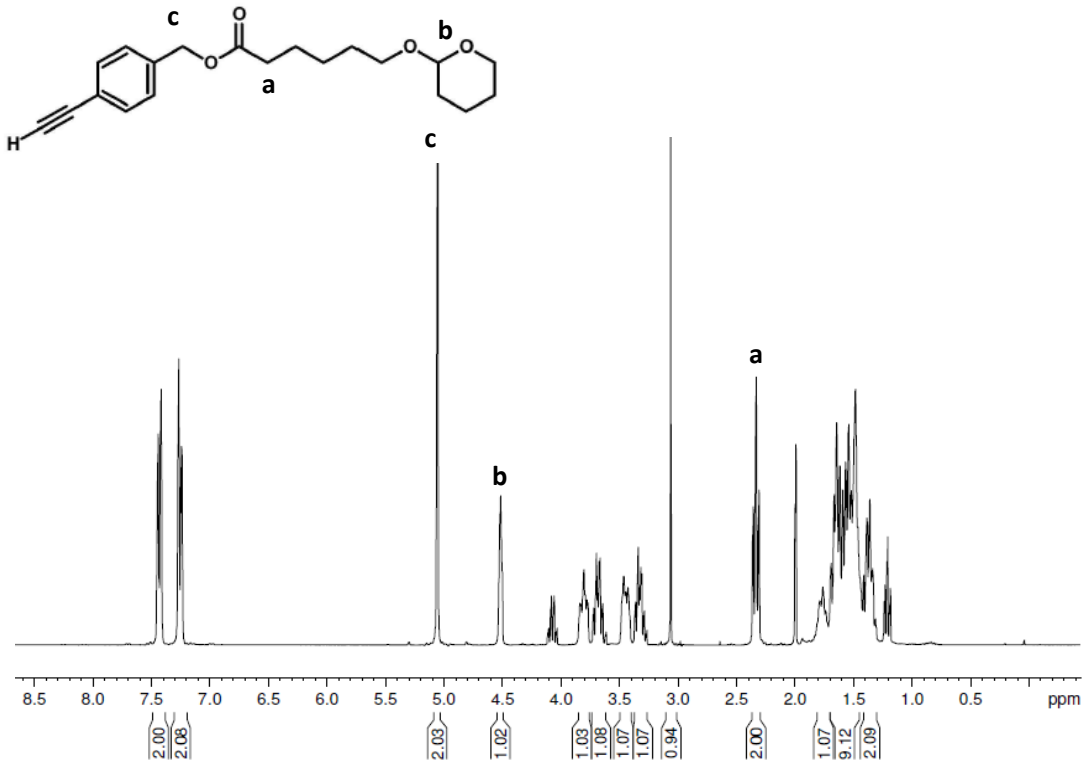

Figure 2.3: ^{1}H NMR spectrum of **2-6**, run in $CDCl_3$ at 300 MHz. Key signals indicating successful ester coupling are indicated.

The next reaction utilized well-known and highly efficient Sonogashira [69,70] coupling conditions to link together the THP-protected alkyne with *p*-iodophenylacetic acid (**2-7**), which is again available commercially, or readily synthesized from *p*-aminophenylacetic acid if larger amounts of compound are desired, to access the carboxyl-terminated 'Dip'-containing compound **2-8** in an average 80% yield over multiple preparations. The success of this reaction was clearly indicated by the presence of the internal alkyne peaks in the ^{13}C NMR (δ=~90 ppm), as well as the increased integration of the aromatic region in the proton spectrum, relative to the aforementioned easily distinguished benzyl methylene proton signal at 5.0 ppm. Another key signal present in both the ^{1}H and ^{13}C NMR was that due to the protons alpha to the terminal carboxylic acid group: these were found as a clear singlet at ~3.6 ppm in the proton spectrum, and ~40 ppm in the ^{13}C. As this is a region of the ^{13}C spectrum in which few other signals appear, the presence of this peak was used as a

quick confirmation that the coupling had occurred for other Dip oligomer syntheses, in which the Sonogashira coupling to form the Dip unit was a key step.

The presence of the terminal carboxylic acid group did limit the solubility of **2-8** and this is certainly a factor in the rather low yield of ester coupling between this compound and the Prenyl-protected hexyl alcohol building block **2-10**. The Prenyl-protected compound, which is new to this work, was conveniently synthesized in two steps *via* **2-9** from the previously-mentioned 6-carbon precursor **2-4**. As mentioned, the ester coupling of **2-10** and **2-8** occurred in relatively low yield (55%), however, the developed conditions once again proved their utility as no major side products were formed, and the unreacted starting materials could be easily separated by chromatography, and re-reacted if desired. The success of the reaction could again be clearly seen in the ^{1}H and ^{13}C NMR; as the Prenyl-derived alkene proton (a multiplet at ~ δ= 5.3 ppm) and carbon signals (δ= 118, 138 ppm) are clearly distinguished, as is the increased integration of the alkyl region in the proton spectrum, including 2 large singlets due to the terminal methyl groups.

Once coupled, the obtained trimer **2-11** had to be THP deprotected, this occurred in high yield and without loss of the Prenyl group, as expected. The product of this particular reaction was used directly in the next step, as the TLC analysis indicated quantitative conversion with no observable side products. However, for those compounds in which the THP removal was not quantitative, ^{1}H and ^{13}C NMR spectra of the purified compound clearly indicated the loss of the THP group. The disappearance of the 4 multiplets integrating for 1 proton each present at ~3.5 ppm in the ^{1}H spectrum, as well as the very downfield (~100 ppm) signal due to the carbon associated with Hb (Figure 2.3) are key evidence.

The terminal alcohol **2-12** could then be ester coupled to the previously-known ‘G(12)’ acid **2-13**; this headgroup was developed during the saturated oligoester work, and can be made easily from tBDMS-protected hydroxyglutaric anhydride and dodecanol [41]. The coupling between the tBDMS-protected G(12) compound **2-13** and the Dip trimer **2-12** was once again seen to be relatively low yielding, however,

considering the molecular weight of the building blocks and the obtained product **2-14**, the sluggish coupling was not completely unexpected, as this had been observed during the reaction optimization work. The success of this particular reaction can be easily assessed by comparing the integration of the large singlet at 0 ppm in the ^{1}H NMR spectrum arising from the trimethylsilyl moiety of tBDMS to the key benzyl methylenes (5.0 ppm, Figure 2.3). In addition, the methine proton geminal to the OtBDMS group is also clearly distinguished as a multiplet at ~5.2 ppm. While the proton NMR as well as certain key signals in the ^{13}C spectrum are most useful for analysis, by this point in the synthesis of these oligoesters the alkyl region of the ^{13}C spectrum becomes very difficult to analyse. This compound in particular has 15 resolvable signals in the 20 – 30 ppm range.

Despite the low yield, the fact that the desired compound (**2-14**) was in hand, well characterized and in a reasonably large amount (~100 mg) was certainly an achievement, as only two steps, the removal of the PRE and tBDMS protecting groups, remained in the synthesis. As mentioned, the final deprotection from the resin was what prevented successful solid-phase synthesis of the Dip compounds, it was therefore approached with caution; removal of the Prenyl group was attempted first, using a catalytic amount of trimethylsilyl triflate (TMSOTf) in DCM at room temperature, conditions developed by others [71]. In the event, it initially appeared that the dreaded decomposition reaction was occurring with this reagent as well, as when added to a clear, colourless solution of the dually-protected oligomer **2-14**, the reaction mixture immediately turned an alarmingly dark greenish brown. TLC analysis of the reaction indicated that the starting material was completely consumed, with only a very low R_f UV-absorbing product visible on the TLC plate. Rapid quenching and extraction of the reaction led to a greenish oil, another not very promising sign. However, when hexanes was added to this residue, a white product immediately precipitated; an NMR taken of this solid pleasantly revealed that TMSOTf had in fact efficiently removed both the Prenyl group, as expected, but also, most surprisingly, the tBDMS moiety as well, unmistakably evidenced by the lack of the large *tert*-butyl singlet in the ^{1}H NMR. This

was a very interesting finding as the reaction was complete in less than 20 minutes, the workup was facile and the desired product was obtained as a solid from precipitation, with the minimal side products produced being removed by filtration. Most importantly, the target Dip-containing oligomer; HO_2C-Hex-Dip-Hex-G(12)-OH was finally in hand, in reasonable yield (14% over 6 steps from **2**-**5**) and in high purity, as observed by HPLC. The high purity of the compound was most pleasing; the initial HPLC of the 'crude' precipitated oligomer was essentially one peak; coupled with the high yield, this indicated that the compound remained intact during the protecting group removal, and that decomposition did not occur to any appreciable extent. This therefore confirmed that the Dip-containing compounds could indeed be synthesized successfully, and the developed procedure of ester coupling, Sonogashira reactions and protecting group chemistry proved to be robust and reliable; a summary of these reaction conditions is presented in Table 2.2. The use of the Prenyl group, coupled with its removal by TMSOTf, is certainly a key development in this synthesis. While other carboxyl protecting groups were tried in other Dip oligomer syntheses in attempts to achieve higher coupling yields (see Appendix 1 for details of other oligomer syntheses), the Prenyl group was ultimately selected as the preferred choice, due to its ease of removal.

REACTION	STANDARD CONDITIONS
Ester coupling	1:2:1 DIC: DiPEA:HOBt Solvents: THF, DMF Temperature: rt – 50^{0}C
Sonogashira coupling	5% Pd[P(Ph_3)$_4$], 10% CuI, 2-5 equivalents NEt_3 Solvents: THF, DMF, Et_2O Temperature: rt – 80^{0}C
Carboxylic acid group protection	Prenyl group: prenyl alcohol + ester coupling conditions
Hydroxyl group protection	THP group: 1.2 equivalents DHP, 0.1 equivalents pTsOH, DCM
Hydroxyl group deprotection	0.1 – 0.3 equivalents pTsOH, 10-30% MeOH/DCM
Carboxylic acid/tBDMS deprotection	0.1 – 0.25% TMSoTf, DCM

Table 2.2: Standard reaction conditions utilized in the Dip oligomer syntheses. Compare with Table 2.1 for the SPS reactions.

With a reliable set of conditions now in hand, a series of Dip-containing oligomers were designed and synthesized. The developed conditions and key building blocks were utilized in a variety of sequences to access a moderately sized library of compounds in reasonable yields. While full experimental details and characterization for all synthesized compounds are available in Appendices 1 and 2, it is worthwhile to present the synthesis of another of the obtained oligomers, the longest isomer, HO_2C-Dec-Dip-Hex-G(12)-OH (**2-15**), as the synthetic approach used for this analog was found to be most effective of all the attempted sequences. As shown in Scheme 2.2, the key development in this synthesis was to build the molecule from both sides, making fairly large 'halves' **2-19** and **2-6** that could be coupled together under Sonogashira conditions to furnish the Dip-containing triester **2-20**. Once THP-deprotected, the free alcohol **2-21** could then be further coupled to the tBDMS-protected G(12) subunit **2-13** (to yield **2-22**) and deprotected using TMSOTf in the usual way, leading to an overall efficient and high-yielding synthesis of the target compound **2-15** (HO_2C-Dec-Dip-Hex-G(12)-OH), with 41% yield over 5 steps from the commercially-available p-iodophenylacetic acid (**2-7**). This particular sequence of reactions was beneficial as it minimized the number of ester couplings that had to occur between larger fragments,

which were found to be sluggish in the other oligomer syntheses, replacing them instead with the consistently higher-yielding Sonogashira reactions. This synthesis also retained the carboxyl-terminus protecting group until the very last step; this minimized the number of chromatographic separations that had to be done on the less-soluble 'exposed' carboxylic acid. In addition, it should be mentioned that increasing familiarity with the reaction conditions and properties of the synthesized compounds also undoubtedly led to a higher-yielding synthesis.

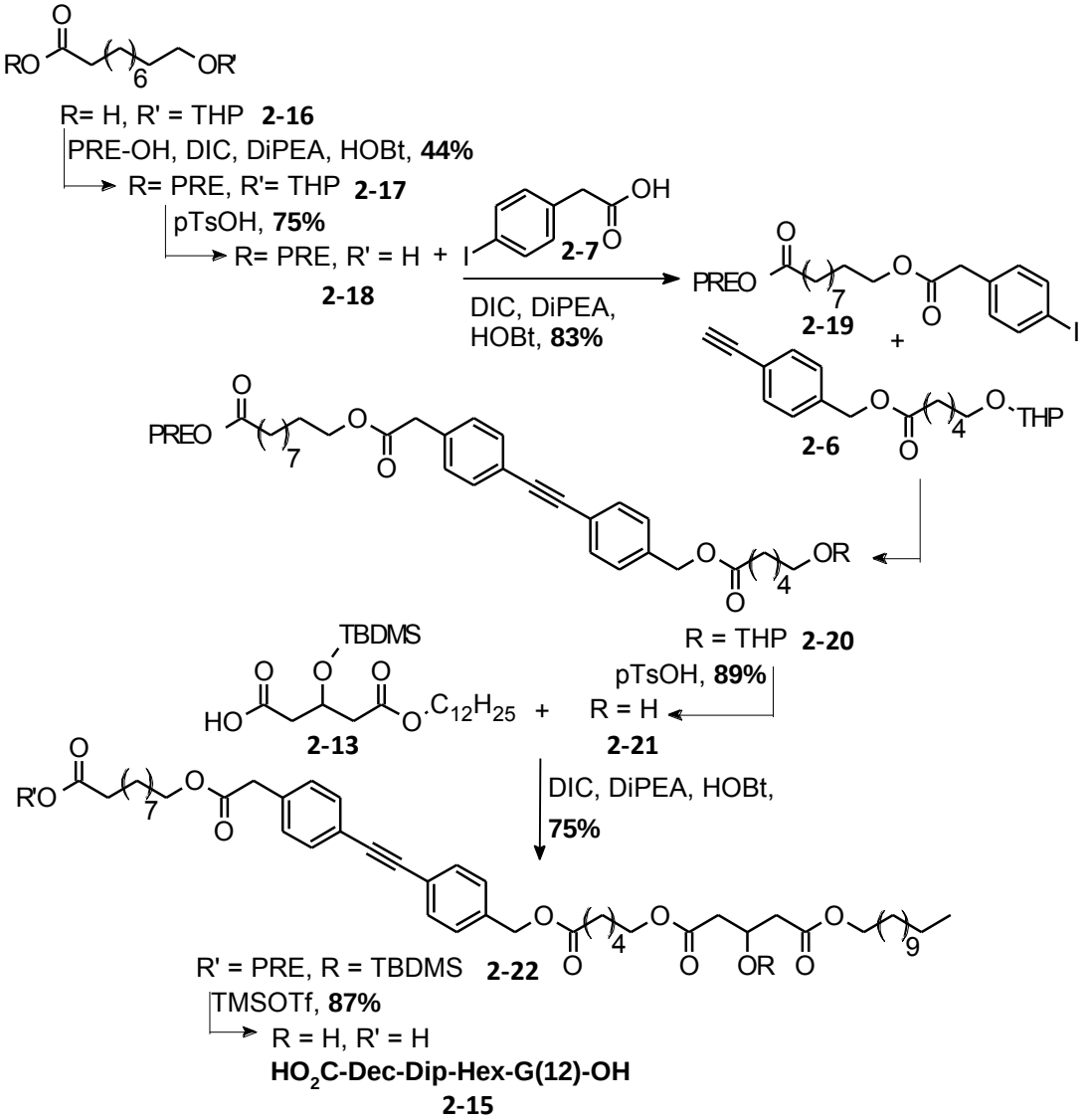

Scheme 2.2: Synthesis of HO_2C-Dec-Dip-Hex-G(12)-OH. Full experimental details and characterization available in Appendices 1 and 2.

The ^{1}H and ^{13}C NMR spectra of HO_2C-Dec-Dip-Hex-G(12)-OH are shown in Figure 2.4A (^{1}H) and Figure 2.4B (^{13}C), the key signals in both spectra are indicated. From this

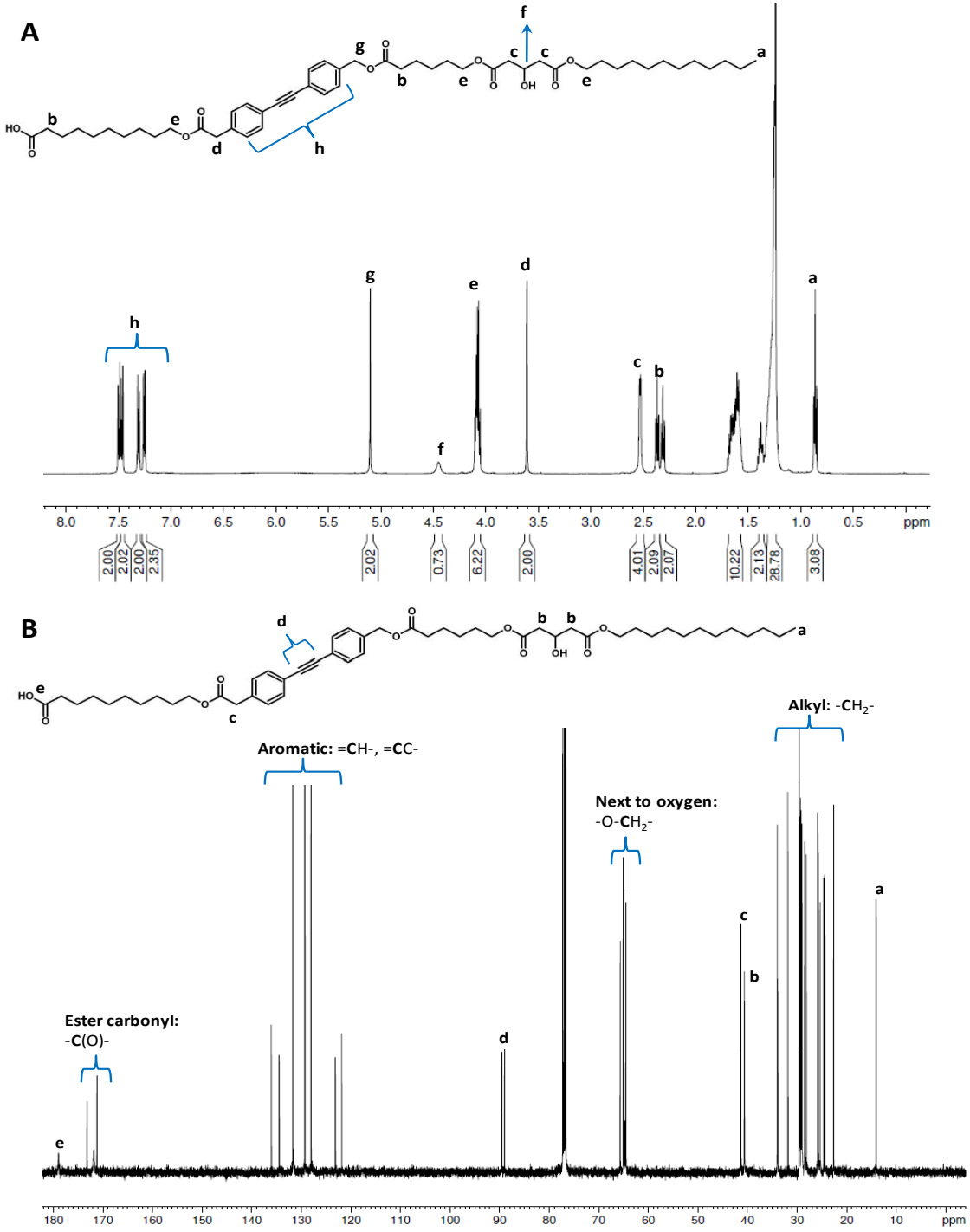

Figure 2.4: NMR spectra of HO_2C-Dec-Dip-Hex-G(12)-OH (**2-15**) taken in $CDCl_3$ **A**: ^{1}H, 500 MHz, the letters correspond to assigned signals on the structure. The large unassigned peaks at ~1.2 and 1.5 ppm are due to the alkyl regions. **B**: ^{13}C spectrum, 125 MHz. Key peaks are assigned, with the brackets indicating regions of similar carbon types.

Figure, one can clearly see how complex the carbon spectra are for the Dip oligoesters; this is due mainly to the dissymmetry of the compounds. Nonetheless, the full assignment of both ^{1}H and ^{13}C spectra are actually rather straightforward if each reaction is followed in turn.

The structures, names and overall yields from commercially-available starting materials of all the Dip oligomers are shown in Table 2.3; six of these 'first-generation'

COMPOUND NAME	STRUCTURE	YIELD	# OF STEPS
HO_2C-Hex-Dip-Hex-G(12)-OH	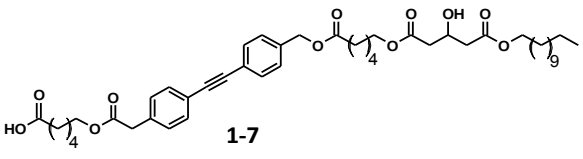 **1-7**	14%	6
HO_2C-Dip-Hex-Hex-G(12)-OH	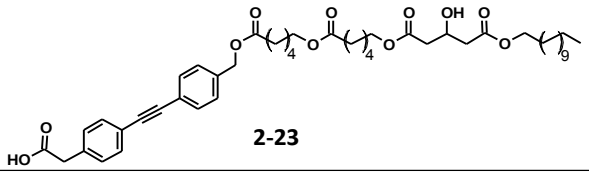 **2-23**	13%	10
HO_2C-Hex-Hex-Dip-G(12)-OH	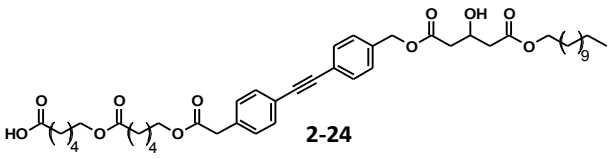 **2-24**	10%	11
HO_2C-Dec-Dip-Hex-G(12)-OH	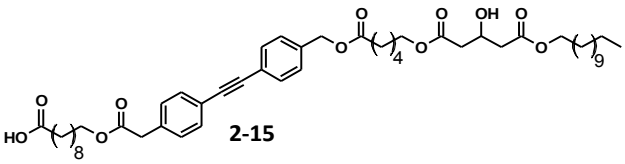 **2-15**	41%	5
HO_2C-Dip-G(12)-OH	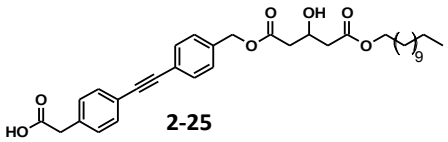 **2-25**	25%	4
HO_2C-Hex-Dip-Hex-G(E3)-OH	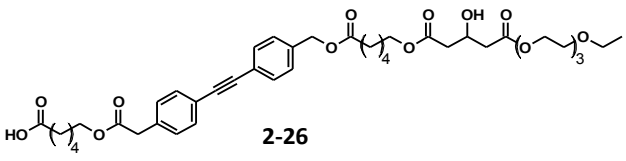 **2-26**	20%	6

Table 2.3: Name, number, structure and overall yields from commercially-available starting materials of the first-generation of Dip oligomers. Full experimental details and characterization available in Appendices 1 and 2.

compounds were made in total. The compounds were designed to test certain structure-activity relationships. Therefore, the library of compounds includes a series of sequence isomers, in which the Dip subunit is placed at varying positions along the oligoester backbone; at the carboxyl terminus (HO_2C-Dip-Hex-Hex-G(12)-OH, **2-23**), in the centre (HO_2C-Hex-Dip-Hex-G(12)- OH) or at the hydroxyl terminus (HO_2C-Hex-Hex-Dip-G(12)-OH, **2-24**). This particular structural series was chosen to see if the placement of the rigidifying element would have any effect on ion transport activity, which could be a possibility considering the anisotropic structure of the bilayer membrane. As certain membrane regions are more ordered than others [72], the Dip subunit could be better tolerated in certain regions, leading to higher activity and the suggestion of a preferred structure. The three sequence isomers are all the same length, therefore, to test whether length of the compounds is a significant factor in their activity, both the previously mentioned ten carbon-containing 'Dec' isomer (HO_2C-Dec-Dip-Hex-G(12)-OH) as well as a short dimer (HO_2C-Dip-G(12)-OH, **2-25**) were made. Finally, in an effort to obtain compounds that were water soluble to at least some degree, as well as to test the effects of increased hydrophilicity, a polyether-containing compound (HO_2C-Hex-Dip-Hex-G(E3)-OH, **2-26**) was also synthesized. The yields of the obtained oligomers were reasonable in all cases, and the final compounds were all purified by HPLC and fully characterized by ^{1}H and ^{13}C NMR, mass spectrometry, UV and fluorescence spectroscopy. The compounds presented themselves as easy to handle, white crystalline solids that were readily soluble in a variety of organic solvents such as THF, methanol and chloroform at usable (millimolar) concentrations.

Overall, the synthesis of this series of compounds was admittedly a fair bit of effort, much more so than would have occurred if a SPS approach had been successful. However, the fact remains that the solid-phase synthesis was unachievable for the Dip compounds, while the developed solution phase protocols were successful, reasonably high yielding and rather efficient, relying on a series of robust reaction conditions and a set of easily-accessed key intermediates. Comparing the two sets of conditions in terms of time invested, it must firstly be mentioned that the number of building blocks utilized

in the Dip oligomer synthesis is higher than that for the saturated oligoesters, so synthesizing the needed precursors added time. The reaction times themselves are actually quite similar between the two sets of conditions, so the extra effort necessary in the solution phase synthesis is due to chromatography, as almost all individual compounds reported in this work have been purified in this manner. This is in fact an advantage, as the purification and characterization of each intermediate indicated which reactions were more successful than others, as well as allowing certain compounds to be used in multiple different syntheses. Finally, as mentioned previously, the reaction conditions and purification of the compounds were continually optimized over time, leading to increasingly efficient syntheses. For example, the synthesis shown in Scheme 2.2 took approximately 3 weeks, which compares favourably with the one week typically necessary to synthesize the oligoesters by SPS.

2.3: Ion transport activity; vesicle assays

As discussed in the Introduction (Figure 1.5), fluorescent vesicle-based ion transport assays, such as the HPTS assay, have been extensively utilized in the study of synthetic ion channels [27]. In this experiment, the pH-sensitive dye (HPTS) is entrapped in large unilamellar vesicles (LUVs) [35,73]; the acid and conjugate base forms of the dye have different excitation wavelengths while their emission wavelength is the same. The HPTS-containing LUVs and the putative channel-forming molecule are suspended in aqueous buffer and placed into the fluorimeter; a burst of NaOH is then added to the suspension. If the tested compound is transport-competent, ions can begin to pass across the membrane, leading to a concomitant increase in the base-form emission of the dye, at the expense of decreased emission from the acid, as the pH gradient is collapsed. The differential emission at both excitation wavelengths can then be plotted as a ratio over time, and the extent of transport over time (N) can be retrieved from the data in procedures mentioned previously [40]. By fitting N to a linear or logarithmic function, apparent rate constants (k) can be obtained. These rates are then reported as

a function of concentration of the assayed compound to compare the activity of a series of tested molecules.

The results of the HPTS assay for the first generation Dip isomers are presented in Figure 2.5 and Table 2.4. The Figure demonstrates the rate (k) versus concentration profile of a selection of the Dip isomers in comparison with one of the previously most

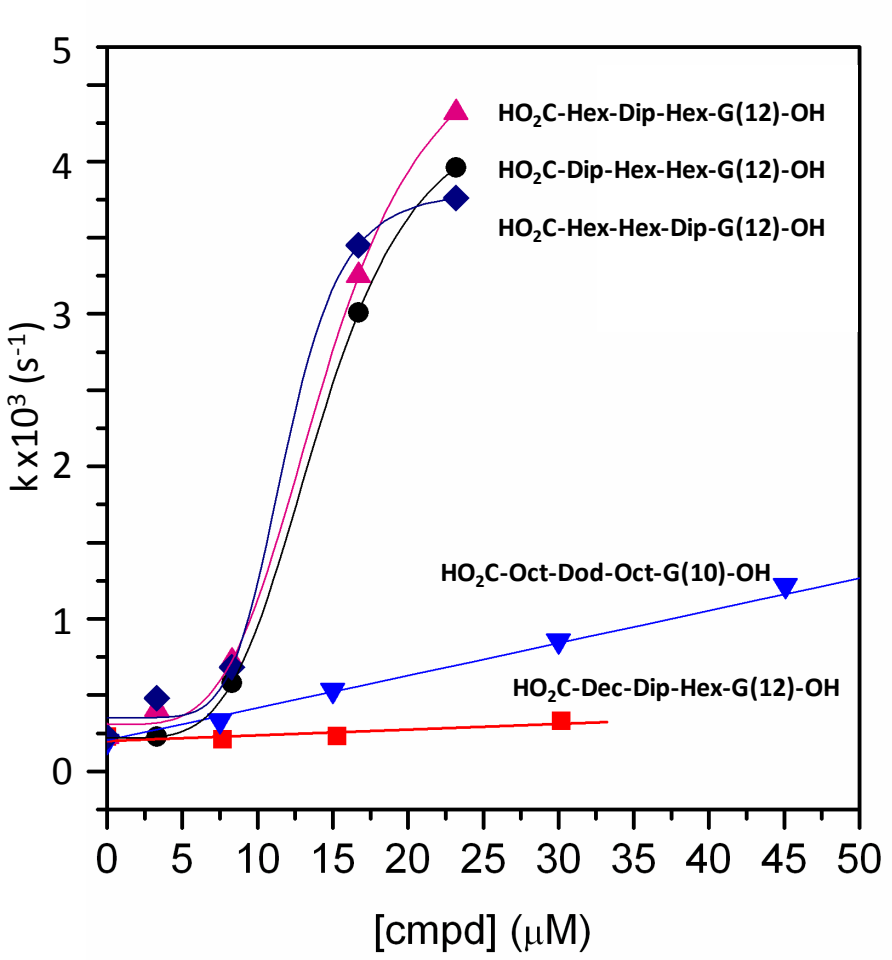

Figure 2.5: Plot of apparent rate constant versus concentration for a selection of first-generation Dip isomers. See Table 2.4 for full dataset. Details of HPTS assay available in Appendix 3.

active saturated oligoesters, HO_2C-Oct-Dod-Oct-G(10)-OH, which was assayed as a control. The Table contains information for all synthesized compounds; in order to compare a large number of compounds in a standardized way, the oligomers are ranked by the concentrations needed to effect a 'benchmark' rate of $1x\ 10^{-3}\ s^{-1}$; clearly a lower required concentration indicates a more active compound. This ranking procedure is

COMPOUND	[COMPOUND] FOR $k = 1 \times 10^{-3} s^{-1}$ (μM)	RELATIVE ACTIVITY
HO_2C-Dip-Hex-Hex-G(12)-OH (2-23)	7	5
HO_2C-Hex-Dip-Hex-G(12)-OH (1-7)	8	4.5
HO_2C-Hex-Hex-Dip-G(12)-OH (2-24)	11	3.3
HO_2C-Oct-Dod-Oct-G(10)-OH	37	1
HO_2C-Dip-G(12)-OH (2-25)	90	0.4
HO_2C-Hex-Dip-Hex-G(E3)-OH (2-26)	>90 (0.5)[a]	<0.4
HO_2C-Dec-Dip-Hex-G(12)-OH (2-15)	n/a (30)[b]	n/a

Table 2.4: Summary of HPTS activity for first generation Dip oligomers, comparison with parent compound (HO_2C-Oct-Dod-Oct-G(10)-OH). a= number in parentheses is rate achieved at highest tested concentration. b= number in parentheses is highest concentration assayed before visible precipitation occurred. Details of HPTS assay available in Appendix 3.

slightly different than that used in previous work, in which the rates of transport at a fixed concentration of oligomer were evaluated [40]. The process used here is advantageous as it gives a clear lower concentration limit of reasonable activity. In addition to having a clear method of comparing amongst compounds, it is important to try to minimize the low, yet inherent variability of the prepared vesicles [27] when utilizing vesicle-based assays. Therefore, each transport experiment for each compound was repeated at least three times, and as often as possible the compounds were assayed on the same day. Importantly, it should be mentioned that the transport results were very reproducible across various trials, usually within 10% of each other, and the vesicles themselves appeared quite stable, being of similar sizes (200 ± 20 nm, as judged by DLS) and exhibiting similar fluorescence intensities of the entrapped dye in subsequent preparations.

When examining the obtained transport data, it is immediately evident that the three shorter Dip-containing sequence isomers (HO_2C-Dip-Hex-Hex-G(12)-OH, HO_2C-Hex-Dip-Hex-G(12)-OH and HO_2C-Hex-Hex-Dip-G(12)-OH) are all significantly more

active than the saturated oligoester parent compound, HO_2C-Oct-Dod-Oct-G(12)-OH. These compounds exhibited activity at concentrations as low as 3 μM, and obtained the 'benchmark' rate at approximately 10 μM or lower, in comparison to the value of nearly 40 μM for the saturated precursor (Table 2.4). The shape of the concentration-rate profiles of the three sequence isomers was fit to a logistic function, allowing for the extraction of an apparent EC_{50} value [27], which averages at approximately 12 μM for the set of compounds.

As the three sequence isomers were in fact the first molecules to be studied in this work, the high activity observed for these compounds was a most satisfying result, but what is the origin of this higher activity? Is it due to the presumed enhanced partitioning of the Dip unit into the membrane, or a lower degree of aggregation in aqueous solution, as this was believed to be the limiting factor controlling activity of the saturated oligoesters [40]. This question can be probed by the pyrene assay [74,75]; this is a fluorescence-based assay used to judge the extent of aqueous aggregation of the monomers in solution (Figure 2.6). The experiment exploits the solvent-sensitivity of

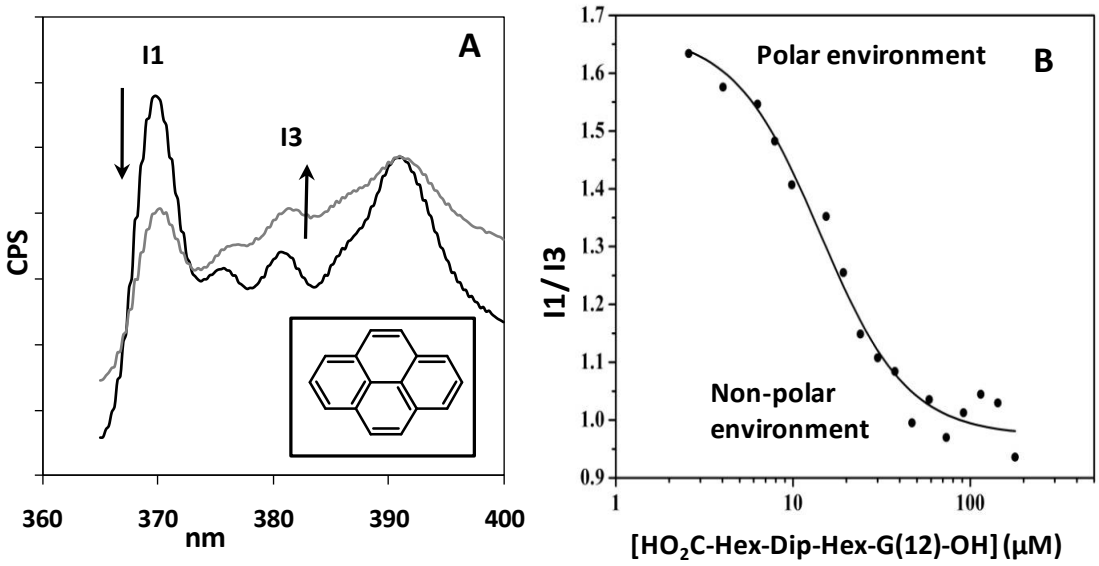

Figure 2.6: The pyrene aggregation assay. **A**: fluorescence emission spectra of pyrene (structure shown in INSET) in aqueous solution in the presence of low (black line) or high (grey line) concentration of an aggregate-forming compound. **B**: ratio of pyrene vibronic band intensities (I1/I3) as a function of the concentration of HO_2C-Hex-Dip-Hex-G(12)-OH (10 mM Na_3PO_4 aqueous buffer, 100 mM NaCl, pH 6.4, 2 μM pyrene). Further details of the assay available in Appendix 3.

pyrene fluorescence; the ratio of the first (I1, ~370 nm) to third (I3, ~380 nm) vibronic bands present in the pyrene spectrum changes depending on whether the compound is in a polar environment, such as the aqueous solution (I1/I3 ~1.5) or in a non-polar environment such as the interior of an aggregate (I1/I3 ~1) (Figure 2.6A). Therefore, the titration of a solution of the compound of interest against a constant concentration of pyrene will result in a curve such as that shown for HO_2C-Hex-Dip-Hex-G(12)-OH in Figure 2.6B. The inflection point of a logistic fit to the data then indicates the cmc (critical micellar concentration) of the assayed compound.

As seen in Figure 2.6B, it is evident that HO_2C-Hex-Dip-Hex-G(12)-OH provides a non-polar environment for pyrene at around 20 μM, indicating that the compound is aggregated at this concentration. Similar 'cmc' values ranging from 12 to 20 μM were reported for the saturated parent compounds [40]. As discussed in the previous report, the obtained values are not conventional 'cmcs', as the transitions are much less abrupt than normally seen for typical micelle-forming surfactants, nevertheless it is evident that the extent of aggregation between the two sets of compounds is very similar. Therefore, the increase in activity seen for the Dip oligoesters in relation to the saturated precursors is not due to decreased aqueous aggregation. Rather, it must be due mainly to enhanced partitioning, a direct consequence of incorporating the rigid Dip unit.

Another factor contributing to the enhanced activity of these molecules is due to their interaction with the lipid molecules themselves. When the compounds enter the bilayer, they are forced into close proximity by the lipid molecules, which prefer to align with each other rather than the invading molecule [1]. This creates a higher local concentration of the compounds in certain regions of the bilayer, these can self-associate and aggregate, ultimately leading to channel formation. Such a process is believed to occur in the well-studied formation of 'raft' domains in membranes, in which certain types of lipids cluster together and exclude others [72,76]. This process would be expected to be enhanced with the Dip compounds as their propensity to self-assemble is higher due to the potential for the aromatic rings to engage in pi-stacking.

In addition, as shown in Figure 2.7, the overall length of these compounds is just long enough to span the membrane used in these studies while allowing the hydrophilic termini to extend into the aqueous solution. Therefore, a degree of membrane thinning

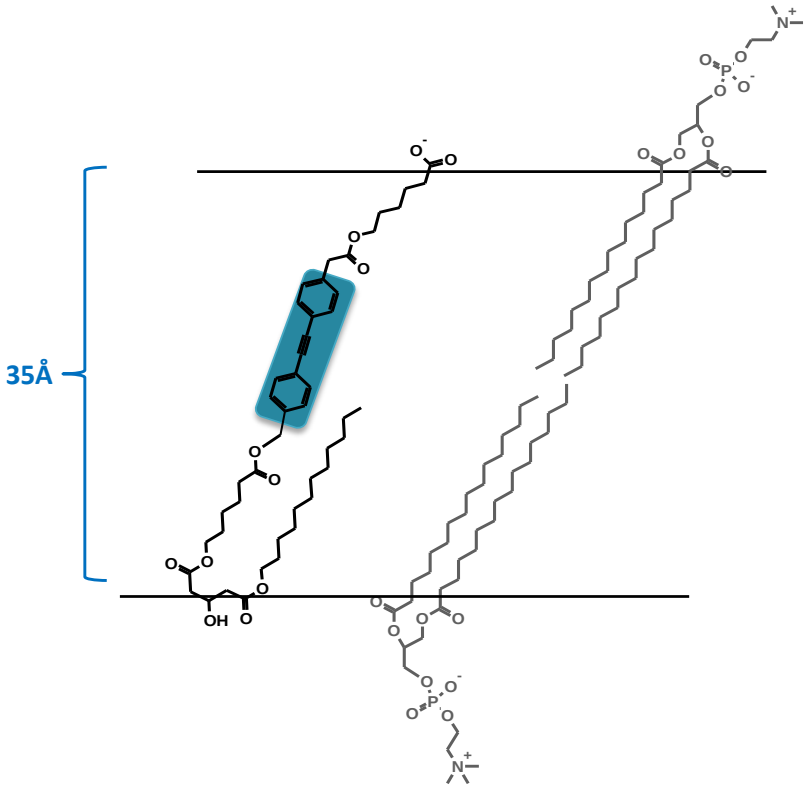

Figure 2.7: Schematic illustration of presumed method of membrane insertion for HO_2C-Hex-Dip-Hex-G(12)-OH.

would be expected to occur around these molecules, as the bilayer lipids prefer this to aqueous exposure [72]; this is believed to occur around membrane proteins which are too short to match the bilayer thickness. The increased stress on the membrane due to this thinning may enhance defect/channel formation. Whatever the underlying mechanism, it is quite remarkable that this relatively simple structural modification was able to effect a greater than 5-fold increase in activity above that previously seen for the saturated oligoesters; this validated the design of these compounds, and indicated that this particular class of structures would be promising for further study.

While this was an exciting finding, another interesting, yet very surprising, result can be observed in Figure 2.5; the almost complete inactivity of the longest isomer, HO_2C-Dec-Dip-Hex-G(12)-OH. This compound did not exhibit any discernable activity at

all, moreover, the concentration that could be tested before visible precipitation occurred in the cuvette used for the assay was very low; approximately 30 µM. This result was striking – after testing the three highly active sequence isomers, the complete lack of activity for the longer compound, which only differs by the presence of four extra methylene groups was completely unexpected, as the previous work on the saturated oligoesters discovered only a minor length effect. However, length effects have been observed to a more prominent extent in earlier work from the Fyles' lab [29], in which a major difference in activity was seen between compounds differing by only a few methylenes as well. Other groups have also reported similar significant length effects [77].

What could be the cause of this substantial difference in activity between the Dip isomers? There are two main possibilities, one of which can be directly tested. The first explanation is HO_2C-Dec-Dip-Hex-G(12)-OH is too hydrophobic, is aggregating to a large extent in the aqueous solution in contact with the vesicles, and is therefore not able to partition effectively into the membrane, as it is monomers that are assumed to partition [40]. This is plausible as precipitation of the compound could be clearly observed at fairly low concentrations in aqueous solution, evidence of its poor water solubility. This hypothesis was tested by making vesicles which were 'pre-loaded' with the compound; a solution of the compound in organic solvent was co-evaporated with the lipid mix, and the vesicles were then prepared in the usual way by sonication and membrane extrusion (see Figure 1.7 in the Introduction for vesicle preparation schematic). The final step in vesicle preparation is size-exclusion chromatography, therefore, one can be confident that the compound is in fact incorporated into the lipid vesicle; as extraneous compound is separated by this process (and remains uncollected on the column). Furthermore, as the hydrophobic Dec isomer would certainly prefer to be dissolved in a less polar medium, it will be located in the bilayer membrane and not the internal aqueous volume. As the compound is now pre-incorporated into the bilayer, this should circumvent its potential poor partitioning; however, these HO_2C-

Dec-Dip-Hex-G(12)-OH-containing vesicles were also HPTS-inactive, indicating that poor partitioning is not solely to blame.

In these experiments, the possibility remains that only a small proportion of the compound, at a concentration too low to effect transport, was successfully incorporated, as it is indeed difficult to assess the actual concentration of compound in the vesicle. Therefore, the partitioning of this compound was also studied by other fluorescence means, as will be discussed below. In addition, there are other ways to assess ion transport activity such as the bilayer clamp technique, which detects single channels; clearly, the concentrations needed for such an assay would be extremely low. The results of this assay for the reported compounds will be discussed in the next section.

Another hypothesis to explain the Dec compound's inactivity is based on a structural argument; perhaps the compound is too long or has some other unknown structural feature that prevents it from forming functional channels. From carboxyl to hydroxyl termini, the overall length of the compound is approximately 40 Å, in comparison to a length of 34 Å for the shorter 'Hex' isomers this is an increase in length of 6 Å, or approximately 15%. As illustrated in the Introduction (Figure 1.10) and Figure 2.7 in this Chapter, these oligoester compounds are assumed to insert into the membrane with the two polar termini projecting into the aqueous medium, allowing the long alkyl tail to 'fold over' into the membrane . The hydrophobic core thickness of the lipids used in these assays is approximately 35 Å, therefore, it is perfectly reasonable that the 40 Å Dec compound is indeed too long. Unlike the previous hypothesis, this theory cannot be directly tested, as the in-membrane structure of these compounds is unknown, as is the case for nearly all synthetic ion channels [24]. Nevertheless, the vast difference in behaviour observed for the Dec compound in comparison to its shorter homologues was most intriguing, and led to much further investigation, as will be discussed.

The ion transport activity of the remaining first generation Dip isomers is also worth examining; both these compounds exhibited similar, fairly low activity, achieving

the benchmark rate at approximately 90 μM. Their similar extent of ion transport activity was somewhat surprising considering their significantly different structures; HO_2C-Dip-G(12)-OH is much shorter than all the other synthesized compounds, while the polyether 'E3' tail of HO_2C-Hex-Dip-Hex-G(E3)-OH renders it the most hydrophilic of the series. The polyether-containing compound was pursued as this particular functionality has been incorporated into many known synthetic ion channel designs; ranging from simple surfactant-type compounds [78], semi-rigid steroidal structures [79] to the very complex, high molecular weight early channels synthesized by Fyles *et al*., shown in Figure 1.8 in the Introduction [45]. This design strategy is based upon molecular recognition, as more electronegative donor atoms lining the pore should help stabilize the transiting ion. In addition, the increased hydrophilicity inherent to HO_2C-Hex-Dip-Hex-G(E3)-OH should equate to enhanced water solubility and less aggregation. While these were all promising reasons to make this particular compound, there also exists in the literature reports that the incorporation of a polyether-type structure as a presumed 'wall', or in this case membrane anchor, would in fact be detrimental to activity [78], as this would cause the ion to bind overly strongly to the channel and not transit through at a high rate [23]. Considering the HPTS results for HO_2C-Hex-Dip-Hex-G(E3)-OH, the latter possibility is the dominant effect, as while the compound did exhibit increased water solubility (as evidenced by the high concentrations that were able to be assayed), the activity remained quite low over this range, and did not achieve the benchmark rate at concentrations up to 90μM, clearly indicating that the polyether tail is indeed detrimental to activity in this case, decreasing it by greater than 10-fold from that seen for the closely related, more hydrophobic homologue HO_2C-Hex-Dip-Hex-G(12)-OH.

In contrast, the short dimer HO_2C-Dip-G(12)-OH was synthesized to test the lower limit of how 'simple' these compounds could become before activity was sacrificed. As mentioned in the Introduction, numerous examples of very simple compounds that exhibit transport activity are known [25]. The interest in making such simple channels is clear; the combination of ease of synthesis and characterization

coupled with the potential to observe high activity is very appealing. However, the main reason this compound was pursued was due to the fact that in previous work in the Fyles lab, it was discovered that a very simple fully-saturated ester dimer; HO_2C-Oct-G(12)-OH, a presumed SPS by-product, had significant HPTS activity [40]. As this would be an example of one of the most structurally simple and synthetically accessible molecules known to form active ion channels, this was a most interesting finding. Concurrently with the studies on the Dip compound, a Chemistry 499 (4^{th} year project) student, Kathleen Genge prepared another ester dimer, HO_2C-Dec-G(12)-OH, which was also shown to exhibit high ion transport activity in both vesicles and planar bilayers [80]. This shows that the original report is likely correct and these very simple compounds form channels, but it calls into question the assertion that the Dip unit is able to increase activity *via* enhanced penetration efficiency, as the saturated compound is much more active than HO_2C-Dip-G(12)-OH. The decreased activity of HO_2C-Dip-G(12)-OH is not an aggregation effect, either, as its 'cmc' was actually found to be much higher (~150 μM) than that of the longer oligomers, as evidenced in the pyrene assay.

In conclusion, the HPTS ion transport results for the first generation Dip isomers led to some interesting findings; three very highly active compounds were discovered, indicating that the Dip subunit was enhancing membrane partitioning and thereby increasing activity by up to five-fold over that previously seen for the saturated precursors, a remarkable result considering the overall structural similarities between these sets of molecules. Equally notable was the complete lack of activity observed for the slightly longer Dec isomer, this striking length effect is unprecedented amongst the progressive iterations of these oligoester compounds, and further studies to elucidate the basis behind this vast difference in activity were of high priority.

2.4: Ion transport activity; bilayer clamp assay

The bilayer clamp assay was described in the Introduction (Figure 1.4); it is a single molecule-detection technique which relates the current observed at a constant

potential (in the milliVolt range) to the flow of ions through an ion channel[37]. The bilayer is a resistor, so in the absence of transporter no current is observed at the applied potential. However, if a transport-competent molecule is introduced into the bilayer, ions can transit across the membrane, completing the circuit and providing an observable current in the picoAmpere (pA) range. Individual ion channels can then be

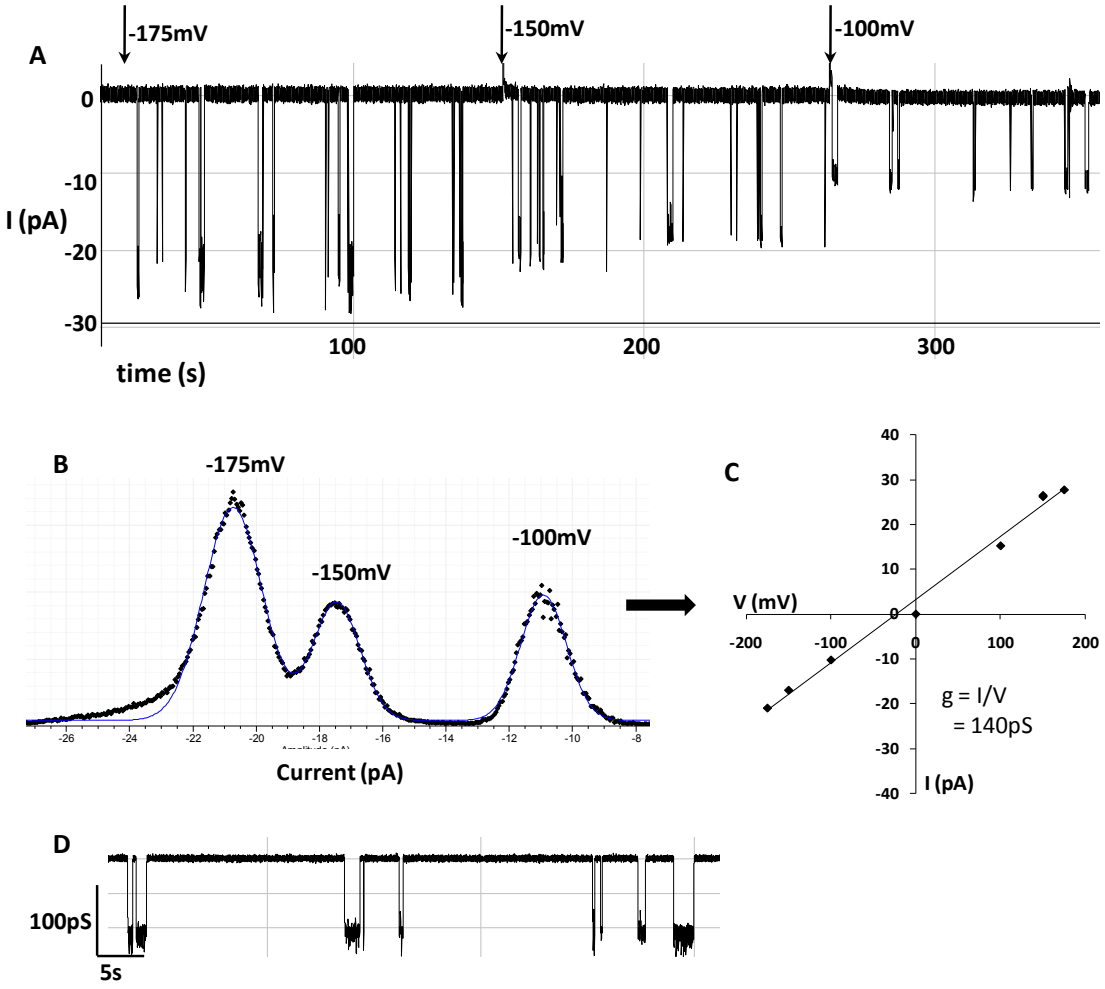

Figure 2.8: Bilayer clamp analysis for 'regular' behaviour observed for HO_2C-Hex-Dip-Hex-G(12)-OH preloaded into a diPhyPC bilayer in 1 M CsCl. **A**: 'raw' bilayer trace displaying current (I) as a function of applied potential (arrows, -175, -150 and -100 mV) over time. **B**: all-points histogram of the trace shown in **A**, displaying the average current observed at each potential; **C**: these values are plotted as an I-V trace, from which the conductance (g) is obtained. **D**: expansion of **A**.

observed as a discrete step-up 'square-top' opening, which has a finite lifetime; a return to the baseline indicates channel closure. If the data obtained are of this 'regular' square-top variety, the bilayer experiment can be remarkably information-rich; the stability of the channel, its concentration and pH dependence, ion selectivity,

conductance and diameter are just some of the many characteristics and properties that can be extracted from such experiments, using well-known procedures [27].

An example of such 'regular', easy to analyse behaviour is shown in Figure 2.8 for HO_2C-Hex-Dip-Hex-G(12)-OH in 1 M CsCl as electrolyte. The observed bilayer trace showing current versus time at various applied potentials is in Figure 2.8A. The baseline, at which no current flows, is at zero, the discrete, downward spikes are single ion channels opening and closing over time. From such a trace, an all-points histogram (Figure 2.8B) can be obtained which displays the current observed at the applied potentials, this can then be plotted as a current-voltage (IV) graph to obtain the conductance value (g, measured in picoSiemens, pS) for the channel (Figure 2.8C). In this particular case, the IV trace is linear, following Ohm's law, the slope of the line gives the experimental conductance value of 140 pS. This indicates that this compound does not exhibit any sort of voltage-gating [1], however, it should be noted that a 'true' voltage-gating study is not possible for this compound, as will be discussed shortly. A section of the bilayer trace in which the y-axis has been converted to conductance is shown in Figure 2.8D; the 'square-top' appearance of these openings can be seen more clearly in this enlargement.

From the 140 pS conductance value obtained, and assuming a channel length of 34 Å, an inner diameter (d) of the putative ion channel can be inferred based on the Hille equation [37], Equation 2.1.

$$1/g = l\,\rho/[\pi(d/2)^2] + \rho/d \qquad \text{Eqn. 2.1}$$

Where g equals the conductance of the single channel, rho is the resistivity of the recording solution, an experimentally-derived value which can be obtained from the literature [81], and l is length of the channel/pore. In the example shown, this correlates to a diameter of approximately 3 Å. As this corresponds to the diameter of an unsolvated Cesium ion, these conductance values indicate this is a 'tight' channel that can pass a 'bare' Cs^+ ion. However, it must be mentioned that the obtained Hille

diameter must be interpreted with caution. Equation 2.1 has been shown to be more applicable to higher conductance values (over a few hundred pS), corresponding to larger channel diameters. Below these conductance values, the diameters obtained from the Hille equation become less physically realistic, as the diameters could be overestimated by up to a factor of five [82].

Analysing the time-component of the exhibited trace by fitting the observed openings to an exponential decay leads to an average lifetime (τ) of the observed channels of approximately 700 milliseconds, indicating reasonably stable channels. Repeating the experiment in a series of electrolytes, in this case KCl and tetramethylammonium chloride (NMe_4Cl) suggests that this compound forms the most regular channels in CsCl.

It is evident that for a trace such as shown in Figure 2.8, the bilayer clamp experiment can provide a wealth of information; in fact, the parameters mentioned are by no means the extent of channel characterization that can occur by using this method. A limiting factor present for the Dip compounds is that the majority of the synthesized oligomers (with the exception of HO_2C-Dip-G(12)-OH), need to be pre-loaded into the lipid in order to observe activity due to their insolubility in water. This prevents key experiments such as a 'true' voltage-gating study from occurring. In the few examples of synthetic ion channels that exhibit voltage-gating, this behaviour was achieved by insertion of the compound from only one side of the bilayer [18]. As this is not possible for compounds that need to be premixed into lipid, the voltage response of the longer Dip oligoesters was indeed expected to be Ohmic. In addition, ion selectivity cannot be accurately judged as the activities are variable in different electrolytes.

While it would be very convenient if all synthesized compounds, or even this particular compound, always exhibited such nicely behaved, ideal square-top activity, this is very much not the case; the behaviour shown in Figure 2.8 is just one type of the many possible activities observed for the various Dip isomers. First, it must be noted that all the synthesized Dip isomers, including the HPTS-inactive Dec isomer, exhibit bilayer activity of some kind, and in the majority of cases, this behaviour does indeed

include the most regular 'square top' variety. The observation of bilayer activity for the Dec isomer was quite interesting, and is attributed to the fact that the compound is pre-loaded into the membrane at concentrations that, while not high enough to elicit a response in the HPTS assay, are clearly sufficient to effect transport in planar lipid bilayers. This is not the only instance of a compound having activity in the bilayer but not in vesicles; this was also observed for example in previous work in the Fyles lab for compounds related to structure **1-2** in Figure 1.3. It is also important to note that in all studied cases, the behaviours observed for each compound are reproducible; as the bilayer clamp is such a sensitive technique, much repetition of the desired experiments must be performed to ensure that the observed activity is indeed a property of the studied molecule [31]. In general, the behaviours fall into three main categories, and as it would be impractical to display even a minority of the bilayer data accumulated for the various Dip isomers it is instructive to consider one particular compound as an example of these behaviours.

The example traces shown in Figure 2.9 are for the shortest compound, HO_2C-Dip-G(12)-OH. This compound is chosen for illustration as it is the only first-generation Dip isomer which did not have to be pre-incorporated into the lipid to observe activity. In the first panel (Figure 2.9A), an example of the first class of observed behaviours, the most regular 'square top' type, is shown. Again, as in Figure 2.8 the baseline at zero is the closed state, while the open state is indicated by the dashed line at level 1. These observed openings are very small (~3 pS), yet occur quite often for this, and other Dip isomers. Usually, these very small openings would be the first type of behaviour to be observed during an experiment, with larger, higher conducting channels following afterwards.

Such higher conducting and more irregular activity is depicted in Figure 2.9B-C. These 'hairy squares', consisting of multiple but irregular openings, made up the majority of the activity observed for the Dip compounds. In Figure 2.9B, the activity at the beginning of this trace appears rather regular, while becoming increasingly irregular over time, both in terms of channel lifetime and conductance values. Multiple step-ups,

i.e. from 0 (closed) to 1 (open) and then from 1 to another open state (2) occur, indicating the opening of multiple channels. Subconductances, which are openings that do not equate to a 'full' step up, and the origin of which is more difficult to assign, are also observed; the portion of Fig. 2.9B between the red arrows gives a good example of this type of activity. Figure 2.9C is another example of the multiple irregular opening

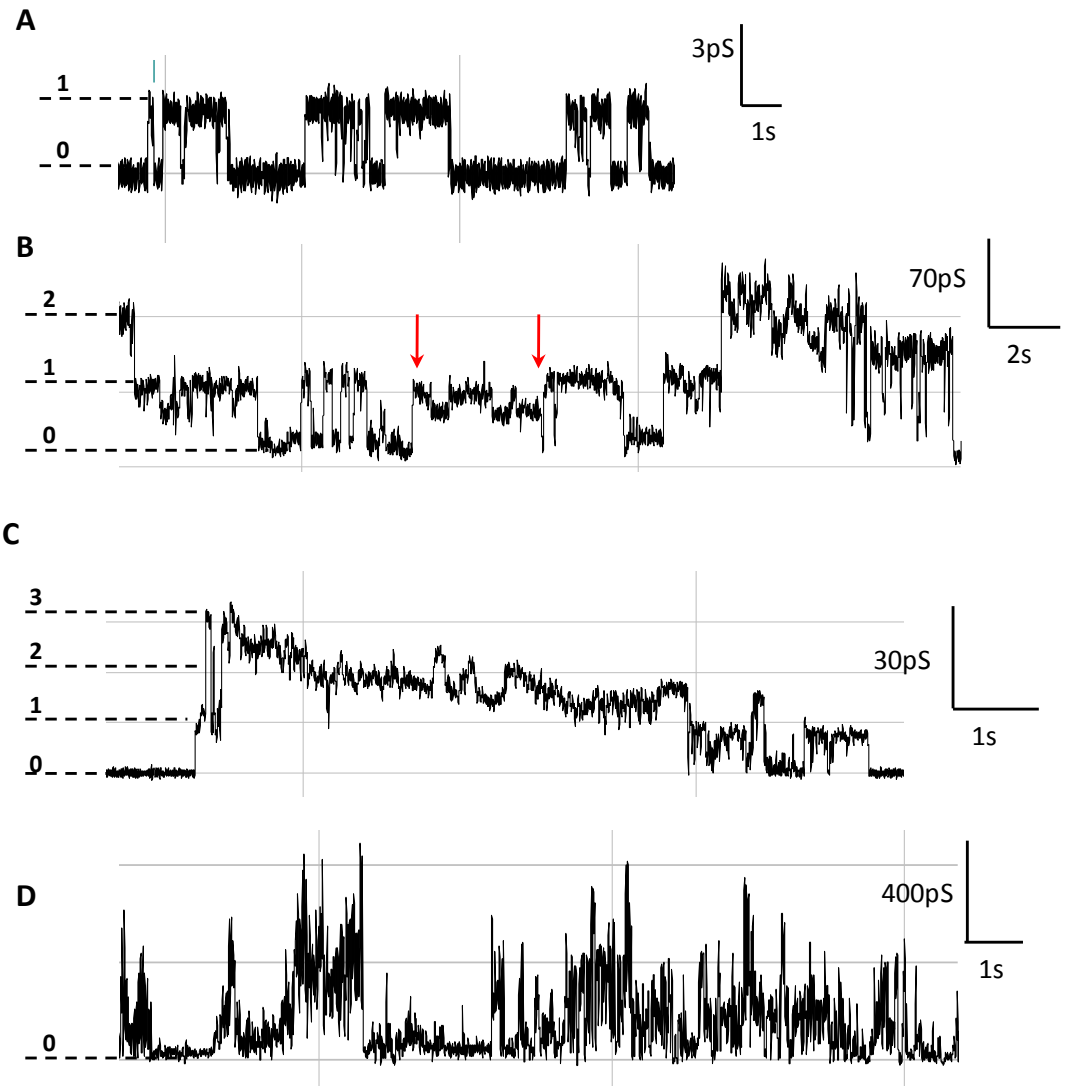

Figure 2.9 : Examples of types of behaviours seen in the bilayer clamp for HO_2C-Dip-G(12)-OH, 0=closed (no current) state, 1, 2, 3= open (conducting) states, multiple levels correspond to multiple open channels. **A**: 1 M CsCl , +175 mV, **B**: 1 M CsCl, +75 mV, red arrows refer to area of multiple irregular openings, further discussion in text. **C:** 1 M CsCl, +150mV, **D:** 1 M KCl, +50 mV. DiPhyPC was the lipid used in all cases. Further experimental details available in Appendix 3.

activity type; in this case, a relatively long lived channel exhibits steadily decreasing conductance over a period of approximately 6 seconds. From the displayed traces, it

can be appreciated that the observed conductances and lifetimes of this irregular behaviour spanned a wide range for this compound. The same is true of each of the 1st-generation Dip isomers, and therefore general conclusions over the series are not possible.

An example of the most irregular type of behaviour observed for the Dip isomers is shown in Figure 2.9D; these types of high-conducting, short lifetime spikes were frequently observed, especially in KCl electrolyte. The very short lifetimes and rapidly changing conductances of these spikes indicates that whatever structures are responsible for them are highly unstable and dynamic, and therefore very difficult to analyse using known protocols [25]. However, the high conductance values of these spikes, frequently in the hundreds of pS, indicate that the structures giving rise to this activity are extremely efficient ion conductors. Therefore, this activity may in fact be even more significant than the more regular square tops, despite the latter's ease of analysis.

Currently, the development of methods to analyse the more irregular types of bilayer clamp behaviour is a generally unexplored field. This may be due to several factors as the existence of regular 'square top' activity has in the past been the defining characteristic of a synthetic ion channel, as this is what is seen for the majority of natural channels. However, it is now clearly appreciated that a variety of different behaviours are possible, and occur, for synthetic ion channels, and that these behaviours contain important information. Methods to extract this information could be an important area of research in the synthetic ion channel field, and attempts have been made to address this issue in other work from the Fyles lab [83, 84]. In a recently-developed process, the various observed activities for a channel compound are first assigned a colour based on their type (for example, square tops are 'green'). The channel lifetime and conductance associated with the observed activity are then extracted, and the coloured activity types are then placed on a grid which plots the conductance against lifetime. This both documents the observed bilayer data in a systematic way, as well as giving a concise visual representation of the obtained data.

This would be most useful when considering the vast amounts of data generated in a bilayer experiment, especially if methods to computationally automate this process are developed.

While this more in-depth analysis is certainly promising and could be utilized in the future to more fully characterize the behaviours observed for the studied Dip compounds, in the present work, the bilayer clamp data was used mainly in a confirmatory sense. In the previous work on the saturated oligoesters, the majority of activity studies were based on vesicle methods, and it was decided that this would be the focus for the Dip compounds as well. Nonetheless, the bilayer clamp experiment was performed for all synthesized first generation Dip isomers and interesting observations were obtained. The presence of discrete, ideally behaved single channel conductances under certain conditions for the majority of the compounds allowed at least some characterization of properties such as channel diameter and voltage response. Perhaps more importantly, in certain cases very high conductance (ion transport efficiency) was observed. The prevalence of irregular behaviour indicates that the channels formed for these compounds are for the most part highly dynamic and changeable species. As the presumed mode of channel formation for this type of 'simple' aggregate channel is based upon random 'collisional activation' [18] in the bilayer, this is not a surprising result, and such time-dependent changes in behaviour are quite common for supramolecular ion channels. In fact, the formation of even somewhat regular channels of a defined structure for structurally simple compounds such as HO_2C-Dip-G(12)-OH is actually quite remarkable, as these molecules are not pre-organized in any way. This illustrates the intriguing behaviours of structurally-simple amphiphilic compounds when interacting with lipid bilayers.

2.5: Photophysical characteristics

2.5.1: Fluorescence in solution

Diphenylacetylene (DPA) is known to be fluorescent [56], however, its photophysics are complex. In particular, DPA is believed to be one of only a few rare compounds which, upon excitation from the ground state (S_0), emit a photon from S_2 (the second excited singlet state) as opposed to S_1 [85,56,28]. Many theoretical and experimental studies into this area have been carried out by Hirata *et al*., Ferrante *et al.* and others, and a detailed discussion of the origin of DPA luminescence is beyond the scope of this report. However, this will not affect the upcoming discussion, as the emission observed for the DPA unit present in the Dip oligoesters exhibits 'regular' fluorescence characteristics such as concentration-dependent intensity and quenching ability, and will therefore be treated as such.

Diphenylacetylene is in fact a fairly 'poor' fluorophore. It has a very low quantum yield; Ferrante *et al*. report a value of approximately 10^{-3} in non-polar solvent at room temperature [85], compared to the maximum value of 1 [59]. Its Stokes shift, the difference between the excitation and emission maxima [59], is also very small (~10 nm), this makes detecting fluorescence experimentally difficult. Finally, its fluorescence lifetime is very short, being of the sub-nanosecond timescale [56,86]. This again makes measuring this property challenging. Despite DPA's non-optimal fluorescence properties, one interesting behaviour it does exhibit is environment-sensitive fluorescence. This is especially prevalent when the DPA subunit has been incorporated into a polymer, as seen in the extensively studied series of conjugated polyphenylethynylenes and conjugated polyelectrolytes (CPEs) developed by Swager *et al*., and Schanze *et al*., as well as others [87,88,89] (Figure 2.10A). These polymers exhibit blue shifted, structured emission in 'good' solvents in which the compounds are well dissolved as monomers; in contrast, in 'poor' solvents in which the compounds aggregate, their emission is red-shifted, broad and decreased in intensity, indicating excimer-like emission from the aggregated compounds [88]. As mentioned in the Introduction, an excimer is a complex between a molecule in its excited state, and one in its ground state; excimers are generally observed to have red-shifted, broadened emissions in relation to the individual monomers [60]. The environment-sensitive

fluorescence of DPA-containing polymers has been exploited in many interesting ways; these compounds have been used extensively as fluorescent sensors [90,87] and membrane probes as their photophysical characteristics are sensitive to pH, temperature, surfactant addition, ionic strength, and other factors [91].

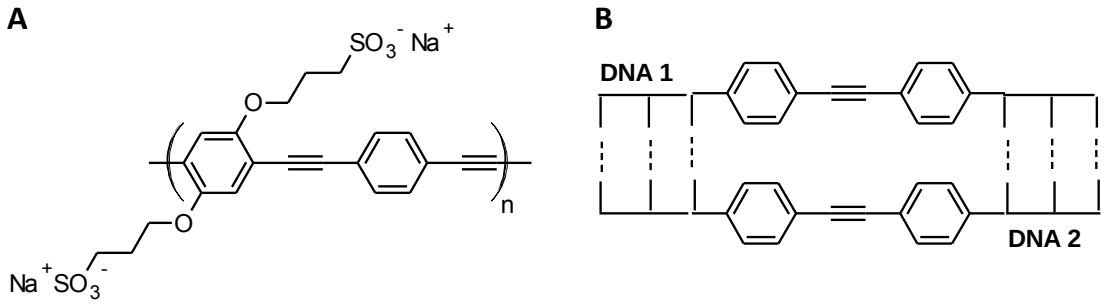

Figure 2.10: Examples of diphenylacetylene (DPA) containing environment-sensitive compounds. **A**: PPE-SO_3^-, a conjugated polyelectrolyte ('CPE') [87]. **B**: DNA-DPA system developed by Letsinger *et al*. [58]; a red-shifting of the emission by ~100 nm was observed when the individual DNA strands base-pair to each other.

While many examples of environment-sensitive excimer emission from DPA-containing polymers exist, this behaviour is usually reported for large, very high molecular weight compounds. In contrast, there are relatively few examples of diphenylacetylene itself [57], or DPA-containing 'small' molecules exhibiting such excimer behaviour; in fact, the first observed instance of diphenylacetylene excimer fluorescence in solution was recently reported for relatively small DNA oligomers synthesized by Letsinger *et al*. [58]. In this study, the authors observed a red-shifted, broad and structureless emission spectrum when two of the DPA-containing DNA strands were hybridized to each other, which they attribute to excimer formation between the stacked DPA subunits which are forced into close proximity due to the DNA base-pairing (Figure 2.10B). This is a most interesting finding, as it indicated that DPA environment-sensitive fluorescence can occur for low-molecular weight oligomers containing only one diphenylacetylene moiety each.

This clearly led to the possibility that similar photophysical behaviour would be observed for the Dip compounds. Environment-sensitive fluorescence would be very useful for a membrane-inserting compound; as the potential to monitor the molecule's

transition from a polar environment, such as aqueous solution, into the non-polar membrane interior would be highly valuable. The ability to probe the compound's membrane association in this manner would have significant implications in mechanistic development, as rates and extent of partitioning could be obtained, as well as potentially leading to some information about the active in-membrane structures themselves. Therefore, it was very satisfying to discover that the Dip compounds do indeed exhibit environment-sensitive fluorescence in solution. As shown in Figure 2.11A, in organic solvents such as THF and methanol, all the studied oligomers displayed a structured emission band at approximately 320 nm. This emission was stable over time and had a very small Stokes shift of approximately 15 nm in comparison to its excitation spectrum (λmax of excitation~ 305 nm); it is assigned to the monomeric state of the Dip molecules as they exist as well-solvated individual compounds in a 'good' solvent, analogous to that seen for the CPEs. The spectral properties exhibited by the Dip compounds in methanol or THF, including absorption spectra (λmax= 288 nm), derived molar extinction coefficient (approximately 2 x 10^4 M^{-1} cm^{-1} depending on the

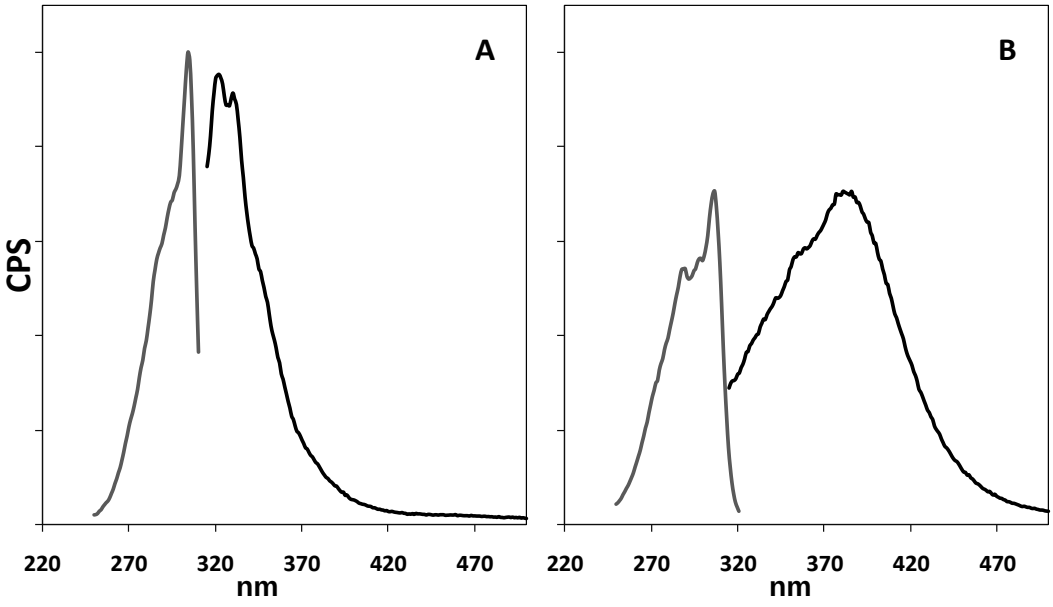

Figure 2.11: Fluorescence excitation (grey lines) and emission (black lines) spectra of 20 μM HO_2C-Dip-Hex-Hex-G(12)-OH in **A**: THF and **B**: aqueous buffer (10 mM Na_3PO_4, 100 mM NaCl, pH 6.4). The scale of the y-axis is the same in both panels. Other Dip isomers exhibit nearly identical behaviour.

compound), excitation and emission wavelengths are in good agreement with that seen previously for unsubstituted diphenylacetylene in solution [92], further indication that these compounds are indeed in a monomer state in these solvents.

In contrast, in aqueous solution the emission is remarkably different, the band is red-shifted by approximately 60 nm and is now centred around 380 nm, while the excitation maximum remains the same as that seen in less-polar solution (Figure 2.11B). The emission is also decreased in intensity and significantly broadened; clearly suggestive of excimer formation. In certain mixtures of solvents, both monomer and excimer emission can be observed, another feature common to excimer formation in aromatic compounds (Figure 2.12A) [61]. The concentrations at which excimer emission are observed are the same at which the compounds exist as aggregates in aqueous solution, as shown by the pyrene assay. This is expected as excimer formation would be facile in an aggregate where the compounds are in close proximity to each other. There is evidence that this emission is due to actual excimer formation (between an excited

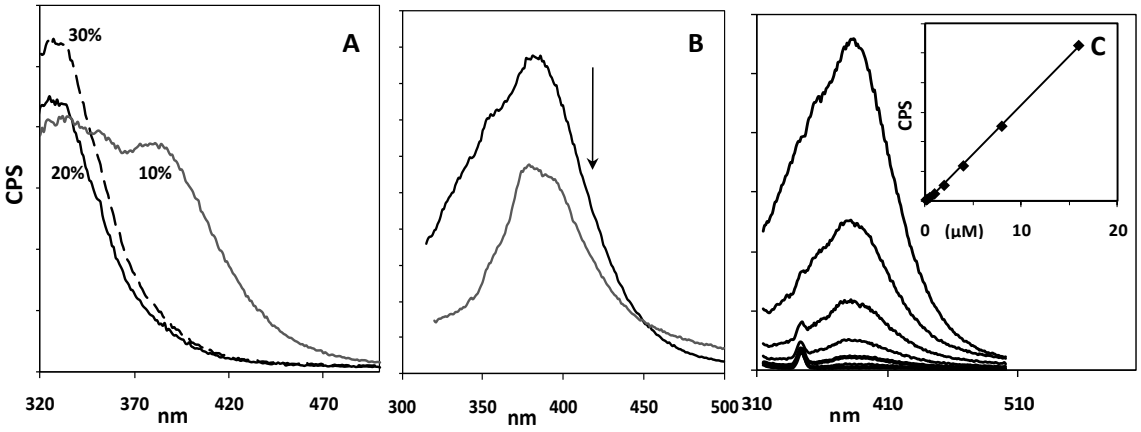

Figure 2.12: Fluorescence emission spectra of 20 μM CO_2H-Dip-Hex-Hex-G(12)-OH in **A:** mixed THF/aqueous buffer solution (10 mM Na_3PO_4, 100 mM NaCl, pH=6.4) 10% THF= grey line, 20% THF= black solid line, 30% THF= black dashed line, **B**: 100% aqueous buffer immediately after mixing (black line) or after 10 mins (grey line), **C**: 100% aqueous buffer, concentration ranges from 16 μM to 0.1 μM. **INSET**: dependence of fluorescence intensity on concentration. λ_{EX} = 305 nm for all panels.

state chromophore and one in its ground state), and not just aggregation-induced self quenching as the 380 nm emission persists in aqueous solution down to very low (0.1 μM) concentrations of compound (Figure 2.12C) far below the 'cmc' derived from the pyrene assay (~20 μM). This result must be interpreted carefully, however, as the

emission intensity in aqueous solution varies over time for the majority of Dip isomers due to the aggregation and eventual precipitation of the minimally water-soluble compounds (Figure 2.12B). In addition, the band shape of the compounds in aqueous solution also changes over time; this must be an indication of numerous species present in aqueous solution. Upon injection into the aqueous medium, the monomers quickly aggregate; the changes in emission intensity and band shape are suggestive of this. Over time, these aggregates evolve to the point where they physically precipitate from the solution, leading to further observed changes in the emission spectra. Overall, while these factors complicated certain experiments such as fluorescence quenching (discussed below), care was taken to correct for this behaviour, minimizing its overall effect on the data.

2.5.2: Fluorescence with vesicles

Regardless of the nature of the actual emitting species, the observation of environment-sensitive fluorescence with the Dip compounds is very significant, as this differential emission can be used to probe the molecules' interaction with a bilayer membrane. Spectral changes upon membrane partitioning have been observed in many cases [59]; blue-shifting of the emission and increase in fluorescence intensity is well-known to occur for tryptophan (**2-27**) [93,94] and other indoles (**2-28**) [95], fluorophores based on an NBD (nitrobenzodioxazole; **2-29**) [96], or dansyl (**2-30**) [59] framework, as well as for certain CPEs [91] (Figure 2.13). Several recent examples such as **2-31**, a flavone derivative [97] and a particularly pertinent report from Gokel *et al.* [98], which studied

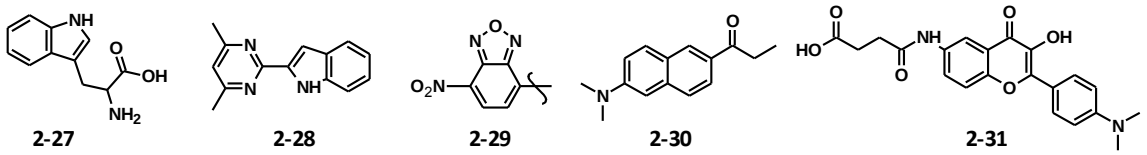

Figure 2.13: Chromophores that exhibit significant spectral changes (blue-shifting, emission enhancement) upon vesicle introduction. **2-27**: Tryptophan, **2-28:** Indole derivative from Ladokhin *et al*., **2-29:** NBD, **2-30**: PRODAN, **2-31:** 'MFL', a flavone derivative.

peptidic ion channels fluorescently labelled with chromophores such as pyrene and NBD suggests that this is a general phenomenon and should occur for the Dip compounds as well.

To test this hypothesis, each Dip oligomer was incubated with a suspension of lipid vesicles in aqueous solution, and their fluorescence spectra collected, Figure 2.14. For the HPTS-active compounds, the fluorescence in water and in the presence of vesicles are dramatically different; the spectrum in vesicles is clearly enhanced at the 320 nm region, and more closely resembles that seen in organic solution (Figure 2.14A-C). This blue-shifting of the emission and intensity increase is analogous to that seen for many fluorescent membrane probes, and indicates that the compound is indeed

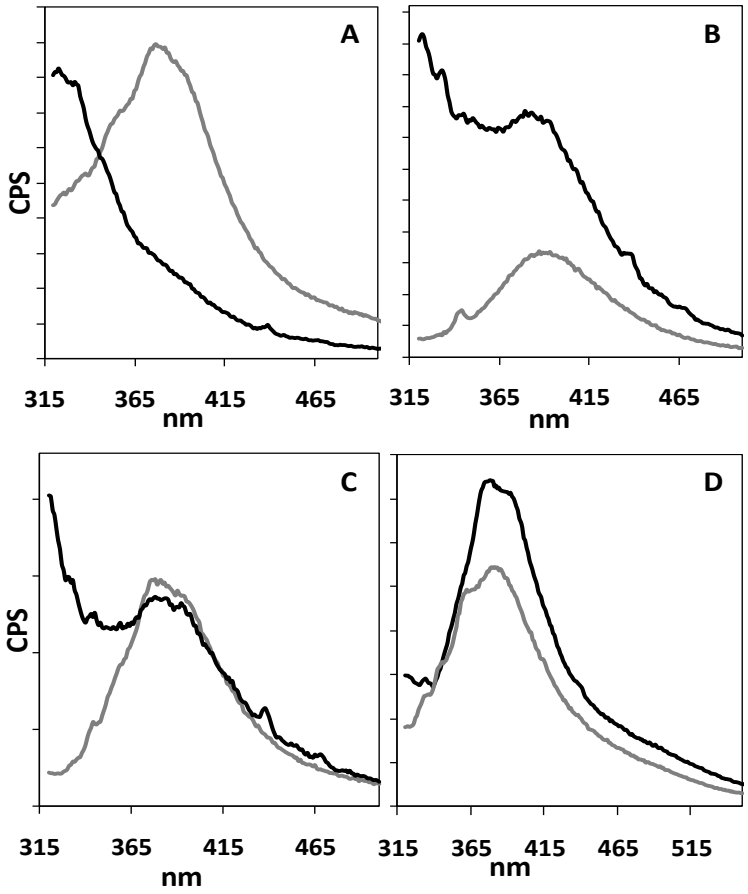

Figure 2.14: Fluorescence emission spectra in aqueous buffer (grey lines) (10 mM Na_3PO_4, 100 mM NaCl, pH 6.4) or after 10 minutes incubation time with lipid vesicles (black lines) for selected 1st-generation Dip isomers. **A**: 22 µM HO_2C-Dip-Hex-Hex-G(12)-OH, **B**: 20 µM HO_2C-Hex-Hex-Dip-G(12)-OH, **C**: 20.5 µM HO_2C-Hex-Dip-Hex-G(12)-OH, **D**: 25 µM HO_2C-Dec-Dip-Hex-G(12)-OH. λ_{EX} = 305 nm for all compounds.

partitioned into the less-polar membrane environment in which it is better solvated and can therefore emit as a monomer. In contrast, the emission spectra of the HPTS-inactive longer isomer (HO_2C-Dec-Dip-Hex-G(12)-OH) before and after vesicle addition are remarkably similar and still dominated by the 380 nm emission. This is an intriguing result, as it indicates that the Dec isomer is not effectively partitioning into the membrane and remains exterior to the vesicle as an aqueous aggregate.

In an effort to further explore this observation, and potentially obtain the kinetics of this process, the vesicle partitioning was monitored over time, as shown in Figure 2.15. In this experiment, the vesicles are introduced into a solution of the compound of interest and the emission at 320 and 380 nm is observed over a period of time. The active isomer (HO_2C-Dip-Hex-Hex-G(12)-OH) exhibits a substantial and immediate increase in fluorescence intensity at 320 nm upon vesicle introduction, which stabilizes after approximately 10 minutes. During this time, the emission at 380 nm, which initially decreases, slowly gains in intensity (Figure 2.15A). The other active isomers exhibit similar intensity changes with time; the emission at 320 nm is always more intense than that at 380 nm (see Appendix 4). In contrast, the inactive Dec isomer displays completely different behaviour (Figure 2.15B); the emission at 380 nm remains dominant and relatively stable over time, strengthening the argument that this

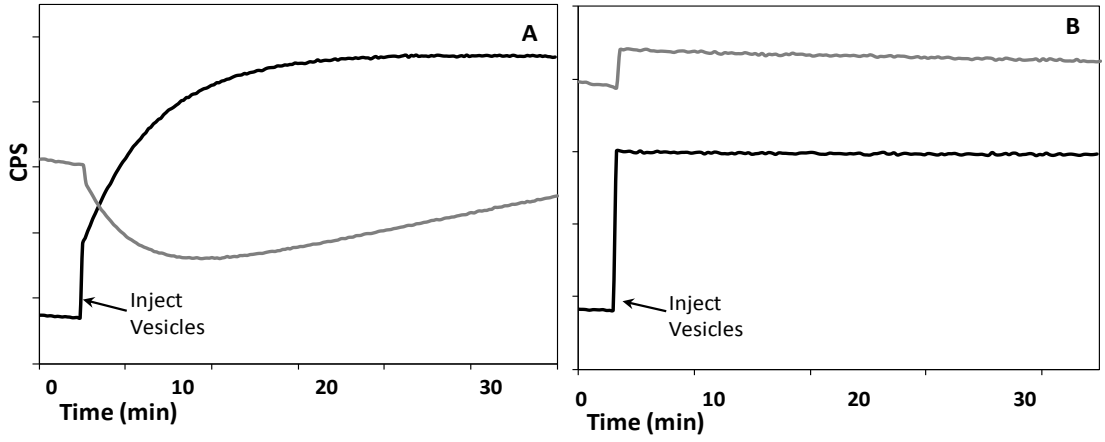

Figure 2.15: **A:** Fluorescence emission ratio at 320 nm (black line) versus 380 nm (grey line) as a function of time of 22 µM HO_2C-Dip-Hex-Hex-G(12)-OH in aqueous buffer (10 mM Na_3PO_4, 100 mM NaCl, pH 6.4) into which a suspension of lipid vesicles was injected at the specified time. **B:** analogous experiments for 25 µM HO_2C-Dec-Dip-Hex-G(12)-OH. λEx= 305 nm for both compounds.

compound remains as an aqueous aggregate and does not partition into the membrane to any appreciable extent.

The results of the experiment shown in Figure 2.15 are interpreted thusly; for HO_2C-Dip-Hex-Hex-G(12)-OH, the dramatic increase in 320 nm emission upon vesicle introduction is indicative of the compound inserting into the membrane as a monomer, while the gradual increase in 380 nm fluorescence over time suggests that the formation of an in-membrane aggregate, the presumed active species, is being observed. This was most exciting as it now gave the possibility that information about the active structure could be obtained by spectroscopic means.

For the inactive Dec isomer, the majority of the compound remains as an aqueous aggregate; this explains the lack of HPTS activity of HO_2C-Dec-Dip-Hex-G(12)-OH; clearly it cannot be active if it is unable to partition to any great extent. These results also rationalize the bilayer clamp study for HO_2C-Dec-Dip-Hex-G(12)-OH, in which it was found to be active, as in this assay the compound is pre-loaded into the lipid bilayer at concentrations apparently high enough to lead to transport activity, overcoming its poor partitioning. Therefore, the dramatic differences in activity between HO_2C-Dec-Dip-Hex-G(12)-OH and the shorter Hex analogs can now be explained based on this partitioning argument.

2.5.3: Quenching studies

Further information about the nature of the compounds' interaction with the membrane was obtained from quenching studies. The rationale behind such studies is evident; if the Dip chromophore is indeed well partitioned into the membrane and buried in a hydrophobic region it should be protected from an externally added aqueous quencher. In contrast, if the observed emission is due to an aqueous species, it should be accessible to the quencher. Therefore, the expectation was that the active compounds in which the 380 nm emission is related to the in-membrane aggregate should not experience quenching at this wavelength when incubated with lipid vesicles,

whereas the inactive Dec isomer would. However, it must be mentioned that the conclusions from these studies were not expected to be so clear-cut; other possibilities such as quenching being observed for compounds associated with, but not partitioned into the membrane, or that due to potential quencher transport through compound-formed channels in the membrane, cannot be excluded outright.

Before the in-vesicle studies could commence, however, an efficient quencher for the Dip chromophore needed to be found. Many known fluorophore-quencher pairs exist; for example, acrylamide is known to effectively quench tryptophan and pyrene fluorescence, it and heavy atoms such as Iodide (for anthracene quenching) and stable radicals such as the nitroxyls (for naphthalene and other polycyclic aromatic hydrocarbons) are amongst the most common [99]. Despite this, not much is known about the quenching of 'isolated' diphenylacetylene moieties (as compared to the conjugated polymer analogs). However, the recent studies carried out by Letsinger *et al*., in which the DPA-DNA hybrids (see Figure 2.10 for structure) were found to be quenched by adjacent purine bases present in the DNA strands indicates that the fluorescence of non-conjugated diphenylacetylene can indeed be quenched [58].

Therefore, a systematic investigation into a suitable diphenylacetylene quencher was carried out; a summary of the findings from these studies is shown in Table 2.5. This study tested a variety of compounds including acrylamide (quenching not observed), cesium (quenching not observed), $NaNO_2$ (quenching at very high concentrations), bromo- and chloro-pyridine (mild quenching at high concentrations) and TEMPO (a stable nitroxyl-radical) (moderate quenching at quite high concentrations), none of which gave completely satisfactory results.

Iodide was also tested and was shown to be an efficient quencher at low (1 mM for 50% quenching) concentrations. However, an oxidation reaction between the Iodide and trace peroxide impurities present in the THF solvent, which has been known to occur [100,101], caused the formation of a bright yellow, unknown complex, possibly containing triiodide (I_3) [100]. This complicated experiments and made using Iodide as a quencher impractical. The results with TEMPO are also worthy of mention as this

compound, when attached to phospholipids, has been used in fluorescence depth quenching (FDQ) experiments to judge the position of compounds in the bilayer membrane [102,103]. Therefore, the fact that the Dip oligoesters can be quenched reasonably effectively by TEMPO allows for the possibility of such studies to be carried out in the future, potentially leading to further information about how these compounds exist in the membrane. In general, it is assumed that the quenching investigations carried out here will be useful to others working with diphenylacetylene as well.

QUENCHER	STRUCTURE /FORMULA	CONCENTRATION RANGE[a]	EFFICACY[b]/NOTES
Acrylamide	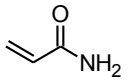	-up to 0.1M	0 (no quenching observed)
Cesium	$CsCl_2$	- 1mM to 45mM	0 (no quenching observed)
4-Chloropyridinium hydrochloride[c]	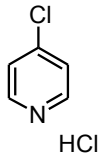	- 1mM to 0.5M	-low (40mM)
Copper	$CuSO_4$	- 0.1mM to 5mM	-very high (1mM)
Iodide	NaI	-0.1 to 5mM	-very high (1mM) -oxidation reaction prevents use
Nitrite	$NaNO_2$	-Up to 50mM	-low (~25mM)
TEMPO[d]	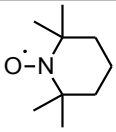	- 1mM to 10mM	-moderate (6mM)

Table 2.5: Summary of quenching data obtained for Dip-containing compounds in MeOH
a= the majority of studies were carried on 0.3 mM of HO_2C-Dip-OTHP (**2-1**)
b= number in brackets is quencher concentration necessary to effect 50% quenching
c= 4-Bromopyridinium hydrochloride gave analogous results
d= studies carried out on oligoesters; results shown for 13 μM of HO_2C-Dec-Dip-Hex-G(12)-OH

Eventually, it was determined that cupric sulphate was the quencher of choice, as this compound was found to efficiently quench the Dip fluorescence in both organic and aqueous solution at fairly low concentrations of quencher (Figure 2.16). As shown in Figure 2.16A for HO_2C-Dec-Dip-Hex(G12)-OH, approximately 1 mM $CuSO_4$ is necessary to obtain significant quenching in methanol solution, this quenching behaviour is linear with concentration and therefore can be fitted satisfactorily to the Stern-Volmer equation by plotting the ratio of fluorescence in absence (I_O) and presence (I_Q) of quencher against quencher concentration [Q] to extract K_{SV}, the Stern-Volmer quenching constant, as per Equation 2.2 [99].

$$I_O/I_Q = K_{SV}[Q] + 1 \qquad \text{Equation 2.2}$$

As shown in Table 2.6, for all studied Dip oligomers in methanol solution, the value of K_{SV} was determined to be in the 10^3 M^{-1} range, consistent with a diffusion-limited collision between a very short lifetime fluorophore and quencher, as the Stern-Volmer constant can also be expressed in terms of fluorescence lifetime of the compound (τ_O) and k_q, the bimolecular rate constant of quenching: Equation 2.3

$$K_{SV} = k_q\tau_O \qquad \text{Equation 2.3}$$

As mentioned, the fluorescence lifetime of diphenylacetylene is in the sub-nanosecond range, therefore, the inference that the Dip compounds undergo mainly dynamic quenching in methanolic solution is reasonable, as this would not exceed diffusion control ($k_q > 10^{10}$) [99].

In comparison, the quenching of the Dip compounds in aqueous solution is very different; as shown in Figure 2.16B, and Table 2.6, the obtained Stern-Volmer constants are 1000 times larger than those obtained in methanol, clearly suggesting that a significant degree of static quenching is occurring in aqueous solution for the Dip

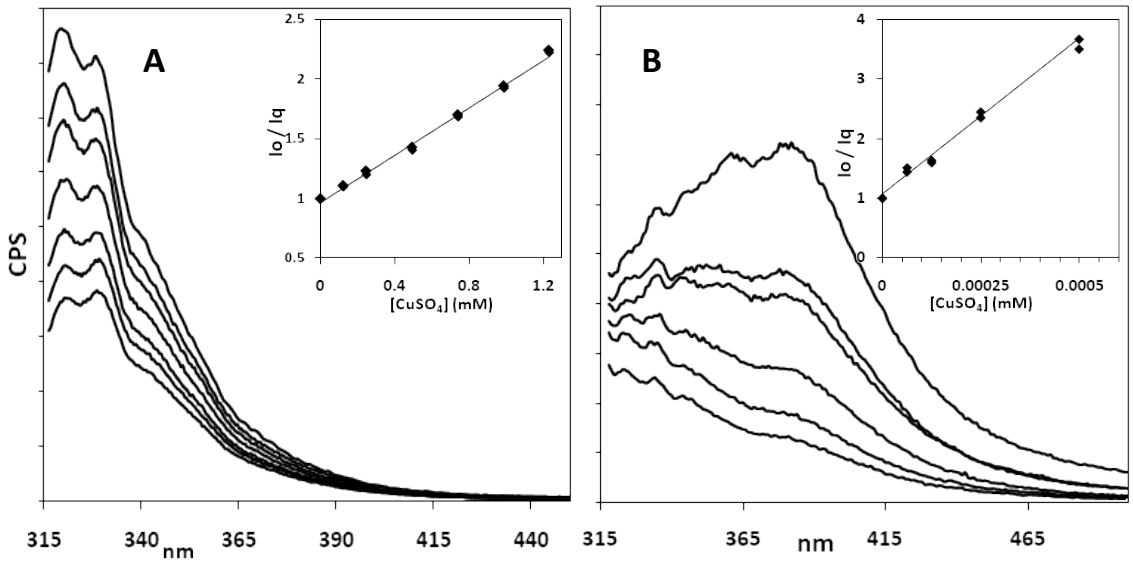

Figure 2.16: Fluorescence quenching in **A**: methanol and **B**: aqueous solution (100 mM NaCl) for 30 µM HO_2C-Dec-Dip-Hex-G(12)-OH. From top to bottom, [$CuSO_4$] = 0, 0.125, 0.25, 0.49, 0.74, 0.98 and 1.23 mM in methanol and 0, 0.0625, 0.125, 0.5 and 1.0 µM in water. **INSET:** Stern-Volmer analysis of quenching data. Constants in methanol had linear fits, while some aqueous-derived constants deviated from linearity, due to changing emission over time. λEx= 305 nm in both panels.

	STERN-VOLMER CONSTANT(K_{sv}) (M^{-1})	
COMPOUND	**AQUEOUS SOLUTION**	**METHANOL SOLUTION**
HO_2C-Dip-Hex-Hex-G(12)-OH	9.5±1.3 x 10^6	1.12±0.05 x 10^3
HO_2C-Hex-Hex-Dip-G(12)-OH	2.2±0.2 x 10^6	6.8±0.2 x 10^2
HO_2C-Dec-Dip-Hex-G(12)-OH	5.26±0.03 x 10^6	1.05±0.02 x 10^3
HO_2C-Dip-G(12)-OH	3.6±0.2 x 10^5	2.0±0.15 x 10^3

Table 2.6: Experimentally-derived Stern-Volmer constants in aqueous solution or in methanol for selected first-generation Dip isomers quenched by $CuSO_4$. Constants in methanol had linear fits, while aqueous-derived constants sometimes deviated from linearity, due to changing emission over time.

oligomers [99]. This is not a completely unexpected result, as exactly this type of behaviour has been observed for the previously-mentioned conjugated polyelectrolytes (CPEs), with which the Dip oligoesters, despite their much lower molecular weight, appear to share many characteristics. The CPEs have been reported to exhibit such 'super-quenching' [104,105] of up to 10^7 M^{-1}, [89] which can be explained by several reasons. Most relevant to this work is that they are polyanionic species which form electrostatic

complexes with the positively-charged compounds used to quench them, an effect which is further enhanced in aqueous solution where the compounds exist mainly as aggregates. This allows a single quencher to access a multitude of fluorophores, increasing quenching efficiency. Certainly, this should explain the vastly more efficient quenching seen in aqueous solution for the Dip chromophore; as the pH of the solution is higher than the pKa of the carboxylic acid terminus, the compounds exist as polyanionic (carboxylate) aggregates. The quencher is a positive ion, so electrostatic interactions between it and the already-formed aggregates are bound to occur, thereby enhancing static quenching. This aggregation-based argument is strongly suggested by the data in Table 2.6 as the short dimer (HO_2C-Dip-G(12)-OH), which aggregates to the least extent ('cmc' ~150 μM), in fact shows the lowest value of K_{SV} of all the studied oligomers in aqueous solution (10^5 for HO_2C-Dip-G(12)-OH, 10^6 for the longer analogs), while having a similar value in methanol.

Clearly, static quenching is a significant factor in aqueous solution; however, it is not expected to lead to any misinterpretations as the data are qualitative in nature. The key conclusion from these solution-phase studies is that $CuSO_4$ had been discovered to be an efficient quencher of both the monomer and excimer fluorescence of the Dip compounds in both methanol and aqueous solution, and could now be applied to the in-vesicle studies. As mentioned previously, the goal of these studies was to further test the hypothesis that the formation of an in-membrane aggregate, which could be a potential active structure, was being directly observed by the increase of 380nm emission in vesicles for the active Dip isomers.

The results of such studies are presented in Figure 2.17 for HO_2C-Dip-Hex-Hex-G(12)-OH, an active molecule, and Figure 2.18 for the HPTS-inactive Dec isomer. Both a 'before and after' scan of the compounds with and without copper and vesicles (Fig. 2.17-18, TOP PANEL) as well as in a time-based experiment (Fig. 2.17-18, BOTTOM PANEL), are shown. For the time-based experiment, the compounds were initially in aqueous solution, in which the 380 nm emission is dominant, as discussed. Vesicles are then added, and the same behaviour is seen as previously (Figure 2.15); the active

compound partitions and the emission at 320 nm dramatically increases, while this does not occur for the inactive analog. Once the quencher is introduced (at concentrations at which it can efficiently quench the Dip 380 nm fluorescence in aqueous solution), it is evident that there is hardly any effect on the emission intensity of HO_2C-Dip-Hex-Hex-G(12)-OH; it is not quenched. As the extent of quenching in the presence of vesicles has decreased from approximately 75% in aqueous solution to almost negligible, this is clear evidence that the compound is indeed partitioned, inaccessible to quencher and that

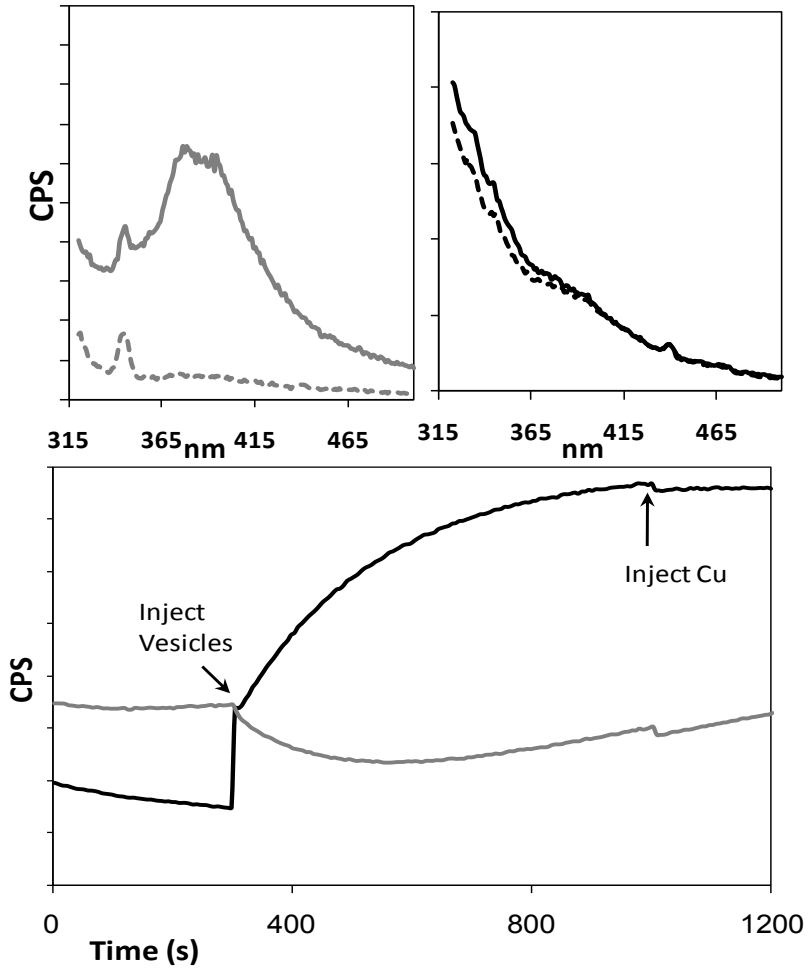

Figure 2.17: **TOP PANEL**: Fluorescence emission spectra of 16 µM HO_2C-Dip-Hex-Hex-G(12)OH in aqueous solution (0.1 mM NaCl) (grey lines) or after incubation with lipid vesicles (black lines) in the absence (solid lines) or presence (dashed lines) of 1 µM $CuSO_4$. **BOTTOM PANEL**: Time-based emission ratio at 320 nm (black line) or 380 nm (grey line) of 16 µM HO_2C-Dip-Hex-Hex-G(12)OH in aqueous solution (0.1 mM NaCl), to which vesicles and 1 µM $CuSO_4$ were added at the indicated times. λEx= 305 nm.

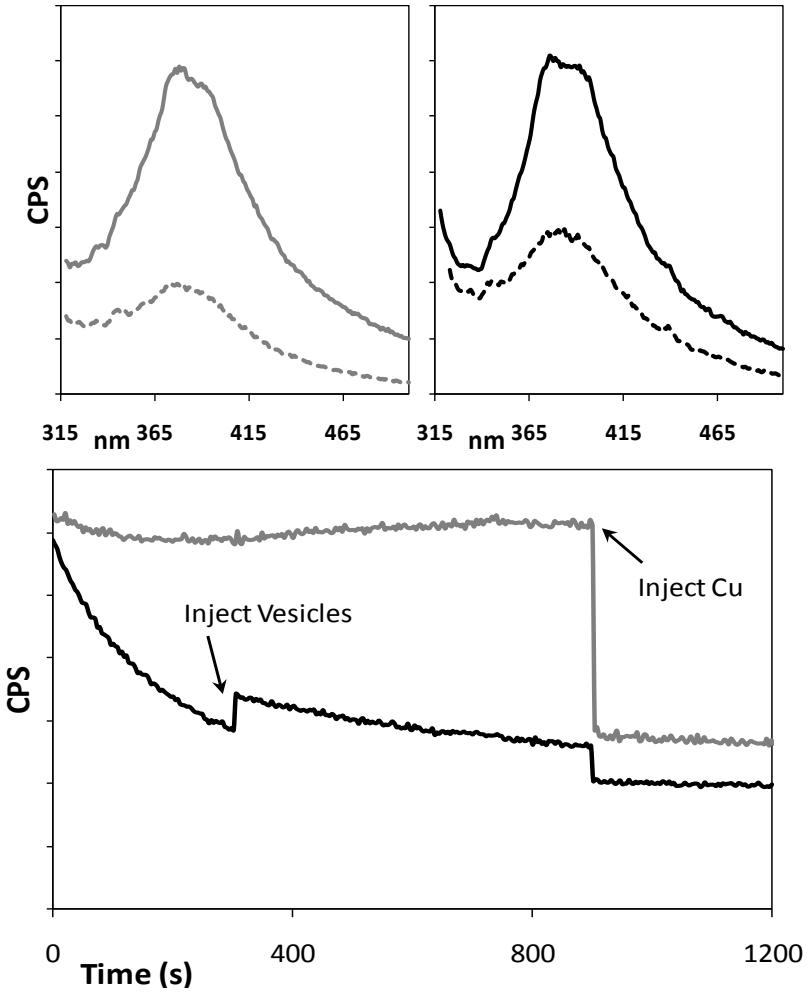

Figure 2.18: **TOP PANEL**: Fluorescence emission spectra of 20 μM HO_2C-Dec-Dip-Hex-G(12)OH in aqueous solution (0.1 mM NaCl) (grey lines) or after incubation with lipid vesicles (black lines) in the absence (solid lines) or presence (dashed lines) of 1 μM $CuSO_4$. **BOTTOM PANEL**: Time-based emission at 320 nm (black line) or 380 nm (grey line) of 20 μM HO_2C-Dec-Dip-Hex-G(12)OH in aqueous solution (0.1 mM NaCl), to which vesicles and 1 μM $CuSO_4$ were added at the indicated times. λEx= 305 nm.

the 380 nm emission observed is due to an in-membrane aggregate. Conversely, the inactive Dec analog exhibits quenching in the presence of vesicles which is practically identical to that observed in aqueous solution alone; clearly the vesicles are not protecting this compound from quenching, and the 380 nm emitting species is predominantly an aqueous aggregate (schematically illustrated in Figure 2.19). This is again consistent with the previous results, indicating the poor partitioning of this compound. As expected, the other studied active Dip isomers exhibit very similar behaviour to that seen for HO_2C-Dip-Hex-Hex-G(12)-OH, and are minimally quenched by

copper in the presence of vesicles.

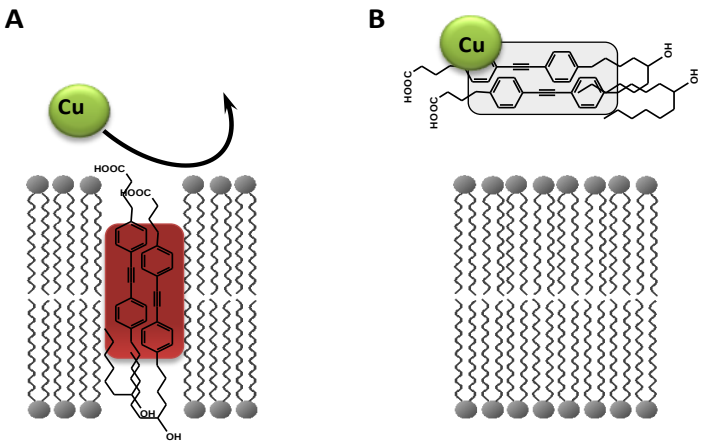

Figure 2.19: Schematic diagram illustrating the results of the in-vesicle quenching assays. **A**: active compounds are inserted into the membrane; 380nm emitting aggregates are protected from quencher. **B**: inactive compound; aggregate remains in aqueous solution and is not protected from quenching.

2.6: Mechanistic implications

Based upon previous work by Fyles *et al*., a working hypothesis to explain the mechanism of action of this class of oligoester aggregate channels was proposed [40] (see Figure 1.10 in the Introduction). As discussed, it is believed that these compounds exist mainly as aggregates in aqueous solution, as evidenced by the pyrene assay. When introduced to lipid vesicles, the transport-competent compounds can partition into the membrane *via* an aqueous monomer, to form an in-membrane monomer. Over time, these monomers can then aggregate in the membrane to form an active ion channel. Conversely, the inactive compounds remain as an aqueous aggregate. In the previous work, it was impossible to directly observe any of these proposed intermediates, as the fully saturated oligoesters did not possess any useful spectroscopic tags.

However, the development of the Dip compounds, and the discovery of their environment-sensitive fluorescence has indeed allowed for the observation of many of these proposed intermediates; furthermore, the detected species are consistent with those of the working hypothesis. As illustrated in Figure 2.20, the evidence for aqueous aggregation can now be directly observed as 380 nm emission in aqueous solution, due

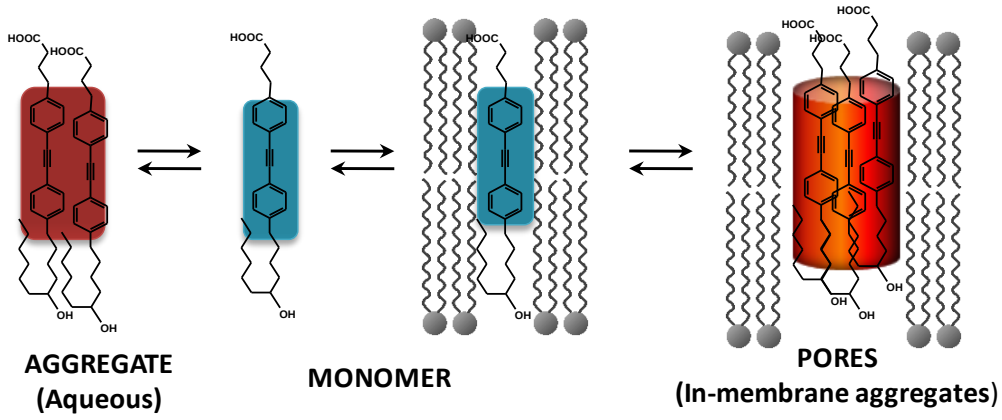

Figure 2.20: Schematic illustration of proposed mechanism of action of Dip-containing aggregate channels. The compounds exist mainly as 380 nm– emitting aggregates in aqueous solution (red rectangle), the active compounds can partition via a presumed aqueous monomer into an in-membrane monomer which emits primarily at 320 nm (blue rectangle). These monomers aggregate in the membrane, forming the active structure (red cylinder).

to an excimer within an aggregate. For the active compounds, a dramatic increase in emission at 320 nm upon vesicle introduction, giving rise to spectra similar to those obtained in organic solution, monitors the partitioning of the compounds into the less-polar membrane interior. Finally, slow recovery of the emission at 380 nm, which cannot be quenched by an aqueous quencher, indicates the in-membrane aggregation of the monomers to potentially form the active structure, a presumed pore-like species. In contrast, the inactive Dec isomer clearly remains stalled in the aqueous aggregate stage, as there is no significant increase in 320 nm emission upon vesicle introduction, and the 380 nm emission present for this compound can be efficiently quenched. These results provide a sound basis to explain the different behaviour exhibited by the active and inactive Dip compounds, as the Dec compound, due to increased hydrophobicity or some other factor, simply cannot partition into the membrane from aqueous solution at a concentration that can effect transport.

Overall, while the model presented in Figure 2.20 remains a hypothesis due to lack of direct structural evidence of the proposed species, these results were very exciting, as the proposed model, which could be used to explain the behaviour of other 'simple structure' aggregate channels now has some experimental evidence.

2.7: Conclusions & future work

The results of the studies on the first generation Dip oligoesters were most promising. While a solid-phase approach, utilized effectively in the work on the fully-saturated precursor compounds, could not be applied here, a well-designed, robust and reliable solution phase procedure was developed that allowed for the synthesis of a suite of compounds which could be purified and extensively characterized. The synthesis is modular and can be applied to many substrates and in a variety of sequences to obtain the desired oligomers, usually in fairly reasonable yields. This solution-phase synthesis has the significant advantage that each intermediate can be isolated and characterized, thereby monitoring potential problems as they arise. In addition, it allows for the possibility to test the isolated advanced intermediates for ion channel activity, as in the past 'by-products' such as the short dimer HO_2C-Oct-G(12)-OH had been discovered to be active [40].

The incorporation of the Dip chromophore led to many advantageous properties and interesting behaviours; firstly, the ability to purify these compounds by HPLC guaranteed their high purity, which ensured that the results observed in the various assays were a consequence of the compounds themselves, and not an impurity. In addition, the increased activity observed in the HPTS assay for the Dip-containing sequence isomers such as HO_2C-Dip-Hex-Hex-G(12)-OH was very significant, as these compounds are up to 5 times more active than the saturated precursors, clearly indicating that enhanced rigidity has a beneficial effect on transport in some instances. However, it was also observed that this rigidity effect is sometimes not enough, as a very striking length effect was observed by the lack of HPTS-activity for the longest oligomer, HO_2C-Dec-Dip-Hex-G(12)-OH. This was correlated to its poor membrane partitioning, based upon the differential environment-sensitive fluorescence observed for the Dip compounds. The environment-sensitive fluorescence is in itself an important finding, as this allows these compounds to be utilized as membrane probes, and is only the second reported instance of a 'simple' diphenylacetylene-based molecule exhibiting excimer-type emission in solution.

In conclusion, the Dip oligomers have done much to strengthen and refine the model proposed to explain the activity of this type of oligoester aggregate channel. The direct spectroscopic observation of key proposed intermediates is useful in further development of this mechanism, which could potentially be extended to other systems. The fluorescence characteristics of the Dip compounds have certainly been an invaluable tool in continuing efforts to elucidate a mechanism which in turn could be used to infer a plausible active structure. Future studies in this regard will be focused on the continued synthesis and characterization of further diphenylacetylene-containing ion transporters, and shall be discussed in the remainder of this work.

Chapter 3 : Synthetic ion channels based on an extended chromophore

3.1: Rationale

As the Dip compounds had indicated that a correlation exists between rigidity and increased ion-transport activity, it was assumed that this could be enhanced further by an even more rigid, multi-aromatic containing compound. In addition, while the environment-sensitive fluorescence of the Dip isomers is a very useful property that had led to a variety of interesting discoveries, the actual fluorescence intensity of the diphenylacetylene chromophore itself is rather low, with a reported fluorescence quantum yield of 3.36×10^{-3} [85]. Increased fluorescence would be advantageous in the possible development of a 'light-up' membrane probe [14], which could monitor the membrane partitioning of the compounds by eye, perhaps in real-time under a fluorescence microscope using larger GUVs. Such assays have been used extensively in various biological applications such as DNA binding by fluorescent dyes [59,106], and to monitor raft formation in mixed-lipid vesicles [43]; this could be an interesting further application in addition to ion transport. Enhanced fluorescence would also allow lower concentrations of compound to be used, possibly minimizing aggregation. In addition, another impetus was the design of a previously-unknown chromophore, with the potential to discover interesting photophysical properties.

3.2: Initial tetra-aromatic design & attempted synthesis

The initial design for the extended chromophore was a tetra-aromatic di-alkyne, chosen as an explicit 'dimer' of the Dip chromophore, and was accordingly named 'Bi(Dip)' (Figure 3.1). This was seen as a natural progression from the Dip structure, and further generations of multi-aromatic containing molecules were envisaged as oligomers of the Dip 'monomer', 'Tri (Dip)' being the next in the intended series. The

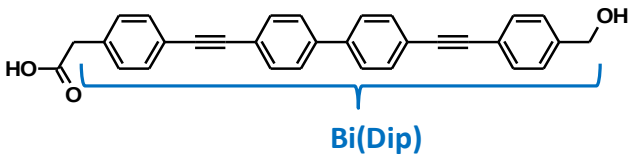

3-1

Figure 3.1: Proposed tetra-aromatic 'Bi(Dip)' structure: HO_2C-Bi(Dip)-OH (**3-1**).

aromatic cores were also meant to be elaborated into oligoesters, therefore, Bi(Dip) retains the same carboxyl and hydroxyl termini as the Dip compounds, in order to utilize the previously-developed set of ester coupling and protection/deprotection reactions (Chapter 2). However, the structure shown in Figure 3.1 (HO_2C-Bi(Dip)-OH, **3-1**) was never intended to be synthesized; such a structure would have poor solubility, due to the bi-polar nature of the charged carboxylate terminus and very hydrophobic multi-aromatic core. In addition, its ester coupling efficiency was presumed to be low, as was observed in previous Dip oligomer syntheses between high molecular weight substrates. Instead, the Bi(Dip) structure would be accessed by a modular approach as utilized in the first generation Dip syntheses; oligomers containing this structure would be built from both sides into large terminal alkyne and halogen-containing 'halves' which could be coupled together using higher-yielding Sonogashira reactions. The formation of the Bi(Dip) moiety would then occur at a late stage in the synthesis. The Prenyl protecting group would also be retained on the carboxyl terminus for as long as possible, limiting the number of reactions performed on the exposed carboxylate.

The attempted synthesis of the first Bi(Dip)-containing target trimer, HO_2C-Hex-Bi(Dip)-G(12)-OH (**3-10**), is shown in Scheme 3.1. The first step required the synthesis of 4, 4'-Bromo-Iodo-biphenyl (**3-3**) from 4-Bromobiphenyl (**3-2**); while appearing rather simple, this compound was in fact the key to access a dissymmetric core structure. Iodo-substituted compounds are well known to undergo Sonogashira coupling much more readily (lower temperatures, shorter reaction times) than their brominated analogs [69]. Therefore, the biphenyl moiety could be selectively functionalized on either side, which laid the groundwork for the rest of the asymmetric synthesis of the target compound. 4, 4'-Bromo-Iodo-biphenyl is a known compound [107], although it is not commercially available. Its synthesis is worth mentioning as the reaction appears as a 'witches brew'

of various reagents, which exists as a deep black solution while it is heating away in acidic nitrobenzene at 90^0C. However, from this black solution, a simple dilution with methanol and filtration led to a fairly high yield (78%) of very pure, shiny white crystals, as reported [107]. The success of the reaction can be easily seen in the ^{13}C NMR, as the carbon *ipso* to the iodo substituent appears characteristically upfield (~90 ppm) from the rest of the aromatic carbons. Once in hand, the iodo substituent could then be selectively Sonogashira coupled to TMS-acetylene; the relatively low temperature (40^0C) and reaction time led to only the desired iodo-coupling (compound **3-4**), with no extra aromatic-containing compounds observed while monitoring the reaction by TLC. In the ^{1}H NMR spectrum, the integration of the 9H singlet due to TMS corresponded to the 8 protons of the aromatic region, clearly indicating mono-substitution. The reaction forming **3-4** was high-yielding (81% after purification), as was the carbonate-facilitated removal of the TMS moiety to provide the terminal alkyne **3-5**; the loss of the TMS signals in the ^{1}H and ^{13}C NMR give clear indication of the success of this reaction. The synthesis continued with another Sonogashira reaction, now coupling the biphenyl-terminal alkyne **3-5** to the Prenyl-protected aromatic iodide **3-6**, which was developed during the Dip syntheses. Again, this reaction was unproblematic, the resulting compound **3-7** was easily purified by chromatography and characterized by NMR; key signals indicating coupling were the Prenyl signals in both spectra, the loss of the terminal alkyne proton (3 ppm) in the ^{1}H NMR, and the appearance of the characteristic internal alkyne carbons at 89 and 90 ppm.

The next step was approached with caution as the yield was expected to be poor, due both to the size of the coupled fragments **3-7** and **3-8** as well as reduced coupling efficiency of bromo-substituted compounds in the Sonogashira reaction. The terminal alkyne **3-8** was again developed during the first generation Dip syntheses, and is accessed *via* ester coupling between 4-ethynylbenzyl alcohol (**2-5**) and HO_2C-G(12)-OTBDMS (**2-13**). In the event, coupling between **3-7** and **3-8** did occur, however, both

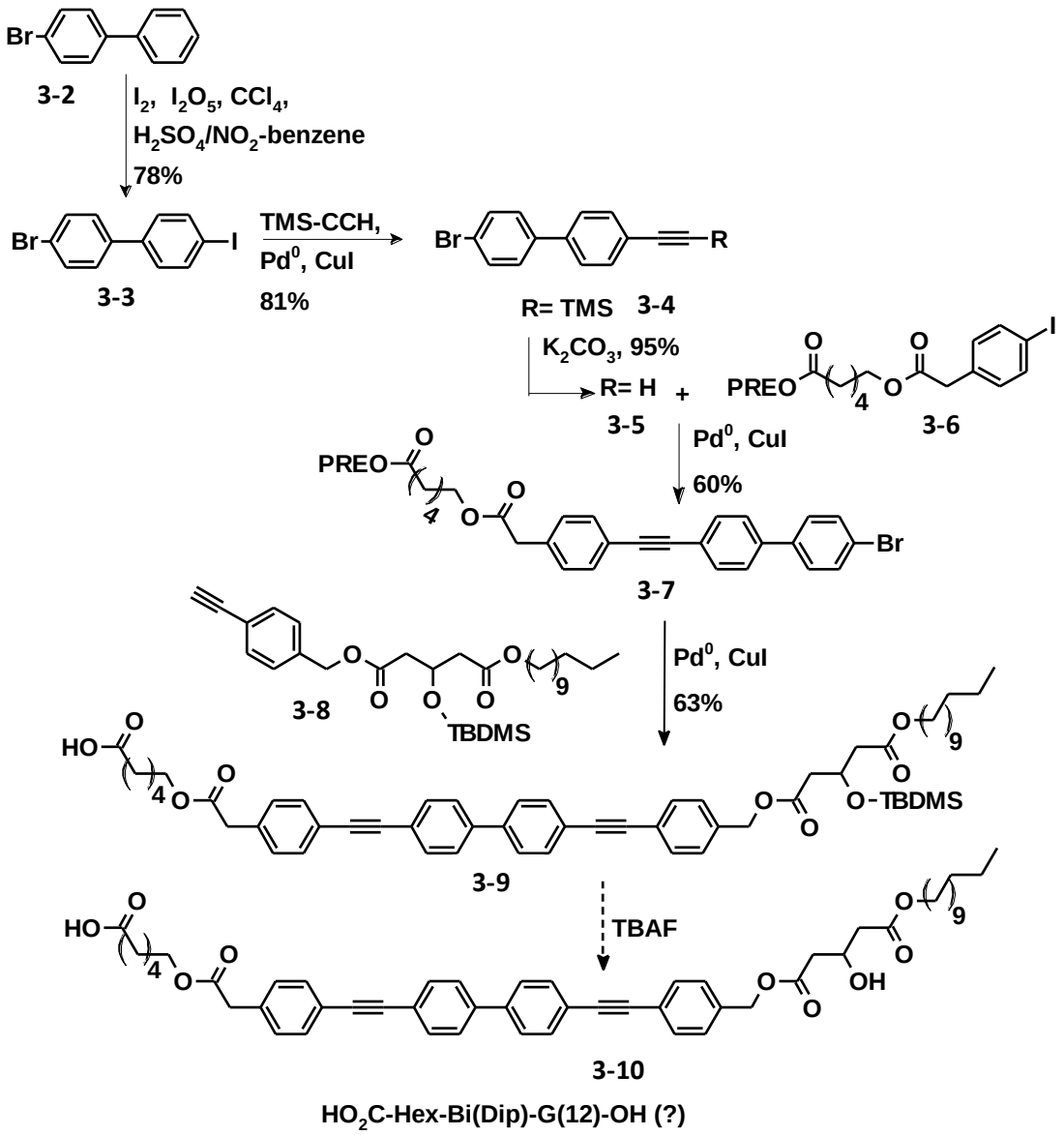

Scheme 3.1: Attempted synthesis of the tetra-aromatic trimer HO_2C-Hex-Bi(Dip)-G(12)-OH (**3-10**). The solid arrows indicate successful reactions, while the identity of the final compound could not be satisfactorily assessed, due to poor solubility. Full experimental details and characterization available in Appendices 1 and 2.

TLC analysis as well as subsequent NMR characterization indicated that the Prenyl group had in fact been removed during the coupling reaction, this was most obvious by TLC as the mobility of the major observed product was much lower than expected. Upon purification, which was non-trivial as expected due to the charged carboxylate, the NMR spectra of **3-9** proved that the Prenyl group had been lost as its signals, such as the

methine proton on the alkene (5.4 ppm) and the terminal methyls (2 large singlets ~1.5 ppm) are unmistakable.

While the loss of the Prenyl group was surprising as it is expected to be removed under acidic conditions, what was less surprising was the poor solubility of the obtained compound **3-9**, however, the synthesis of the target compound was nearing completion; only the removal of tBDMS moiety present on the 'G'-hydroxyl terminus remained. The product of this reaction, assumed to be the desired final compound HO_2C-Hex-Bi(Dip)-G(12)-OH (**3-10**), was exceedingly difficult to work with; chromatography proved almost impossible both by 'regular' polarity silica as well as on a reverse-phase column (HPLC). The highly-fluorescent product eventually obtained was found to have very poor solubility in a wide range of organic solvents, and its NMR spectra were in fact collected in D_6-dmso at elevated temperature [108]. Even under these conditions, proof of structure for HO_2C-Hex-Bi(Dip)-G(12)-OH could not be obtained; the NMR spectra were consistent with the desired structure, but not conclusive. Therefore, the synthesis was ultimately deemed unsuccessful, and a new approach had to be found.

This first attempted synthesis is discussed as it is a good example of the issues surrounding the synthesis of such 'rigid-rod' multi-aromatic compounds. Their poor solubility with increasing length is well-known [109], especially for un-functionalized rods which do not have solubilising groups attached to them. This has been encountered in other synthetic ion channel work by the Matile lab in the early development of their 'octiphenyl' compounds (structure shown in Figure 3.2); the very low yields of these molecules in reactions such as biaryl couplings were attributed to the poor solubility of the almost completely aromatic intermediates [110]. In future work, Matile *et al*. continued to elaborate and functionalize these compounds, eventually leading to the very interesting class of 'beta-barrel multifunctional pores', which have shown a variety of behaviours such as ligand-gating, and are in fact the 'sugar sensors' discussed in the Introduction [17].

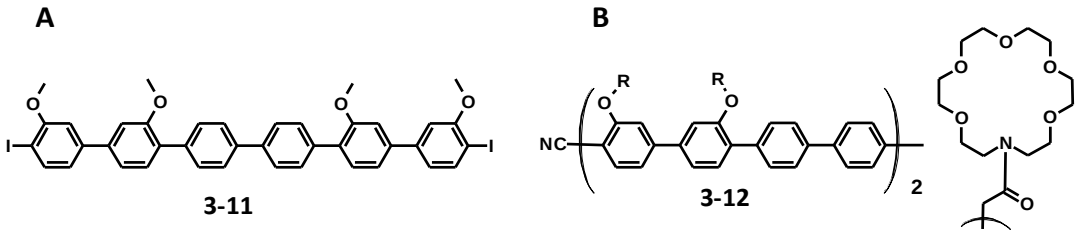

Figure 3.2: Early examples of the octiphenyl class of ion channels developed by Matile *et al*. **A**: **3-11**, a highly-insoluble intermediate in the synthesis of the octiphenyl rod **3-12** shown in **B**.

Returning to the Bi(Dip) compound, while the unsuccessful synthesis was a setback, an encouraging observation was that the intermediates were indeed highly fluorescent both as solids and in solution, this could be visualized by a simple UV light, something not possible for the Dip chromophore. This suggested that such structures were a promising first attempt which required some further optimization.

3.3: Modified design & synthesis: the 'Trip' scaffold

The next design iteration involved removing one of the phenyl rings to make a triphenyl ('Trip') scaffold (illustrated as part of compound **3-17**), as shown in Scheme 3.2. The Trip subunit itself is named analogously to the Dip moiety; the methylenes on either side of the aromatic ring and terminal alkyne are included in the 'core' structure, while the termini are not; compound **3-17** is therefore PREO_2C-Trip-OH. This structure, and oligomers containing it, were expected to have higher solubility than the tetra-aromatic 'Bi(Dip)' compound as the dissymmetry of the Trip molecule could lead to decreased packing and possibly decreased aggregation. The simple removal of a phenyl ring, leading to a less-extended aromatic core should also be beneficial in this regard, while still presumably retaining high fluorescence.

The synthetic plan for the Trip scaffold, and its eventual incorporation into di- or tri-esters, was completely different from that developed for the Bi(Dip) compounds, despite sharing the same key starting material, 4, 4'-Bromo-Iodo-biphenyl (**3-3**). As mentioned, the main consideration is retaining the carboxyl-terminus Prenyl protecting

group for as long as possible, thereby increasing solubility. In the Bi(Dip) synthesis, the elevated temperatures utilized in the Sonogashira coupling of the bromo-substituted **3-7** resulted in the loss of the Prenyl moiety, this was clearly to be avoided. In the new planned synthesis, the bromo-containing compound which undergoes this high temperature coupling would be a simple aromatic without any esters present. It was also decided to synthesize the Trip scaffold first, and then further extend the structure by appending various alkyl 'tails': the Trip unit would then be a common building block that could be diversified into numerous compounds. The synthesis is shown in Scheme 3.2, while further experimental details and full characterization of all compounds are available in Appendices 1 and 2.

The synthesis begins with the facile Sonogashira coupling of propargyl alcohol ($HCCCH_2OH$) to the aforementioned biphenyl compound **3-3**. This reaction was performed on a relatively large scale (2.5 g of starting alkyne), and in high yield (89%) to obtain a reasonably large amount of the desired mono-functionalized biphenyl alkyne **3-13**. The successful coupling to only the iodo substituent was again observed in the ^{1}H NMR spectrum by the correct integration of the methylene protons α to the alcohol (2H, δ= 4.51 ppm, doublet) in relation to the aromatic signals (8H, ~7.5 ppm, complex multiplet).

The next step was the high-temperature Sonogashira coupling of the bromo-substituted **3-13**, as mentioned this compound is a relatively simple aromatic without any potentially labile groups such as the Prenyl moiety. In the event, the reaction between **3-13** and an excess of the readily-available TMS acetylene (TMS-CCH) was in fact very successful considering it involved a bromo-substituted starting material, resulting in a good yield of the easily purified and characterized desired product, **3-14**. The ^{13}C NMR was most useful in judging the success of the reaction, the presence of 4 alkyne carbons, and specifically the appearance of the new signals from the TMS acetylene at ~95 and 100 ppm were clear indication. In addition, while the only difference in the proton spectrum between starting material **3-13** and the desired product **3-14** is the large singlet at 0ppm due to the TMS group, the relative integration

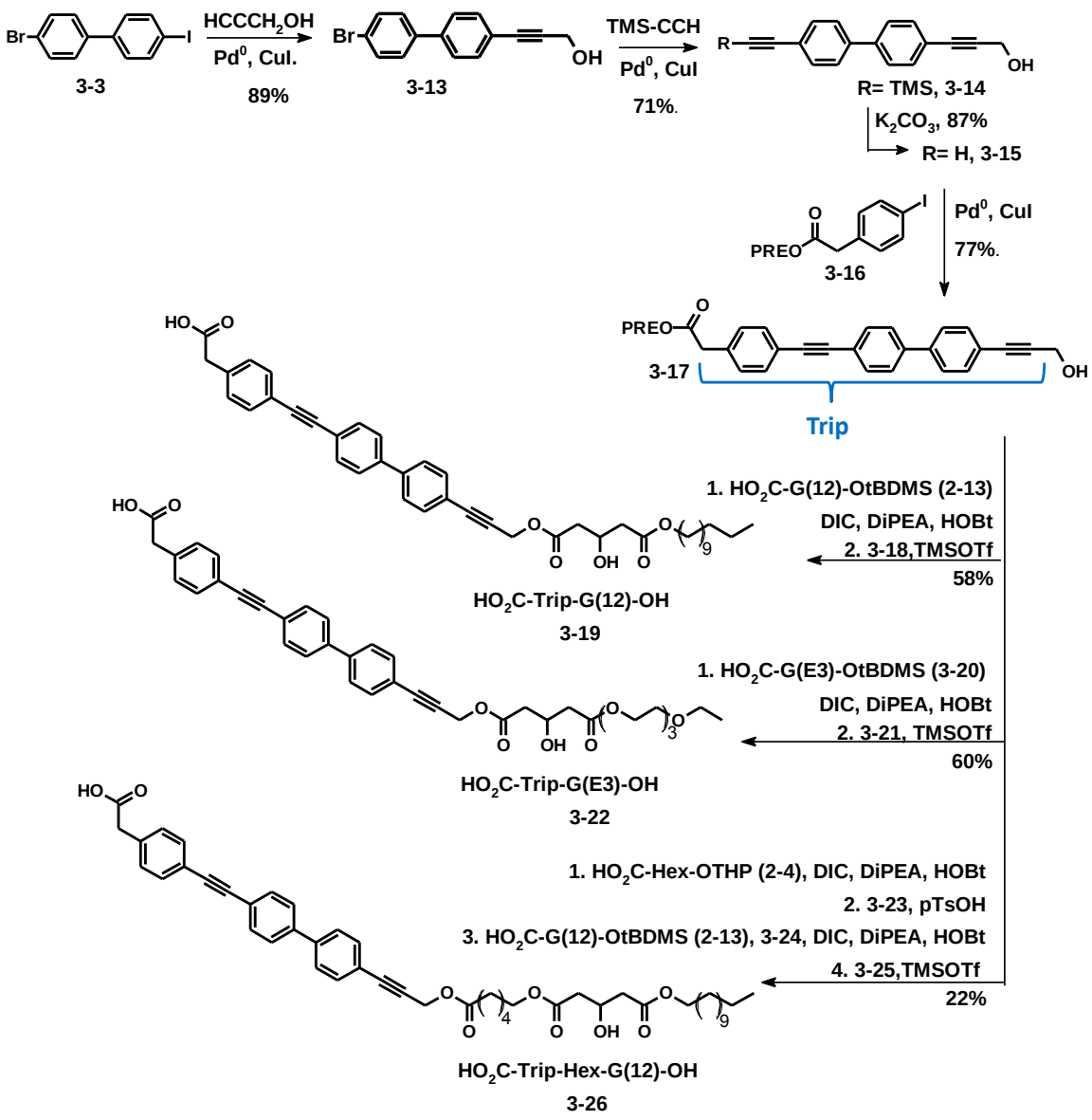

Scheme 3.2: Synthesis of the Trip scaffold and Trip-containing molecules.

between this obvious signal and the aromatic region can also be used as an indicator.

After simple, unproblematic TMS deprotection, the terminal alkyne **3-15** underwent yet another (room temperature) Sonogashira reaction with the Prenyl-protected aromatic iodide **3-16**, to furnish the Prenyl-protected 'Trip' scaffold $PREO_2C$-Trip-OH (**3-17)**. Compound **3-16** was made simply by ester coupling prenyl alcohol (HO-$CH_2CHC(CH_3)_2$) to 4-iodo-phenylacetic acid (**2-7**), the details of which are available in Appendix 1.

The purification of $PREO_2C$-Trip-OH (**3-17**) was pleasantly facile, and it is well soluble in a variety of organic solvents, and is fluorescent both as a solid and in solution. As $PREO_2C$-Trip-OH is used as a model compound in further studies into the Trip molecules, and is in fact a novel chromophore, its structural characterization is worth discussing, therefore its ^{1}H and ^{13}C NMR spectra are presented in Figure 3.3. The ^{1}H NMR (Figure 3.3A) is fairly uncomplicated, and the key indicator of successful coupling is the correct integration (2H each) between the 'Trip' methylenes Hb and Hc, the aromatic region also integrates to the expected 12 protons. The carbon spectrum is significantly more complicated, although just as with the Dip compounds each signal can indeed be assigned; key signals are the 4 internal alkyne carbons visible at ~90 ppm, the Prenyl group carbons (138, 118, 62, 25, 17 ppm) and the ester carbonyl present at the expected 170 ppm.

With the Trip scaffold in hand, it could now be extended into dimeric or trimeric ester molecules by utilizing the same series of ester coupling and deprotection reactions as discussed previously. The alkyl 'tails' appended to the hydroxyl terminus of $PREO_2C$-Trip-OH were also known from previous work; HO_2C-G(12)-OtBDMS (**2-13**), the more hydrophilic HO_2C-G(E3)-OtBDMS (**3-20**) and the 6 carbon THP-protected hydroxyacid HO_2C-Hex-OTHP (**2-4**). In total three different structures were targeted; the dimers HO_2C-Trip-G(12)-OH (**3-19**) and HO_2C-Trip-G(E3)-OH (**3-22**) and the trimer HO_2C-Trip-Hex-G(12)-OH (**3-26**). In all cases, the ester coupling reactions between the protected alkyl tails and the Trip scaffold were fairly good yielding; 71% for the reaction yielding **3-21**, 73% for **3-18**, and ~60% for each of the 2 steps leading to **3-25,** *via* **3-23** and **3-24**. This was pleasantly surprising considering the low yields and sluggish couplings encountered in previous Dip syntheses carried out on two large fragments. Key evidence from the NMR were the integral values of the Trip methylenes (Hb and Hc, Figure 3.3A) in relation to the methine proton geminal to the tBDMS group, or α to the carbonyl of the newly formed ester.

The final step in all three syntheses was the simultaneous removal of the Prenyl and tBDMS protecting groups using TMS triflate; this facile and convenient one-step

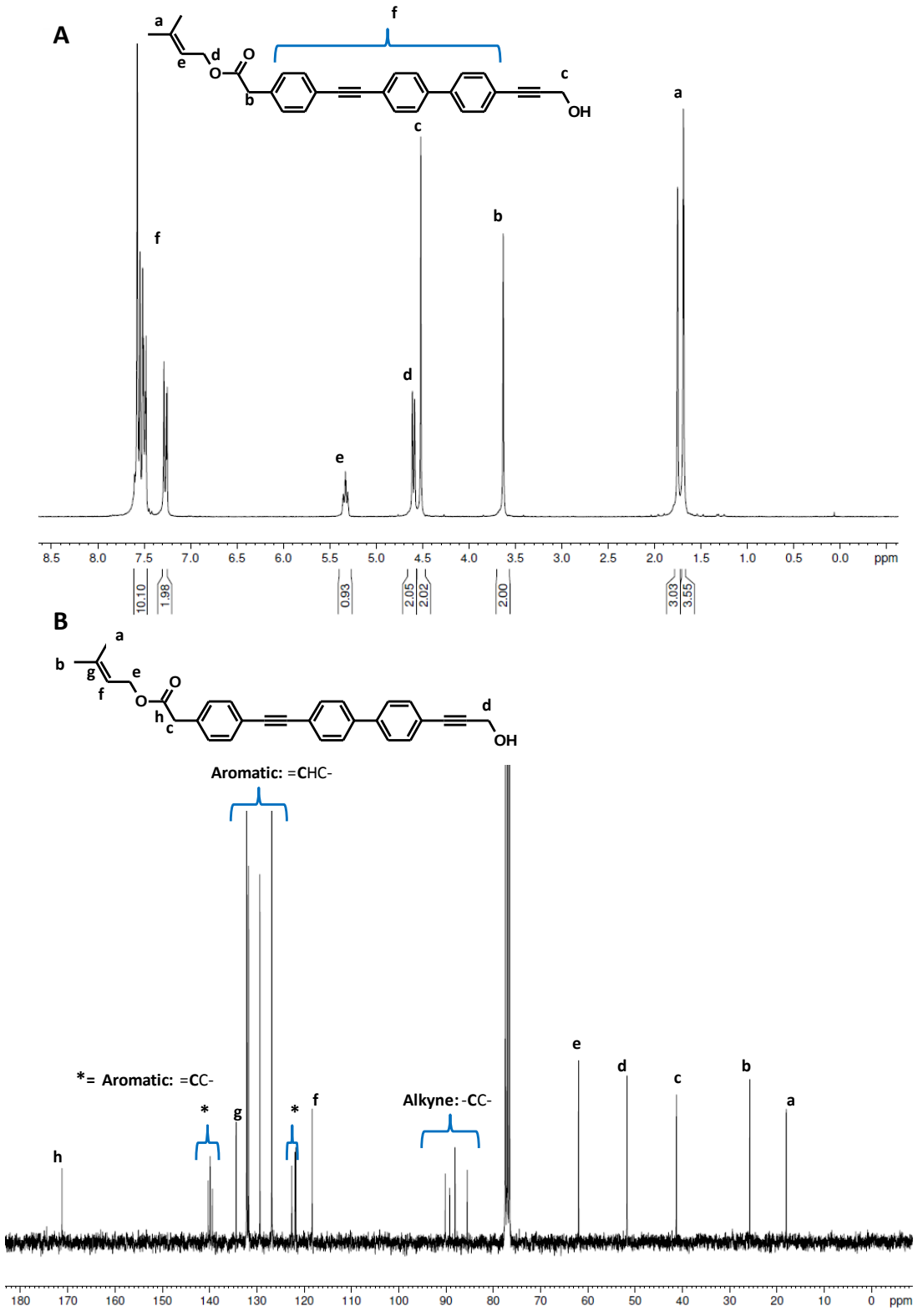

Figure 3.3: NMR spectra of PREO$_2$C-Trip-OH (**3-17**), taken in $CDCl_3$. **A**: ^{1}H, 300 MHz, **B**: ^{13}C, 75 MHz.

reaction was discussed in Chapter 2. As discovered during the Dip syntheses, the main advantage of this procedure is that the resultant carboxylic acid products can be usually precipitated from a non-polar solvent such as hexanes to yield a fairly high purity compound, while any side products are evaporated or filtered away. The joint deprotection was successful for all three Trip-containing esters as evidenced by TLC (very low R_f spot that required acidic conditions for mobility), however, in the case of HO_2C-Trip-G(E3)-OH, the compound did not precipitate as expected, unlike the other two molecules. This is most likely due to the polyether 'E3' tail present on this molecule, as the final compound itself was indeed a waxy semi-solid. The polyether tail also made purification by chromatography somewhat challenging, as the compound did not elute cleanly from the column; this could be easily visualized by a handheld UV lamp as a large, 'streaky' fluorescent band. Despite this complication, the desired HO_2C-Trip-G(E3)-OH was eventually obtained in high purity, and it is expected that its purification could be easily optimized if desired.

The protecting group removal and purification of the other two Trip compounds was unproblematic, and all three were then further purified by HPLC and fully characterized by NMR, MS, UV and fluorescence (Appendices 1 and 2). The overall yields were reasonable, the Trip scaffold proved amenable to the previously developed set of reaction conditions, and the reactions themselves were clean (minimal side products formed). Most importantly, however, was the fact that the Trip compounds retained favourable properties throughout the syntheses, with the final, deprotected oligomers being soluble in conventional solvents such as methanol and chloroform at usable (millimolar) concentrations. This was in stark contrast to the poor solubility exhibited by the Bi(Dip)-containing molecule **3-10** shown in Scheme 3.1. Therefore, it did appear that the rather simple structural change from the Bi(Dip) scaffold to the Trip structure did indeed circumvent the solubility problem, leading to the successful synthesis and characterization of the three target molecules.

3.4: Ion transport activity

3.4.1: Vesicle assays

In the vesicle-based HPTS ion transport assay (as described in the Introduction, Figure 1.5), the only of the three Trip molecules that exhibited ion transport activity was the polyether-tailed compound, HO_2C-Trip-G(E3)-OH (Table 3.1). The other Trip-containing isomers were completely inactive, with 'rates' no higher than that of the THF or MeOH controls. This negligible activity is most likely due to their high extent of aggregation in aqueous solution, as the more hydrophobic compounds (HO_2C-Trip-G(12)-OH and the HO_2C-Trip-Hex-G(12)-OH) could only be tested up to very low concentrations before visible precipitation could be seen in the fluorescence cuvette used for the assay (approximately 49 and 36 μM respectively, see Table 3.1). Again, this result was not entirely surprising based on the structure of these compounds, as their aqueous solubility was indeed expected to be lower than that of the more hydrophilic

COMPOUND	[COMPOUND] FOR $k = 1 \times 10^{-3} s^{-1}$ (μM)	RELATIVE ACTIVITY
HO_2C-Hex-Dip-Hex-G(12)-OH (**1-7**)	8	1
HO_2C-Trip-G(E3)-OH (**3-22**)	20	0.4
HO_2C-Trip-G(12)-OH (**3-19**)	n/a (49)[a]	n/a
HO_2C-Trip-Hex-G(12)-OH (**3-26**)	n/a (36)[a]	n/a

Table 3.1: Summary of HPTS activity for Trip isomers, comparison with Dip compound (HO_2C-Hex-Dip-Hex-G(12)-OH). *a*= number in brackets is highest concentration assayed before visible precipitation occurred. Details of HPTS assay available in Appendix 3.

polyether-containing HO_2C-Trip-G(E3)-OH. However, another factor must also be considered to explain the lack of activity of the other two molecules, as pre-incorporating HO_2C-Trip-Hex-G(12)-OH into vesicles did not lead to enhanced transport behaviour (see Appendix 4). This was not due to lack of partitioning or membrane association, however, as the vesicles produced after the standard procedures were

visibly fluorescent under UV light, and fairly emissive in the fluorimeter. As will be discussed shortly, the compound has almost no fluorescence in aqueous solution; therefore, it must be at least associated with the membrane to a certain extent.

Examining the HPTS-activity of HO_2C-Trip-G(E3)-OH, (Table 3.1 and Figure 3.4), indicates that the compound is active at fairly low concentrations, as above-baseline activity was observed at concentrations ranging from 3 to 9 µM (Figure 3.4A). At concentrations above 9 µM, however, the rate appears to level off, with only minor rate increases from 20 µM to the maximum tested concentration of approximately 150 µM being observed (Figure 3.4B). The concentration-rate profile does not seem to follow a logistic function, as previously observed for the Dip isomers, attempts at such a fit resulted in very poor r^2 values. Rather, the activity seems to saturate, as the rate at 150 µM is only 1.5 fold greater than that at 15 µM, despite the 10 fold increase in concentration. Fitting the data to a saturation model was consistent with this, resulting in a Vmax of 0.0155 s^{-1} and a concentration at half maximal activity of 9.81 µM (r^2 = 0.94). It must also be emphasized that the activity of HO_2C-Trip-G(E3)-OH is modest; the maximum rate achieved of 0.0155 s^{-1} is approximately 40% of that exhibited by the most active Dip isomer (Table 3.1). Therefore, the increased rigidity of the Trip scaffold was evidently not increasing activity as had been hoped.

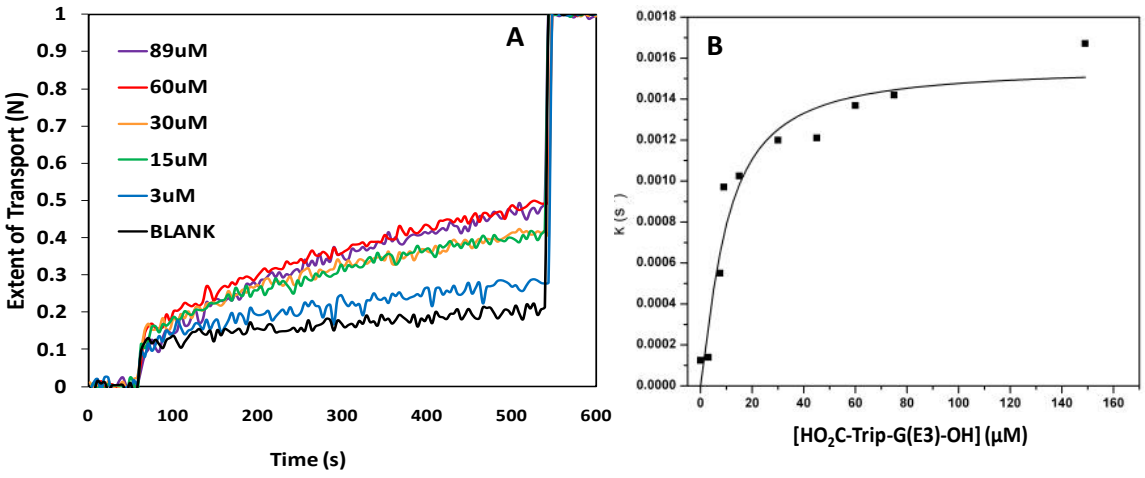

Figure 3.4: HPTS results for HO_2C-Trip-G(E3)-OH. **A**: raw data, **B**: plot of rate as a function of concentration.

As this type of saturation behaviour has been associated with membrane-disrupting or surfactant-type molecules [27], the carboxyfluorescein (CF) assay was carried out to test for this type of activity. As described in the Introduction (Figure 1.6), this assay measures the extent of CF efflux out of lipid vesicles; molecules that can disrupt the membrane to a large enough extent to allow CF to escape the vesicle are making pores of diameters greater than 10 Å in the membrane, the approximate size of CF. As seen in Figure 3.5, this does appear to be the case for the polyether-tailed Trip compound, as extensive CF efflux equal to that of the commercial surfactant Triton X-100 is observed for HO_2C-Trip-G(E3)-OH at relatively low concentrations (~80 µM, Figure 3.5A). The extent of CF release shown in Figure 3.5B was calculated using the equation shown in Figure 1.6 in the Introduction, taking the Triton and methanol 'blank' values as the upper and lower limits, respectively. Similarly to the HPTS results, the extent of CF release appeared to 'saturate' at approximately 80 µM, with the half-maximal response at approximately 25 µM. After 80 µM, further increases in compound concentration up to 260 µM actually reduced the extent of CF efflux, although this is most likely due to poor solubility of the Trip compound at these high concentrations.

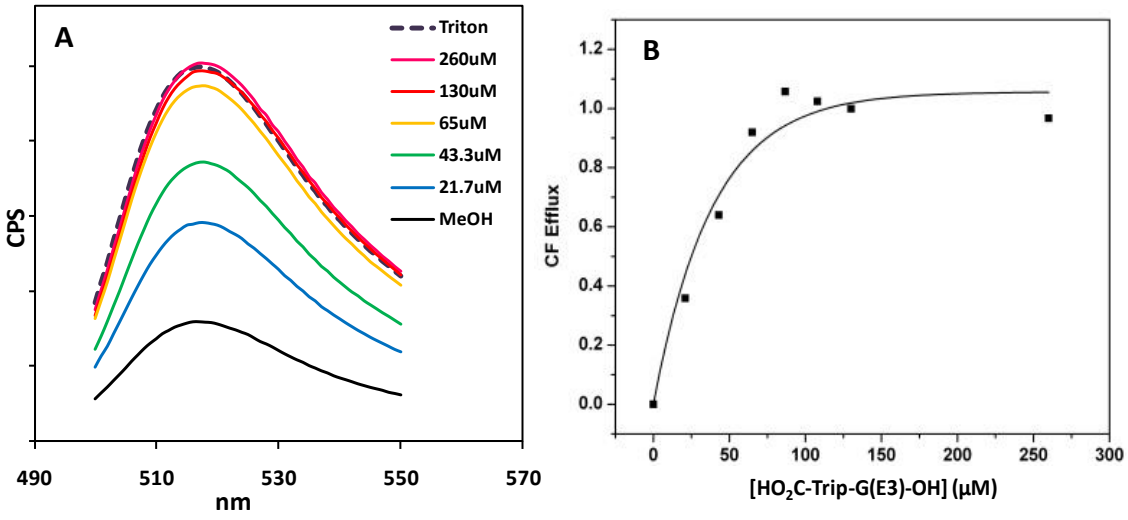

Figure 3.5: Carboxyfluorescein assay for HO_2C-Trip-G(E3)-OH. **A**: raw data, **B**: fraction CF release as calculated in Figure 1.6.

3.4.2: Bilayer clamp assay

The HPTS and CF results indicate that HO_2C-Trip-G(E3)-OH behaves as a membrane disruptor or surfactant at high concentrations, instead of an ion channel. Structurally, HO_2C-Trip-G(E3)-OH certainly resembles a 'classic' surfactant, which are able to solubilise membranes due to their amphiphilic nature. A comparison of the structure of Triton X-100 (**3-27** in Figure 3.6), the surfactant used to lyse the vesicles in the HPTS assay, with that of HO_2C-Trip-G(E3)-OH indicates that the same polyether tail is used, although the one on Triton is longer by 6 ethylenedioxy units. The general structure is very similar; a hydrophilic polyether tail appended to a hydrophobic aromatic core. Triton is known to form micelles at fairly low concentrations (200 μM) [111]; this is in reasonable agreement with the 80 μM observed to cause complete membrane lysis by HO_2C-Trip-G(E3)-OH. Therefore, it would appear that the behaviour observed for HO_2C-Trip-G(E3)-OH can be explained by comparison with Triton; they are both membrane-lysing surfactants.

However, the story becomes more interesting when one considers that Triton itself, as well as other molecules built upon a Triton scaffold (**3-28**) [112] or highly reminiscent of it (**3-29**,**3-30**) [113,78], have exhibited single-channel conductance behaviour in the bilayer clamp assay (see Figure 3.6 for structures). The original observation of Triton single channels was published in 1977 by Schlieper and De Robertis; the reported activity shows fairly long-lived (up to a few minutes), predominantly 'square-topped' type behaviour with conductances ranging from 100 to 400 pS, in 0.1 M KCl or NaCl as electrolyte and PC as lipid [114]. Shorter lifetime openings were also observed, as

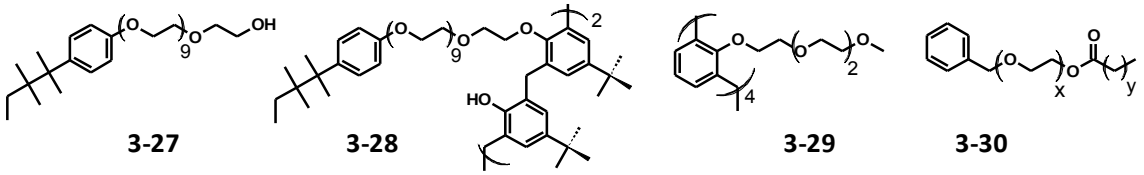

3-27 **3-28** **3-29** **3-30**

Figure 3.6: Triton and 'Triton-like' channel-forming molecules. **3-27** Triton-X-100 , **3-28** and **3-29**, calixarenes reported by Cragg *et al*. [112,113], **3-30**; aromatic polyethers from Schafer *et al*. [78]; x=4,5, y= 6,8,10,12.

were multiple step-ups, indicating the presence of multiple single channels. Other electrolytes were tested, and these Triton channels were found to be selective for cations over anions. Interestingly, the Triton channels were also observed to show voltage-dependent conductance, as the IV plot flattened out and was no longer linear at voltages above ±70 mV. The authors also tested other known commercial surfactants, none of which was able to produce such single channel bilayer activity. Triton was also seen to produce single channel activity in further work from other groups [115,116]; Pasternak *et al*. in fact observed very similar conductances and long-lived square tops as in the original report, although in this case the observed behaviours are much more varied, with conductances ranging from 10 pS to over 1 nS, and the longer-lived events are interspersed with shorter, 'flicker' types as well [115]. In addition, the voltage-gating reported by Schlieper and De Robertis was not observed.

In all reports of Triton single channels, the concentrations of compound used are very low (down to subnanomolar), clearly far below its cmc of 0.2 mM; evidently at very low concentration, this known surfactant forms discrete channels. If Triton could form channels, this implied that HO_2C-Trip-G(E3)-OH may also be a discrete ion channel at the proper, low concentrations. Therefore, the behaviour of HO_2C-Trip-G(E3)-OH in the bilayer clamp experiment was explored, and will be discussed shortly.

The other Triton-inspired structures presented in Figure 3.6 have all also been reported to exhibit single-channel behaviour in the bilayer clamp under a variety of conditions. Intriguingly, while some variation exists amongst the compounds, in general the reported activity is mainly of the 'long-lived square-top' type; although compound **3-30**, where x= 4 and y= 12 exhibited some shorter 'spikes' in LiCl. For example, the calixarene-substituted Triton **3-28** developed by Cragg *et al*., which is the most structurally similar to Triton; exhibits both very small (26 pS) and larger (200 pS), square-top conductances at fairly high concentrations of compound (up to 64 μM), although only in NaCl electrolyte. Interestingly, when these authors tested Triton at these concentrations, they observed only membrane rupture [112]. This brings up the important point that there is indeed a great deal of controversy surrounding the Triton

single-channel literature [62,63], as the methods used to introduce Triton to the bilayer are unconventional, and that activity is not seen when the compound is injected into an aqueous solution in contact with the lipid bilayer. Pre-mixing the compound with lipid is acceptable and understandable for compounds that are not water soluble, but this should not be necessary for Triton, which is readily water soluble. Furthermore, recent attempts to reproduce the Triton single-channel behaviour have so far been met with limited success, and the concentrations necessary to avoid membrane rupture are difficult to assess.

Overall, it is evident that the activity of Triton, and the nature of its ion conducting states, is not understood, and any further information that could be provided would be most useful. Perhaps HO_2C-Trip-G(E3)-OH, which resembles Triton in structure and appears to behave as a surfactant in vesicles, could aid in this regard. Alternatively, any similarities in bilayer activity observed between the two molecules would be interesting, as the reported activity for the majority of the "Triton-like" channels is fairly similar (long-lived square tops).

Examples of some of the types of activity observed for HO_2C-Trip-G(E3)-OH are presented in Figure 3.7; the compound is active, and very regular square tops can indeed be observed for HO_2C-Trip-G(E3)-OH under certain conditions; the 'proof' of single ion channel activity. This therefore confirms that similarly to Triton, this compound can act in a 'dual role' as both a surfactant and discrete ion channel. Unlike Triton, however, which predominately shows fairly regular square tops, the Trip compound is much less regular, and shows a variety of behaviours depending on the conditions used. Importantly, and again unlike Triton, these activities occur when the compound is injected from solution into the bilayer apparatus, this is preferable to pre-loading into lipid as the concentration can be better controlled.

The activity exhibited by HO_2C-Trip-G(E3)-OH varies significantly from short-lived, high-conducting but very irregular 'spikes' (Figure 3.7A) through 'hairy square' irregular yet longer-lived openings (Figure 3.7C) to very regular, almost 'idealized'

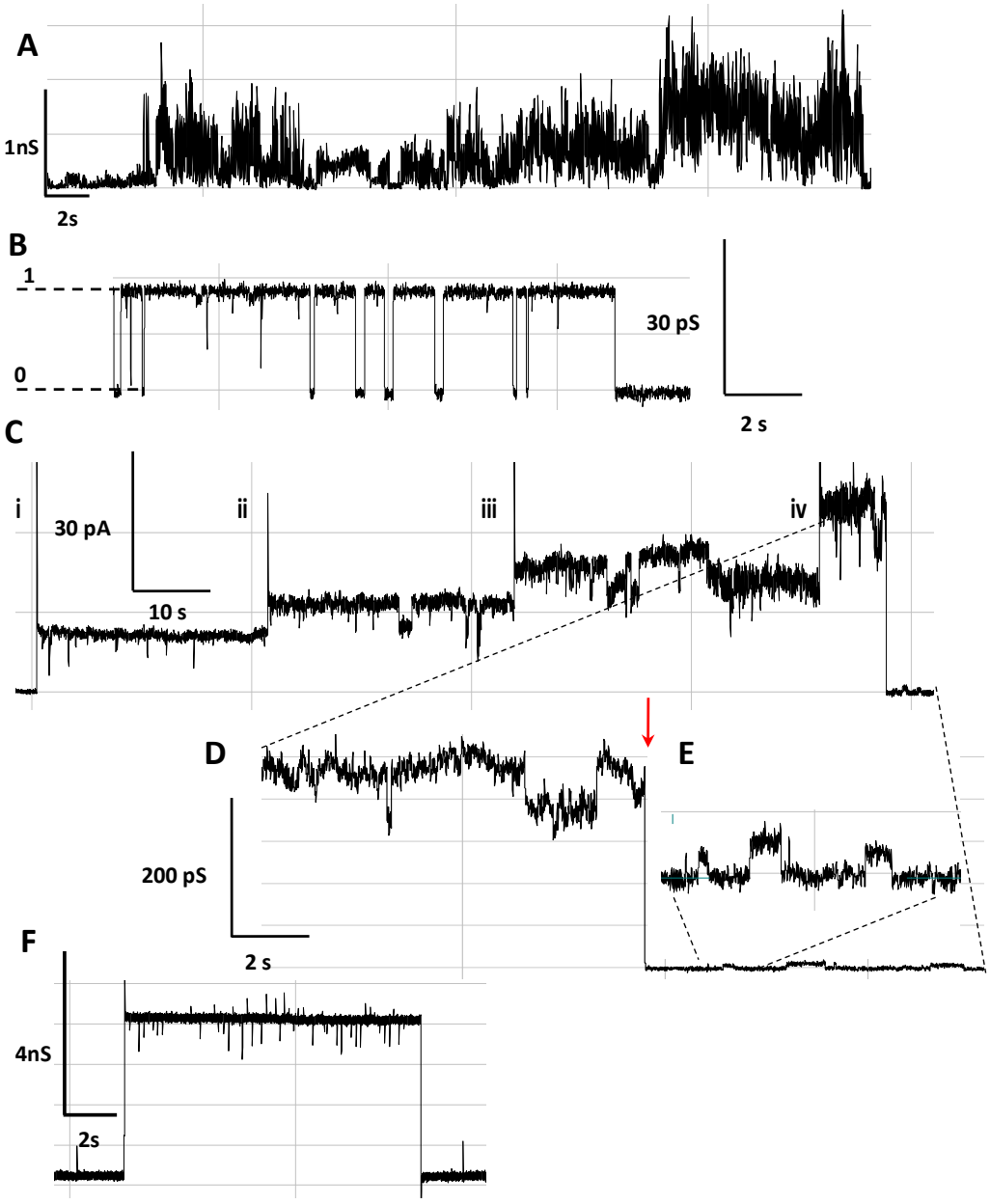

Figure 3.7: Bilayer clamp data for HO_2C-Trip-G(E3)-OH. Conditions; **A**: 1 M KCl, +90 mV, **B:** 1 M CsCl, +175 mV; 0= closed, 1= open. **C**: 1 M NMe_4Cl, (i) 50 mV, (ii) 75 mV, (iii) 100 mV, (iv) 150 mV **D**: expansion of **B** (150 mV region); red arrow indicates spontaneous channel closure, potential is still being applied. **E:** expansion of **C**. **F**: 1 M KCl, +10 mV.

square tops of fairly low conductance (~30 pS for the trace shown in Figure 3.7B). In most cases, multiple types of behaviours are observed in a single trace over a very short period of time, indicating the presence of a variety of active structures. The large, long-lived opening observed in Figure 3.7C remained open and responsive to voltage for

several minutes, reaching a conductance of almost 400 pS before abruptly closing at the point indicated in the Figure (red arrow); after this time, very small openings (~20 pS, Figure 3.7E) were observed. This particular trace is interesting, as the observed behaviours are remarkably similar to those seen for two of the 'Triton-like' channels shown in Figure 3.6. Both compound **3-28** as well as **3-30** (x= 4, y= 12) showed square tops with conductances of 26 pS, as well as larger openings of great than 100 pS, under very similar conditions. The fact that these compounds are so similar to each other, as well as to HO_2C-Trip-G(E3)-OH could suggest some sort of active structure common to all three.

Analogously to the Dip isomers, attempts to generalize the activity observed for HO_2C-Trip-G(E3)-OH were difficult: each type of behaviour (spikes, square tops, irregular 'hairy' squares and openings) occurred in approximately equivalent proportions in each electrolyte used (KCl, CsCl, NMe_4Cl), no electrolyte gave consistently one type of behaviour. This indicates that despite its increased rigidity, many different channel conformations are still possible for HO_2C-Trip-G(E3)-OH. In addition, the other two Trip-containing compounds were completely inactive in the bilayer clamp, just as in the vesicle assays. Therefore, the hypothesis that increased rigidity both enhances activity and leads to more stable, regular channels is not confirmed.

However, while the lifetimes and 'appearance' of the activities did vary greatly and cannot be easily categorized, an exciting trend that did emerge was the consistently high conductances produced by this compound. In fact, in 75% of the traces collected for HO_2C-Trip-G(E3)-OH, conductances of over 100 pS were predominant, regardless of type of activity observed, and in over 20% of total experiments, the predominant behaviour showed conductances greater than 1 nS. This is significant, as these types of very large pores are fairly rare in the synthetic ion channel literature [83], and were not reported for any of the 'Triton-like' channels shown in Figure 3.6; perhaps the increased rigidity of the Trip channel is having a beneficial effect after all. In certain cases, such as that illustrated in Figure 3.7F, truly 'giant' pores were formed, the example shown has a Hille diameter greater than 10 Å, assuming a channel length of 3.5 nm [37]. This correlates

very well to the results of the CF assay shown earlier (Figure 3.5), indicating that the large openings observed in this experiment are in fact due to channel formation, and not membrane rupture. Actually, membrane rupture was not often observed during the bilayer experiments carried out for HO_2C-Trip-G(E3)-OH; only a minor proportion of the obtained traces ended in this manner, further demonstration that the compound is not just a surfactant. Even the extremely high conductances obtained by the giant pore shown in Figure 3.7F did not cause membrane rupture; the channel closed spontaneously and the bilayer returned to its previous baseline level. In general, these high-conducting events were seen most often in NMe_4Cl, which makes sense as it is the largest of the three tested cations, thereby implying some size-based ion selectivity, as was in fact proposed for the Triton-like channel **3-28** in Figure 3.6. However, this cannot be the case for HO_2C-Trip-G(E3)-OH, as the most long-lived, 'square-top' type of behaviour such as the example in Figure 3.7F occurred in KCl. Overall, HO_2C-Trip-G(E3)-OH was shown to have some very interesting bilayer activity, which proves it acts as an ion channel at low concentrations, similar to the results obtained for the commercial surfactant Triton.

3.4.3: Non-linear current-voltage response

The most exciting result obtained from the bilayer studies on HO_2C-Trip-G(E3)-OH is the apparent suggestion of a non-linear current-voltage response shown by this compound. The long-lived openings frequently observed for HO_2C-Trip-G(E3)-OH provided the opportunity to conduct a 'macroscopic' IV (current-voltage) trace over an extended period of time; one such trace is shown in Figure 3.8A . In this particular experiment, the potential was changed every minute or so, the current over each time interval was remarkably stable. The average current at each time period was then plotted in an IV trace, shown in Figure 3.8B. It is evident from this Figure that the current response is non-linear and that significantly higher currents are being passed at positive potentials; for example, the current at +100 mV is almost 4 times greater in

magnitude as that at -100 mV. This 'rectification' [1] behaviour can also be clearly seen when the current is converted to conductance (g), as shown in Figure 3.8C. Again comparing the behaviour at ±100 mV, the conductance at positive potential is nearly 1.6 nS, while that at -100 mV is only 400 pS.

While not all experiments carried out on HO_2C-Trip-G(E3)-OH resulted in voltage-dependent conductance, this was in fact observed in quite a few cases; approximately one-third of the obtained traces gave at least some indication of a non-linear IV response, and it occurred in all tested electrolytes. Two further examples are illustrated in Figure 3.9; Figure 3.9A is interesting as during this experiment the channels exhibited several examples of rectification which were opposite in sign. Channels were formed that exhibited higher conductance at negative potential (~300 pS at +50 mV

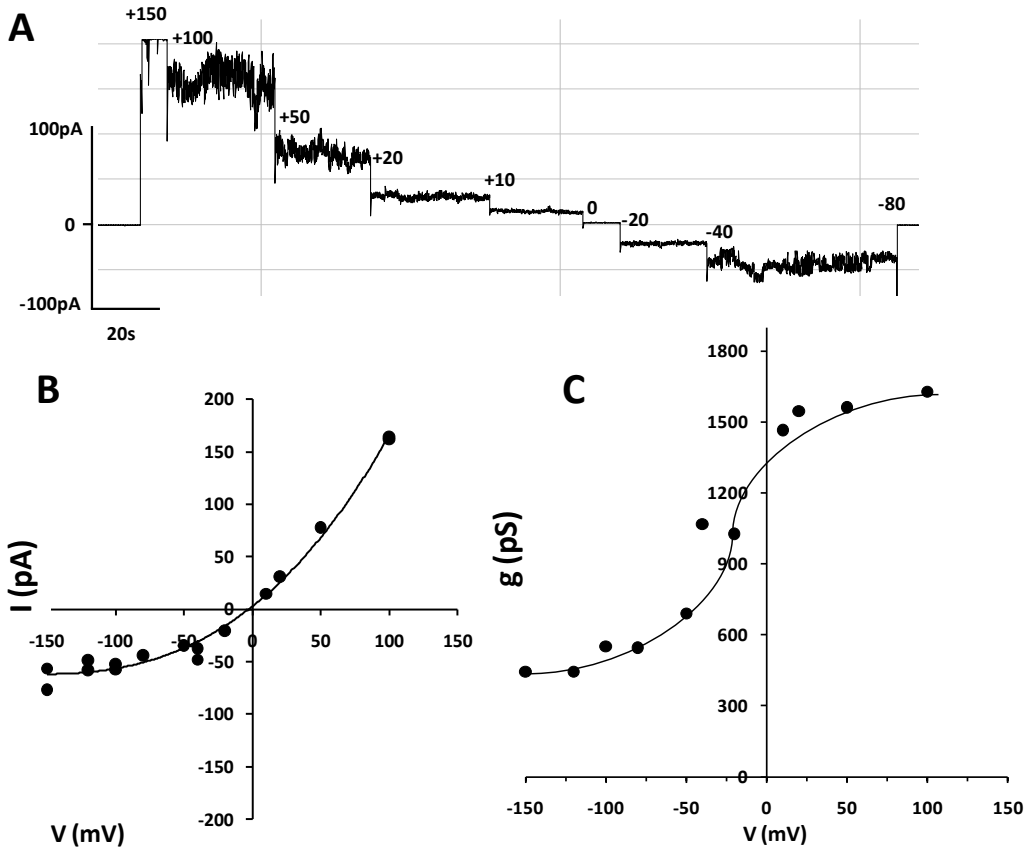

Figure 3.8: Voltage-gated behaviour of HO_2C-Trip-G(E3)-OH, 1 M NMe_4Cl, diPhyPC lipid. **A**: 'raw data trace indicating the potential steps applied over each time period. **B**: IV trace of average obtained current at each time period as a function of voltage. **C**: gV trace of data. The lines in **B** and **C** are to guide the eye.

versus 600 pS at -50 mV, as shown), but also in a short time later in the same experiment, higher conductance at positive applied potential was observed. Figure 3.9B is yet another instance of positive rectification; this example is interesting as the activity observed in this trace was of the highly irregular, very short lived 'spike' type, it is shown in Figure 3.7 as trace 'A'. As for the longer-lived openings, an analysis of average current over a time period of applied potential was used to obtain the conductance values. As the importance and prevalence of non-ideal 'square-top' behaviour in bilayer clamp data is becoming increasingly apparent (Chapter 2, and Ref [83]), the fact that nonlinear IV behaviour can be extracted from such data is significant.

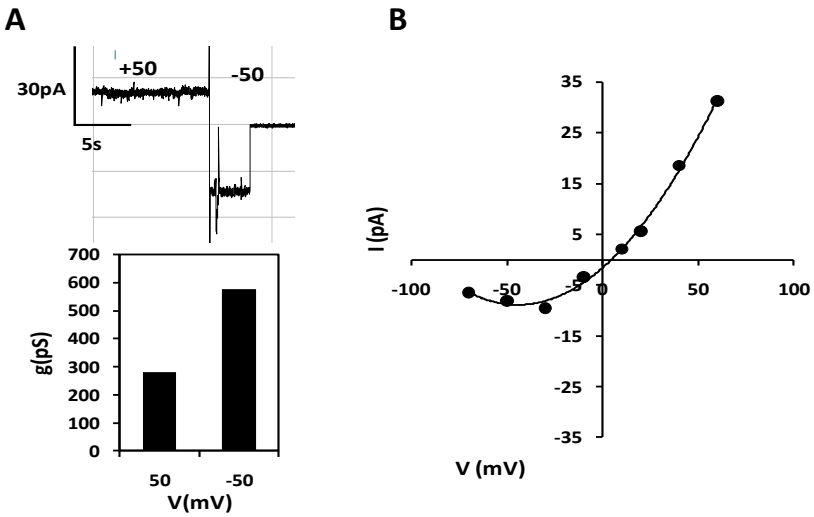

Figure 3.9: Voltage-gating and rectification behaviour of HO_2C-Trip-G(E3)-OH. **A:** 1 M NMe_4Cl, **B**: 1 M KCl, IV response of trace 'A' in Figure 3.7. DiPhyPC was the lipid used for both examples. The line in **B** is to guide the eye.

As mentioned in the Introduction and Chapter 2, voltage-gating and rectification are very rarely observed for synthetic ion channels, while being almost exclusively observed in natural channels. Several examples have been mentioned [20], including the 'bola-amphiphile' (2-headed amphiphile) compound **1-4** synthesized in the Fyles lab, the structure of which is shown in Figure 1.9B. When introduced to the bilayer from only one side, this compound was shown to carry significant currents at negative potentials only; over time, the IV response eventually became linear as the compound lost its asymmetry of insertion in the membrane [18]. This compound has significantly different 'headgroups' present at each terminus; it is singly charged at one end (carboxylate),

while doubly anionic at the other (succinate). It is believed that in order to exhibit a voltage-gated response, a significant dipole must be present on the compound, and its overall structure must be asymmetric [1]. Furthermore, in order to form a voltage-gated complex, the compound must preferentially insert into the membrane from one side and in one 'direction', with all carboxylate termini on one side of the bilayer, for example. Considering these criteria, it is reasonable that HO_2C-Trip-G(E3)-OH exhibits a voltage-gated response; it is clearly asymmetric, can be introduced into the bilayer from one 'side' by injection into the aqueous solution, and does contain a dipole. Directional insertion is favoured by the presence of the carboxylate terminus, as it would be less likely to traverse the membrane than the uncharged hydroxyl terminus. Therefore, considering the repeated observation of a non-linear current-voltage response under a variety of conditions in multiple independent experiments, it can be stated with confidence that HO_2C-Trip-G(E3)-OH is a rare example of a voltage-gated synthetic ion channel. Intriguingly, this once again brings up comparisons to Triton X-100, as it too was observed to exhibit a voltage-gated response, although as mentioned, this was not conclusively observed by other authors.

3.5: Photophysical characterization

3.5.1: Fluorescence in solution

While the ion-transport activity for the Trip isomers revealed some interesting observations, the other key impetus to make these structures was to examine their fluorescence properties, as the extended chromophore should lead to enhanced fluorescence intensity over that seen for the Dip molecules. This enhanced fluorescence was indeed already apparent during the synthesis of the Trip molecules, as mentioned. Analogous to the Dip isomers, the fluorescence emission of the Trip chromophore was expected to be environment-sensitive, potentially aiding in developing a mechanistic model to explain their activity. Considering the 'dual roles' of

the Trip compounds as well as other polyether-containing molecules as both ion channels as well as membrane disruptors, a mechanistic framework would be most desirable. Finally, as mentioned previously, a significant fluorescence response upon interaction with vesicles could lead to the application of these molecules as 'light-up' membrane probes.

As the 'Trip' chromophore has not yet been reported in the literature, its photophysical characteristics were unknown. It was therefore satisfying to observe that in organic solutions such as THF or methanol, these compounds exhibit much increased fluorescence over that seen for the Dip isomers, with fluorescence intensities enhanced by at least an order of magnitude (Figure 3.10A). The Trip compounds also exhibit much higher extinction coefficients (ε ~90 000 M^{-1} cm^{-1} compared with 25 000 M^{-1} cm^{-1}), red-shifted absorption (λMax= 313 versus 289 nm), excitation and emission

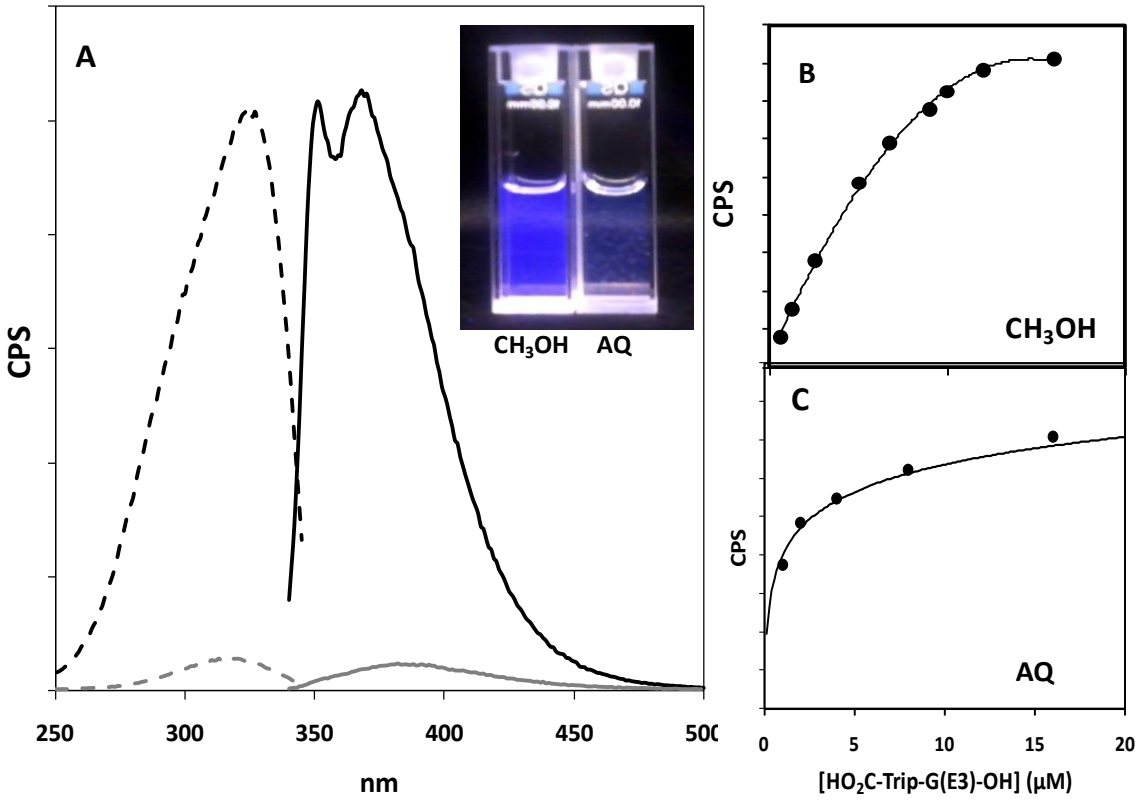

Figure 3.10: HO_2C-Trip-G(E3)-OH fluorescence in methanol or aqueous solution. **A**: Excitation (dashed lines) or emission (solid lines) spectra of 14 µM compound in CH_3OH (black line) and aqueous buffer (10 mM Na_3PO_4, 100 mM NaCl, pH=6.4) (grey line). INSET: photograph under UV light of the same solutions as in the graph. **B**: Fluorescence emission intensity as a function of compound concentration in CH_3OH, **C**: in aqueous. Lines in **B** and **C** are to guide the eye.

spectra in comparison with the Dip isomers, as expected (see Appendix 4 for absorption spectrum and determination of ε). In methanol, the fluorescence intensity is linearly dependent on concentration in the range of 1 to 16 µM (Figure 3.10B), above which the fluorescence intensity began to approach instrument saturation. Some evidence of self-quenching can also be observed above this concentration, as the concentration-intensity response deviates from linearity; similar behaviour was observed in the absorption spectra. The fluorescence emission at <1 µM was still significant. Quenching studies were also carried out, and the Trip fluorophore can indeed be quenched by $CuSO_4$ in methanolic solution. This quenching is not as efficient as that seen for the Dip fluorophore, requiring copper concentrations of approximately 5 mM to effect 50% quenching, corresponding to a Stern-Volmer constant of approximately 230 M^{-1} (See Appendix 4 for data). A comparison of key spectroscopic parameters between the Dip and Trip fluorophores is presented in Table 3.2 for two representative compounds in methanol.

PROPERTY	DIP	TRIP
Extinction coefficient (M^{-1} cm^{-1})	2.5±0.1 x 10^4	9.08±0.27 x 10^4
Absorption: λMax (nm)	288	315
Excitation: λMax (nm)	305	325
Emission: λMax (nm)	322	370
CPS at λMax_{EM} [a]	ca. 300 000	> 3 000 000
Quenched by $CuSO_4$ / K_{SV} (M^{-1})	Yes / 1.12±0.05 x 10^3	Yes / 2.29±0.11 x10^2

Table 3.2: Summary comparison of representative photophysical parameters of the Dip and Trip fluorophores in methanolic solution. a= The reported values are for 16 µM HO_2C-Trip-G(E3)-OH compared with the same concentration of HO_2C-Dip-6-6-(G12)-OH with same slit widths (3nm); the CPS are above the instrument limit for the Trip compound.

An actual comparison of the fluorescence intensities between the two fluorophores is challenging. Quantitative measurements, i.e. quantum yield, were not carried out for the Dip and Trip compounds, while qualitative comparisons such as intensity counts (CPS) are not valid as the fluorimeter slit widths had to be decreased

from 3 nm (Dip compounds) to 1 nm for the Trip fluorophore in order to avoid instrument saturation. Nevertheless, this observation can be used to roughly compare the two fluorophores; at the same concentration (16 μM), at slit widths of 3 nm, the fluorescence intensity of a Dip-containing oligomer is approximately 3 x 10^5 CPS, while it is greater than 3 million for the Trip compounds. Therefore, the rough estimate of a 10-fold increase in fluorescence intensity for the Trip fluorophore is reasonable. Another qualitative comparison is that unlike the Dip compounds, all the synthesized Trip isomers were visibly fluorescent at low micromolar concentrations under a simple UV light, as can been seen in the inset of Figure 3.10A.

While the extended Trip chromophore exhibited the desired fluorescence enhancement in organic solution, this high fluorescence intensity was much reduced in water, as clearly demonstrated in Figure 3.10A. The low fluorescence in aqueous solution was not completely unexpected, due to the previously observed visible aggregation of these molecules in water. The most hydrophilic of the three Trip isomers (HO_2C-Trip-G(E3)-OH) exhibited low, yet detectable aqueous fluorescence, while for the longest, most hydrophobic trimer (HO_2C-Trip-Hex-G(12)-OH), this fluorescence was negligible, suggesting some sort of aggregation-induced self-quenching, as seen for many fluorescent dyes [59]. This was suggested by the non-linear dependence of the fluorescence intensity on concentration; as illustrated in Figure 3.10C for HO_2C-Trip-G(E3)-OH, this non-linearity begins at concentrations higher than 5 μM, indicating self-quenching due to aggregation occurs above this concentration. For the Dip compounds, the extent of aqueous aggregation was quantified by the pyrene assay (Figure 2.6), however, this assay cannot be carried out on the Trip isomers, due to the overlapping fluorescence of the Trip and pyrene fluorophores. Therefore, the data obtained from the concentration-response plot shown in Figure 3.10C was used to infer a 'cmc' of 5 μM for HO_2C-Trip-G(E3)-OH [96]. Similar analysis could not occur for the more hydrophobic compounds, as their aqueous fluorescence was only 10% of the already low value obtained for HO_2C-Trip-G(E3)-OH, making it barely detectable. However, even at these very low intensities, the fluorescence response was clearly not linear with

concentration, and the maximum fluorescence intensity was reached at concentrations as low as 3 μM. As mentioned, the cmc of the known surfactant Triton X-100 is 0.2 mM, therefore, the Trip compounds are all vastly less soluble in aqueous solution than is Triton X-100.

Besides aggregation, another possible explanation for the very low fluorescence of the Trip compounds in aqueous solution is that water is actually quenching the fluorescence of the molecule by some specific solvent effect such as the formation of hydrogen bonds [59]. This effect has been proposed to explain the decreased fluorescence intensity in aqueous solution of a number of recently-developed membrane probes including **2-28** and **2-31**, (structures shown in Figure 2.13) [117,97]. This effect is also believed to occur for the well-known fluorescently labelled phospholipid anthroyl-PC [118] (Figure 3.11, compound **3-31**); Tocanne *et al*. have used this molecule to

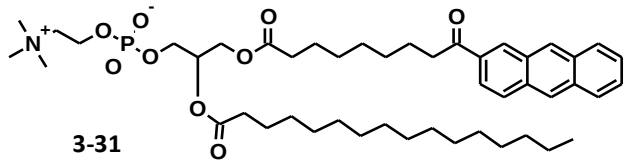

3-31

Figure 3.11: Structure of anthroyl-PC (**3-31**).

sense the presence of water deep within bilayer membranes, providing evidence that bilayer membranes are not strictly impermeable to water. In these systems, it is believed that hydrogen bonding between the polar groups of the molecules and the solvent occurs, which causes quenching by a variety of not-completely understood mechanisms.

To determine whether this was a factor for the Trip fluorophore, a 'Stern-Volmer' type experiment was carried out on the Prenyl-protected Trip model compound PREO_2C-Trip-OH (**3-17**), the results of which are shown in Figure 3.12. In this experiment, a constant concentration of compound in MeOH was titrated against increasing concentrations of aqueous buffer; solvent mixtures starting from 5% aqueous component to 100% were tested. Selected scans are shown in Figure 3.12A; from this data, it is evident that the 'water quenching' does not follow a linear Stern-Volmer type

relationship, as the fluorescence intensity remains unchanged up to 40% water (22 M), and then suddenly decreases by half at 45% water (24.8 M). Rather, the observed behaviours are much more consistent with an aggregation-type 'cmc' process. As the plot in Figure 3.12B illustrates, the change in fluorescence intensity with increasing water concentrations clearly follows a logistic function, and is highly reminiscent of the data obtained from a pyrene aggregation assay (Figure 2.6), used to determine cmcs. Therefore, it appears that above some critical concentration of water (24.5 M, as determined from the midpoint of the transition in Fig. 3.12B), the Trip-containing compound collapses into an aggregate, which is the cause of its decreased fluorescence in aqueous solution.

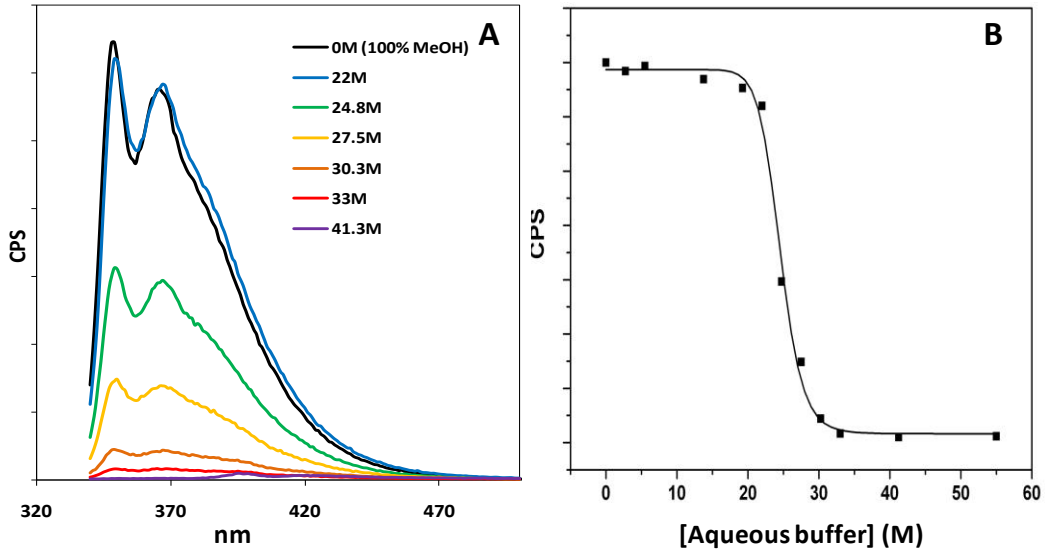

Figure 3.12: Aqueous aggregation of PREO$_2$C-Trip-OH. **A**: Fluorescence emission spectra (Ex~325 nm) for 14 µM compound in aqueous/MeOH mixtures, concentrations of water as marked. **B**: fluorescence intensity as a function of water concentration, fit to a logistic function, $r^2 > 0.99$.

While the 'water quenching' did not follow a linear Stern-Volmer relationship, such a relationship was observed when $CuSO_4$ was used as quencher, analogously to the results seen in MeOH for the Trip isomers, as well as the Dip compounds. In further analogy to the Dip molecules, the quenching observed in aqueous solution was significantly more efficient than in MeOH, with 50% quenching observed at approximately 0.25 mM. This correlates to a K_{SV} value of approximately 1000 M^{-1}

obtained in water, compared with a K_{SV} of 230 M^{-1} in MeOH (see Appendix 4 for spectra). The fact that quenching by copper was observed in both media for the Trip chromophore was most welcome, as this indicated that the same experiments as carried out for the Dip compounds, in particular quenching in the presence of vesicles, could be conducted on the Trip molecules as well.

Besides its much lower intensity, the fluorescence observed for the Trip compounds in aqueous solution is significantly red-shifted in comparison to that present in MeOH, shifting by 20 nm for HO_2C-Trip-G(E3)-OH, as shown in Figure 3.10A. This significant red-shift and decrease in intensity is immediately suggestive of excimer formation, analogous to that observed for the Dip isomers. However, it is clear that for the Trip molecules, even if excimer emission is being observed, the extremely low intensity of this emission makes it of little practical utility. Significantly more interesting is that the Trip compounds with a free carboxyl terminus exhibit solvatochromism that can be correlated to the polarity of the solvent, judged by Reichardt's E_T scale [119]. As shown in Figure 3.13 for HO_2C-Trip-G(E3)-OH, plotting the wavelength of maximum emission against the solvent polarity results in a fairly good linear correlation (r^2= 0.94), with the emission maximum shifting from 349 nm in hexanes to 385 nm in water. The linear relationship and significant blue shift in less polar solution suggest that HO_2C-Trip-G(E3)-OH is a highly-sensitive polarity probe. This was an exciting result, as it indicated that the Trip compound's environment-sensitive fluorescence could be even more useful than the Dip isomers' excimer emission in determining properties such as membrane partitioning. For the Dip compounds, both the aqueous aggregates as well as the in-membrane aggregates emitted at around 380 nm, however, for the Trip compound, the spectral differences between the aqueous aggregates (emission at 385 nm) and in-membrane aggregates (emission in a non-polar solvent, potentially ~360 nm) should be significant.

Many 'polarity probe' fluorophores are known [59], and many have indeed been incorporated into bilayer membranes to probe the polarity of the bilayer environment [120]. In the synthetic ion channel literature, Gokel *et al*. have used this method to study

the in-membrane location of a variety of fluorescent 'hydraphile' [121] and more recently, peptidic [98] channels, including the dansyl-substituted compound **3-32** (Figure 3.14) which showed a linear dependence of emission maxima on E_T in solution [98].

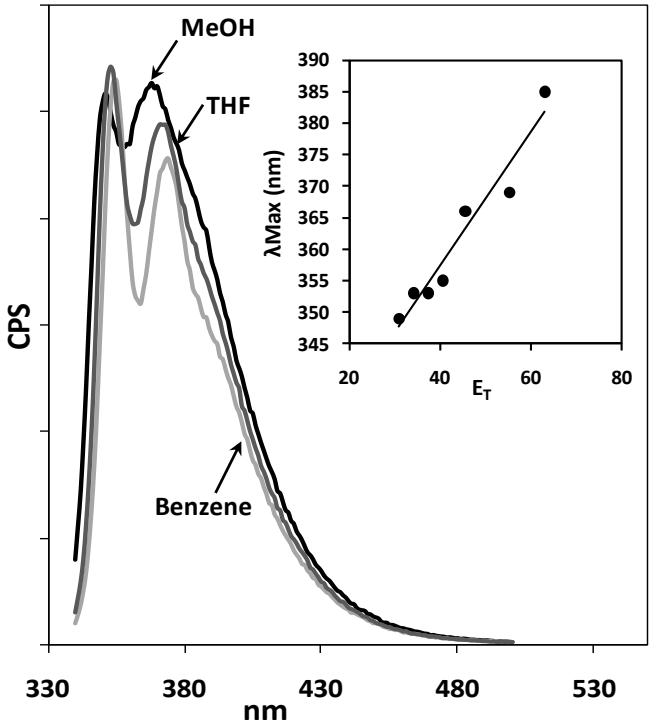

Figure 3.13: Solvatochromism of HO_2C-Trip-G(E3)-OH. Fluorescence emission spectra (λEx~325 nm) of 16 µM compound in selected solvents. INSET: λMax as a function of solvent polarity for all solvents tested.

The compound was then introduced into vesicles, and the obtained maxima were plotted onto the line obtained in the solvent studies. From this fit, the authors were able to infer a polarity value for the environment surrounding the dansyl chromophore of approximately 44, similar to the E_T value of DMF. For comparison, the E_T value of

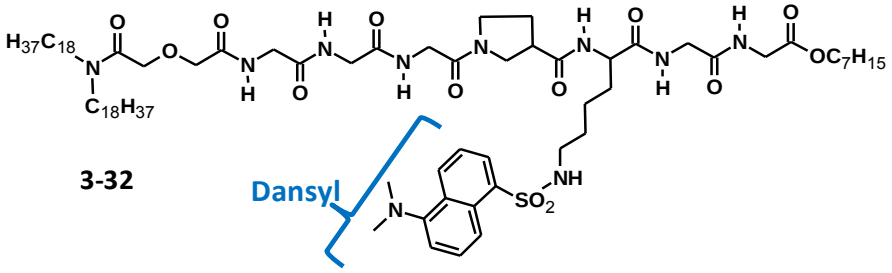

Figure 3.14: Solvatochromic dansyl-containing peptidic ion channel **3-32** developed by Gokel *et al*.

water is 63.1, while for the very non-polar solvent hexanes it is 31 [119]. As the polarities of the various regions of the bilayer are known at least to an approximation [5], the obtained in-vesicle E_T value indicated that the dansyl group was located in a region of medium polarity, such as the glyceryl ester region [98]. These intriguing results suggested that such data could be obtained for the Trip compounds.

3.5.2: Fluorescence with vesicles; pre-incorporation

The polarity-dependent fluorescence observed for HO_2C-Trip-G(E3)-OH was almost completely mirrored by the behaviour of the longer trimer HO_2C-Trip-Hex-G(12)-OH, as its emission maxima again showed a red-shift in increasingly polar solution, illustrated in LEFT:Figure 3.15. In previous studies, this compound had been pre-incorporated into lipid vesicles, therefore, its fluorescence spectra in such vesicles were known. These HO_2C-Trip-Hex-G(12)-OH-containing vesicles were found to be visibly fluorescent under a simple UV light, and reasonably emissive in the fluorimeter. The vesicles retain similar characteristics as their non-Trip containing counterparts, such as diameter (approximately 200 nm, judged by DLS) and turbidity, suggesting that the Trip compound is well-tolerated in the vesicle. While it cannot be said with certainty that the compound adopts an in-membrane structure, it is certainly associated with the membrane, and not within the internal volume of the vesicle, as the compound is not fluorescent in aqueous solution. These compound-incorporated vesicles therefore presented the opportunity to conduct an analysis analogous to the one reported by Gokel *et al.*, thereby inferring the polarity around the Trip fluorophore in a membrane environment.

As illustrated in LEFT:Figure 3.15 and Table 3.3, the fluorescence emission maxima of HO_2C-Trip-Hex-G(12)-OH were also well-correlated to solvent polarity, with the maxima shifting from 348 nm in hexanes to 405 nm in aqueous solution. Interestingly, when pre-loaded into vesicles, the compound has two equivalent maxima at 356 and 375 nm, indicating that the Trip compound is acting as two 'separate' fluorophores and probing two membrane environments with different E_T values. As the

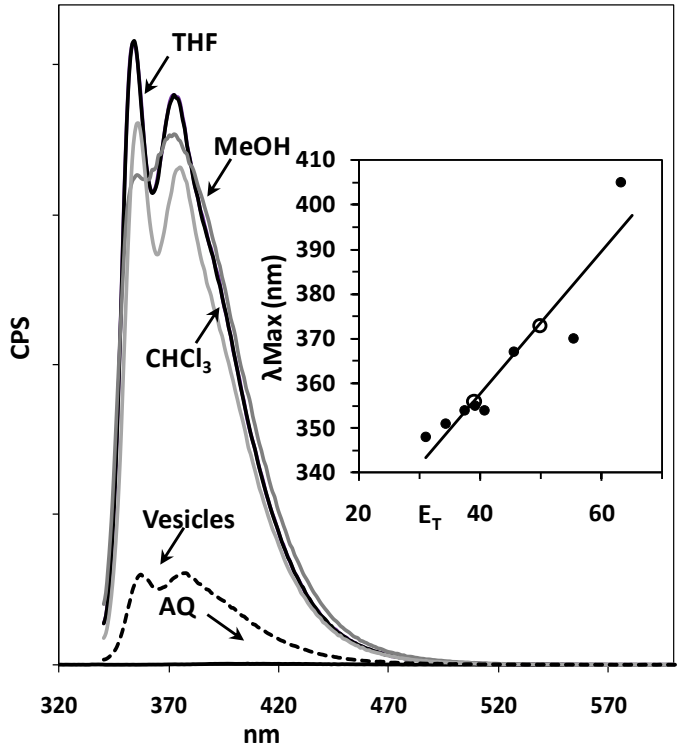

SOLVENT	E_T	λMax_{EM} (nm)
Water	63.1	405
MeOH	55.4	370
ACN	45.6	367
DCM	40.7	354
$CHCl_3$	39.1	355
THF	37.4	354
Benzene	34.3	351
Hexanes	31	348
VESICLES[a]	39, 50	356, 373

LEFT:Figure 3.15: Solvent effects for HO_2C-Trip-Hex-G(12)-OH. Fluorescence emission spectra (λEx~325 nm) for 17 μM compound in selected solvents, and pre-loaded into vesicles at 0.5 mol%, or approximately 3.5 μM. INSET: λMax as a function of solvent polarity. Open circles= tested solvents, black circles= fit of vesicle wavelengths onto linear relationship. RIGHT: Table 3.3: E_T values and emission maxima as shown in Fig. 3.15. a= inferred from fit of data.

molecule can rotate about a number of bonds including the biphenyl single bond, a loss of conjugation leading to independent fluorophore emission is reasonable. Furthermore, the length of the Trip scaffold from carboxyl terminus to hydroxyl terminus is approximately 20 Å, so it can clearly extend through different regions of the bilayer.

Once the maxima are plotted onto the linear emission-polarity relationship, they correspond to derived in-vesicle 'E_T' values of 38.8 (39) and 49.8 (50), very similar to the E_T values of $CHCl_3$ (39.1) and Butanol (49.7), respectively. The derived value of 39 is lower than that observed by Gokel *et al*. for the dansyl peptide **3-32** (44), and suggests that at least a portion of the Trip fluorophore is in a region of fairly low polarity. The compound must therefore be inserted into the membrane to at least a certain extent, although clearly not deeply enough to form any sort of ion-conducting pore or defect. This interpretation could be used to rationalize the lack of transport activity observed

for HO_2C-Trip-Hex-G(12)-OH, even when pre-loaded into vesicles. This is supported by the other derived E_T value of 50, which indicates a fairly polar environment. This portion of the fluorophore must be very near the aqueous interface, although a conformation in which the compound protrudes significantly into the aqueous environment would not be expected due to the hydrophobicity of this molecule. Furthermore, the blue-shift of the second in-vesicle maximum (375 nm) is still significant in relation to the aqueous emission (405 nm); therefore, a membrane-associated, semi-inserted species lying 'diagonally' in the membrane could be a plausible structure. While this remains speculation, these in-vesicle polarity studies are significant, as they clearly indicate that the Trip fluorophore can be used as a polarity probe in membranes, to at least infer a location of the compound in the bilayer. In general, while the lack of usefully-detectable excimer emission was initially seen as a drawback of the Trip molecules, their solvatochromism clearly makes up for this.

As shown in LEFT:Figure 3.15, the fluorescence intensity observed when HO_2C-Trip-Hex-G(12)-OH is introduced to vesicles is significantly enhanced over that seen in aqueous solution. The extent of fluorescence enhancement cannot be quantitatively determined due to the fact that the concentration of compound in the vesicle is unknown, however, if 100% vesicle incorporation is assumed, as is reasonable considering the hydrophobicity of this compound, this corresponds to approximately 3.5 μM of compound in the assayed vesicle suspension. Comparison with the fluorescence observed for 3.5 μM of HO_2C-Trip-Hex-G(12)-OH in MeOH solution indicates that the fluorescence intensity is actually fairly similar between the two. Therefore, pre-loading the compound into the vesicle ensures complete partitioning, and a significant fluorescence response. This indicates that if the partitioning step can be bypassed, the Trip-containing compounds can indeed act as 'light-up' membrane probes under these conditions.

3.5.3: Fluorescence with vesicles; partitioning from aqueous solution

While the results obtained for HO_2C-Trip-Hex-G(12)-OH indicated that fluorescence enhancement upon vesicle binding was indeed occurring, and can be significant, this particular example is not a good indicator as the compound is pre-loaded into vesicles. As the concentration of compound in the vesicle can only be inferred, the extent of fluorescence enhancement in the presence of vesicles in relation to that observed in aqueous cannot be accurately determined. In addition, in order to be of practical use as a sensor, the compound should 'find' the vesicle in aqueous solution and bind/partition into it [14]. As the transport assays had suggested that HO_2C-Trip-G(E3)-OH was indeed able to partition into the membrane from aqueous solution, in which its fluorescence is very weak, it was of interest to see if the compound could accomplish this to a great enough extent to 'light up' when introduced to vesicles, and thus be accurately quantified. As seen in Figure 3.16, this does appear to be the case, at least to an extent, for HO_2C-Trip-G(E3)-OH, as there is a moderate increase (approximately 2-fold) in fluorescence emission intensity when vesicles are present over that seen in aqueous solution, without need for pre-loading compound into the vesicle. This suggests that this compound is indeed partitioning into the bilayer membrane, as would be expected as it is both bilayer and HPTS transport active, which can clearly only occur for a membrane-inserted structure. Further indication that the compound is

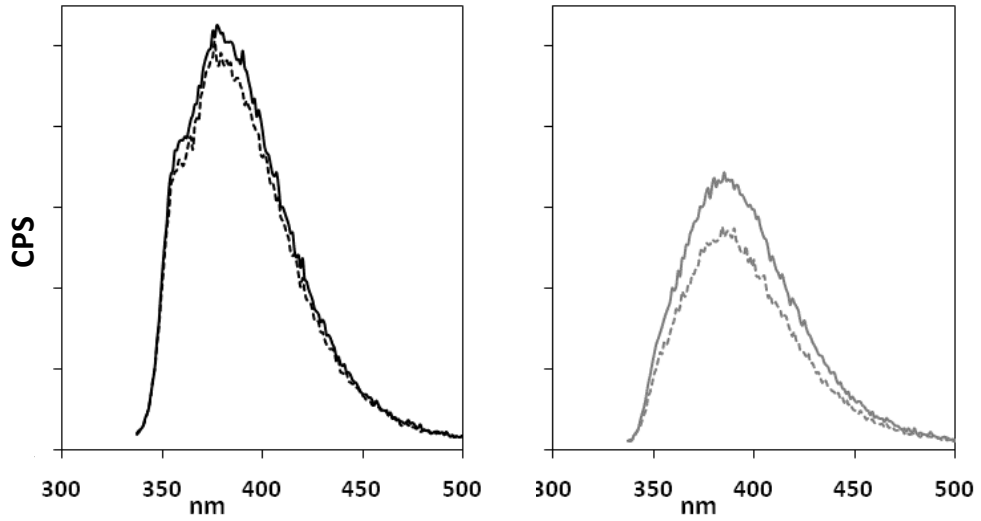

Figure 3.16: Fluorescence emission spectra of 15 µM HO_2C-Trip-G(E3)-OH in aqueous buffer (10 mM BisTris, 100 mM NaCl, pH 6.4) in the presence (black) or absence (grey) of lipid vesicles, with the addition of 200 µM $CuSO_4$ (dashed lines). λEx= 325 nm.

inserted into the bilayer comes from the fact that the quenching seen with externally-added aqueous copper, which was found to quench Trip fluorescence in both aqueous and organic solution (section 3.5.1, and Appendix 4), is decreased when the compound is introduced to vesicles (Figure 3.16). These results are similar to that seen for the Dip isomers, as discussed in Chapter 2.

While these results were promising, it is evident from Figure 3.16 that the fluorescence observed in vesicles, while increased over that in aqueous solution, is still only a fraction of that in MeOH or THF (approximately 10%, compare with Figure 3.10). This would clearly need to be increased further in order to be of practical use, i.e., to actively visualize partitioning 'by eye'. As mentioned, the fact that the fluorescence intensity does not approach that observed in organic solution can be attributed to the propensity of these compounds to aggregate in aqueous solution. Aggregation-induced self-quenching is a significant factor for all the Trip compounds, as shown in the aqueous titration results of Figure 3.12, as well as the non-linear concentration-emission response observed for all the Trip isomers (see Figure 3.10 for HO_2C-Trip-G(E3)-OH). Therefore, despite its increased hydrophilicity, in aqueous solution the majority of HO_2C-Trip-G(E3)-OH must still remain as a highly-aggregated, minimally emissive complex which is unwilling to dissociate into its component monomers and partition into the membrane. As partitioning of a larger aggregate is unlikely [40,64], and the driving force of aggregate break-up is low, the fluorescence enhancement upon vesicle introduction remains minimal.

That aqueous aggregation is responsible for the modest fluorescence enhancement and poor partitioning observed for the Trip compounds is further supported by the observation that the fluorescence intensity of the Trip isomers is dramatically increased at the end of the HPTS assay when Triton X-100 is added to lyse the vesicles (Figure 3.17). Significantly, this effect is most prominent for the most hydrophobic molecule, HO_2C-Trip-Hex-G(12)-OH. When the surfactant (Triton X-100) is added, the fluorescence intensity of the Trip compounds increases to almost that seen in organic solution, where the compound exists as well-solvated, separated monomers.

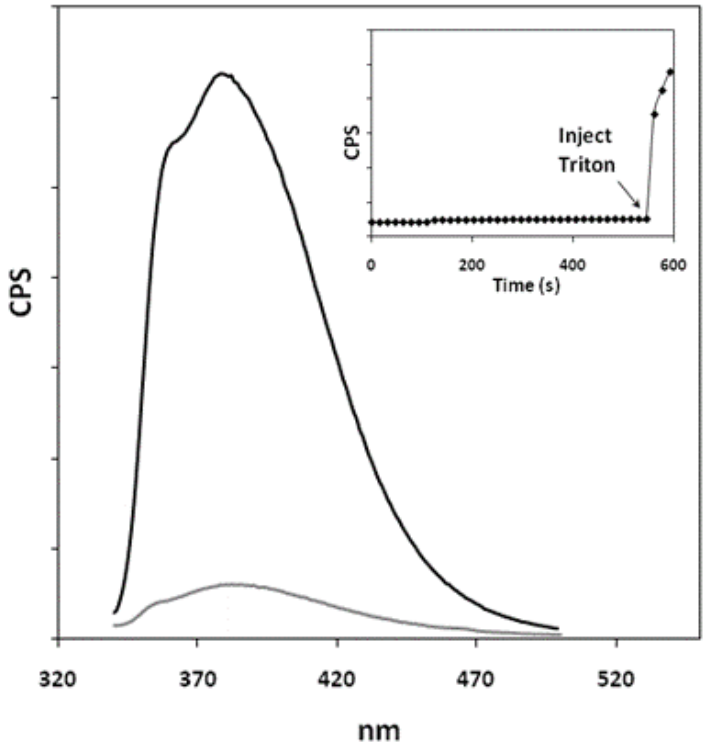

Figure 3.17: Fluorescence emission spectra of 25 μM HO_2C-Trip-Hex-G(12)-OH after 10 minutes incubation time with lipid vesicles in aqueous buffer (10 mM Na_3PO_4, 100 mM NaCl, pH 6.4) in the presence (black) or absence (grey) of Triton X-100. INSET: Emission over time of 25 μM HO_2C-Trip-Hex-G(12)-OH with vesicles, showing response to Triton addition. λEx= 325 nm.

This suggests that Triton acts as a 'solvent' for the Trip molecules, de-aggregating them to the extent that they can once again fluoresce as monomers. This type of fluorescence enhancement upon surfactant binding has indeed been observed by other authors studying CPEs [122], most significantly in a report by Chen *et al*., in which almost identical behaviour was seen for a polysulfonate-containing CPE interacting with dodecyltrimethylammonium bromide, another well-known surfactant [91].

These results demonstrate that the fluorescence response upon vesicle introduction has the potential to be greatly enhanced if the extent of partitioning could be increased, presumably by decreasing these compounds' aqueous aggregation, in-line with the working hypothesis developed previously, illustrated in Figure 2.20 in Chapter 2 [40]. It would therefore be of value to actually quantify the extent of partitioning occurring for HO_2C-Trip-G(E3)-OH to judge the maximum response possible. This can be achieved by determining a partitioning constant (Kp), using a procedure initially

developed by Haugland and Huang [123], and extended further by Wimley *et al*. [124]. In the experiment, a constant concentration of fluorescent compound is titrated against increasing concentrations of lipid vesicles. If the probe exhibits increased fluorescence intensity in the presence of vesicles, the change in emission intensity as a function of lipid concentration can be used to obtain Kp, using Equation 3.1.

$$1/I_i=([W]/K_pI_o) \cdot 1/[L] + 1/I_o \qquad \text{Eqn. 3.1}$$

By generating a double reciprocal plot of the fluorescence intensity ($1/I_i$) as a function of lipid concentration ($1/[L]$), a line with slope equal to the concentration of water [W] over the partitioning constant (Kp) multiplied by the fluorescence intensity upon maximal partitioning (I_o), is obtained. Kp is therefore equal to the concentration of water (55 M) multiplied by the x intercept [123].

Importantly, in order for equation 3.1 to be applicable, the partitioning must reach saturation (I_o). Therefore, as can be seen in Figure 3.18, a partitioning constant

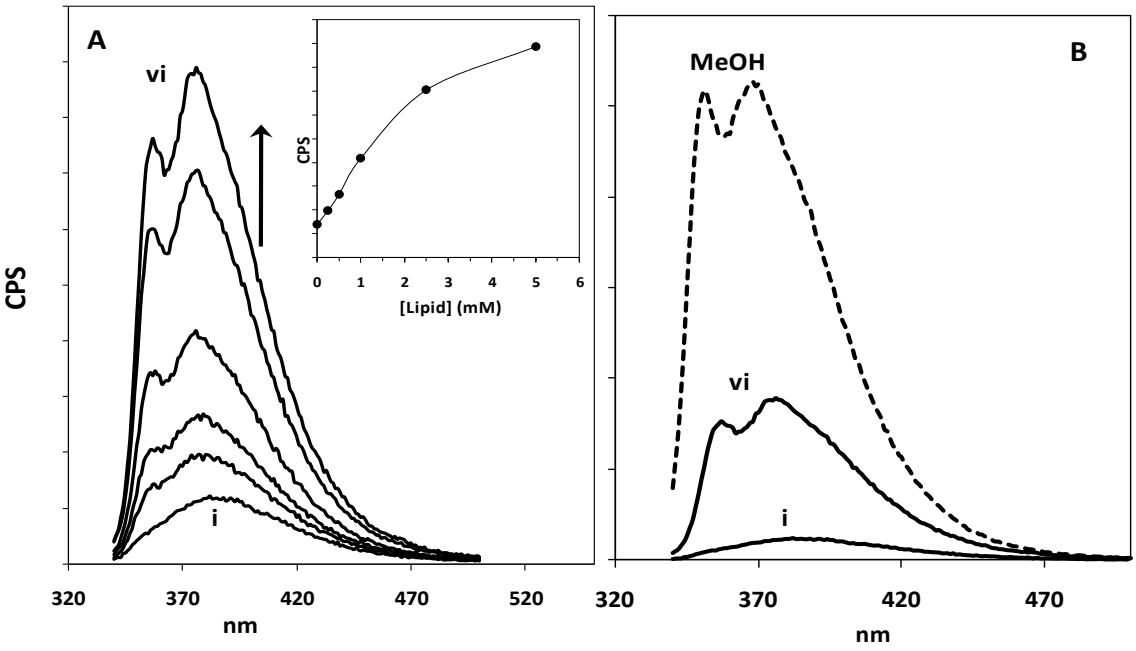

Figure 3.18: Partitioning of 16 µM HO_2C-Trip-G(E3)-OH from aqueous solution into lipid vesicles. **A**: From i to vi, lipid concentrations= 0, 0.25, 0.5, 1, 2.5, 5 mM. INSET: Plot of CPS versus lipid concentration, saturation was not reached, Kp not determined. **B**: comparison of maximal fluorescence in vesicles (curve vi as marked in **A**) compared with that in MeOH (dashed black line) and aqueous (curve i).

could not be obtained for HO_2C-Trip-G(E3)-OH. While the fluorescence intensity increases with increasing lipid concentration ([L] = 0-5 mM), eventually leading to an emission intensity nearly 8-fold higher than that observed in aqueous solution, saturation is not reached. At the highest lipid concentration tested (5 mM), the turbidity of the test solutions was so pronounced that the scattering from the vesicles [125] could not be ignored, and further increases in concentration were not feasible. Despite the inability to determine Kp, the results obtained from the partitioning experiment for HO_2C-Trip-G(E3)-OH are significant for several reasons. Firstly, they give at least a rough approximation of the affinity of this compound for lipid vesicles; clearly, the driving force for partitioning, while higher than that observed for HO_2C-Trip-Hex-G(12)-OH, is still not sufficient to ensure complete partitioning. For the more hydrophobic molecule, the lack of partitioning can be easily explained by its high hydrophobicity. This inhibits the dissolution of aqueous aggregates into aqueous monomers competent for efficient partitioning into the membrane; evidently HO_2C-Trip-G(E3)-OH is still not hydrophilic enough. This suggests further modifications to the Trip molecules should continue to increase their hydrophilicity, in order to decrease aggregation.

Furthermore, the previously-mentioned up to 8-fold increase in fluorescence intensity observed for HO_2C-Trip-G(E3)-OH in the presence of vesicles makes it in fact possible to monitor partitioning 'by eye'; the samples with the two highest concentrations of vesicles (curves **v**, **vi** in Figure 3.18) are indeed visibly fluorescent under UV light. However, scope for improvement remains, as the fluorescence intensity of even the 'most partitioned' sample is still only 40% of that observed in MeOH, indicating that self-quenching is still a factor (Figure 3.18B).

The relatively poor partitioning observed for HO_2C-Trip-G(E3)-OH also has consequences when considering the vesicle-based activity assays discussed above. In this work, the concentration of lipid as vesicles utilized in the HPTS assay is always 0.5 mM, this corresponds to curve **iii** in Figure 3.18A; clearly, the compound is nowhere near fully partitioned at this lipid concentration, nor at any practically useful lipid

concentration. In the aforementioned report by Gokel *et al*., the authors observe similar incomplete partitioning for their molecules, and thereby suggest that the ion transport activity observed for these compounds is indeed only a fraction of what could be possible[98]. This is an interesting hypothesis, and could certainly be tested for the Trip compounds by repeating the HPTS experiment at increasing concentrations of lipid. If a direct correlation between extent of partitioning and HPTS activity was found, this would be a most interesting result, and other inactive compounds could be re-tested for activity in light of this finding.

Finally, the titration reveals another interesting point, which is the shift of the emission maxima from that initially seen in water (385 nm) to 375 nm, and the growth of a new band at 356 nm. A blue-shifting of emission maximum was shown to occur for this compound in less-polar solvents in the solution studies of Figure 3.13. This further confirms that partitioning is being directly observed in the experiment shown in Figure 3.18. When the emission maximum of 375 nm obtained from the partitioning assay for HO_2C-Trip-G(E3)-OH was plotted onto the linear E_T-emission wavelength relationship shown in Figure 3.13, the resulting 'in-vesicle' E_T value was 57. The same analysis for the peak at 356 nm corresponded to an E_T value of 39; interestingly, this is exactly the same as the value derived for HO_2C-Trip-Hex-G(12)-OH (LEFT:Figure 3.15). Therefore, these results support a fairly well-buried location for the Trip fluorophore in both molecules, as was indicated by the reduced quenching efficiency observed in the presence of vesicles for HO_2C-Trip-G(E3)-OH (Figure 3.16). As the one compound is active, and the other is not, the observation of the same derived E_T value for both Trip molecules is most intriguing; suggesting that extent of membrane insertion cannot be used to rationalize the difference in activity for these two compounds.

However, while HO_2C-Trip-Hex-G(12)-OH had two equivalent maxima, HO_2C-Trip-G(E3)-OH has only one, at 375 nm. The derived E_T value at this wavelength (57) is very high, greater than that for the second HO_2C-Trip-Hex-G(12)-OH maximum (50), and similar to the E_T value of MeOH (55.4), a polar solvent. A portion of the fluorophore must therefore be experiencing a very polar environment, perhaps protruding into the

phosphocholine headgroup region. Interestingly, the derived E_T value corresponds exactly to that reported for glycerol, a polyalcohol; could this be an indication that the polyether tail of HO_2C-Trip-G(E3)-OH is in fact interacting with a portion of the Trip fluorophore, thereby increasing the polarity of its local environment? Another possibility open to this compound, but not HO_2C-Trip-Hex-G(12)-OH, is that the high polarity E_T value in this case is indeed reporting an aqueous aggregate, as the fluorescence intensity of HO_2C-Trip-G(E3)-OH in aqueous solution is relatively high in comparison to the longer analog, and the blue-shift of 10 nm is not as significant as that seen for HO_2C-Trip-Hex-G(12)-OH (32nm, LEFT:Figure 3.15). As the compound does not partition completely into the vesicle from water, this is a reasonable suggestion.

Any presumed structure must remain speculation, and the variety of activities observed in the bilayer clamp experiment clearly indicates that there are in fact many possible active structures. However, the E_T data obtained for the Trip compounds are an intriguing piece of the puzzle. The fact remains that both compounds can indeed report their environments, and that these environments are different in polarity. Whether this is due to depth of compound insertion into the membrane, aggregation in aqueous solution or in the membrane, or local structural variation of the compounds themselves is currently unknown. Overall, the partitioning and E_T studies reveal that as for the Dip compounds, there are a number of possibilities available to HO_2C-Trip-G(E3)-OH when introduced to lipid vesicles in aqueous solution. Some remains in aqueous solution (evidenced by incomplete partitioning and potentially the high E_T value of 57), some associates with the membrane but does not insert very deeply (potentially giving rise to the derived E_T of 57), and some inserts to a depth sufficient to experience a fairly non-polar environment (E_T of 39, equivalent to the polarity of chloroform). This further-inserted species must be able to cause a defect in the membrane which allows transport, and eventually, at higher concentrations, membrane rupture.

3.6: Conclusions & future work

In conclusion, a series of triphenyl-containing molecules based on a completely novel, highly fluorescent 'Trip' chromophore was synthesized. These compounds retain good solubility properties, are solvatochromic, and can be characterized and assayed in a variety of ways. While their HPTS-derived ion transport activity was found to be modest (or non-existent), the active compound, HO_2C-Trip-G(E3)-OH, proved to be an interesting molecule. Its transport results in both the bilayer clamp and in-vesicle assays demonstrate the formation of highly conducting pores, which eventually disrupt the membrane to a similar extent as does a known surfactant. However, the compound is not simply a surfactant, as the observation of discrete, 'square-top' like conductances in the bilayer clamp experiment indicate that it does behave as an ion channel under certain conditions. A variety of other less-regular behaviours were also observed. In the majority of cases, the conductances produced by each type of activity were very high, up to 4 nS, confirming the presence of very large pores as suggested by the CF assay. Most excitingly, the apparent non-linear current-voltage response exhibited by HO_2C-Trip-G(E3)-OH makes it one of only a few known voltage-gated synthetic ion channels. The membrane-disrupting behaviour of HO_2C-Trip-G(E3)-OH is also most interesting, and could indeed be an asset in potential biological applications, as this sort of membrane-disrupting activity has been proposed as a mechanism by which ion transporting molecules can act as anti-bacterial agents [5].

The environment-sensitive fluorescence, and in particular the ability to determine an approximate polarity of the membrane environment surrounding the Trip fluorophore is a most exciting result. The fact that the derived E_T values and therefore local environments differ between the active and inactive compounds could form a basis to explain their completely different ion transport behaviour. The ability to monitor the partitioning of these compounds by substantially increasing fluorescence is also significant. The up to 8-fold increase in fluorescence intensity upon membrane partitioning observed for HO_2C-Trip-G(E3)-OH, from a very low background level in aqueous solution, is approaching a practically-usable level. The Trip fluorophore in general, and HO_2C-Trip-G(E3)-OH in particular, forms a good basis for further study into

increasingly rigid, fluorescent ion channels with potential applications in membrane sensing.

The data presented in this Chapter clearly demonstrate that the Trip molecules aggregate in aqueous solution at concentrations below 5 μM, and that this aggregation severely diminishes both their fluorescence intensity as well as partitioning ability. As extent of partitioning could be correlated to ion-transport activity, this is a serious limitation. For future iterations of these Trip-containing molecules, the main goal should therefore be to increase their extent of membrane partitioning. This necessitates further structural modifications to try to strike a balance between a compound that is hydrophilic enough to dissolve to a reasonable extent in aqueous solution, yet be hydrophobic enough that its partitioning will be favourable. The Trip molecules are certainly promising, and it is hoped that further modifications will allow them to reach their full transport and membrane-partitioning potential.

Chapter 4 : Second-generation Dip containing compounds

4.1: Rationale & design

While the Trip compounds had demonstrated some interesting properties and behaviours (Chapter 3), their overall poor ion transport activity prompted the return to the diphenylacetylene 'Dip' chromophore to develop a second generation of these types of compounds. In addition to exploring which components were necessary for the highest ion transport activity, the potential to recover the environment-sensitive excimer emission inherent to the Dip compounds was another impetus. While the first generation of Dip isomers were reasonably active, especially as compared to the fully saturated precursors (Chapter 2), in relation to small-molecule natural channel-formers such as gramicidin, their activity remains modest [40]. In addition, while the bilayer clamp studies did indicate a variety of behaviours including regular, reproducible 'square-top' type conductances, a property that had not yet been achieved for the Dip-containing oligomers was any evidence of voltage-gating. Perhaps modifying the existing Dip structures, especially at the carboxyl and hydroxyl termini could lead to this highly desired property, as well as increased ion transport ability. Finally, as the synthetic conditions to access the Dip molecules had by this point been well established, it was believed that a large suite of compounds could be made quickly, allowing for a structure-activity relationship study which could lead to some mechanistic insights, an ongoing impetus for this work.

In the first generation of Dip compounds, the design strategy relied heavily on the precursor, fully-saturated analogs, as the length and building blocks were chosen to mimic these as closely as possible. In previous work, it was found that the glutaric-anhydride derived 'G' hydroxyl terminus played a role in increasing activity, as all of the most active fully-saturated oligoesters contained this substituent. However, as recently suggested [126] the 'G' headgroup could be introducing increased complexity into the system due to its chirality, as the resultant oligomers are therefore a mixture of

enantiomers. While it is unknown how this could be affecting the Dip molecules' behaviours, the opportunity to simplify these compounds further should be addressed. Therefore, it was decided to modify one of the previously most active Dip isomers, HO_2C-Hex-Dip-Hex-G(12)-OH by a variety of means including changing the length of the analogs, incorporating different charges at the termini, and removing the 'G' subunit (Figure 4.1). The 'core' structure (RO_2C-Hex-Dip-Hex-OR') was therefore retained, and different substituents were appended at either end of the molecules. The majority of manipulations were carried out on the hydroxyl terminus, as the negatively charged carboxylate was desired. However, an analog in which the Prenyl group was retained at the carboxyl terminus was also synthesized and tested for activity.

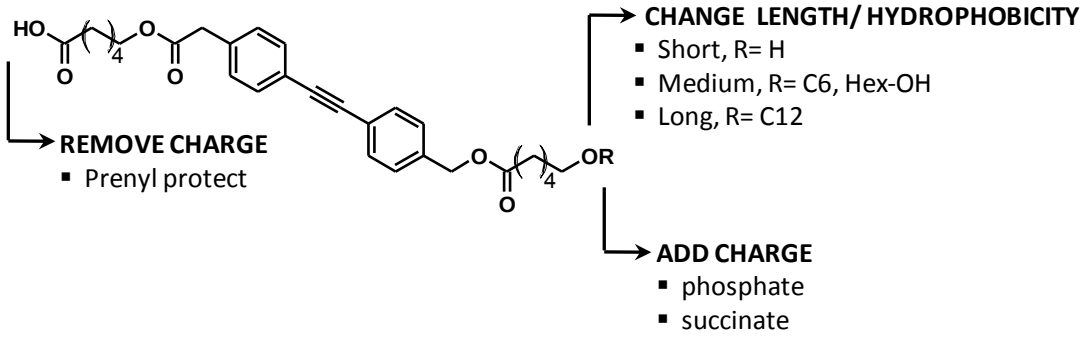

Figure 4.1: Planned sites of modification leading to 2nd-generation Dip isomers.

For the choice of hydroxyl terminus substituents, one consideration was overall length; as a dramatic length effect had been observed for the first-generation Dip isomers, it was of interest to see if this was still the case for this series of compounds. This 'length effect' is most likely due to the difference in hydrophobicity of the compounds which correlates to their extent of aqueous aggregation; the more hydrophobic compounds aggregate more, and partition less. Therefore, to probe this question further, a set of isomers ranging from the longest, most hydrophobic twelve-carbon containing 'C12' oligomer (HO_2C-Hex-Dip-Hex-C12), medium (HO_2C-Hex-Dip-Hex-C6, HO_2C-Hex-Dip-Hex-Hex-OH) to shortest, most hydrophilic oligomer (HO_2C-Hex-Dip-Hex-OH) were designed (Figure 4.1). Besides the differences in hydrophobicity provided by the length and number of the appended alkyl tails, this series also probes

another key question concerning the need for polarity at both termini, as HO_2C-Hex-Dip-Hex-C6 and HO_2C-Hex-Dip-Hex-Hex-OH differ by only a single hydroxyl group.

Another factor of interest was to synthesize compounds with an overall dissymmetric charge distribution, as this type of structure is expected to lead to voltage-gated ion-transport behaviour, as mentioned, and observed previously. In particular, a phosphate-terminated compound was thought to be most promising, due to the dual negative charge present on the phosphate group at pH 6-8, conditions at which the transport studies are conducted, in comparison to the singly charged carboxylate terminus. A succinic acid analog, while only singly-charged, was also thought to be a worthwhile target to complete the series from neutral (OH), singly-charged (COO^-) to dually-charged (PO_3^{2-}) termini. While the majority of these compounds were designed to retain the carboxylic acid terminus, as some charge was assumed necessary, this assumption was also tested in one case ($PREO_2C$-Hex-Dip-Hex-C6), leading to a compound with no overall charge. Finally, as mentioned, the 'G' subunit was not incorporated into any of the 2^{nd}-generation Dip analogs, which was a major departure from the first series of these molecules.

4.2: Synthesis

The synthetic strategy was designed to be as modular as possible, involving the synthesis of several key intermediates which could be elaborated into the final products using the well-established ester coupling, deprotection and Sonogashira reactions outlined in Chapter 2 (Table 2.2). As shown in Scheme 4.1, the key intermediates, compounds **4-1** and **3-6** were known from the first generation Dip syntheses, and could be made reliably in multi-gram quantities, while many of the other reagents and conditions had literature precedent. The syntheses begin with the alkyne-containing precursor **4-1**. This comes directly from THP deprotection of the previously-mentioned terminal alkyne **2-6**, which is synthesized by ester coupling between 4-ethynylbenzyl alcohol (**2-5**) and the known [41] building block HO_2C-Hex-OTHP (**2-4**) (78% over 2 steps).

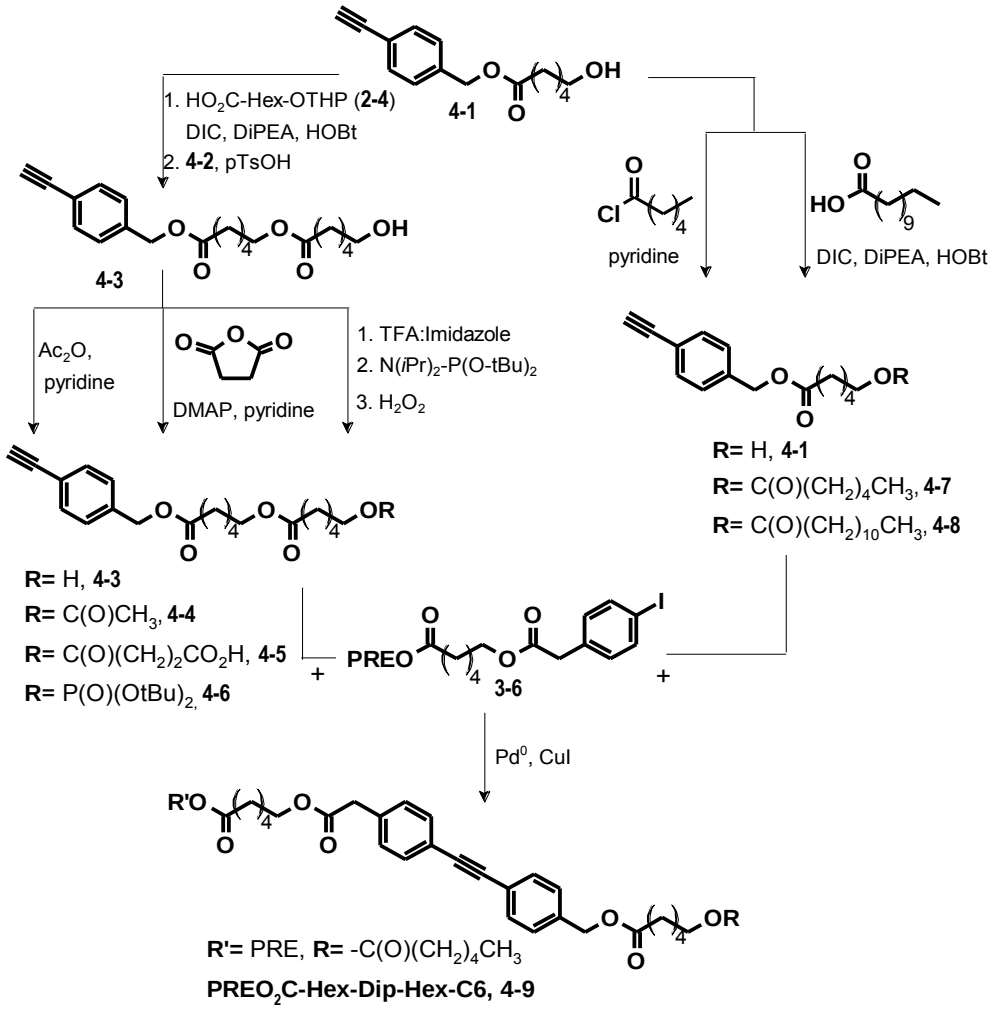

R'= PRE, **R=** H, **4-10**
R'= PRE, **R=** C(O)$(CH_2)_5$OH, **4-11**
R'= PRE, **R=** C(O)$(CH_2)_{10}CH_3$, **4-12**
R'= PRE, **R=** C(O)$(CH_2)_5$OC(O)CH_3, **4-13**
R'= PRE, **R=** C(O)$(CH_2)_5$OC(O)$(CH_2)_2CO_2$H, **4-14**
R'= PRE, **R=** C(O)$(CH_2)_5$OP(O)$(OtBu)_2$, **4-15**

TMSOTf

R'= R= H, **HO_2C-Hex-Dip-Hex-OH, 4-16**
R'= H, **R=** C(O)$(CH_2)_5$-OH, **HO_2C-Hex-Dip-Hex-Hex-OH, 4-17**
R'= H, **R=** C(O)$(CH_2)_4CH_3$, **HO_2C-Hex-Dip-Hex-C6, 4-18**
R'= H, **R=** C(O)$(CH_2)_{10}CH_3$, **HO_2C-Hex-Dip-Hex-C12, 4-19**
R'= H, **R=** C(O)$(CH_2)_5$OC(O)CH_3, **HO_2C-Hex-Dip-Hex-Hex-OAc, 4-20**
R'= H, **R=** C(O)$(CH_2)_5$OC(O)$(CH_2)_2CO_2$H, **HO_2C-Hex-Dip-Hex-Hex-OSucc, 4-21**
R'= H, **R=** C(O)$(CH_2)_5$OP(O)$(OH)_2$, **HO_2C-Hex-Dip-Hex-Hex-OPhos, 4-22**

Scheme 4.1: Synthesis summary, compound naming, numbering and structures for 2nd-generation Dip isomers. Full experimental details and characterization available in Appendices 1 and 2.

From this compound, diversification into two synthetic streams involving standard ester or acyl chloride coupling conditions led to aromatic terminal alkynes containing a variety of oligoester alkyl tails, both hydroxyl (**4-3**) or alkyl-terminated (**4-7**, **4-8**). In all cases, these reactions were high yielding and un-problematic, leading to easily purified intermediates. Characterization by ^{1}H and ^{13}C NMR was unambiguous, key signals included the ester carbonyls in the ^{13}C, which were usually distinguishable for each new ester bond formed, as well as the protons on either side of the ester bonds in the ^{1}H spectra. Appearing at approximately 4 ppm (α to the oxygen) or 2.5 ppm (α to the carbonyl), the integration of these two sets of methylene protons clearly indicated whether any extra alkyl 'tail' remained with the product. These could also be compared with the integration of the benzyl methylenes at 5 ppm, as discussed in Chapter 2.

After purification, the alkyl-terminated alkynes **4-7** and **4-8** were then ready for Sonogashira coupling with the iodo compound **3-6**, the other key intermediate, yielding the 'Dip'-containing Prenyl-protected oligomers **4-9** and **4-12**. The starting alkyne (**4-1**) was also coupled to **3-6**, leading to the shortest trimer **4-10**. For all the oligomers, successful Sonogashira coupling was easily determined by the appearance of the expected aromatic peaks and internal alkyne carbon signals (~90 ppm) in the ^{13}C. In the ^{1}H spectrum, the disappearance of the terminal alkyne H at 3.0 ppm, as well as the appearance of the easily identified Prenyl signals including the characteristic alkene proton at ~5.3 ppm were useful markers. After purification, all these molecules could then be de-protected with TMS triflate using the previously developed conditions to give the final products HO_2C-Hex-Dip-Hex-OH (**4-16)**, HO_2C-Hex-Dip-Hex-C6 (**4-18)** and HO_2C-Hex-Dip-Hex-C12 (**4-19)** in overall reasonable yields ranging from 20 to 39% over a maximum of five steps from the starting commercially-available alkyne **2-5** (see Table 4.1 for details).

Returning to the other synthetic stream, the hydroxyl-terminated analog **4-3** was synthesized from **4-1** *via* **4-2** by a facile ester coupling to HO_2C-Hex-OTHP (**2-4**) and THP deprotection (72% over 2 steps). Once in hand, **4-3** required the installation of various substituents to make the acetate (**4-4**), succinic acid (**4-5**) and phosphate (**4-6**) -

containing triesters. In all cases, these reactions followed literature procedures adapted to the compounds of interest [127,128]. Satisfyingly, all the resultant alkynes retained good solubility properties and were easily purified by column chromatography; this was most appreciated in the case of the succinic acid derivative **4-5**, as the negative charge could have potentially led to solubility issues. Once synthesized, the headgroup-modified alkynes could then re-join the other synthetic stream and be coupled to **3-6**, adding to the suite of Prenyl-protected oligomers (**4-11**, **4-13**, **4-14**, **4-15**). Standard Prenyl deprotection with TMS triflate resulted in a total of four different tetraesters (**4-17**, **4-20**, **4-21**, and **4-22**) varying in charge distribution and hydrophobicity in overall acceptable yields. All the synthesized oligoesters from both streams were then purified by HPLC and fully characterized by NMR, Mass spectrometry, UV and fluorescence spectroscopy (see Appendices 1 and 2 for full synthesis and characterization). The structures, names, numbering and overall yields from commercially-available 4-ethynylbenzyl alcohol (**2-5**) of the second generation Dip oligomers are available in Table 4.1.

During the course of the synthesis of the phosphate-terminated oligomer (HO_2C-Hex-Dip-Hex-Hex-OPhos), it was pleasant to discover that TMS triflate once again acted as a 'wonder' reagent, as it cleanly and efficiently removed the *tert*-butyl protecting groups present on the dually-protected precursor **4-15** concurrently with the Prenyl group. This further broadens the scope of this very useful reagent, as other reagents used to remove *tert*-butyl groups such as trifluoroacetic acid have been observed to interact adversely with the diphenylacetylene moiety (Chapter 2). Considering the minute quantities of TMS triflate needed for deprotection (successful reaction has been achieved with as little as 0.1 mol%), and cleanliness of the reaction, this reagent is most promising as a general deprotection agent for acid-sensitive protecting groups, especially for diphenylacetylene-containing compounds. The *tert*-butyl-protected phosphate-terminated alkyne **4-6** was also interesting from a spectroscopic point of view, as the change in ^{31}P NMR shifts from that expected for a phosphonate (~130 ppm) to that of an phosphate triester (-20 to 0 ppm expected, -9 ppm observed) clearly

indicated that the oxidation with H_2O_2 had been achieved. The change in shifts between the *t*-butyl protected compound **4-15** (-9 ppm) to the deprotected phosphate in the final oligomer HO_2C-Hex-Dip-Hex-Hex-OPhos (1.76 ppm) was also indicative of a successful reaction.

COMPOUND NAME	STRUCTURE	YIELD	# OF STEPS
HO_2C-Hex-Dip-Hex-OH	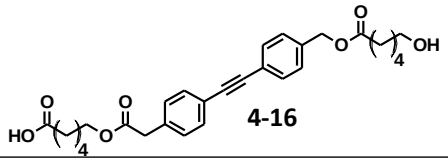 **4-16**	20	4
HO_2C-Hex-Dip-Hex-Hex-OH	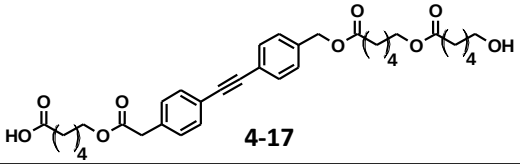 **4-17**	30	6
HO_2C-Hex-Dip-Hex-Hex-C6	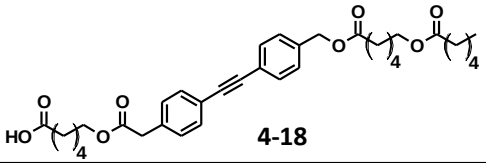 **4-18**	39	5
HO_2C-Hex-Dip-Hex-Hex-C12	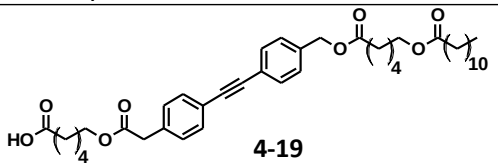 **4-19**	32	5
HO_2C-Hex-Dip-Hex-Hex-OAc	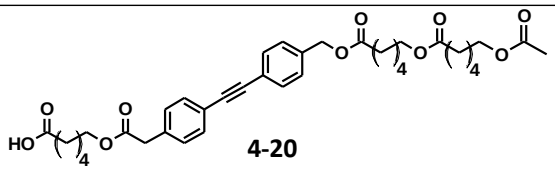 **4-20**	33	7
HO_2C-Hex-Dip-Hex-Hex-OSucc	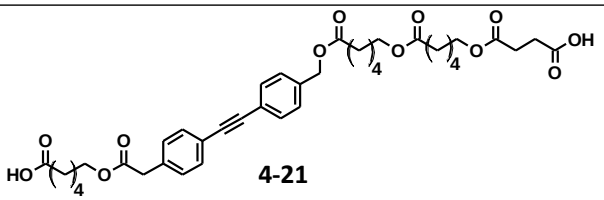 **4-21**	22	7
HO_2C-Hex-Dip-Hex-Hex-OPhos	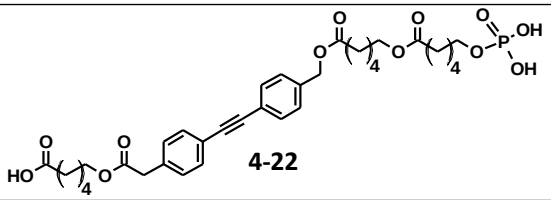 **4-22**	21	7

Table 4.1: Names, structures and yields of second-generation Dip containing compounds from 4-ethynylbenzyl alcohol (**2-5**).

4.3: Ion transport activity; HPTS assay

The structures of the 2nd-generation Dip compounds were intentionally designed to test various hypotheses about what is necessary to achieve high ion-transport activity. As mentioned previously, the search for a 'minimum' active structure, especially when considering structurally 'simple' channel-forming molecules, is a much-pursued topic. This is not to suggest that one can *a priori* predict function based on structure, especially in the field of synthetic ion channel research, where a large diversity of active channel-forming molecules are known. However, for the Dip isomers, certain compounds were presumed to exhibit higher activity than others. For example, as mentioned previously, the longest, most hydrophobic analog (HO_2C-Hex-Dip-Hex-C12) was expected to have poor transport activity due to its propensity to aggregate, similar to that seen for the longest first-generation Dip isomer, HO_2C-Dec-Dip-Hex-G(12)-OH (Chapter 2). Furthermore, as the return to the Dip fluorophore meant that excimer emission could now once again be observed for this compound, poor ion-transport activity was expected to be correlated to its inefficient membrane partitioning, as assayed by fluorescence spectroscopy. In contrast, the highly-charged succinic acid and phosphate-terminated compounds were expected to be of the 'correct' length and overall polarity to exhibit high activity and efficient membrane partitioning behaviour. Overall, it was hoped that structure-activity trends would emerge that could lend further support to the previously-proposed mechanistic framework developed for the Dip isomers, and possibly indicate a 'privileged structure' for these types of oligoester channels.

The results of the HPTS vesicle assay for all the 2nd generation Dip oligomers are shown in Figure 4.2 and Table 4.2. As in Chapter 2, the Table lists the concentrations of compound necessary to effect the 'benchmark' rate of $k= 1x10^{-3}$ s^{-1}, as well as ranking the compounds in order of highest to lowest activity in comparison to the parent structure (HO_2C-Hex-Dip-Hex-G(12)-OH), one of the most active 1st-generation analogs. For the least active compounds which did not achieve the benchmark rate, two different criteria were used. For the compounds that exhibited some activity, the

number listed is the rate achieved at the highest tested concentration (as seen for HO_2C-Hex-Dip-Hex-Hex-OSucc). Alternatively, the maximum testable concentration itself is listed for the analogs that did not exhibit any activity whatsoever ($PREO_2C$-Hex-Dip-Hex-C6 and HO_2C-Hex-Dip-Hex-C12).

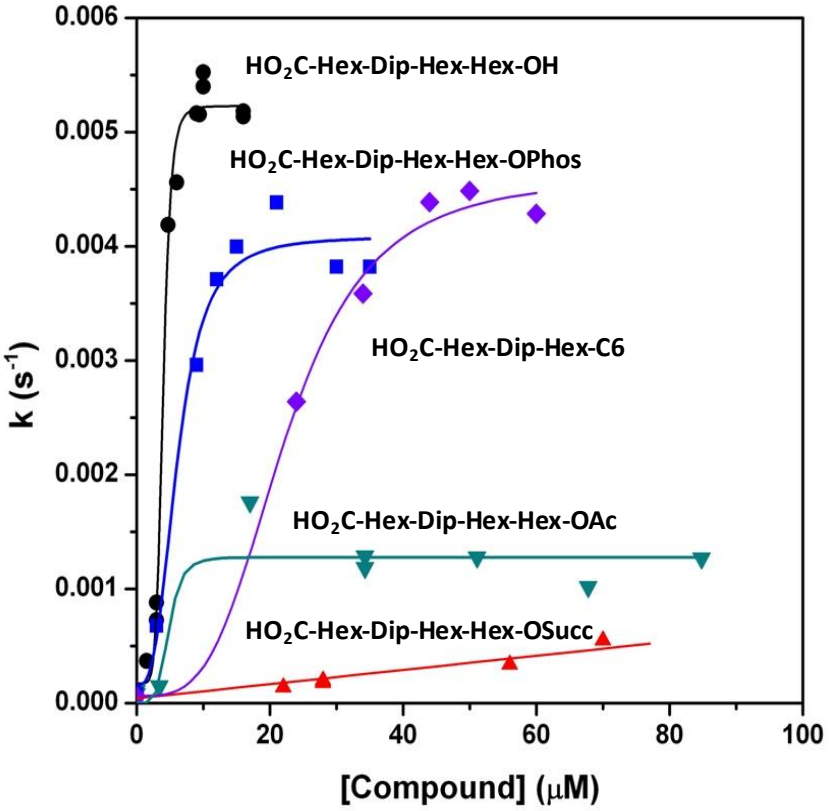

Figure 4.2: Plot of apparent rate constant versus concentration for a selection of 2nd-generation Dip isomers. The lines shown are fits of the data to either logistic or linear functions. See Table 4.2 for full dataset. Details of HPTS assay available in Appendix 3.

4.3.1: Structure-activity correlations

Figure 4.2 illustrates the varying concentration-rate responses of all the active compounds. Examining the data leads to several observations which both confirm as well as contradict the structure-activity hypotheses. Firstly, it is evident that the inclusion of the 'G' subunit at the hydroxyl terminus is not necessary to achieve high activity, as the most active compound in the series, HO_2C-Hex-Dip-Hex-Hex-OH, does

COMPOUND	[COMPOUND] FOR $k = 1 \times 10^{-3} s^{-1}$ (μM)	RELATIVE ACTIVITY
HO_2C-Hex-Dip-Hex-Hex-OH (4-17)	4	2
HO_2C-Hex-Dip-Hex-Hex-OPhos (4-22)	5	1.5
HO_2C-Hex-Dip-Hex-G(12)-OH (1-7)	8	1
HO_2C-Hex-Dip-Hex-C6 (4-18)	15	0.5
HO_2C-Hex-Dip-Hex-Hex-OAc (4-20)	30	0.3
HO_2C-Hex-Dip-Hex-OH (4-16)	80	0.1
HO_2C-Hex-Dip-Hex-Hex-OSucc (4-21)	>70 (0.5)[a]	<0.1
HO_2C-Hex-Dip-Hex-C12 (4-19)	n/a (~50)[b]	n/a
$PREO_2C$-Hex-Dip-Hex-C6 (4-9)	n/a (35)[b]	n/a

Table 4.2: Summary of HPTS activity for head-group modified Dip isomers, comparison with parent compound (HO_2C-Hex-Dip-Hex-G(12)-OH). *a*= number in brackets is rate achieved at highest tested concentration. *b*= number in brackets is highest concentration assayed before visible precipitation occurred. Details of HPTS assay available in Appendix 3.

not contain it. This was a surprising result, as the extensive work carried out previously on the saturated oligoester ion channels suggested that the presence of the G headgroup tended to enhance activity [40]. However, as HO_2C-Hex-Dip-Hex-Hex-OH is more than twice as active as the parent structure, and indeed ranks as the most active of all the Dip-containing isomers (exhibiting activity at concentrations as low as 1 μM), this is clearly not the case for the Dip compounds. This result was most exciting for several reasons; the very high activity of this compound was obviously welcome, as the concentrations needed were now approaching a range that could become potentially useful in biological assays or other applications, as well as comparing favourably with the activity of other recent 'simple' channel-formers, such as the 'aplosspans' studied by Gokel *et al*., which exhibited activity in the CF assay at approximately 0.5 μM (an example of which is shown as compound **4-23** in Figure 4.3) [62,63]. It was also gratifying to observe that a minor structural modification led to such an enhancement of activity, suggesting that further alterations to this compound could lead to further gains in

activity, or other interesting behaviours. In addition, the resulting compound was no longer chiral, removing this as a potential source of complication. Finally, on a more practical level, the removal of the G headgroup simplified the synthesis and improved yields (the final coupling with the G-alkyl groups was notoriously sluggish and usually the lowest-yielding step). Overall, this compound is most promising and can act as a new 'lead' structure, from which the next set of Dip isomers could be based.

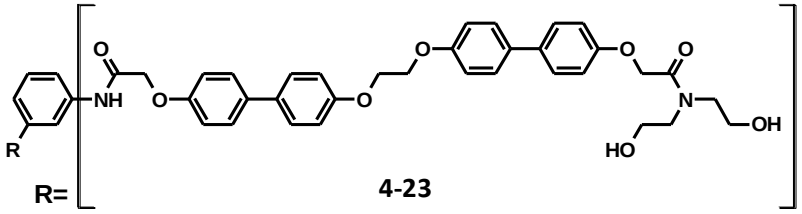

Figure 4.3: Structure of **4-23**, one of the 'aplosspan'-type synthetic ion channels developed by Gokel *et al*.[62,63].

While at first glance the structures of HO_2C-Hex-Dip-Hex-Hex-OH and the parent first-generation Dip isomer (HO_2C-Hex-Dip-Hex-G(12)-OH) appear quite dissimilar, suggesting that their high activity must be due to very different active structures, when considering the previously-proposed model (Figure 2.20), it can be argued that the removal of the G(12) subunit is indeed a 'minor' structural alteration, and that the observed activity of HO_2C-Hex-Dip-Hex-Hex-OH should not in fact be so surprising. As illustrated in Figure 4.4, and discussed in both the Introduction and Chapter 2, the 1st-generation Dip isomers [64] as well as the saturated precursor oligoesters [40] are speculated to insert into the membrane with the hydroxyl terminus 'headgroup' projecting into the polar region made up of the lipid phosphate groups on one side of the bilayer. Therefore, the length of all the first-generation Dip isomers (except the longest Dec isomer) was designed to be approximately the same (~35 Å) from the carboxylic acid terminus to the G hydroxyl group. The alkyl tail appended to the G subunit was then expected to 'fold over' into the membrane to act as an anchor to further embed the compound in the bilayer. The overall length of HO_2C-Hex-Dip-Hex-

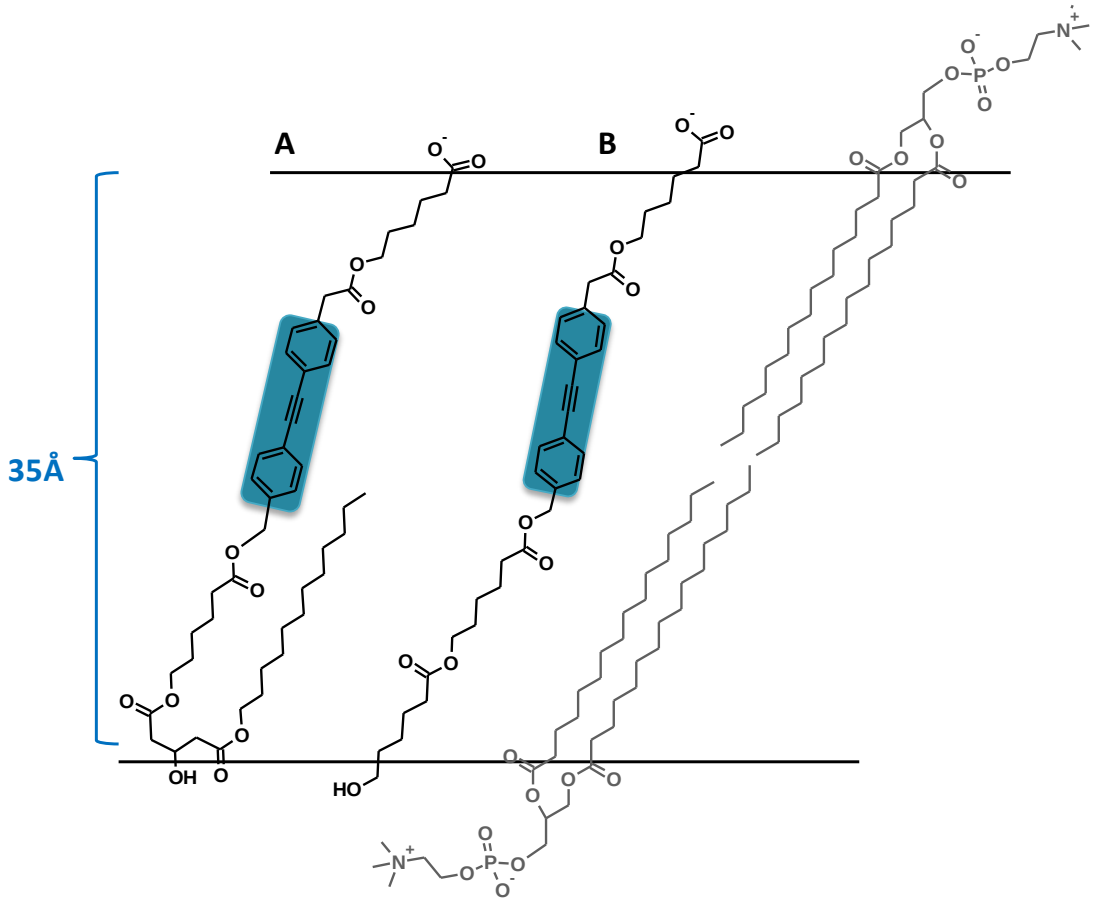

Figure 4.4: Schematic illustration of proposed transmembrane orientation of first-generation Dip isomer HO_2C-Hex-Dip-Hex-G(12)-OH (**A**) compared with the most active second-generation Dip compound HO_2C-Hex-Dip-Hex-Hex-OH (**B**). The lipid pair (in grey) is shown for scale.

Hex-OH in its fully-extended form is approximately 37 Å, very similar to the 'core' of the 1st-generation Dip compounds and clearly matching the bilayer thickness, allowing both polar termini to be in contact with the polar lipid headgroups. This suggests that the alkyl tail in the G-containing isomers is in fact extraneous, and that further anchoring into the membrane is unnecessary. This result is consistent with the findings of London *et al*. [129], who in an extensive study used fluorescence depth quenching (FDQ) to ascertain the penetration depth of various fluorescent membrane probe molecules, and found that the presence of long alkyl tails did not much influence the depth of partitioning of the probes.

Another point to discuss about HO_2C-Hex-Dip-Hex-Hex-OH is the actual shape of its HPTS concentration-response graph (Figure 4.5). As seen for the first-generation Dip isomers, this curve clearly follows a logistic function ($r^2 > 0.99$), giving an EC_{50} value of

3.9 μM. The initial concentration-rate response (before it levels off) is exponential, indicating that these compounds form "Class I" channels [27] and can therefore be fit to the Hill equation (Equation 4.1);

$$\log Y = n\log C_m - n\log K_D \qquad \text{Eqn 4.1}$$

Plotting this initial rate response (fractional activity, 'Y') as a function of monomer concentration (C_m) in a log-log graph (Hill analysis [27]), leads to a Hill coefficient (*n*) of 2, indicating that active structures are formed from at least two monomers aggregating, presumably in the membrane. This rather low number seems to suggest that the channels formed by HO_2C-Hex-Dip-Hex-Hex-OH are much simpler in structure than those seen for the previous set of Dip isomers, which exhibited Hill coefficients ranging from four to eleven [64], and is similar to results seen for other aggregate-type channels [63]. As a simpler, more defined aggregate could potentially lead to more well-

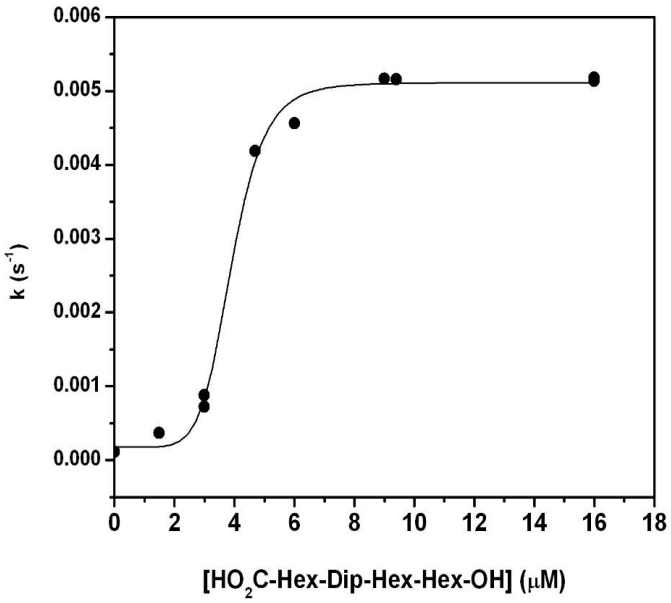

Figure 4.5: An expansion of Figure 4.2, showing the HPTS concentration-rate response of HO_2C-Hex-Dip-Hex-Hex-OH in detail. The line shown is a fit of the data to a logistic function.

behaved activity in other assays such as the bilayer clamp, this was an appealing interpretation. However, the assumption that monomers aggregate to give active structures is not easily tested, and this remains a challenge for many studied systems.

The high ion transport activity of HO_2C-Hex-Dip-Hex-Hex-OH suggests that its polarity, hydrophobicity and length are well-optimized. It would therefore be valuable to elucidate which component of the oligomer is responsible for this high activity. The importance of head group polarity in enhancing activity can be clearly seen by comparison of the high activity observed for HO_2C-Hex-Dip-Hex-Hex-OH (EC_{50} = 3.9 μM) and that of its very closely related homolog HO_2C-Hex-Dip-Hex-C6 (EC_{50} = 22.4 μM from logistic fit, r^2= 0.99). These molecules differ by only the terminal hydroxyl group, yet one is over three times more active than the other (Table 4.2). This pronounced difference in activity was a very interesting observation, and it clearly cannot be correlated with overall length, as this is approximately 37 Å for both molecules. This must therefore be due to the presence of polar termini, as they can interact favourably with the polar lipid headgroups. This is further demonstrated by the phosphate-terminated oligomer HO_2C-Hex-Dip-Hex-Hex-OPhos, which is nearly as active as the hydroxyl-terminated compound (k= $1x10^{-3}s^{-1}$ at 5 μM, EC_{50} = 6.1 μM). In addition, the increased hydrophilicity of the hydroxyl and phosphate terminated compounds should also decrease their extent of aqueous aggregation, thereby increasing partitioning and activity.

The importance of headgroup polarity is perhaps made most evident by the complete inactivity of the only compound in the series which lacks the carboxylate terminus; $PREO_2C$-Hex-Dip-Hex-C6. This compound did not exhibit any above-baseline activity whatsoever, and the concentrations that were able to be tested before visible precipitation occurred were the second-lowest of the entire set of Dip and Trip isomers (35 μM). This increased propensity to aggregate must be due to the lack of charge on the carboxyl terminus, as now the repulsive forces created by the interacting negative charges are absent. In addition, there are now no polar groups present on the ends of the molecule to interact favourably with the lipid phosphate headgroups. Comparing the activity of $PREO_2C$-Hex-Dip-Hex-C6 with that of the free carboxyl-terminal HO_2C-Hex-Dip-Hex-C6 clearly illustrates another example how a fairly minor structural modification can lead to very different levels of ion transport activity. Therefore, the

structure-activity correlations observed for this series of molecules further supports the hypothesis that the extent of aggregation in aqueous solution governs partitioning and thus activity.

As headgroup polarity is clearly important for enhanced activity, it is interesting to consider the effect of headgroup *charge*. The overall positive results obtained for HO_2C-Hex-Dip-Hex-Hex-OH suggested that the length and polarity of this compound were most conducive to high activity; it was presumed that the charged phosphate and succinic acid-containing compounds (HO_2C-Hex-Dip-Hex-Hex-OPhos, HO_2C-Hex-Dip-Hex-Hex-OSucc) would also show high activity. As can be seen in Figure 4.2 and Table 4.2, this was certainly the case for the phosphate-terminated compound, as discussed. This compound had significant activity down to approximately 3 μM, which was the lowest tested concentration, although its maximal rate ($4.4x10^{-3}$ s^{-1}) is less than that attained by HO_2C-Hex-Dip-Hex-Hex-OH ($5.2x10^{-3}$ s^{-1}). This again indicates that the G subunit is unnecessary for activity, and that the length, rigidity and polarity of these new compounds appear close to optimal. Considering the concentration-response trace for HO_2C-Hex-Dip-Hex-Hex-OPhos in detail reveals that it too can be fit satisfactorily to a logistic function (r^2= 0.98), from which an EC_{50} value of 6.1 μM, and a Hill coefficient of 3 (2.99) can be obtained. Interestingly, there is a sharp increase in activity at approximately 20 μM or so, after which it begins to decrease (Figure 4.2). This behaviour is consistent with the compound precipitating out of solution at higher concentrations [27]; as the solubility of this particular compound was indeed seen to be lower than other analogs such as HO_2C-Hex-Dip-Hex-Hex-OH, this result is not entirely unexpected.

In contrast, strikingly different results were seen for the succinic acid-containing compound; HO_2C-Hex-Dip-Hex-Hex-OSucc, as it was essentially inactive, with the maximum rate attained being only half of the 'benchmark' rate of $1x10^{-3}$ s^{-1}. In comparison to the phosphate-terminated compound, the maximum testable concentration (70 μM) for HO_2C-Hex-Dip-Hex-Hex-OSucc was actually quite high, suggesting that aggregation and precipitation from solution before 'reasonable'

concentrations could be reached cannot be blamed for its inactivity. Actually, it must be mentioned that visible precipitation was never observed for HO_2C-Hex-Dip-Hex-Hex-OSucc; concentrations above 70 μM were not tested as the very low activity seen at these relatively high concentrations clearly ranked this compound as 'inactive'. In addition, as some, albeit minimal, activity was seen, it has to be assumed that the compound is partitioning into the bilayer to at least a certain extent, so the explanation for the lack of activity used in the first generation Dip isomers to explain the behaviour of HO_2C-Dec-Dip-Hex-G(12)-OH cannot be invoked here. In fact, the observation of this very low activity was so unexpected that it even led to the speculation that the compound was not characterized correctly, and did not contain the expected terminal carboxylic acid group, as this did indeed prove difficult to observe in the ^{13}C NMR. However, as seen in the Experimental details (Appendices 1 and 2), the obtained mass spectrum was such a close match to the expected value that this argument must also be rejected.

Upon further consideration, a potential explanation which was not obvious initially once again returns to a possible length and polarity mismatch between this compound and the bilayer. In its fully extended form, the OSucc compound is approximately 42 Å from end to end (Figure 4.6). This is clearly in the realm of 'too long', as it is in fact even longer than the longest first-generation Dip isomer, HO_2C-Dec-Dip-Hex-G(12)-OH, which was also seen to be inactive in vesicle assays at least, although as mentioned this is due mainly to its inefficient membrane partitioning. For HO_2C-Hex-Dip-Hex-Hex-OSucc, the negative charge and high polarity of the succinate group would presumably prevent the headgroup from partitioning deeper into the membrane than the midpolar region, as seen for other charged membrane probe molecules studied by London *et al*.[129]. This would limit the compound's potential to re-orient in some sort of 'folded over' conformation to attain a better fit into the bilayer, as would be possible for other, less-polar analogs. While it must again be emphasized that the lack of direct structural evidence for any of the active channels leaves these arguments as

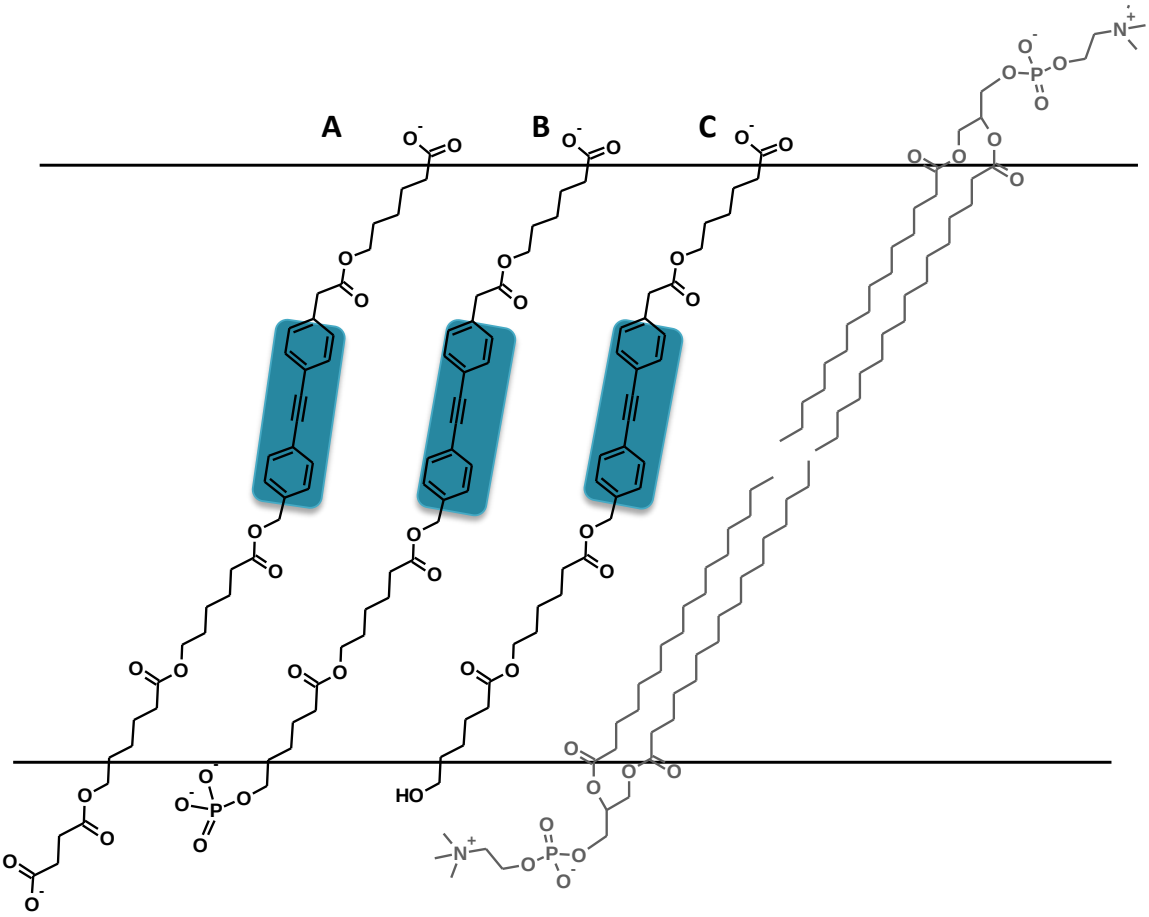

Figure 4.6: Proposed transmembrane orientations of **A**: HO_2C-Hex-Dip-Hex-Hex-OSucc, **B**: HO_2C-Hex-Dip-Hex-Hex-OPhos, **C**: HO_2C-Hex-Dip-Hex-Hex-OH.

speculation, the dramatic difference in activity between HO_2C-Hex-Dip-Hex-Hex-OSucc, -OPhos and -OH are reminiscent of the activity differences observed in the first generation Dip isomers, which were clearly linked to a length and hydrophobicity effect. Further studies such as fluorescence-based membrane partitioning assays were much anticipated for this compound to potentially help explain these results, and shall be discussed shortly.

Further structure-activity analyses of the second-generation Dip isomers again clearly indicated that a significant length and hydrophobicity effect was prevalent for many of these compounds. Comparing the hexyl-terminated analog (HO_2C-Hex-Dip-Hex-C6), which showed reasonably high activity, with both the shortest trimer (HO_2C-Hex-Dip-Hex-OH) and the longest, dodecyl-containing compound (HO_2C-Hex-Dip-Hex-C12), it is immediately evident that there is a fine balance between length and

hydrophobicity that must be maintained in order to obtain high activity. The shortest trimer is only about 29 Å long in its fully-extended conformation; this is clearly not a membrane-spanning length, and therefore the minimal HPTS activity observed for this compound must be due to numerous monomers associating on both sides of the membrane. The low activity seen for HO_2C-Hex-Dip-Hex-OH can be compared to the previous work on fully saturated oligoesters, in which short dimers such as HO_2C-Oct-Dod-OH (26 Å) were found to be relatively inactive in the HPTS assay.

As mentioned previously, the presence of detectable activity indicates that HO_2C-Hex-Dip-Hex-OH can effectively partition into the membrane to at least a certain extent. This, however, cannot be said of the longest, dodecyl-terminated oligomer, as its HPTS-based ion transport activity was negligible. While there was some indication of above-baseline activity during one experimental attempt, the concentration needed to see even this minimal level of activity, as well as the lack of reproducibility of this result, quite unusual for the HPTS assay, suggests that this particular instance can be excluded from consideration. In this case, analogous to that seen for HO_2C-Dec-Dip-Hex-G(12)-OH, the longest 1^{st}-generation isomer, the increased hydrophobicity of the compound is clearly leading to a high extent of aggregation in aqueous solution, preventing membrane partitioning and abolishing ion transport activity. As discussed in the upcoming section, the fluorescence-based membrane partitioning studies also support this conclusion.

4.4: Ion-transport activity; bilayer clamp assay

The bilayer clamp assay is usually considered to be the only unambiguous method to test for single channel ion transport activity [29], and the majority of novel synthetic ion channels are therefore characterized in this manner. However, as mentioned previously, this assay is extremely time-consuming, as each compound must be tested in a variety of conditions repeatedly, to be certain that the activity seen is truly due to the compound in question. The goal of the 2^{nd}-generation Dip isomer

studies was to quickly screen various compounds to develop a structure-activity relationship, for which vesicle-based transport assays are well suited. Considering this, the bilayer clamp assay was therefore only performed on a selection of the second-generation Dip isomers which were thought to exhibit the most interesting properties. Compounds were chosen at both ends of the activity series; the most active HO_2C-Hex-Dip-Hex-Hex-OH as well as the inactive C12 isomer were studied, as was the reasonably active HO_2C-Hex-Dip-Hex-C6, as this compound was a good 'intermediate' between the other analogs. The phosphate-terminated isomer was also assayed, both for its high activity as well as with the expectation that it might exhibit voltage-gated behaviour.

Overall, the bilayer clamp results confirmed those seen in the vesicle assays; the compounds that exhibited HPTS activity were bilayer-active, while the C12 compound was found to be inactive in both assays, most likely due to inefficient membrane partitioning. This differs from what was seen for the first generation Dip isomers, in which the longest isomer (HO_2C-Dec-Dip-Hex-G(12)-OH) displayed bilayer-clamp activity, despite being inactive in vesicles (Chapter 2). Reasons behind this difference are not known for certain, but can most likely be attributed to the increased hydrophobicity of HO_2C-Hex-Dip-Hex-C12 as compared to the first generation compound, in which the glutaric-anhydride headgroup containing two extra carbonyls and a hydroxyl group was present.

Before analysing their activity, an important note to mention about the more hydrophilic compounds (HO_2C-Hex-Dip-Hex-Hex-OH and -OPhos) is that they did not have to be pre-mixed into the lipid to exhibit activity, unlike the majority of the other Dip and Trip isomers, including HO_2C-Hex-Dip-Hex-C6 and the inactive C12 molecule. Rather, they could be introduced into the aqueous solution in contact with the bilayer by injection from a methanol or THF solution of the compound. Introducing compounds from injection is significantly preferred to pre-mixing, as the concentration can be better controlled, and certain properties such as ion selectivity and voltage-gating can be assessed. This achieved another goal of the second-generation Dip isomer studies; to synthesize compounds hydrophilic enough to not completely precipitate out of aqueous

solution, but hydrophobic enough to effectively partition into the membrane and effect transport.

Considering their behaviour; it was observed that the most HPTS-active compound, HO_2C-Hex-Dip-Hex-Hex-OH, exhibited the most reproducible behaviour of one dominant type, as shown in Figure 4.7. The top panel of this Figure illustrates the main activity type observed for this compound; discretely opening and closing 'hairy' square tops with reasonably large conductances on the order of approximately 200-500 pS. In over 70% of the analysed traces, this 'hairy square' activity was the predominant type of behaviour. This was the case in all three tested electrolytes, although it was most prominent in CsCl, in which nearly 90% of all traces consisted of this type of activity as the major type. The conductance range was also fairly narrow over the set of analysed traces; approximately 60% of the analysed experiments had g values in the 100- 500 pS range, while in 16% of cases, fairly large pores with

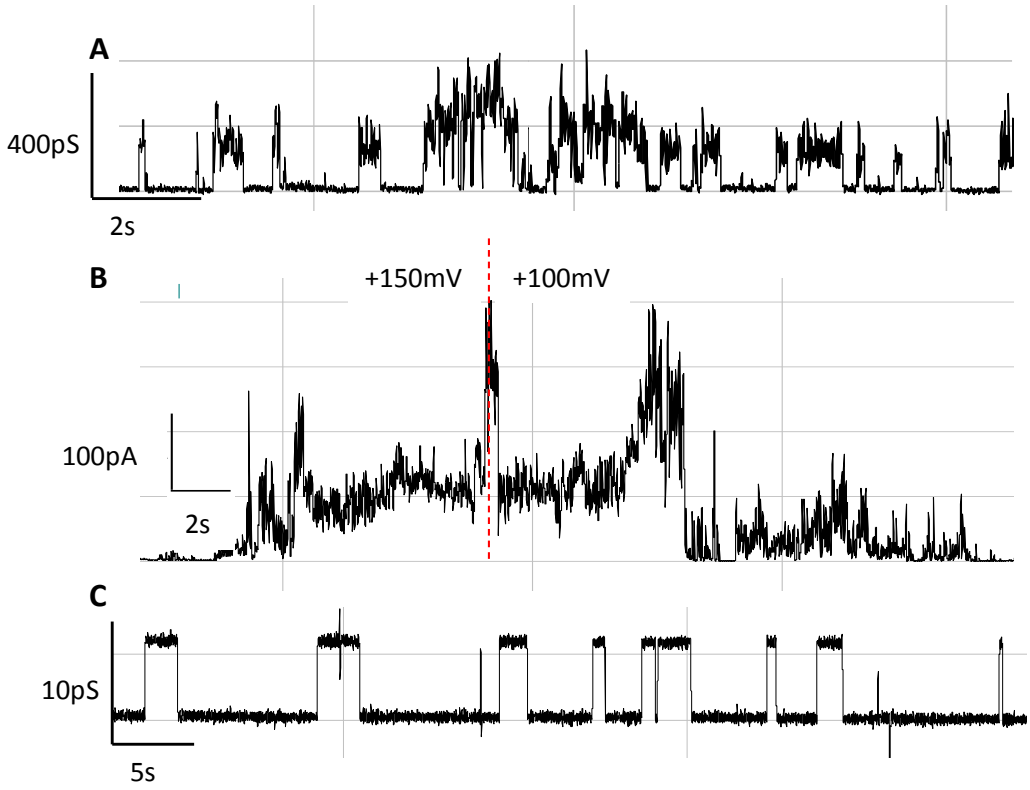

Figure 4.7: Bilayer clamp results for HO_2C-Hex-Dip-Hex-Hex-OH. Conditions: **A**: 1 M CsCl, +40 mV, **B**: 1 M NMe_4Cl, red dashed line marks switch from +150 mV to +100 mV, **C**: 1 M CsCl, +100 mV. DiPhyPC was the lipid in all cases.

conductances greater than 1 nS were observed. In almost all traces, even when the activity became more irregular and the conductance increased, the activity still returned to the baseline. This can be seen in Figure 4.7B, in which the observed long-lived opening, which reached a conductance value of over 2 nS, responds to applied potential and then abruptly closes; activity continued after this time.

These 'hairy square'-type openings, while still somewhat irregular, can in fact be analysed in many cases by using the established protocols designed for the most regular 'square top' behaviours. Therefore, lifetimes, open probabilities and assumed diameters can be obtained for many of the observed traces. This makes HO_2C-Hex-Dip-Hex-Hex-OH fairly 'well-behaved' in comparison to some of the other compounds studied in this work. One property that was not observed, however, was any evidence of voltage-gating. Individual long-lived openings did not appear to be voltage-sensitive, and an 'average analysis' such as performed for the Trip compound in Chapter 3 could not be applied here, as HO_2C-Hex-Dip-Hex-Hex-OH did not exhibit a constant current over a period of time long enough to be analysed by this method.

The other types of 'common' activity observed for the first generation Dip isomers and the Trip compounds include very short-lived spikes, long-lived 'always on' openings and very regular 'square tops'. These types of behaviours made up the minority of the activity seen for HO_2C-Hex-Dip-Hex-Hex-OH, with the most regular square tops making up only 5% of all observed behaviour (Figure 4.7C). However, while rare, these square tops are interesting as their conductance and lifetimes are in fact very similar to other examples of square tops observed for both the first generation Dip isomers as well as the Trip compounds; compare Figure 2.9A for HO_2C-Dip-G(12)-OH and Figure 3.7B for HO_2C-Trip-G(E3)-OH. Therefore, it appears that the most regular channels formed have very low conductances (10-30 pS), and similar lifetimes (1-5 s). Intriguingly, this is exactly the finding of a recent comprehensive review of the reported bilayer clamp literature carried out by Fyles and Chui [83]. Apparently, the vast majority of reported 'square top' activity observed for a wide variety of compounds studied by different groups fall into this conductance and lifetime range.

As discussed in Chapter 2, while regular behaviour is much easier to analyse, other, more irregular behaviour can be just as information-rich, and perhaps even more significant. For example, the other highly HPTS-active, phosphate-terminated compound was indeed extremely irregular; examples of this compound's activity are shown in Figure 4.8. Almost a third of all analysed traces terminate by membrane rupture; this is the only compound of all those studied in which this occurred to such a high extent. The most regular type of 'square top' activity was never observed for HO_2C-Hex-Dip-Hex-Hex-OPhos, however, there were instances in which the activity was reasonably regular; the activity in Figure 4.8A is quite similar to that observed for HO_2C-Hex-Dip-Hex-Hex-OH in Figure 4.7A. This trace again shows relatively large discrete openings of approximately 400 pS, with lifetimes on the order of a few hundred milliseconds. This type of activity, if present, usually occurred at the beginning of an experiment. However, this activity was the minority of that observed for HO_2C-Hex-Dip-Hex-Hex-OPhos, being the predominant behaviour in only 14% of all traces. Another

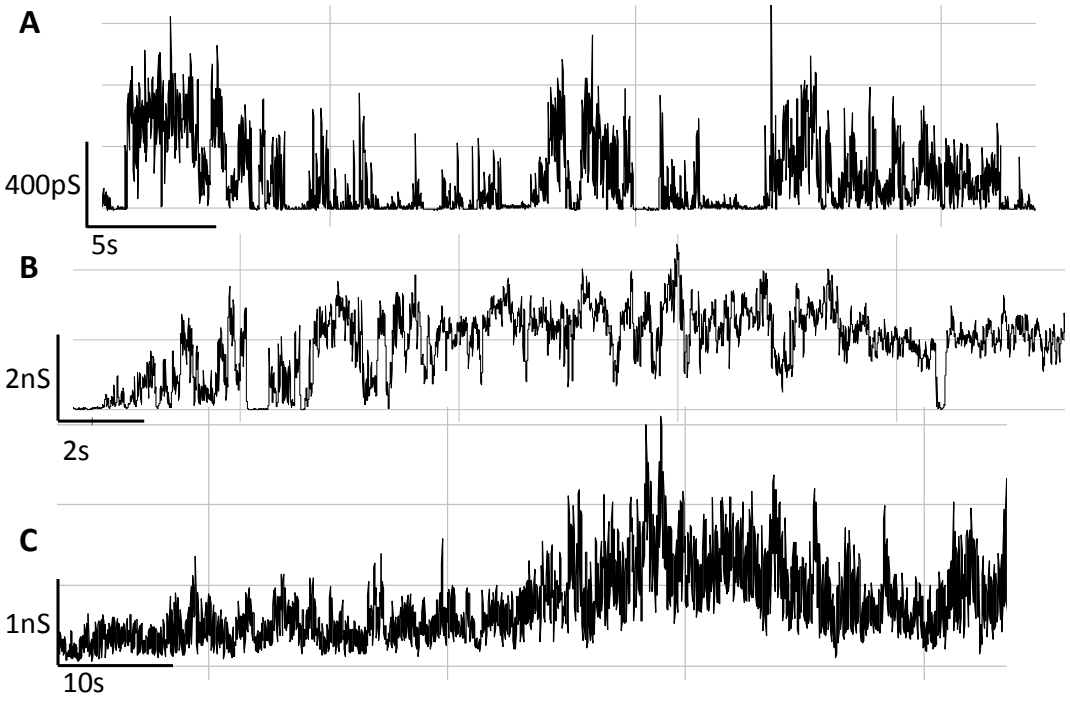

Figure 4.8: Bilayer clamp results for HO_2C-Hex-Dip-Hex-Hex-OPhos. Conditions; diPhyPC lipid, **A**: 1 M KCl, +50 mV, **B**: 1 M CsCl, +25 mV, **C**: 1 M KCl, +40 mV.

17% of all traces had the very short lifetime 'spike' activity seen often for the first generation Dip isomers; the conductances of these spikes were rather variable.

The most representative behaviour (46% of all traces) can be seen in Figure 4.8B; very large, irregular openings with long lifetimes that seldom returned to the baseline were consistently observed; the extreme case can be seen in Figure 4.8C, in which the pore never closes and becomes increasingly large over time. While this type of activity usually resulted in membrane rupture, these 'always on' channels remained intact for an extended period of time of up to several minutes. Over this time, the conductances of these pores were observed to reach values of greater than 2 nS; according to the Hille equation (Eqn 2.1) [27,37], this corresponds to a channel diameter of approximately 1 nm, amongst some of the largest pore openings seen for the Dip and Trip compounds. Very large conductances were actually fairly common for HO_2C-Hex-Dip-Hex-Hex-OPhos; extremely high g values of greater than 1 nS were the predominant conductance observed in 18% of analysed traces. These very high conductance openings occurred most often in KCl electrolyte, and on one particular occasion, a trace was collected in which truly 'giant' pores were observed, with the conductance spiking to almost 10 nS for a short period of time (10 s). Similarly to the highly conducting 'spike' activity discussed in Chapter 2; these very large opening events are significant: the trace in Figure 4.8C in particular indicates a long-lived, highly conducting opening. While suffering from the same analytical difficulties as encountered with other 'irregular' behaviour, these very efficient ion conductors should be probed in more detail, considering the rarity of such very high conductances in the synthetic ion channel literature [83,38,39]. The predominance of these large conductance irregular 'hairy squares' must mean that they are a property inherent to the compound, and that it does not form the small, very regular square tops observed for other Dip and Trip isomers.

Analogously to the Trip studies, the frequency of membrane rupture suggests that HO_2C-Hex-Dip-Hex-Hex-OPhos eventually acts as a surfactant in the membrane, although this may be due to the compound being present at too high of a concentration. Unlike the majority of studied compounds, HO_2C-Hex-Dip-Hex-Hex-

OPhos was unique in that its activity only occurred after a fairly long period of time. Over this longer period of time, additional compound was added in hopes of observing activity before having to reform the membrane, as any particular bilayer can only be used for a finite period. It is therefore plausible that too much compound was added and not given enough time to effectively partition and associate into active structures; this should be avoided in any further bilayer study into this compound.

Despite its interesting activity, the phosphate-terminated oligomer was somewhat disappointing in that it did not display any voltage-gating behaviour in any of the analysed traces. Repeated attempts were made to characterize the voltage response of individual openings, as well as the 'average analysis' discussed previously; the conductances were found to vary significantly over time at each potential, complicating this analysis. Where clear IV correlations were observed, they were for the most part linear. Due to its dissymmetric nature and differential charge distribution at either terminus, HO_2C-Hex-Dip-Hex-Hex-OPhos seemed a promising candidate to display voltage-gating, therefore this was an unfortunate result. However, considering how few voltage-gated synthetic ion channels are known in the literature, this is clearly a challenging property to achieve. In addition, the lack of voltage-gating can be rationalized by the very large pores consistently formed by this compound. If greater than 1nm pores are being formed in the membrane, individual monomers can therefore clearly transition through this pore to the other side of the membrane. Even if any preferential insertion of the compound into the membrane occurred initially, this would eventually be removed through this 'flip-flop' mechanism. As an asymmetric distribution of compounds leading to an overall dipole is assumed to be required for voltage-gated behaviour, this rationalizes the lack of such behaviour observed for HO_2C-Hex-Dip-Hex-Hex-OPhos.

Without over-generalizing, it can be concluded that the bilayer-clamp activity of the studied 2nd-generation Dip isomers was in line with what was observed for the first-generation analogs; similar types of activity were seen, as could be expected due to the structural similarity of these two sets of compounds. The most prevalent activity

observed was of the somewhat regular, 'hairy square-top' variety, with both shorter and longer-lived behaviours making up the minority of observed activity. The most regular behaviour was observed for the most highly HPTS-active compound, HO_2C-Hex-Dip-Hex-Hex-OH, while the phosphate-terminated analog formed very large, 'always on'-type channels, although its activity was highly variable. These compounds did not need to be pre-loaded into lipid, a significant improvement over the majority of the first-generation Dip isomers. Importantly, the assay did agree with the HPTS data and confirmed which compounds were active and inactive, indicating that the use of the assay as a confirmatory screen for the studied compounds was justified in this context.

4.5: Photophysical characteristics

4.5.1: Fluorescence in solution

In addition to developing highly-active compounds, the other main motivation to return to the Dip-containing structure was to recover the excimer fluorescence that had proven so useful in the first generation of these compounds (Chapter 2). The differential fluorescence between excimer and monomer emission observed in aqueous solution in the presence and absence of lipid vesicles suggested that membrane partitioning could be directly observed, lending support to the proposed working model. The moderately large library of 2nd-generation Dip isomers available, which presumably would still exhibit excimer emission could therefore aid in continuing efforts to further refine and test this working model.

As seen in Figure 4.9, the second-generation Dip isomers display at least some degree of environment-sensitive fluorescence. In methanol solution, the emission spectra of these compounds are very similar; all exhibit the expected monomer-type emission at approximately 320 nm. This similarity extends to their excitation and absorption spectra (see Appendix 4) as well as their emission intensity at similar

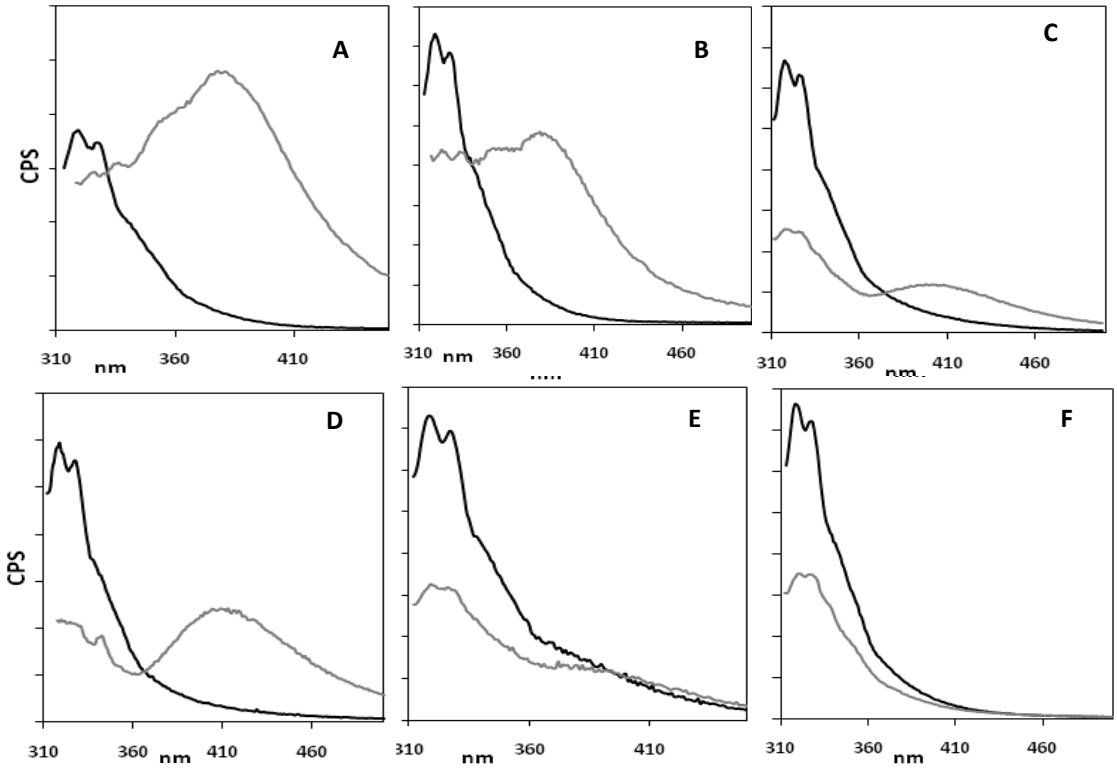

Figure 4.9: Fluorescence emission spectra in CH_3OH (black lines) or aqueous buffer (grey lines) (10 mM BisTris, 100 mM NaCl, pH 6.4) for head-group modified Dip isomers. **A**: 25 µM HO_2C-Hex-Dip-Hex-C6, **B**: 25 µM HO_2C-Hex-Dip-Hex-C12, **C**: 16 µM HO_2C-Hex-Dip-Hex-OH, **D**: 17 µM HO_2C-Hex-Dip-Hex-Hex-OH, **E**: 15 µM HO_2C-Hex-Dip-Hex-Hex-OPhos, **F**: 18 µM HO_2C-Hex-Dip-Hex-Hex-OSucc. Excitation wavelengths varied minimally around 305 nm (302-305) for all compounds in both solvents. Fluorescence intensity varied over time in aqueous solution.

concentrations, suggesting that in organic solvents, the Dip chromophore in its monomer state is not much affected by the various structural modifications present in these compounds. The overall emission intensity remains low for the oligomers, as expected for the Dip chromophore, however, sufficient signal could be seen at approximately 10-25 µM of compound which is within the range used for the HPTS assay. As for the first-generation Dip isomers, the monomer emission for these analogs can be quenched by Cu 2^+ ions at millimolar concentrations, yielding Stern-Volmer constants of approximately 1100 M^{-1} (Figure 4.10). While these relatively large Stern-Volmer constants are suggestive of static quenching [99], full analysis of their quenching behaviour was not the goal of these studies, which were to find an efficient quencher that could be used to study membrane partitioning behaviour, just as for the first-

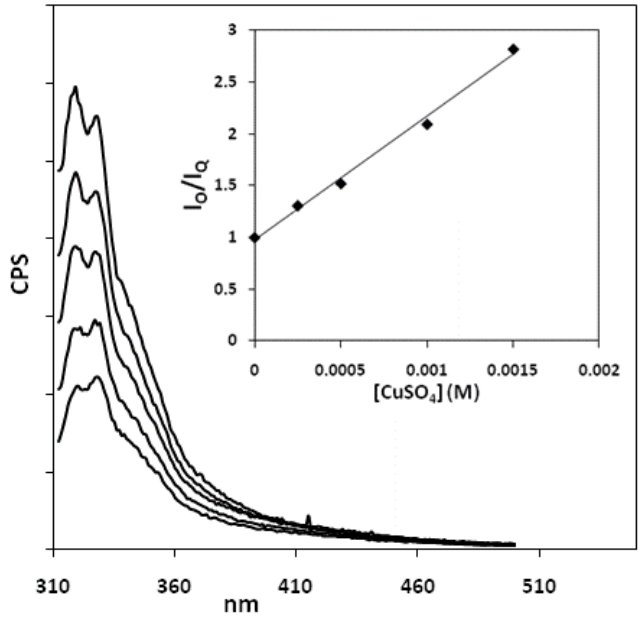

Figure 4.10: Fluorescence quenching in CH_3OH for 17 µM HO_2C-Hex-Dip-Hex-Hex-OH. From top to bottom, [$CuSO_4$] = 0, 0.25, 0.5, 1, 1.5 mM. INSET: Stern-Volmer analysis of quenching data, $K_{SV} = 1.19 \pm 0.08 \times 10^3\ M^{-1}$.

generation Dip isomers. However, the constants are in fact reasonable when considering the sub-nanosecond lifetime of diphenylacetylene in solution [85,56].

While the differences between the Dip isomers in organic solution are minimal, the same cannot be said for their behaviour in aqueous solution. As seen in Figure 4.9, the emission spectra of these compounds in water vary greatly amongst the oligomers; especially when considering the extent of excimer emission. For the previous set of Dip isomers, the fluorescence in aqueous solution was dominated by the excimer emission present at approximately 380 nm. While this still occurs for certain 2nd-generation Dip compounds such as HO_2C-Hex-Dip-Hex-C6 (Fig. 4.9A), for others this excimer emission is completely abolished, as seen for HO_2C-Hex-Dip-Hex-Hex-OSucc (Fig. 4.9F). There are also intermediate instances, in which the compounds exhibit significant fluorescence intensity at both the shorter (~320 nm) and longer wavelengths (HO_2C-Hex-Dip-Hex-Hex-OH and HO_2C-Hex-Dip-Hex-OH, Fig. 4.9C, D). While the shapes of the emission spectra differ greatly for the various compounds, some overall trends can be observed, such as the generally lower fluorescence intensity in aqueous solution as compared to that seen in methanol. This has been observed for the majority of the compounds

discussed in this work, including the first-generation Dip isomers (Chapter 2) as well as the Trip compounds (Chapter 3). This behaviour can again be rationalized in terms of compound aggregation, instead of water quenching, as the experiments carried out on the Trip compounds in Chapter 3 (Figure 3.12) clearly indicate. Further evidence specific to the 2nd generation Dip isomers include the fact that the aqueous emission is unstable over time for the majority of these compounds, indicating that there are a variety of species present in solution which rather slowly evolve over time. Unfortunately, this highly unstable emission prohibited an accurate 'water quenching' experiment as performed for the Trip compound discussed in Chapter 3. Furthermore, if hydrogen bonding were to blame, this effect should also be seen in methanol solution, as was in fact observed for the indole compound **2-28** shown in Figure 2.13. This is not the case for the Dip isomers, as the fluorescence emission in methanol is very similar in band shape and intensity to that seen in less-polar solvents such as THF and chloroform. Finally, if specific water-compound interactions were occurring, it is assumed that this effect would be more pronounced for the more polar compounds, such as the succinic-acid derivative, which can more readily partake in H-bonding; examining Figure 4.9 indicates that this is not the case, as the decrease in intensity is similar (approximately 50% of that seen in methanol) for the majority of isomers.

For the second-generation Dip oligomers, the single case in which excimer emission is increased over monomer emission is HO_2C-Hex-Dip-Hex-C6 (Figure 4.9A), however, this emission intensity is seen to decrease over time, this in fact occurs for all the studied compounds, as mentioned. The time-dependent changes vary amongst the isomers; certain compounds exhibit enhanced 380 nm emission over time, while for others the excimer emission continues to decrease. Further complications arise from the fact that the actual *shape* of the emission spectra change over time; this can vary from a subtle decrease in intensity at certain wavelengths (Figure 4.11A) to the extreme behaviour witnessed for HO_2C-Hex-Dip-Hex-Hex-OAc, in which the emission spectrum changes so dramatically over a period of approximately 10 minutes that the final spectrum does not remotely resemble the initial spectrum (Figure 4.11B). Overall, it is

once again clear that the variety of monomer to aggregate equilibria that occur in aqueous solution for these compounds greatly complicates their analyses, a problem which is well-recognized for such amphiphilic compounds [130].

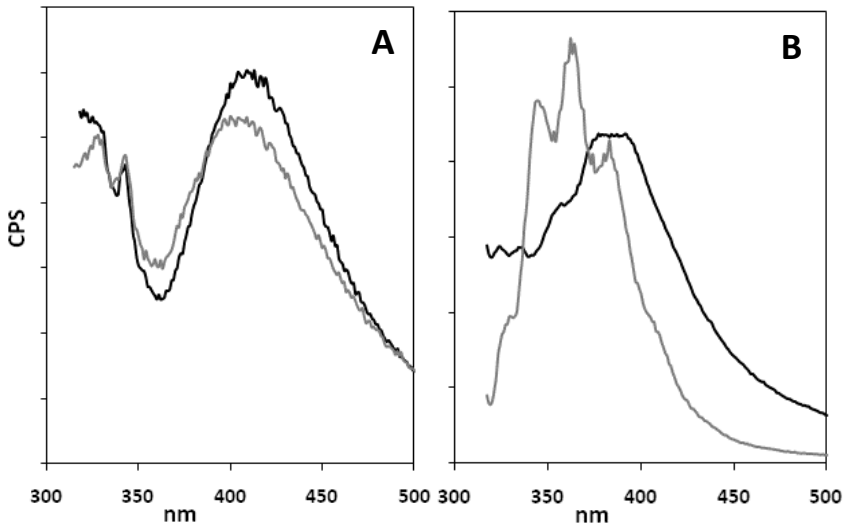

Figure 4.11: Fluorescence emission spectra in aqueous buffer (10 mM BisTris, 100 mM NaCl, pH 6.4) immediately after mixing (black lines) or after 10 minutes stirring time (grey lines) for **A**: HO_2C-Hex-Dip-Hex-Hex-OH and **B**: HO_2C-Hex-Dip-Hex-Hex-OAc.

Despite these complications, is it possible to rationalize the varied emission profiles of these compounds in aqueous solution based on structural criteria? Certain observations are easily explained; for example, an evident correlation exists between compound hydrophobicity and excimer intensity. The least polar of the studied isomers, HO_2C-Hex-Dip-Hex-C6 and the longer C12-terminated analog exhibit the highest extent of excimer emission, see Figure 4.9 panel A and B. As the non-polar alkyl tails of these compounds would allow them to aggregate to a great extent, predominant excimer emission for these compounds is not surprising. On the other end of the scale, the succinic acid-terminated oligomer HO_2C-Hex-Dip-Hex-Hex-OSucc exhibits the lowest degree of excimer-like emission; it is in fact barely detectable, and its aqueous emission is almost identical to its spectrum in methanol, despite the aforementioned decreased fluorescence intensity. The multiple negative charges present on the succinate headgroup of this compound would be expected to repel each other, thereby decreasing its propensity to aggregate. The aggregation explanation is consistent with

the behaviour seen for the intermediate cases as well; the longer, more hydrophobic tetramer (HO_2C-Hex-Dip-Hex-Hex-OH, Fig. 4.9D) shows higher excimer fluorescence than the shorter trimer HO_2C-Hex-Dip-Hex-OH, Fig. 4.9C).

While the extent of excimer emission seen for the varying compounds does correlate reasonably with their hydrophobicity, thereby suggesting that aggregation is a key factor, these results immediately lead to a very interesting, and perplexing, observation. Throughout this work, it has been assumed that a higher extent of aggregation (visualized by the amount of excimer emission) limits the compounds' ability to partition into the membrane and therefore their potential activity, as has been observed when comparing the activity of molecules such as HO_2C-Hex-Dip-Hex-C12 and HO_2C-Hex-Dip-Hex-C6. This is consistent with the high activity seen for the phosphate-terminated molecule, which exhibits very low excimer fluorescence. However, the succinic-acid compound clearly does not agree with this hypothesis as it is marginally HPTS-active despite displaying what appears to be almost exclusively monomer-type emission in aqueous solution, implying minimal aggregation. Minimal aggregation is also implied by the observation that, as discussed, no visible precipitation could be seen for this compound at concentrations up to approximately 70 μM (the highest concentration tested), quite high in comparison with most of the other Dip and Trip isomers. The succinic acid-terminated compound is therefore an interesting case, as it is the only compound of the entire Dip and Trip series that does not seem to fit into the 'aggregation limits activity' hypothesis, leading to speculation as to the cause of its minimal ion transport activity. As discussed above, a reasonable explanation may be that the compound is too long, and therefore its partitioning into the bilayer is unfavourable as the formed in-membrane species would not be well-matched to the hydrophobic and hydrophilic regions of the bilayer. Whatever the mechanism, it is clear that while aqueous aggregation can decrease activity of an active compound, lack of aggregation, as seen for HO_2C-Hex-Dip-Hex-Hex-OSucc, does not guarantee activity.

A final important feature common to the majority of the second-generation Dip isomers is their ability to be efficiently quenched by Cu^{2+} in aqueous solution, just as in

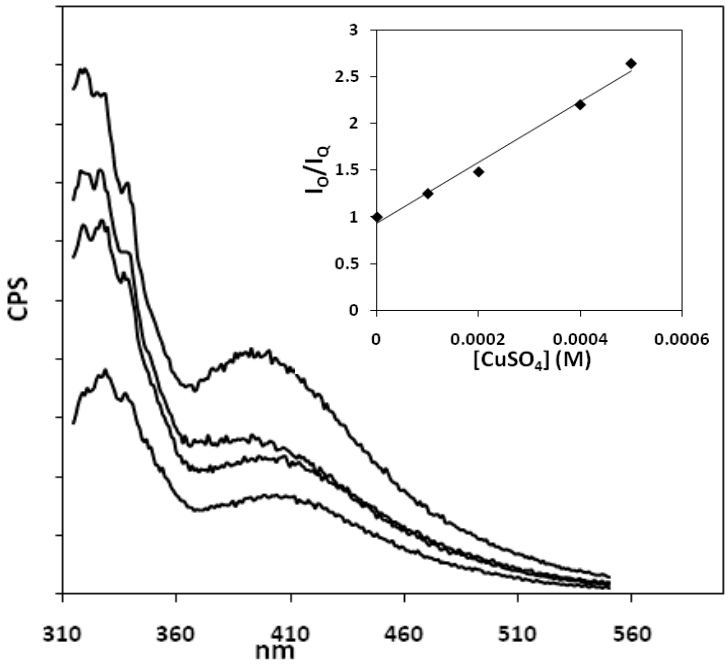

Figure 4.12: Fluorescence quenching in aqueous buffer (10 mM BisTris, 100 mM NaCl, pH 6.4) for 17 µM HO_2C-Hex-Dip-Hex-Hex-OH. From top to bottom, [$CuSO_4$] = 0, 0.1, 0.2, and 0.5 mM. λEX= 305 nm. INSET: Stern-Volmer analysis of quenching data at 320nm, K_{SV} = 3.28±0.07 x 10^3 M^{-1}. The fluorescence at ~400 nm did not follow a linear Stern-Volmer relationship.

methanol. For all tested compounds, the concentrations needed to effect reasonable quenching occurred at approximately 0.05 to 0.2 mM, 10 times lower than that required in methanol. For the more polar oligomers exhibiting appreciable monomer fluorescence in aqueous solution, the response to quenching at 320nm was seen to follow a linear Stern-Volmer relationship, suggesting Stern-Volmer constants on the order of 3x10^3 M^{-1} (see Figure 4.12, inset). As this is a similar value to that seen in MeOH for quenching of the monomer, this is consistent with the lesser extent of aggregation observed for the more hydrophilic compounds. Unfortunately, the instability of the longer wavelength emission over time prevented full Stern-Volmer analysis for the excimer in most cases; as seen in Figure 4.12, the quenching response at ~400 nm to concentration is clearly not linear. Nevertheless, the key finding from the solution-phase quenching studies is that copper can indeed be used as a quencher for both monomer and excimer emissions at reasonably low concentrations, making it amenable to further membrane partitioning studies with vesicles.

4.5.2: Fluorescence with vesicles; membrane partitioning studies

In the first-generation of Dip isomers, it was demonstrated that membrane partitioning could be directly observed by monitoring the differential emission intensities between monomer and excimer. The most active compounds exhibited a dramatic increase in 320 nm (monomer) emission when vesicles were introduced, while for the inactive compound (HO_2C-Dec-Dip-Hex-G(12)-OH), the excimer emission at 380 nm continued to dominate, without changing over time. In addition, quenching studies performed in the presence of vesicles indicated that the active compounds were well-protected from quenching in vesicles as compared to when they were free in solution, again suggesting a membrane-inserted state for these molecules. It was therefore hoped that similar behaviour would be observed for the second-generation Dip isomers in these types of assays, potentially rationalizing their activity, as well as strengthening the mechanistic proposal.

As can be seen in Figure 4.13, there is evidence that all the active compounds exhibit membrane association and/or partitioning, as suggested by the increase in 'monomer' emission upon vesicle introduction. The increase in emission intensity, change in band structure and blue-shifting of the wavelength observed all clearly indicate a less-polar environment is being provided for the chromophore. Interestingly, incubation with vesicles also affects the longer-wavelength emission for these compounds, as analogous changes in intensity, λmax and band structure are observed in this region as well. This is quite pronounced for the phosphate-terminated compound (Figure 4.13D), in which two structured bands at approximately 370 and 390 nm emerge over ten minutes of stirring with vesicles. Such pronounced changes in the presumed excimer emission were not seen for the 1^{st}-generation Dip compounds, and indicate that the aqueous and in-membrane aggregates present in the second-generation Dip isomers may have different spectroscopic properties. This suggests the exciting possibility that the in-membrane aggregate can now be detected and analysed separately from the aqueous aggregate, which would be extremely significant in terms

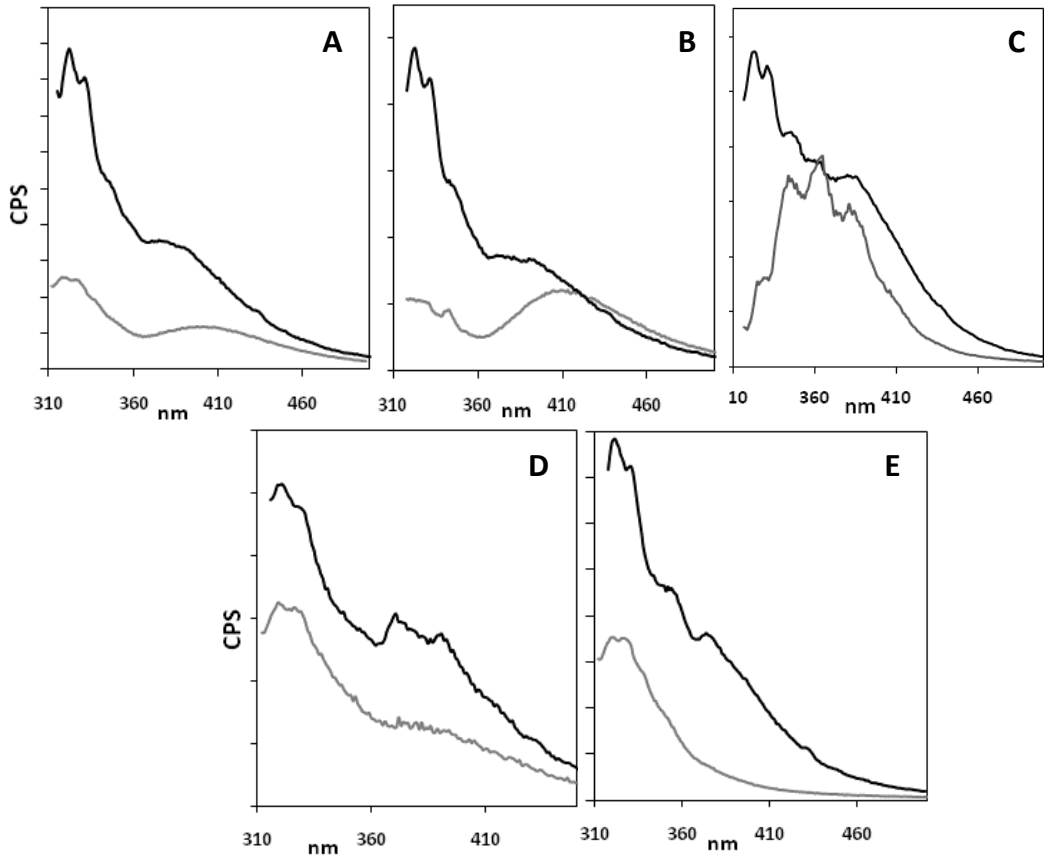

Figure 4.13: Fluorescence emission spectra in aqueous buffer (grey lines) (10 mM Na_3PO_4, 100 mM NaCl, pH 6.4) or after 10 minutes incubation time with lipid vesicles (black lines) for selected head-group modified Dip isomers. **A**: 16 µM HO_2C-Hex-Dip-Hex-OH, **B**: 17 µM HO_2C-Hex-Dip-Hex-Hex-OH, **C**: 18.5 µM HO_2C-Hex-Dip-Hex-OAc, **D**: 15 µM HO_2C-Hex-Dip-Hex-Hex-OPhos, **E**: 18 µM HO_2C-Hex-Dip-Hex-Hex-OSucc. Excitation wavelengths varied minimally around 305 nm (302-305) for all compounds. Data for HO_2C-Hex-Dip-Hex-C6 and HO_2C-Hex-Dip-Hex-C12 available in Fig. 4.14.

of elucidating and characterizing a possible active structure. Unfortunately, this intriguing observation complicates matters, as it suggests that the current method of monitoring the same wavelength in both aqueous solution and with vesicles as an indication of membrane partitioning may not be accurate; for example, for HO_2C-Hex-Dip-Hex-Hex-OH, the shift in the excimer emission upon vesicle introduction is almost 30 nm, which is quite significant (Figure 4.13B). This is even more evident for the acetate-terminated compound (Figure 4.13C), where it is clearly inappropriate to monitor at one specific wavelength, as the spectra in aqueous and with vesicles are completely different. In these systems, monitoring at the aqueous emission maximum clearly does not give an accurate reading of the amount of excimer emission occurring

in the presence of vesicles. The decision to remain at one standard wavelength for each compound was made in order to simplify the analysis, as it has been suggested that this is the most accurate way to carry out these types of experiments [125]. However, it is now evident that in future work, the experiment must be carried out in a different manner. A 'multi-dye' type experiment, in which numerous emission wavelengths can be monitored concurrently, would be most useful in this regard. However, despite this limitation, the data is still significant from a qualitative point of view, and clearly indicates a significant degree of membrane association and partitioning for the studied compounds.

While this partitioning occurs to varying degrees amongst the active compounds, even those in which the transport activity is quite low, the only compound in which the emission at 320 nm does not significantly increase upon vesicle addition is the completely transport-inactive HO_2C-Hex-Dip-Hex-C12. This can be further illustrated when comparing the emission at both 320 and 380 nm over a period of time between the reasonably active HO_2C-Hex-Dip-Hex-C6 and its longer C12-terminated analog (Figure 4.14). These two compounds were chosen as model substrates for the majority of the fluorescence assays as their structures are quite similar, differing only in the length of alkyl tail, but their length or hydrophobicity differences were clearly sufficient to lead to vastly different ion-transport activity in both the HPTS and bilayer clamp assays. As shown in Figure 4.14, the membrane partitioning results obtained for these compounds are completely analogous to the results seen for the first generation Dip isomers; the longer, inactive molecules (HO_2C-Hex-Dip-Hex-C12 in this case, HO_2C-Dec-Dip-Hex-G(12)-OH for the first generation isomers) exhibit mainly 380 nm emission that does not change over time; the emission spectra before and after vesicle incubation look very similar for these compounds (Bottom panel, Figure 4.14). In contrast, the emission at 320 nm for the active compounds (HO_2C-Hex-Dip-Hex-C6 in this case) is significantly enhanced over that seen in aqueous solution, with the fluorescence spectrum after vesicle incubation strongly resembling that seen for the monomers in methanol (Top panel, Figure 4.14). In addition, the slow growth of the excimer emission

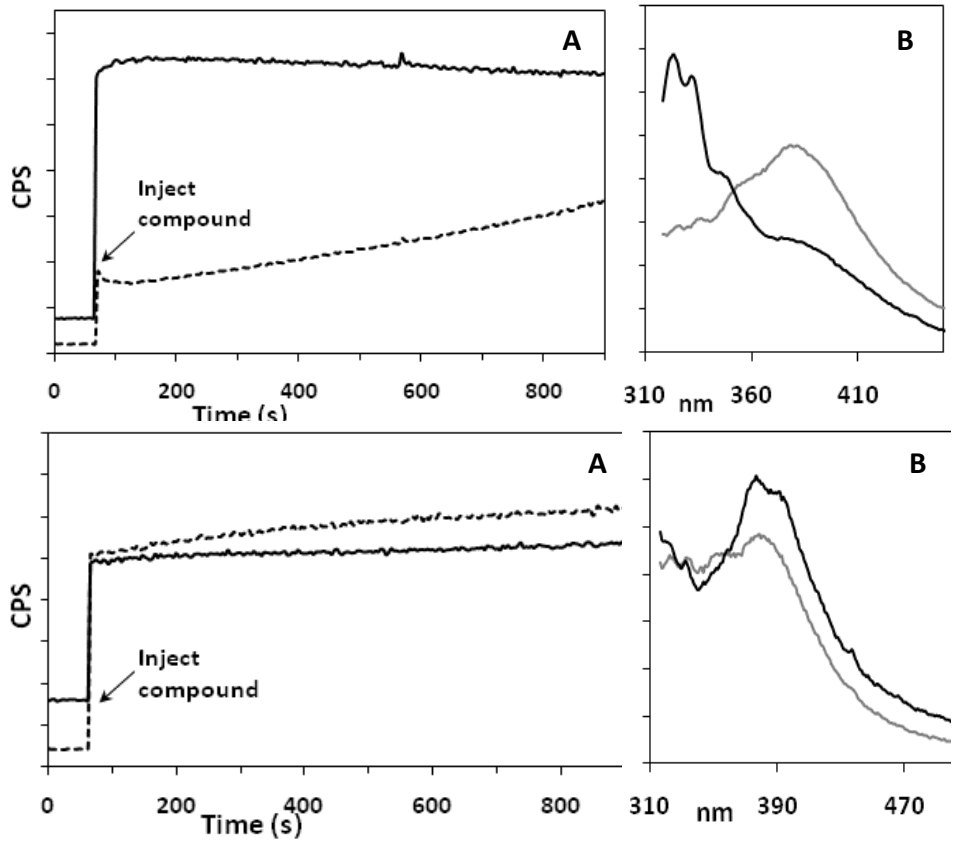

Figure 4.14: **TOP PANEL**: **A**: Fluorescence emission ratio at 320 nm (solid line) versus 380 nm (dashed line) as a function of time of 25 μM HO_2C-Hex-Dip-Hex-C6 injected at the specified time into an aqueous suspension of lipid vesicles (10 mM Na_3PO_4, 100 mM NaCl, pH 6.4). λEx= 305 nm. **B**: fluorescence emission spectra of the same solution before (grey line) and after (black line) vesicle incubation. **BOTTOM PANEL**: analogous experiments for 25 μM HO_2C-Hex-Dip-Hex-C12.

at 380 nm over time is exactly the same sort of behaviour seen for the active 1st-generation isomers, and tracks the slow aggregation of monomers in the membrane. Importantly, in contrast to the other headgroup-modified compounds shown in Figure 4.13, the wavelength maxima for excimer emission in aqueous solution and in the presence of vesicles are only slightly different for both HO_2C-Hex-Dip-Hex-C6 and HO_2C-Hex-Dip-Hex-C12, indicating that comparing fluorescence intensity at a constant wavelength is an accurate gauge of excimer emission in these cases. This is another reason why these compounds were chosen for extensive study, as further discussed in the next Chapter.

4.5.3: Quenching in vesicles

As the differential emission ratios observed for HO_2C-Hex-Dip-Hex-C6 and its C12 analog supported the proposed working hypothesis suggested in Chapter 2 (Figure 2.20), this was an exciting result. Further support for the model came from the quenching assays, illustrated in Figure 4.15, in which the extent of quenching in aqueous solution for both active (HO_2C-Hex-Dip-Hex-C6) and inactive (HO_2C-Hex-Dip-Hex-C12) model compounds are shown in the presence and absence of vesicles. While the 380 nm band is efficiently quenched for both compounds in aqueous solution, the extent of quenching in vesicles for the active compound is decreased from greater than

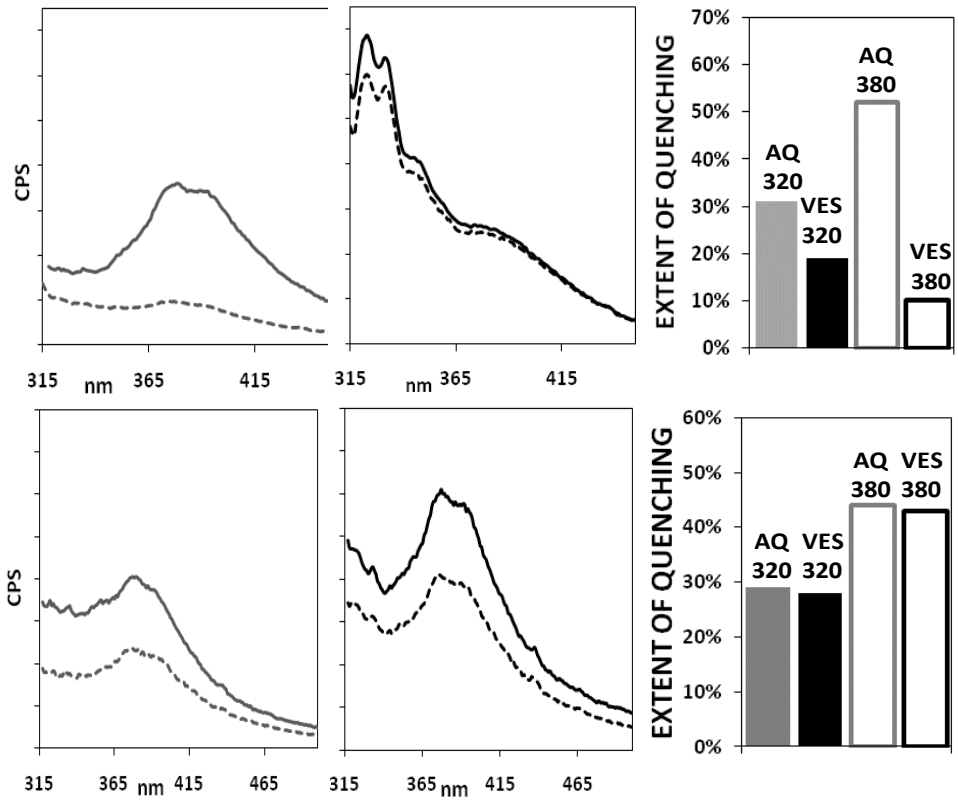

Figure 4.15: **TOP PANEL**: Fluorescence emission spectra of 25 µM HO_2C-Hex-Dip-Hex-C6 (λEx= 305 nm) in aqueous solution (10 mM BisTris, 100 mM NaCl, pH 6.4) in the absence (grey) or presence (black) of lipid vesicles with the addition of 0.1 mM $CuSO_4$ (dashed lines). The bar graph shows the extent of quenching at both 320 and 380 nm, in the presence and absence of vesicles, as marked. **BOTTOM PANEL**: analogous experiments for 25 µM HO_2C-Hex-Dip-Hex-C12.

50% in aqueous solution to less than 10% in the presence of vesicles. A similar decrease is observed for the emission at 320 nm, although this comparison may not be accurate

as the 320 nm emission in aqueous solution is not well-defined for HO_2C-Hex-Dip-Hex-C6. These results are strongly suggestive of a membrane-partitioned compound, which is protected from the externally added aqueous quencher. In contrast, the results observed for HO_2C-Hex-Dip-Hex-C12 clearly suggest that the majority of the compound remains external to the vesicle as an aqueous aggregate, as the extent of quenching with and without vesicles is almost exactly the same. Overall, this data indicates that the mechanism proposed in Chapter 2 is plausible, and that the different emission ratios observed for these compounds indicate their degree of membrane partitioning, which can be directly correlated with their ion-transport activity.

When attempting to extend the quenching assays to the rest of the second-generation Dip isomers, it becomes obvious that the same limitations that complicated their membrane-insertion studies would be a factor here as well. The fact that the emission maxima vary so significantly between aqueous and in-vesicle solutions makes choosing a 'standard' wavelength at which to compare the data quite challenging. In order to be consistent with the previous assays, it was decided to conduct the emission ratios at the maximal wavelengths present in the aqueous spectra of the various compounds. While this affects the data in a quantitative sense, i.e. the actual 'extent of quenching' percentages, the qualitative observations are certainly valid. As for the membrane-insertion assays, if quantitative data are required, it would be worthwhile to re-visit these quenching assays as a 'multi-dye' experiment to see how the obtained values compare.

Figure 4.16 and Table 4.3 give an overall summary of the extent of monomer and excimer-type emission present for the Dip compounds in both aqueous and vesicle-containing solution, in the presence and absence of ~0.1 mM copper as quencher. The fluorescence intensity (CPS) is used to compare both within compounds (for example with and without quencher) and between compounds, as the fluorescence intensities at the same concentration are fairly similar amongst them. It is useful to present the data in this fashion as it illustrates which species are dominant for which compound under various conditions. However, this is a static view, which does not take into account the

dynamic processes that occur for these compounds, which are clearly significant. Nonetheless, continuing with a qualitative analysis, it can be seen that certain trends emerge. Firstly, the dramatic enhancement of emission at 320 nm for the active compounds upon incubation with vesicles is evident in this Figure, as is the substantial increase in 380 nm emission; these behaviours have already been discussed. Considering the quenching data, it is immediately evident that the emission at 380 nm is significantly less quenched in the presence of vesicles than in aqueous solution; for the acetate-terminated compound, the extent of quenching was decreased three-fold, from greater than 60% in water to less than 20% with vesicles (Figure 4.16C). This indicates that the excimer emission observed in vesicles is due to a membrane-inserted species which is

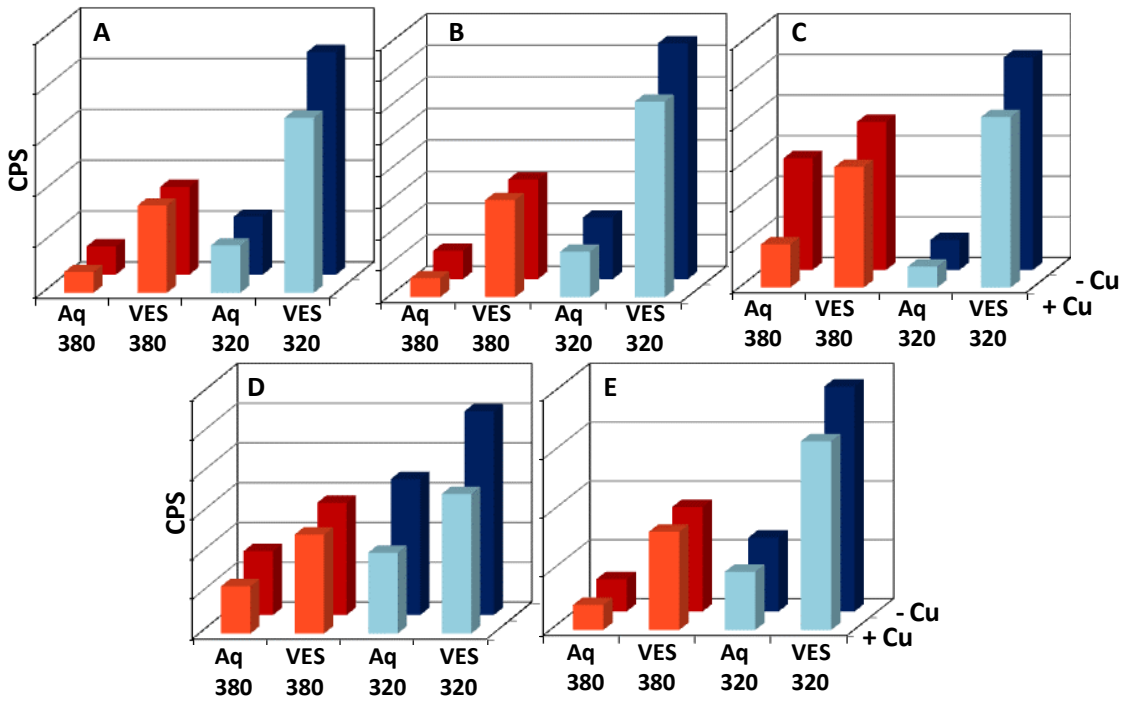

Figure 4.16: Fluorescence emission summary for selected head-group modified Dip isomers. **A**: 16 µM HO_2C-Hex-Dip-Hex-OH, **B**: 17 µM HO_2C-Hex-Dip-Hex-Hex-OH, **C**: 18.5 µM HO_2C-Hex-Dip-Hex-Hex-OAc, **D**: 15 µM HO_2C-Hex-Dip-Hex-Hex-OPhos, **E**: 18 µM HO_2C-Hex-Dip-Hex-Hex-OSucc. Conditions as marked. [$CuSO_4$] = 0.1 mM for all compounds except HO_2C-Hex-Dip-Hex-Hex-OPhos, for which it was 0.2 mM. Excitation wavelengths varied minimally around 305 nm (302-305) for all compounds.

inaccessible to the aqueous quencher. As discussed, this behaviour has been seen previously for the active Dip isomers of both generations, and was therefore not surprising to observe this for compounds such as HO_2C-Hex-Dip-Hex-Hex-OH or -OPhos,

as they are active ion transporters, and would be expected to exhibit an in-membrane aggregate emission that could be due to the active structure. However, this behaviour is seen for all the compounds in Figure 4.16, even the minimally active HO_2C-Hex-Dip-Hex-Hex-OSucc; in fact, the relative proportions of 380 nm-emitting species present in vesicles with and without copper look almost identical for the various isomers. This is a most interesting result, suggesting that the presence of an in-membrane aggregate is not in itself sufficient for transport activity. This is the first indication throughout this work that perhaps the 380 nm emitting species is not indicative of the active structure, an intriguing observation which will be further discussed in the next Chapter. The results are still consistent with what has been previously observed, as the only compound which was completely inactive (HO_2C-Hex-Dip-Hex-C12) saw no protection from quenching in vesicles. Therefore, the increase in emission intensity and the protection of this emission from quenching observed for the other oligomers must be indicative of a membrane-inserted aggregate. However, the detected aggregate is not necessarily correlated with transport activity; i.e. detected aggregation is not a sufficient condition for activity.

Further interesting observations occur when examining the quenching behaviour at 320 nm; in all cases the quenching seen in vesicles is quite similar to that observed in aqueous solution, with an average reduction in vesicles of approximately 10%. This clearly indicates that the 320 nm emitting species is accessible to the copper ions in solution, and is therefore not partitioned into the membrane interior. While this could suggest that the compound remains in aqueous solution, it is much more likely that the compound is associated with the membrane in some way, presumably adhering to the outside of the vesicle; the enhanced emission at 320 nm in the presence of vesicles is strongly suggestive of this. These membrane-associated monomers could then slowly partition into the membrane and aggregate over time, as indicated by the slow increase in emission at 380 nm seen for all the active second-generation Dip isomers. This particular mechanism of activity; i.e. membrane association of monomers followed by slow insertion and aggregate formation has been recently invoked to explain the

behaviours exhibited by both membrane-inserting CPEs [131] as well as other fluorescent ion channels [98], and it is consistent with the behaviours seen for the Dip isomers.

COMPOUND	λEM (CH_3OH)	λEM (AQ)	λEM (VES)	QUENCHING 320		QUENCHING 380	
				AQ	VES	AQ	VES
HO_2C-Hex-Dip-Hex-Hex-OH	319	407	321	30%	18%	34%	15%
HO_2C-Hex-Dip-Hex-Hex-OPhos	319	319	319	41%	28%	29%	12%
HO_2C-Hex-Dip-Hex-C6	324	377	322	31%	19%	52%	10%
HO_2C-Hex-Dip-Hex-Hex-OAc	320	372	321	28%	20%	61%	19%
HO_2C-Hex-Dip-Hex-OH	317	317	321	19%	19%	39%	14%
HO_2C-Hex-Dip-Hex-C12	322	377	377	29%	28%	44%	43%
HO_2C-Hex-Dip-Hex-Hex-OSucc	319	319	319	22%	19%	39%	14%

Table 4.3: Summary of fluorescence emission properties for 2nd-generation Dip isomers. For quenching studies, the extent of quenching (with $CuSO_4$) was measured at the maximum emission wavelengths determined in CH_3OH (~320 nm) or aqueous (AQ) solution (~380 nm). Extent of quenching at both wavelengths in the presence (VES) or absence (AQ) of lipid vesicles was then compared. Excitation wavelengths varied minimally around 305 nm (301-305 nm). Emission intensity in aqueous solution was found to vary over time for some compounds. Experimental details available in Appendix 3.

4.5.4: Quantifying partitioning

Another method used to characterize the behaviour of the second generation Dip compounds when introduced to vesicles was to actually quantify the extent of partitioning by obtaining a Kp value. This assay was described in Chapter 3 (section 3.5.3); it involves titrating a constant concentration of compound against increasing concentrations of lipid. As the fluorescence intensity of the Dip oligomers increases upon membrane incorporation, this increase can be fit to Equation 3.1 to obtain the partitioning constant [123]. Importantly, the fluorescence response must reach saturation in order for Equation 3.1 to be applicable; this prevented the calculation of a Kp value for the compound (HO_2C-Trip-G(E3)-OH) tested in Chapter 3.

For the 2nd-generation Dip molecules, this experiment was carried out on HO_2C-Hex-Dip-Hex-C6 and HO_2C-Hex-Dip-Hex-Hex-OH, these compounds were chosen as they were both active, and clearly both able to partition, yet their activities differed by 3-fold despite the very minor structural variation present between them. It was therefore of interest to explore how the presence of a single extra oxygen atom in HO_2C-Hex-Dip-Hex-Hex-OH can lead to such an increase in activity above that exhibited by HO_2C-Hex-Dip-Hex-C6; could this be correlated to their affinity for the membrane? The results of this experiment are shown in Figure 4.17 for HO_2C-Hex-Dip-Hex-C6 and Figure 4.18 for HO_2C-Hex-Dip-Hex-Hex-OH. The demonstrated scans were taken after a 3 minute incubation period, and not repeated afterwards, they therefore illustrate a 'static' picture. This was done to try to minimize the time-dependent emission changes that can occur for these compounds. In particular, the slow growth of the 380 nm emission in the presence of vesicles (once partitioned) was not monitored in this assay.

For both compounds, the fluorescence increase was observed to reach

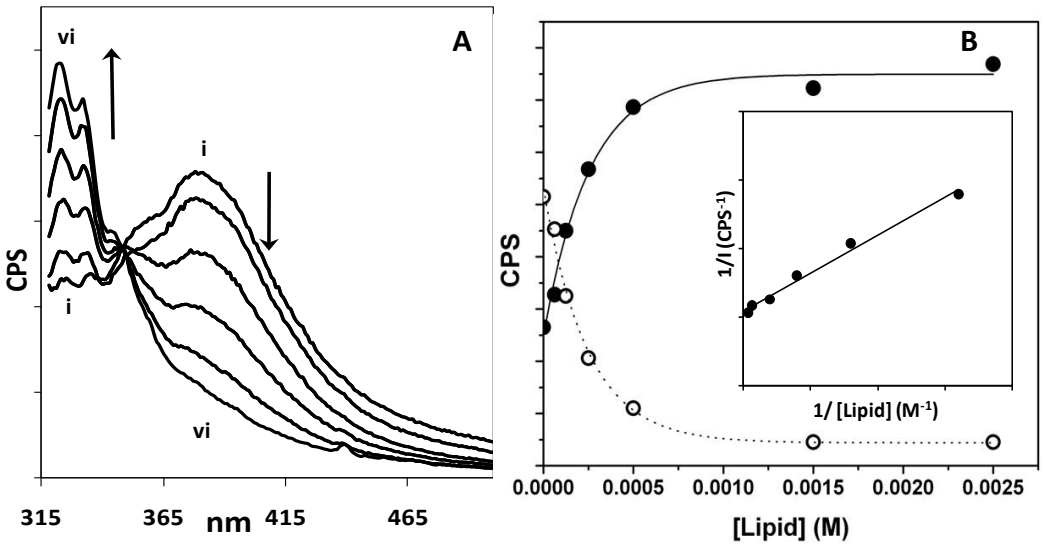

Figure 4.17: Fluorescence partition assay for HO_2C-Hex-Dip-Hex-C6. **A**: Fluorescence emission spectra of 17 µM compound (λEx= 305 nm) titrated against increasing concentration of lipid vesicles. From i to vi, lipid concentrations= 0.0625, 0.125, 0.25, 0.5, 1.5, 2.5 mM. **B**: Plot of CPS at 320 nm (closed circles) and 380 nm (open circles) as a function of lipid concentration, double reciprocal plot (INSET) used to determine Kp using Eqn 3. 1, r^2= 0.99.

saturation, thereby allowing the derivation of the partitioning constant. For HO_2C-Hex-Dip-Hex-C6, the increase in 320 nm emission correlated exactly with the decrease in 380

nm emission; the curves even pass through a common isoemissive point at approximately 350 nm. This indicates that the aqueous aggregate and the membrane-bound compound are the only two detected species in this case [132]. Analysis of the titration data by plotting the double reciprocal of fluorescence intensity as a function of lipid concentration, as shown in Figure 4.17B, gave a linear relationship; the x-intercept of this line multiplied by the concentration of water is equal to Kp (see equation 3.1) [123]. The derived Kp value for HO_2C-Hex-Dip-Hex-C6 is therefore 1.05 ±0.04 x 10^6. This value can also be used to determine an 'EC_{50}': the lipid concentration needed to incorporate half the probe population; [W]/Kp, which is equal to 53 μM in this case. These values suggest that HO_2C-Hex-Dip-Hex-C6 has a moderate affinity for the membrane, but more importantly, that the compound is completely partitioned into the membrane at the lipid concentrations utilized for the HPTS assay (0.5 mM lipid). This indicates that the transport activity observed for HO_2C-Hex-Dip-Hex-C6 is the 'maximum' possible, unlike that observed for HO_2C-Trip-G(E3)-OH, in which only a fraction of the compound was successfully partitioned into the membrane at the utilized lipid concentrations. Interestingly, the Kp value for HO_2C-Hex-Dip-Hex-C6 is strikingly similar to the Kp and lipid EC_{50} values obtained by Haugland and Huang in the original report for several common membrane probes. For example, these authors report a Kp value of 1.3 x 10^6 for the well-known membrane probe DPH (1,6-diphenyl- 1,3,5-hexatriene, compound **4-24** in Table 4.4). In addition, the Kp and EC_{50} values obtained for HO_2C-Hex-Dip-Hex-C6 are also very similar to those obtained by Gokel *et al*. for the fluorescent peptides discussed in Chapter 2. In this case, the tested compound (**4-25**) had an NBD-fluorophore attached to the peptidic backbone, and was found to have a Kp of 1.29 x 10^6, corresponding to an EC_{50} of 43 μM (see Table 4.4 for structure) [98]. The continuing similarities between these compounds are most interesting.

The partitioning data for HO_2C-Hex-Dip-Hex-Hex-OH are presented in Figure 4.18; in this case the isoemissive point is much less defined, although it seems to occur

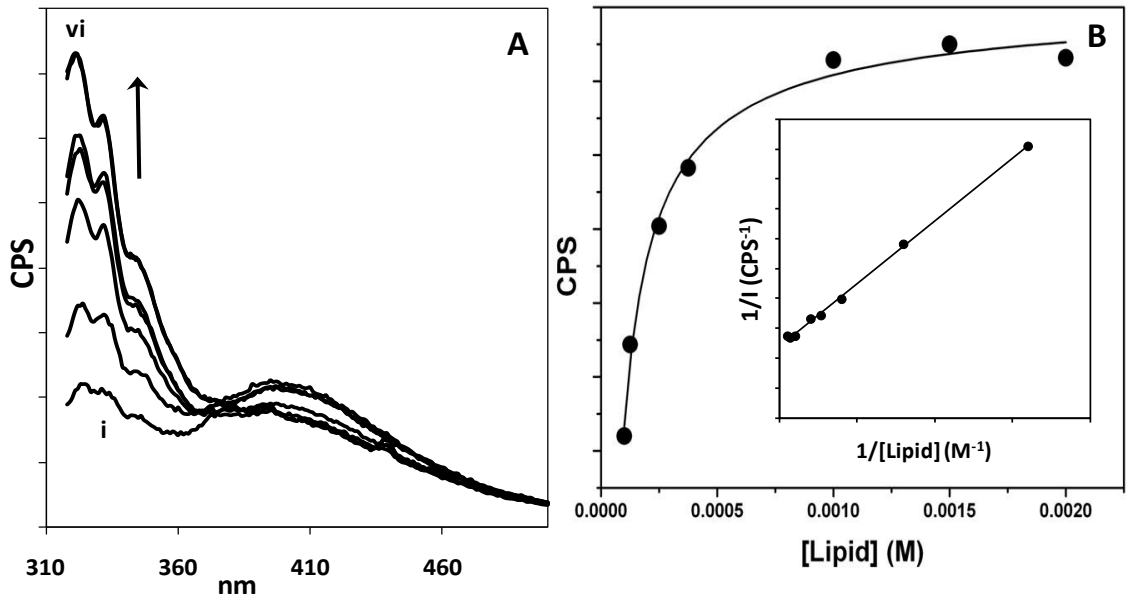

Figure 4.18: Fluorescence partition assay for HO_2C-Hex-Dip-Hex-Hex-OH. **A**: Fluorescence emission spectra of 17 µM compound (λEx= 305 nm) titrated against increasing concentration of lipid vesicles. From i to vi, lipid concentrations= 0.0625, 0.125, 0.25, 0.375, 0.5, 1.5, 2.5 mM. **B**: Plot of CPS at 320 nm as a function of lipid concentration, double reciprocal plot (INSET) used to determine Kp using Eqn 3.1, r^2= 0.99.

at approximately 370 nm. Furthermore, the increase in emission at 320 nm is not accompanied by a concomitant decrease in emission at 400 nm; rather, the emission intensity at this wavelength remains fairly constant over time. This is an interesting observation, and suggests that the species present at 400 nm is not being bound by the vesicles. This is consistent with the previous observation that the compound has minimal aqueous aggregation, and is mainly monomer in aqueous solution (Figure 4.13B), as only the 320nm emission changes with lipid. When fit to Equation 3.1, the Kp and lipid EC_{50} value obtained for HO_2C-Hex-Dip-Hex-Hex-OH are 3.18 ±0.01 x 10^5 and 174 µM, respectively. These are lower than those observed for HO_2C-Hex-Dip-Hex-C6, as well as DPH and the Gokel NBD-peptide **4-25**; apparently HO_2C-Hex-Dip-Hex-Hex-OH has a significantly *lower* affinity for the membrane than do these other compounds. This is reasonable considering the structures of the various compounds, as Haugland and Huang did indeed observe lower Kp values for more polar molecules; the propionic-acid terminated analog of DPH (compound **4-26** in Table 4.4) has a Kp of 6.5 x 10^5, while that for the positively-charged aniline derivative (TMA-DPH, compound **4-27**) was lower

still, at 2.4 x 10^5 (structures and partitioning data of comparison compounds are shown in Table 4.4). Clearly, the hydrophobicity and polarity of the molecules plays an important role in partitioning, as expected. Despite the lower Kp value obtained for HO_2C-Hex-Dip-Hex-Hex-OH, it is still maximally partitioned at the lipid concentration utilized for the HPTS assay, as seen for HO_2C-Hex-Dip-Hex-C6.

COMPOUND & STRUCTURE	Kp	EC_{50}[a] (μM)
HO_2C-Hex-Dip-Hex-C6: see Table 4.1	1.05±0.04 x10^6	53
HO_2C-Hex-Dip-Hex-Hex-OH: see Table 4.1	3.19±0.01 x10^5	174
DPH[b] **4-24** 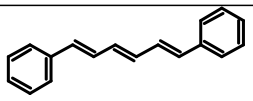	1.3 x10^6	43
DPH-Propionic acid[b] **4-26** 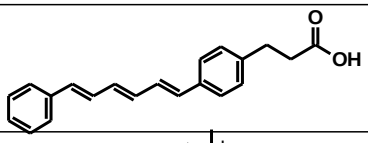	6.5 x10^5	85
TMA-DPH[b] **4-27** 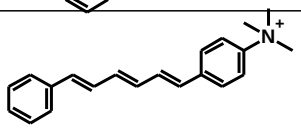	2.4 x10^5	230
NBD-Peptide[c] 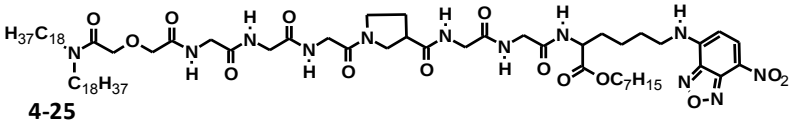 **4-25**	1.29 x10^6	43

Table 4.4: Partitioning data for various membrane probes. a= value corresponds to lipid concentration needed to incorporate 50% of the probe molecule. b= determined by Haugland and Huang [123], c= determined by Gokel *et al*. [98].

Comparing directly the data obtained for HO_2C-Hex-Dip-Hex-C6 and the hydroxyl-terminated analog further illustrates that ability to partition is not the only deciding factor in determining ion transport activity. This was concluded based upon the minimal HPTS activity of the succinate analog, despite its evident ability to partition. That the less polar HO_2C-Hex-Dip-Hex-C6 partitions more efficiently into the non-polar membrane is not surprising, and the fact that the compounds both do this to a fairly high extent is consistent with the argument that efficient partitioning can be correlated with ion transport activity. Once partitioned, however, the in-membrane structures of

these compounds must be significantly different enough to lead to a 3-fold difference in activity. The previously-mentioned hypothesis that the terminal hydroxyl group facilitates a transmembrane structure due to the potential to interact favourably with the polar lipid headgroups could be a plausible explanation for this behaviour. Nevertheless, the ability to obtain Kp values for the Dip isomers that are reasonably similar to those observed for other membrane-inserting compounds is significant, and indicates that the transport activity observed for these compounds is an accurate reflection of the maximum activity possible.

4.6: Conclusions & future work

In this Chapter, the synthesis and characterization of a series of headgroup-modified Dip-containing oligomers has been discussed. The developed syntheses were modular, high yielding and very time-efficient, enabling a large suite of compounds to be made and tested to examine possible structure-activity correlations. In many cases, the vesicle-based ion transport activity was seen to agree quite well with structural considerations, as well as with the results obtained by the bilayer-clamp technique. While certain structures, such as the succinic-acid terminated compound exhibited behaviour that was initially unexpected, careful consideration of length, hydrophobicity and charge effects could indeed rationalize this observed behaviour. The most significant achievement stemming from the work on the second-generation Dip compounds is believed to be the development and synthesis of the highly transport-active HO_2C-Hex-Dip-Hex-Hex-OH. As mentioned previously, this compound is most promising due to its high activity, reasonably regular single-channel conductances and ease of synthesis, and should continue to be studied in the future. As the synthetic methodology to access these compounds is now very well-established, further modifications can easily be made to the existing structure, in hopes of achieving certain desirable properties such as voltage-gated transport activity.

While the transport activity for the second-generation Dip isomers is reasonably well understood, their photophysical characteristics are not as easily rationalized. Certain trends are observed; for example, it is clear that all the active compounds, even if their activity is minimal, can associate with or partition into the membrane to a certain extent, as evidenced by the changes in emission observed upon vesicle introduction, as well as the quenching protection afforded to the compounds in the presence of vesicles. In contrast, the completely inactive isomer (HO_2C-Hex-Dip-Hex-C12), in which the emission at 380 nm dominates, does not exhibit any significant changes to its spectrum when incubated with vesicles, and its fluorescence can be quenched in the presence of vesicles. Its lack of partitioning therefore explains its inactivity. However, the extent of partitioning cannot be used as a clear indicator of enhanced activity, as the higher Kp value for the less-active HO_2C-Hex-Dip-Hex-C6 compared with its more active analog HO_2C-Hex-Dip-Hex-Hex-OH indicates. Nonetheless, the increased emission at 320 nm in the presence of vesicles for all the active compounds is clearly significant, indicating a less polar environment for the chromophore. This further strengthens the utility of the Dip chromophore as an effective membrane probe, and supports the conclusion that increased emission at 320 is a good indication of membrane partitioning, which can be correlated to ion transport activity in certain cases.

Throughout this work, the majority of the photophysical characterization of the various compounds has remained qualitative; this is necessary due to the complex behaviours associated with these molecules. It is now evident that the second-generation Dip compounds, despite their relatively similar structures, exhibit fluorescence characteristics which vary significantly amongst the series, which makes rationalizing their behaviour challenging. However, as mentioned, there is scope for further experimental refinement which could possibly aid in their analysis. In particular, the use of a multi-wavelength emission ratio is most promising; such an experiment was in fact utilized for the first generation Dip isomers to monitor the HPTS assay concurrently with membrane insertion dynamics (data available in Appendix 4). As

spectral changes occur for the headgroup modified compounds at both the 'monomer' and 'excimer' wavelength regions, individual monitoring of each of these regions could potentially lead to interesting findings such as whether the in-membrane and aqueous aggregates can be separately detected. This remains a promising goal for future work. In general, the most useful results come from direct comparison between the length isomers HO_2C-Hex-Dip-Hex-C6 and HO_2C-Hex-Dip-Hex-C12. These compounds have many favourable properties which makes them a good choice as model compounds for further study. Their fluorescence emission intensity is reasonably stable over time, they are structurally similar while exhibiting completely different ion transport activity, and most importantly, their wavelength maxima for excimer emission between aqueous and in-vesicle solution are fairly similar, which allows accurate monitoring of membrane insertion. Further studies involving these compounds will be discussed in the next Chapter.

When considering the structure-activity relationships present in the entire set of second-generation Dip isomers, several overall trends can be observed. Firstly, it is evident that some degree of charge at one terminus at least is essential for activity; compare HO_2C-Hex-Dip-Hex-C6 ('baseline' rate achieved at 15 µM) with $PREO_2C$-Hex-Dip-Hex-C6 (inactive). Furthermore, it appears that having polarity at both termini, as for the phosphate and hydroxyl-terminated analogs, is beneficial; this seems intuitive as it supports the design criteria – synthetic ion channels that are meant to span the membrane 'should' have the same sort of polarity as the bilayer itself. Finally, there is a clear length/hydrophobicity effect present in these compounds. The longest or most hydrophobic compounds are essentially inactive (HO_2C-Hex-Dip-Hex-C12) and the shortest compound (HO_2C-Hex-Dip-Hex-OH) exhibits minimal activity, while the highest activity is observed for compounds measuring approximately 37 Å (HO_2C-Hex-Dip-Hex-Hex-OH).

While these trends are clear and can be rationally explained, in all cases there are a number of effects occurring simultaneously, and the subtle interplay between them cannot be completely deconvoluted; how to tell for certain if it is the length of

HO_2C-Hex-Dip-Hex-C12 that is causing its inactivity or the hydrophobicity *due* to its length, for example. Another intriguing question arises when comparing HO_2C-Hex-Dip-Hex-C6 and its hydroxyl-terminated analog HO_2C-Hex-Dip-Hex-Hex-OH – can a greater than 3-fold increase in activity really be due to such a minor variation, especially as it is the less-active compound that partitions more efficiently?

While these are important questions, and could possibly be addressed by the synthesis and analysis of a greater number of compounds, the overall goal of synthesizing the 2nd-generation Dip isomers was to obtain structure-activity relationships that could suggest key elements important for activity, which was indeed achieved. The vastly differing activity amongst these isomers has pointed out what features are beneficial and which are detrimental, information that can be applied in designing further Dip-containing compounds. Most promisingly, these studies have led to the development of two very highly active compounds; HO_2C-Hex-Dip-Hex-Hex-OH and its phosphate-terminated analog. As mentioned, these compounds are the most active of all the molecules synthesized in this work, and are now almost 10 times as active as the precursor fully-saturated oligoesters. Importantly, these compounds are also amongst the most structurally-simple molecules known to form functional ion channels; an ongoing objective in this work. In contrast to many known structures their synthesis involves only up to 4 steps from readily available key precursors, which is a significant benefit when attempting to build a library of compounds. Their purification and characterization is also straightforward, and their structures known to a high degree of confidence, which can be difficult for larger, more complex channel-formers. It is hoped in the future that these beneficial features will allow these compounds to find further use both as ion transporters and in other interesting, possibly biological, applications.

In conclusion, the goals laid out at the beginning of this Chapter have been achieved; a series of compounds was efficiently synthesized and characterized, leading to the discovery of two highly-active ion transporters. Their photophysical

characteristics, while complex, are undoubtedly interesting, and certainly provide many opportunities for future work on this topic.

Chapter 5 : Time-resolved studies and mechanistic implications

5.1: Rationale

Over the past few decades of synthetic ion channel research, a great variety of compounds have been synthesized that have achieved the stated goals of transporting ions, as well as in certain cases exhibiting higher levels of regulation such as voltage or ligand-gating. Certainly, progress towards the goal of achieving 'bio-mimetic' ion transport has been made, as well as notable developments in other fields such as therapeutic and sensor applications. In addition, the functional characterization of synthetic ion channels utilizing vesicles and planar bilayers has led to much information about what these molecules do. However, an area of synthetic ion channel research that has not been as extensively developed is the proposal of a mechanism or model to account for the various active and inactive structures that form when the compounds are introduced to a bilayer, and how these interconvert over time. This makes it difficult to predict or understand how designed structures actually work. From the present research in particular, it is evident that a number of aggregates, both active and inactive, occur in both the aqueous solution and in the membrane, and that these species have different properties over time. Both the identity of these species, as well as the time scales involved in their interconversion would be very interesting to discover.

The reasons behind the lack of mechanistic details provided for many synthetic ion channels are numerous, and most are centered on the fact that the channels made by monomer aggregation are transient in nature [25]. As shown in many studies including this work, the properties of these aggregate channels are highly variable over time. For the Dip isomers, the fluorescence spectra, bilayer activity and membrane insertion studies are all time-dependent. Other factors complicating mechanistic development are that in most cases, the active structure exists only in the membrane and is a minor species which is structurally different than the monomers that comprise it, therefore,

structural studies on supramolecular ion channels are very difficult to perform [27]. In addition, the activity observed for these types of channels is highly dependent on the experimental parameters such as type of lipid and electrolyte used, concentration and pH of the solution, amongst others. Interestingly, this situation is actually more complicated with structurally simpler molecules such as the ones discussed here. While a large, unimolecular 'barrel' type compound such as the octiphenyl beta-barrels developed by Matile *et al*. [30] clearly suggests an active structure, this is much more difficult to predict for an aggregate channel made up of a number of monomers. This too can be observed in the current work; with Hill coefficients [27] (possibly indicating the number of monomers making up the active channel) ranging from two to eleven [64], the implied structures available to the Dip isomers are numerous; this is also evident from the variety of behaviours witnessed in the bilayer clamp experiment. Considering these factors, which are certainly not unique to the Dip compounds, it is therefore understandable that the active structures, as well as inactive intermediates, are unknown for the majority of synthetic ion channels.

Due to this lack of structural evidence, the development of a plausible model to help understand how current synthetic ion channels work, and on which to base future compound design is clearly an important goal, and is being actively pursued. In the Fyles group, a working hypothesis has been proposed based initially on the observations from the fully-saturated oligoesters, illustrated in Figure 1.10. This hypothesis was further developed in this work involving the Dip compounds, as their environment-sensitive fluorescence has allowed the visualization and tracking of certain proposed species (Figure 2.20 in Chapter 2, re-drawn here as Figure 5.1). The Dip compounds are especially well-suited to a mechanistic study, as a wide variety of these molecules are available and they display varying properties which can be related to their structure in a discernable way; for example, the lack of excimer emission in aqueous solution for the more hydrophilic compounds such as HO_2C-Hex-Dip-Hex-Hex-OPhos (Chapter 4). These structure-activity relationships, as well as the probe qualities of these molecules, indicate that further mechanistic details could be extracted from these compounds. If

some idea as to the active or inactive species as well as their interconversion could be gained from the differential fluorescence characteristics of the Dip molecules, this could be used to design future compounds more efficiently and effectively.

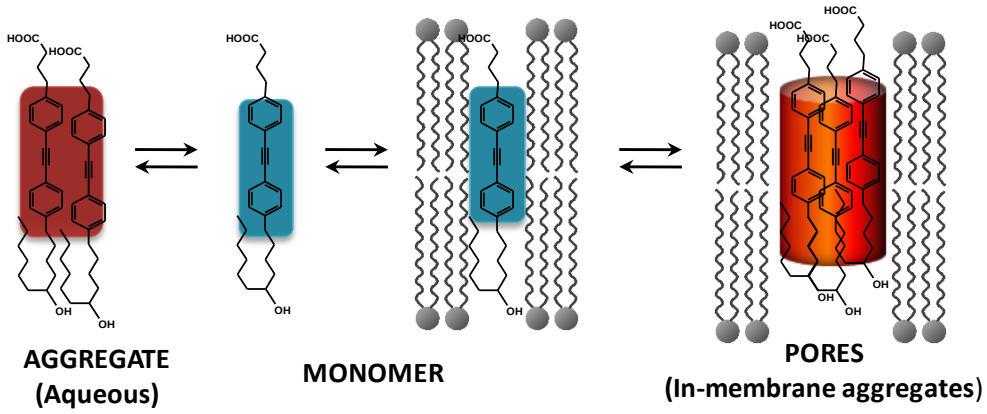

Figure 5.1 : Copy of Figure 2.20, working hypothesis to explain the activity of the Dip oligomers.

5.2: Time-dependent ion transport activity

An underlying theme observed repeatedly for most of the compounds synthesized for this work is that their fluorescence and aggregation behaviours are highly time-dependent. While the majority of these behaviours are expected due to the dynamic properties of such aggregate channels, it would be desirable to explain them based on a mechanistic argument, such as discerning and assigning distinct species which are responsible for the various spectra or bilayer activity. In particular, the key impetus was to differentiate between and spectroscopically identify the in-membrane and aqueous aggregates shown to exist for the Dip compounds and assign these as distinct species. If the observed transport behaviour could be linked to these different spectra this would be a step towards determining the structure of an active species.

It was expected that examining the transport activity over time for the Dip compounds while simultaneously monitoring their fluorescence emission would provide valuable information towards this goal. Such a 'multi-dye' experiment which monitored HPTS activity concurrently with fluorescence emission of both monomer (320 nm) and excimer (380 nm) had indeed been carried out for the first generation Dip isomers (see

Appendix 4); the duration of this experiment was only the length of a single HPTS run (10 minutes). However, during the course of studying the activity of the second-generation Dip oligomers, it became evident that the processes that occur for these molecules occur over a much longer time scale. The partitioning assays such as the one shown in Figure 4.14 have been conducted for up to one hour, and the emission at both wavelengths is still changing over this very long period of time. In order to discover when the system stabilizes, an experiment was conducted in which the Dip-containing compounds HO_2C-Hex-Dip-Hex-C6 and C12 were pre-loaded into vesicles at 0.3 mol%. The fluorescence emission at both the monomer and excimer wavelengths of these vesicles in aqueous solution was then monitored over a period of time. As the vesicle preparation (including size-exclusion chromatography) leads to all compound being present in the membrane, the initial emission of these compound-containing vesicles should therefore be stable. After 5 minutes in the fluorimeter, additional oligomer was added from organic solution into the vesicle suspension (indicated by the arrow in Figure 5.2), and the resulting changes were monitored for one hour.

The results of this experiment are shown in Figure 5.2A for HO_2C-Hex-Dip-Hex-C6 and Figure 5.2B for HO_2C-Hex-Dip-Hex-C12. As expected, for the first 5 minutes, the emission intensity of both monomer and excimer remain stable, and very similar between the two compound-containing vesicles. Once the additional solution of compound is introduced, however, the response between the two oligomers is completely opposite: the transport-active HO_2C-Hex-Dip-Hex-C6 immediately partitions into the membrane, evidenced by the pronounced increase in 320 nm (monomer) emission. In contrast, the inactive C12 analog displays immediate increase in emission at 380 nm, due to formation of aqueous aggregates. As previously demonstrated in Chapter 4 (Figure 4.14), the following changes in emission ratio over time are much more pronounced for the active compound; once the initial jump is over, minimal changes occur for HO_2C-Hex-Dip-Hex-C12, while the 380 nm emission continues to increase significantly, at the expense of monomer emission, for HO_2C-Hex-Dip-Hex-C6.

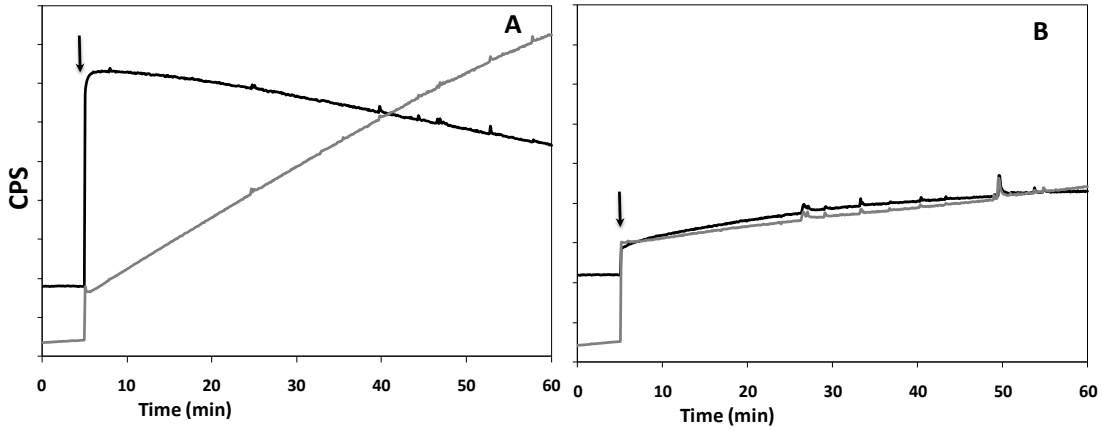

Figure 5.2: Fluorescence emission at 320 nm (black lines) and 380 nm (grey lines) (λEx= 305 nm) for an aqueous suspension of vesicles pre-loaded with **A**: 0.3% HO_2C-Hex-Dip-Hex-C6, or **B**: 0.3% HO_2C-Hex-Dip-Hex-C12. The arrow indicates the addition of 15 μM HO_2C-Hex-Dip-Hex-C6 in **A**, and 20 μM HO_2C-Hex-Dip-Hex-C12 in **B**. The vertical scale is the same for both panels.

For HO_2C-Hex-Dip-Hex-C6, what is most surprising is that these changes continue for such a long period of time; the implications of these long time-scale processes, especially the continuing increase in 380 nm emission, will be discussed in an upcoming section. Interestingly, similar very slow membrane-association dynamics of up to several hours have been observed in systems previously discussed such as the fluorescent peptides of Gokel *et al*. [98] (Figure 3.14 and Table 4.4), certain CPEs [131] and NBD-labelled phospholipids studied by Moreno *et al*. [130]. The similarities observed between these molecules and the Dip compounds further illustrate the need to develop a functional model to track and possibly identify the various intermediates present in these systems, which could be used to explain both partitioning and ion transport behaviour.

Further consideration of Figure 5.2 brings up an interesting question: if the observed changes in the species present occur over such a long time, are the ion transport rates the same over this period? This was probed by conducting a long time-scale HPTS assay, in which an aqueous 'stock' solution of compound and vesicles was made and left to incubate. Every 10 minutes for an hour, an HPTS experiment was run; therefore, the compound had between 3 and 60 minutes in contact with the vesicles. This assay was designed to track both the extent of partitioning (as evidenced by the monomer and excimer emissions), as well as the ion transport activity over time. It was

expected, therefore, that the active compound (HO_2C-Hex-Dip-Hex-C6) would display an increase in ion transport over time, in conjunction with the increased emission at 380 nm (as seen in Figure 5.2A).

The results of this experiment for HO_2C-Hex-Dip-Hex-C6 are shown in Figure 5.3. The first panel (Figure 5.3A) shows the extent of transport obtained at 10 minute intervals; an immediate and striking observation is the rapid *decrease* in ion-transport activity over time from relatively highly active in the first time period (T= 0) to minimally active half an hour later. As in the long-term membrane partitioning results shown in Figure 5.2A, during this rapid decrease in the ion transport activity, the emission at 380 nm continued to increase (Figure 5.3B), eventually becoming nearly equal in intensity to the 320nm, membrane-associated monomer emission (Figure 5.3C). Intriguingly, the transport rate recovers from almost negligible (less than 5×10^{-4} s^{-1}) to greater than that seen initially (4.5×10^{-3} s^{-1}) once another aliquot of compound is added to the solution at 60 mins (Figure 5.3D). This seems to indicate that 'fresh' compound can re-initiate the transport process.

The negative correlation between 380 nm emission and transport rate was completely unexpected, and had immediate ramifications; clearly, the mechanism of action previously proposed for the Dip compounds (Figure 5.1) is not correct in this case. The model suggests that for the active molecules, once the initial partitioning is demonstrated by the immediate increase in 320 nm fluorescence, the slow growth of a 380 nm-emitting species tracks the evolution of an in-membrane aggregate, the presumed active structure. Transport activity and increasing 380 nm emission over time are therefore linked in this model. The current results indicate that while the 380 nm-emission may still be linked to transport, as the aggregate emission is complex and made up of several species, it is now clear that whatever component is causing the *long-term* increase in 380 nm emission for HO_2C-Hex-Dip-Hex-C6, cannot be responsible for transport.

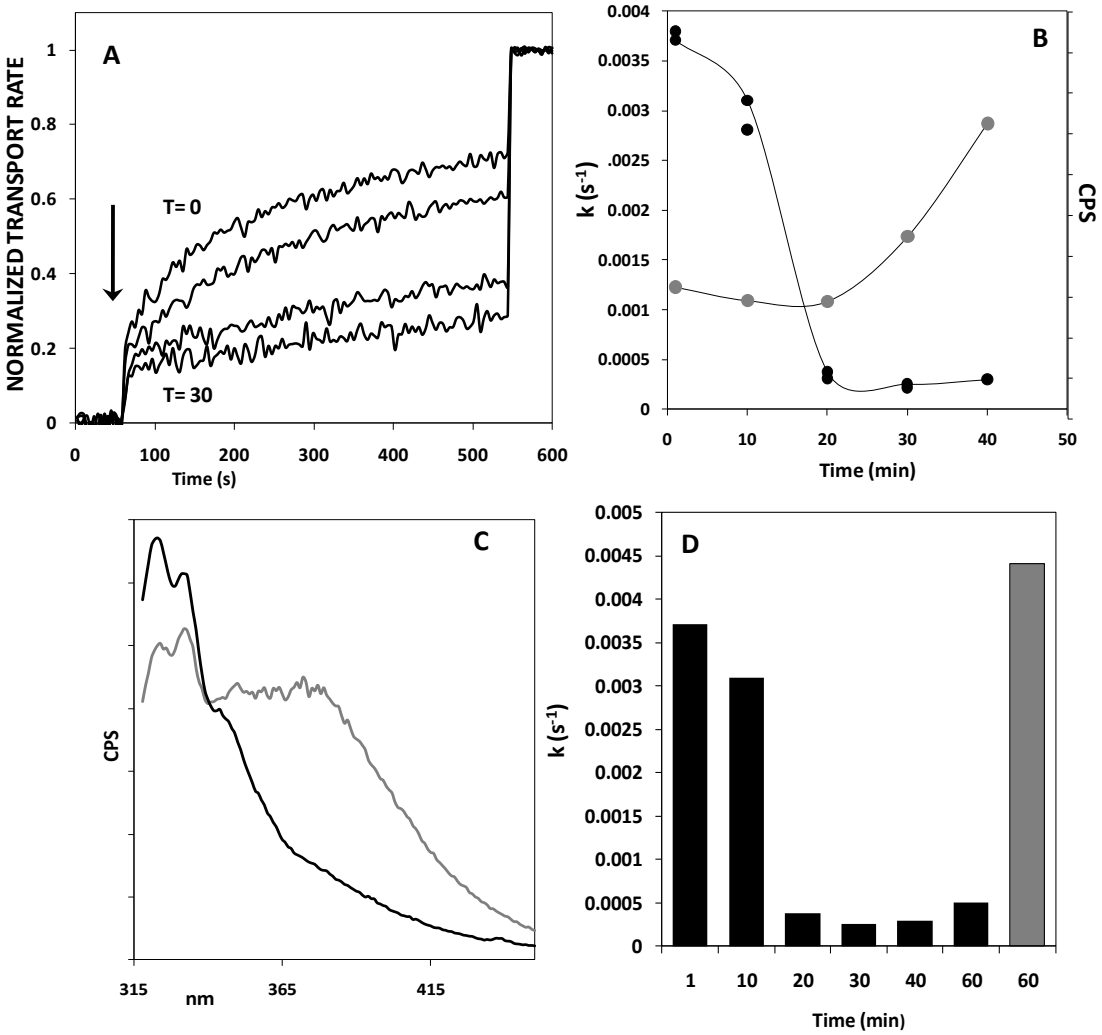

Figure 5.3: Results of long time-scale HPTS activity assay for 22 µM HO_2C-Hex-Dip-Hex-C6. **A**: Decreasing HPTS activity over time; from initial scan at t= 0 minutes, to 10, 20 and 30 minutes. **B**: Rates of HPTS activity (Black circles) compared with increase in emission at 380 nm (grey circles). **C**: Fluorescence emission (λEx= 305 nm) at t= 0 minutes (black line) and t= 40 minutes (grey line). **D**: Bar graph illustrating the same data as in **B** (black bars), indicating the effect of an additional 22 µM of compound (grey bar).

What could the nature of this species be? A plausible explanation is that the continued increase in 380 nm emission observed for HO_2C-Hex-Dip-Hex-C6 is the slow transitioning of the molecule from an active, pore-like aggregate to some other, more stable aggregate which is no longer transport active, yet still emits at 380 nm. This terminally-formed aggregate would therefore act as a 'sink' species for all the introduced compound. This suggestion is supported by the results of the long-term HPTS assay shown in Figure 5.3D: if the decrease in activity is indeed due to the initially

added compound being sequestered as a transport-incompetent 'sink' aggregate, the addition of 'fresh' compound should re-start the transport process, as it does. Further examination of the data provides more evidence; the fact that the transport rate only increases to approximately 1.3 times that initially seen, despite twice as much compound now being theoretically available in the solution, clearly indicates that a certain proportion of the molecule is now present as a stable, in-membrane aggregate which can no longer cause transport. While an alternative interpretation could be that the excess compound is simply precipitating upon introduction into the solution, previous results confirm that the initial membrane association/partitioning of the monomers is a favourable and rapid process. The Kp results of Figure 4.17 are particularly indicative of this, as they show that the compound is fully partitioned at the lipid concentrations used in the assay. Therefore, the formation of the final in-membrane 'sink' species is more consistent with the data.

The long-term HPTS assay was repeated for the highly active 2nd-generation Dip oligomers HO_2C-Hex-Dip-Hex-Hex-OH and -OPhos; the results for the hydroxyl compound are shown in Figure 5.4. For both compounds, the rate of transport

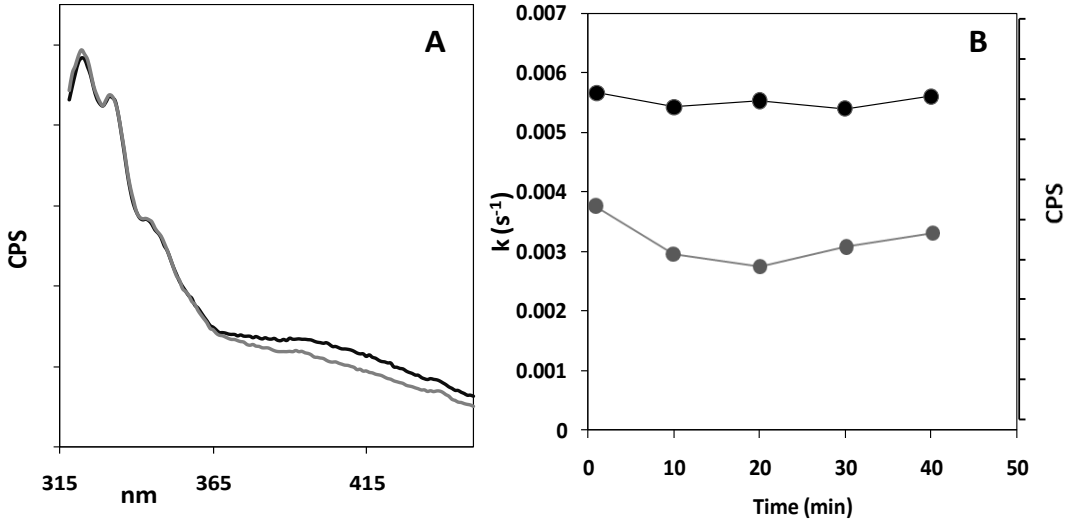

Figure 5.4: Results of long time-scale HPTS activity assay for 10 µM HO_2C-Hex-Dip-Hex-Hex-OH. **A**: Fluorescence emission spectra (λEx= 305 nm) of compound incubated with an aqueous solution of vesicles taken at t= 1 min (black line), and t= 40 min (grey line). **B**: HPTS rates over time (black circles), compared with emission at 390 nm (grey circles). HO_2C-Hex-Dip-Hex-Hex-OPhos exhibited identical behavior.

remained constant over time, as did the excimer emission. This indicates that whatever forces are driving the formation of the inactive in-membrane species for HO_2C-Hex-Dip-Hex-C6, they are not present for these compounds. The reasons for this are currently unclear; perhaps the increased hydrophobicity of HO_2C-Hex-Dip-Hex-C6 favours the formation of a more closely-packed aggregate through which ions cannot pass.

5.3: Fluorescence lifetime studies

The time-based transport results clearly indicate that in addition to having an aqueous aggregate; or more likely a variety of aqueous aggregates, present for the Dip isomers, many in-membrane aggregates including active and inactive species can also form, as seen for HO_2C-Hex-Dip-Hex-C6. This finding complicated matters; as the stated goal was to separate and identify the in-membrane and aqueous aggregates, this becomes more difficult if their spectroscopic properties are so similar. Although the steady-state emission spectra are indeed broad and only 'centred around' 380 nm, the subtle differences in wavelength and band-shape in the various environments are clearly not enough on which to base structural arguments. To this end, time-resolved fluorescence techniques were pursued; if different lifetimes could be observed for the Dip compounds in various environments, perhaps they could be associated with particular species or conformations of the Dip molecules in the membrane. For example, if the lifetimes obtained for the aggregates present in aqueous solution were unlike those seen in vesicles, this would be a basis on which to analyse the different aggregates. If the lifetimes varied to a great enough extent, time-resolved emission spectra (TRES) [59] could be collected; these extract discrete emission spectra for each obtained lifetime and could be used to potentially observe emission from the various aggregate states. This would be significant data, as the broad emission seen in both vesicles and aqueous solution must certainly be comprised of numerous similar spectra which cannot be deconvoluted. Time-resolved fluorescence assays such as time-correlated single photon counting (TCSPC) [133,59], the technique used in this work, are extensively utilized in many fields as the data obtained from these studies yield

information not accessible by steady-state methods. As with most fluorescence properties, the fluorescence lifetime of a molecule is highly dependent on its environment, and it is common to observe multiple lifetimes depending on the environment available to the chromophore [59]. Therefore, the experimental rationale is as follows; determine whether the Dip compounds have detectable lifetimes in organic solution, aqueous solution and in vesicles, and if so, try to separate and analyse the obtained lifetimes.

The first step was to establish if the Dip compounds had a detectable lifetime in methanol, where they exist as monomers. In previous work by others, the lifetimes of diphenylacetylene itself and other substituted diphenylacetylenes in solution have been found to be in the sub-nanosecond range [85]. As the time-resolution of the instrument used in this study was approximately 1 ns [134], it was therefore not surprising that a discernable lifetime could not be detected for the tested Dip oligomers in methanol. As demonstrated in Figure 5.5A and Table 5.1 for HO_2C-Dec-Dip-Hex-G(12)-OH, the obtained decay completely overlaps the instrument response function (IRF), therefore, an accurate lifetime cannot be reported under these conditions, although the 'sub-

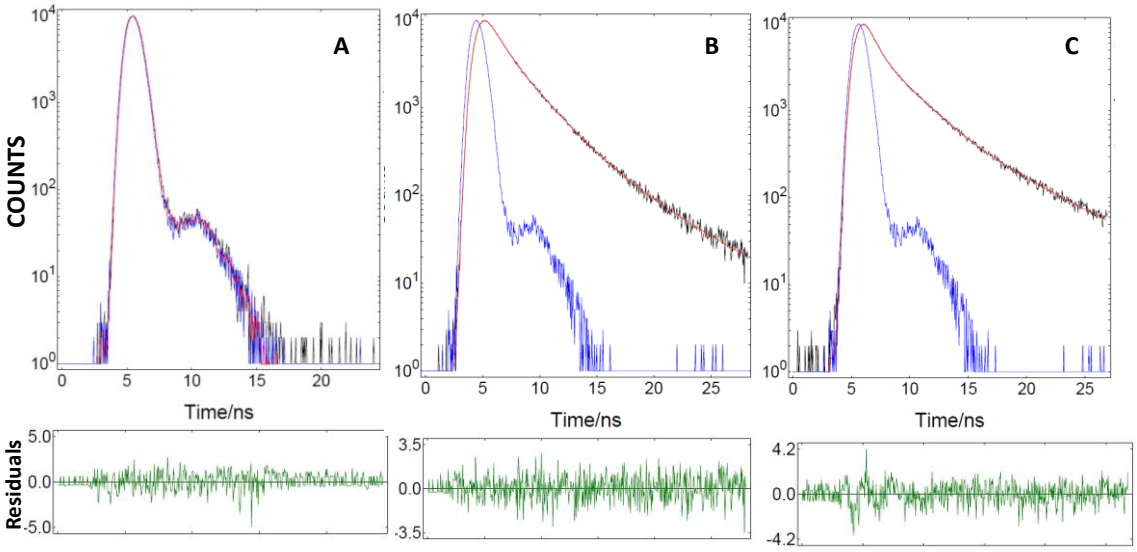

Figure 5.5: TCSPC results for HO_2C-Dec-Dip-Hex-G(12)-OH. **A**: 20 µM compound in methanol, **B**: 20 µM compound in phosphate buffer (10 mM Na_3PO_4, 100 mM NaCl, pH=6.4), **C**: 1 mol% compound pre-loaded into vesicles. λEx= 276 nm, λEm= 380 nm. Blue line= IRF, black line= experimental decay curve, red line= calculated fit of the data. Further experimental details are available in Appendix 3.

CONDITIONS	τ_1 (ns)	%	τ_2	%	τ_3	%	χ^2
Methanol solution	0.06	99	1.65	1	n/a	n/a	0.880
Aqueous solution	1.01	20	2.39	65	6.05	15	1.005
Preloaded into vesicles	0.44	24	2.27	50	6.50	26	1.056

Table 5.1: TCSPC fitting results for HO_2C-Dec-Dip-Hex-G(12)-OH.

nanosecond' result is consistent with previous reports. In contrast, Figure 5.5B shows the obtained decay profile of the same compound in aqueous solution; here more than one lifetime is clearly detectable. The obtained decay profile was found to fit well to a tri-exponential decay; short (1.01 ns), medium (2.39 ns) and long (6.05 ns) components were derived from the data (see Table 5.1). As mentioned, the shortest component is not accurately determined, as it is also near the IRF; however, a bi-exponential decay did not give a reasonable fit to the data. The difference in decay profiles in water and in MeOH for HO_2C-Dec-Dip-Hex-G(12)-OH is striking; evidently the compound is experiencing a significant environmental change in aqueous solution which causes the lifetimes to lengthen. Significantly, a similar, tri-exponential decay consisting of short, medium and long-lived components was observed when the compound was pre-loaded into vesicles (Figure 5.5C); the compound was pre-loaded to ensure that it was in the membrane as HO_2C-Dec-Dip-Hex-G(12)-OH does not partition freely from aqueous solution. The aversion of this compound to water is actually a benefit in this experiment as one can now be confident that the behaviours seen are due to the compound in the membrane, and not residual in the surrounding solution. In addition, as the compound is now 'maximally' partitioned, its emission should be stable over time, analogously to the results seen for the pre-incorporated partitioning assays carried out in Figure 5.2.

The TCSPC results were most exciting as an increase in lifetime upon vesicle binding is commonly observed for a variety of fluorophores [117,135,118]. The mechanisms behind this phenomenon are numerous, but one often proposed and most applicable to

this work is that the compound now exists in a more rigid environment [59]. As the lifetime (τ) is the reciprocal of all de-excitation processes [59], the increase in rigidity would cause a decrease in molecular motions, and a concomitant decrease in de-excitation processes such as solvent relaxation, thus leading to an increased fluorescence lifetime. This explanation has been used to rationalize the increase in lifetimes observed for the 'classic' membrane probe DPH (compound **4-24** in Table 4.4) interacting with vesicles consisting of lipids below their phase transition temperatures; i.e. in more rigid membranes [136]. This effect is even more pronounced when cholesterol, known to rigidify membranes, is added to vesicles [137]. The fluorescence decay behaviours observed for HO_2C-Dec-Dip-Hex-G(12)-OH in both aqueous solution and in vesicles are completely consistent with this explanation. In both media, the compound exists as an aggregate, in which the diphenylacetylene moieties would experience a more structured environment than that found when they are freely dissolved in methanol. The fluorescence lifetimes therefore corroborate with the previous results indicating the 380 nm emission is due to aggregate formation, and the fact that this can be followed in both steady-state and time-resolved studies is most significant.

Besides lengthening the lifetime, the other important observation derived from this experiment is that the lifetimes in both aqueous solution and in vesicles are multi-exponential; this has often been interpreted as indicating a variety of environments available to the fluorophore [137,94], although this remains an actively-debated topic [135]. In the present case, all the data strongly indicate that numerous environments; i.e. aggregates, are present for the Dip compounds in both aqueous solution and in vesicles. Therefore, the first objective of the studies; the determination of lifetimes for the Dip compounds was successful. However, the actual values of the derived lifetimes are very similar in both media. Therefore, the possibility of assigning different in-membrane and aqueous aggregates based on their different lifetimes is not feasible in this particular system.

While not feasible for HO_2C-Dec-Dip-Hex-G(12)-OH, it was thought that perhaps other compounds would prove more amenable to analysis and hence new compounds were selected for study. As mentioned, HO_2C-Hex-Dip-Hex-C6 and its longer homolog HO_2C-Hex-Dip-Hex-C12 are a good comparison set; the shorter compound is ion-transport active and clearly partitions into the membrane, while the longer C12 analog is inactive and does not partition from water. Therefore, this system should give a clear indication as to which lifetimes correspond to the in-membrane aggregate and which to the aqueous aggregate. In addition, the recently discovered negative correlation between ion transport and increasing 380 nm emission observed for HO_2C-Hex-Dip-Hex-C6 made it clear that multiple in-membrane species are present for this compound, and it would be interesting to see if they could be separately identified. Finally, another key impetus in these experiments was to judge if the lifetimes themselves changed over time, a property that has been observed for the majority of behaviours associated with the Dip compounds. This could possibly indicate the interconversion of one species to another.

The experiment carried out for HO_2C-Hex-Dip-Hex-C6 and HO_2C-Hex-Dip-Hex-C12 involved measuring the fluorescence decays at ten minute intervals of an aqueous suspension of vesicles to which the compounds had been introduced. It is necessary to stress that the compounds have *not* been pre-loaded into the vesicle in these cases; therefore, the partitioning behaviours of the compounds will play an important role. The same solution was scanned over the whole time period, and was kept at a constant temperature, in the dark, between scans. The emission was monitored at 380 nm; therefore only excimer-like emission from aggregates was detected. It was expected that the lifetimes detected for the compounds should differ, both from each other and over time, reflecting the variable partitioning and aggregation behaviours of the oligomers.

The results for HO_2C-Hex-Dip-Hex-C6 are shown in Figure 5.6 and Table 5.2; it is immediately evident that the decay profiles change appreciably over time. In the initial scan (Fig. 5.6A), the most significant contribution to the decay is the shortest-lived

component (τ_1; <1 ns), while in the scan taken 70 minutes later (Fig. 5.6C), the longest-lived component (τ_3; ~3.9 ns) dominates. Scans taken at intermediate times (20 minutes, Fig. 5.6B) show this transition clearly. This is further illustrated in Figure 5.7; the longest-lived species increases from approximately 25% of the total emission, to almost 90%, this occurs at the expense of the shortest lived component, which contributes only 1% to the observed lifetime by the final scan, while the proportion of

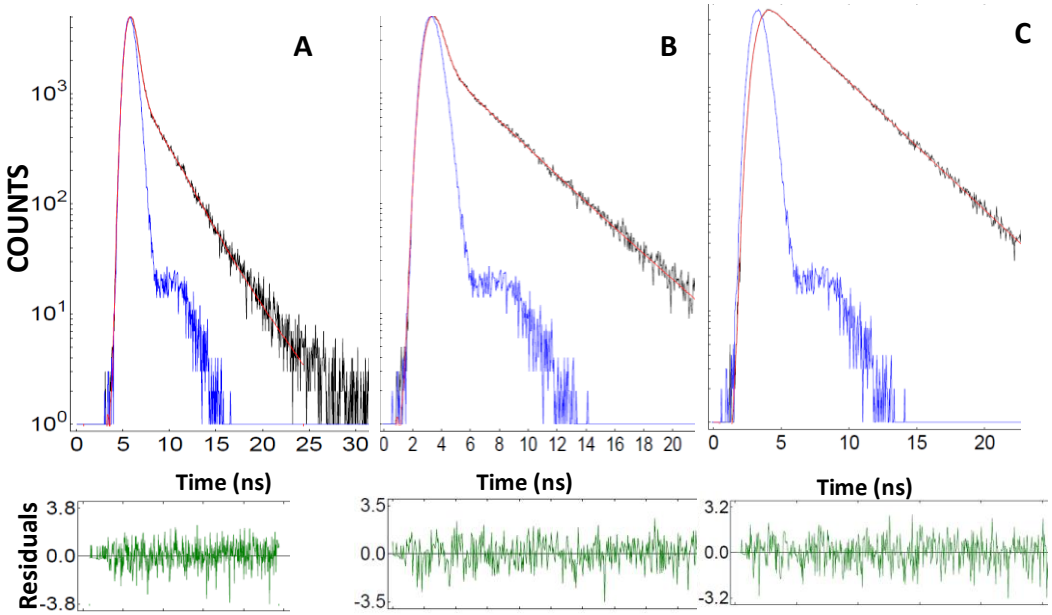

Figure 5.6: Change in fluorescence decay profiles over time for 20 µM HO_2C-Hex-Dip-Hex-C6 incubated with a suspension of lipid vesicles in aqueous phosphate buffer (10 mM Na_3PO_4, 100 mM NaCl, pH 6.4). Scans were taken after **A**: 1 min, **B**: 20 mins, **C**: 70 mins of mixing time.

COMPOUND	TIME (min)	τ_1 (ns)	%	τ_2	%	τ_3	%	χ^2
HO_2C-Hex-Dip-Hex-C6	1	0.19	62	2.35	12	3.91	26	0.941
	20	0.18	43	1.79	10	3.74	47	0.995
	70	0.11	1	2.54	14	3.87	86	0.947
HO_2C-Hex-Dip-Hex-C12	1	0.29	26	1.41	41	2.91	33	1.007
	20	0.26	32	1.49	42	3.34	25	1.184
	70	0.29	42	1.60	39	3.51	19	1.130

Table 5.2: Initial, intermediate and final lifetimes and proportions of each species obtained from the TCSPC experiment for 20 µM HO_2C-Hex-Dip-Hex-C6 and 20 µM HO_2C-Hex-Dip-Hex-C12.

the mid-lifetime species (τ_2; ~ 2 ns) remains fairly constant over the time interval. Over the entire experiment, the fitted curves fit most satisfactorily to tri-exponential functions, however, for the final few time periods the shortest-lived component is almost undetectable by a visual inspection of the data (full dataset for the experiment available in Appendix 4). The lifetimes of the individual components were fairly similar over the experimental time period (Table 5.2), although as mentioned previously the

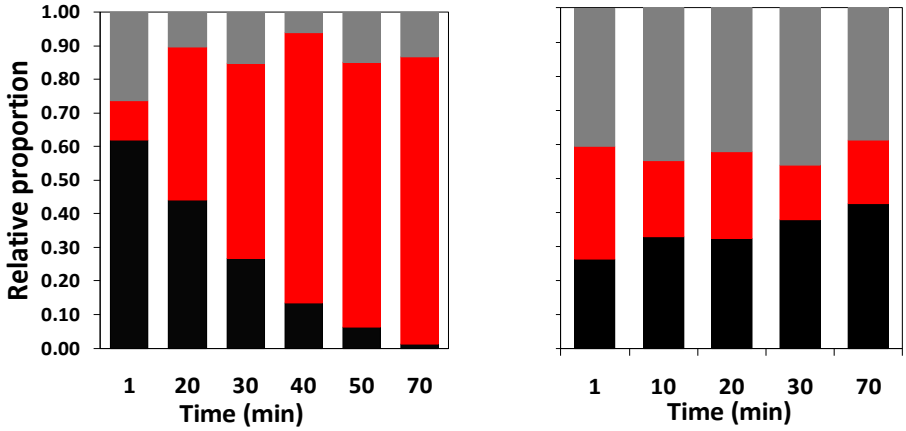

Figure 5.7: Change in relative proportions of each lifetime component over time. LEFT PANEL: 20 µM HO_2C-Hex-Dip-Hex-C6, RIGHT PANEL: 20 µM HO_2C-Hex-Dip-Hex-C12. Black = τ1 (shortest-lived component), Grey = τ2 (mid lifetime component), Red = τ3 (longest lived component).

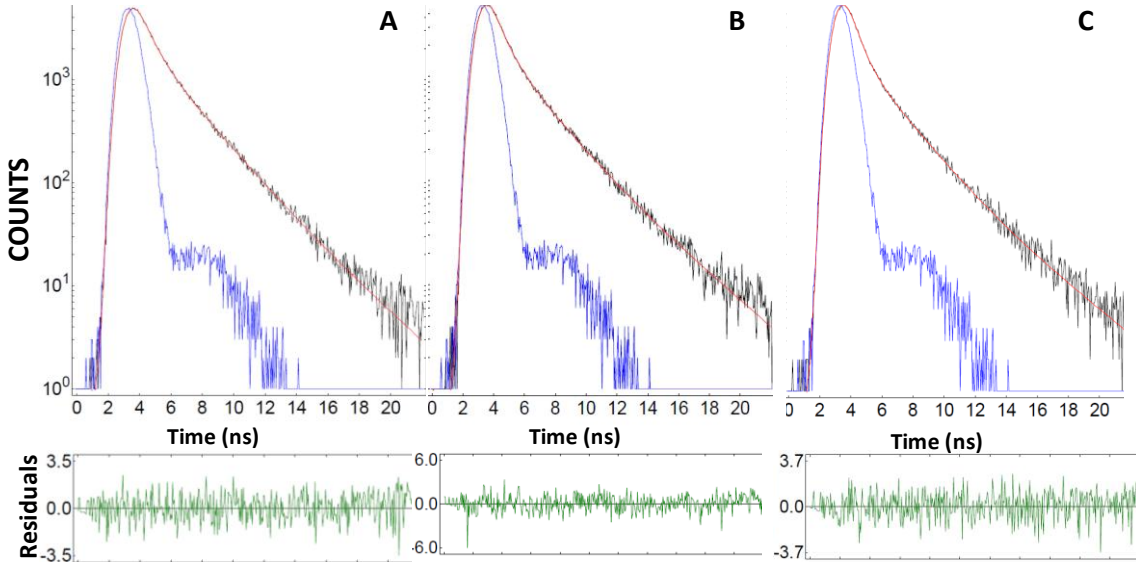

Figure 5.8: Change in fluorescence decay profiles over time for 20 µM HO_2C-Hex-Dip-Hex-C12 incubated with a suspension of lipid vesicles in aqueous phosphate buffer (10 mM Na_3PO_4, 100 mM NaCl, pH 6.4). Scans were taken after **A**: 1 min, **B**: 20 mins, **C**: 70 mins of mixing time.

lifetime of the shortest-lived component cannot be accurately measured, as it is below the resolution of the instrument.

Intriguingly, HO_2C-Hex-Dip-Hex-C12 does indeed behave differently; as shown in Figure 5.8, Table 5.2 and Figure 5.7. Its fluorescence decays remain very similar over the same time period; the decays are still tri-exponential, and numerical values of the short (<1 ns), mid (~1.5 ns) and long (~3.4 ns) components are in the same general range as those seen for the shorter oligomer. However, in contrast to HO_2C-Hex-Dip-Hex-C6, the relative proportions of each component detected for HO_2C-Hex-Dip-Hex-C12 do not vary significantly during the experiment (Figure 5.7). In fact, close inspection of the data suggests the exact opposite behaviour as that seen for HO_2C-Hex-Dip-Hex-C6 is occurring for this HO_2C-Hex-Dip-Hex-C12; the shortest-lived component is now gaining intensity at the expense of the longest-lived one, although the changes are less pronounced than that seen for the shorter analog, and in this case τ_2 changes slightly as well.

The differences in the fluorescence lifetime behaviour for these compounds are significant; clearly HO_2C-Hex-Dip-Hex-C6 is undergoing a greater degree of change in the distribution of 380 nm-emitting species than is HO_2C-Hex-Dip-Hex-C12. This is completely consistent with the steady-state results as shown in Figure 5.2; the active compound partitions quickly, and the 380 nm emission changes slowly over time. Could this be an indication that the processes detected by both the steady-state fluorescence increase as well as SPC-derived lifetime changes are related somehow? This is suggested from Figure 5.9, in which the relative proportion of $\tau 3$ (the longest-lived component) increases at a similar rate as does the steady-state 380 nm emission. This could indicate that for HO_2C-Hex-Dip-Hex-C6, the events being monitored by both techniques are the same; the slow evolution over time from an active in-membrane aggregate to an inactive one. Analogously, the minimal change in both lifetimes and steady-state 380 nm emission observed for HO_2C-Hex-Dip-Hex-C12 are consistent as well; this compound does not partition, and remains as a relatively stable set of aqueous aggregates, the proportions of which do not change significantly over time.

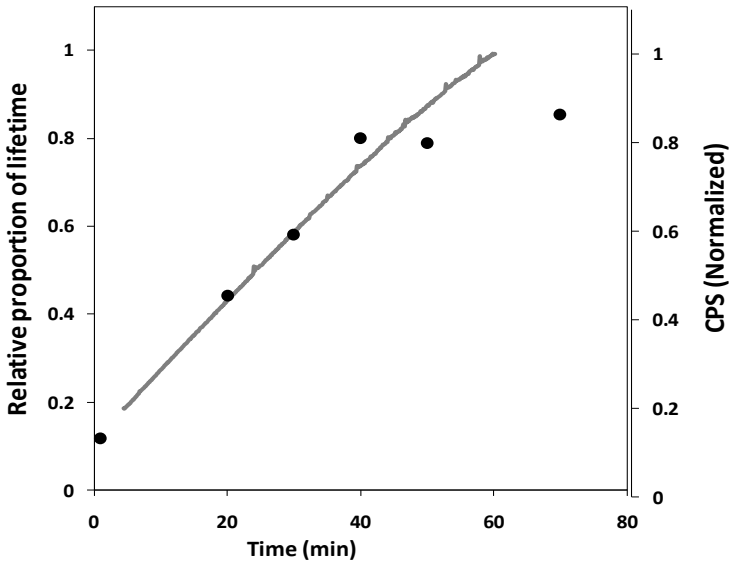

Figure 5.9: Proportion of longest lived species (τ3) (black circles)(LEFT AXIS) as a function of time for 20 μM HO_2C-Hex-Dip-Hex-C6, compared with growth of 380 nm emitting species over time for 15 μM of HO_2C-Hex-Dip-Hex-C6 added to an aqueous suspension of vesicles to which 0.3 mol% of the compound had already been pre-loaded (grey line) (RIGHT AXIS).

To summarize the results of the SPC experiments, it has been shown that the Dip compounds exhibit environment-sensitive fluorescence decays which depend on whether they exist as monomers (un-quantifiable, sub-nanosecond lifetime obtained in methanol), or as aggregates (detectable, tri-exponential decays). The lengthening and distribution of lifetimes observed in aqueous solution and in vesicles relative to that in methanol corroborates the steady-state results that aggregates are present for these compounds in both media, which provide a more rigid environment for the fluorophore and lead to slower fluorescence relaxation. Furthermore, there are multiple aggregates present in both cases which experience a number of different environments. Overall, the change in the decay profiles both between active and inactive molecules, and over time for each of them, suggests a variety of equilibria and dynamic processes are occurring for these compounds. For both oligomers, the observed differences in lifetimes may be significant enough to allow the collection of TRES in the future; this would de-convolute the complicated steady-state spectra and allow each lifetime to be associated with its own spectrum [118,59].

5.4: Mechanistic implications

As mentioned, the time-dependent ion transport and TCSPC results shown here indicate that the model previously-developed for the saturated oligoesters of Luong *et al*. and extended to the first-generation Dip compounds cannot be applied to HO_2C-Hex-Dip-Hex-C6, and this is presumably the case for the other Dip and Trip molecules that show significant in-membrane aggregation. In previous studies on the Dip and Trip compounds, the ion-transport assays occurred only over a 10 minute time period. The eventual formation of the proposed inactive 'sink' aggregate, which occurs over a longer period of time, does therefore not affect the reported ion transport results. Over long time periods, however, the loss of transport activity due to the formation of this inactive species can no longer be ignored, as seen for HO_2C-Hex-Dip-Hex-C6. In general, it is now clear that there are numerous competing pathways available to the putative channel-former when introduced into an aqueous suspension of vesicles. Not only is aqueous aggregation limiting its activity, as previously proposed, but even if the molecule can indeed partition to an appreciable extent, its de-activation over time by the formation of the inactive, stable 'sink' must also now be taken into account. The nature of this species is unknown, but it is certainly an aggregate, as it emits at 380 nm.

Evidently, the previously proposed working hypothesis, while still correct in its overall sequence of events, is too simplistic, and a greater degree of complexity is needed to explain fully the observed behaviours. In particular, a greater number of both aqueous and in-membrane 380 nm-emitting species are necessary to account for the multiple fluorescence lifetimes observed. In addition, the implications of the variable time-scales over which these lifetimes change must be rationalized.

For the inactive HO_2C-Hex-Dip-Hex-C12 oligomer, the situation actually remains fairly similar to that of the previous model; the molecule does not partition into the membrane and remains in the aqueous solution as a variety of interconverting aggregates of which the overall proportions remain stable over time. All the data obtained for this compound are self-consistent; the partitioning assay, SPC results and quenching studies all point to this conclusion, and it can be tied back to the structure-

activity relationships discussed in Chapter 4. This compound is too hydrophobic, making the dissolution of the initially-formed aqueous aggregate unfavourable. These conclusions can without a doubt be extended to the other hydrophobic, inactive Dip and Trip derivatives such as HO_2C-Dec-Dip-Hex-G(12)-OH and HO_2C-Trip-Hex-G(12)-OH which show similar behaviour to HO_2C-Hex-Dip-Hex-C12 in other studies.

When considering an active compound such as HO_2C-Hex-Dip-Hex-C6, the complexity increases. The TCSPC results indicate at least two, if not three, 380 nm-emitting components are present in vesicles. These species evolve slowly over time, at similar timescales as the decrease in ion transport activity. The time-scale of the decrease in proportion of the shortest-lifetime component (τ_1) appears to match most closely with the decrease in ion transport activity, therefore, if a 380 nm-emitting species is responsible for transport, it may be due to this species (Figure 5.7LEFT). Conversely, the evolution of the longest-lived component (τ_3), suggests that this lifetime is tracking the formation of an inactive in-membrane aggregate, as its increase over time is well-correlated time-wise with ion-transport decrease (Figure 5.9). The mid-length component (τ_2), is also assumed to be an inactive species, although it is yet more difficult to assign as its decay characteristics do not change significantly over time; it could be some sort of intermediate through which the active aggregate transitions to the inactive one. Overall, there is no direct evidence that any of the emitting species is transport active, and clearly at least two are not.

Is it possible to propose a new model that takes into account the increased number of in-membrane aggregates and the possible evolution from active to inactive species? Any such discussion must include the time-scales involved for these transitions, which are very slow. Partitioning itself is assumed to be efficient, as is the formation of the initially active aggregate channel, as the highest activity is evident during the initial HPTS trial, i.e. within a few minutes of initial mixing. The initially formed state must therefore adopt a conformation that allows facile partitioning into the membrane. At pH 7 the carboxylate is charged and unlikely to rapidly penetrate through the bilayer; from the relatively rapid rate, it is likely the carboxylate resides

near the aqueous interface. The compounds are introduced to the vesicle from only one side; this partitioning will initially lead to an asymmetric distribution of monomers present in only one of the bilayer leaflets. As the rigid Dip moiety would be expected to lead the insertion, the initially inserted monomer could therefore adopt a "U"-shaped conformation (see Figure 5.10A). Alternatively, the insertion could lead directly to a

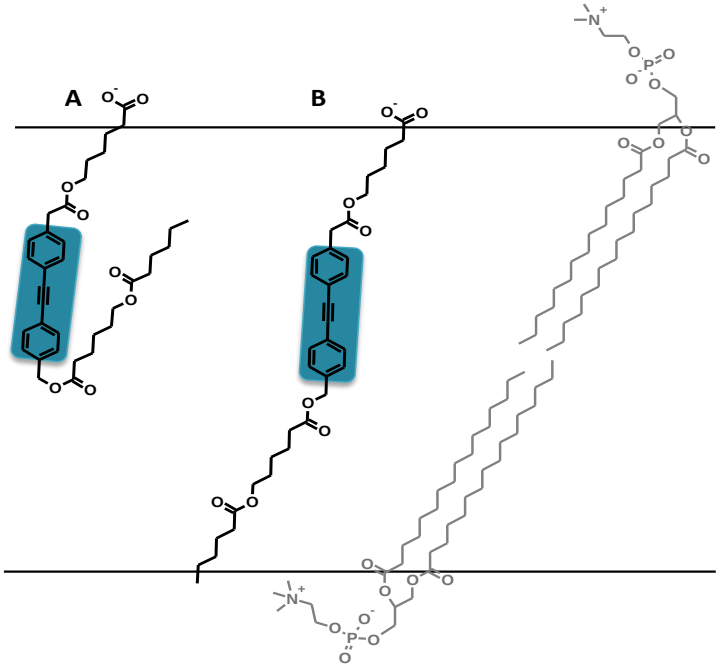

Figure 5.10: Proposed structures of 320 nm-emitting species initially inserted into bilayer. **A**: "U"-shaped monomer. **B**: linear transmembrane-inserted monomer. The compounds and lipids are drawn to scale.

membrane-spanning structure (Figure 5.10B). The structure-activity correlations observed in Chapter 4 indicated that while polar functionality at both termini are beneficial for activity, this is not necessary, as HO_2C-Hex-Dip-Hex-C6 is still fairly active in comparison to compounds such as HO_2C-Hex-Dip-Hex-Hex-OPhos. Therefore, a transmembrane structure may not be needed, and as the insertion of a U-monomer would be expected to occur more rapidly than linear insertion, the U-monomer is presented as a possible initially-formed species.

Once inserted, these U-monomers could quickly diffuse together to form a low-numbered aggregate (Figure 5.11). Lateral diffusion occurs very quickly (~10^{-7} s) in individual bilayer leaflets[2], and the compounds would already be expected to be in

close proximity due to the 'segregating' effect of the lipids [43,1]. This segregation is due to the tendency of the lipids to exclude compound 'additives' in order to pack more efficiently, as the packing would be decreased around the introduced molecule. The compounds therefore become sequestered in certain lower-ordered regions of the bilayer, leading to an area of higher local concentration of compound and increased defect formation [1]. These regions would therefore be most conducive to channel formation.

As shown in Figure 5.11, there are multiple possibilities for this initially formed low-numbered aggregate, which shall be considered a dimer for this discussion. The U-shaped and linear monomers could both form homo-dimers, (Figure 5.11A and C), or a mixed U-linear dimer could result (Figure 5.11B). The U-dimer (Figure 5.11B) is the least lipid-like in shape, and this aggregate could certainly deform the bilayer to a great enough extent to open an ion-conducting pathway. These U-dimers would also be expected to form quickly as the U-monomers could rapidly insert, and then laterally diffuse together. They would also be presumed to be unstable due to the high extent of

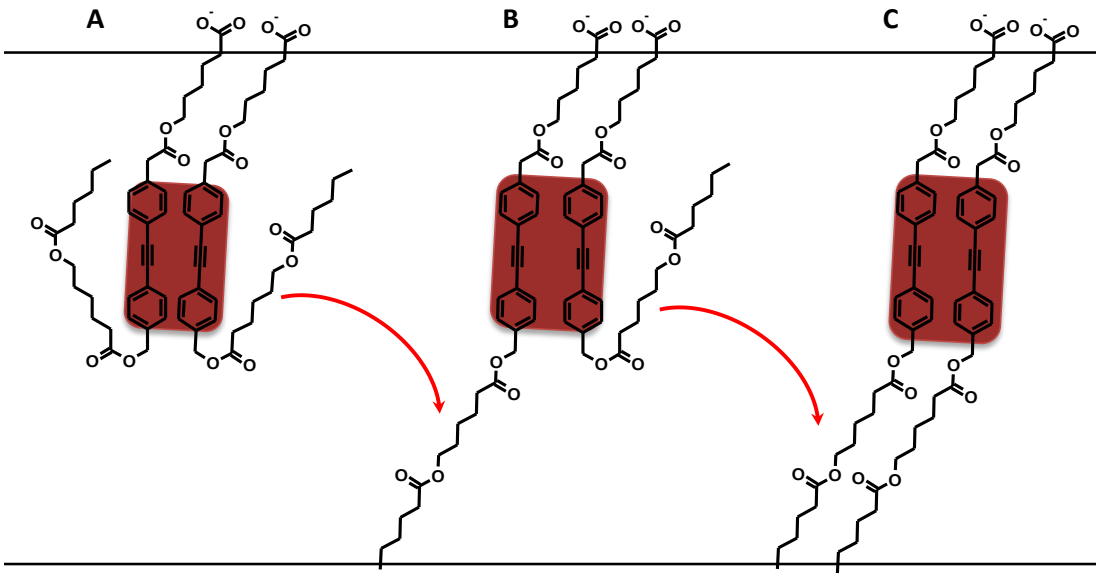

Figure 5.11: Initially-formed dimers. **A**: rapidly-formed U-homodimer, a potential active structure, **B**: mixed linear-U dimer formed either from slower linear insertion of monomer, or slow opening of U-monomer (red arrow). **C**: linear homodimer, presumed to be the slowest forming of the initial species. The lipid pair is omitted for clarity.

membrane deformation, and could therefore diffuse away from each other quickly. This would result in a short-lived active structure, as suggested by the rapid decrease in the proportion of the shortest-lived species in the TCSPC results. The U-dimer or aggregate could therefore be a plausible active structure, potentially corresponding to τ1 in the TCSPC studies.

Over time, these unstable, yet potentially active U-monomers could 'open-up' to form the linear homodimer, *via* a mixed U-linear aggregate (Figure 5.11B to C). The linear-linear dimer is the most lipid-like in shape and would pack well into the bilayer, increasing its stability. This could eventually lead to a cluster of such molecules which are too tightly-packed to conduct ions. In addition, this clustering would lead to a more rigid environment for the Dip fluorophore, thereby lengthening its lifetime. Finally, these aggregates would be expected to form rather slowly due either to slow initial transmembrane insertion (Figure 5.10) or slow re-arrangement of the U-monomers. This aggregate of transmembrane monomers could therefore be the species responsible for τ2 in the TCSPC studies.

The transition to the finally formed, most stable inactive structure occurs over a period of almost 40 minutes. Therefore, even the presumed slow rearrangements shown in Figure 5.11 cannot adequately account for the formation of this 'sink' species. It is therefore proposed that the final inactive aggregate, potentially corresponding to τ3 in the TCSPC studies, comes about through a flip-flop mechanism. Flip-flop is the process by which a phospholipid transitions fully from one leaflet of the bilayer to the other [2] (Figure 5.12). As this involves the movement of the polar headgroup of the lipid through the hydrophobic interior of the bilayer, it is an inherently unfavourable process; consequently, it occurs over a very slow time scale of hours to days. For example, a recently-reported half-life of flip-flop for PC, the lipid used in the majority of this work, was found to be over 70 hours [138]. Flip-flop is an important mechanism in natural membranes, as it is involved in maintaining membrane asymmetry, and specialized enzymes, 'flippases' have therefore evolved to increase its rate, leading to half-lives of several minutes [139]. Several other compounds, including natural lipids such as DHA

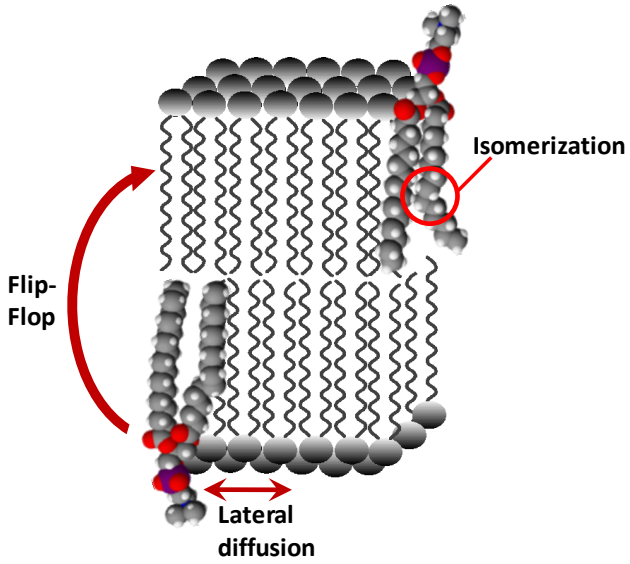

Figure 5.12: Examples of some of the processes that can occur in a phospholipid bilayer, including flip-flop, the crossing of a lipid from one bilayer leaflet to the other. Adapted from Ref. [2].

(docosohexenoic acid) [138,140] and synthetic peptides [139] have also been observed to increase the rate of flip-flop. In general, it is believed that increased membrane disorder, such as that occurring around multiply-unsaturated lipids or pore-forming compounds such as melittin [139] and amphotericin [141] can lead to increased rates of flip-flop [142]. The rate increases are variable amongst the cited examples, although the general trends are that pore-mediated flip-flop occurs faster than the 'defect'-mediated rate. The synthetic peptide mentioned above, which forms a pore, brought this rate up to approximately 1 min^{-1}; this is similar to the rates achieved by flippases.

The fact that increased rates of flip-flop are observed with both multiply unsaturated and pore-forming molecules is most pertinent to results observed for the Dip compounds. While the Dip oligomers could be mediating flip-flop of the phospholipids, which would be interesting in its own right, the observed behaviours imply that the compounds themselves undergo this process. The Dip compounds are rigid, multiply-unsaturated and certainly form defects in the membrane – and in most cases these defects must be initially pore-like in structure, allowing for ion transport. In addition, the time-scales involved in flip-flop correlate well with the formation of the final, inactive 380nm-emitting 'sink' species. Therefore, as shown in Figure 5.13, the

final ‘resting state’ of the Dip compound in the membrane could indeed come about from a flip-flop mechanism. Once partitioned, the initially inserted U-monomer would undergo a slow flip-flop to the other side of the bilayer (Fig. 5.13A to B). From here, the flip-flopped monomer could aggregate with a transmembrane monomer; the driving force for this process would be to decrease membrane perturbation (Fig. 5.13C). Finally, the stable, inactive transmembrane ‘sink’ aggregate forms by rearrangement of the U-monomer (Fig. 5.13D).

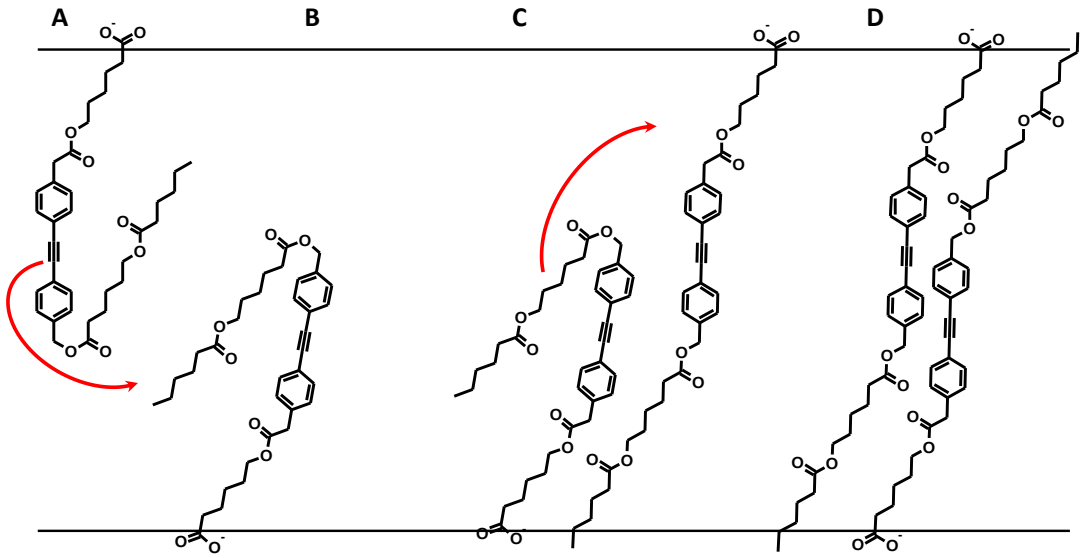

Figure 5.13: Potentially slow structural reorganizations. **A**: initial U-monomer undergoes slow flip-flop to monomer in other bilayer leaflet (**B**). Once formed, this monomer aggregates to a transmembrane linear monomer (**C**); rearrangement to form the stable, final transmembrane linear ‘sink’ aggregate (**D**) with carboxylates on both sides of the bilayer finally occurs.

This structure is postulated as the final aggregate due to similar arguments as that for the transmembrane dimer shown in Figure 5.11C: it is lipid-like in shape, thereby leading to minimal bilayer perturbation. It can pack tightly together and close the ion-conducting pore. Finally, it is no longer dissymmetric, with the carboxylates present on both sides of the bilayer. Therefore, the charge repulsion felt by the individual compound monomers is no longer present, giving rise to the most stable, yet slowest formed, of the possible species.

5.5: New model

In light of the presented data, a new model to explain the Dip compounds' behaviours is illustrated in Figure 5.14. The general format remains similar to that previously proposed, however, the increased number of aqueous and in-membrane aggregates is now taken into account. For the inactive compounds, the situation remains similar; a number of interconverting aqueous aggregates exist, and the compounds do not partition into the membrane, Fig. 5.14A. For the active molecules, the partitioning from A to B occurs efficiently, initially forming a U-shaped monomer on one side of the bilayer leaflet which is presumed to emit at 320 nm, as seen by the rapid increase in emission intensity at this wavelength (Fig. 5.14B). The U-monomers quickly laterally diffuse into low-numbered aggregates, potentially giving rise to the 380 nm-

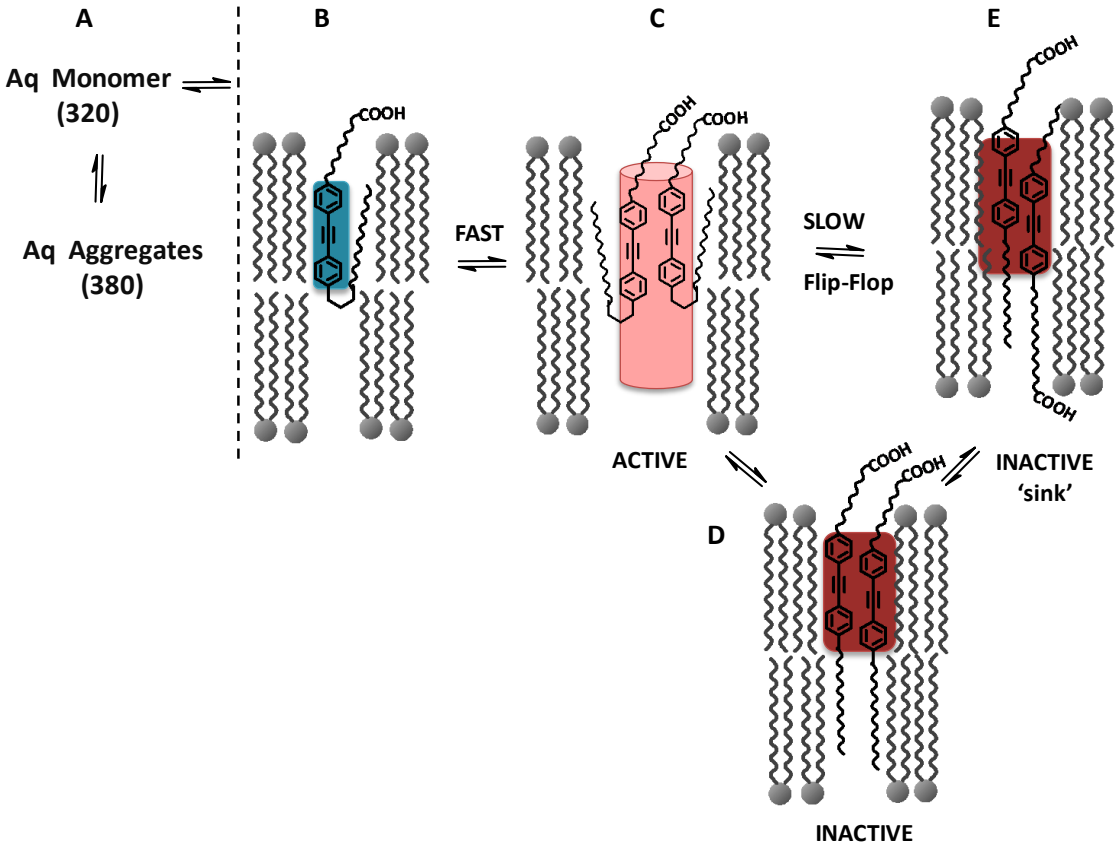

Figure 5.14: Schematic illustration of the proposed new model. **A**: the compounds aggregate when initially introduced into aqueous solution, from which the active compounds partition *via* an aqueous monomer into the bilayer (**B**). Once partitioned, the initially formed U-monomers (blue rectangle in **B**), laterally diffuse to form the U-aggregate, opening an ion conducting pathway (red cylinder) (**C**). Slower rearrangement (to form **D**) and eventual flip-flop (to form **E**, the final 'sink' aggregate) then occurs, forming the transmembrane species (red rectangle in **D** and **E**), which are transport inactive. Other intermediates are also possible.

emitting shortest lived species (τ1), and transport activity (Fig. 5.14C). Finally, over time, the U-monomers 'open up' and rearrange via a flip-flop process to form larger, close-packed aggregates which are transport inactive (Fig. 5.14D and E). The finally-formed, most stable species, potentially correlated with the longest-lived component in TCSPC (τ3) could be the transmembrane aggregate shown in Figure 5.14E. This 'sink' compound would form very slowly, as it would require flip-flop of the monomer to occur (Figure 5.13). It no longer has a dissymmetric charge distribution, as carboxylate headgroups are positioned on either side of the bilayer. Once formed, it would most likely be the most stable possible species, as the individual compound monomers would be close-packed, the bilayer would be least perturbed, and the repulsion felt when the carboxylates are forced into close contact would be minimized.

An interesting question arises when considering the proposed new model. Can the initially formed U-aggregates perturb the bilayer to a great enough extent to open an ion-conducting pathway and effect transport, despite being present in only one leaflet? Examining Figure 5.10 indicates that indeed this could be the case, due both to the rigidity of the Dip subunits as well as the preference to keep the carboxylate headgroup in a high polarity region. Furthermore, it is well-known that the disorder in a bilayer increases towards its centre, as the alkyl chains undergo a variety of processes such as cis-trans isomerizations at very fast time scales (~10^{10} s^{-1}) (see Figure 5.12) [2]. Therefore, the lipids would certainly undergo such processes to accommodate the inserted compound, forming 'kinks' and further increasing the spaces available for an ion as it passes through the membrane. These increasingly disordered regions are also associated with higher degrees of hydration, as water molecules can also penetrate more readily [1]; this would further enhance ion transport. As a Dip U-monomer which is inserted into a single leaflet (as in Figure 5.10A) should therefore be sufficient to effect transport, this suggests another interesting concept. While it has been assumed that the dimer or a higher aggregate is responsible for transport, this could in fact be achieved by the monomer itself if it inserted deeply enough into the membrane, as it too would

be expected to deform the bilayer. As with all postulated structures, this remains hypothesis at present.

5.6: Conclusions

In conclusion, this Chapter has shown that a time-based approach is a very effective way to analyse the diverse processes that occur for the Dip and Trip compounds. The picture that emerges is undoubtedly complex, and multiple species are involved in the various dynamics of aggregation, partitioning and re-aggregation in the membrane; as demonstrated by the numerous fluorescence lifetimes present for both the active and inactive compounds in various media. This indicates that the fluorophores are experiencing a number of microenvironments in both aqueous solution and in the presence of vesicles, as different aggregates form and interconvert over time. For the inactive compound (HO_2C-Hex-Dip-Hex-C12), this interconversion leads to an overall stable population of aggregates. In contrast, the lifetime changes over time, as well as the steady-state fluorescence increase at 380 nm for the active compound (HO_2C-Hex-Dip-Hex-C6) can be used to postulate both active and inactive structures formed by this molecule. Despite being more complicated than previously thought, the model proposed in Figure 5.14 is supported by the collected data. It is therefore a reasonable 'working hypothesis' to account for the various active and inactive species present, and how they interconvert over time.

Chapter 6 : Conclusions, future directions & significance

The goals outlined at the beginning of this Thesis were to study the effect of rigidity on synthetic ion channel activity, and to work towards elucidating a mechanism or model to rationalize any such effects. This involved the synthesis of approximately 18 diphenylacetylene-containing oligoester compounds, based both on a modified diphenylacetylene scaffold ('Dip'), as well as a novel, triaromatic 'Trip' chromophore. The synthetic methods developed for both series of compounds are a significant achievement, as they allowed for the efficient and rapid synthesis of a large library of compounds that differed in structural properties such as length, hydrophobicity and charge. This provided a solid framework upon which a structure-activity survey could be based.

The synthesized compounds were amenable to study by a wide variety of assays, including ion transport studies such as HPTS and the bilayer clamp that are the cornerstone of synthetic ion channel research. The activities of the compounds varied fairly significantly. Highly active compounds such as the phosphate and hydroxyl-terminated 2nd-generation Dip isomers discussed in Chapter 4 (Figure 4.2) were discovered. The results from these molecules indicate that rigidity does indeed play a beneficial role in enhancing ion transport activity, as they are much more active than the 'fully saturated' oligoester precursor compounds. Just as interesting, however, is the complete inactivity of compounds such as HO_2C-Dec-Dip-Hex-G(12)-OH and HO_2C-Hex-Dip-Hex-C12, that differ marginally from their highly-active analogs such as HO_2C-Hex-Dip-Hex-G(12)-OH and HO_2C-Hex-Dip-Hex-C6, respectively (Chapter 2, Figure 2.5, Chapter 4, Figure 4.2). These differences in activity, while unexpected initially, could in most instances be rationalized by structural arguments such as increased hydrophobicity due to the longer alkyl chains. It was also found that increased rigidity does not enhance transport in all cases, as some of the very rigid Trip-containing compounds such as HO_2C-Trip-G(12)-OH (Table 3.1) are completely inactive. The subtle interplay between charge, length, polarity and hydrophobicity was most interesting to

observe in these studies, and gave an indication as to what structural features are beneficial in attaining high transport activity.

From the in-vesicle ion transport assays, the most significant finding must certainly be the high activity and generally favourable properties of HO_2C-Hex-Dip-Hex-Hex-OH. As discussed in Chapter 4, this compound is now nearly 10 times more active than the previous 'benchmark' fully-saturated oligoester developed by Fyles *et al.* [41]. The concentrations at which this compound is active (~1 μM) are approaching those of biologically-relevant compounds, and studies to test this compound in biological applications such as anti-bacterial activity are underway in the Fyles lab [143]. It is hoped that this molecule may be useful in such applications, but in any case will certainly be a promising lead candidate for the next generation of Dip-containing synthetic ion channels.

The activity of the synthesized compounds was also evaluated in planar bilayers, usually considered the unequivocal evidence that the molecule is indeed an ion channel. Once again, the activity of the compounds was shown to vary; however, some exciting findings resulted from the bilayer studies as well. Perhaps the most notable is the behaviour of the triphenyl-containing compound HO_2C-Trip-G(E3)-OH (Figure 3.7). This compound exhibited very highly-conducting openings which in some cases correspond to pores on the order of 10 Å in diameter; these types of openings are very rare in the reported literature. In addition, the suggestion of voltage-dependent transport present for this compound is very exciting, as this type of behaviour is rarer still for synthetic ion channels (Figure 3.8). The regulation of synthetic ion channels could lead to potential technological applications such as sensing, as has been discussed for the 'sugar sensors' of Matile *et al.* [17]. Therefore, further study and development of HO_2C-Trip-G(E3)-OH or similar analogs could lead to such applications as well.

In addition to transport studies, the chromophores present in the Dip and Trip compounds made an entirely new set of experiments possible which could not occur for the previously-developed saturated oligoesters. The environment-sensitive fluorescence of both chromophores, whether the excimer-like emission exhibited by the

Dip molecules, or the solvatochromism present for the Trip compounds, led to a great deal being discovered about these molecules and how they interact with the bilayer membrane. It was shown that for both sets of compounds, a significant blue-shift and increase in fluorescence intensity can track insertion into the bilayer. For the Dip compounds, this allowed the extraction of a partitioning constant (Kp), thereby quantifying the affinity of these molecules for the membrane (Table 4.4). This could be carried out on the rest of the Dip oligomers to quantitatively correlate activity with extent of partitioning. Equally significant, the solvatochromism shown by the Trip molecules can infer their location in the membrane by the extraction of an apparent E_T value for the environment surrounding the chromophore (LEFT:Figure 3.15). This, in addition to the significant increase in fluorescence intensity of up to 8-fold when partitioned into vesicles over that observed in aqueous solution could lead to the Trip molecules' application as 'light-up' membrane probes.

Studies such as fluorescence quenching, membrane partitioning and time-resolved single-photon counting were utilized to try to understand what happens to a putative channel-forming compound when introduced to the lipid bilayer. The studies indicate that the picture is complex, as is expected for aggregate channels that consist of multiple monomers that randomly collide in the membrane to form an active species. Many species form both in aqueous solution and in the membrane, and the identities of these species certainly change over time. This can be seen in the decrease in fluorescence intensity and change in band shape over time, as well as the change in fluorescence lifetimes discussed in Chapter 5. The combined fluorescence behaviours of these compounds were used to modify the previously-proposed working hypothesis developed for the fully-saturated oligoester precursor compounds (Figure 1.10 and Figure 2.20). In contrast to the fully-saturated analogs, the fluorescence of the compounds studied in this work meant that the proposed intermediates along a pathway such as depicted in Figure 5.14 could be detected. While the identity of each possible intermediate, both active and inactive, remains speculation, the data obtained

through studies such as the long timescale TCSPC studies of Chapter 5 are a positive step towards achieving this goal.

In the future, the proposed model could be tested and refined further by extending the experiments conducted in Chapter 5 to the rest of the synthesized Dip and Trip isomers, potentially discovering further correlations between lifetime and fluorescence changes and activity. In addition, the interesting photophysical characteristics of these compounds make them amenable to a variety of other assays. Experiments such as fluorescence anisotropy [59] and red-edge excitation spectra (REES) [144,6], would both indicate the type of environment present around the fluorophores, while TRES would associate each lifetime component with a steady-state emission spectrum. In addition, as mentioned previously, the Dip compounds can also be moderately quenched by the stable nitroxyl radical TEMPO. This indicates that fluorescence depth quenching (FDQ) studies could be performed with the Dip oligomers to further elucidate their position in the membrane. Finally, an experiment related to that developed by McIntyre and Sleight [145], and extensively utilized by many groups studying membrane dynamics using fluorescent, NBD-labelled lipids [146,138,139], could potentially be developed. In this interesting assay, vesicles containing the NBD-labelled lipids are quickly exposed to sodium dithionite ($Na_2S_2O_4$), which reduces the nitro group, irreversibly quenching its fluorescence. The excess dithionite is then removed from the vesicles using size-exclusion chromatography; this is to ensure that only NBD that resides in the outer bilayer leaflet is quenched, as dithionite has low membrane permeability [145]. This procedure has been used in a number of reports previously mentioned concerning membrane flip-flop. This method could therefore be applied to the Dip and Trip compounds to assess if they indeed exhibit 'flippase'-type activity and increase the rate of flip-flop, which could indirectly indicate that the compounds themselves were undergoing this process as well.

In conclusion, it is well appreciated that such 'structurally-simple' aggregate channels will have complex dynamics associated with them; minimal structural pre-organization makes this inevitable. The ability to synthesize compounds such as the Dip

and Trip isomers, which allow such a variety of assays to occur, is certainly a significant achievement towards the continuing goal of designing and creating active ion channels, as well as establishing how they function. This is therefore the most significant contribution of this work; the development of highly active, relatively simple synthetic ion channels which can be studied in ways not previously possible.

Bibliography

1. Fyles, T. M. *Chemical Society Reviews* **2007,** *36,* 335-347.
2. Yeagle, R. L., Ed. *The Structure of Biological Membranes,* 2nd ed.; CRC Press: Boca Raton USA, 2005.
3. Hauser, H.; Pascher, I.; Pearson, R. H.; Sundell, S. *Biochimica et Biophysica Acta* **1981,** *650,* 21-51.
4. Pearson, R. H.; Pascher, I. *Nature* **1979,** *281,* 499-501.
5. Gokel, G.; Carasel, I. A. *Chemical Society Reviews* **2007,** *36,* 378-389.
6. Rawat, S. S.; Kelkar, D. A.; Chattopadhyay, A. *Biophysical Journal* **2004,** *87,* 831-843.
7. Tien, H. T.; Ottova, A. L. *Journal of Membrane Science* **2001,** *189,* 83-117.
8. Davis, J. T.; Okunolaa, O.; Quesada, R. *Chemical Society Reviews* **2010,** *39,* 3843-3862.
9. Hucho, F.; Weise, C. *Angewandte Chemie International Edition* **2001,** *40,* 3100-3116.
10. Brotherhood, P. R.; Davis, A. P. *Chemical Society Reviews* **2010,** *39,* 3633-3647.
11. Hubner, C. A.; Jentsch, T. J. *Human Molecular Genetics* **2002,** *11* (20), 2435-2445.
12. MacKinnon, R. *Angewandte Chemie International Edition* **2004,** *43,* 4265-4277.
13. Doyle, D. A.; Cabral, J. M.; Pfuetzner, R. A.; Kuo, A.; Gulbis, J. M.; Cohen, S. L.; Chait, B. T.; MacKinnon, R. *Science* **1998,** *280,* 69-77.
14. Demchenko, A. P. *Introduction to Fluorescence Sensing;* Springer: Berlin, 2009.
15. Leevy, W. M.; Weber, M. E.; Schlesinger, P. H.; Gokel, G. W. *Chemical Communications* **2005,** 89-91.
16. Renkes, T.; Schafer, H. J.; Siemens, P. M.; Neumann, E. *Materials Science and Engineering C* **2002,** *22,* 275-275.
17. Matile, S.; Tanaka, H.; Litvinchuk, S. *Topics in Current Chemistry* **2007,** *277,* 219-250.
18. Fyles, T. M.; Loock, D.; Zhou, X. *Journal of the American Chemical Society* **1998,** *120* (13), 2997-3003.
19. Goto, C.; Yamamura, M.; Satake, A.; Kobuke, Y. *Journal of the American Chemical Society* **2001,** *123,* 12152-12159.
20. Kobuke, Y.; Nagatani, T. J. *Journal of Organic Chemistry* **2001,** *66,* 5094-5101.
21. Jog, P. V.; Gin, M. S. *Organic Letters* **2008,** *10* (17), 3693-3696.
22. Litvinchuk, S.; Tanaka, H.; Miyatake, T.; Pasini, D.; Tanaka, T.; Bollot, G.; Mareda, J.; Matile, S. *Nature Materials* **2007,** *6,* 576-580.
23. Gokel, G. W.; Mukhopadhyay, A. *Chemical Society Reviews* **2001,** *30,* 274-286.
24. Matile, S.; Jentzsch, A. V.; Montenegro, J.; Fin, A. *Chemical Society Reviews* **2011,**

40, 2453-2474.

25. Matile, S.; Abhigyan, S. A.; Sorde, N. *Tetrahedron* **2004,** *60,* 6405-6435.
26. Mcnally, B. A.; Leevy, M. W.; Smith, B. D. *Supramolecular Chemistry* **2007,** *19* (1), 29-37.
27. Matile, S.; Sakai, N. The Characterization of Synthetic Ion Channels and Pores. In *Analytical Methods in Supramolecular Chemistry;* Schalley, C. A., Ed.; Wiley-VCH: Weinheim, 2007; pp 391-418.
28. Nakano, A.; Xie, Q.; Mallen, L.; Echegoyen, L.; Gokel, G. W. *Journal of the American Chemical Society* **1990,** *112,* 1287-1289.
29. Fyles, T. M.; Knoy, R.; Mullen, K.; Sieffert, M. *Langmuir* **2001,** *17,* 6669-6674.
30. Matile, S. *The Chemical Record* **2001,** *1,* 162-172.
31. Sakmann, B., Neher, E., Eds. *Single-Channel Recording,* 2nd ed.; Plenum Press: NY USA, 1995.
32. Buchmann, M. B.; Fyles, T. M.; Sutherland, T. *Bioorganic and Medicinal Chemistry* **2004,** *12,* 1315-1324.
33. Eggers, P. K.; Fyles, T. M.; Mitchell, K. D.; Sutherland, T. *Journal of Organic Chemistry* **2003,** *68,* 1050-1058.
34. Ashley, R. H., Ed. *Ion Channels: A Practical Approach;* University Press, Oxford, 1995.
35. New, R. R. *Liposomes: A Practical Approach;* IRL Press: Oxford, 1990.
36. Fyles, T. M.; Tong, C. C. *New Journal of Chemistry* **2007,** *31,* 655-661.
37. Hille, B. *Ion Channels of Excitable Membranes,* 3rd ed.; Sinauer Associates: USA, 2001.
38. Ma, L.; Melegari, M.; Colombini, M.; Davis, J. T. *Journal of the American Chemical Society* **2008,** *130,* 2938-2939.
39. Ma, L.; Harrell, W. A.; Davis, J. T. *Organic Letters* **2009,** *11* (7), 1599-1602.
40. Fyles, T. M.; Luong, H. *Organic and Biomolecular Chemistry* **2009,** *7,* 733-738.
41. Fyles, T. M.; Luong, H. *Organic and Biomolecular Chemistry* **2009,** *7,* 725-732.
42. Fyles, T. M.; Hu, C. *Supramolecular Chemistry* **2001,** *1,* 207-215.
43. Bagatolli, L. A. *Biochimica et Biophysica Acta - Biomembranes* **2006,** *1758* (10), 1541-1556.
44. Li, X.; Shen, B.; Yao, X.-Q.; Yang, D. *Journal of the American Chemical Society* **2009,** *131,* 13676-13680.
45. Carmichael, V. E.; Dutton, P. J.; Fyles, T. M.; James, T. D.; Swan, J. A.; Zojaji, M. *Journal of the American Chemical Society* **1989,** *111,* 767-769.
46. Koert, U. *Physical Chemistry Chemical Physics* **2005,** *7,* 1501-1506.
47. Fyles, T. M.; Hu, C.; Knoy, R. *Organic Letters* **2001,** *3,* 1335-1337.
48. Fyles, T. M.; Hu, C.-W.; Luong, H. *Journal of Organic Chemistry* **2006,** *71,* 8545-8551.

49. Luong, H. *Towards Voltage-Gated Ion Channels Synthesized by Solid Phase Organic Synthesis;* Doctoral Dissertation; University of Victoria: Victoria, 2008.
50. Avallone, E.; Izzo, I.; Vuolo, G.; Costabile, M.; Garrisi, D.; Pasquato, L.; Scrimin, P.; Tecilla, P.; De Riccardis, F. *Tetrahedron* **2003,** *44,* 6121-6124.
51. Zhang, J.; Jing, B.; Regen, S. L. *Journal of the American Chemical Society* **2003,** *125,* 13984-13987.
52. Arnt, L.; Tew, G. N. *Journal of the American Chemical Society* **2002,** *124,* 7664-7665.
53. Arnt, L.; Tew, G. N. *Langmuir* **2003,** *19,* 2404-2408.
54. Tedesco, M. M.; Ghebremariam, B.; Sakai, N.; Matile, S. *Angewandte Chemie International Edition* **1999,** *38* (4), 540-543.
55. McMaster, M. *HPLC; A Practical User's Guide;* Wiley-VCH: NY USA, 1994.
56. Hirata, Y. *Bulletin of the Chemical Society of Japan* **1999,** *72,* 1647-1664.
57. Brocklehurst, B.; Bull, D. C.; Evans, M.; Scott, P. M.; Stanney, G. *Journal of the American Chemical Society* **1975,** *97* (11), 2977-2978.
58. Letsinger, R. L.; Wu, T.; Yang, J.-S.; Lewis, F. D. *Photochemical and Photobiological Sciences* **2008,** *7,* 854-859.
59. Lakowicz, J. R., Ed. *Principles of Fluorescence Spectroscopy,* 3rd ed.; Springer: NY USA, 2006.
60. Valeur, B. Molecular Fluorescence. In *Encyclopedia of Applied Spectroscopy;* Andrews, D. L., Ed.; Wiley-VCH: Weinheim, 2009.
61. Martinez-Manez, R.; Sancenon, F. *Chemical Reviews* **2003,** *103* (11), 4419-4476.
62. Wang, W.; Li, R.; Gokel, G. W. *Chemical Communications* **2009,** 911-913.
63. Wang, W.; Ruiqiong, L.; Gokel, G. W. *Chemistry - a European Journal* **2009,** *15,* 10543-10553.
64. Moszynski, J. M.; Fyles, T. M. *Organic and Biomolecular Chemistry* **2010,** *8,* 5139-5149.
65. Merrifield, R. B. *Journal of the American Chemical Society* **1963,** *85,* 2149-2154.
66. Kuisle, O.; Quinoa, E.; Riguera, R. *Journal of Organic Chemistry* **1999,** *64,* 8063-8075.
67. Zaragoza Dorwald, F. *Organic Synthesis on Solid Phase,* 2nd ed.; Wiley-VCH: Weinhem, 2002.
68. Greene, T. W.; Wuts, P. G. *Protective Groups in Organic Synthesis,* 3rd ed.; John Wiley & Sons: NY USA, 1999.
69. Chinchilla, R.; Najera, C. *Chemical Reviews* **2007,** *107,* 874-922.
70. Sonogashira, K.; Tohda, Y.; Hagihara, N. *Tetrahedron Letters* **1975,** *16,* 4467-4470.
71. Nishizawa, M.; Yamamoto, K.; Seo, H.; Imagawa, H.; Sugihara, T. *Organic Letters* **2002,** *4,* 1947-1949.
72. Bagatolli, L. A.; Ipsen, J. H.; Simonsen, A. C.; Mouritsen, O. G. *Progress in Lipid Research* **2010,** *49,* 378-389.

73. Mayer, L. D.; Hope, M. J.; Cullis, P. R. *Biochimica et Biophysica Acta* **1986,** *858,* 161-168.
74. Kalyanasundaram, K.; Thomas, J. K. *Journal of the American Chemical Society* **1977,** *99,* 2039-2044.
75. Yihwa, C.; Kellermann, M.; Becherer, M.; Hirsch, A.; Bohne, C. *Photochemical and Photobiological Sciences* **2007,** *6,* 525-531.
76. Bouvrais, H.; Pott, T.; Bagatolli, L. A.; Ipsen, J. H.; Meleard, P. *Biochmica et Biophysica Acta* **2010,** *1798,* 1333-1337.
77. Sakai, N.; Mareda, J.; Matile, S. *Accounts of Chemical Research* **2005,** *38* (2), 79-87.
78. Renkes, T.; Schafer, H. J.; Siemens, P. M.; Neumann, E. *Angewandte Chemie International Edition* **2000,** *39* (14), 2512-2515.
79. DiGiorgio, A. F.; Otto, S.; Bandyopadhyay, P.; Regen, S. L. *Journal of the American Chemical Society* **2000,** *122,* 11029-11030.
80. Genge, K. *The Ion Transport Activity of a Simple Oligoester Dimer;* Undergraduate Thesis; University of Victoria, 2010.
81. Lobo, V. M., Ed. *Handbook of Electrolyte Solutions;* Elsevier, 1989.
82. Smart, O. S.; Breed, J.; Smith, G. R.; Sansom, M. S. *Biophysical Journal* **1997,** *72,* 1109-1126.
83. Chui, J. K.; Fyles, T. M. Ionic Currents of Synthetic Channels: Analysis, Lessons, and Recommendations. **Submitted 2011**.
84. Chui, J. K.; Fyles, T. M. *Chemical Communications* **2010,** *46,* 4169-4171.
85. Ferrante, C.; Kensy, U.; Dick, B. *Journal of Physical Chemistry* **1993,** *97,* 13457-13463.
86. Benniston, A. C.; Harriman, A.; Rostron, J. P. *Physical Chemistry Chemical Physics* **2005,** *7,* 3041-3047.
87. Liu, Y.; Ogawa, K.; Schanze, K. S. *Journal of Photochemistry and Photobiology C: Photochemistry Reviews* **2009,** *10,* 173-190.
88. Jiang, H.; Taranekar, P.; Reynolds, J. C.; Schanze, K. S. *Angewandte Chemie International Edition* **2009,** *48,* 4300-4316.
89. Pinto, M. R.; Kristal, B. M.; Schanze, K. S. *Langmuir* **2003,** *19,* 6523-6533.
90. Ding, L.; Chi, E. Y.; Schanze, K. S.; Lopez, G. P.; Whitten, D. G. *Langmuir* **2010,** *26* (8), 5544-5550.
91. Chen, L. H.; Xu, S.; McBranch, D.; Whitten, D. *Journal of the American Chemical Society* **2000,** *122,* 9302-9303.
92. Nagano, Y.; Ikoma, T.; Akiyama, K.; Tero-Kubota, S. *Journal of the American Chemical Society* **2003,** *125,* 14103-14112.
93. Szabo, A. G.; Rayner, D. M. *Journal of the American Chemical Society* **1980,** *102,* 554-563.
94. Caesar, C. E.; Esbjorner, E. K.; Lincoln, P.; Norden, B. *Biochemistry* **2006,** *45,* 7682-

7692.

95. Kyrychenko, A.; Herbich, J.; Wu, F.; Thummel, R. P.; Waluk, J. *Journal of the American Chemical Society* **2000,** *122,* 2818-2827.
96. Cardoso, R. M.; Filipe, H. A.; Gomes, F.; Moriera, N. D.; Vaz, W. L.; Moreno, M. J. *Journal of Physical Chemistry B* **2010,** *114,* 16337-16346.
97. Postupalenko, V. Y.; Shvadchak, V. V.; Duportail, G.; Pivovarenko, V. G.; Klymchenko, A. S.; Mely, Y. *Biochimica et Biophysica Acta* **2011,** *1808,* 424-432.
98. You, L.; Gokel, G. W. *Chemistry - a European Journal* **2008,** *14,* 5861-5870.
99. Eftink, M. R. Fluorescence Quenching: Theory and Applications. In *Topics in Fluorescence Spectroscopy, Volume 2: Principles;* Lakowicz, J. R., Ed.; Plenum Press, 1991; pp 53-126.
100. Bragg, A. E.; Schwartz, B. J. *Journal of Physical Chemistry B* **2008,** *112,* 483-494.
101. Mizuno, M.; Tanaka, J.; Harada, I. *Journal of Physical Chemistry* **1981,** *85,* 1789.
102. Chattopadhyay, A.; London, E. *Biochemistry* **1987,** *26,* 36-45.
103. Brown, D. A.; London, E. *Journal of Membrane Biology* **1998,** *164,* 103-114.
104. Zhou, Q.; Swager, T. M. *Journal of the American Chemical Society* **1995,** *117,* 12593-12602.
105. Zhou, Q.; Swager, T. M. *Journal of the American Chemical Society* **1995,** *117,* 7017-7018.
106. Dai, N.; Kool, E. T. *Chemical Society Reviews* **2011,** Advance Article: DOI 10.1039/C0CS00162G.
107. Moroda, A.; Togo, H. *Tetrahedron* **2006,** *62,* 12408-12414.
108. 500MHz NMR collected by Mrs. Christine Greenwood, NMR technician, University of Victoria.
109. Schwab, P. F.; Levin, M. D.; Michl, J. *Chemical Reviews* **1999,** *99* (7), 1863-1934.
110. Winum, J.-Y.; Matile, S. *The Journal of the American Chemical Society* **1999,** *121,* 7961-7962.
111. Mohr, A.; Talbiersky, P.; Korth, H.-G.; Sustmann, R.; Boese, R.; Blser, D.; Rehage, H. *Journal of Physical Chemistry B* **2007,** *111* (45), 12985-12992.
112. Iqbal, K. S.; Allen, M. C.; Fucassi, F.; Cragg, P. J. *Chemical Communications* **2007,** 3951-3953.
113. Lawal, O.; Iqbal, K.; Mohamadi, A.; Razavi, P.; Dodd, H. T.; Allen, M. C.; Siddiqui, S.; Fucassi, F.; Cragg, P. J. *Supramolecular Chemistry* **2009,** *21* (1-2), 55-60.
114. Schlieper, P.; De Robertis, E. *Archives of Biochemistry and Biophysics* **1977,** *184,* 204-208.
115. Rostovtseva, T. K.; Bashford, C. L.; Lev, A. A.; Pasternak, C. A. *Journal of Membrane Biology* **1994,** *141,* 83-90.
116. Alder, G. M.; Arnold, W. M.; Bashford, C. L.; Drake, A. F.; Pasternak, C. A.; Zimmerman, U. *Biochimica et Biophysica Acta* **1991,** 111-120.

117. Kyrychenko, A.; Wu, F.; Thummel, R. P.; Waluk, J.; Ladokhin, A. S. *Journal of Physical Chemistry B* **2010,** *114,* 13574-13584.

118. Perochon, E.; Lopez, A.; Tocanne, J. F. *Biochemistry* **1992,** *31,* 7672-7682.

119. Reichardt, C. *Chemical Reviews* **1994,** *94,* 2319-2358.

120. Davenport, L. *Methods in Enzymology* **1997,** *278,* 487-512.

121. Abel, E.; Maguire, G. E.; Murillo, O.; Suzuki, I.; De Wall, S. L.; Gokel, G. W. *Journal of the American Chemical Society* **1999,** *121* (39), 9043-9052.

122. Kaur, P.; Yue, H.; Wu, M.; Liu, M.; Treece, J.; Waldeck, D. H. *Journal of Physical Chemistry B* **2007,** *111,* 8589-8596.

123. Huang, Z.; Haugland, R. P. *Biochemical and Biophysical Research Communications* **1991,** *181* (1), 166-171.

124. White, S. H.; Wimley, W. C.; Ladokhin, A. S.; Hristova, K. *Methods in Enzymology* **1998,** *295,* 62-87.

125. Ladokhin, A. S.; Jayasinghe, S.; White, S. H. *Analytical Biochemistry* **2000,** No. 285, 235-245.

126. Dr. Jeffery T. Davis, comment to the author, Pacifichem 2010.

127. Lei, X.; Porco, J. A. *Organic Letters* **2004,** *6,* 795-798.

128. Gomez, C.; Chen, J.; Wang, S. *Tetrahedron Letters* **2009,** *50,* 6691-6692.

129. Kachel, K.; Asuncion-Punzalan, E.; London, E. *Biochimica et Biophysica Acta* **1998,** *1374,* 63-76.

130. Estronca, L. M.; Moreno, M. J.; Laranjinha, J. A.; Almeida, L. M.; Vaz, W. L. *Biophysical Journal* **2005,** *88,* 557-565.

131. Ding, L.; Chi, E. Y.; Chemburu, S.; Ji, E.; Schanze, K. S.; Lopez, G. P.; Whitten, D. G. *Langmuir* **2009,** *25* (24), 13742-13751.

132. Steed, J. W.; Atwood, J. L. *Supramolecular Chemistry,* 2nd ed.; John Wiley & Sons: UK, 2009.

133. Birch, D. S.; Imhof, R. E. Time-Domain Fluorescence Spectroscopy Using Time-Correlated Single-Photon Counting. In *Topics in Fluorescence Spectroscopy, Volume 1: Techniques;* Lakowicz, J. R., Ed.; Plenum Press: New York USA, 1991.

134. Li, R.; Carpentier, E.; Newell, E. D.; Olague, L. M.; Heafey, E.; Yihwa, C.; Bohne, C. *Langmuir* **2009,** *25* (24), 13800-13808.

135. Greiner, A. J.; Pillman, H. A.; Worden, R. M.; Blanchard, G. J.; Ofoli, R. Y. *Journal of Physical Chemistry B* **2009,** *113,* 13263-13268.

136. Duportail, G.; Weinreb, A. *Biochimica et Biophysica Acta* **1983,** *736,* 171-177.

137. Gratton, E.; Parasassi, T. *Journal of Fluorescence* **1995,** *5* (1), 51-57.

138. Armstrong, V. T.; Brzustowicz, M. R.; Wassall, S. R.; Jenski, L. J.; Stillwell, W. *Archives of Biochemistry and Biophysics* **2003,** *414,* 74-82.

139. Fatta, E.; Nir, S.; Parente, R. A.; Szoka, F. C. *Biochemistry* **1994,** *33,* 6721-6731.

140. Carley, A. N.; Kleinfeld, A. M. *Biochemsitry* **1999,** *45,* 10437–10445.

141. Schneider, E.; Haest, C. W.; Plasa, G.; Deuticke, B. *Biochimica et Biophysica Acta* **1986,** *855,* 325-336.
142. Missner, A.; Pohl, P. *ChemPhysChem* **2009,** *10,* 1405-1414.
143. Parvizi, P. *Unpublished results;* University of Victoria, 2011.
144. Chattopadhyay, A.; Mukherjee, S. *Biochemistry* **1993,** *32,* 3804-3811.
145. McIntyre, J. C.; Sleight, R. G. *Biochemistry* **1991,** *30,* 11819-11827.
146. Moreno, M. J.; Estronca, L. M.; Vaz, W. L. *Biophysical Journal* **2006,** *91,* 873-881.
147. Fraser, R. R.; Hanbury, P.; Reyes-Zamora, C. *Canadian Journal of Chemistry* **1967,** *45,* 2481-2487.

Appendix 1: Synthetic experimental details

General procedures

Most chemicals and solvents were used as received from known suppliers, except THF and DMF which were dried and distilled before use. All NMR spectra were recorded on a Bruker Advance 500 (500 MHz ^{1}H and 125 MHz ^{13}C) or Bruker AC300 (300 MHz ^{1}H and 75 MHz ^{13}C). Chemical shifts are reported relative to tetramethylsilane in ppm All 500 MHz NMR were collected by Mrs. Christine Greenwood, NMR technician, UVic. UV spectra were run on a Cary 5 UV-VIS spectrometer in a 10 x 10 mm quartz cell. ESI Mass spectra were recorded on a Waters MicroMass Q-TOF instrument running in negative ion mode. HPLC was performed using an HP Series 1100 instrument, with either a Macherey-Nagel "Nucleosil" RP C18 analytical (4 mm x 250 mm) or a Grace Davison "Alltima" RP C18 semi-prep (10 mm x 150 mm) column. Solvents used (ACN, CH_3OH; HPLC-grade, H_2O; Milipore) were filtered through a Milipore sub-micrometre filter before use. HPLC elution was monitored at various UV wavelengths (typically 254, 280 and 220 nm) and fluorometrically (λEx = 310, λEm = 330 nm). Fluorescence spectra were run on a PTI QM-2 instrument at T = 20^{0}C in 10 x 10 mm quartz cells equipped with a micro stir rod.

Sonogashira coupling [70]: To a round bottomed flask equipped with a septum, 1.2–1.5 equivalents (in relation to the alkyne starting material) of the iodo-containing reactant and 6–10% CuI were dissolved in dry DMF, which was then deoxygenated under vacuum. The alkyne reactant was then added to the flask, which was kept in the dark. $Pd(PPh_3)_4$ (3–5%) was then added, followed by 2–5 equivalents of NEt_3. The reaction was then stirred under N_2 at temperatures ranging from rt to 50^{0}C, for 10–24 h, depending on the reagents used. Reactions were monitored by TLC (silica gel, EtOAc/hexanes as eluent, visualized by UV, *p*-anisaldehyde and/or vanillin stain). Once complete, reactions were cooled if necessary, diluted with EtOAc and washed with saturated EDTA (2–3 times), H_2O (once), saturated NaCl

(once), dried over sodium sulfate, and concentrated under vacuum. Unless noted otherwise, the crude products were purified by column chromatography on silica gel, typically using EtOAc/hexanes as eluent.

Ester coupling: To a solution of 1.3–2 equivalents of either the alcohol or acid building block in relation to 1 equivalent of the other (excess reagent choice determined by ease of synthesis or availability) in THF or DMF (depending on substrate) were added 1.3–2 eq. of DIC, HOBt and 2.6–4 eq. of DIPEA. The reaction was sealed under an atmosphere of N_2, and stirred for 16–24 h at temperatures varying between rt and 50^0C. Reaction completion was monitored by TLC. Once complete, the reaction was cooled (if necessary), filtered to remove DIU, and diluted with DCM or EtOAc. The organic phase was extracted with H_2O (twice), saturated $NaHCO_3$ (twice), rinsed with sat. NaCl (once), dried with anhydrous sodium sulfate, and concentrated under vacuum. Unless noted otherwise, the crude product was purified by column chromatography on silica gel, typically using EtOAc/hexanes as eluent.

THP removal: pTsOH (5–25%) was added to a solution of compound in ~10–30% CH_3OH: DCM, which was stirred at rt for 1–3 h, as monitored by TLC. Once complete, the reaction was diluted with DCM, washed with H_2O (once), saturated $NaHCO_3$ (twice), and saturated NaCl (once), then dried over sodium sulfate and concentrated under vacuum. If necessary, further purification was carried out as noted.

Fluoride deprotection: ~5–10 equivalents of 1.0 M TBAF in THF were added to a solution of compound in THF, which was then stirred at rt for 1–3 h, as monitored by TLC. Once complete, the reaction was quenched by the addition of H_2O, diluted into EtOAc, washed with 10% aqueous HCl, (once), then H_2O (until neutral) and saturated NaCl (once), then dried over sodium sulfate and concentrated under vacuum. Further purification was carried out as noted.

Prenyl deprotection*:* Adapted [71]: 0.025–0.1 equivalents TMSOTf were added to the compound dissolved in DCM, which was stirred at rt. Once complete (as monitored by TLC, generally < 1 h), the reaction mixture was diluted further into DCM, washed with

H_2O, saturated $NaHCO_3$ and saturated NaCl, then dried over sodium sulfate and concentrated under vacuum. Further purification was carried out as noted.

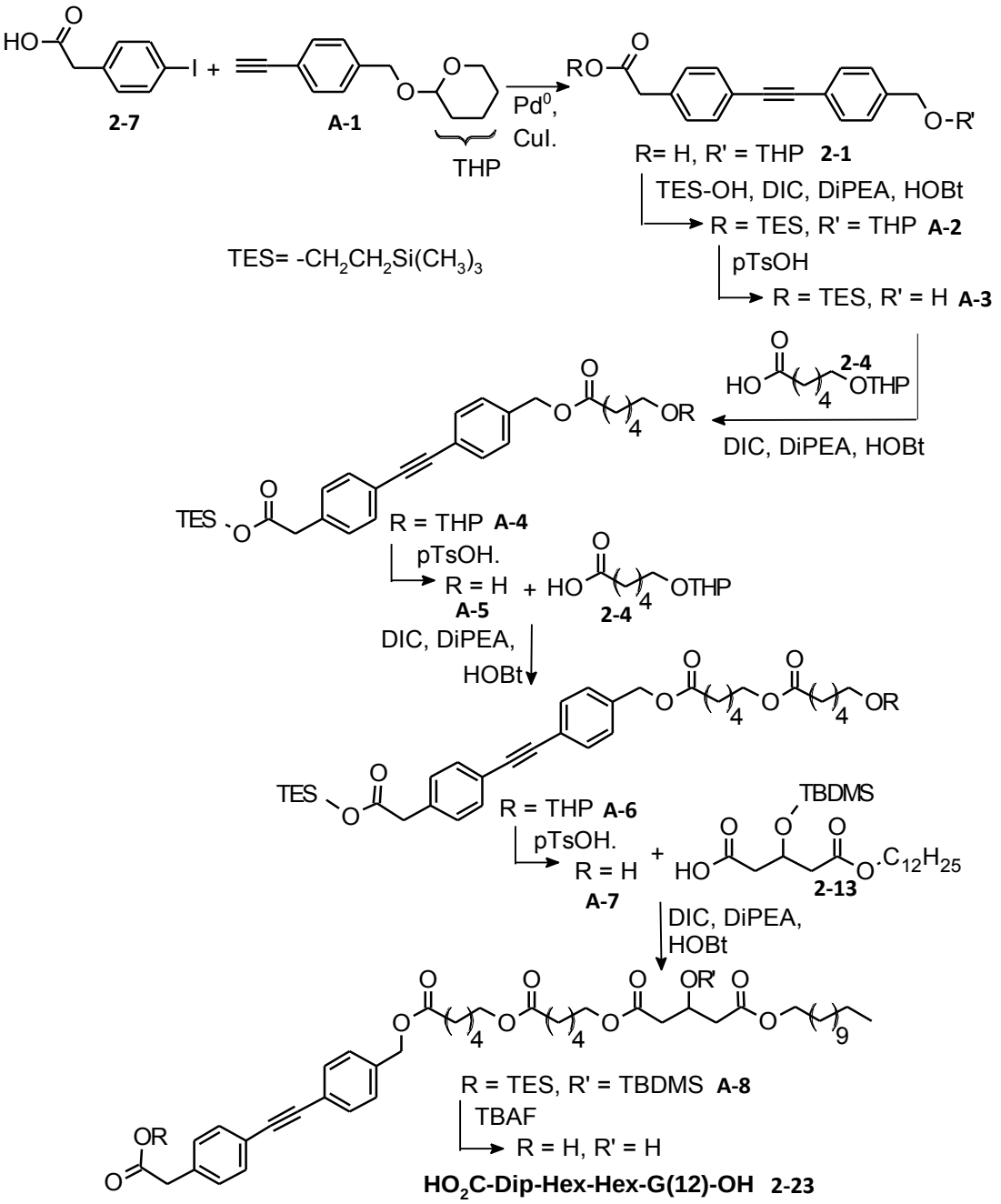

Scheme A1.1: Synthesis of **HO_2C-Dip-Hex-Hex-G(12)-OH (2-23)**

A-1: Previously synthesized [147] but no spectral data reported. 1.0 equivalent of 4-ethynylbenzyl alcohol, 1.2 equivalents DHP, 0.1 equivalents TsOH, stirred in DCM at 0^0C – rt for 0.5 – 2hr. Once complete, the reaction was diluted with DCM, extracted

against saturated $NaHCO_3$ (twice), washed with H_2O and saturated NaCl (until neutral), then dried over sodium sulfate and concentrated under vacuum. Purification by silica gel column (elution at ~5% EtOAc/hexanes). Yields average ~90% (multiple preparations) of a clear, colourless oil. NMR ($CDCl_3$): ^{1}H: 7.46 (d, 2H, *J*= 8Hz), 7.31 (d, 2H, *J*= 8Hz), 4.77 (d, 1H, *J*= 13Hz), 4.68, (t, 1H, *J*= 4Hz), 4.49 (d, 1H, *J*= 13Hz), 3.89 (m, 1H), 3.53 (m, 1H), 3.06 (s, 1H), 1.85-1.55 (m, 6H). ^{13}C: 139.2, 132.1, 127.5, 121.1, 97.8, 83.6, 77.1, 68.3, 62.1, 30.5, 25.4, 19.3.

2-1: Sonogashira coupling: 1.2 – 1.5 equivalents **2-7**, 1.0 equivalent **A-1**, 5% $Pd(PPh_3)_4$, 10% CuI, DMF, 2-5 eq. NEt_3, Stir at 40 – 50^{0}C for 16 – 24 hr. Standard workup, purification by silica gel column; (elution at ~15% EtOAc/hexanes, 1% AcOH added to all eluting solvents). Yields **2-1** (74 – 90%, multiple preparations) of clear, colourless crystals, which can be re-crystallized from slow evaporation of THF/pentane. MP: 151 – 153^{0}C. NMR ($CDCl_3$): ^{1}H : 7.49 (m, 4H), 7.34, (d, 2H, *J*= 8Hz), 7.27 (d, 2H, *J*= 8 Hz), 4.78 (d, 1H, *J*= 13Hz), 4.71 (t, 1H, *J*= 1Hz), 4.50 (d, 1H, *J*= 13Hz), 3.91 (m, 1H), 3.66 (s, 2H), 3.55 (m, 1H), 1.89 – 1.52 (m, 6H). ^{13}C: 176.6, 138.6, 133.3, 131.8, 131.6, 129.4, 127.6, 122.4, 122.3, 97.8, 89.6, 88.9, 68.5, 62.1, 40.8, 30.5, 25.4, 19.3.

A-2: Ester coupling: 1.0 equivalent (1.5 g, 4.2 mmol) of **2-1**, 3 equivalents TES-OH, DIC, HOBt, 5 equivalents DIPEA in THF. Stirred at 40^{0}C for 16 hr. Standard workup, purification by silica gel column (elution at ~5% EtOAc/hexanes). Yields 1.81g (90%) of a white, waxy solid. MP: 46 – 48^{0}C. NMR ($CDCl_3$): ^{1}H: 7.48 (m, 4H), 7.32 (d, 2H, *J*= 8Hz), 7.26 (d, 2H, *J*= 8Hz), 4.78 (d, 1H, *J*= 13Hz), 4.69 (t, 1H, *J*= 4Hz), 4.50 (d, 1H, *J*= 13Hz), 4.15 (m, 2H), 3.91 (m, 1H), 3.59 (s, 2H), 3.54 (m, 1H), 1.86-1.53 (m, 6H), 0.95 (m, 2H), 0.00 (s, 9H). ^{13}C: 171.3, 138.6, 134.3, 131.7, 131.6, 129.3, 127.6, 122.3, 122.0, 97.8, 89.4, 89.1, 68.4, 63.3, 62.2, 41.5, 30.5, 25.5, 19.3, 17.2, -1.5.

A-3: THP removal conditions: 1.0 equivalent (1.4 g, 3.0 mmol) of **A-2**, 0.3 equivalents

TsOH in 10% CH_3OH/DCM. Stirred for 3 hr at rt. Standard workup, used without further purification. Yields 1.05 g (95%) of a white solid. NMR ($CDCl_3$): ^{1}H: 7.48 (m, 4H), 7.32 (d, 2H, *J*= 8Hz), 7.26 (d, 2H, *J*= 8Hz), 4.69 (d, 2H, *J*= 4Hz), 4.16 (m, 2H), 3.58 (s, 2H), 1.85 (t, 1H, *J*= 4Hz), 0.95 (m, 2H), 0.0 (s, 9H). ^{13}C: 171.4, 140.9, 134.9, 131.7, 129.3, 126.8, 122.4, 121.9, 89.3, 89.2, 64.9, 63.3, 41.5, 17.2, -1.6.

A-4: Ester coupling conditions: 1.0 equivalent (1.0 g, 2.7 mmol) of **A-3**, 2.0 equivalents **2-4**, DIC, HOBt, 4.0 equivalents DIPEA in DMF. Stirred at 40^{0}C for 24 hr. Standard workup, purification by silica gel column (elution at ~10% EtOAc/hexanes). Yields 1.23 g (79%) of pale yellow crystals, MP < rt. NMR ($CDCl_3$): ^{1}H: 7.47 (m, 4H), 7.30 (d, 2H, *J*= 8Hz), 7.25 (d, 2H, *J*= 8Hz), 5.09 (s, 2H), 4.54 (t, 1H, *J*= 4Hz), 4.17 (m, 2H), 3.83 (m, 1H), 3.71 (m, 1H), 3.58 (s, 2H), 3.47 (m, 1H), 3.35 (m, 1H), 2.36 (t, 2H, *J*= 7Hz), 1.68-1.36 (m, 12H), 0.95 (m, 2H), 0.00 (s, 9H). ^{13}C: 173.4, 171.2, 136.1, 134.4, 131.7, 131.6, 129.3, 127.9, 123.1, 121.8, 98.8, 89.5, 89.0, 67.2, 65.6, 63.2, 62.3, 41.4, 34.2, 30.7, 29.3, 25.8, 25.4, 24.8, 19.6, 17.2, -1.6.

A-5: THP removal conditions: 1.0 equivalent (1.2 g, 2.1 mmol) of **A-4**, 0.2 equivalents TsOH in 25% CH_3OH/DCM. Stirred for 2.5 hr at rt. Standard workup, used without further purification. Yields 0.99 g (97%) of a white solid. MP = 48 – 50^{0}C. NMR ($CDCl_3$): ^{1}H: 7.48 (m, 4H), 7.30 (d, 2H, *J*= 8Hz), 7.25 (d, 2H, *J*= 8Hz), 5.09 (s, 2H), 4.16 (m, 2H), 3.61 (m, 4H), 2.37 (t, 2H, *J* = 7Hz), 1.66 (m, 2H), 1.56 (m, 2H), 1.45 (s, br, 1H), 1.38 (m, 2H), 0.95 (m, 2H), 0.00 (s, 9H). ^{13}C: 173.4, 171.3, 136.1, 134.5, 131.7, 131.6, 129.3, 128.0, 123.1, 121.8, 89.5, 89.0, 65.6, 63.3, 62.6, 41.5, 34.1, 32.2, 25.2, 24.6, 17.2, -1.6.

A-6: Ester coupling conditions: 1.0 equivalent (0.63 g, 1.3 mmol) of **A-5**, 2.0 equivalents **2-4** [41], DIC, HOBt, 4.0 equivalents DIPEA in THF. Stirred at 40^{0}C for 24 hr. Standard workup, purification by silica gel column (1:1 EtOAc/hexanes). Yields 0.68 g (76%) of a clear, colourless, viscous oil. NMR ($CDCl_3$): ^{1}H: 7.48 (m, 4H), 7.30 (d, 2H,

J= 8Hz), 7.24 (d, 2H, *J*= 8Hz), 5.09 (s, 2H), 4.54 (t, 1H, *J*= 4Hz), 4.16 (m, 2H), 4.03 (t, 2H, *J*= 7Hz), 3.83 (m, 1H), 3.69 (m, 1H), 3.58 (s, 2H), 3.46 (m, 1H), 3.36 (m, 1H), 2.36 (t, 2H, *J*= 7Hz), 2.28 (t, 2H, *J*= 7Hz), 1.75-1.32 (m, 18H), 0.95 (m, 2H), 0.00 (s, 9H). ^{13}C: 173.7, 173.2, 171.2, 136.1, 134.4, 131.7, 131.6, 129.3, 128.1, 123.1, 121.8, 98.8, 89.6, 89.0, 67.3, 65.7, 63.9, 63.3, 62.3, 41.5, 34.2, 34.0, 30.7, 29.4, 28.3, 25.8, 25.5, 25.4, 24.8, 24.5, 19.6, 17.2, -1.6.

A-7: THP removal conditions: 1.0 equivalent of **A-6**, 0.3 equivalents TsOH in 20% CH_3OH/DCM. Stirred for 3 hr at rt. Standard workup, used without further purification. Yields 0.42 g (96%) of a clear, pale yellow oil. NMR ($CDCl_3$): ^{1}H: 7.48 (m, 4H), 7.30 (d, 2H, *J*= 8Hz), 7.26 (d, 2H, *J*= 8Hz), 5.10 (s, 2H), 4.17 (m, 2H), 4.04 (t, 2H, *J*= 7Hz), 3.65 (m, 3H), 3.59 (s, 2H), 2.36 (t, 2H, *J*= 7Hz), 2.29 (t, 2H, *J*= 7Hz), 1.69 – 1.53 (m, 7H), 1.43 – 1.34 (m, 5H), 0.96 (m, 2H), 0.0 (s, 9H). ^{13}C: 173.8, 173.4, 171.4, 136.2, 134.6, 131.8, 129.4, 128.1, 123.3, 121.9, 89.1, 65.8, 64.1, 63.4, 62.7, 41.6, 34.3, 34.2, 32.4, 28.4, 25.6, 25.3, 24.7, 24.6, 17.4, -1.5.

A-8: Ester coupling conditions: 1.0 equivalent **A-7** (0.34 g, 0.56 mmol), 2.0 equivalents **2-13** [48], DIC, HOBt, 4.0 equivalents DIPEA in DMF. Stirred at 40^{0}C for 24 hr. Standard workup, purification by silica gel column (elution at ~5% EtOAc/hexanes). Yields 0.341 g (60%) of a clear, pale yellow oil. NMR ($CDCl_3$): ^{1}H: 7.48 (m, 4H), 7.30 (d, 2H, *J*= 8Hz), 7.26 (d, 2H, *J*= 8Hz), 5.09 (s, 2H), 4.51 (quintet, 1H, *J*= 6Hz), 4.17 (m, 2H), 4.03 (m, 6H), 3.59 (s, 2H), 2.52 (m, 4H), 2.36 (t, 2H, *J*= 7Hz), 2.27 (t, 2H, *J*= 7Hz), 1.69 – 1.57 (m, 10H), 1.37 (m, 4H), 1.23 (s, 18H), 0.96 (m, 2H), 0.86 (t, 3H, *J*= 7Hz), 0.82 (s, 9H), 0.04 (s, 6H), 0.00 (s, 9H). ^{13}C: 173.5, 173.1, 171.2, 171.0, 136.1, 134.5, 131.7, 129.3, 128.0, 123.2, 121.8, 89.6, 89.0, 66.3, 65.6, 64.7, 64.3, 64.0, 63.2, 42.5, 42.4, 41.5, 34.0, 31.9, 29.6, 29.5, 29.4, 29.3, 29.2, 28.5, 28.3, 28.2, 25.9, 25.6, 25.5, 24.6, 24.5, 22.6, 17.9, 17.3, 14.1, -1.6, -4.9.

2-23: Fluoride deprotection conditions: 6 equivalents of 1.0 M TBAF in THF were

added to **A-8** in THF. Stirred for 3hr at rt. Standard workup. The crude residue was purified on Florisil (EtOAc/hexanes, 1% AcOH added to all eluting solvents). While the reaction appeared quantitative by TLC, the purification was problematic, leading to a 59% yield (0.12 g) of a pale blue solid, which was further purified by RP-HPLC (1:1ACN: CH_3OH as eluting solvents) to yield a crystalline white solid. UV: λ_{max} (CH_3OH)= 288 nm (ε= 24 813 $M^{-1}cm^{-1}$. Fluorescence: λ_{max}Ex (CH_3OH)= 305 nm, λ_{max}Em (CH_3OH)= 322 nm. NMR (1:1 $CDCl_3$: CD_3OD, 500MHz): ^{1}H: 7.48 (d, 2H, *J*= 8Hz), 7.40 (d, 2H, *J*= 8Hz), 7.34 (d, 2H, *J*= 8Hz), 7.30 (d, 2H, *J*= 8Hz), 5.12 (s, 2H), 4.42 (m, 1H), 4.07 (m, 6H), 3.61 (s, br, 2H), 2.53 (m, 4H), 2.40 (t, 2H, *J*= 7Hz), 2.31 (t, 2H, *J*= 7Hz), 1.70 – 1.59 (m, 10H), 1.39 (m, 4H), 1.26 (s, 18H), 0.88 (t, 3H, *J*= 7Hz). ^{13}C: 175.4, 174.9, 172.9, 172.8, 139.9, 137.4, 132.6, 132.3, 130.4, 129.1, 124.6, 121.8, 90.9, 89.2, 66.7, 66.0, 65.8, 65.5, 65.3, 42.7, 42.6, 35.0, 34.9, 32.9, 30.7, 30.7, 30.6, 30.5, 30.4, 30.3, 29.6, 29.3, 29.2, 26.9, 26.5, 26.4, 25.6, 23.6, 14.5. MS (-ve ESI): Calc'd for $C_{46}H_{63}O_{11}$= 791.4376 amu, obtained = 791.455 amu. Overall yield over 10 steps from 4-ethynylbenzyl alcohol = 13%

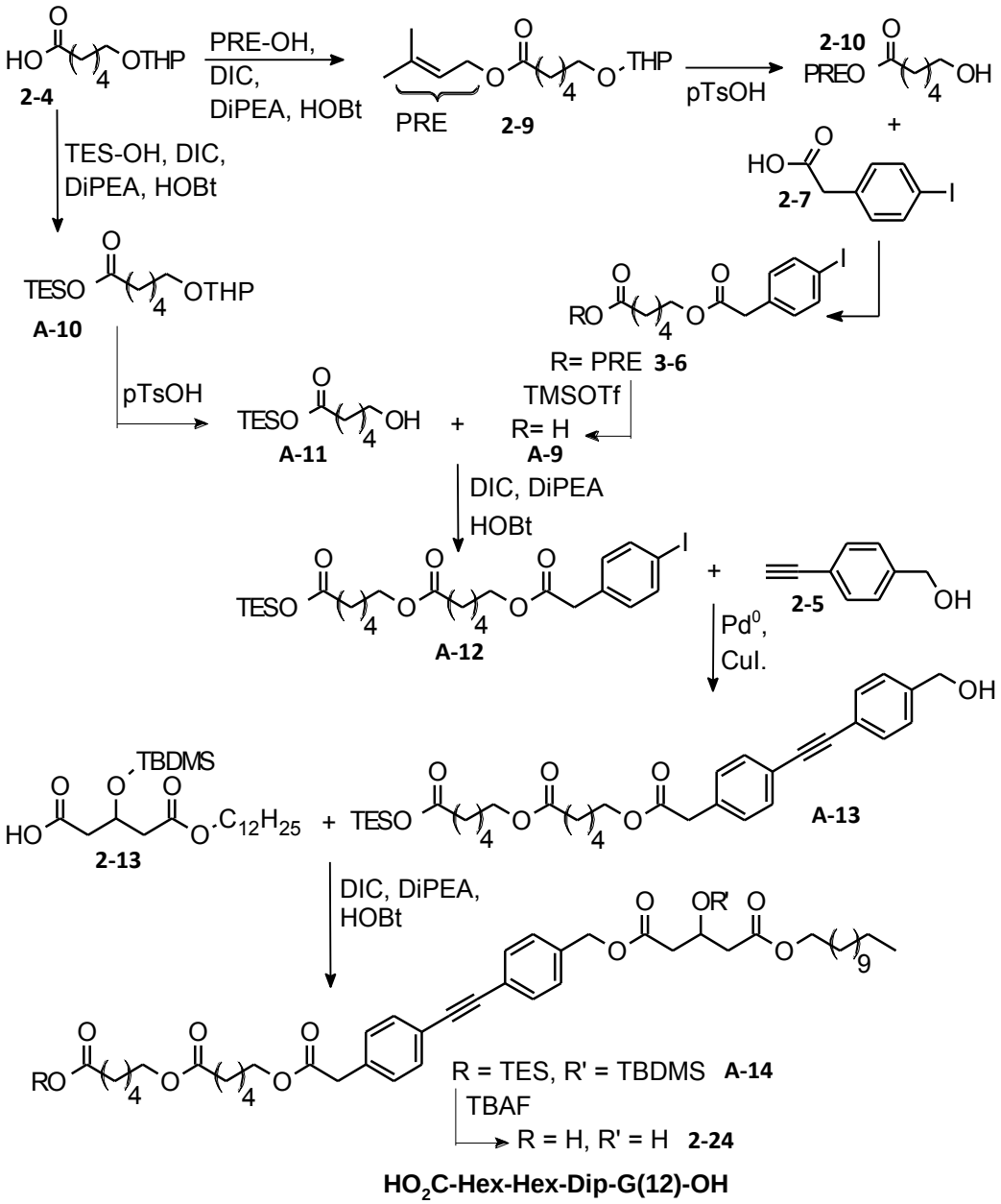

Scheme A1.2: Synthesis of **HO_2C-Hex-Hex-Dip-G(12)-OH** (**2-24**)

2-9: Ester coupling conditions: 1.0 equivalent (0.5 g, 2.3 mmol) of **2-4**, 1.2 equivalents PRE-OH, DIC, HOBt, 2.4 equivalents DiPEA in THF as solvent. Stirred at rt for 18 hr. Yields 0.49 g (74%) of clear colourless oil. NMR ($CDCl_3$): ^{1}H: 5.31 (m, 1H), 4.53 (m, 3H), 3.83 (m, 1H), 3.70 (m, 1H), 3.46 (m, 1H), 3.35 (m, 1H), 2.28 (t 2H, *J*= 7Hz), 1.79 (m, 1H), 1.73 (s, 3H), 1.68 (s, 3H), 1.66 – 1.49 (m, 9H), 1.36 (m, 2H). ^{13}C:

173.7, 138.9, 118.7, 98.8, 67.3, 65.8, 62.3, 61.2, 34.3, 30.7, 29.4, 25.8, 25.7, 25.5, 24.8, 19.6, 17.9.

2-10: THP removal conditions: 1.0 equivalent (0.45 g, 1.59 mmol) of **2-9**, 0.1 equivalent TsOH in 10% CH_3OH/DCM. Stirred at rt for 2 hr. Standard workup, purification by silica gel column (elution at ~15% EtOAc/hexanes) yields 0.32 g (86%) of a clear, colourless oil. NMR ($CDCl_3$): ^{1}H: 5.26 (m, 1H), 4.49 (d, 2H, *J*= 7Hz), 3.54 (t, 2H, *J*= 7Hz), 2.33 (s, br, 1H), 2.24 (t, 2H, *J*= 7Hz), 1.68 (s, 3H), 1.63 (s, 3H), 1.58 (m, 2H), 1.50 (m, 2H), 1.31 (m, 2H).^{13}C: 173.8, 138.9, 118.6, 62.3, 61.2, 34.2, 32.2, 25.7, 25.2, 24.6, 17.9.

3-6: Ester coupling conditions: 1.0 equivalent (1.4 g, 6.0 mmol) of **2-7**, 1.5 equivalents of **2-10**, DIC, HOBt, 3.0 equivalents DiPEA in THF. Stirred at 40^{0}C for 16 hr. Standard workup, purification by silica gel column (elution at ~7% EtOAc/hexanes). Yields 1.76 g (73%) of a clear, colourless oil. NMR ($CDCl_3$): ^{1}H: 7.61 (dt, 2H, *J*= 8, 2Hz), 7.00 (d, 2H, *J*= 8Hz), 5.31 (m, 1H), 4.54 (d, 2H, *J*= 7Hz), 4.05 (t, 2H, *J*= 7Hz), 3.51 (s, 2H), 2.26 (t, 2H, *J*= 7Hz), 1.73 (s, 3H), 1.68 (s, 3H), 1.60 (m, 4H), 1.31 (m, 2H).^{13}C: 173.5, 171.0, 139.0, 137.6, 133.7, 131.3, 118.6, 92.6, 64.8, 61.3, 40.9, 34.1, 28.2, 25.8, 25.4, 24.5, 18.0.

A-9: Prenyl deprotection conditions: 1.0 equivalent (0.5 g, 1.2 mmol) **3-6**, 0.05 equivalents TMSOTf in DCM, stirred at rt for 1 hr. During this time, the reaction turned dark brown/purple. Standard workup yielded a brown oil, from which a white solid precipitated with the addition of hexanes, yielding 0.359 g (83%) of **A-9**, which was used without further purification. NMR ($CDCl_3$): ^{1}H: 11.38 (s, br, 1H), 7.61 (d, 2H, *J*= 8Hz), 6.99 (d, 2H, *J*= 8Hz), 4.05 (t, 2H, *J*= 7Hz), 3.52 (s, 2H), 2.31 (t, 2H, *J*= 7Hz), 1.60 (m, 4H), 1.33 (m, 2H). ^{13}C: 179.7, 171.2, 137.6, 133.7, 131.3, 92.7, 64.9, 40.9, 33.9, 28.2, 25.3, 24.2.

A-10: Ester coupling conditions: 1.0 equivalent (1.43 g, 6.62 mmol) of **2-4**, 1.5 equivalents TES-OH, DIC, HOBt, 3.0 equivalents DiPEA in THF. Stirred at rt for 16 hr. Standard workup, purification by silica gel column (elution at ~4% EtOAc/hexanes) yields 1.71 g, (82%) as a clear colourless oil. NMR ($CDCl_3$): ^{1}H: 4.54 (m, 1H), 4.12 (m, 2H), 3.83 (m, 1H), 3.69 (m, 1H), 3.46 (m, 1H), 3.34 (m, 1H), 2.26 (t, 2H, *J*= 7Hz), 1.81-1.34 (m, 12H), 0.94 (m, 2H), 0.01 (s, 9H).^{13}C: 173.5, 98.5, 67.0, 62.1, 61.9, 34.2, 30.5, 29.2, 25.7, 25.3, 24.6, 19.4, 17.1, -1.7.

A-11: THP deprotection conditions: 1.0 equivalent (0.4 g, 1.3 mmol) of **A-10**, 0.1 equivalent TsOH in 10% CH_3OH/DCM. Stirred at rt for 2.5 hr. Standard workup, purification by silica gel column (elution at ~20% EtOAc/hexanes) yields 0.272 g, (93%) of **A-11** as a clear, colourless oil. NMR ($CDCl_3$): ^{1}H: 4.12 (m, 2H), 3.60 (t, 2H, *J*= 6Hz), 2.26 (t, 2H, *J*= 7Hz), 1.90 (s, br, 1H), 1.66 – 1.49 (m, 4H), 1.35 (m, 2H), 0.94 (m, 2H), 0.00 (s, 9H).^{13}C: 173.9, 62.5, 62.4, 34.3, 32.2, 25.2, 24.6, 17.2, -1.6.

A-12: Ester coupling conditions: 1.0 equivalent (0.36 g, 0.97 mmol) of **A-9**, 1.4 equivalents of **A-11**, DIC, HOBt, 2.8 equivalents DiPEA in THF. Stirred at rt for 16 hr. Standard workup, purification by silica gel column (elution at ~10% EtOAc/hexanes) yields 0.52 g (92%) as a clear, colourless oil. NMR ($CDCl_3$): ^{1}H: 7.62 (d, 2H, *J*= 8Hz), 7.01 (d, 2H, *J*= 8Hz), 4.14 (m, 2H), 4.05 (m, 4H), 3.52 (s, 2H), 2.26 (m, 4H), 1.69-1.55 (m, 8H), 1.41-1.26 (m, 4H), 0.96 (m, 2H), 0.02 (s, 9H).^{13}C: 173.6, 173.4, 170.9, 137.6, 133.6, 131.2, 92.5, 64.8, 64.1, 62.4, 40.8, 34.3, 34.0, 28.3, 28.2, 25.5, 25.4, 24.5, 24.4, 17.3, -1.5.

A-13: Sonogashira coupling conditions: 1.0 equivalent (0.35 g, 0.59 mmol) of **A-12**, 1.5 equivalents **2-5**, 5% $Pd(PPh_3)_4$, 10% CuI, 3.0 equivalents NEt_3 in deoxygenated DMF. Stirred in the dark under N_2 at rt for 16 hr. Standard workup, purification by silica gel column (elution at ~35% EtOAc/hexanes), yields 0.299 g, (85%) as a pale yellow semi-solid. NMR ($CDCl_3$): ^{1}H: 7.48 (m, 4H), 7.33 (d, 2H, *J*= 8Hz), 7.25 (d, 2H, *J*=

8Hz), 4.69 (d, 2H, *J*= 1Hz), 4.14 (m, 2H), 4.06 (m, 4H), 3.61 (s, 2H), 2.26 (m, 4H), 1.91 (s, br, 1H), 1.67 – 1.56 (m, 8H), 1.35 (m, 4H), 0.96 (m, 2H), 0.03 (s, 9H).^{13}C: 173.7, 173.5, 171.2, 141.1, 134.3, 131.7, 129.3, 126.8, 122.4, 122.0, 89.3, 89.1, 64.9, 64.8, 64.2, 62.5, 41.3, 34.3, 34.1, 28.4, 28.2, 25.6, 25.5, 24.6, 24.5, 17.3, -1.5.

A-14: Ester coupling conditions: 1.0 equivalent (0.25 g, 0.42 mmol) of **A-13**, 1.3 equivalents **2-13**, DIC, HOBt, 2.6 equivalents DIPEA in DMF. Stirred at 50^{0}C for 24 hr. Standard workup, purification by silica gel column (elution at ~15% EtOAc/hexanes) yields 0.26 g (61%) as a pale yellow oil. NMR ($CDCl_3$): ^{1}H: 7.48 (m, 4H), 7.30 (d, 2H, *J*= 8Hz), 7.25 (d, 2H, *J*= 8Hz), 5.09 (m, 2H), 4.56 (quintet, 1H, *J*= 6Hz), 4.14 (m, 2H), 4.10 – 4.00 (m, 6H), 3.61 (s, 2H), 2.61 (d, 2H, *J*= 6Hz), 2.54 (d, 2H, *J*= 6Hz), 2.27 (t, 4H, *J*= 7Hz), 1.67 – 1.56 (m, 10H), 1.38 (m, 4H), 1.24 (s, br, 18H), 0.96 (m, 2H), 0.86 (t, 3H, *J*= 7Hz), 0.82 (s, 9H), 0.03 (m, 6H), 0.02 (s, 9H).^{13}C: 173.6, 173.4, 171.1, 170.9, 170.7, 135.8, 134.4, 131.7, 131.6, 129.3, 128.0, 123.1, 121.9, 89.6, 89.2, 66.2, 65.8, 64.7, 64.6, 64.1, 62.4, 42.4, 42.3, 41.3, 34.2, 34.0, 31.8, 29.6, 29.5, 29.4, 29.3, 29.2, 28.5, 28.3, 28.2, 25.9, 25.6, 25.5, 25.4, 24.5, 24.4, 22.6, 17.8, 17.3, 14.1, -1.6, -4.9.

2-14: Fluoride deprotection conditions: 1.0 equivalent (0.2 g, 0.2 mmol) of **A-14**, 10 equivalents of 1.0 M TBAF in THF, stirred at rt for 3 hours. Standard workup, purification by silica gel chromatography (elution at ~30% EtOAc/hexanes, 1% AcOH added to all eluting solvents) yields the desired oligomer (0.115 g, 73%) as an off-white solid. The compound was further purified by RP-HPLC (1: 1 ACN: CH_3OH as eluting solvents) to yield a white powder. UV: λ_{max} (CH_3OH)= 286 nm (ε= 24 813 M^{-1} cm^{-1}). Fluorescence: λ_{max}Ex (CH_3OH)= 305 nm, λ_{max}Em (CH_3OH)= 322 nm. NMR (1:1 $CDCl_3$: CD_3OD, 500 MHz): ^{1}H: 7.47 (m, 4H), 7.33 (d, 2H, *J*= 8Hz), 7.25 (d, 2H, *J*= 8Hz), 5.13 (s, 2H), 4.46 (m, 1H), 4.09 – 4.01 (m, 6H), 3.63 (s, 2H), 2.60 (m, 2H), 2.53 (m, 2H), 2.28 (t, 4H, *J*= 7Hz), 1.66 – 1.58 (m, 10H), 1.40 – 1.23 (m, 23H), 0.85 (t, 3H, *J*= 7Hz).^{13}C: 175.0, 172.7, 172.6, 172.2, 136.7, 135.2, 132.4, 132.3, 130.1, 128.8, 123.9, 122.7, 90.1, 89.7, 66.7, 65.7, 65.6, 65.5, 65.1, 42.1, 41.9, 34.7, 32.6, 30.3, 30.3, 30.2,

30.1, 30.0, 29.9, 29.2, 28.9, 28.8, 26.6, 26.2, 26.0, 25.3, 25.1, 23.3, 14.5. MS (-ve ESI): Calc'd for $C_{46}H_{63}O_{11}$ = 791.4376 amu, obtained = 791.478 amu. Overall yield over 11 steps from **2-4**: 10%

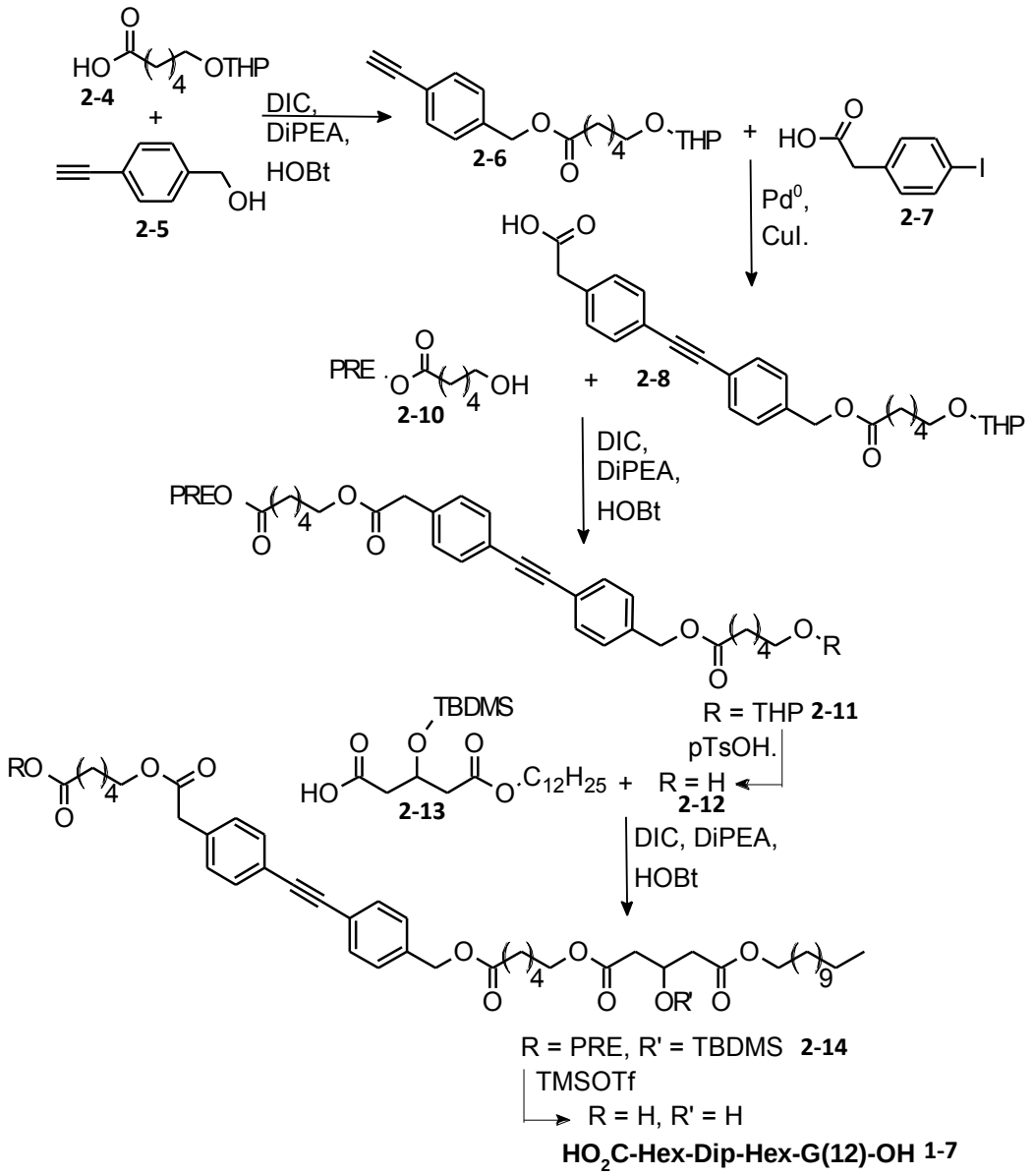

Scheme A1.3: Synthesis of **HO_2C-Hex-Dip-Hex-G(12)-OH** (**1-7**).

2-6: Ester coupling conditions: 1.0 equivalent (1.18 g, 8.92 mmol) of **2-5**, 1.5 equivalents of **2-4**, DIC, HOBt, 3.0 equivalents DIPEA in THF. Stir at rt for 16 hr.

Standard workup, purification by silica gel column (elution at ~5% EtOAc/hexanes), yields 2.41 g (82%) of a clear, pale yellow oil. NMR ($CDCl_3$): ^{1}H: 7.43 (d, 2H, *J*= 7Hz), 7.26 (d, 2H, *J*= 7Hz), 5.05 (s, 2H), 4.50 (m, 1H), 3.81 (m, 1H), 3.67 (m, 1H), 3.44 (m, 1H), 3.34 (m, 1H), 3.06 (s, 1H), 2.33 (t, 2H, *J*= 7Hz), 1.77 – 1.34 (m, 12H).^{13}C: 173.3, 136.8, 132.2, 127.9, 121.9, 98.8, 83.2, 77.6, 67.2, 65.4, 62.3, 34.1, 30.7, 29.3, 25.8, 25.4, 24.7, 19.6.

2-8: Sonogashira coupling conditions: 1.0 equivalent of **2-6**, 1.3 equivalents **2-7**, 4% $Pd(PPh_3)_4$, 8% CuI, 2.0 equivalents NEt_3, in DMF. Stir at rt for 16hr. After standard workup, the crude residue (a brown oil) was treated with diethyl ether, from which a white precipitate was isolated by filtration. This procedure lead to a suitably pure compound in ~80% yield (78 – 83, three separate preparations), which could be further purified by column chromatography on silica gel (EtOAc/hexanes, 1% AcOH added to all eluting solvents). NMR (d_6-acetone): ^{1}H: 7.53 (m, 4H), 7.43 (d, 2H, *J*= 8Hz), 7.37 (d, 2H, *J*= 8Hz), 5.15 (s, 2H), 4.55 (m, 1H), 3.78 (m, 1H), 3.67 (m, 3H), 3.43 (m, 1H), 3.35 (m, 1H), 2.40 (t, 2H, *J*= 7Hz), 1.81 – 1.39 (m, 12H). ^{13}C: 173.5, 172.4, 138.2, 136.7, 132.4, 132.3, 130.6, 129.0, 123.7, 122.4, 99.2, 90.2, 89.6, 67.6, 65.8, 62.2, 41.1, 34.5, 31.5, 30.1, 26.6, 26.4, 25.5, 20.2.

2-11: Ester coupling conditions: 1.0 equivalent (0.25g, 0.76 mmol) of **2-10**, 1.2 equivalents of **2-8**, DIC, HOBt, 2.4 equivalents DIPEA in THF. Stirred at 40^{0}C for 24 hr. Standard workup, purification by silica gel column (elution at ~20% EtOAc/hexanes) yields 0.32 g (55%) of a pale yellow, clear oil. NMR ($CDCl_3$): ^{1}H: 7.47 (m, 4H), 7.29 (d, 2H, *J*= 8Hz), 7.24 (d, 2H, *J*= 8Hz), 5.31 (m, 1H), 5.09 (s, 2H), 4.54 (m, 3H), 4.06 (t, 2H, *J*= 7Hz), 3.83 (m, 1H), 3.71 (m, 1H), 3.59 (s, 2H), 3.47 (m, 1H), 3.35 (m, 1H), 2.36 (t, 2H, *J*= 7Hz), 2.27 (t, 2H, *J*= 7Hz), 1.78 (m, 1H), 1.73 (s, 3H), 1.68 (s, 3H), 1.67 – 1.29 (m, 17H). ^{13}C: 173.4, 173.3, 171.1, 138.9, 136.1, 134.3, 131.7, 131.6, 129.3, 127.9, 123.1, 121.8, 118.5, 98.8, 89.5, 89.0, 67.2, 65.5, 64.7, 62.3, 61.2, 41.2, 34.1, 34.0, 30.7, 29.3, 28.2, 25.8, 25.7, 25.4, 25.3, 24.7, 24.4, 19.6, 17.9.

2-12: THP deprotection conditions: 1.0 equivalent (0.32g, 0.42 mmol) of **2-11**, 0.2 equivalents TsOH in 20% CH_3OH/DCM, stirred at rt for 3 hr. Standard workup yields 0.28 g (>95%, quantitative conversion by TLC) of a clear, pale yellow oil, which was used directly without further purification to synthesize **2-14**.

2-14: Ester coupling conditions: 1.0 equivalent (0.28 g, 0.41 mmol) of **2-12**, 1.5 equivalents **2-13**, DIC, HOBt, 3.0 equivalents DIPEA in THF. Stirred at rt for 30 hr (sluggish coupling, poor conversion by TLC). Standard workup, purification by silica gel column (elution at ~10% EtOAc/hexanes) yields 0.21 g (53%) of a clear, colourless oil. NMR ($CDCl_3$): ^{1}H: 7.44 (m, 4H), 7.25 (d, 2H, *J*= 8Hz), 7.20 (d, 2H, *J*= 8Hz), 5.27 (m, 1H), 5.05 (s, 2H), 4.50 (m, 3H), 4.07 – 3.96 (m, 6H), 3.56 (s, 2H), 2.48 (m, 4H), 2.32 (t, 2H, *J*= 7Hz), 2.23 (t, 2H, *J*= 7Hz), 1.69 (s, 3H), 1.64 (s, 3H), 1.57 (m, 10H), 1.38 – 1.19 (m, 22H), 0.82 (t, 3H, *J*= 7Hz), 0.77 (s, 9H), 0.00 (m, 6H). ^{13}C: 173.5, 173.2, 171.1, 171.0, 171.0, 138.9, 136.1, 134.4, 131.7, 129.3, 128.0, 123.2, 121.9, 118.6, 89.6, 89.0, 66.3, 65.7, 64.8, 64.7, 64.2, 61.2, 42.5, 42.4, 41.3, 34.1, 34.0, 31.9, 29.6, 29.5, 29.4, 29.3, 29.2, 28.5, 28.3, 28.2, 25.9, 25.7, 25.6, 25.5, 25.4, 24.5, 22.6, 17.9, 17.8, 14.1, -4.9.

1-7: Prenyl deprotection conditions: 1.0 equivalent (0.115 g, 0.197 mmol) of **2-14**, 0.05 equivalents TMSOTf in DCM, stirred at rt for 1 hr. Standard workup yields a yellow oil, from which an off-white solid precipitated upon hexanes addition. Further purification by silica gel column (elution at ~20% EtOAc/hexanes, 1% AcOH added to all eluting solvents) yields 0.073 g (76%) of a pale blue powder, which was further purified by RP-HPLC (1: 1 ACN/CH_3OH as eluting solvents) to afford a white crystalline solid. UV: λ_{max} (CH_3OH)= 289 nm (ε= 24 800 M^{-1} cm^{-1}). Fluorescence: λ_{max}Ex (CH_3OH)= 305 nm, λ_{max}Em (CH_3OH)= 322 nm. NMR ($CDCl_3$): ^{1}H: 7.49 (m, 4H), 7.31 (d, 2H, *J*= 8Hz), 7.25 (d, 2H, *J*= 8Hz), 5.11 (s, 2H), 4.44 (quintet, 1H, *J*= 6Hz), 4.12 – 4.06 (m, 6H), 3.61 (s, 2H), 2.59 (m, 1H), 2.53 (m, 4H), 2.35 (m, 4H), 1.69 – 1.52 (m,

10H), 1.41 – 1.32 (m, 4H), 1.25 (s, br, 18H), 0.86 (t, 3H, *J*= 7Hz). ^{13}C: 173.2, 171.9, 171.8, 171.2, 136.1, 134.4, 131.8, 131.7, 129.3, 128.1, 123.2, 121.9, 89.6, 89.1, 65.7, 65.0, 64.8, 64.7, 64.6, 41.3, 40.6, 34.0, 33.6, 31.9, 29.6, 29.5, 29.5, 29.3, 29.2, 28.5, 28.2, 25.9, 25.4, 25.3, 24.5, 24.2, 22.7, 14.1. MS (-ve ESI): Calc'd for $C_{46}H_{63}O_{11}$= 791.4376 amu, obtained = 791.467 amu. Overall yield in 6 steps from **2-5**: 14%

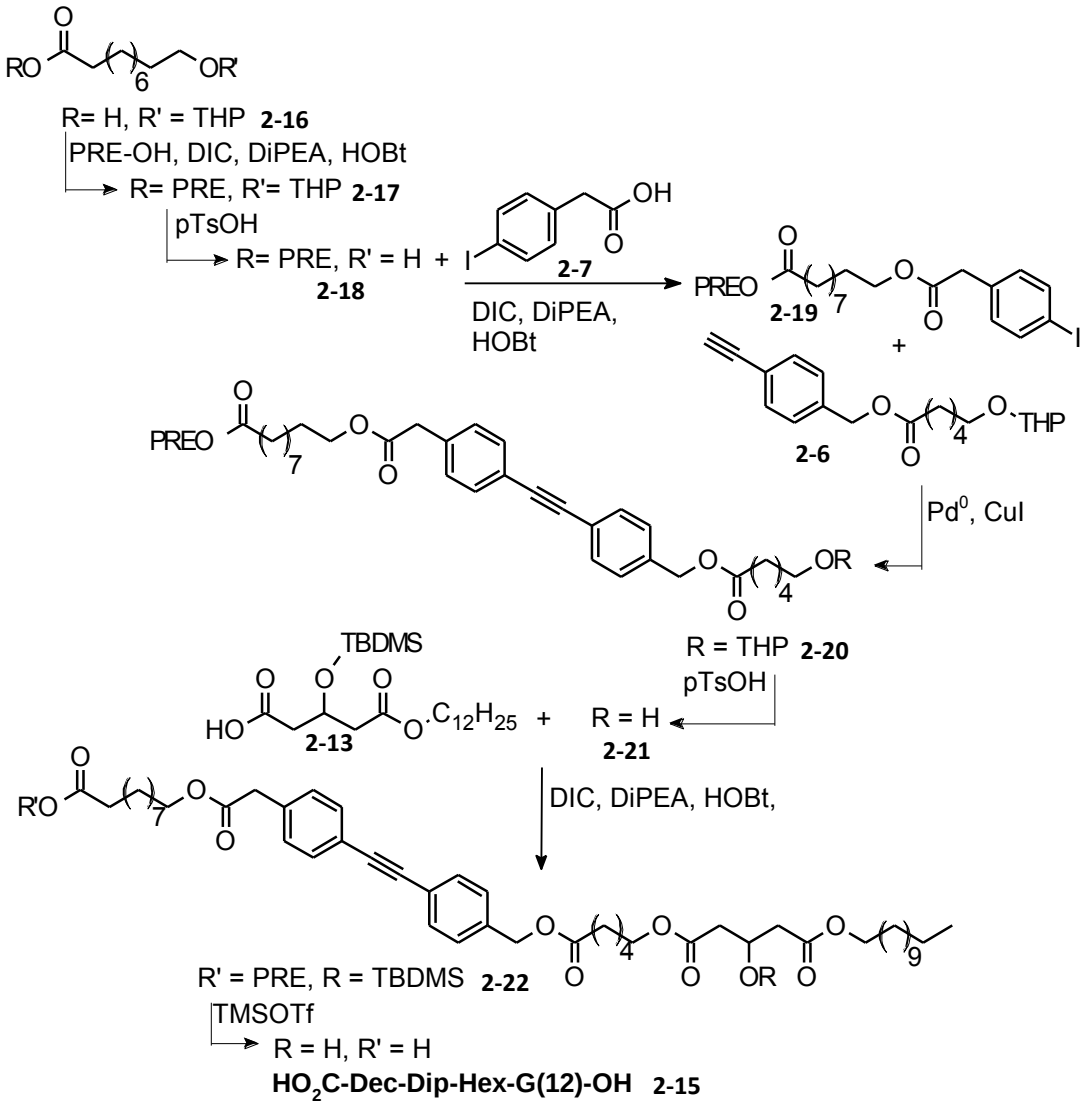

Scheme A1.4: Synthesis of **HO_2C-Dec-Dip-Hex-G(12)-OH** (**2-15**)

2-17: Ester coupling conditions: 1.0 equivalent (2.0 g, 7.4mmol) of **2-16**, 2.0 equivalents PRE-OH, 0.5 DiPEA in THF. Stirred for 24 hr at 40^{0}C. Standard workup, purification by silica gel (elution at ~ 3% EtOAc/hexanes, 1% AcOH added to all

eluting solvents). Sluggish coupling and a seemingly unstable starting material lead to a poor (1.1 g, 44%) yield of a clear, colourless oil. NMR ($CDCl_3$): ^{1}H: 5.31 (t7, 1H, *J*= 6, 1Hz), 4.53 (m, 3H), 3.58 (m, 1H), 3.70 (m, 1H), 3.47 (m, 1H), 3.35 (m, 1H), 2.26 (t, 2H, *J*= 7Hz), 1.73 (s, 3H), 1.68 (s, 3H), 1.67 – 1.50 (m, 10H), 1.27 (s, 10H). ^{13}C: 173.8, 138.8, 118.8, 98.9, 67.7, 62.3, 61.1, 34.4, 30.8, 29.7, 29.3, 29.2, 29.1, 26.2, 25.7, 25.5, 24.9, 19.7, 17.9.

2-18: THP removal conditions: 1.0 equivalent (0.85 g, 2.50 mmol) **2-17**, 0.2 equivalents TsOH in 20% CH_3OH/DCM. Stirred for 1 hour at rt. Standard work up, purification by silica gel plug, (15% EtOAc/hexanes) yields 0.64 g (75%) of a clear, colourless oil. NMR ($CDCl_3$): ^{1}H: 5.32 (t7, 1H, *J*= 7, 1Hz), 4.55 (d, 2H, *J*= 7Hz), 3.61 (t, 2H, *J*= 7Hz), 2.27 (t, 2H, *J*= 7Hz), 1.74 (s, 3H), 1.69 (s, 3H), 1.62 – 1.49 (m, 4H), 1.35 – 1.27 (m, 11H). ^{13}C: 173.9, 138.9, 118.7, 62.9, 61.2, 34.3, 32.7, 29.4, 29.3, 29.1, 29.0, 25.7, 25.6, 24.9, 17.9.

2-19: Ester coupling conditions: 1.0 equivalent (0.45 g, 1.75 mmol) of **2-18,** 1.5 equivalents of **2-7**, DIC, HOBt, and 3.0 equivalents DIPEA in DMF. Stirred for 16 hr at rt. Standard work up, purification by silica gel plug (15% EtOAc/hexanes) yields 0.709 g (83%) of a clear, colourless oil. NMR ($CDCl_3$): ^{1}H: 7.62 (d, 2H, *J*= 8Hz), 7.01 (d, 2H, *J*= 8Hz), 5.32 (m, 1H), 4.55 (d, 2H, *J*= 7Hz), 4.05 (t, 2H, *J*= 7Hz), 3.53 (s, 2H), 2.28 (t, 2H, *J*= 7Hz), 1.74 (s, 3H), 1.69 (s, 3H), 1.62 – 1.53 (m, 4H), 1.25 (s, br, 10H).^{13}C: 173.8, 170.9, 138.9, 137.5, 133.8, 131.2, 118.7, 92.5, 65.1, 61.2, 40.9, 34.3, 29.2, 29.1, 29.0, 28.5, 25.7, 24.9, 17.9.

2-20: Sonogashira coupling conditions: 1.6 equivalents of **2-6**, 5% $Pd(PPh_3)_4$, 10% CuI, and 3.0 equivalents NEt_3 were added to a solution of 1.0 equivalent (0.41 g, 0.84 mmol) of **2-19** in deoxygenated THF. Reaction was stirred under N_2 at rt for 10 hrs. Standard work up, purification by silica gel column (elution at ~10% EtOAc/hexanes) yields 0.495 g (85%) of a pale yellow oil. NMR ($CDCl_3$): ^{1}H: 7.48 (m, 4H), 7.31 (d, 2H,

J= 8Hz), 7.26 (d, 2H, *J*= 8Hz), 5.32 (t7, 1H, *J*= 6, 1Hz), 5.10 (s, 2H), 4.55 (m, 3H), 4.07 (t, 2H, *J*= 7Hz), 3.84 (m, 1H), 3.72 (m, 1H), 3.61 (s, 2H), 3.48 (m, 1H), 3.36 (m, 1H), 2.37 (t, 2H, *J*= 7Hz), 2.27 (t, 2H, *J*= 7Hz), 1.75 (s, 3H), 1.69 (s, 3H), 1.65 – 1.50 (m, 14H), 1.45 -1.35 (m, 2H), 1.26 (s, 10H).^{13}C: 173.9, 173.4, 171.2, 138.9, 136.2, 134.5, 131.7, 129.3, 128.0, 123.1, 121.9, 118.7, 98.9, 89.5, 89.0, 67.3, 65.6, 65.1, 62.4, 61.2, 41.3, 34.3, 34.2, 30.7, 29.4, 29.3, 29.1, 29.0, 28.5, 25.8, 25.8, 25.7, 25.5, 24.9, 24.8, 19.7, 17.9.

2-21: THP removal conditions: 1.0 equivalent (0.48 g, 0.69 mmol) of **2-20,** 0.3 equivalents TsOH in 20% CH_3OH/DCM. Stirred for 1 hr at rt. Standard work up, purification by silica gel column (elution ~ 30% EtOAc/hexanes) yields 0.373 g (89%) of a white solid. MP = 63 – 65^{0}C. NMR ($CDCl_3$): ^{1}H: 7.49 (m, 4H), 7.31 (d, 2H, *J*= 8Hz), 7.26 (d, 2H, *J*= 8Hz), 5.32 (t7, 1H, *J*= 6, 1Hz), 5.10 (s, 2H), 4.55 (d, 2H, *J*= 7Hz), 4.07 (t, 2H, *J*= 7Hz), 3.63 (m, 4H), 2.38 (t, 2H, *J*= 7Hz), 2.27 (t, 2H, *J*= 7Hz), 1.74 (s, 3H), 1.69 (s, 3H), 1.65 – 1.55 (m, 8H), 1.44 – 1.34 (m, 3H), 1.26 (s, 10H). ^{13}C: 173.9, 173.4, 171.2, 138.9, 136.1, 134.5, 131.7, 131.7, 129.3, 128.0, 123.2, 121.9, 118.7, 89.6, 89.0, 65.7, 65.1, 62.6, 61.2, 41.4, 34.3, 34.2, 32.3, 29.3, 29.1, 29.1, 28.5, 25.8, 25.7, 25.3, 24.9, 24.6, 17.9.

2-22: Ester coupling conditions: 1.0 equivalent (0.25 g, 0.41 mmol) of **2-21**, 1.5 equivalents **2-13**, DIC, HOBt, 3.0 equivalents DIPEA. Stirred in THF for 16 hr at rt. Standard work up, purification by silica gel column (elution at ~15% EtOAc/hexanes) yields 0.316 g (75%) of a clear, colourless oil. NMR ($CDCl_3$): ^{1}H: 7.48 (m, 4H), 7.31 (d, 2H, *J*= 8Hz), 7.25 (d, 2H, *J*= 8Hz), 5.32 (m, 1H), 5.10 (s, 2H), 4.53 (m, 3H), 4.09 – 4.00 (m, 6H), 3.60 (s, 2H), 2.52 (m, 4H), 2.36 (t, 2H, *J*= 7Hz), 2.27 (t, 2H, *J*= 7Hz), 1.74 (s, 3H), 1.69 (s, 3H), 1.67 – 1.56 (m, 9H), 1.43 – 1.20 (m, 32H), 0.86 (t, 3H, *J*= 7Hz), 0.82 (s, 9H), 0.04 (s, 6H). ^{13}C: 173.8, 173.1, 171.1, 171.0, 170.9, 138.8, 136.0, 134.5, 131.7, 129.3, 128.0, 123.2, 121.9, 118.7, 89.6, 89.0, 66.3, 65.6, 65.1, 64.6, 64.2, 61.1, 42.5, 42.5, 41.3, 34.3, 34.0, 31.9, 29.6, 29.5, 29.4, 29.3, 29.2, 29.2, 29.1, 29.0, 28.5,

28.4, 28.2, 25.9, 25.7, 25.7, 25.6, 25.5, 24.9, 24.5, 22.6, 17.9, 17.8, 14.1, -4.9.

2-15: Prenyl deprotection: 0.1 equivalents TMSOTf was added to a solution of 1.0 equivalent (0.18 g, 0.18 mmol) of **2-22** in DCM. The reaction turned greenish brown immediately. Reaction was complete after 20 mins. After standard workup, hexanes was added to the crude residue (a greenish oil), from which a white solid immediately precipitated. This was then filtered, rinsed with hexanes and dried to yield 0.133 g (87%) of the desired compound. The product was further purified by RP-HPLC (1:1 ACN/CH_3OH as eluting solvents) to yield a white powder. UV: λ_{max} (CH_3OH) = 288 nm, (ε = 24 800 M^{-1} cm^{-1}). Fluorescence: λ_{max}Ex (CH_3OH) = 305 nm, λ_{max}Em (CH_3OH) = 322 nm. NMR ($CDCl_3$, 500 MHz): ^{1}H: 7.50 (d, 2H, *J*= 8Hz), 7.46 (d, 2H, *J*= 8Hz), 7.31 (d, 2H, *J*= 8Hz), 7.26 (d, 2H, *J*= 8Hz), 5.10 (s, 2H), 4.45 (m, 1H), 4.10 – 4.05 (m, 6H), 3.61 (s, 2H), 2.53 (m, 4H), 2.37 (t, 2H, *J*= 7Hz), 2.31 (t, 2H, *J*= 7Hz), 1.68 – 1.57 (m, 10H), 1.41 – 1.36 (m, 2H), 1.25 (m, 29H), 0.86 (t, 3H, *J*= 7Hz). ^{13}C: 178.9, 173.2, 171.9, 171.2, 136.1, 134.5, 131.7, 131.7, 129.3, 128.0, 123.2, 121.9, 89.6, 89.0, 65.7, 65.1, 65.0, 64.7, 64.5, 41.3, 40.7, 34.0, 33.9, 31.9, 29.6, 29.5, 29.5, 29.4, 29.3, 29.2, 29.1, 29.0, 29.0, 28.9, 28.5, 28.4, 28.2, 25.8, 25.7, 25.4, 24.6, 24.4, 22.6, 14.1. MS (-ve ESI): Calc'd for $C_{50}H_{71}O_{11}$ = 847.5002 amu, obtained; 847.429 amu. Overall yield in 7 steps from **2-16**: 11%

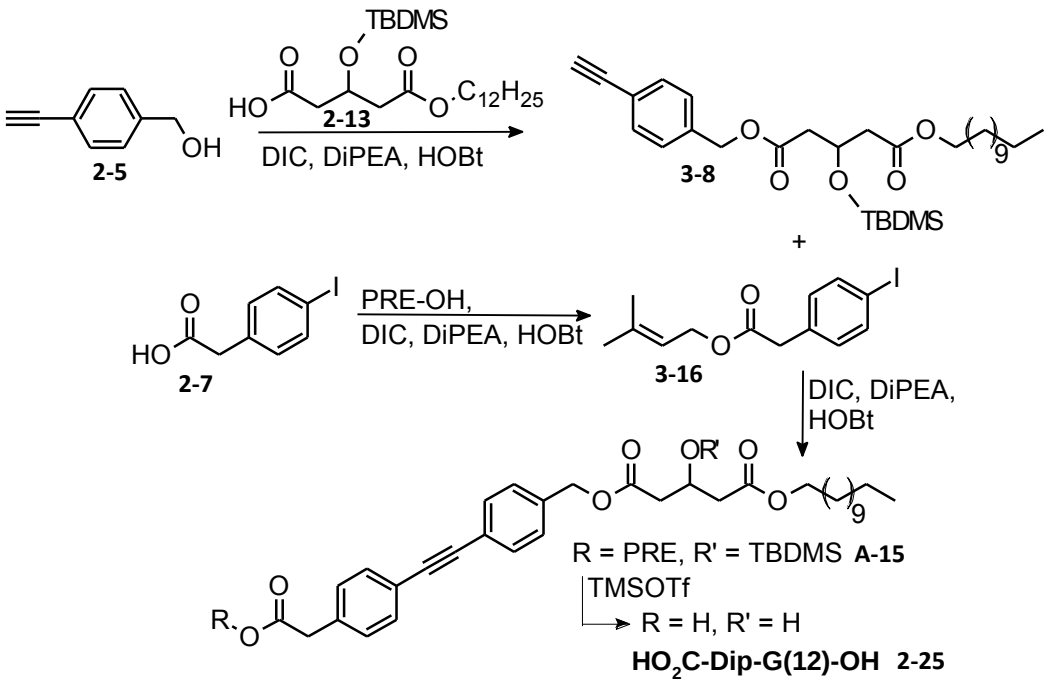

Scheme A1.5: Synthesis of **HO_2C-Dip-G(12)-OH** (**2-25**).

3-8: Ester coupling condition: 1.0 equivalent (0.07 g, 0.53 mmol) of **2-5** was added to 1.4 equivalents of **2-13**, 1.4 equivalents of DIC and 0.5 equivalents of DIPEA in DMF. The reaction was stirred at rt for 16 hrs, after which was diluted with EtOAc, washed with H_2O, $NaHCO_3$ (sat), and NaCl (sat), dried over sodium sulfate and concentrated under vacuum. Purification by silica gel chromatography (elution at ~3% EtOAc/hexanes) yielded 196 mg (68%) of **3-8** as a pale yellow oil. NMR($CDCl_3$): ^{1}H: 7.46 (d, 2H, *J*= 8Hz), 7.29 (d, 2H, *J*= 8Hz), 5.09 (m, 2H), 4.55 (p, 1H, *J*= 6Hz), 4.03 (m, 2H), 3.07 (s, 1H), 2.60 (d, 2H, *J*= 6Hz), 2.53 (d, 2H, *J*= 6Hz), 1.65 – 1.55 (m, 2H), 1.25 (s, 18H), 0.87 (t, 3H, *J*= 6Hz), 0.82 (s, 9H), 0.04 (s, 3H), 0.02 (s, 3H). ^{13}C: 170.9, 170.7, 136.5, 132.3, 127.9, 122.0, 83.2, 77.6, 66.3, 65.7, 64.7, 42.5, 42.4, 31.9, 29.6, 29.5, 29.5, 29.3, 29.2, 28.5, 25.9, 25.6, 22.7, 17.9, 14.1, -5.0.

3-16: Ester coupling conditions: to a solution of 1.0 equivalent (1.29 g, 4.92 mmol) of **2-7** in ACN 2.0 equivalents HOBt, 2.0 equivalents DIC and 3 equivalents of DIPEA were added, and the reaction was allowed to stir at rt for 30 mins. After this time, 2.0

equivalents (1.05 mL) of prenyl alcohol were added, and the reaction continued to stir at rt for 16 hours. Standard work up conditions, followed by silica gel chromatography (elution at 10% EtOAc/hexanes) yields 1.44 g (84%) of **3-16** as white crystals. MP = 42-44^{0}C. NMR ($CDCl_3$): ^{1}H: 7.63 (d, 2H, *J*= 8Hz), 7.02 (d, 2H, *J*= 8Hz), 5.36 (m, 1H), 4.58 (d, 2H, *J*= 7Hz), 3.54 (s, 2H), 1.74 (s, 3H), 1.68 (s, 3H). ^{13}C: 171.0, 139.4, 137.6, 133.7, 131.3, 118.3, 92.6, 61.9, 40.8, 25.8, 18.0.

A-15: Sonogashira coupling conditions: 1.0 equivalent (0.171 g, 0.310 mmol) of **3-8**, 1.3 equivalents (0.150 g) of **3-16**, 5mol% (0.018 g) $Pd(PPh_3)_4$, 10mol% (0.059 g) CuI and 2.0 equivalents NEt_3 were added to dry, deoxygenated THF. The reaction was stirred at rt for 16 hours, after which it was diluted with EtOAc, extracted twice against saturated EDTA, washed once with H_2O and once with NaCl (sat), dried over sodium sulfate and concentrated under vacuum. Silica gel chromatography (elution at ~15% EtOAc/hexanes) yielded 0.142 g (61%) of **A-15** as a brown oil. NMR($CDCl_3$): ^{1}H: 7.48 (m, 4H), 7.31 (d, 2H, *J*= 8Hz), 7.27 (d, 2H, *J*= 8Hz), 5.32 (m, 1H), 5.10 (m, 2H), 4.59 – 4.52 (m, 3H), 4.03 (m, 2H), 3.61 (s, 2H), 2.61 (d, 2H, *J*= 6Hz), 2.54 (d, 2H, *J*= 6Hz), 1.74 (s, 3H), 1.68 (s, 3H), 1.62 – 1.57 (m, 2H), 1.24 (s, 18H), 0.86 (t, 3H, *J*= 6Hz), 0.82 (s, 9H), 0.05 (s, 3H), 0.04 (s, 3H). ^{13}C: 171.2, 171.0, 170.8, 139.4, 135.8, 134.4, 131.7, 131.7, 129.3, 128.1, 123.2, 121.9, 118.3, 89.6, 89.0, 66.3, 65.8, 64.7, 61.9, 42.5, 42.4, 41.3, 31.9, 29.6, 29.5, 29.4, 29.3, 29.2, 28.5, 25.9, 25.8, 25.6, 22.7, 18.0, 17.9, 14.1, -4.9.

2-25: Prenyl deprotection conditions: 1.0 equivalent (0.125 g, 0.170 mmol) of **A-15**, 15% (~10uL) TMSOTf, in 5mL DCM. Stirred for 10 mins, diluted with DCM, washed with H_2O, NaCl(sat), dried over sodium sulfate, rotovapped. The beige solid was then sonicated with hexanes and filtered, yielding 0.070 g (73%) of **2-25** as a white solid. This was then purified by HPLC (semi-prep column, 75% ACN:CH_3OH, retention time~4mins) to yield white crystals. UV (CH_3OH); λ_{max}Abs=287 nm. Fluorescence (CH_3OH); λ_{max}Ex= 302 nm, λ_{max}Em= 320 nm. NMR: ^{1}H ($CDCl_3$): 7.50 (m, 4H), 7.32 (d, 2H, *J*= 8Hz), 7.27 (d, 2H, *J*= 8Hz), 5.15 (s, 2H), 4.48 (p, 1H, *J*= 6Hz), 4.09 (t, 2H, *J*= 7Hz), 3.67

(s, 2H), 2.61 (d, 2H, *J*= 7Hz), 2.54 (d, 2H, *J*= 7Hz), 1.64 (m, 2H), 1.25 (s, 18H), 0.87 (t, 3H, *J*= 7Hz). ^{13}C (125MHz, 1:1 $CDCl_3$:MeOD): 173.9, 173.5, 137.9, 137.1, 133.6, 133.6, 131.4, 130.0, 125.3, 123.8, 91.5, 90.8, 67.9, 66.9, 66.8, 43.4, 33.8, 31.6, 31.5, 31.5, 31.4, 31.3, 31.2, 30.5, 27.8, 24.6, 15.7.MS (-ve ESI): Calc'd for $C_{34}H_{43}O_7$ = 563.3009 amu, obtained = 563.3237 amu. Overall yield over 4 steps from **2-5** = 25%.

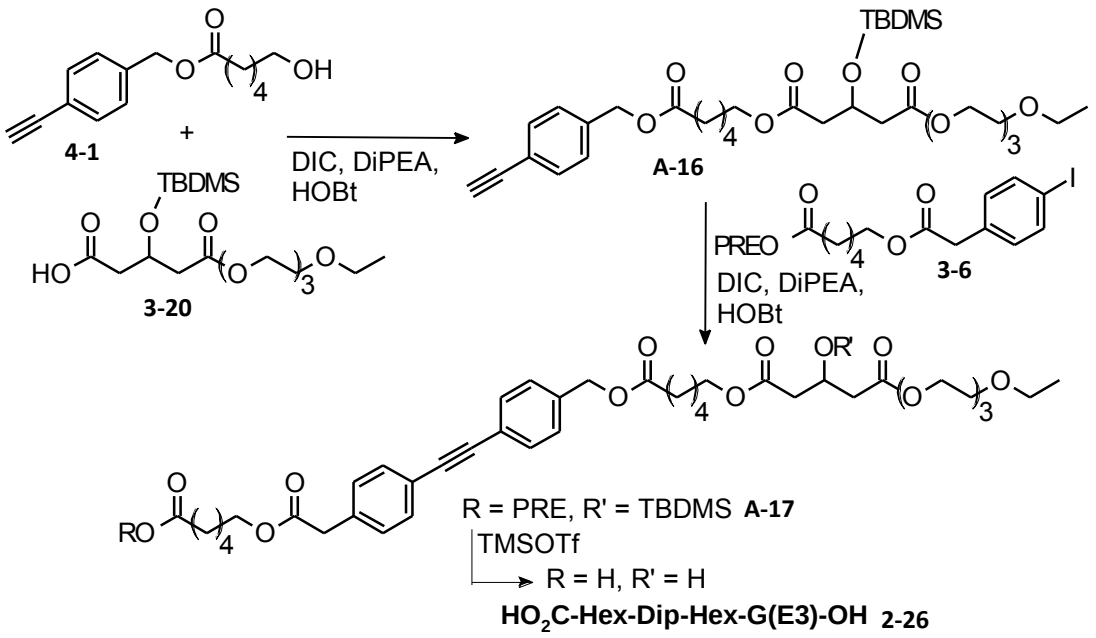

Scheme A1.6: Synthesis of **HO_2C-Hex-Dip-Hex-G(E3)-OH** (**2-26**).

3-20: 1.0 equivalent (0.52 mL, 3.70 mmol) of tri(ethylene glycol) monoethyl ether and 1.1 equivalent glutaric anhydride were refluxed in toluene for 16hr. After completion, the reaction was rotovapped to remove toluene, re-dissolved in DCM, washed with H_2O, NaCl (sat), dried over sodium sulfate and concentrated under vacuum. The crude product was then further purified by silica get chromatography (1:1 DCM:hexanes + 1% AcOH) to yield 1.21 g (81%) of **3-20** as a clear, pale blue oil, which solidified below 0^0C. NMR ($CDCl_3$) ^{1}H: 4.52 (p, 1H, *J*= 6Hz), 4.21 (m, 2H), 3.69 – 3.48 (m, 12H), 2.57 (m, 4H), 1.18 (t, 3H, *J* = 7Hz), 0.82 (s, 9H), 0.05 (s, 6H). ^{13}C: 170.8, 70.6, 70.5, 70.4, 69.7, 68.9, 66.6, 66.1, 63.6, 42.3, 42.2, 17.9, 15.1, -4.9, -4.9.

A-16: Ester coupling conditions; 1.0 equivalent (0.12 g, 0.49 mmol) **4-1**, 1.5 equivalents **3-20**, 1.5 equivalents DIC, HOBt and 3 equivalents DIPEA were stirred in THF at rt for 40 hrs. Standard workup, purification by silica gel chromatography (elution at 30% EtOAc/hexanes) gave 0.245 g (77%) of **A-16** as a clear, colourless oil. NMR ($CDCl_3$): ^{1}H: 7.45 (dt, 2H, *J*= 8, 1Hz), 7.27 (d, 2H, *J*= 8Hz), 5.08 (s, 2H), 4.51 (p, 1H, *J*= 6Hz), 4.19 (m, 2H), 4.01 (m, 2H), 3.68 – 3.53 (m, 12H), 3.07 (s, 1H), 2.55 (m, 2H), 2.51 (m, 2H), 2.35 (t, 2H, *J*= 7Hz), 1.63 (m, 3H), 1.35 (m, 3H), 1.18 (t, 3H, *J*= 7Hz), 0.81 (s, 9H), 0.03 (s, 6H). ^{13}C: 173.1, 171.0, 170.9, 136.7, 132.3, 127.9, 121.9, 83.2, 77.6, 70.7, 70.6, 69.8, 69.0, 68.9, 66.6, 66.2, 65.5, 64.2, 63.6, 42.5, 42.4, 34.0, 28.2, 25.8, 25.6, 25.5, 24.5, 17.9, 15.1, -4.9, -4.9.

A-17: Sonogashira coupling conditions; 1.0 equivalent (0.215 g, 0.330 mmol) of **A-16** 1.4 equivalents **3-6,** 5% $Pd(PPh_3)_4$, 10% CuI and 2 equivalents NEt_3 were stirred in THF at rt for 24 hrs, then at 40^{0}C for a further 24 hrs. Coupling was seen to be inefficient by TLC. Standard workup, purification by silica gel chromatography (elution at ~15% Acetone/hexanes) gave 0.172 g (54%) of the desired compound as a clear yellow oil. NMR ($CDCl_3$): ^{1}H: 7.48 (m, 4H), 7.31 (d, 2H, *J*= 8Hz), 7.24 (d, 2H, *J*= 8Hz), 5.31 (m, 1H), 5.09 (s, 2H), 4.52 (m, 3H), 4.19 (m, 2H), 4.05 (m, 4H), 3.67 – 3.47 (m, 14H), 2.54 (m, 4H), 2.36 (t, 2H, *J*= 7Hz), 2.28 (t, 2H, *J*= 7Hz), 1.74 (s, 3H), 1.69 (s, 3H), 1.67 – 1.57 (m, 8H), 1.43 – 1.29 (m, 4H), 1.19 (t, 3H, *J*= 7Hz), 0.82 (s, 9H), 0.04 (s, 6H). ^{13}C: 173.5, 173.2, 171.1, 171.0, 170.9, 139.0, 136.1, 134.4, 131.7, 129.3, 128.0, 123.2, 121.9, 118.6, 89.6, 89.0, 70.7, 70.6, 69.8, 69.0, 66.6, 66.2, 65.7, 64.8, 64.3, 63.6, 61.3, 42.4, 42.3, 41.3, 34.1, 34.0, 28.2, 25.7, 25.6, 25.5, 25.4, 24.5, 17.9, 17.8, 15.1, -4.8, -4.9.

2-26: Prenyl deprotection conditions; 1.0 equivalent (0.15 g, 0.16 mmol) of **A-17** and 0.25 equivalents of TMSoTf were stirred in DCM at rt for 40 mins. Standard extractive workup lead to a green oil, from which a yellow solid precipitated upon sonication with acetone/hexanes. This crude product was purified by silica gel chromatography (elution at 30% acetone/hexanes, 2% AcOH added to all eluting solvents) to yield 0.09 g (75%) of

a white, waxy solid. This was further purified by RP-HPLC (semi-prep column, 1:1 ACN:CH_3OH) to yield a colourless waxy solid. UV (CH_3OH); λ_{max}Abs= 286 nm. Fluorescence (CH_3OH); λ_{max}Ex= 302 nm, λ_{max}Em= 320 nm. NMR ($CDCl_3$): ^{1}H: 7.47 (m, 4H), 7.30 (d, 2H, *J*= 8Hz), 7.24 (d, 2H, *J*= 8Hz), 5.09 (s, 2H), 4.45 (p, 1H, *J*= 6Hz), 4.25 (m, 2H), 4.08 (m, 4H), 3.68 (t, 2H, *J*= 6Hz), 3.58 (m, 10H), 3.49 (q, 2H, *J*= 6Hz), 2.53 (m, 4H), 2.36 (t, 2H, *J* = 7Hz), 1.71 – 1.58 (m, 8H), 1.35 (m, 4H), 1.18 (t, 3H, *J* = 7Hz). ^{13}C: 173.2, 171.6, 171.2, 136.1, 134.4, 131.7, 131.7, 129.3, 128.1, 123.1, 121.9, 89.6, 89.1, 70.6, 70.5, 70.5, 69.7, 68.9, 66.6, 65.7, 64.7, 64.5, 63.7, 41.3, 40.8, 40.7, 34.0, 28.2, 25.4, 24.5, 15.1. MS (-ve ESI): calc'd for $C_{42}H_{55}O_{14}$ = 783.3597 amu, obtained = 783.3397 amu. Overall yield over 6 steps from 4-ethynylbenzyl alcohol = 20%.

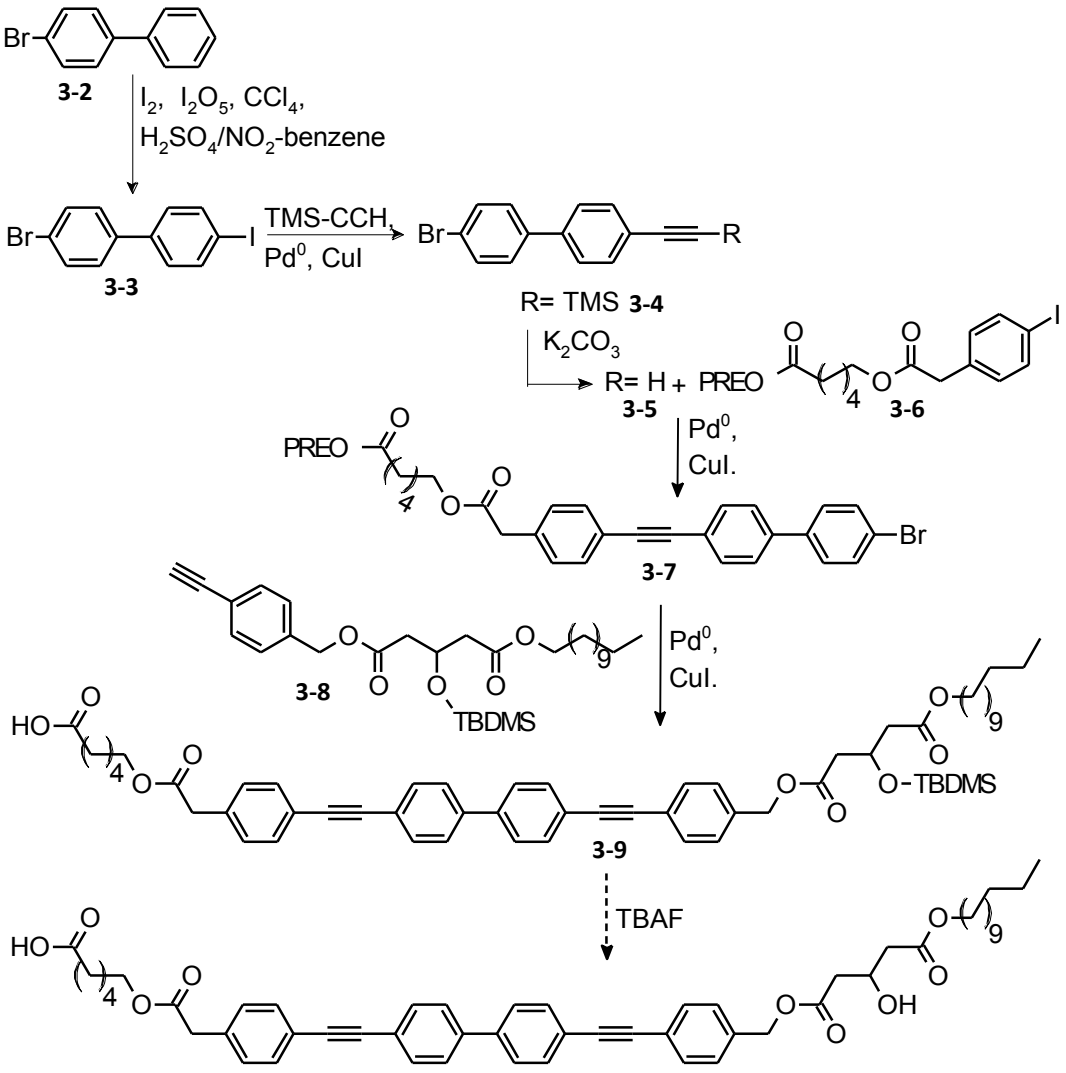

Scheme A1.7: Attempted synthesis of **HO_2C-Hex-Bi(Dip)-G(12)-OH** (**3-10**).

3-3: From [107]. 1.0 equivalent (6.97 mmol, 2.32 g) I_2O_5, 1.6 equivalents **3-2**, 3.50 equivalents I_2, in 5 mL CCl_4, 50% Aq. H_2SO_4 in nitrobenzene (10 mL) were stirred at 90^0C for 48 hrs. After this time, the reaction mixture was cooled and diluted with CH_3OH, from which white shiny crystals precipitated. These were filtered to yield 2.05 g (78%) of **3-3**. MP= 169-170^0C (lit. 166 – 168^0C). NMR ($CDCl_3$): agrees with literature.

3-4: Sonogashira conditions; 1.0 equivalent (1.087 g, 3.040 mmol) **3-3**, 1.1 equivalent TMS acetylene, 5% $Pd(PPh_3)_4$, 10% CuI and 2 equivalents NEt_3 were stirred in THF at 40^0C for 16 hrs. Standard work-up followed by silica gel chromatography (elution at 100% hexanes) lead to 0.805 g (81%) of **3-4** as shiny white crystals. MP= 131-132^0C. NMR ($CDCl_3$) ^{1}H: 7.57 – 7.42 (m, 8H), 0.27 (s, 9H). ^{13}C: 139.9, 139.2, 132.5, 131.9, 128.6, 126.7, 122.5, 121.9, 104.6, 95.3, 0.01.

3-5: TMS deprotection: 1.0 equivalent (0.733 g, 2.230 mmol) of **3-4** and 1.1 equivalent K_2CO_3 were stirred in 1:1 DCM: CH_3OH for 0.5 hrs. Once complete, the reaction was diluted with DCM, washed with 1 M Aq. HCl (twice), H_2O (twice), sat. NaCl (once), dried over sodium sulfate and rotovapped. This yielded 0.544 g (95%) of **3-5** as white crystals, which were used without further purification. MP= 144-146^0C. NMR ($CDCl_3$) ^{1}H: 7.58 – 7.49 (m, 6H), 7.43 (td, 2H, *J*= 8, 2Hz), 3.14 (s, 1H). ^{13}C: 140.3, 139.2, 132.7, 131.9, 128.6, 126.8, 122.0, 121.4, 83.4, 78.1.

3-7: Sonogashira coupling conditions; 1.0 equivalent (0.217 g, 0.850 mmol) **3-5**, 1.3 equivalents **3-6**, 5% $Pd(PPh_3)_4$, 10% CuI and 2 equivalents NEt_3 were stirred in DMF at 40^0C for 16 hrs. Standard work-up followed by silica gel chromatography with DCM as eluent lead to a mixture of products, further chromatography (elution at 5% EtOAc/hexanes) lead to 0.290 g (60%) of **3-7** as shiny pinkish crystals. MP= 174-178^0C. NMR ($CDCl_3$) ^{1}H: 7.62-7.46 (m, 10H), 7.29 (d, 2H, *J*= 8Hz), 5.35 (m, 1H), 4.58 (d, 2H, *J*= 7Hz), 4.11 (t, 2H, *J*= 7Hz), 3.64 (s, 2H), 2.31 (t, 2H, *J*= 7Hz), 1.77 (s, 3H), 1.72 (s, 3H), 1.65 (m, 4H), 1.36 (m, 2H). ^{13}C: 171.2, 171.0, 140.1, 139.9, 135.9, 134.4, 132.2, 131.7, 129.3, 128.6, 128.4, 128.1, 126.8, 123.1, 122.6, 122.4, 122.0, 90.1, 89.9, 89.7, 89.4, 66.3, 65.8, 64.7, 42.5, 42.4, 41.3, 31.9, 29.6, 29.5, 29.5, 29.3, 29.2, 28.5, 28.2, 25.9, 25.6, 25.4, 24.3, 22.6, 17.9, 14.1, -4.9.

3-9: Sonogashira coupling conditions; 1.0 equivalents (0.20 g, 0.35mmol) **3-7**, 1.5 equivalents **3-8**, 5% $Pd(PPh_3)_4$, 10% CuI and 2 equivalents NEt_3 were stirred in DMF at

80^0C for 24 hrs. TLC analysis of the reaction showed a very low Rf, highly fluorescent spot as the major product, suggesting loss of the Prenyl group. Standard work-up followed by silica gel chromatography (elution at 99% EtOAc/1% AcOH) lead to 0.215 g (63%) of a yellow solid **3-9**, which NMR showed had indeed lost the Prenyl group. NMR ($CDCl_3$) ^{1}H: 7.53 – 7.39 (m, 14H), 7.27 (d, 2H, *J*= 8Hz), 7.20 (d, 2H, *J*= 8Hz), 5.05 (m, 2H), 4.53 (m, 1H), 4.04 (m, 4H), 3.56 (s, 2H), 2.57 (d, 2H, *J*= 6Hz), 2.49 (d, 2H, *J*= 6Hz), 1.56 (m, 6H), 1.19 (s, br, 22H), 0.79 (m, 12H), 0.00 (2s, 6H). ^{13}C: 171.2, 171.1, 170.6, 140.1, 139.9, 135.9, 134.4, 132.2, 132.1, 131.7, 129.3, 128.6, 128.4, 128.1, 126.8, 123.1, 122.6, 122.4, 122.0, 90.1, 89.9, 89.7, 89.4, 66.3, 65.9, 64.7, 42.5, 42.4, 41.3, 31.9, 29.6, 29.5, 29.4, 29.3, 29.2, 28.5, 28.2, 25.9, 25.6, 25.4, 24.3, 22.6, 17.9, 14.1, -4.9.

3-10: Silyl deprotection conditions; 1.0 equivalent (0.19 g, 0.22 mmol) **3-9**, 4 equivalents TBAF in THF were stirred in THF at rt for 1 hr. Purification (silica gel chromatography) was difficult due to poor solubility of the highly fluorescent presumed product. Elution at 9:1:1 EtOAc:CH_3OH:AcOH lead to ~100 mg of a beige solid, which proved marginally soluble in dmso. ^{1}H NMR (D6-dmso, 70^0C): suggestive of product formation, but lack of solubility prevented further analysis.

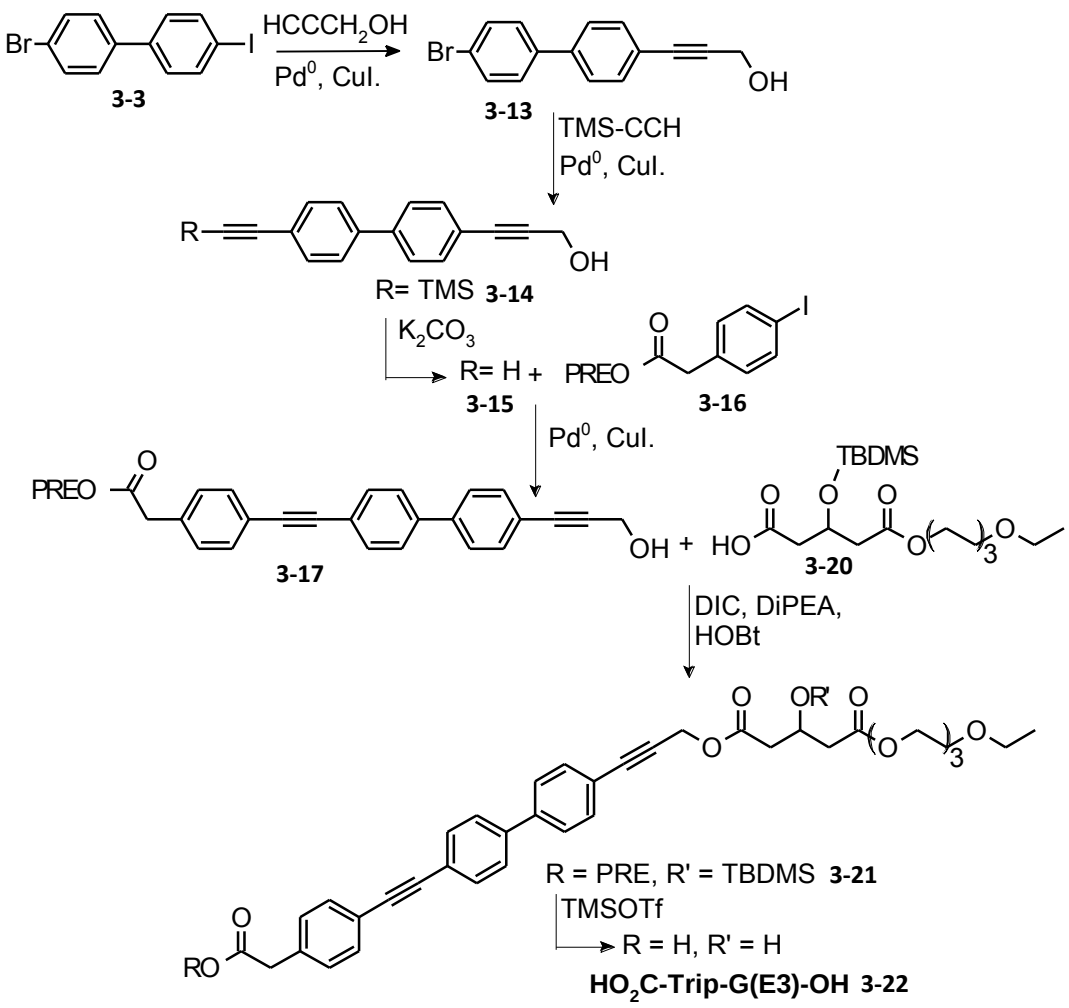

Scheme A1.8: Synthesis of **HO_2C-Trip-G(E3)-OH** (**3-22**).

3-13: Sonogashira coupling conditions: 1.0 equivalent (2.50 g, 6.90 mmol) of **3-3** (4-Bromo, 4'-Iodobiphenyl), 2.0 equivalents (0.81 mL) propargyl alcohol, 5% $Pd(PPh_3)_4$, 10% CuI and 2 equivalents NEt_3 were stirred in THF at rt for 20 hrs. Standard work-up followed by silica gel chromatography (elution at 20% EtOAc/hexanes) lead to 1.78 g (89%) of **3-13** as creamy white needles. MP= 153-154^{0}C. NMR ($CDCl_3$) ^{1}H: 7.55 (dt, 2H, *J*= 8, 2Hz), 7.49 (s, 4H), 7.42 (dt, 2H, *J*= 8, 2 Hz), 4.51 (d, 2H, *J*= 6Hz), 1.68 (t, 1H, *J*= 6Hz). ^{13}C: 139.9, 139.1, 132.2, 131.9, 128.6, 126.8, 121.9, 121.8, 88.1, 85.4, 51.7.

3-14: Sonogashira coupling conditions; 1.0 equivalent (0.4 g, 1.4 mmol) of **3-13**, 2.0 equivalents (0.39 mL) TMS-acetylene, 5% $Pd(PPh_3)_4$, 10% CuI and 2 equivalents NEt_3 were stirred in DMF at 70^0C for 48 hrs. Standard work-up followed by silica gel chromatography (elution at ~15% EtOAc/hexanes) lead to 0.296 g (71%) of **3-14** as dull yellow flakes. MP= 158-160^0C. NMR ($CDCl_3$) ^{1}H: 7.52 (m, 8H), 4.51 (s, 2H), 0.26 (s, 9H). ^{13}C: 140.3, 140.1, 132.5, 132.2, 126.8, 126.7, 122.5, 121.8, 104.8, 95.3, 88.1, 85.5, 51.7, -0.1.

3-15: TMS deprotection: 1.0 equivalent (0.28 g, 9.20 mmol) of **3-14** and 1.0 equivalent (127mg) K_2CO_3 were stirred in 1:1 DCM: CH_3OH for 3.5 hrs. Once complete, the reaction was diluted with DCM, washed with 1 M Aq. HCl (twice), H_2O (twice), sat. NaCl (once), dried over sodium sulfate and rotovapped. This yielded 0.186 g (87%) of **3-15** as a tan powder, which was used without further purification. NMR ($CDCl_3$) ^{1}H: 7.52 (m, 8H), 4.52 (s, 2H), 3.14 (s, 1H), 1.72 (s, br, 1H). ^{13}C: 140.5, 140.2, 132.6, 132.2, 126.9, 126.8, 121.9, 121.4, 88.1, 85.5, 83.4, 78.1, 51.7.

3-17: Sonogashira coupling conditions; 1.0 equivalent (0.15 g, 6.47 mmol) of **3-15**, 1.4 equivalents (0.30 g) **3-16** 5% $Pd(PPh_3)_4$, 10% CuI and 2 equivalents NEt_3 were stirred in Et_2O at rt for 16 hrs. Standard work-up, purification by silica gel chromatography (elution at ~ 40% EtOAc/hexanes) yields 0.218 g (77%) of **3-17** as a pale yellow solid. MP= 140^0C (decomp). NMR ($CDCl_3$) ^{1}H: 7.52 (m, 10H), 7.27 (d, 1H, *J*= 8Hz), 5.33 (m, 1H), 4.59 (d, 2H, *J*= 7Hz), 4.52 (s, 2H), 3.63 (s, 2H), 1.75 (s, 3H), 1.69 (s, 3H). ^{13}C: 171.2, 140.3, 139.9, 139.4, 134.4, 132.2, 132.1, 131.7, 129.4, 126.9, 122.6, 121.9, 121.8, 118.3, 90.2, 89.2, 88.1, 85.5, 61.9, 51.7, 41.3, 25.8, 18.0.

3-21: Ester coupling conditions; 1.0 equivalent (0.20 g, 4.61 mmol) of **3-17**, 1.2 equivalents (0.24 g) of **3-20**, 1.3 equivalents DIC, HOBt and 2.6 equivalents DiPEA were stirred in ACN at rt for 24 hrs. Standard work-up and purification by silica gel chromatography (elution at ~30% EtOAc/hexanes) yields 0.276 g (71%) of **3-21** as a

yellow oil. NMR ($CDCl_3$) ^{1}H: 7.57 – 7.48 (m, 10H), 7.27 (d, 2H, *J*= 8Hz), 5.33 (m, 1H), 4.92 (s, 2H), 4.58 (m, 3H), 4.22 (td, 2H, *J*= 6, 1Hz), 3.70 – 3.47 (m, 14H), 2.63 (m, 4H), 1.75 (s, 3H), 1.68 (s, 3H), 1.19 (t, 3H, *J*= 7Hz), 0.84 (s, 9H), 0.09 (s, 3H), 0.07 (s, 3H). ^{13}C: 171.2, 170.8, 170.3, 140.6, 139.8, 139.4, 134.4, 132.4, 132.1, 131.7, 129.4, 126.9, 126.8, 122.7, 121.9, 118.3, 90.2, 89.2, 86.3, 83.7, 70.7, 70.6, 69.8, 69.0, 66.6, 66.1, 63.6, 61.9, 52.8, 42.3, 42.3, 41.3, 25.8, 25.7, 18.0, 17.9, 15.2, -4.8, -4.9.

3-22: Prenyl deprotection conditions; 1.0 equivalent (0.20 g, 0.24mmol) of **3-21** and 5µL TMSOTf were stirred in DCM for 0.5hr. The reaction was then diluted with DCM and washed with H_2O, during this time the solution went from a dark green to a pale yellow. The mixture was then washed with sat. NaCl, dried over sodium sulfate and concentrated under vacuum. The crude product (0.125 g, ~80% yield) was then purified by silica gel chromatography (elution at 98% Et_2O/2% AcOH). Purification was poor, as the compound did not cleanly elute from the column, leading to a poor recovery (~50% yield, 0.078 g) of purified **3-22** as a pale yellow, waxy solid. The compound was further purified by HPLC (semi-prep column, 75% CH_3OH: 25% ACN) to yield a virtually unchanged pale yellow, waxy solid. UV (CH_3OH); λ_{max}Abs=315 nm (ε=90 806 $M^{-1}cm^{-1}$). Fluorescence (CH_3OH); λ_{max}Ex= 325 nm, λ_{max}Em= 370 nm. NMR ($CDCl_3$) ^{1}H: 7.57 – 7.48 (m, 10H), 7.27 (d, 2H, *J*= 8Hz), 4.95 (s, 2H), 4.52 (p, 1H, *J*= 6Hz), 4.27 (m, 2H), 3.72 – 3.48 (m, 14H), 2.62 (m, 4H), 1.19 (t, 3H, *J*= 7Hz). ^{13}C: 175.6, 171.6, 170.9, 140.6, 139.9, 133.7, 132.4, 132.1, 131.8, 129.5, 126.9, 126.8, 122.6, 122.3, 121.3, 90.1, 89.4, 86.5, 83.5, 70.6, 70.5, 69.8, 68.9, 66.7, 64.7, 63.8, 53.1, 40.8, 40.7, 40.6, 15.1. MS (-ve ESI): calc'd for $C_{38}H_{39}O_{10}$ = 655.2549 amu, obtained = 655.2659 amu. Overall yield over 7 steps starting from **3-2** = 16%.

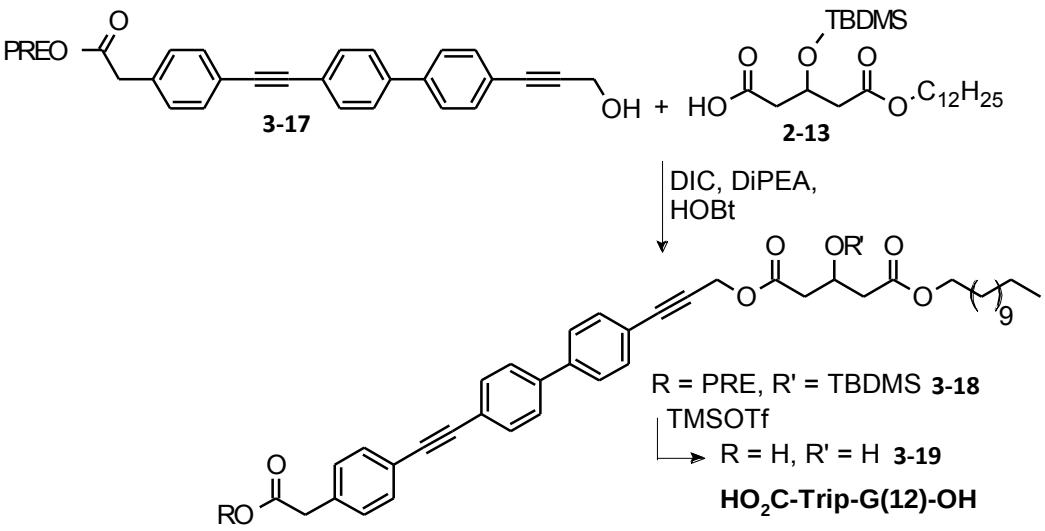

Scheme A1.9: Synthesis of **HO_2C-Trip-G(12)-OH** (**3-19**).

3-18: Ester coupling conditions; 1.0 equivalent (0.20 g, 0.46 mmol) of **3-17**, 1.3 equivalents (0.26 g) **2-13**, 1.3 equivalents DIC, HOBt and 2.6 equivalents of DIPEA were stirred at rt in ACN for 18hr. Standard work-up, purification by silica gel chromatography (elution ~7% EtOAc:hexanes) yields 0.285 g (73%) of a clear, colourless oil, which solidified under vacuum to give a white foam. MP < rt. NMR ($CDCl_3$): ^{1}H: 7.58 – 7.48 (m, 10H), 7.27 (d, 2H, *J*= 8Hz), 5.33 (m, 1H), 4.92 (s, 2H), 4.60 (m, 3H), 4.05 (m, 2H), 3.63 (s, 2H), 2.65 (d, 2H, *J*= 6Hz), 2.57 (d, 2H, *J*= 6Hz), 1.75 (s, 3H), 1.69 (s, 3H), 1.61 (m, 2H), 1.25 (s, 18H), 0.86 (m, 12H), 0.10 (s, 3H), 0.08 (s, 3H). ^{13}C: 171.2, 170.9, 170.4, 140.5, 139.8, 139.4, 134.4, 132.4, 132.1, 131.7, 129.4, 126.9, 126.8, 122.7, 121.9, 121.4, 118.4, 90.2, 89.2, 86.3, 83.8, 66.2, 64.8, 61.9, 52.8, 42.5, 42.3, 41.3, 31.9, 29.6, 29.6, 29.5, 29.3, 29.3, 28.6, 25.9, 25.8, 25.7, 22.7, 18.0, 17.9, 14.1, -4.9.

3-19: Prenyl deprotection conditions; 1.0 equivalent (0.20 g, 0.24 mmol) **3-18** and 0.1 equivalent TMSOTf were stirred in DCM for 20 mins. Upon addition of TMSOTf, the reaction mixture turned from a pale yellow solution to a dark bluish-green, which reverted back to the pale yellow color upon quenching with water. After washing the organic layer with water twice, it was dried over sodium sulfate and rotary evaporated. The crude residue was then re-suspended in hexanes and sonicated, from which a pale

greenish-yellow solid precipitated. This product was then purified by silica gel chromatography (elution at 20% acetone/hexanes, 2% AcOH added to all eluting solvents), to yield 0.130 g (79%) of a white solid. The product was then further purified by RP-HPLC (semi-prep column, 1:1 ACN:CH_3OH) to yield transparent crystals. UV (CH_3OH); λ_{max}Abs= 313 nm (ε= 90 800 M^{-1} cm^{-1}). Fluorescence (CH_3OH); λ_{max}Ex= 325 nm, λ_{max}Em= 370 nm. NMR ($CDCl_3$) ^{1}H (500MHz): 7.57 – 7.49 (m, 10H), 7.28 (d, 2H, *J*= 8Hz), 4.96 (s, 2H), 4.49 (p, 1H, *J*= 6Hz), 4.09 (t, 2H, *J*= 7Hz), 3.67 (s, 2H), 2.63 (m, 2H), 2.56 (d, 2H, *J*= 6Hz), 1.64 – 1.53 (m, 3H), 1.24 (s, 18H), 0.86 (t, 3H, *J*= 7Hz). ^{13}C (125MHz): 173.9, 172.1, 171.2, 140.9, 140.2, 133.8, 132.7, 132.4, 132.1, 129.7, 127.1, 127.0, 122.9, 122.6, 121.6, 90.4, 89.7, 86.8, 83.7, 65.4, 64.9, 53.4, 40.7, 40.6, 32.1, 29.9, 29.8, 29.7, 29.6, 29.5, 28.8, 26.1, 22.9, 14.3, MS (-ve ESI): calc'd for $C_{42}H_{47}O_7$ = 663.3327 amu, obtained = 663.3408 amu. Overall yield over 7 steps from **3-2** = 19%

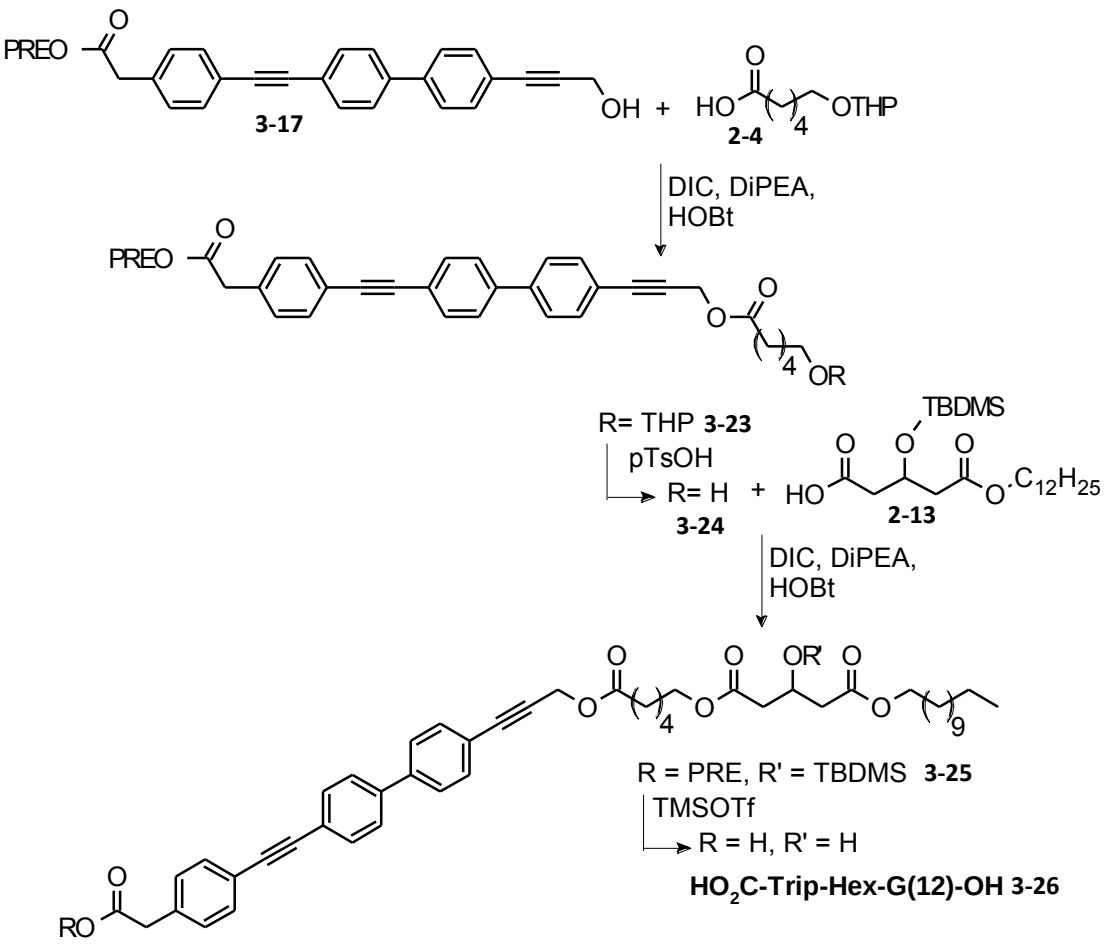

Scheme A1.10: Synthesis of **HO_2C-Trip-Hex-G(12)-OH** (**3-26**).

3-23: Ester coupling conditions; 1.0 equivalent (0.18 g, 0.42 mmol) **3-17**, 2.0 equivalents (0.18 g) **2-4**, 2 equivalents DIC, HOBt and 3.5 equivalents DIPEA were stirred in THF for 14 hrs at rt. Standard work-up, purification by silica gel chromatography (elution at 10% EtOAc/hexanes) gave 0.152 g (58%) of **3-23** as a white semi-solid. NMR ($CDCl_3$): ^{1}H: 7.57 – 7.48 (m, 10H), 7.25 (d, 2H, *J*= 8Hz), 5.32 (m, 1H), 4.92 (s, 2H), 4.28 (d, 2H, *J*= 7Hz), 4.55 (m, 1H), 3.84 (m, 1H), 3.72 (m, 1H), 3.62 (s, 2H), 3.46 m, 1H), 3.37 (m, 1H), 2.39 (t, 2H, *J*= 7Hz), 1.74 (s, 3H), 1.68 (s, 3H), 1.64 – 1.39 (m, 12H). ^{13}C: 172.9, 171.0, 140.5, 139.8, 139.3, 134.4, 132.4, 132.0, 131.7, 129.3, 126.8, 126.7, 122.6, 121.9, 121.4, 118.3, 98.8, 90.2, 89.2, 86.1, 83.9, 67.2, 62.3, 61.9, 52.6, 41.2, 33.9, 30.7, 29.3, 25.8, 25.7, 25.4, 24.6, 19.6, 17.9.

3-24: THP removal conditions; 1.0 equivalent (0.14 g, 0.22mmol) **3-23** and 0.2 equivalents TsOH were stirred in 20% CH_3OH:DCM for 2 hrs at rt. Standard work up led to 0.108 g (89%) of the desired compound, which was used directly in the next reaction without further purification.

3-25: Ester coupling conditions; 1.0 equivalent (0.10 g, 0.18 mmol) **3-24**, 1.5 equivalents DIC, HOBt, 3 equivalents of DIPEA and 1.5 equivalents (0.12 g) of **2-13** were stirred in THF for 48 hrs at 40^0C. TLC monitoring indicated no further reaction occurred after approximately 16hrs. Standard workup, purification by silica gel chromatography (elution at ~10% EtOAc/hexanes) led to 0.102 g (58%) of the product as a clear colorless oil. NMR ($CDCl_3$): ^{1}H: 7.52 – 7.42 (m, 10H), 7.21 (d, 2H, *J*= 8Hz), 5.27 (m, 1H), 4.88 (s, 2H), 4.53 (d, 2H, *J*= 7Hz), 4.48 (t, 2H, *J*= 7Hz), 3.99 (m, 4H), 3.57 (s, 2H), 2.48 (m, 4H), 2.34 (t, 2H, *J*= 7Hz), 1.69 – 1.52 (m, 11H), 1.19 (s, br, 22H), 0.81 (m, 12H), -0.01 (s, 6H). ^{13}C: 172.7, 171.2, 171.1, 171.0, 140.6, 139.8, 139.4, 134.4, 132.4, 132.1, 131.7, 129.4, 126.9, 126.8, 122.7, 121.9, 121.4, 118.3, 90.2, 89.2, 86.2, 83.9, 66.3, 64.7, 64.3, 61.9, 52.7, 42.5, 42.5, 41.3, 33.9, 31.9, 29.6, 29.5, 29.5, 29.3, 29.2, 28.5, 28.2, 25.9, 25.8, 25.6, 25.5, 24.5, 22.7, 18.0, 17.9, 14.1, -4.9.

3-26: Prenyl deprotection conditions; 1.0 equivalent (0.060 g, 0.060 mmol) **3-25** and 0.2 equivalents TMSOTf were stirred in DCM for 40 mins at rt. Upon addition of TMSOTf, the reaction mixture turned from a pale yellow solution to a dark green, which reverted back to the pale yellow color upon quenching with water. After washing the organic layer with water twice, it was dried over sodium sulfate and rotary evaporated. The crude residue was then re-suspended in 1:1 EtOH: hexanes and sonicated, from which a pale yellow solid precipitated to yield 0.043 g (73%) of crude product. This was then further purified by RP-HPLC (semi-prep column, 3:1 ACN:CH_3OH) to yield white crystals. UV (CH_3OH); λ_{max}Abs= 312 nm (ε= 90 806 M^{-1} cm^{-1}). Fluorescence (CH_3OH); λ_{max}Ex= 327 nm, λ_{max}Em= 365 nm. NMR ($CDCl_3$) ^{1}H: 7.57 – 7.49 (m, 10H), 7.28 (d, 2H, *J*= 8Hz), 4.93

(s, 2H), 4.44 (p, 1H, *J*= 6Hz), 4.10 (m, 4H), 3.67 (s, 2H), 2.53 (m, 4H, *J*= Hz), 2.40 (t, 2H, *J*= 7Hz), 1.75 – 1.57 (m, 6H), 1.42 (m, 2H), 1.25 (s, 18H), 0.87 (t, 3H, *J*= 7Hz). ^{13}C: 175.4, 172.8, 171.9, 171.8, 140.6, 139.9, 133.5, 132.4, 132.1, 131.8, 129.5, 126.9, 126.8, 122.6, 122.3, 121.4, 90.0, 89.4, 86.2, 83.9, 65.0, 64.8, 64.6, 52.8, 40.6, 33.9, 31.9, 29.6, 29.5, 29.4, 29.3, 29.2, 28.5, 28.2, 25.9, 25.4, 24.4, 22.7, 14.1. MS (-ve ESI): calc'd for $C_{48}H_{58}O_9$ =778.4037 amu, obtained = 778.4346 amu. Overall yield over 9 steps from **3-2** = 7%

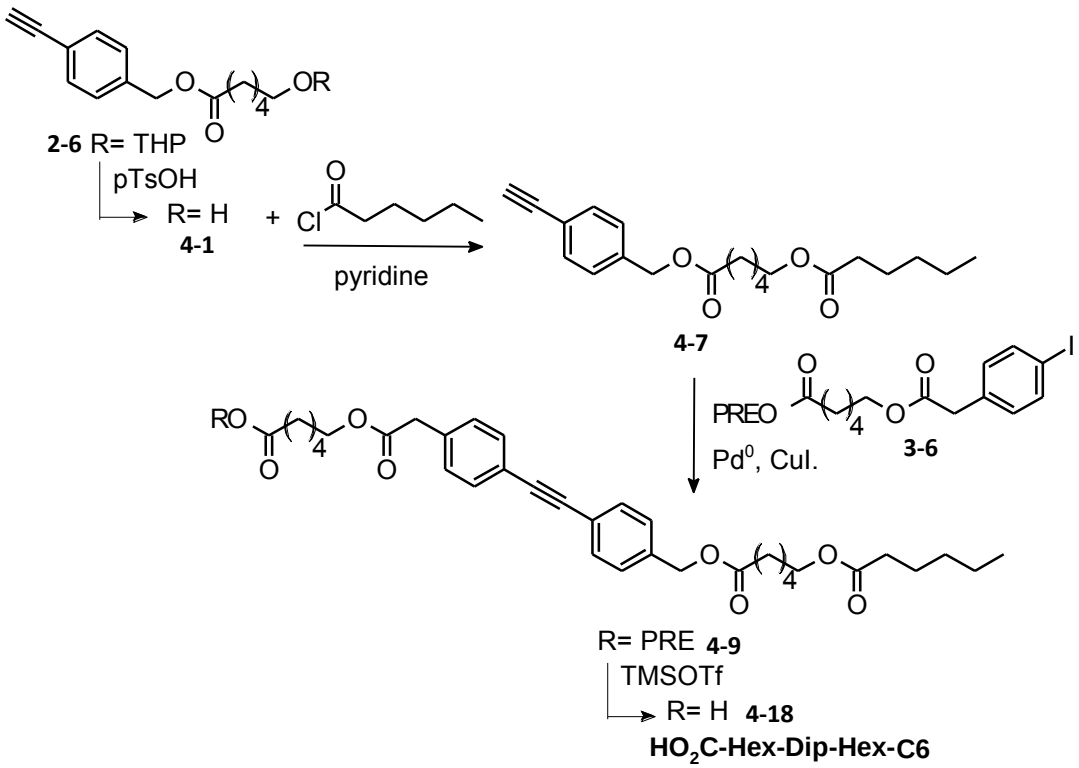

Scheme A1.11: Synthesis of **HO_2C-Hex-Dip-Hex-C6** (**4-18**).

4-1: THP removal conditions: 1.0 equivalent (3.0 g, 9.1 mmol) of **2-6** and 0.2 equivalents TsOH were stirred in 10% CH_3OH/DCM for 2.5hours. Standard workup led to 2.2 g (95%) of the product as a clear, colorless oil, which solidified in the freezer as white needles, and was used without further purification. MP < rt. NMR ($CDCl_3$): ^{1}H: 7.46 (d, 2H, *J*= 8Hz), 7.28 (d, 2H, *J*= 8Hz), 5.08 (s, 2H), 3.61 (m, 3H), 3.07 (s, 1H), 2.36 (t, 2H, *J*= 7Hz), 1.67 – 1.38, m, 6H). ^{13}C: 173.4, 136.7, 132.3, 127.9, 121.9, 83.2, 77.6, 65.6, 62.6, 34.1, 32.3, 25.2, 24.6.

4-7: 1.0 equivalent (0.25 g, 1.02 mmol) of **4-1** and 1.5 equivalents (0.12 mL) pyridine were stirred in DCM in a septum-sealed round-bottomed flask under N_2 at 0^0C. 1.5 equivalents (0.20 mL) of hexanoyl chloride was then added by syringe. Once the reaction was complete (0.5 hr, as monitored by TLC), the reaction mixture was diluted with DCM, washed with H_2O (twice), sat. NaCl (twice), dried over sodium sulfate and rotary evaporated. The crude product was purified by silica gel chromatography (elution at ~5% EtOAc/hexanes) to yield 0.34 g (80%) of **4-7** as a pale greenish, clear oil. NMR ($CDCl_3$): ^{1}H: 7.47 (dt, 2H, *J* = 8, 2Hz), 7.27 (d, 2H, *J*= 8Hz), 5.09 (s, 2H), 4.04 (t, 2H, *J*= 7Hz), 3.07 (s, 1H), 2.36 (t, 2H, *J*= 7Hz), 2.26 (t, 2H, *J*= 7Hz), 1.69 – 1.57 (m, 6H), 1.42 – 1.27 (m, 6H), 0.88 (t, 3H, *J*= 7Hz). ^{13}C: 173.9, 173.2, 136.7, 132.3, 127.9, 121.9, 83.2, 77.6, 65.6, 63.9, 34.3, 34.1, 31.3, 28.3, 25.5, 24.7, 24.5, 22.3, 13.9.

4-9: Sonogashira coupling conditions; 1.0 equivalent (0.20 g, 0.45 mmol) of **3-6**, 1.3 equivalents (0.20 g) of **4-7**, 5% $Pd(PPh_3)_4$, 10% CuI and 2 equivalents NEt_3 were stirred in THF at rt for 24hrs. Standard workup, purification by silica gel chromatography (elution at ~20% EtOAc/hexanes) gave 0.26 g (87%) of the desired compound as orange waxy needles. NMR ($CDCl_3$): ^{1}H: 7.48 (m, 4H), 7.30 (d, 2H, *J*= 8Hz), 7.24 (d, 2H, *J*= 8Hz), 5.31 (m, 1H), 5.09 (s, 2H), 4.54 (d, 2H, *J*= 7Hz), 4.05 (m, 4H), 3.59 (s, 2H), 2.37 (t, 2H, *J*= 7Hz), 2.26 (m, 4H), 1.73 (s, 3H), 1.68 (s, 3H), 1.61 (m, 10H), 1.42 – 1.24 (m, 9H), 0.87 (t, 3H, *J*= 7Hz).^{13}C: 173.9, 173.5, 173.2, 171.2, 139.0, 136.1, 134.4, 131.8, 131.7, 129.3, 128.1, 123.2, 121.9, 118.6, 89.6, 89.0, 65.7, 64.8, 63.9, 61.3, 41.3, 34.3, 34.2, 34.1, 31.3, 28.3, 28.2, 25.8, 25.5, 25.4, 24.7, 24.5, 22.3, 18.0, 13.9.

4-18: Prenyl deprotection conditions; 1.0 equivalent (0.22 g, 0.33 mmol) of **4-9** and 0.1 equivalent TMSOTf were stirred in DCM at rt for 0.5 hr. Upon addition of TMSOTf, the reaction mixture turned from a pale orange solution to a dark green, which reverted back to the pale orange color upon quenching with water. After washing the organic layer with water twice, it was dried over sodium sulfate and rotary evaporated. The

crude residue was then purified by silica gel chromatography (elution at ~20% EtOAc/hexanes, 2% AcOH added to all eluting solvents) to yield 0.14 g (71%) of the desired compound as an off-white powder, which was then further purified by RP-HPLC (semi-prep column, 3:1 ACN:CH_3OH) to yield white crystals. UV (CH_3OH); λ_{max}Abs= 286 nm (ε= 31 909 M^{-1} cm^{-1}). Fluorescence (CH_3OH); λ_{max}Ex= 302 nm, λ_{max}Em= 318 nm. NMR ($CDCl_3$) ^{1}H: 7.48 (m, 4H), 7.31 (d, 2H, *J*= 8Hz), 7.27 (d, 2H, *J*= 8Hz), 5.10 (s, 2H), 4.07 (m, 4H), 3.61 (s, 2H), 2.39 – 2.24 (m, 6H), 1.63 (m, 10H), 1.43 – 1.24 (m, 9H), 0.88 (t, 3H, *J*= 7Hz). ^{13}C: 174.0, 173.3, 171.2, 136.1, 134.4, 131.8, 131.7, 129.3, 128.0, 123.2, 121.9, 89.6, 89.1, 65.7, 64.7, 64.0, 41.3, 34.3, 34.1, 31.3, 28.3, 28.2, 25.5, 25.4, 24.7, 24.5, 24.2, 22.3, 13.9. MS (-ve ESI): calc'd for $C_{35}H_{43}O_8$ = 591.2958 amu, obtained = 591.2957 amu. Overall yield over 5 steps from **2-5** = 39%

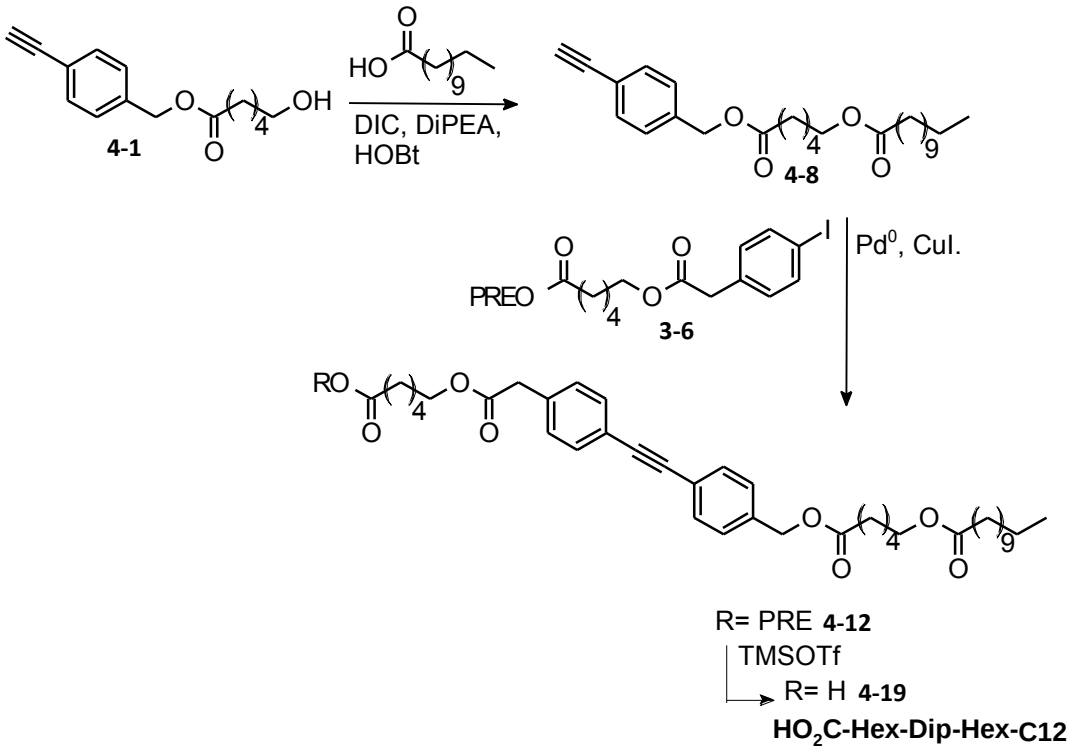

Scheme A1.12: Synthesis of **HO_2C-Hex-Dip-Hex-C12** (**4-19**).

4-8: Ester coupling conditions; 1.0 equivalent (0.15 g, 0.61mmol) of **4-1**, 1.5 equivalents (0.20 g) of Lauric acid, 1.5 equivalents DIC, HOBt and 3 equivalents DIPEA were stirred in

THF for 15 hr at rt. Standard workup and purification by silica gel chromatography (elution at 5% EtOAc/hexanes) led to 0.183 g (70%) of **4-8** as a clear, colorless oil. NMR ($CDCl_3$): ^{1}H: 7.47 (d, 2H, *J*= 8Hz), 7.27 (d, 2H, *J*= 8Hz), 5.09 (s, 2H), 4.03 (t, 2H, *J*= 7Hz), 3.07 (s, 1H), 2.36 (t, 2H, *J*= 7Hz), 2.26 (t, 2H, *J*= 7Hz), 1.69 – 1.57 (m, 6H), 1.24 (s, br, 18H), 0.86 (t, 3H, *J*= 7Hz). ^{13}C: 173.9, 173.2, 136.7, 132.3, 127.9, 121.9, 83.2, 77.6, 65.6, 63.9, 34.3, 34.1, 31.9, 29.6, 29.5, 29.3, 29.2, 29.1, 28.3, 25.5, 24.9, 24.5, 22.7, 14.1.

4-12: Sonogashira coupling conditions; 1.0 equivalent (0.115 g, 0.258 mmol) **3-6,** 1.2 equivalents (0.138 g) of **4-8**, 5% $Pd(PPh_3)_4$, 10% CuI and 2 equivalents NEt_3 were stirred in THF at rt for 22hrs. Standard workup, purification by silica gel chromatography (elution at ~15% EtOAc/hexanes) gave 0.128 g (67%) of the desired compound as pale yellow crystals. NMR ($CDCl_3$): ^{1}H: 7.47 (m, 4H), 7.29 (d, 2H, *J*= 8Hz), 7.25 (d, 2H, *J* = 8Hz), 5.31 (m, 1H), 5.09 (s, 2H), 4.55 (d, 2H, *J*= 7Hz), 4.05 (m, 4H), 3.59 (s, 2H), 2.36 (t, 2H, *J*= 7Hz), 2.26 (m, 4H), 1.73 (s, 3H), 1.68 (s, 3H), 1.57 (m, 9H), 1.23 (s, br, 21H), 0.85 (t, 3H, *J*= 7Hz). ^{13}C: 173.9, 173.5, 173.2, 171.1, 138.9, 136.1, 134.4, 131.7, 131.7, 129.3, 128.0, 123.2, 121.9, 118.6, 89.6, 89.0, 65.7, 65.5, 64.8, 63.9, 61.2, 41.3, 34.3, 34.1, 31.9, 29.6, 29.5, 29.3, 29.2, 29.1, 28.3, 28.2, 25.7, 25.5, 25.4, 24.9, 24.5, 22.7, 17.9, 14.1.

4-19: Prenyl deprotection conditions; 1.0 equivalent (0.10 g, 0.13 mmol) of **4-12** and 0.2 equivalents TMSOTf were stirred in DCM for 20 minutes. Upon addition of TMSOTf, the reaction mixture turned from a pale yellow solution to a dark green, which reverted back to the pale yellow color upon quenching with water. After washing the organic layer with water twice, it was dried over sodium sulfate and rotary evaporated. The crude residue was then sonicated with hexanes, from which 0.08 g (88%) of the product precipitated as a green solid. This was then further purified by RP-HPLC (semi-prep column, 1:1 ACN:CH_3OH) to yield white crystals. UV (CH_3OH); λ_{max}Abs= 287 nm (ε= 34 926 M^{-1} cm^{-1}). Fluorescence (CH_3OH); λ_{max}Ex= 303 nm, λ_{max}Em= 319 nm. NMR (500 MHz, $CDCl_3$) ^{1}H: 7.49 (dt, *J*= 8, 2Hz), 7.47 (dt, 2H, *J*= 8, 2Hz), 7.31 (d, 2H, *J*= 8Hz), 7.25 (d, 2H, *J*= 8Hz), 5.09 (s, 2H), 4.08 (t, 2H, *J*= 7Hz), 4.03 (t, 2H, *J*= 7Hz), 3.60 (s, 2H), 2.36 (t, 2H,

J= 7Hz), 2.33 (t, 2H, *J*= 7Hz), 2.26 (t, 2H, *J*= 7Hz), 1.69 – 1.57 (m, 12H), 1.36 (m, 4H), 1.23 (s, br, 16H), 0.86 (t, 3H, *J*= 7Hz). ^{13}C (125 MHz): 176.6, 174.0, 173.3, 171.2, 136.2, 134.5, 131.8, 131.7, 129.3, 128.1, 123.2, 121.9, 89.6, 89.1, 65.7, 64.7, 63.9, 41.4, 34.4, 34.1, 33.3, 31.9, 29.6, 29.5, 29.3, 29.2, 29.1, 28.3, 28.2, 25.5, 25.4, 24.9, 24.5, 24.2, 22.7, 14.1. MS (-ve ESI): calc'd for $C_{41}H_{55}O_8$ = 675.3897 amu, obtained = 675.3804 amu. Overall yield over 5 steps from **2-5** = 32%

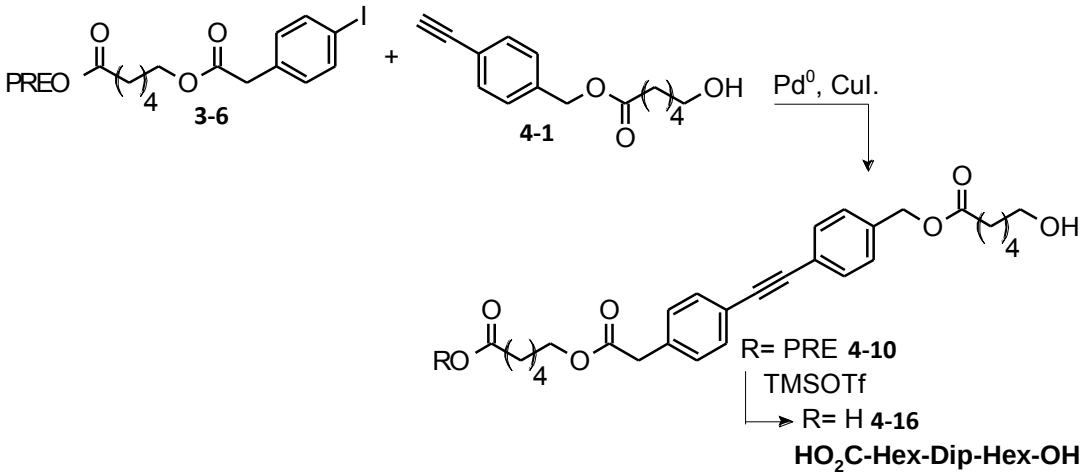

Scheme A1.13: Synthesis of **HO_2C-Hex-Dip-Hex-OH** (**4-16**).

4-10: Sonogashira coupling conditions: 1.0 equivalents (0.20 g, 0.45 mmol) of **3-6**, 1.2 equivalents **4-1**, 5% $Pd(PPh_3)_4$, 10% CuI and 2 equivalents NEt_3 were stirred in THF at 40^{0}C for 20 hrs. Standard workup, purification by silica gel chromatography (elution at 35% EtOAc/hexanes) yields 0.205 g (81%) of the product as orange crystals. NMR ($CDCl_3$): ^{1}H: 7.48 (m, 4H), 7.31 (d, 2H, *J*= 8Hz), 7.25 (d, 2H, *J*= 8Hz), 5.32 (t7, 1H, *J*= 6, 1Hz)), 5.10 (s, 2H), 4.55 (d, 2H, J= 7Hz), 4.08 (t, 2H, J= 7Hz), 3.62 (m, 4H), 2.37 (t, 2H, J= 7Hz), 2.28 (t, 2H, J= 7Hz), 1.74 (s, 3H), 1.69 (s, 3H), 1.67 – 1.54 (m, 8H), 1.44 – 1.29 (m, 4H).^{13}C: 173.5, 173.4, 171.2, 139.0, 136.1, 134.4, 131.8, 131.7, 129.3, 128.1, 123.1, 121.9, 118.6, 89.6, 89.1, 65.7, 64.8, 62.6, 61.3, 41.3, 34.2, 34.1, 32.3, 29.7, 28.2, 25.8, 25.4, 25.2, 24.6, 24.5, 18.0.

4-16: Prenyl deprotection conditions; 1.0 equivalent (0.17 g, 0.30 mmol) **4-10** and 0.2 equivalents TMSoTf were stirred in DCM at rt for 30mins. Standard workup, purification

by silica gel chromatography (elution at 40% acetone/hexanes, 2% AcOH added to all eluting solvents, poor recovery due to adherence to the column) led to 0.048 g (32%) of the product as a white solid. Further purification by RP-HPLC (semi-prep column, 1:1 ACN:CH_3OH) yielded a colourless solid. UV (CH_3OH); λ_{max}Abs= 286 nm (ε=31 705 M^{-1} cm^{-1}). Fluorescence (CH_3OH); λ_{max}Ex= 301 nm, λ_{max}Em= 318 nm. NMR ($CDCl_3$) ^{1}H: 7.49 (m, 4H), 7.31 (d, 2H, *J*= 8Hz), 7.25 (d, 2H, *J*= 8Hz), 5.11 (s, 2H), 4.06 (m, 3H), 3.63 (m, 4H), 2.35 (m, 4H), 1.70 – 1.54 (m, 8H), 1.43 – 1.31 (m, 4H). ^{13}C: 178.2, 173.4, 171.2, 136.1, 134.4, 131.8, 131.7, 129.3, 128.1, 123.1, 121.9, 89.6, 89.1, 65.7, 64.7, 62.6, 41.3, 34.2, 33.6, 32.2, 28.2, 25.3, 25.2, 24.6, 24.2. MS (-ve ESI): calc'd for $C_{29}H_{33}O_7$ = 493.2226 amu, obtained = 493.2171 amu. Overall yield in 4 steps from **2-5** = 20%

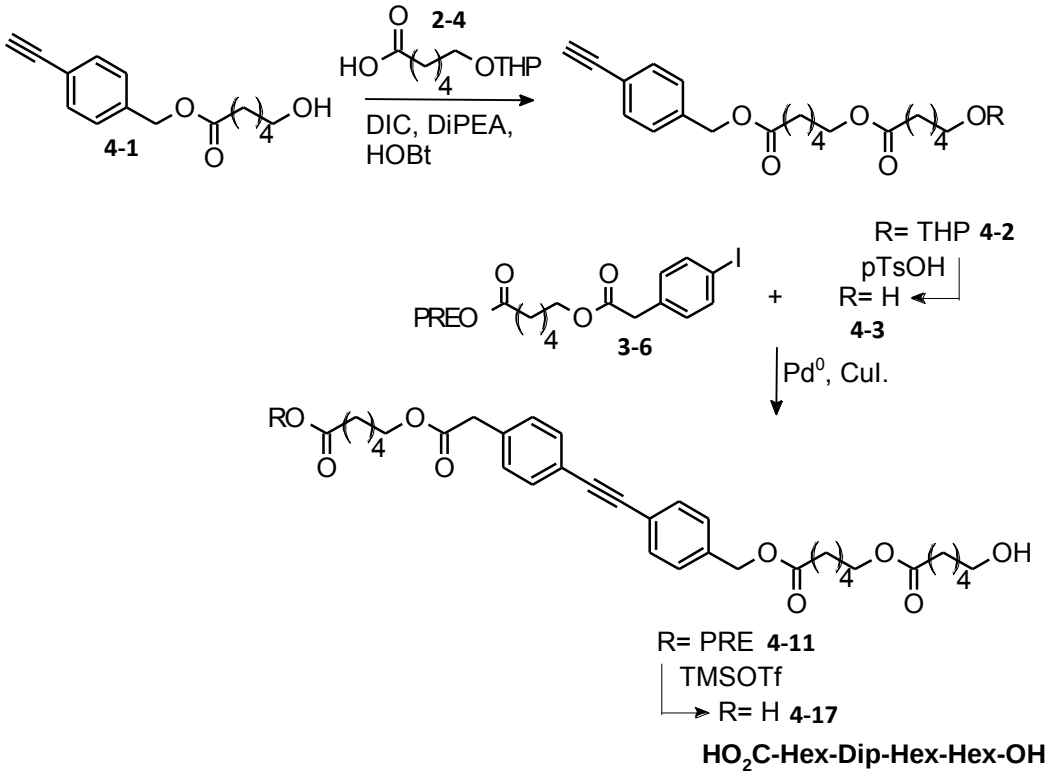

Scheme A1.14: Synthesis of **HO_2C-Hex-Dip-Hex-Hex-OH** (**4-17**).

4-2: Ester coupling conditions; 1.0 equivalent (1.50 g, 6.09 mmol) of **4-1**, 1.8 equivalents **2-4**, 1.8 equivalents DIC, HOBt and 3.6 equivalents DIPEA were stirred in THF at rt for 48hr. Standard workup, purification by silica gel chromatography (elution at 15%

EtOAc/hexanes) led to 2.19 g (81%) of the product as a clear, colourless oil. NMR ($CDCl_3$) ^{1}H: 7.45 (dt, 2H, *J*= 8, 2Hz), 7.27 (td, 2H, *J*= 8, 2Hz), 5.07 (s, 2H), 4.54 (m, 1H), 4.02 (t, 2H, *J*= 7Hz), 3.83 (m, 1H), 3.70 (m, 1H), 3.46 (m, 1H), 3.65 (m, 1H), 3.07 (s, 1H), 2.34 (t, 2H, *J*= 7Hz), 2.27 (t, 2H, *J*= 7Hz), 1.79 – 1.50 (m, 14H), 1.42 – 1.32 (m, 4H). ^{13}C: 173.7, 173.1, 136.7, 132.3, 127.9, 121.9, 98.8, 83.2, 77.6, 67.3, 65.5, 63.9, 62.3, 34.2, 34.0, 30.7, 29.4, 28.3, 25.8, 25.5, 24.8, 24.5, 19.7.

4-3: THP removal conditions; 1.0 equivalent (1.70 g, 3.82 mmol) of **4-2** and 0.2 equivalents pTsOH were stirred in 20% CH_3OH/DCM at rt for 3.5hr. Standard workup, purification by silica gel chromatography (elution at 40% EtOAc/hexanes) led to 1.21 g (89%) of the product as a clear, colourless oil. NMR ($CDCl_3$) ^{1}H: 7.45 (d, 2H, *J*= 8Hz), 7.25 (d, 2H, *J*= 8Hz), 5.07 (s, 2H), 4.02 (t, 2H, *J*= 7Hz), 3.59 (m, 3H), 3.06 (s, 1H), 2.34 (t, 2H, *J*= 7Hz), 2.27 (t, 2H, *J*= 7Hz), 1.67 – 1.51 (m, 8H), 1.41 – 1.31 (m, 4H). ^{13}C: 173.8, 173.2, 136.7, 132.3, 127.9, 121.9, 83.2, 77.6, 65.6, 64.1, 62.5, 34.2, 34.1, 32.3, 28.3, 25.5, 25.3, 24.6, 24.5.

4-11: Sonogashira coupling conditions; 1.0 equivalent (0.139 g, 0.390 mmol) **4-3**, 1.2 equivalents **3-6**, 5% $Pd(PPh_3)_4$, 10% CuI and 2.0 equivalents NEt_3 were stirred in THF for 20hr at 40^{0}C. Standard workup, purification by silica gel chromatography (elution at 60% EtOAc/hexanes) yields 0.186 g (71%) of the product as a pale solid. NMR ($CDCl_3$) ^{1}H: 7.47 (m, 4H), 7.30 (d, 2H, *J*= 8Hz), 7.23 (d, 2H, *J*= 8Hz), 5.31 (m, 1H), 5.09 (s, 2H), 4.53 (d, 2H, *J*= 7Hz), 4.04, m, 4H), 3.61 (m, 4H), 2.36 (t, 2H, *J*= 7Hz), 2.27 (m, 4H), 1.73 (s, 3H), 1.67 (s, 3H), 1.67 – 1.54 (m, 12H), 1.39 – 1.31 (m, 6H). ^{13}C: 173.7, 173.5, 173.3, 171.2, 139.0, 136.1, 134.4, 131.7, 129.3, 128.1, 123.2, 121.9, 118.6, 89.6, 89.0, 65.7, 64.8, 64.1, 62.6, 61.3, 41.3, 34.2, 34.1, 34.0, 32.3, 28.3, 28.2, 25.7, 25.5, 25.4, 25.3, 24.7, 24.5, 17.9.

4-17: Prenyl deprotection conditions: 1.0 equivalent (0.14 g, 0.21 mmol) of **4-11** and 0.2 equivalents TMSOTf were stirred in DCM at rt for 1 hr. Standard workup led to a green oil, from which a yellow solid precipitated upon sonication with acetone/hexanes. This

crude product was purified by silica gel chromatography (elution at 1:1 acetone/hexanes, 2% AcOH added to all eluting solvents) to yield 0.090 g (75%) of a white solid. This was further purified by RP-HPLC (semi-prep column, 3:1 ACN:CH_3OH) to yield white crystals. UV (CH_3OH); λ_{max}Abs= 286 nm (ε= 24 347 M^{-1} cm^{-1}). Fluorescence (CH_3OH); λ_{max}Ex= 301 nm, λ_{max}Em= 318 nm. NMR ($CDCl_3$) ^{1}H: 7.48 (m, 4H), 7.31 (d, 2H, *J*= 8Hz), 7.25 (d, 2H, *J*= 8Hz), 5.10 (s, 2H), 4.06 (m, 5H), 3.63 (m, 4H), 2.32 (m, 6H), 1.69 – 1.52 (m, 12H), 1.42 – 1.32 (m, 6H). ^{13}C: 173.8, 173.3, 171.2, 136.1, 134.4, 131.8, 131.7, 129.3, 128.1, 123.1, 121.9, 89.6, 89.0, 65.7, 64.8, 64.1, 62.6, 41.3, 34.2, 34.0, 32.2, 28.3, 28.2, 25.5, 25.4, 25.3, 24.6, 24.5, 24.3. MS (-ve ESI): calc'd for $C_{35}H_{43}O_9$ = 607.2907 amu, obtained = 607.2767 amu. Overall yield over 6 steps from **2-5** = 38%

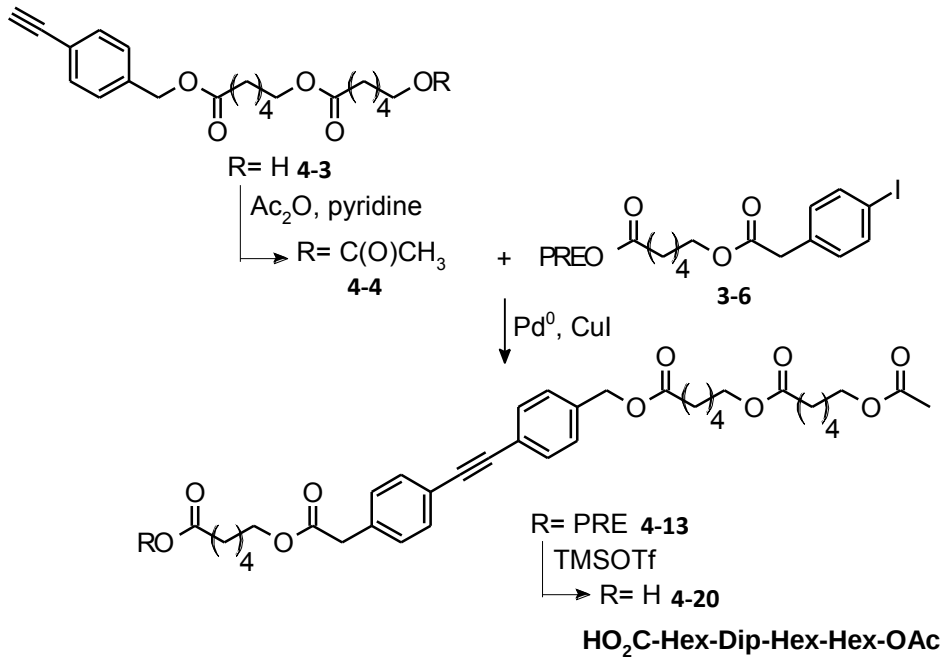

Scheme A1.15: Synthesis of **HO_2C-Hex-Dip-Hex-Hex-OAc** (**4-20**).

4-4: 1.0 equivalent (0.135 g, 0.370 mmol) of **4-3**, 2.0 equivalents Acetic anhydride and 2.0 equivalents pyridine were stirred in dry DCM for 20 hr at rt. Once complete, the reaction was diluted into DCM, washed with H_2O, sat. $NaHCO_3$ and sat. NaCl, dried over sodium sulfate and evaporated under vacuum. The crude product (a yellow oil, 0.199 g, > 100% yield) was used directly in the next step without further purification as there

were no other alkyne-containing compounds present. NMR ($CDCl_3$) ^{1}H: 7.44 (dt, 2H, *J*= 8, 2H), 7.25 (d, 2H, *J*= 8Hz), 5.06 (s, 2H), 4.01 (t, 2H, *J*= 7Hz), 3.06 (s, 1H), 2.34 (t, 2H, *J*= 7Hz), 2.26 (t, 2H, *J*= 7Hz), 1.99 (s, 3H), 1.67 – 1.56 (m, 8H), 1.39 – 1.31 (m, 4H). ^{13}C: 173.5, 173.1, 171.1, 136.7, 132.2, 127.9, 121.9, 83.2, 77.6, 65.5, 64.2, 64.0, 34.1, 34.0, 28.3, 25.5, 24.5, 24.5, 22.1.

4-13: Sonogashira coupling conditions; 1.0 equivalent (0.15 g, 0.37 mmol) of **4-4**, 1.0 equivalent **3-6**, 5% $Pd(PPh_3)_4$, 10% CuI and 2.0 equivalents NEt_3 were stirred in THF at rt for 48hr. Standard workup, purification by silica gel chromatography (elution at 30% EtOAc/hexanes) led to 0.17 g (64%) of the product as a clear yellow oil. NMR ($CDCl_3$) ^{1}H: 7.49 (m, 4H), 7.31 (d, 2H, *J*= 8Hz), 7.25 (d, 2H, *J*= 8Hz), 5.32 (m, 1H), 5.10 (s, 2H), 4.55 (d, 2H, *J*= 7Hz), 4.05 (m, 6H), 3.61 (s, 2H), 2.37 (t, 2H, *J*= 7Hz), 2.27 (m, 4H), 2.02 (s, 3H), 1.74 (s, 3H), 1.69 (s, 3H), 1.67 – 1.57 (m, 12H), 1.42 – 1.29 (m, 6H). ^{13}C: 173.5, 173.5, 173.2, 171.1, 139.0, 136.1, 134.4, 131.7, 129.3, 128.1, 123.2, 121.9, 118.6, 89.6, 89.0, 65.7, 64.8, 64.3, 64.1, 61.3, 41.3, 34.1, 34.0, 28.3, 28.3, 28.2, 25.8, 25.5, 25.4, 24.6, 24.5, 20.9, 17.9.

4-20: Prenyl deprotection conditions; 1.0 equivalent (0.086 g, 0.132 mmol) of **4-13** and 0.2 equivalents TMSOTf were stirred in DCM at rt for 20 mins. Standard workup led to a green oil, from which 0.070 g (91%) of a pale green solid precipitated upon sonication with EtOAc/hexanes. This crude product was further purified by RP-HPLC (semi-prep column, 3:1 CH_3OH:ACN) to yield a white crystalline solid. UV (CH_3OH); λ_{max}Abs= 286 nm. Fluorescence (CH_3OH); λ_{max}Ex= 300 nm, λ_{max}Em= 318 nm. NMR (500 MHz, $CDCl_3$) ^{1}H: 7.49 (dt, 2H, *J*= 8,2Hz), 7.46 (dt, 2H, *J*= 8,2Hz), 7.31 (d, 2H, *J*= 8Hz), 7.25 (d, 2H, *J*= 8Hz), 5.09 (s, 2H), 4.08 (t, 2H, *J*= 7Hz), 4.03 (m, 4H), 3.60 (s, 2H), 2.36 (t, 2H, *J*= 7Hz), 2.33 (t, 2H, *J*= 7Hz), 2.28 (t, 2H, *J*= 7Hz), 2.02 (s, 3H), 1.62 (m, 12H), 1.35 (m, 6H). ^{13}C (125 MHz): 177.6, 173.8, 173.5, 171.5, 171.4, 136.3, 134.4, 132.0, 131.9, 129.5, 128.3, 123.4, 121.1, 89.8, 89.3, 65.9, 64.9, 64.5, 64.3, 41.6, 34.4, 34.3, 33.7, 28.5, 28.5, 28.4, 25.7,

25.6, 24.8, 24.7, 24.4, 21.2. MS (-ve ESI): calc'd for $C_{37}H_{45}O_{10}$ = 649.3013 amu, obtained = 649.3036 amu. Overall yield in 7 steps from **2-5** = 33%

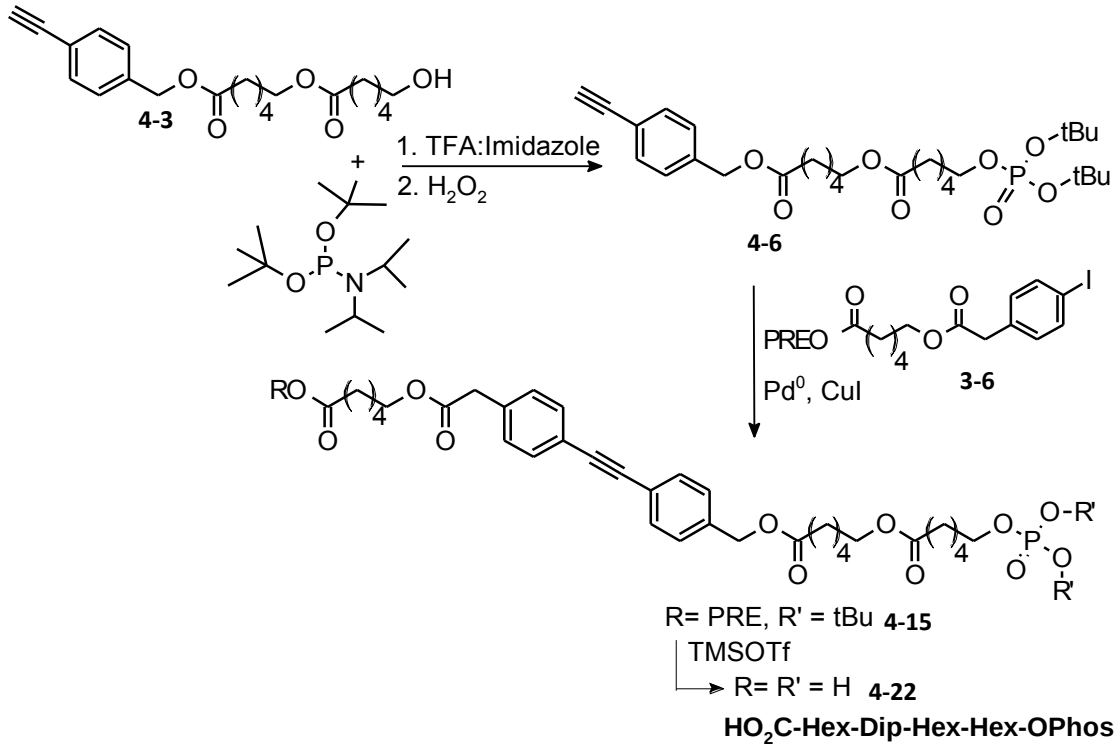

Scheme A1.16: Synthesis of **HO_2C-Hex-Dip-Hex-Hex-OPhos** (**4-22**).

4-6: Adapted from [128]: 4.6 equivalents (3.17 mmol) of TFA and 4.6 equivalents of imidazole were stirred in THF under N_2 at rt for 10 mins, in which time a white slurry formed. 1.5 equivalents (1.04 mmol) of di-tert-butyl-*N,N*-di-isopropyl phosphoramidite were then added by syringe over a further 10mins. 1.0 equivalent (0.25 g, 0.69 mmol) of **4-3** was then added dropwise by syringe to the mixture, which was then stirred at rt under N_2 until no further consumption of starting material was observed (20hr total reaction time, however, no further reaction after 1.5 hr). The reaction mixture was then cooled to 0^oC, and 3.5 equivalents of 30% H_2O_2 were added. This reaction was complete after 30 mins, after which it was quenched by the addition of sat. $NaHCO_3$, diluted with H_2O and extracted against EtOAc, dried over sodium sulfate and rotary evaporated. Purification by silica gel chromatography yielded 0.245 g (64%) of a clear, colourless oil. NMR ($CDCl_3$) ^1H: 7.45 (d, 2H, *J*= 8Hz), 7.27 (d, 2H, *J*= 8Hz), 5.07 (s, 2H),

4.02 (t, 2H, *J*= 7Hz), 3.91 (q, 2H, *J*= 7Hz), 3.06 (s, 1H), 2.34 (t, 2H, *J*= 7Hz), 2.26 (t, 2H, *J*= 7Hz), 1.68 – 1.58 (m, 8H), 1.45 (s, 18H), 1.41 – 1.31 (m, 4H). ^{13}C: 173.5, 173.1, 136.7, 132.3, 127.9, 121.9, 83.2, 81.9, 81.9, 77.6, 66.5, 66.4, 65.5, 64.0, 34.1, 34.0, 29.9, 29.8, 28.3, 25.5, 25.2, 24.5. ^{31}P (200 MHz): -8.99 (s, 1P).

4-15: Sonogashira coupling conditions; 1.0 equivalent (0.20 g, 0.36 mmol) of **4-6**, 1.3 equivalents **3-6**, 5% $Pd(PPh_3)_4$, 10% CuI and 2.0 equivalents NEt_3 were stirred at rt for 24 hrs, then at 40^{o}C for a further 24 hrs. Standard workup, purification by silica gel chromatography (elution at 20% acetone/hexanes) yielded 0.218 g (69%) of a clear, pale yellow oil. NMR ($CDCl_3$) ^{1}H: 7.46 (m, 4H), 7.29 (d, 2H, *J*= 8Hz), 7.23 (d, 2H, *J*= 8Hz), 5.29 (t7, 1H, *J*= 7, 1Hz), 5.08 (s, 2H), 4.53 (d, 2H, *J*= 7Hz), 4.03 (m, 4H), 3.91 (q, 2H, *J*= 7Hz), 3.59 (s, 2H), 2.35 (t, 2H, *J*= 7Hz), 2.26 (m, 4H), 1.71 (s, 3H), 1.67 (s, 3H), 1.65 – 1.54 (m, 12H), 1.44 (s, 18H), 1.41 – 1.28 (m, 4H). ^{13}C: 173.5, 173.4, 173.2, 171.1, 138.9, 136.1, 134.4, 131.7, 131.7, 129.3, 128.0, 123.1, 121.9, 118.6, 89.6, 89.0, 81.9, 81.8, 66.5, 66.4, 65.6, 64.8, 64.0, 61.2, 41.3, 34.1, 34.0, 34.0, 29.9, 29.8, 28.3, 28.2, 25.7, 25.5, 25.4, 25.2, 24.5, 17.9. ^{31}P (200 MHz): -9.01 (s, 1P).

4-22: Prenyl deprotection conditions; 1.0 equivalent (0.14 g, 0.16 mmol) of **4-15**, and 0.4 equivalents TMSOTf were stirred at rt in DCM for 20 mins. Standard extractive workup led to a yellow oil, from which 0.091 g (83%) of a white, waxy solid precipitated upon sonication with hexanes. This was further purified by RP-HPLC (semi-prep column, 100% CH_3OH) to yield a white crystalline solid. UV (CH_3OH); λ_{max}Abs=287 nm (ε=31 705 M^{-1} cm^{-1}). Fluorescence (CH_3OH); λ_{max}Ex=301 nm, λ_{max}Em= 318 nm. NMR: ^{1}H (CD_3OD): 7.49 (m, 4H), 7.37 (d, 2H, *J*= 8Hz), 7.31 (d, 2H, *J*= 8Hz), 5.14 (s, 2H), 4.11 (t, 2H, *J*= 7Hz), 4.06 (t, 2H, *J*= 7Hz), 3.90 (q, 2H, *J*= 6Hz), 3.68 (s, 2H), 2.41 (t, 2H, *J*= 7Hz), 2.29 (m, 4H), 1.69 – 1.58 (m, 12H), 1.45 – 1.33 (m, 6H). ^{13}C (125 MHz, CD_3OD): 177.6, 175.7, 175.1, 173.3, 138.3, 136.5, 132.8, 130.8, 129.4, 124.5, 123.3, 90.5, 90.1, 66.8, 66.7, 66.1, 65.4, 42.0, 35.2, 35.0, 34.9, 31.6, 31.5, 29.5, 29.5, 26.7, 26.7, 29.5, 25.9, 25.8, 25.7. ^{31}P (200

MHz, CD_3OD): 1.76 (s, 1P). MS (-ve ESI): calc'd for $C_{35}H_{44}O_{12}P$ = 687.2570 amu, obtained = 687.2717 amu. Overall yield over 7 steps from **2-5** = 21%

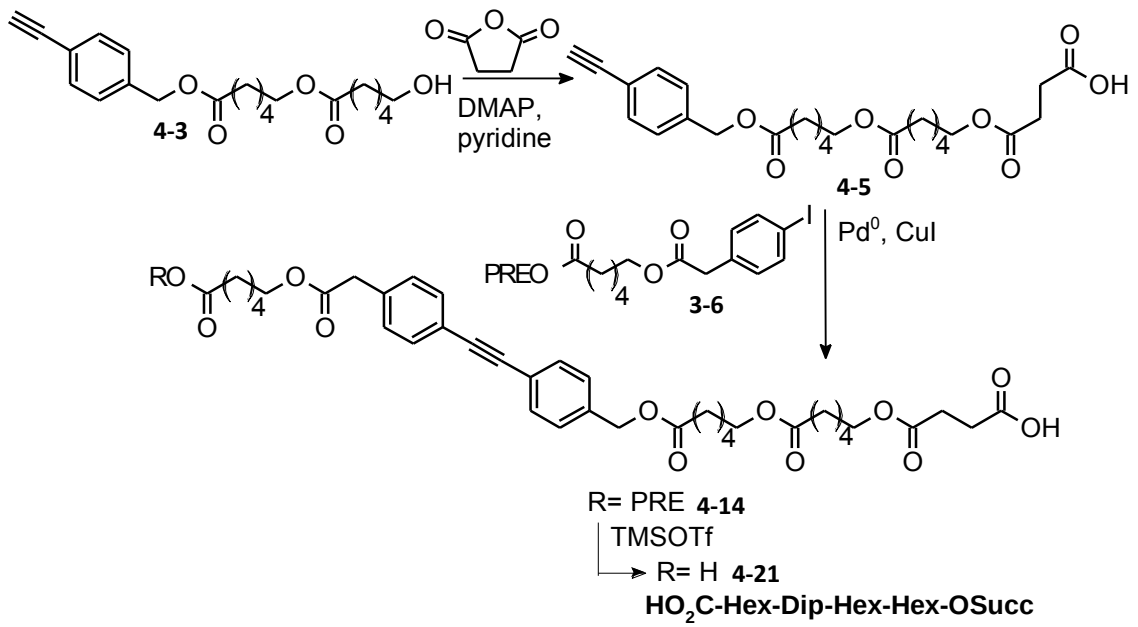

Scheme A1.17: Synthesis of **HO_2C-Hex-Dip-Hex-Hex-OSucc** (**4-21**).

4-5: Adapted from[127]: 1.0 equivalent (0.25 g, 0.69 mmol) of **4-3**, 4.0 equivalents succinic anhydride, 5.0 equivalents pyridine and 1.0 equivalent DMAP were stirred in dry DCM for 24 hrs at rt. The reaction mixture was then diluted with DCM, extracted against water, sat. $NaHCO_3$ and sat. NaCl, dried over sodium sulfate and concentrated under vacuum. The crude product was purified by silica gel chromatography (elution at 30% EtOAc/hexanes, 2% AcOH added to all eluting solvents) to yield 0.242 g (76%) of a clear, colourless oil. NMR ($CDCl_3$) ^{1}H: 9.01 (s, br, 1H), 7.45 (dt, 2H, *J*= 8, 2Hz), 7.27 (d, 2H, *J*= 8Hz), 5.07 (s, 2H), 4.04 (m, 4H), 3.07 (s, 2H), 2.60 (s, br, 4H), 2.35 (t, 2H, *J*= 7Hz), 2.27 (t, 2H, *J*= 7Hz), 1.67 – 1.56 (m, 8H), 1.40 – 1.30 (m, 4H). ^{13}C: 173.7, 173.3, 172.3, 136.7, 132.3, 127.9, 121.9, 83.2, 77.7, 65.6, 64.6, 64.1, 34.1, 34.0, 32.1, 29.1, 28.3, 28.2, 25.5, 25.2, 24.6, 24.5.

4-14: Sonogashira coupling conditions; 1.0 equivalent (0.21 g, 0.46 mmol) of **4-5**, 1.2 equivalents **3-6**, 5% $Pd(PPh_3)_4$, 10% CuI and 2.5 equivalents NEt_3 were stirred in THF at rt for 20hrs. Standard workup, purification by silica gel chromatography (40% EtOAc/hexanes, 2% AcOH added to all eluting solvents) lead to 0.252 g (73%) of the

compound as a clear colourless oil, which solidified under vacuum into a white waxy solid. NMR ($CDCl_3$) ^{1}H: 7.48 (m, 4H), 7.30 (d, 2H, *J*= 8Hz), 7.23 (d, 2H, *J*= 8Hz), 5.31 (m, 1H), 5.09 (s, 2H), 4.54 (d, 2H, *J*= 7Hz), 4.05 (m, 6H), 3.60 (s, 2H), 2.62 (m, br, 4H), 2.36 (t, 2H, *J*= 7Hz), 2.27 (m, 4H), 1.73 (s, 3H), 1.68 (s, 3H), 1.66 – 1.56 (m, 12H), 1.41 – 1.29 (m, 6H). ^{13}C: 173.7, 173.6, 173.3, 172.1, 171.2, 139.0, 136.1, 134.4, 131.7, 131.7, 129.3, 128.1, 123.2, 121.9, 118.6, 89.6, 89.1, 65.7, 64.8, 64.6, 64.2, 61.3, 41.3, 34.1, 34.0, 29.0, 28.3, 28.2, 25.7, 25.5, 25.4, 24.5, 17.9.

4-21: Prenyl deprotection conditions; 1.0 equivalent (0.15 g, 0.19 mmol) of **4-14** and 0.2 equivalents TMSoTf were stirred in DCM at rt for 1 hr. Standard workup led to a green oil, from which 97mg (71%) of a white solid precipitated upon sonication with 1:1 Et_2O/hexanes. Further purification by RP-HPLC (semi-prep column, 15% CH_3OH/ACN) to yield a white crystalline solid. UV (CH_3OH); λ_{max}Abs=286 nm (ε= 32 283 M^{-1} cm^{-1}). Fluorescence (CH_3OH); λ_{max}Ex= 301 nm, λ_{max}Em= 317 nm. NMR (500 MHz, $CDCl_3$) ^{1}H: 7.51 (dt, 2H, *J*= 8, 2Hz), 7.47 (dt, 2H, *J*= 8, 2Hz), 7.32 (d, 2H, *J*= 8Hz), 7.26 (d, 2H, *J*= 8Hz), 5.11 (s, 2H), 4.06 (m, 6H), 3.61 (s, 2H), 2.65 (m, br, 2H), 2.59 (m, br, 2H), 2.38 (t, 2H, *J*= 7Hz), 2.27 (m, 4H), 1.67 – 1.56 (m, 12H), 1.36 (m, 4H), 1.27 (m, 2H). ^{13}C (125 MHz, $CDCl_3$): 173.9, 173.5, 172.4, 171.3, 136.4, 134.8, 132.0, 131.9, 129.5, 128.3, 123.4, 122.2, 89.8, 89.3, 65.9, 64.9, 64.9, 64.3, 41.9, 34.4, 34.3, 29.2, 28.4, 28.3, 25.7, 25.5, 24.8, 24.7, 24.3. MS (-ve ESI): calc'd for $C_{39}H_{47}O_{12}$ = 707.3068 amu, obtained = 707.3105 amu. Overall yield in 4 steps from **2-5** = 22%

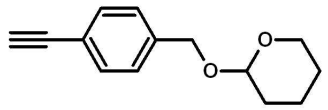

A-1

^{1}H NMR ($CDCl_3$) 300 MHz

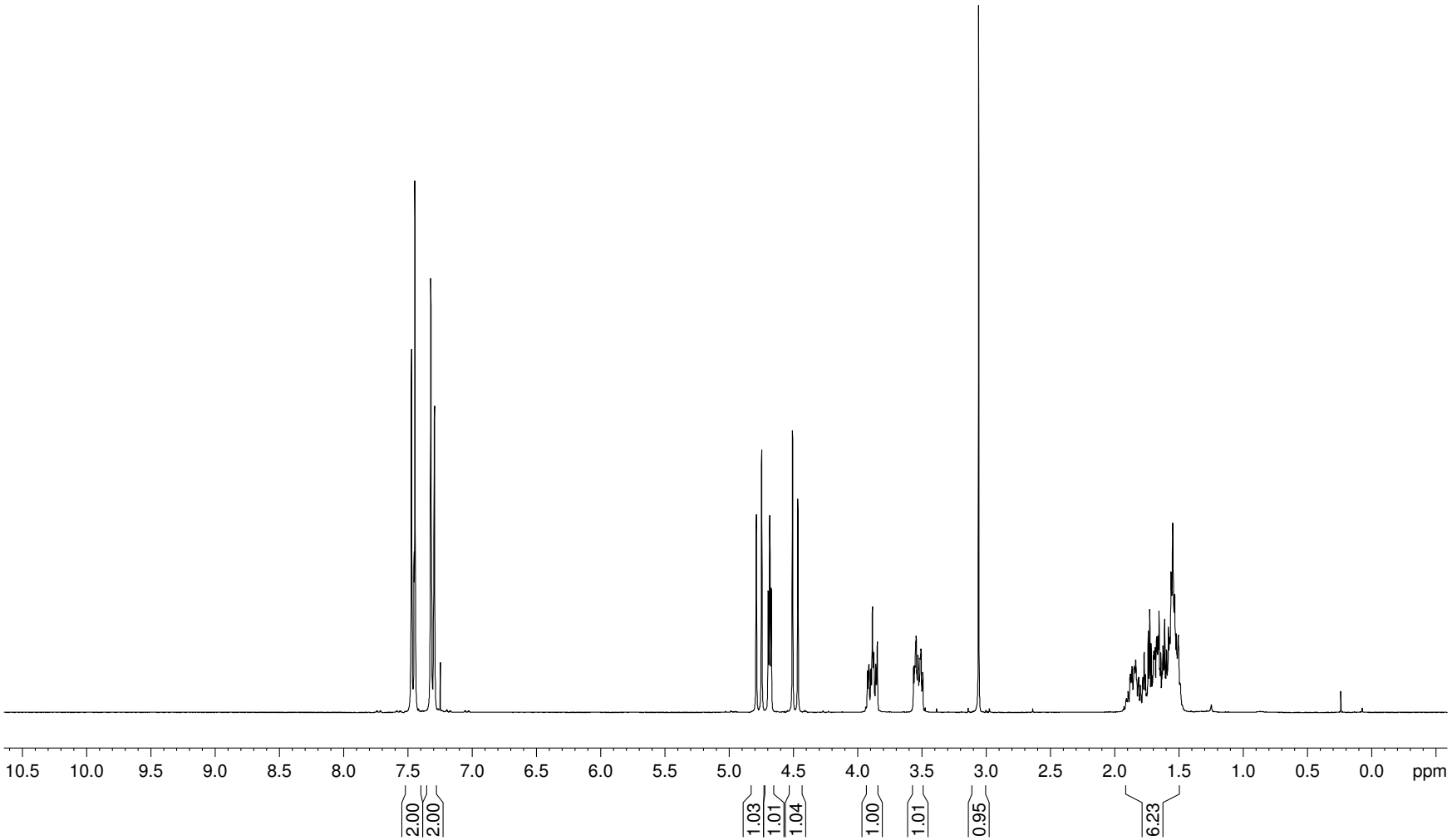

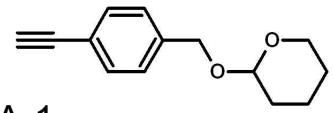

A-1

^{13}C NMR ($CDCl_3$) 75 MHz

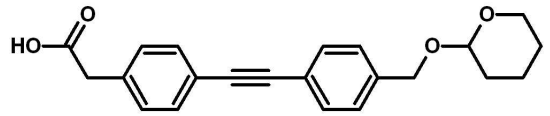

2-1

^{1}H NMR ($CDCl_3$) 300 MHz

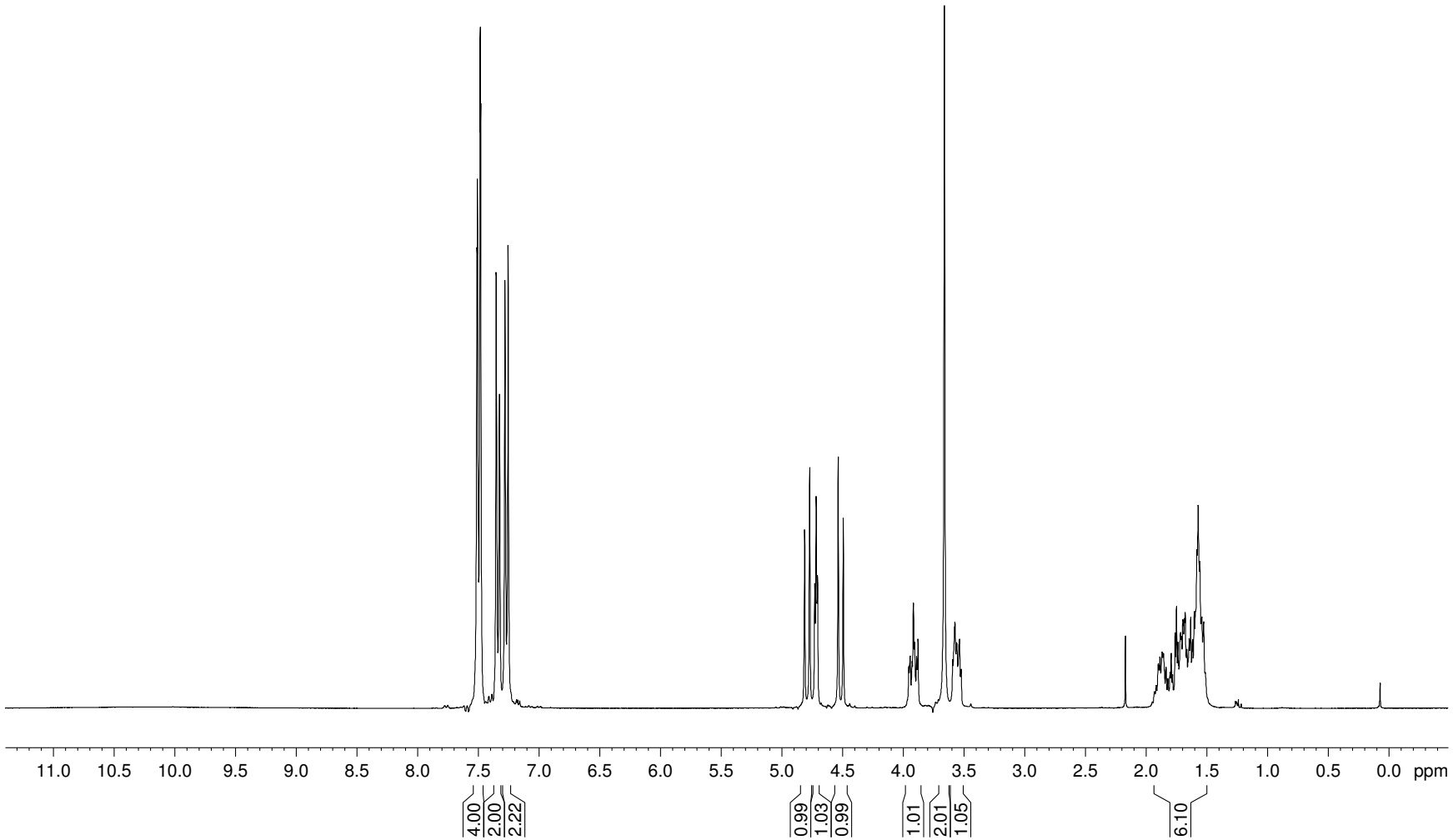

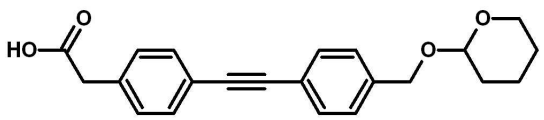

2-1

^{13}C NMR ($CDCl_3$) 75 MHz

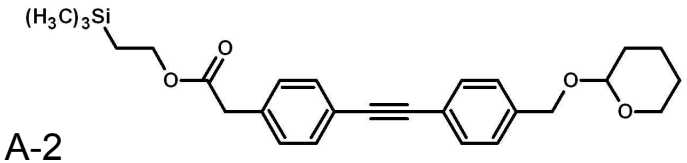

A-2

^{1}H NMR ($CDCl_3$) 300 MHz

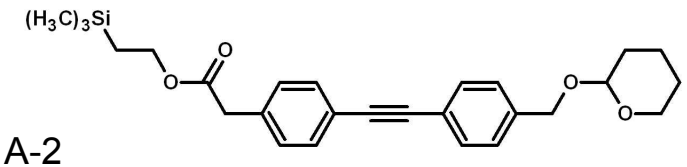

A-2

^{13}C NMR ($CDCl_3$) 75 MHz

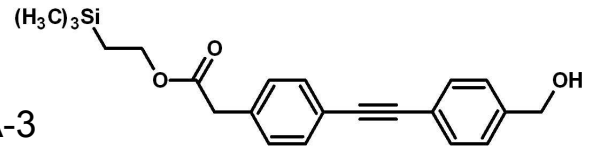

A-3

^{1}H NMR ($CDCl_3$) 300 MHz

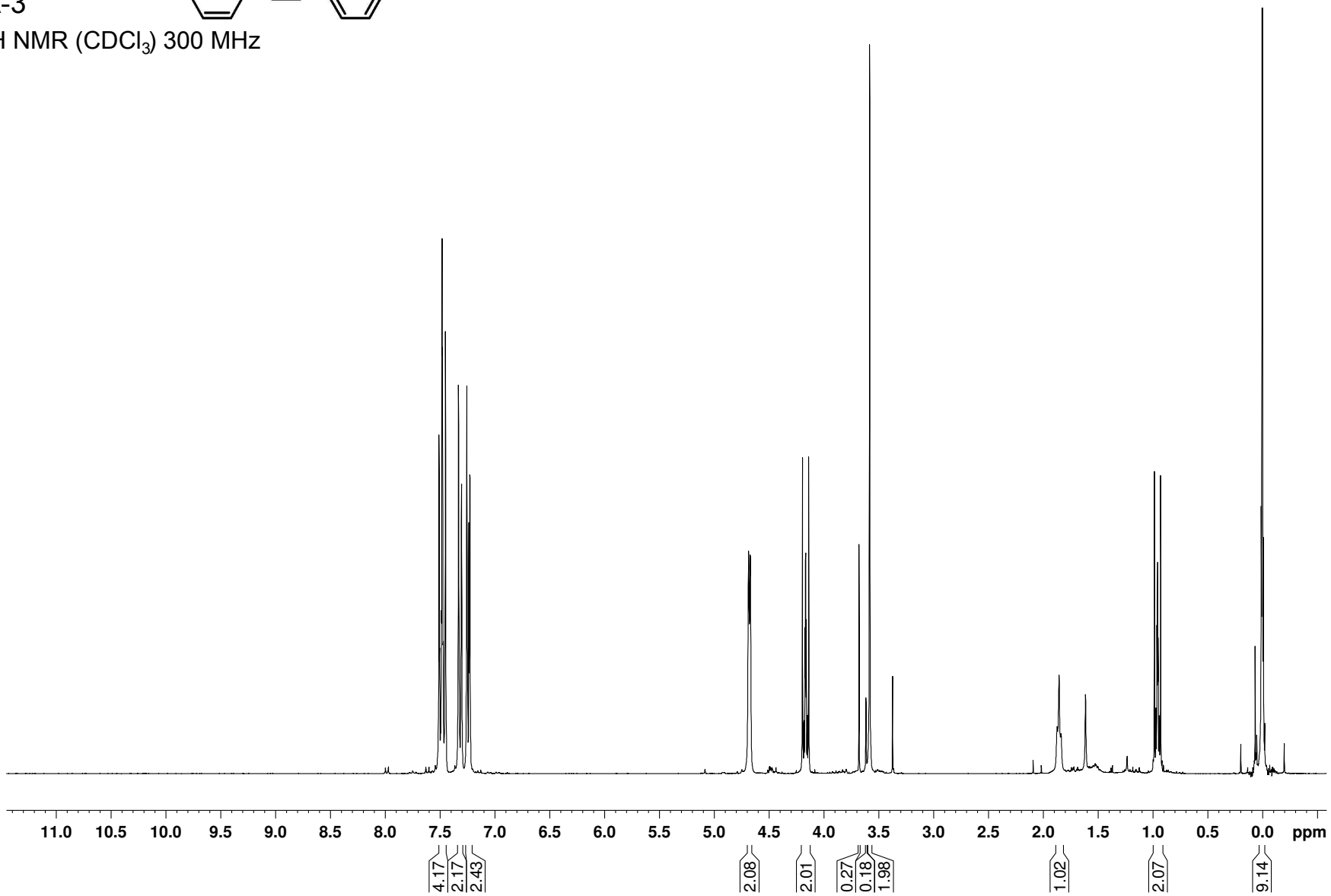

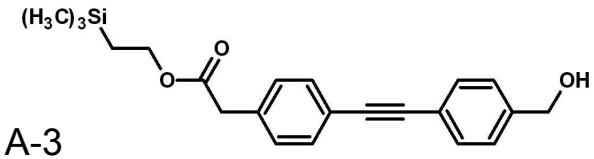

A-3

^{13}C NMR ($CDCl_3$) 75 MHz

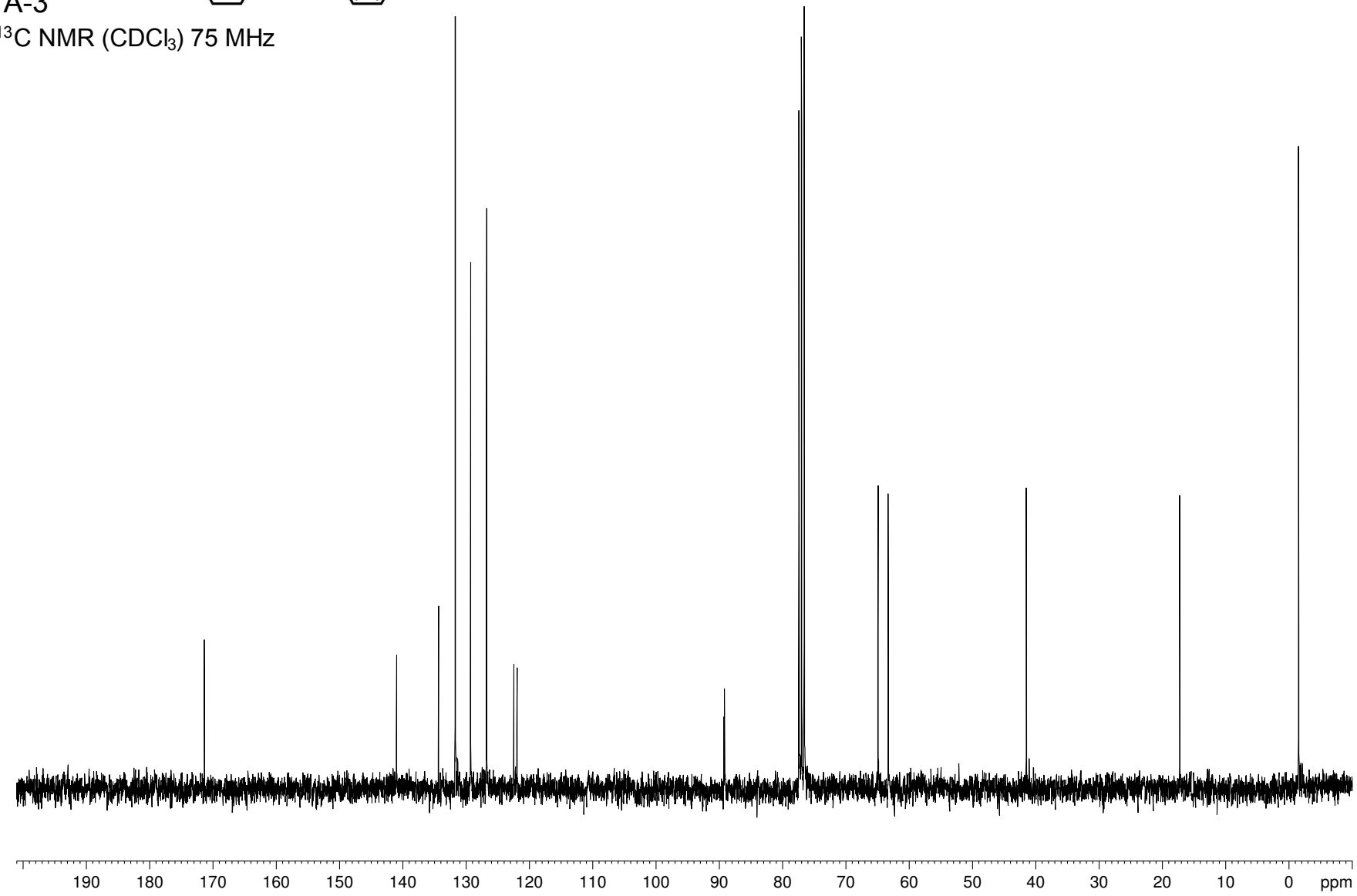

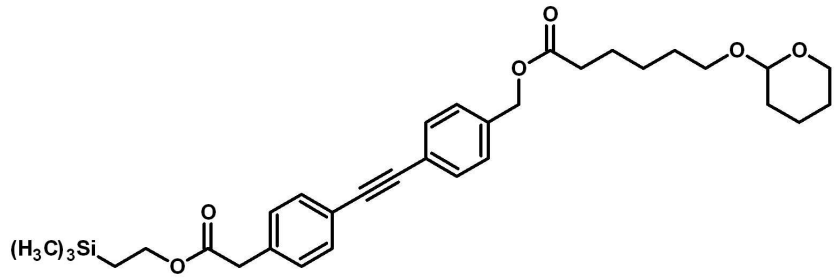

A-4

^{1}H NMR ($CDCl_3$) 300 MHz

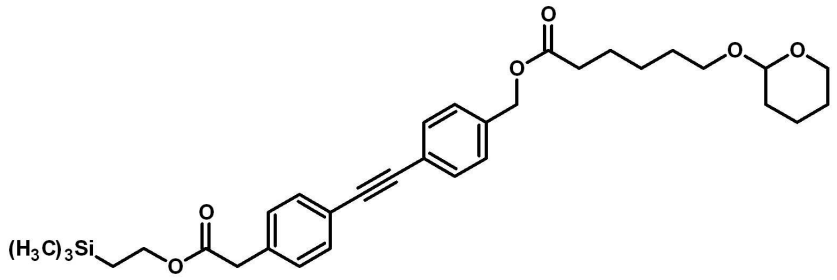

A-4

^{13}C NMR ($CDCl_3$) 75 MHz

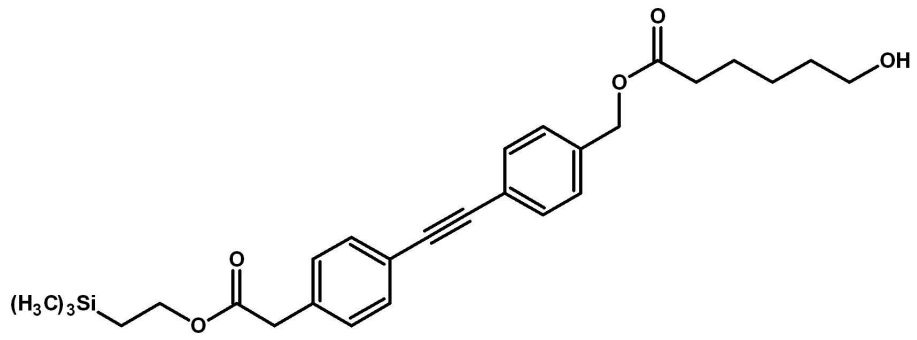

A-5

^{1}H NMR ($CDCl_3$) 300 MHz

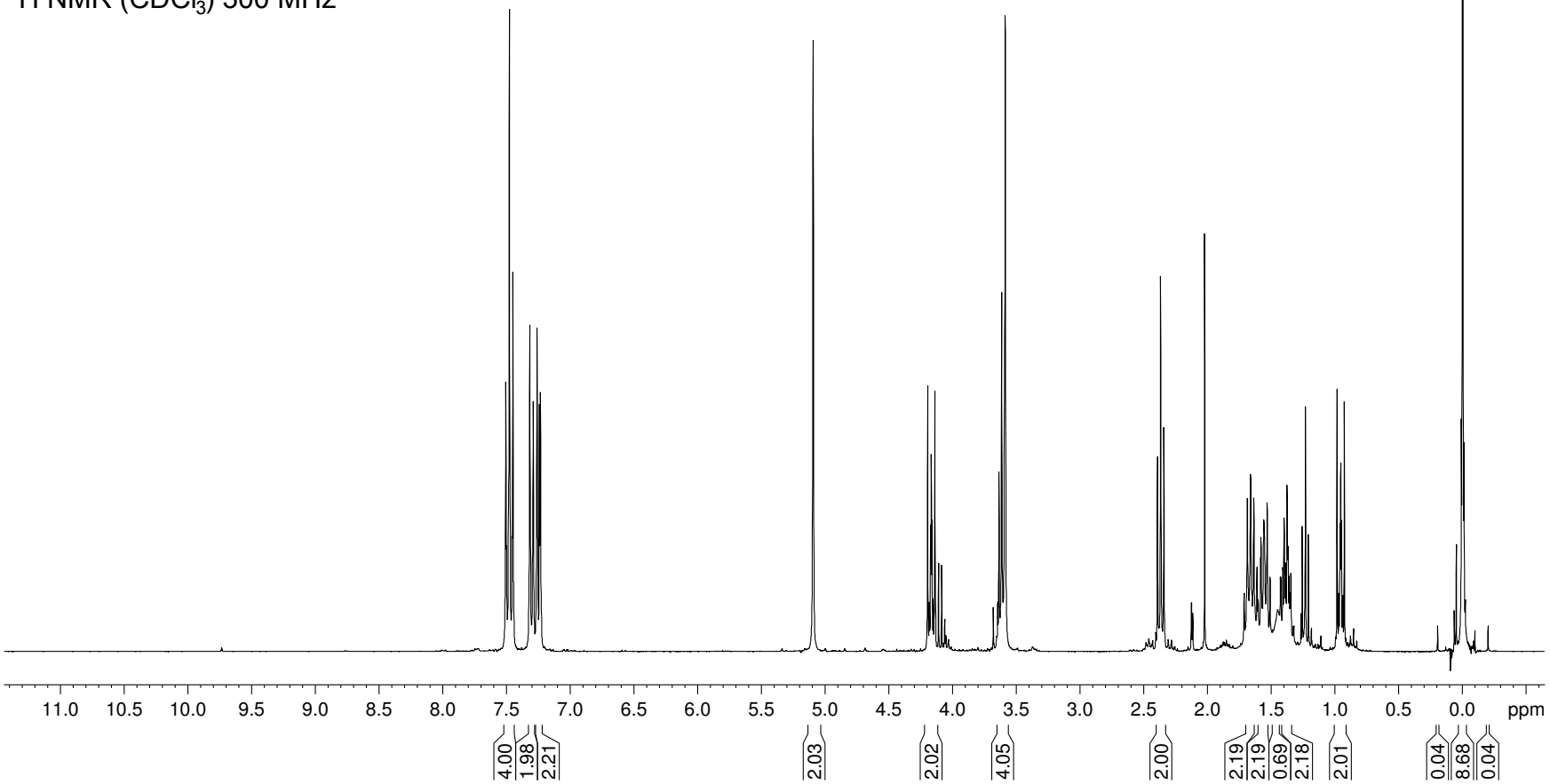

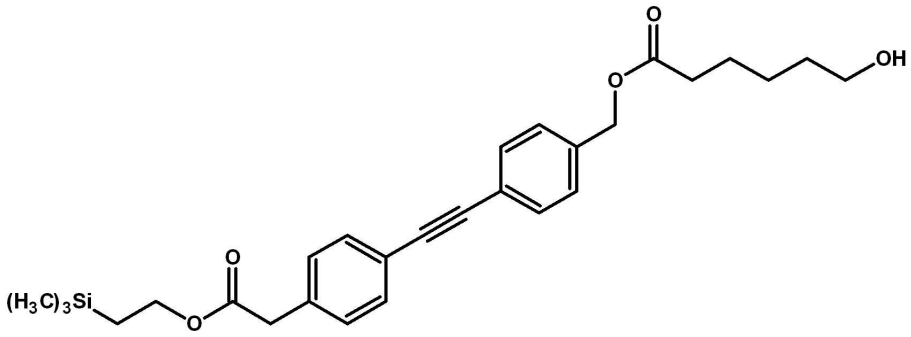

A-5

^{13}C NMR ($CDCl_3$) 75 MHz

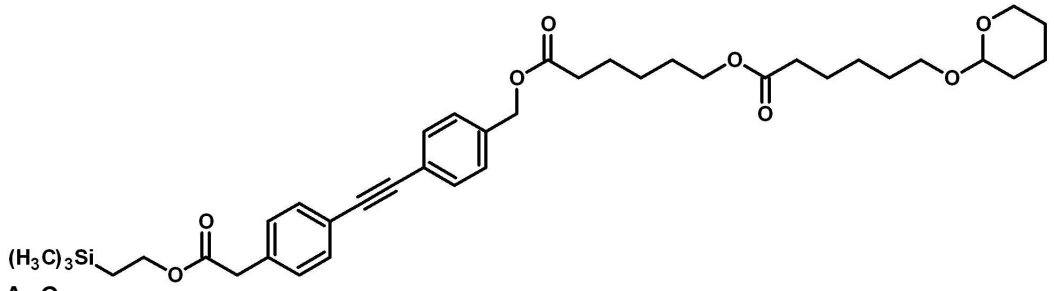

A-6

^{1}H NMR ($CDCl_3$) 300 MHz

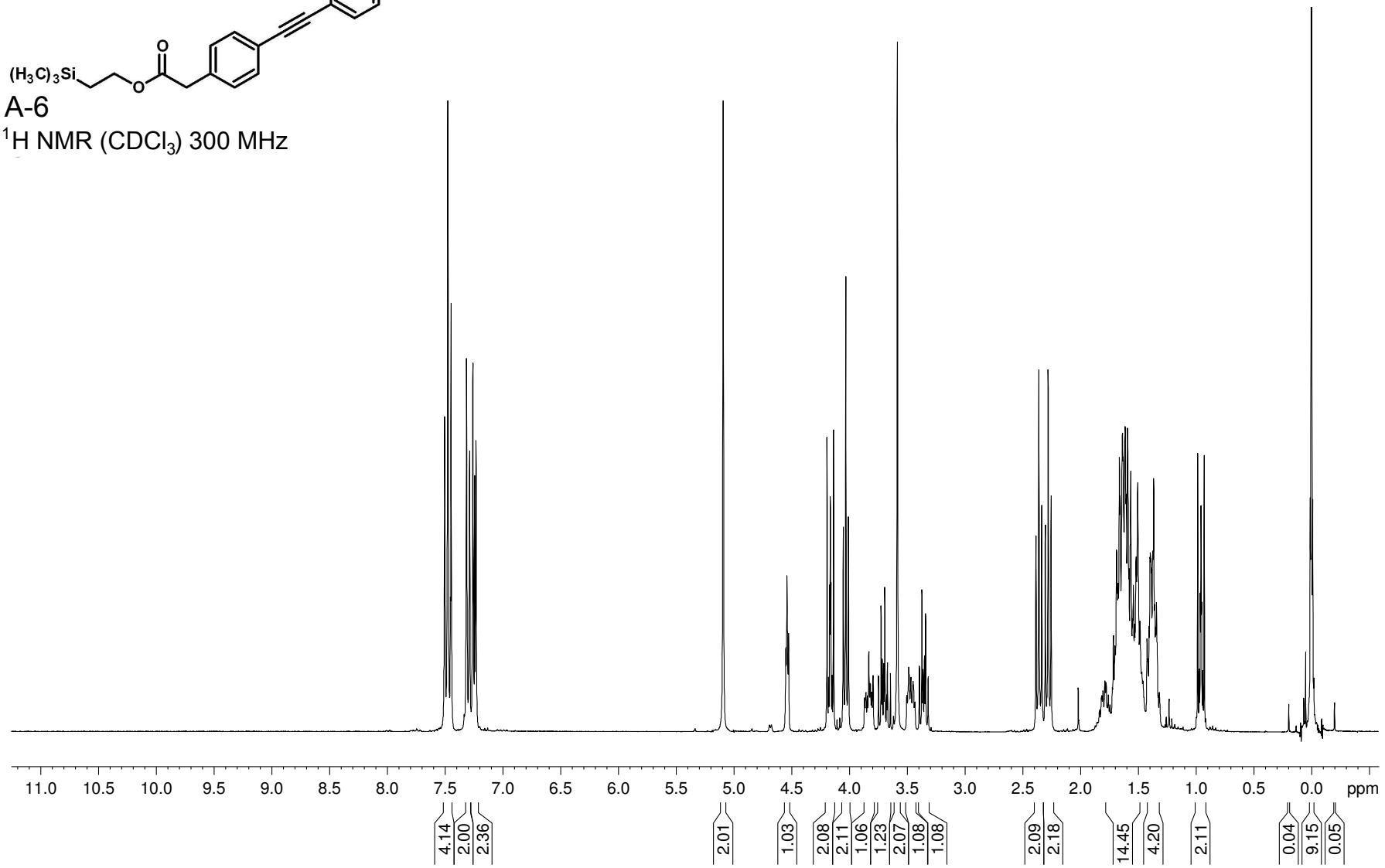

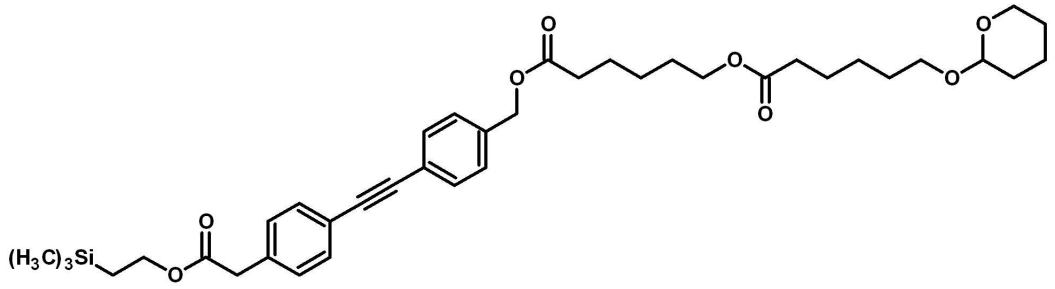

A-6

^{13}C NMR ($CDCl_3$) 75 MHz

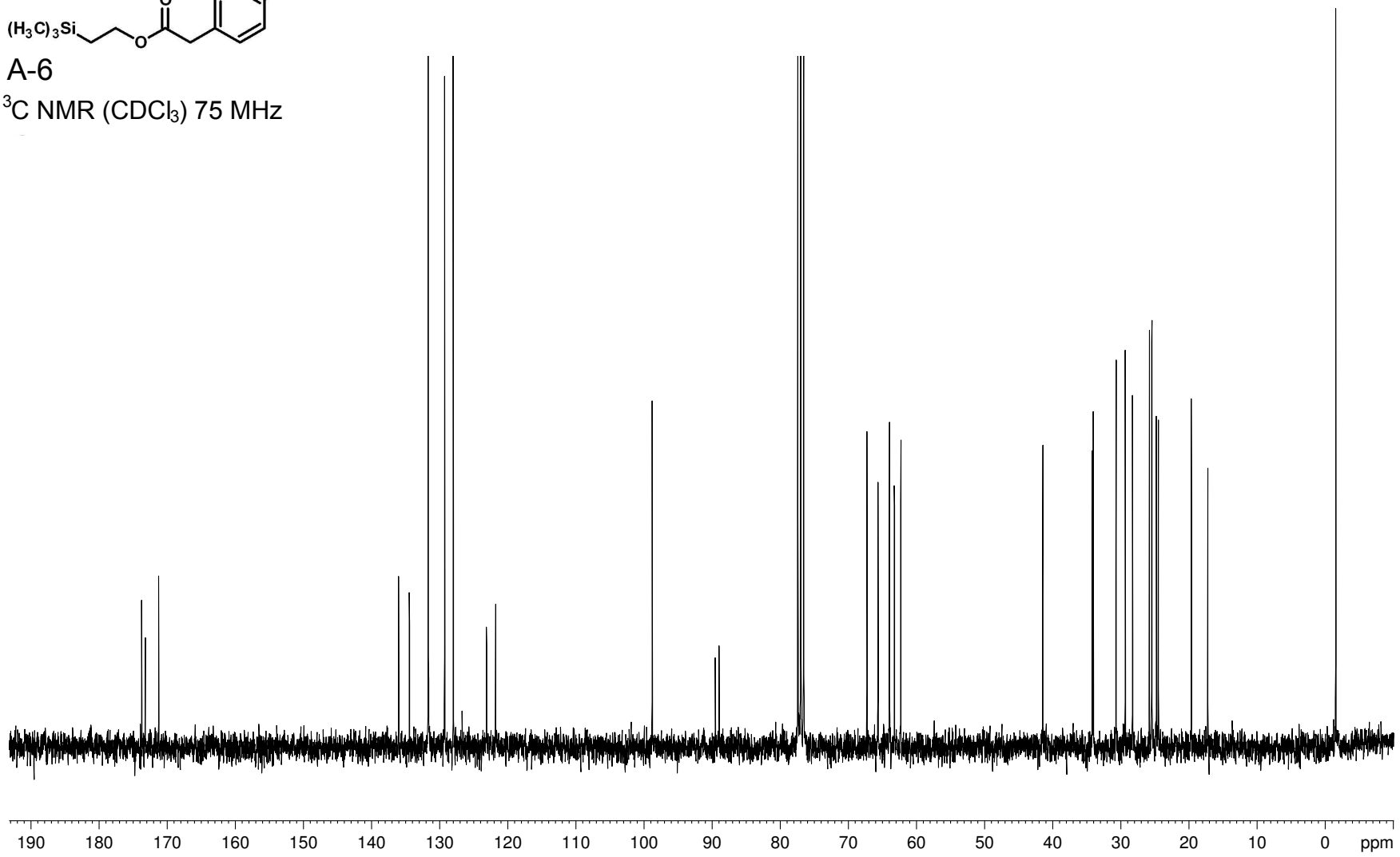

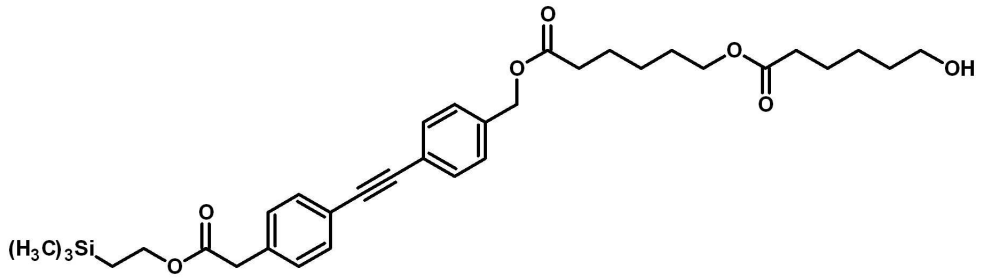

A-7

^{1}H NMR ($CDCl_3$) 300 MHz

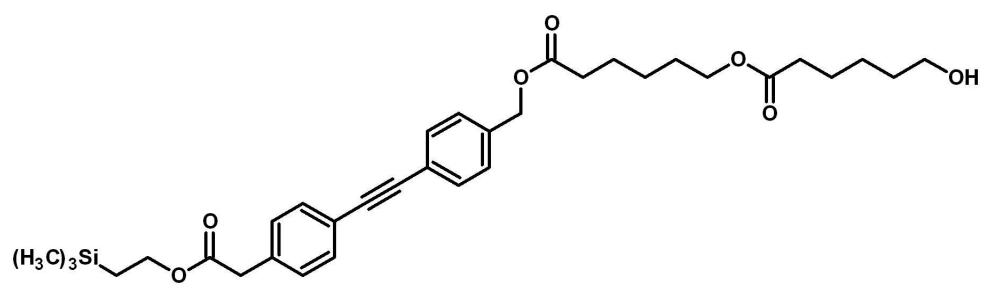

A-7

^{13}C NMR ($CDCl_3$) 75 MHz

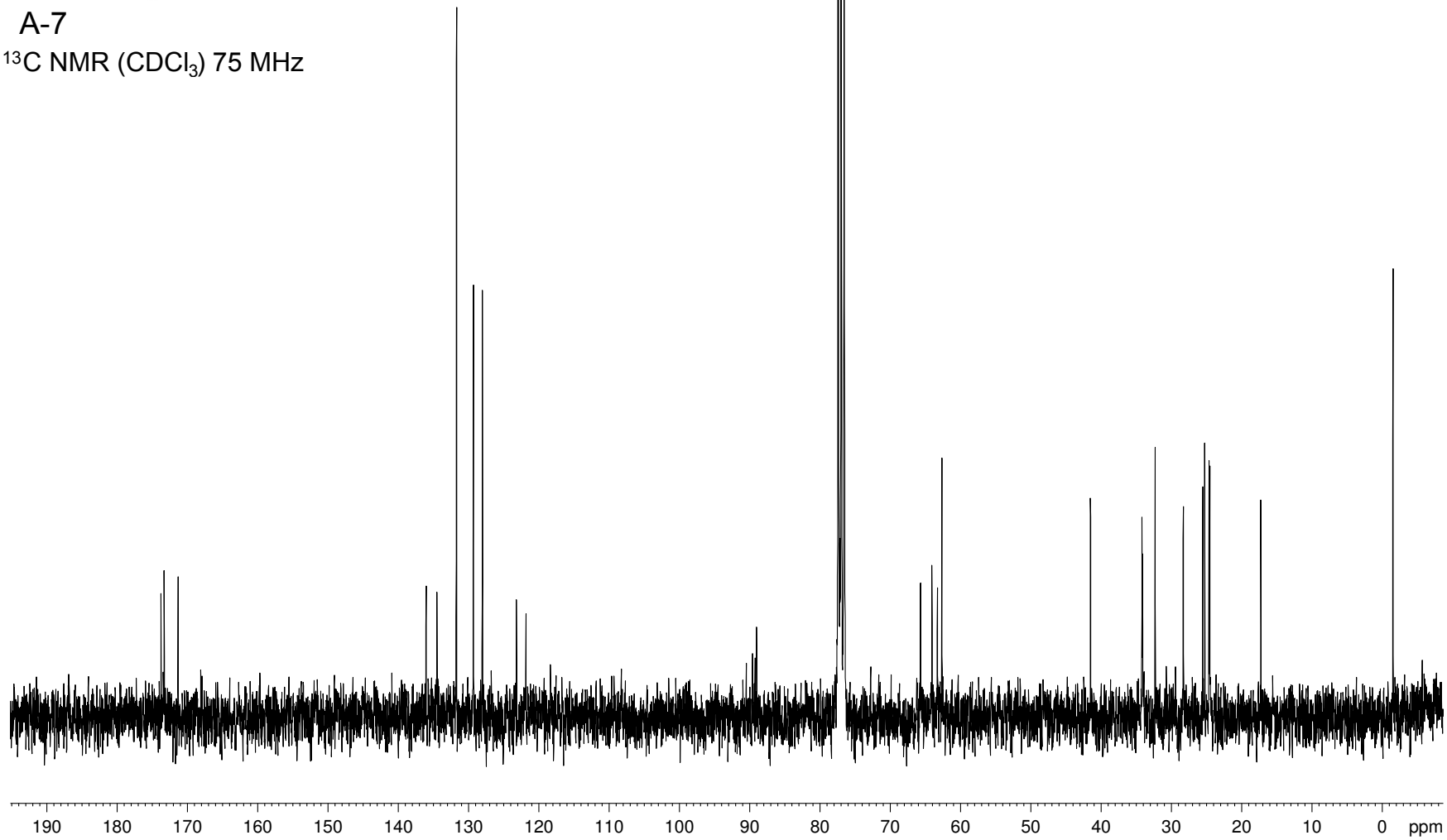

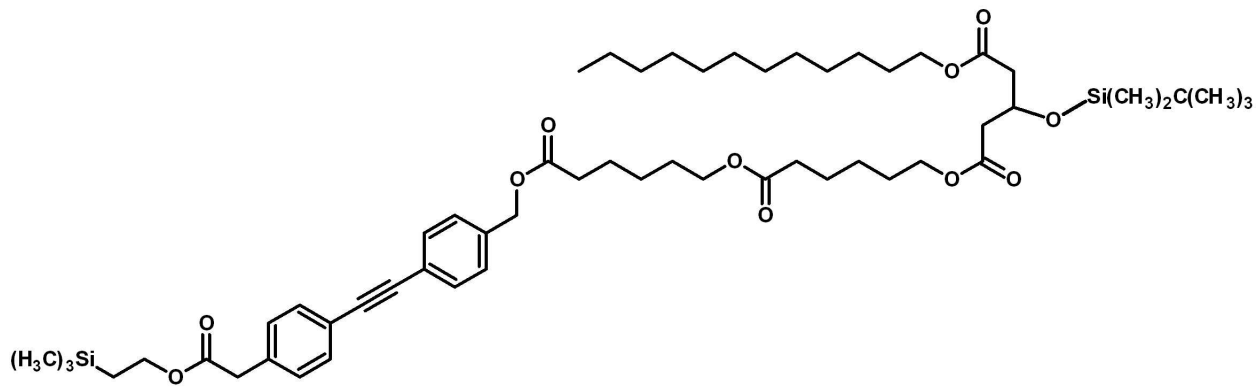

A-8

^{1}H NMR ($CDCl_3$) 300 MHz

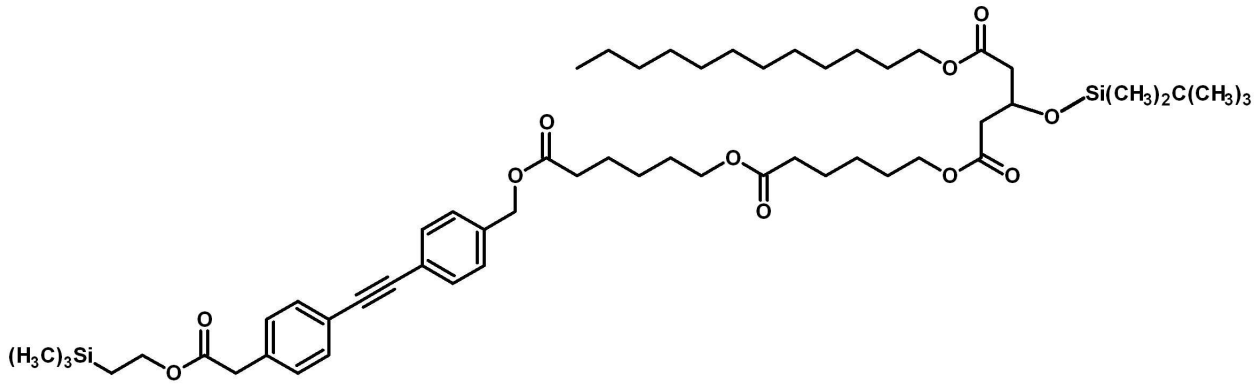

A-8

^{13}C NMR ($CDCl_3$) 75 MHz

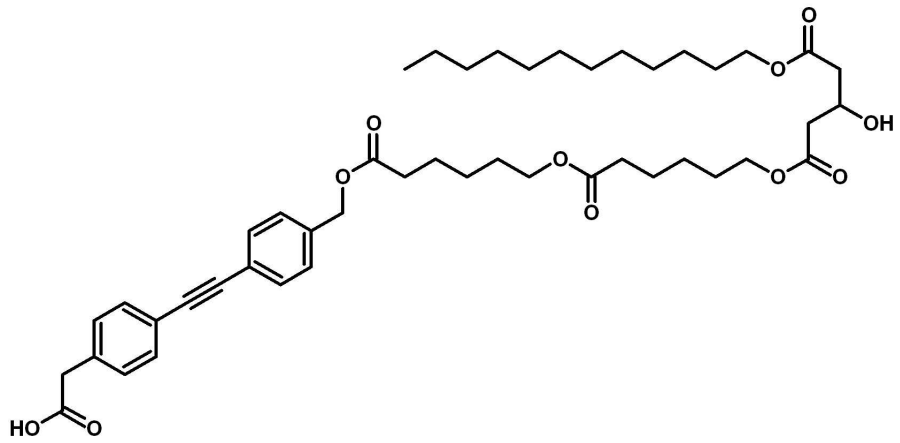

HO_2C-**Dip-Hex-Hex-G(12)**-OH
2-23

^1H NMR (1:1 $CDCl_3$: CD_3OD) 500 MHz

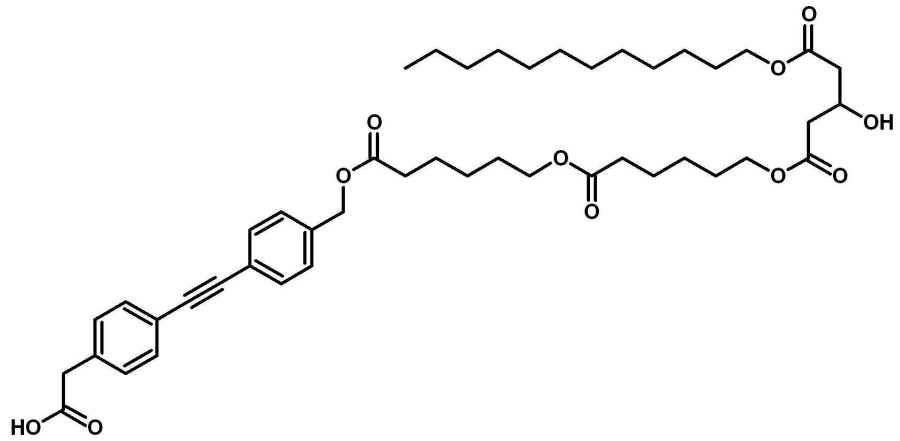

HO_2C-**Dip-Hex-Hex-G(12)**-OH

2-23

^{13}C NMR (1:1 $CDCl_3$: CD_3OD) 125 MHz

HO_2C-**Dip-Hex-Hex-G(12)**-OH

2-23

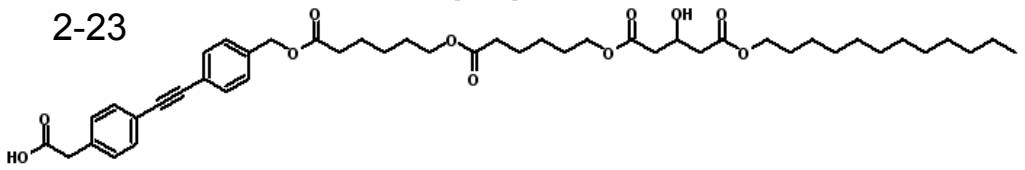

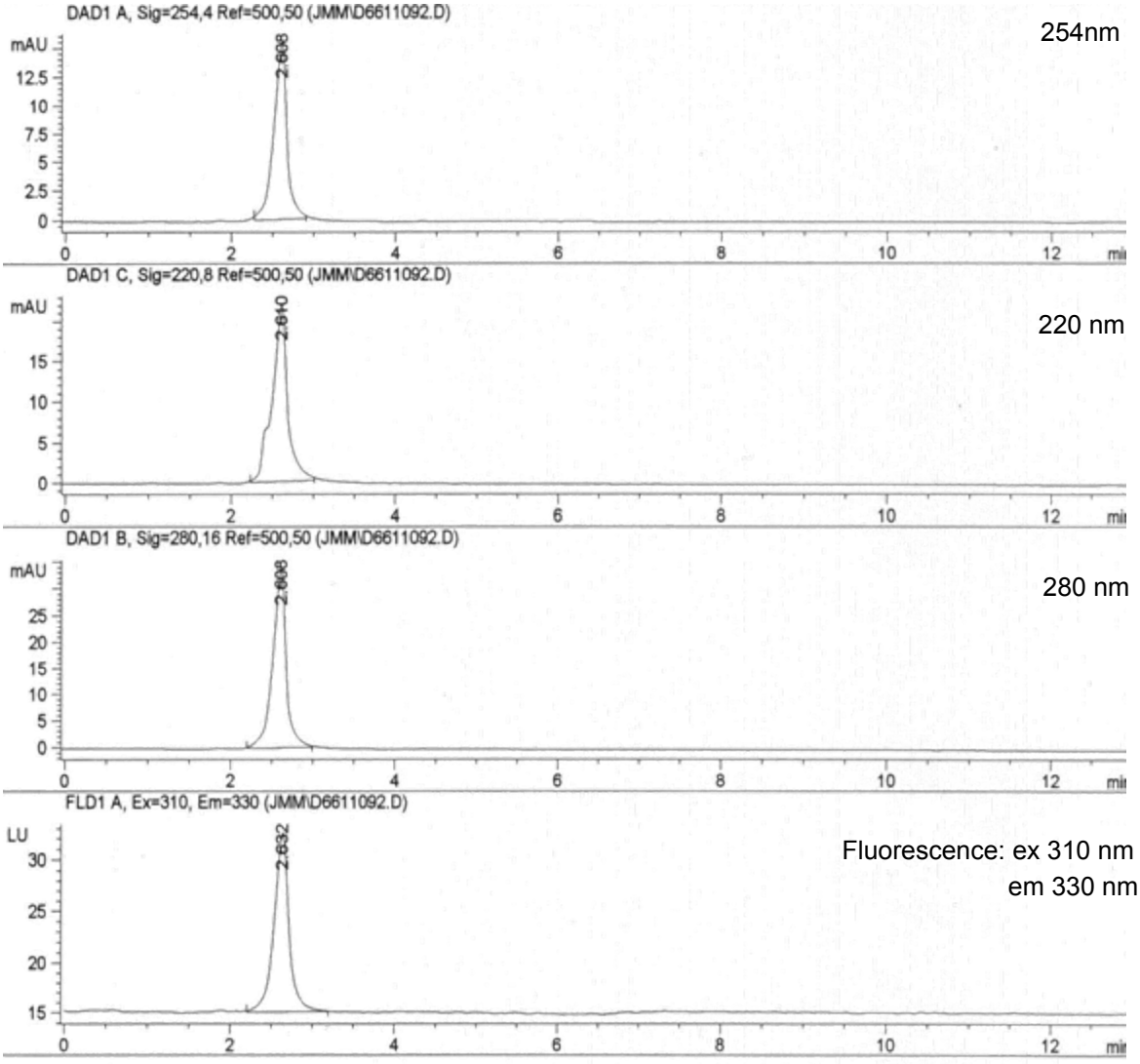

-HPLC trace of purified sample (used for transport and fluorescence studies)

-CONDITIONS: HP series 1100 HPLC

-Macherey-Nagel RP C^{18} "Nucleosil" analytical column (4 mm x 250 mm)

-1:1 CH_3OH: ACN as eluting solvents, flow 1mL/min

HO_2C-**Dip-Hex-Hex-G(12)**-OH

2-23

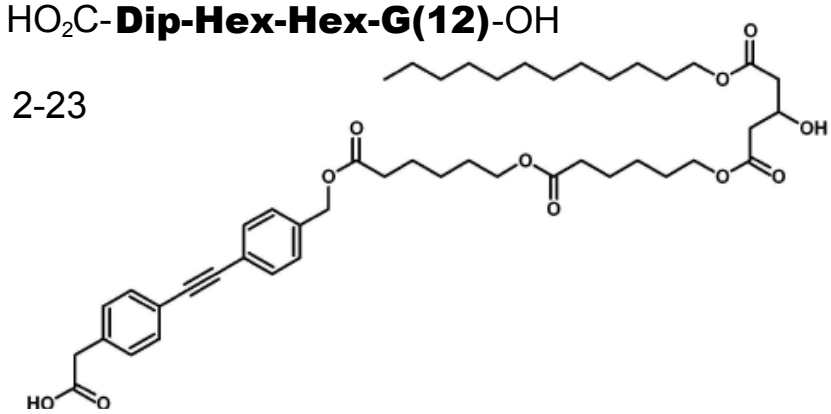

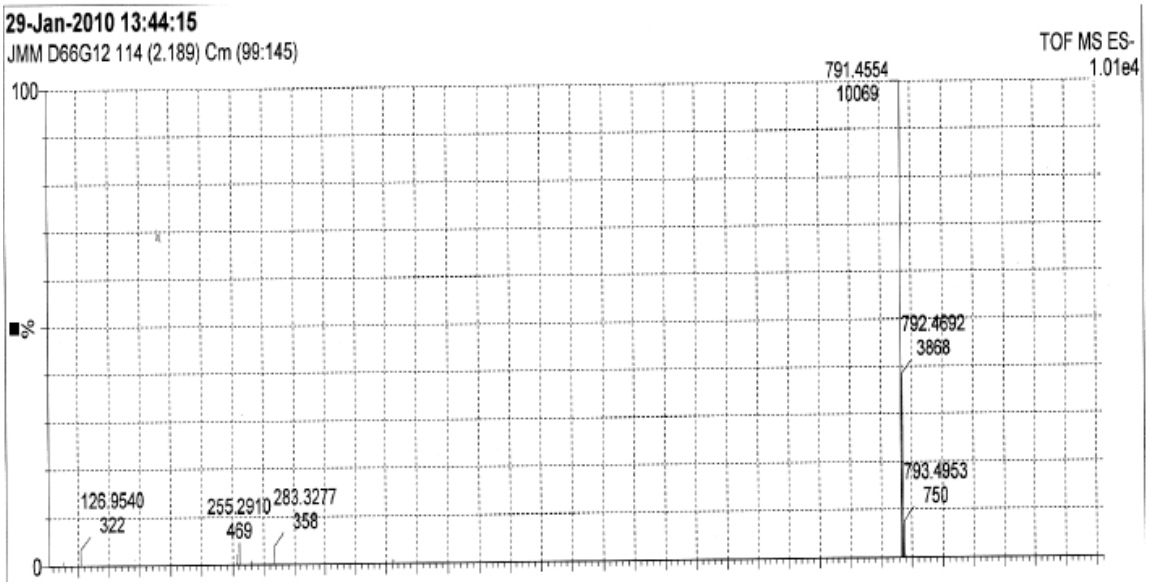

MS: -ve ion ESI, Q-TOF-2 instrument

Calc'd for$C_{46}H_{63}O_{11}$= 791.4376 amu, obtained = 791.455 amu

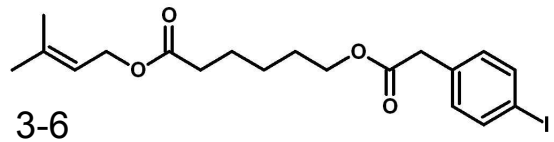

3-6

^{1}H NMR ($CDCl_3$) 300 MHz

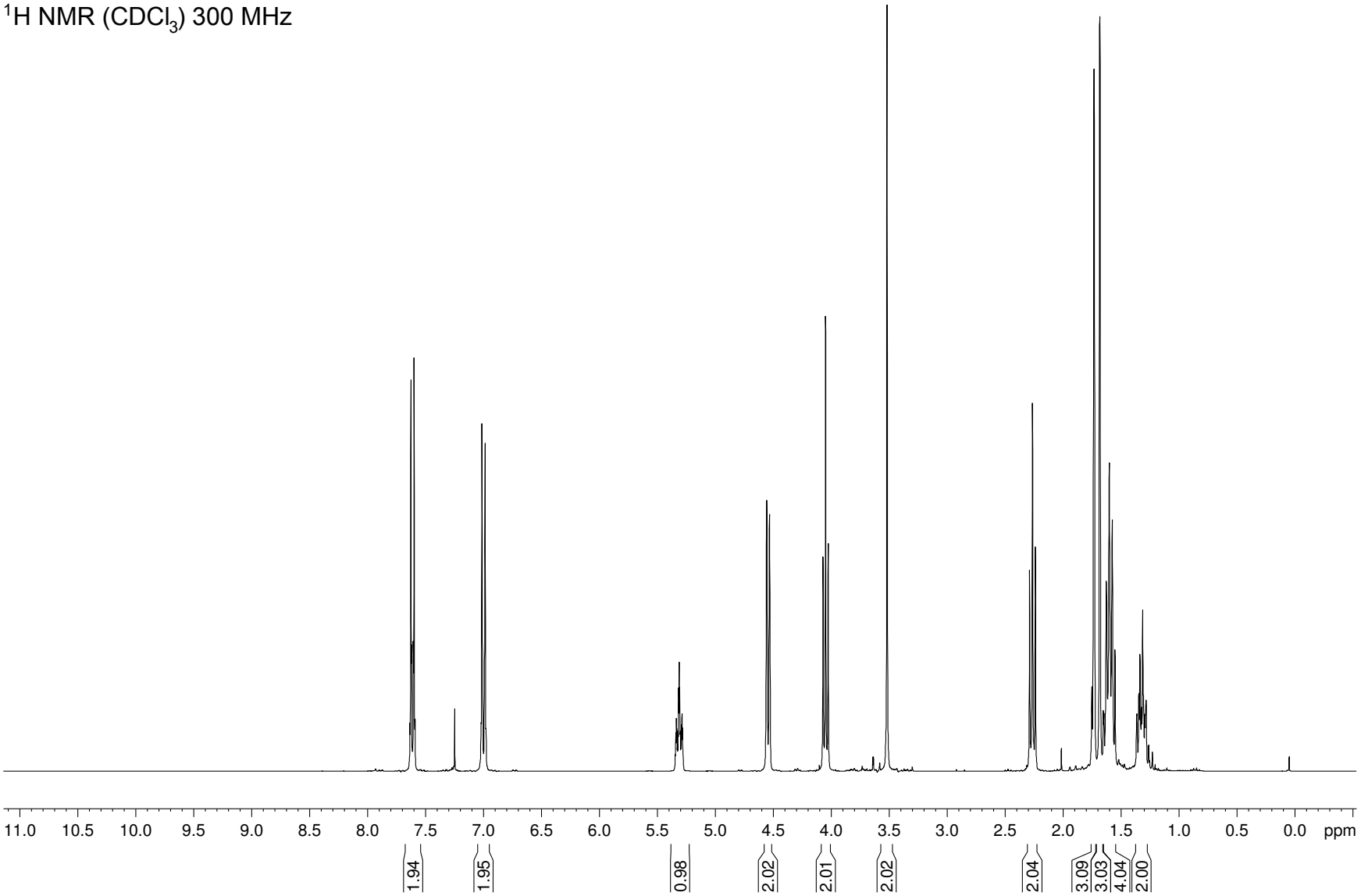

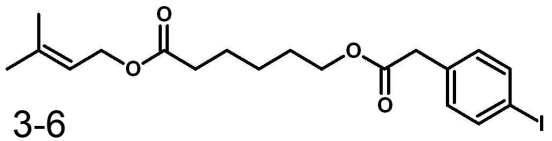

3-6

^{13}C NMR ($CDCl_3$) 75 MHz

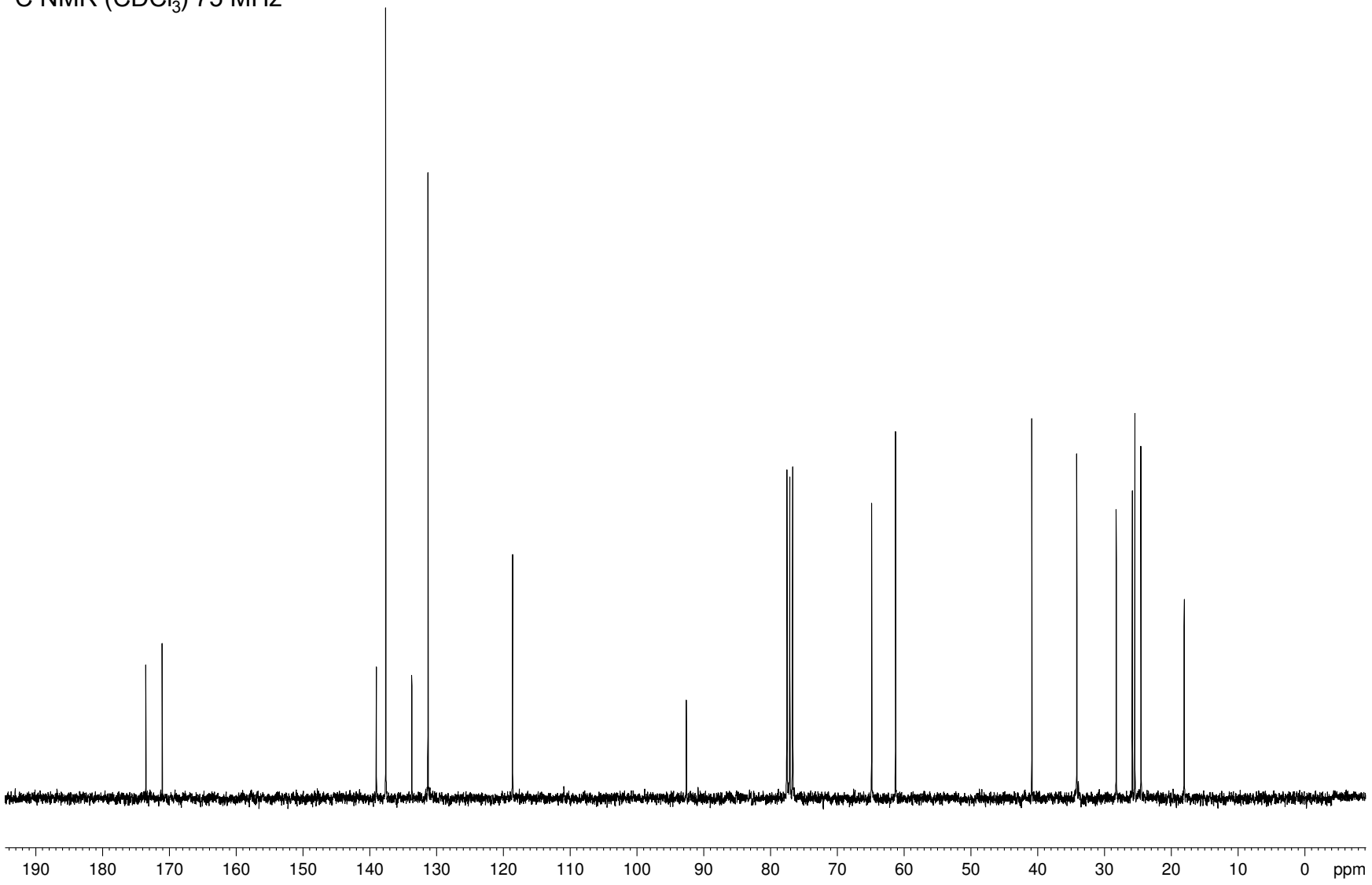

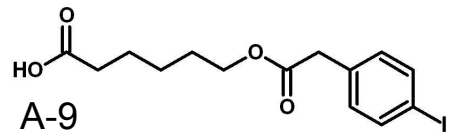

A-9

^{1}H NMR ($CDCl_3$) 300 MHz

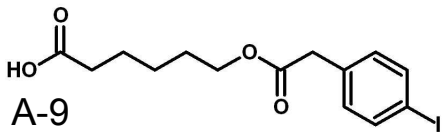

A-9

^{13}C NMR ($CDCl_3$) 75 MHz

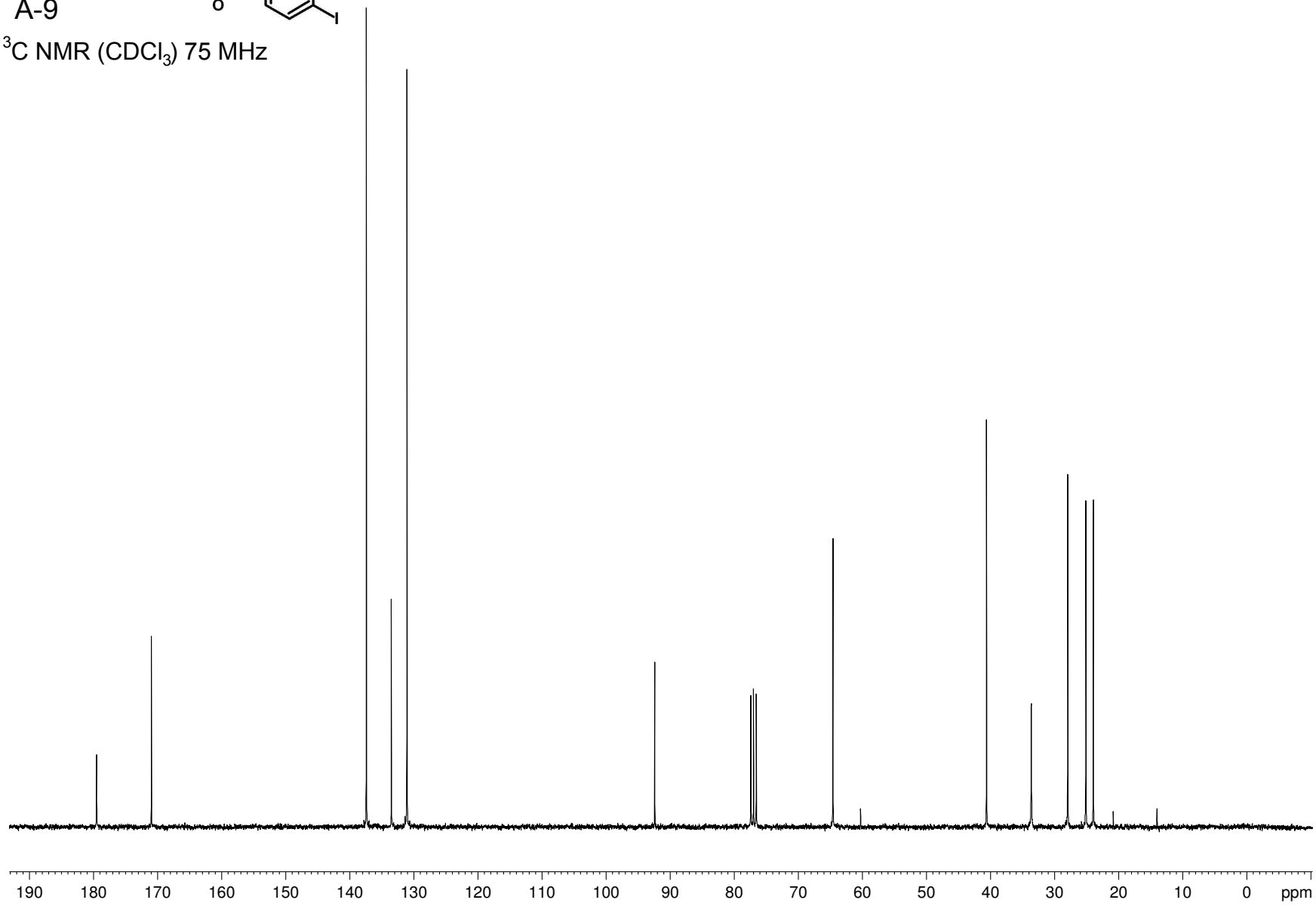

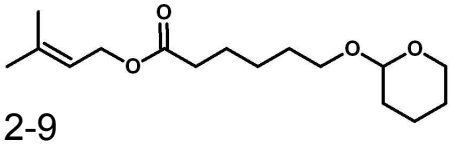

2-9

^{1}H NMR ($CDCl_3$) 300 MHz

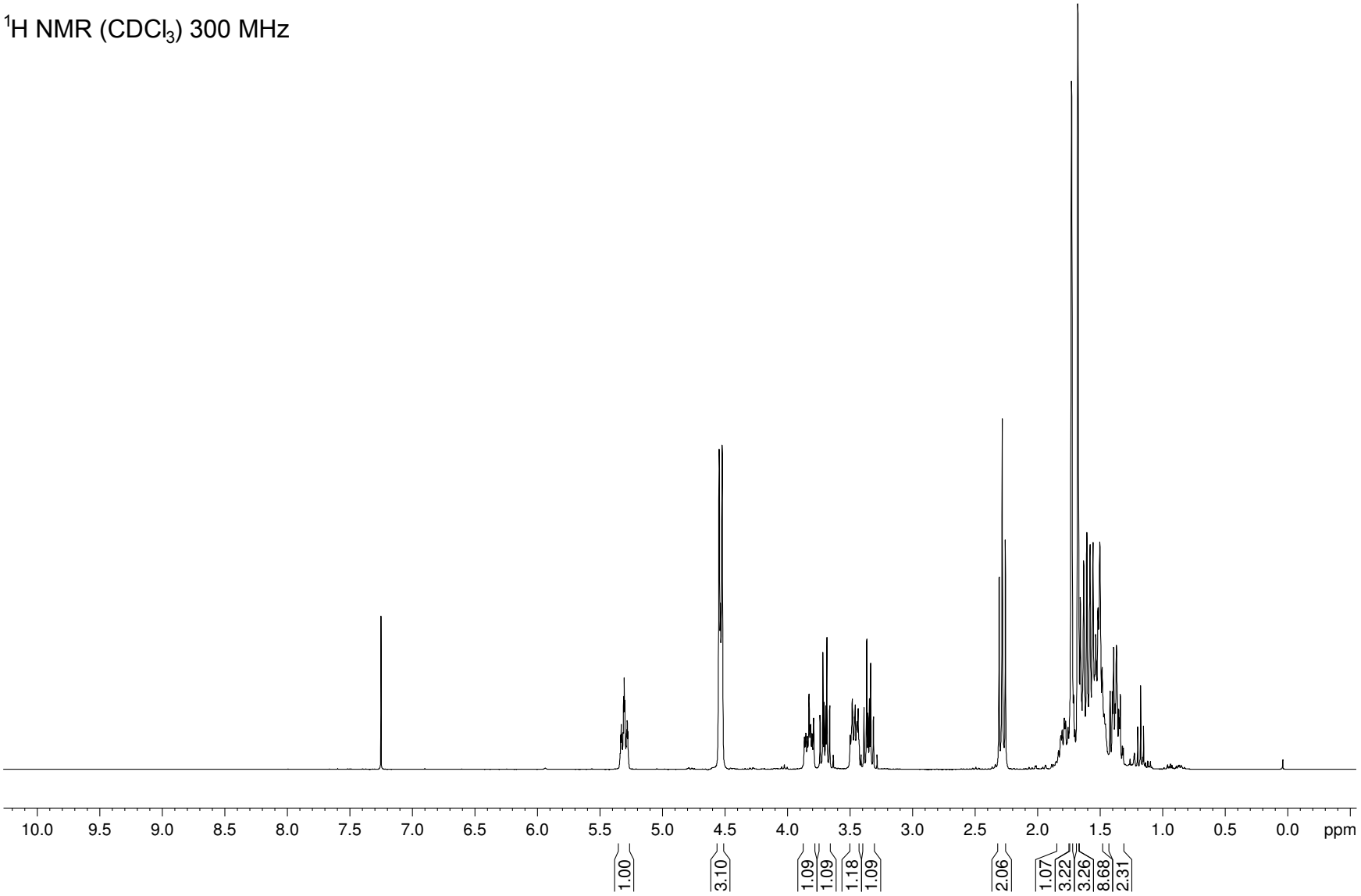

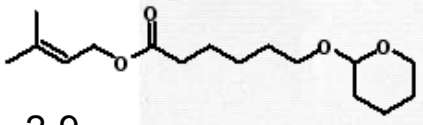

2-9

^{13}C NMR ($CDCl_3$) 75 MHz

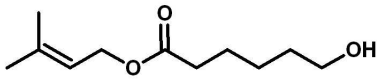

2-10

^{1}H NMR ($CDCl_3$) 300 MHz

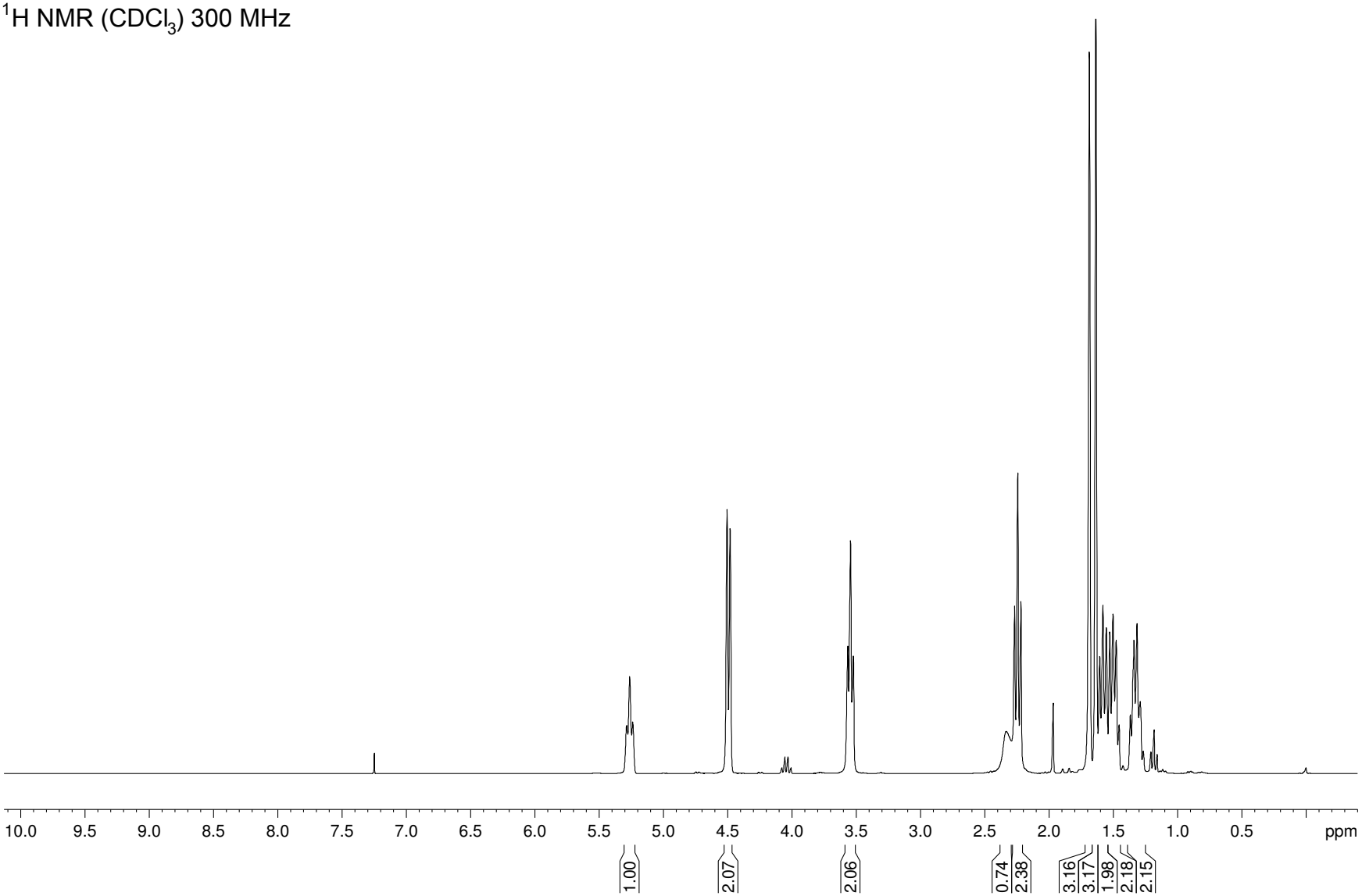

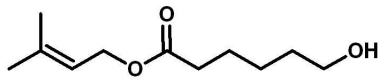

2-10

^{13}C NMR ($CDCl_3$) 75 MHz

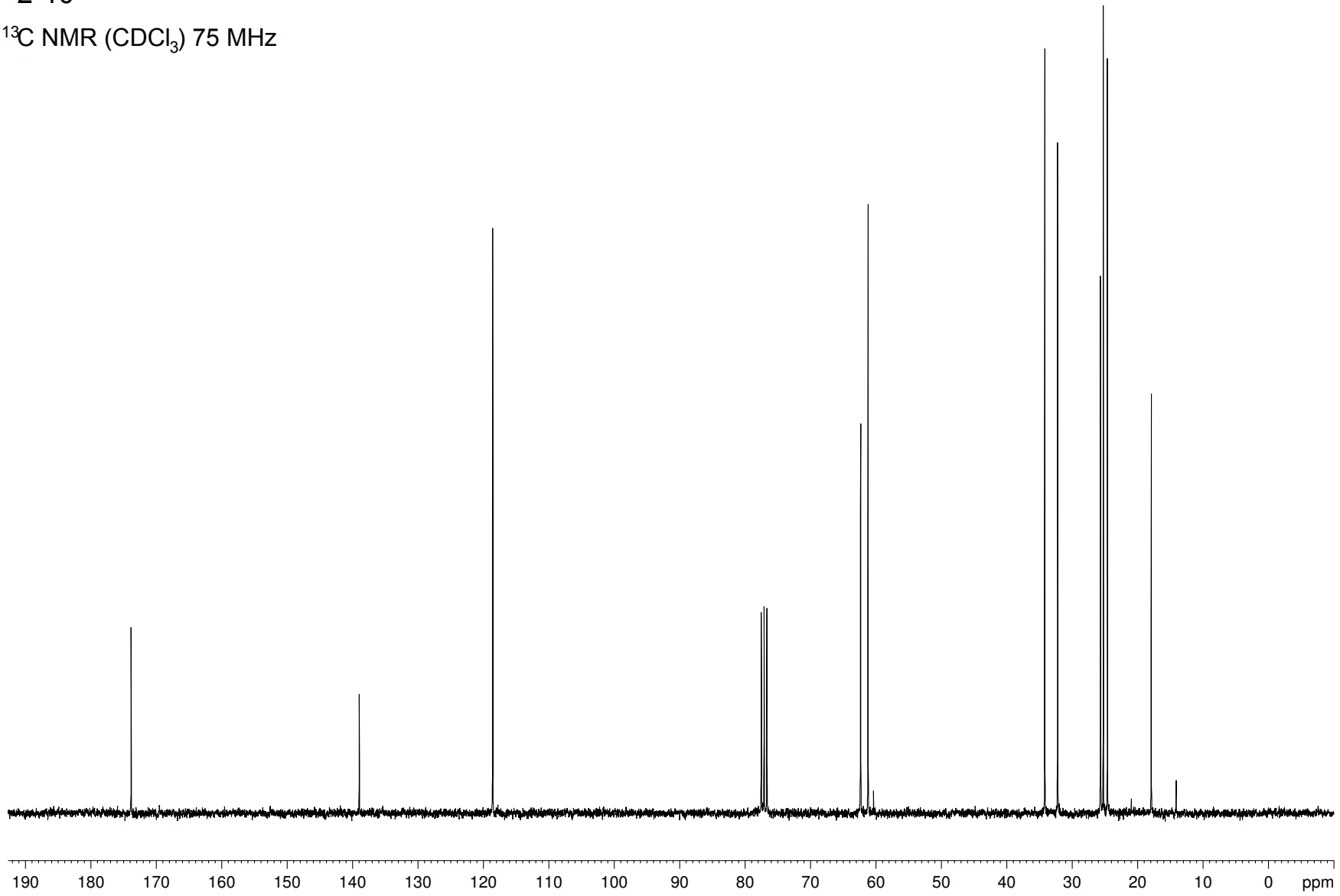

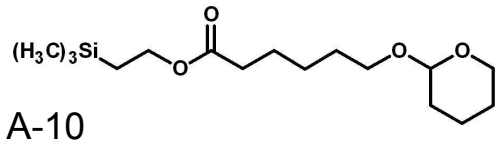

A-10

^{1}H NMR ($CDCl_3$) 300 MHz

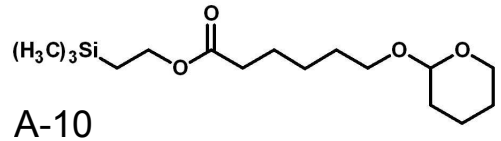

A-10

^{13}C NMR ($CDCl_3$) 75 MHz

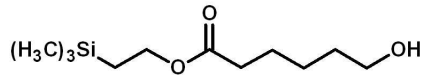

A-11

^{1}H NMR ($CDCl_3$) 300 MHz

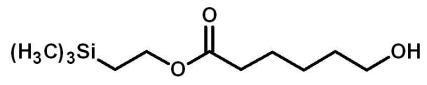

A-11

^{13}C NMR ($CDCl_3$) 75 MHz

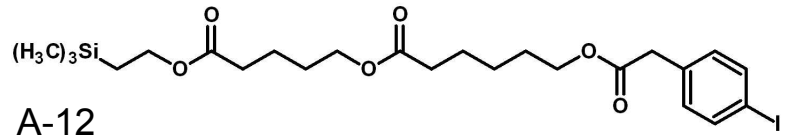

A-12

^{1}H NMR ($CDCl_3$) 300 MHz

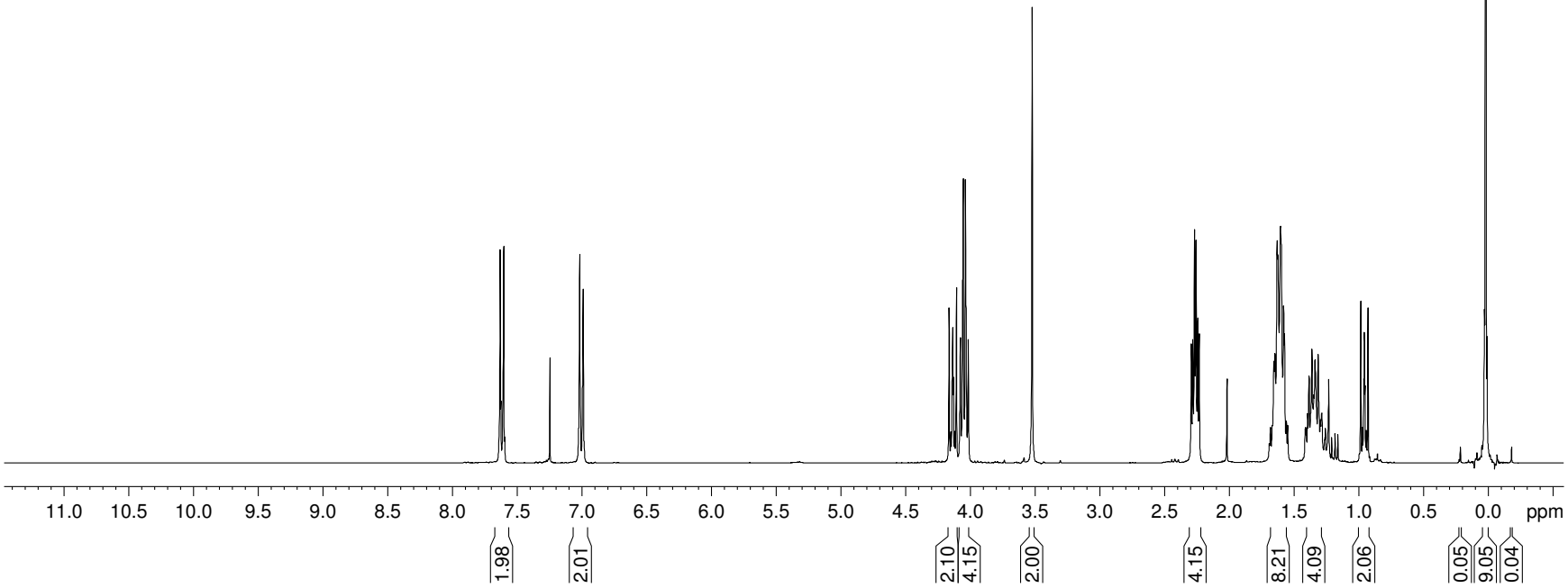

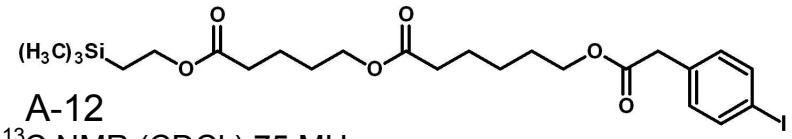

A-12

^{13}C NMR ($CDCl_3$) 75 MHz

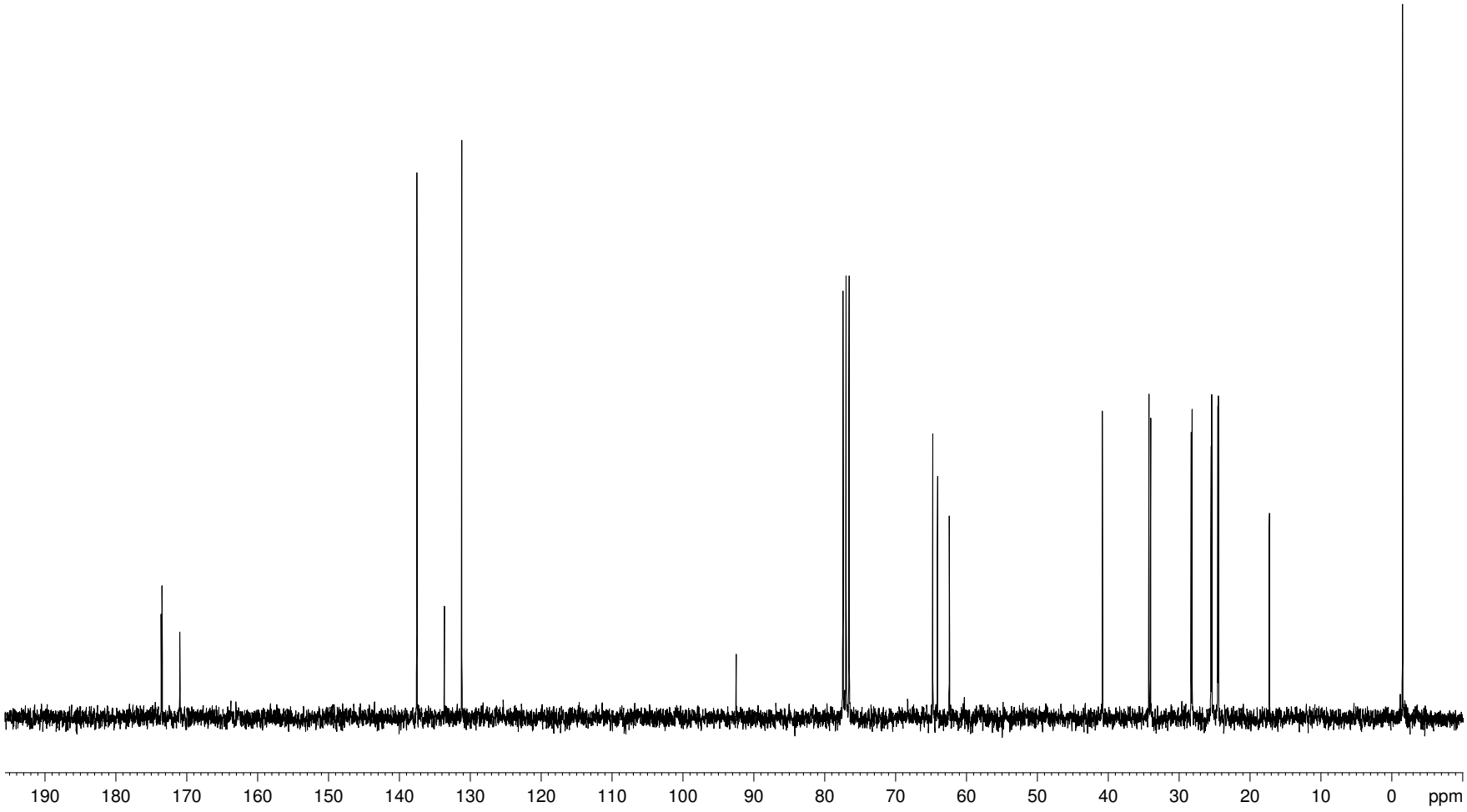

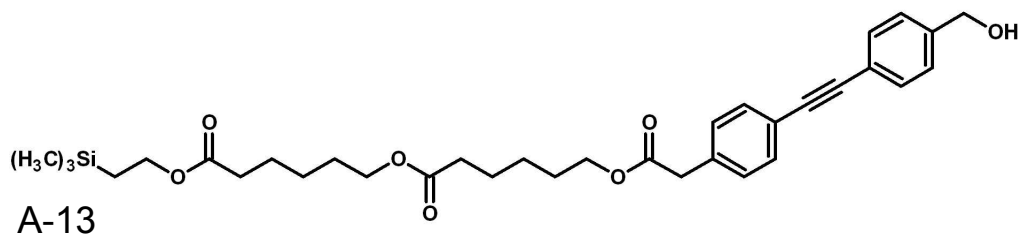

A-13

^{1}H NMR ($CDCl_3$) 300 MHz

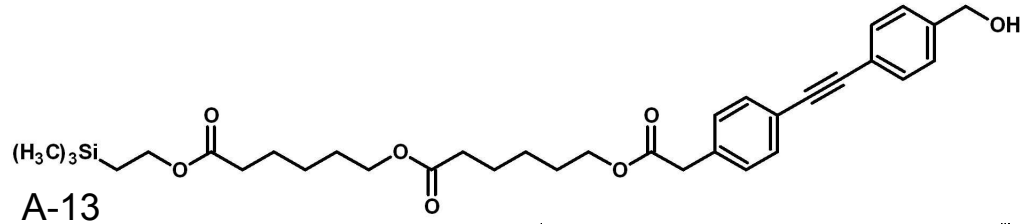

A-13

^{13}C NMR ($CDCl_3$) 75 MHz

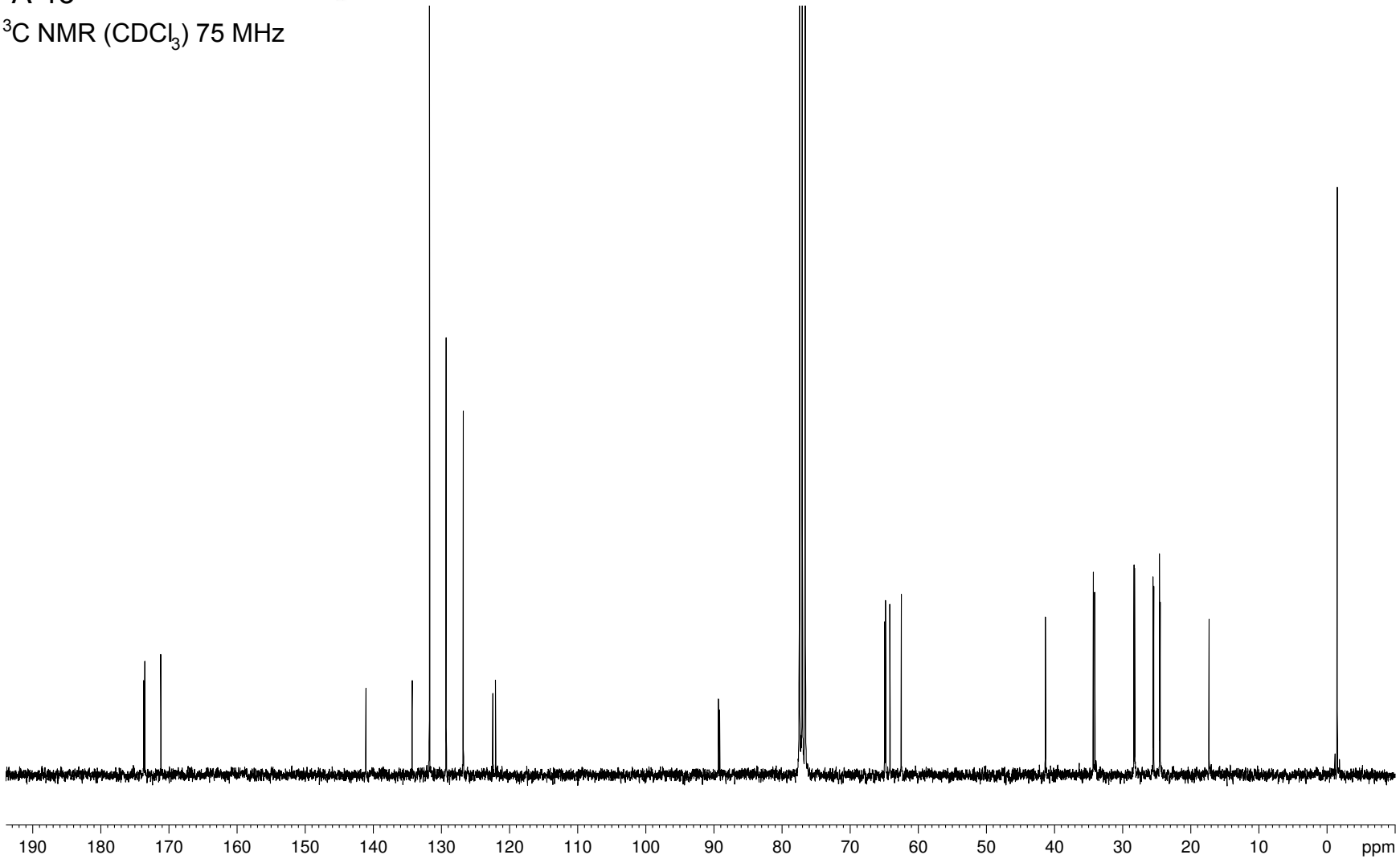

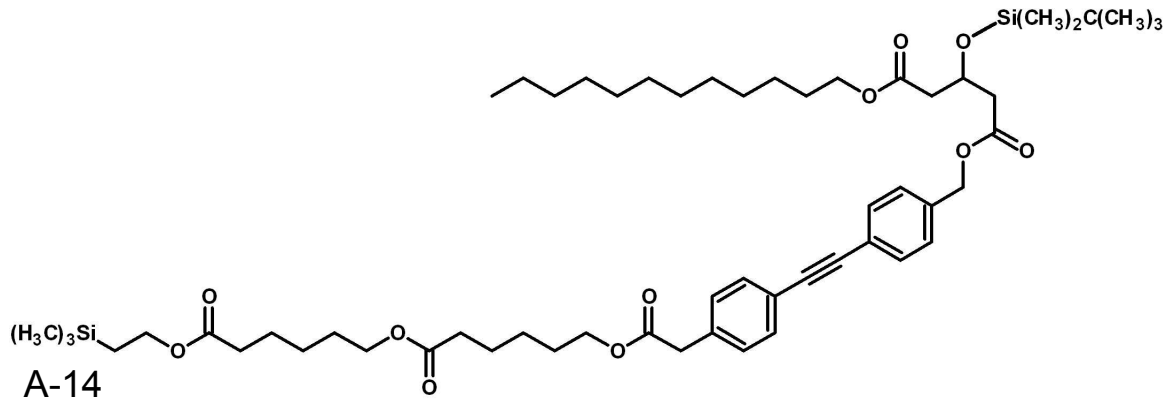

A-14

^{1}H NMR ($CDCl_3$) 300 MHz

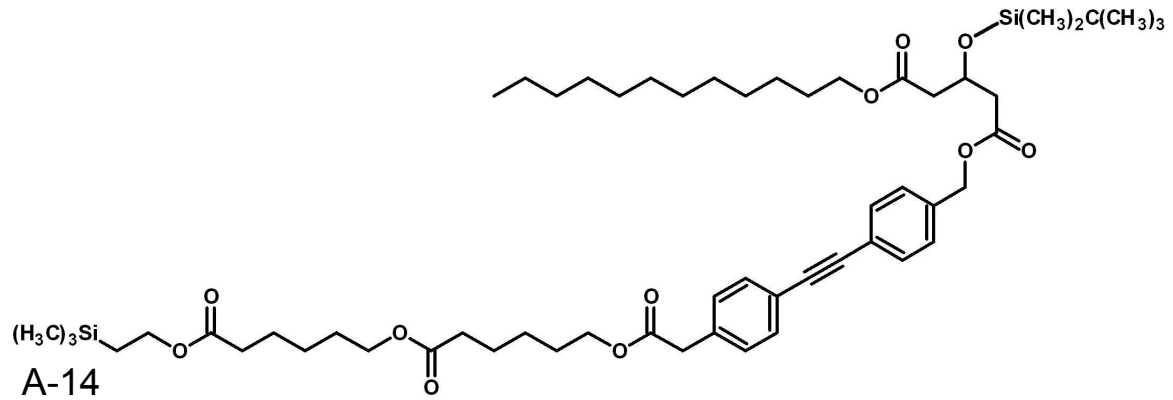

A-14

^{13}C NMR ($CDCl_3$) 75 MHz

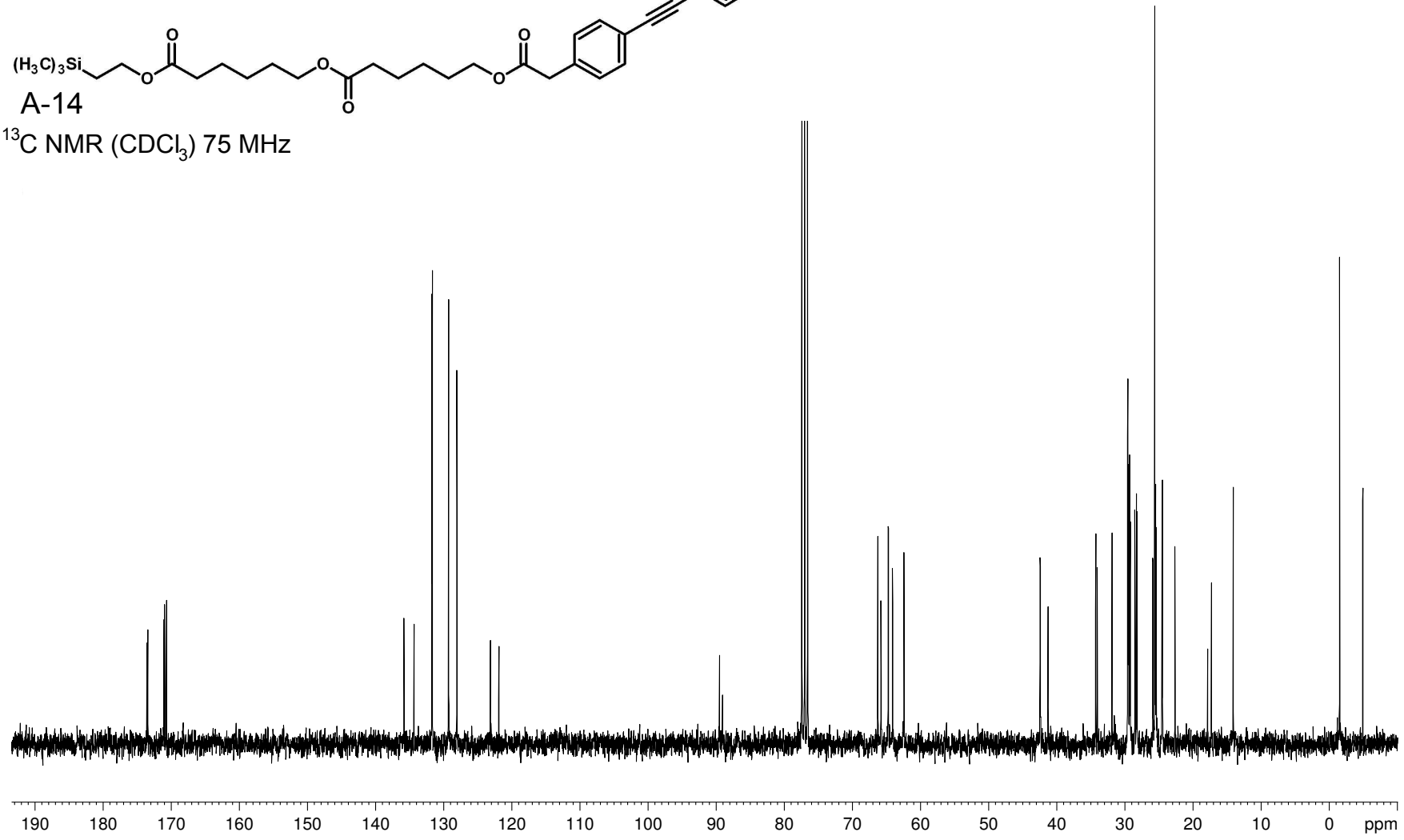

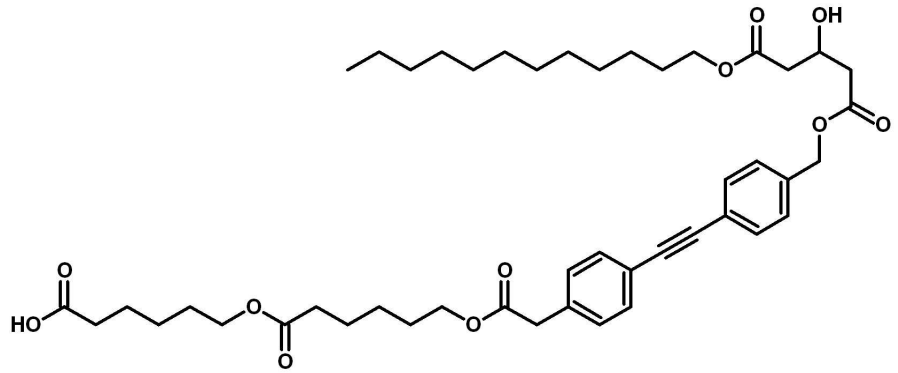

HO_2C-**Hex-Hex-Dip-G(12)**-OH

2-24

^1H NMR (1:1 $CDCl_3$: CD_3OD) 500 MHz

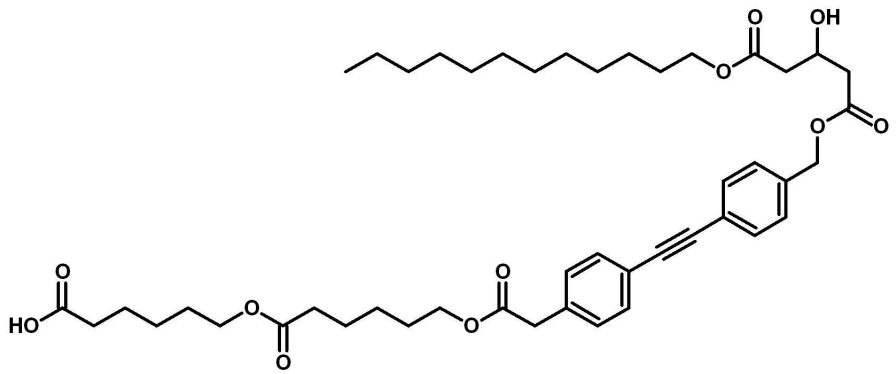

HO_2C-**Hex-Hex-Dip-G(12)**-OH

2-24

^{13}C NMR (1:1 $CDCl_3$: CD_3OD) 125 MHz

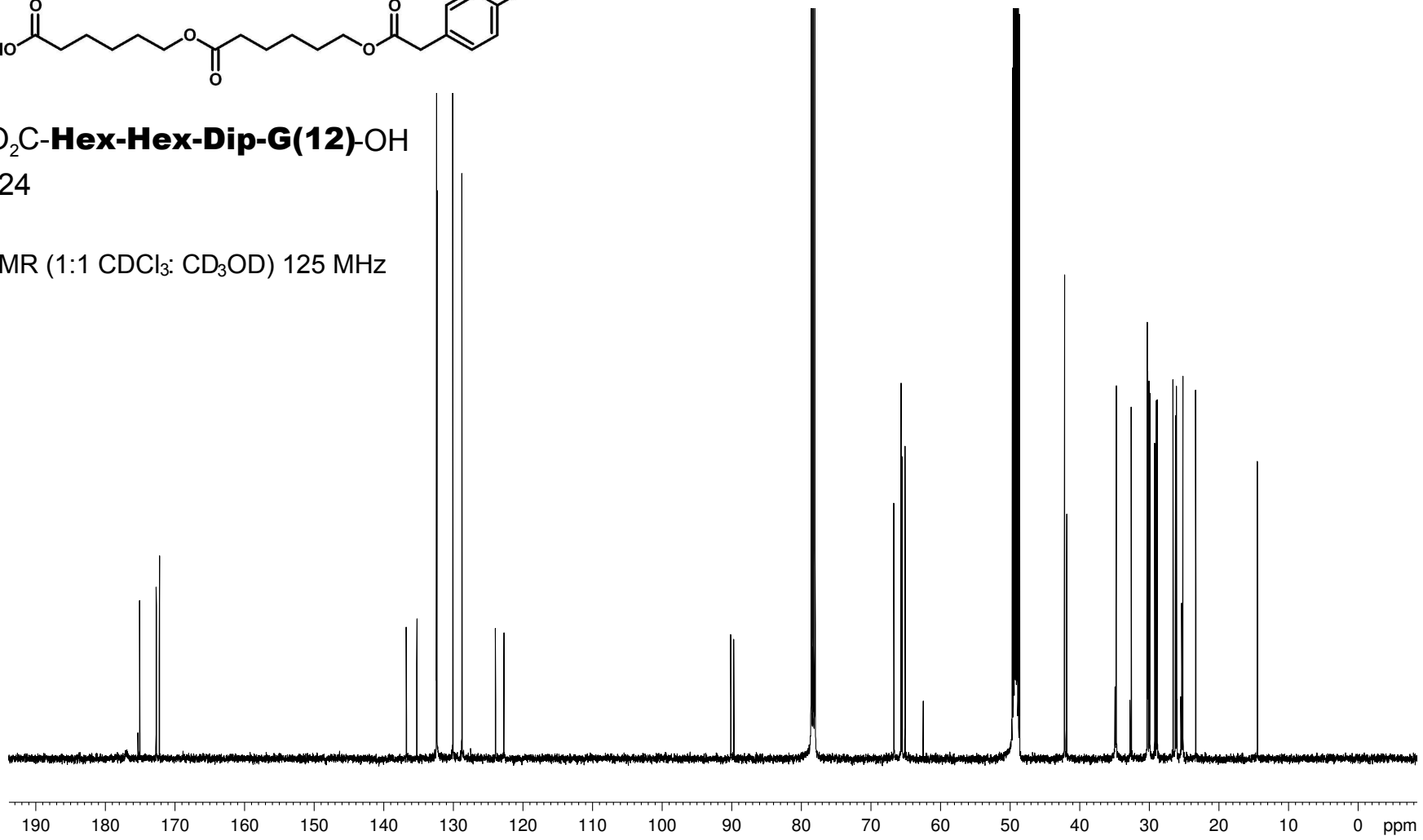

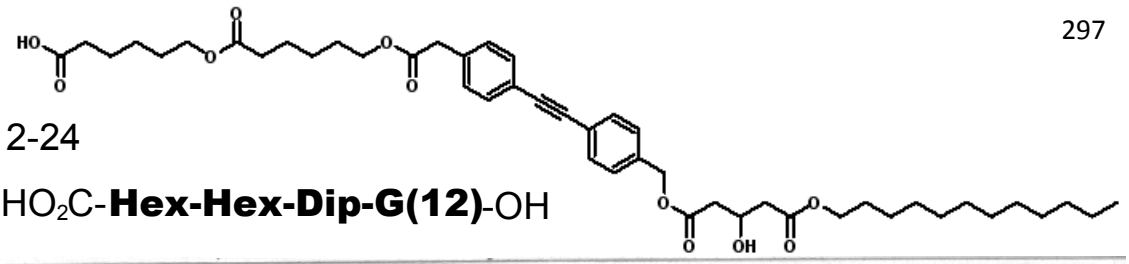

2-24

HO_2C-**Hex-Hex-Dip-G(12)**-OH

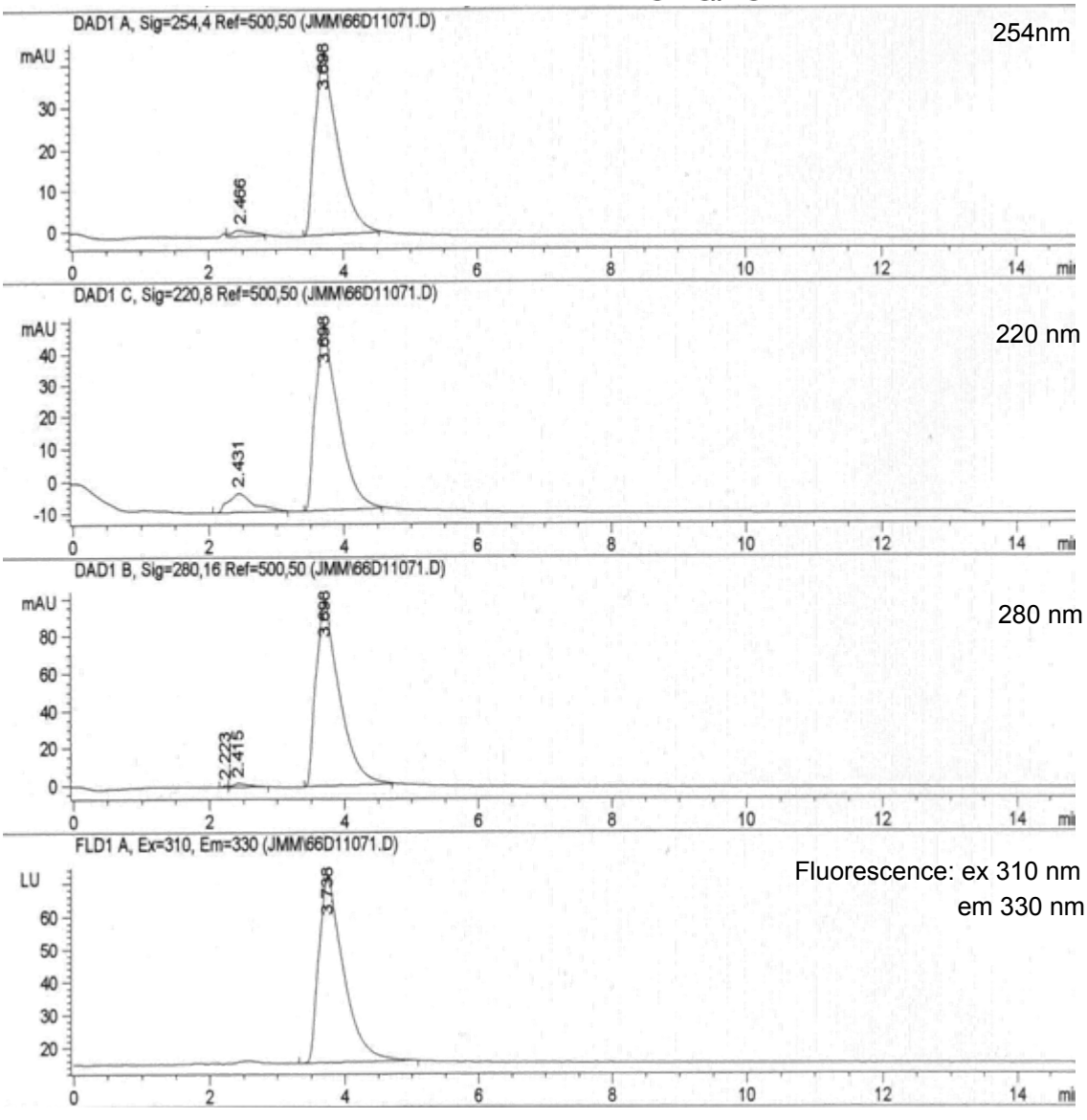

-HPLC trace of purified sample (used for transport and fluorescence studies)
-CONDITIONS: HP series 1100 HPLC
-Macherey-Nagel RP C^{18} "Nucleosil" analytical column (4 mm x 250 mm)
-1:1 CH_3OH: ACN as eluting solvents, flow 1mL/min

HO_2C-**Hex-Hex-Dip-G(12)** -OH

2-24

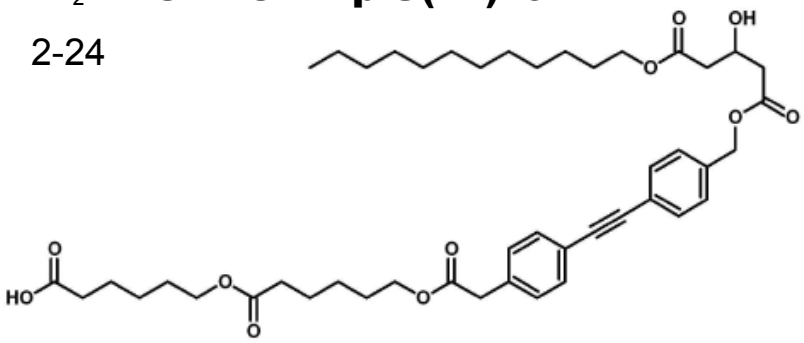

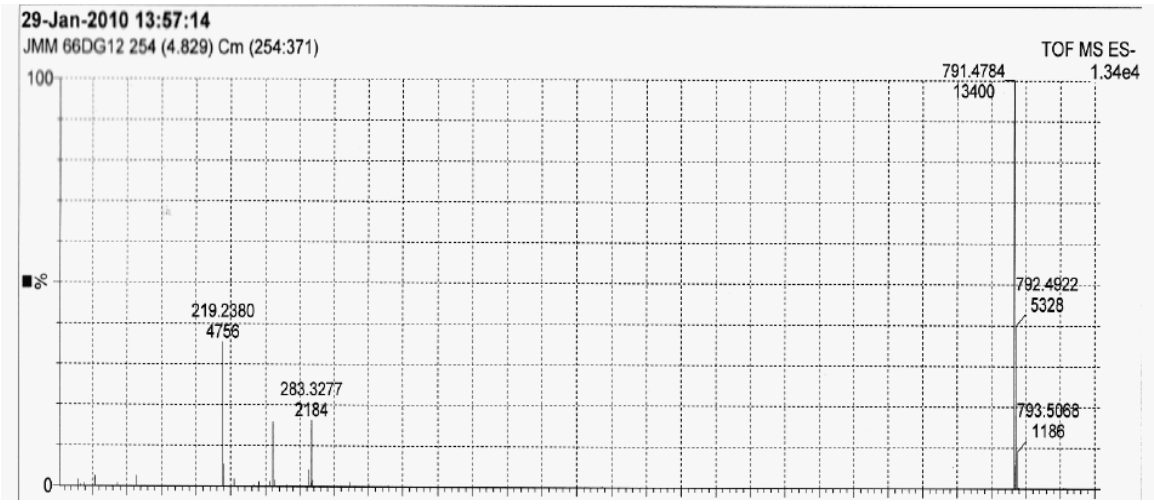

MS: -ve ion ESI, Q-TOF 2 instrument

Calc'd for C46H63O11 = 791.4376 amu, obtained = 791.478 amu

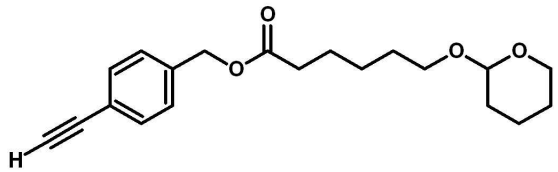

2-6

^{1}H NMR ($CDCl_3$) 300 MHz

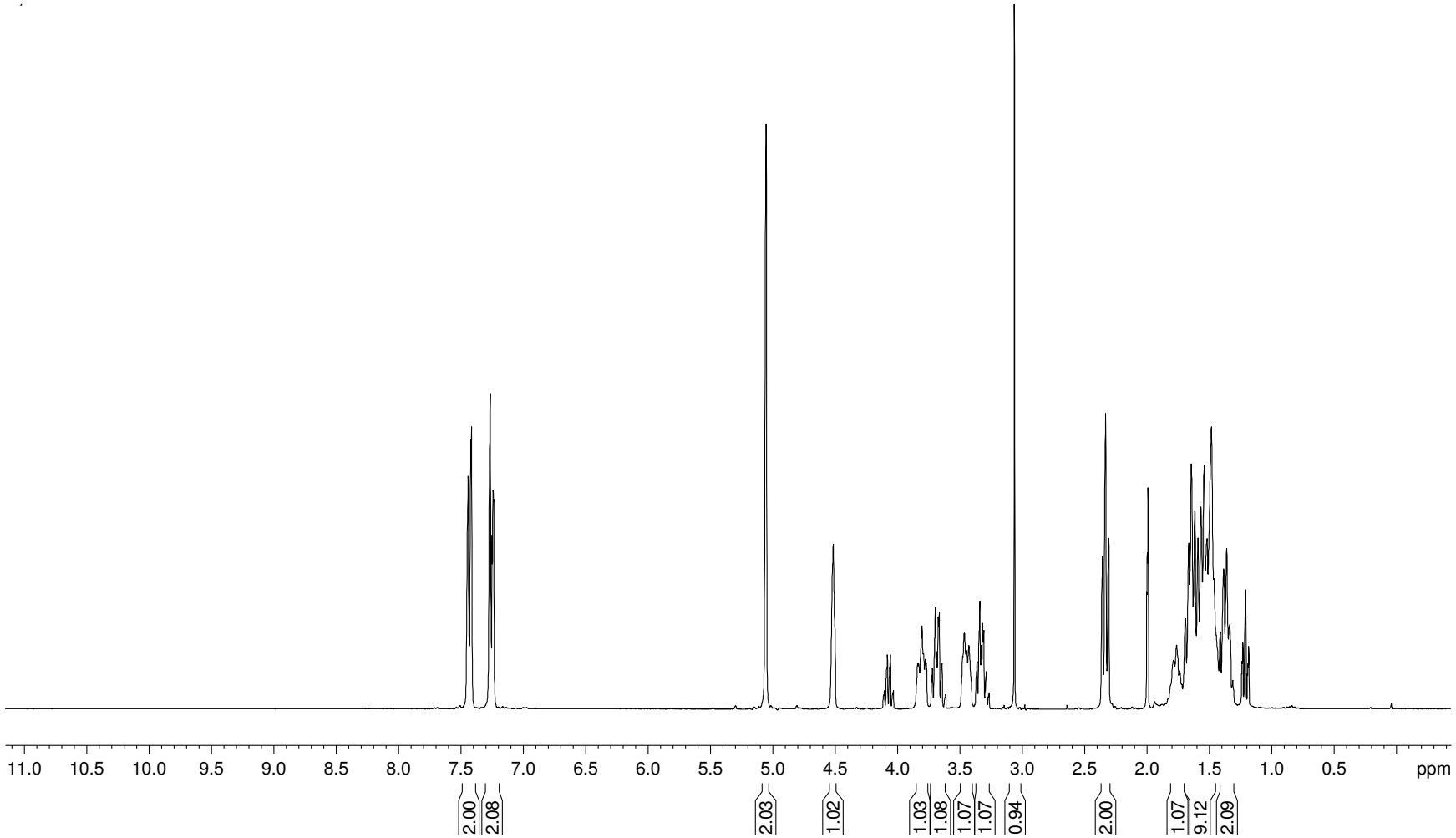

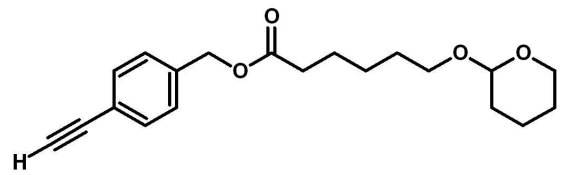

2-6

^{13}C NMR ($CDCl_3$) 75 MHz

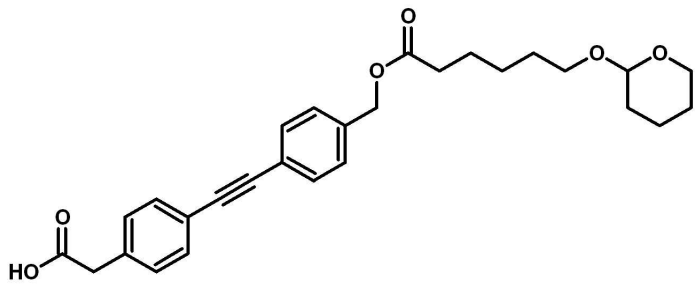

2-8

^{1}H NMR [$(CD_3)_2CO$] 300 MHz

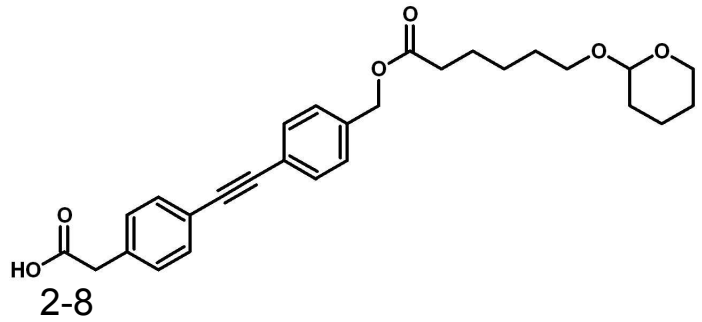

2-8

^{13}C NMR [$(CD_3)_2CO$] 75 MHz

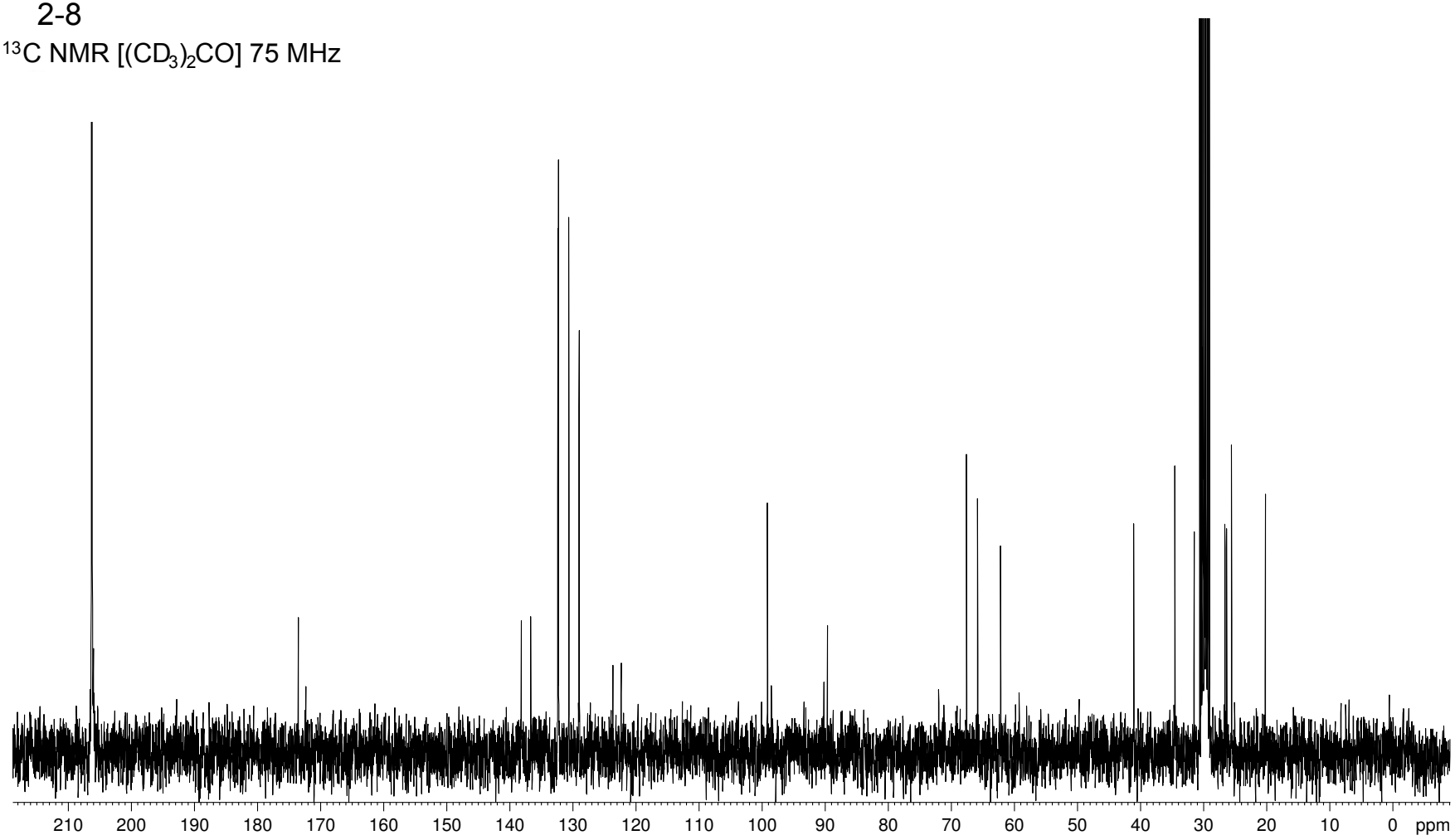

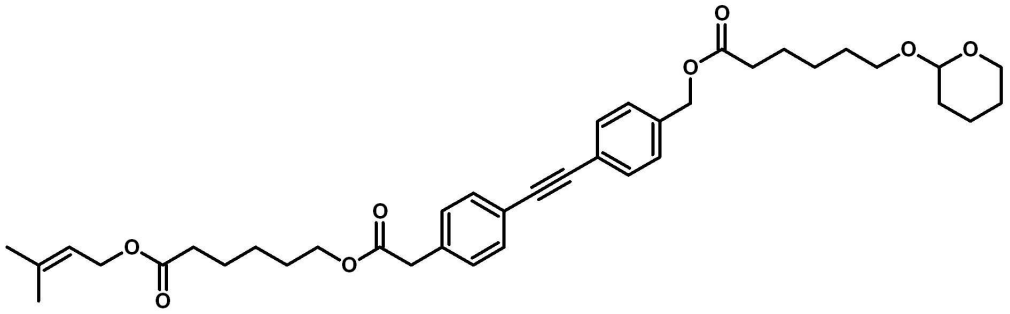

2-11

^{1}H NMR ($CDCl_3$) 300 MHz

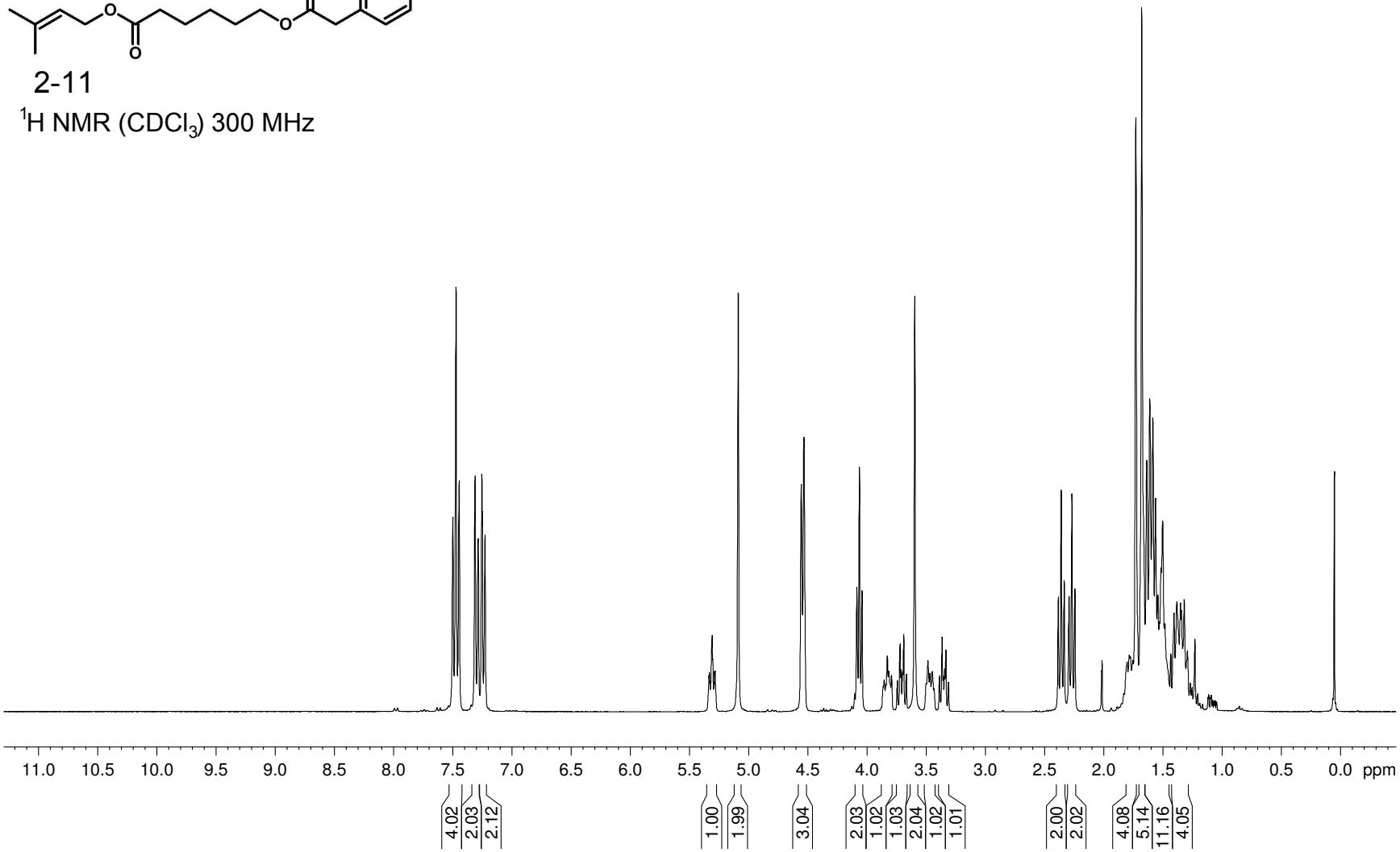

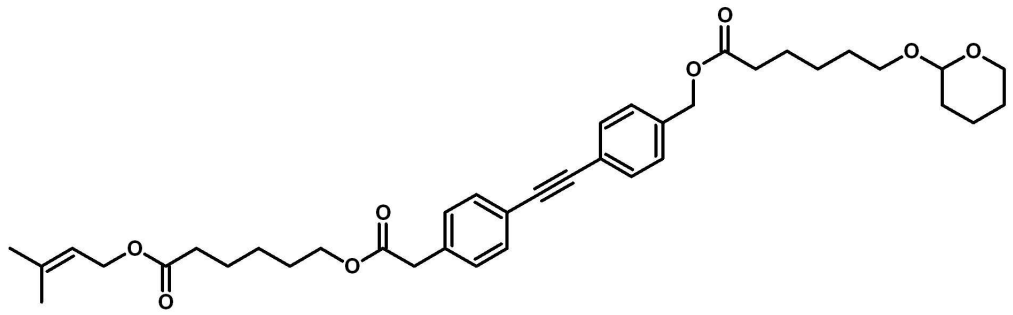

2-11

^{13}C NMR ($CDCl_3$) 75 MHz

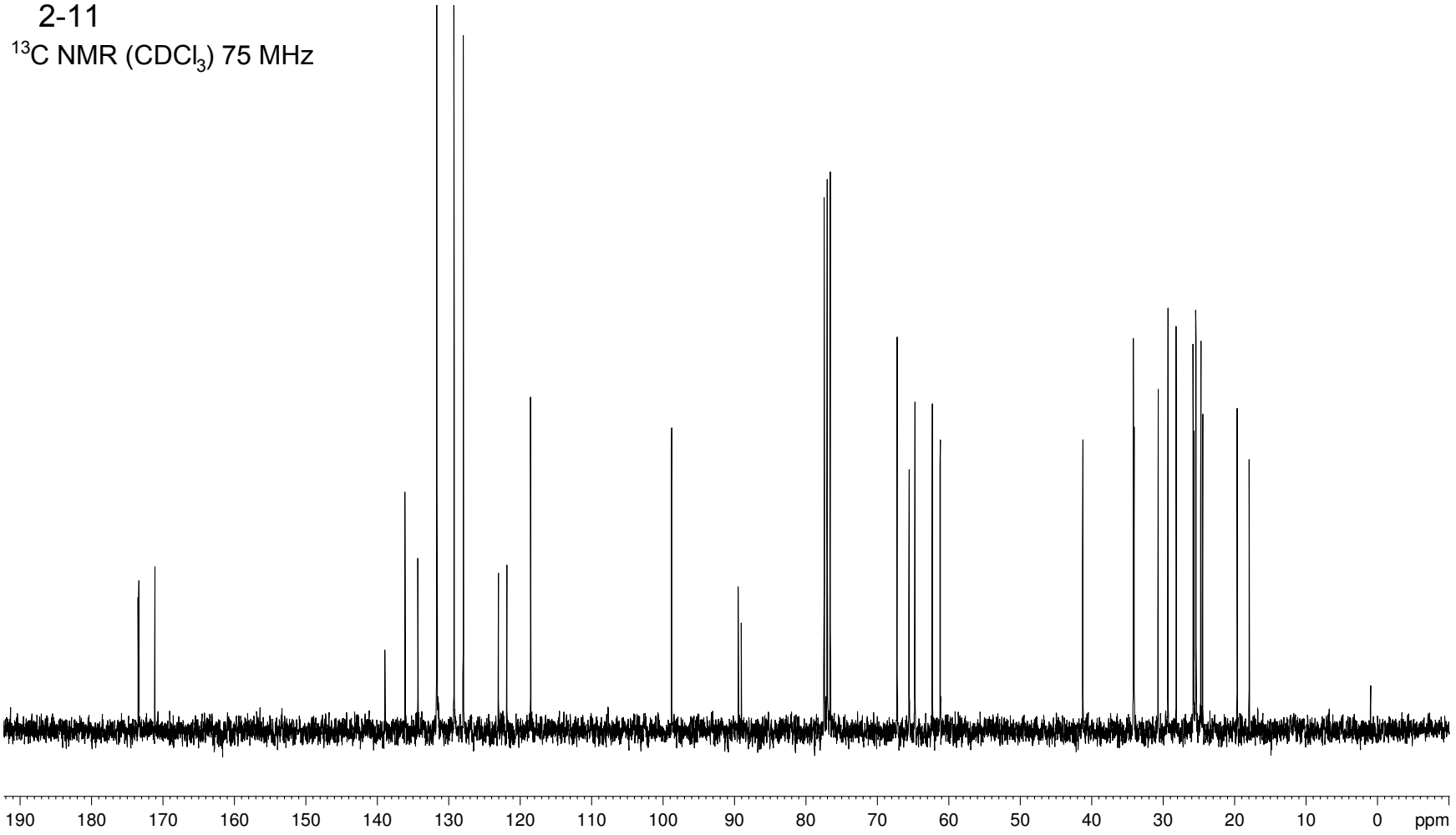

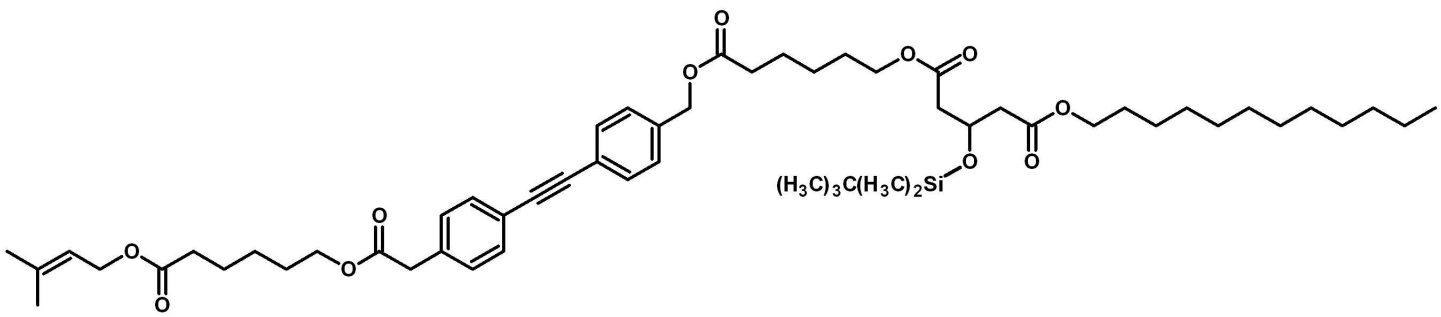

2-14

^{1}H NMR ($CDCl_3$) 300 MHz

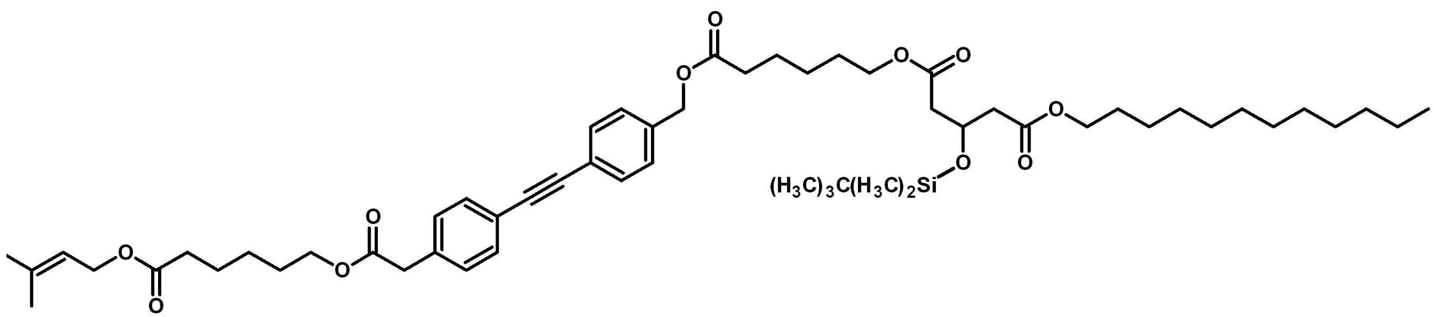

2-14

^{13}C NMR ($CDCl_3$) 75 MHz

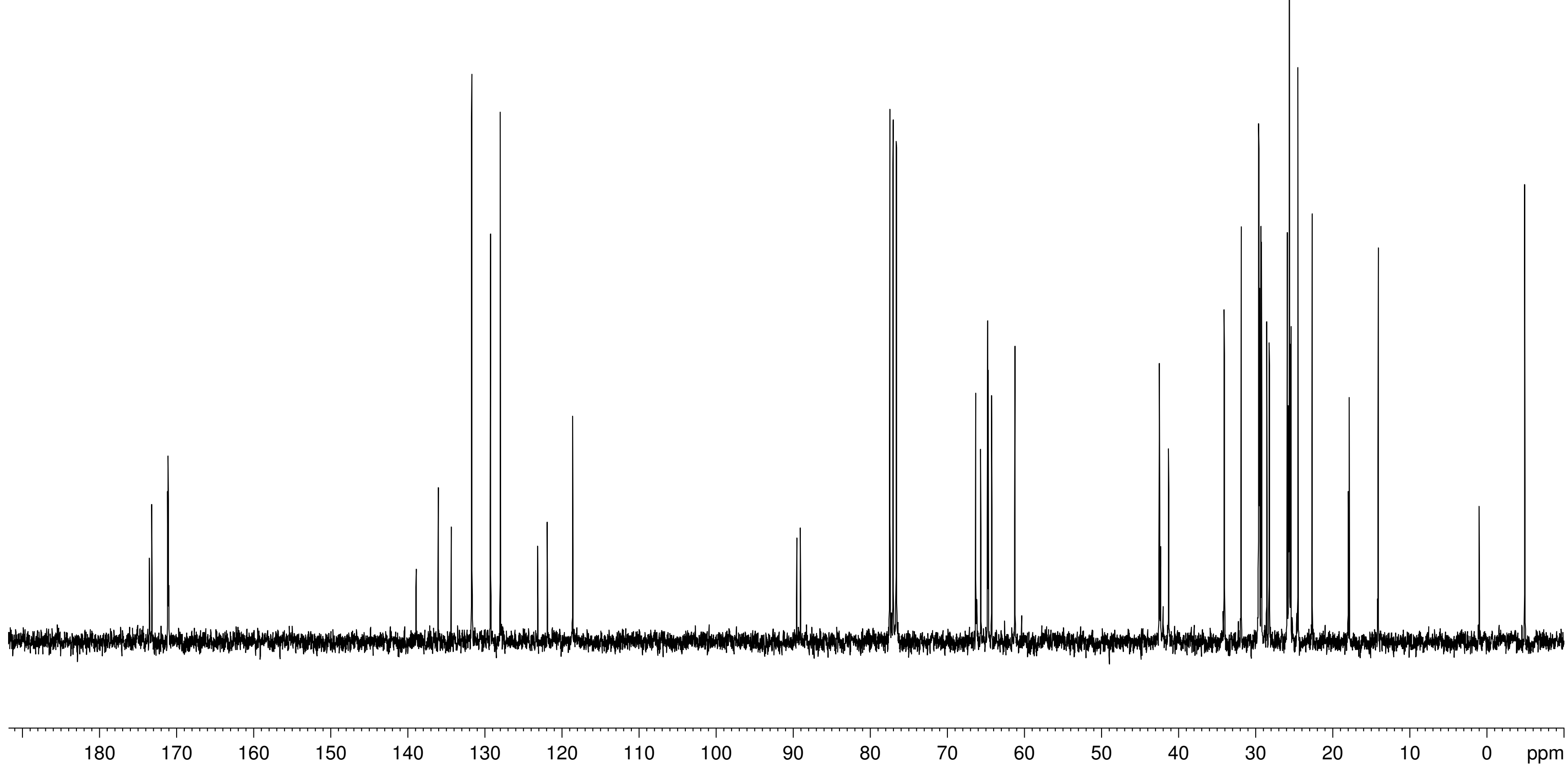

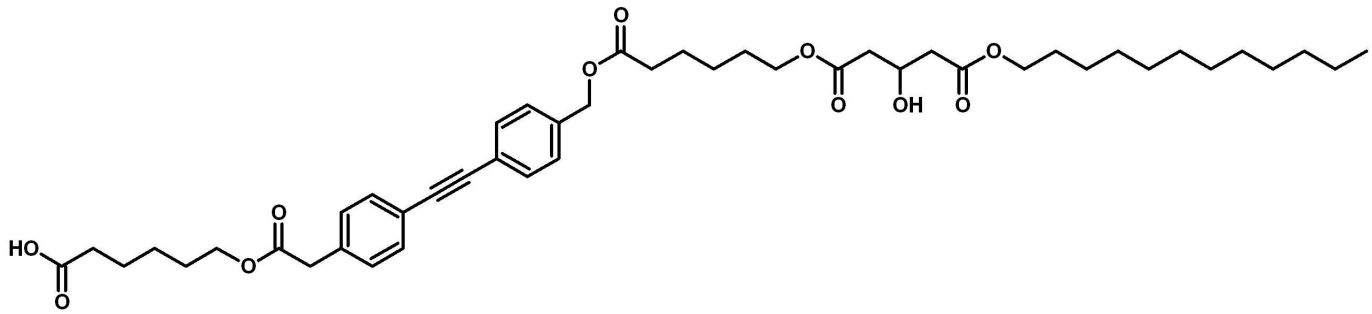

HO_2C-**Hex-Dip-Hex-G(12)**-OH

1-7

^1H NMR ($CDCl_3$) 300 MHz

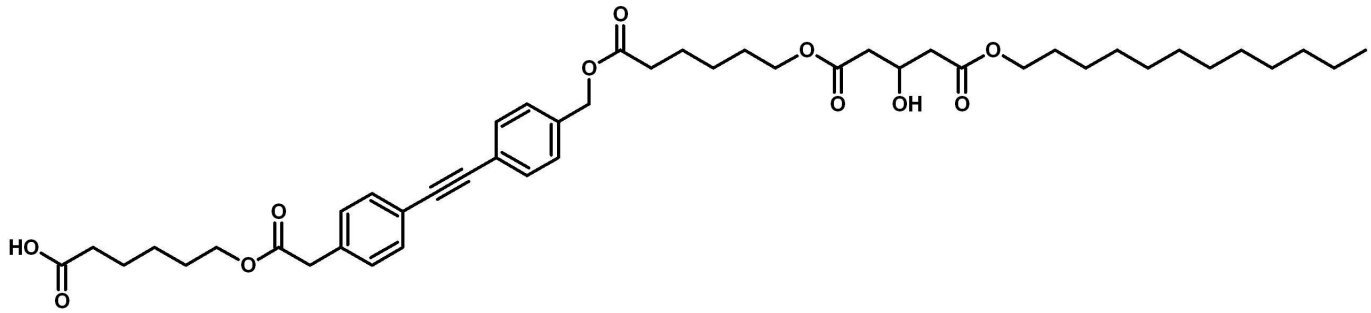

HO_2C-**Hex-Dip-Hex-G(12)**-OH

1-7

^{13}C NMR ($CDCl_3$) 75 MHz

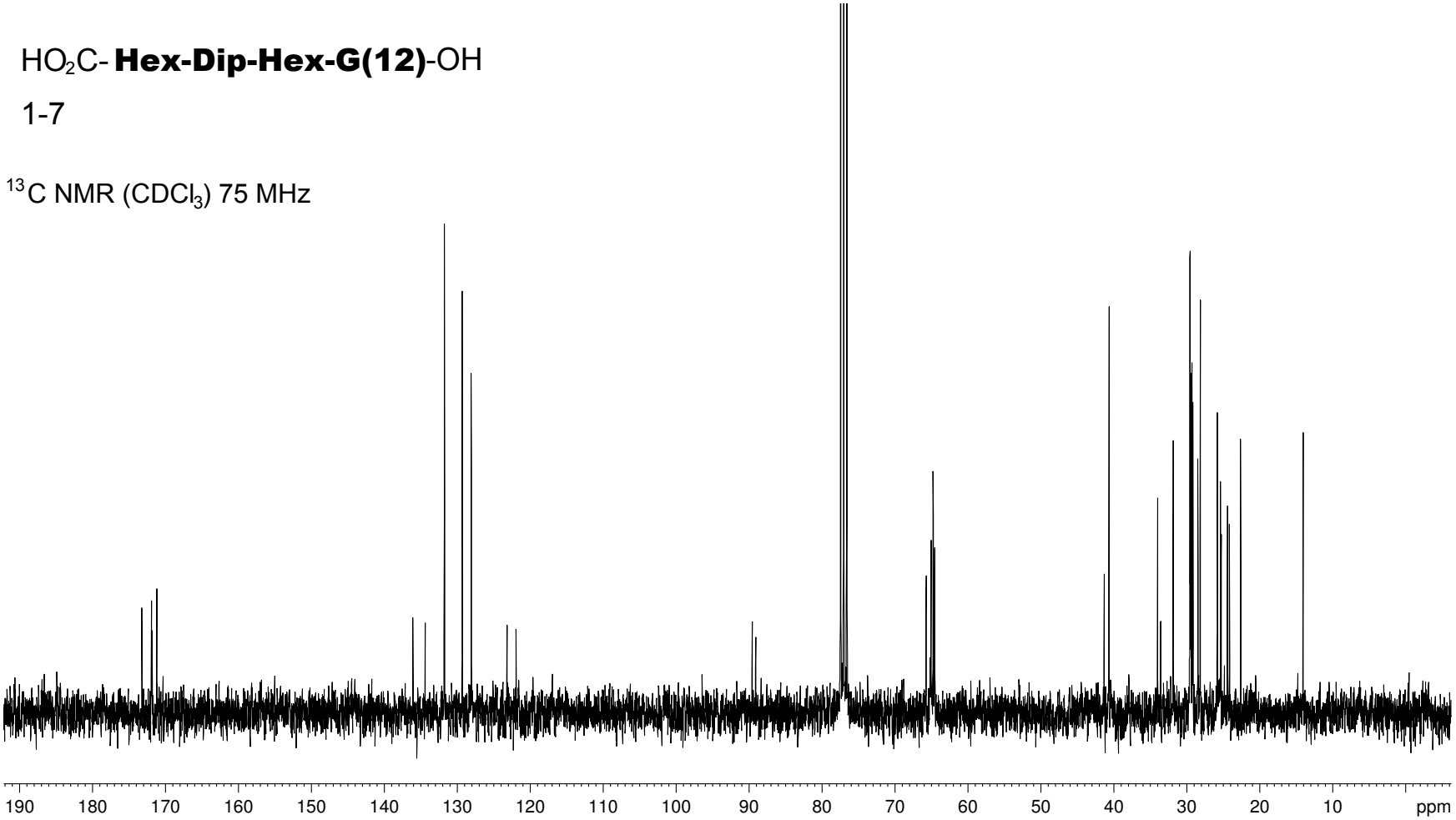

HO_2C-**Hex-Dip-Hex-G(12)**-OH

1-7

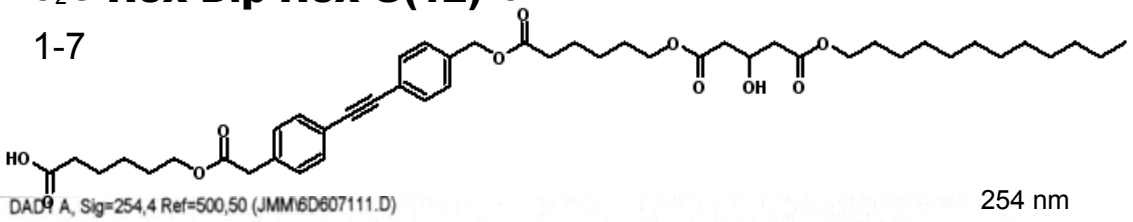

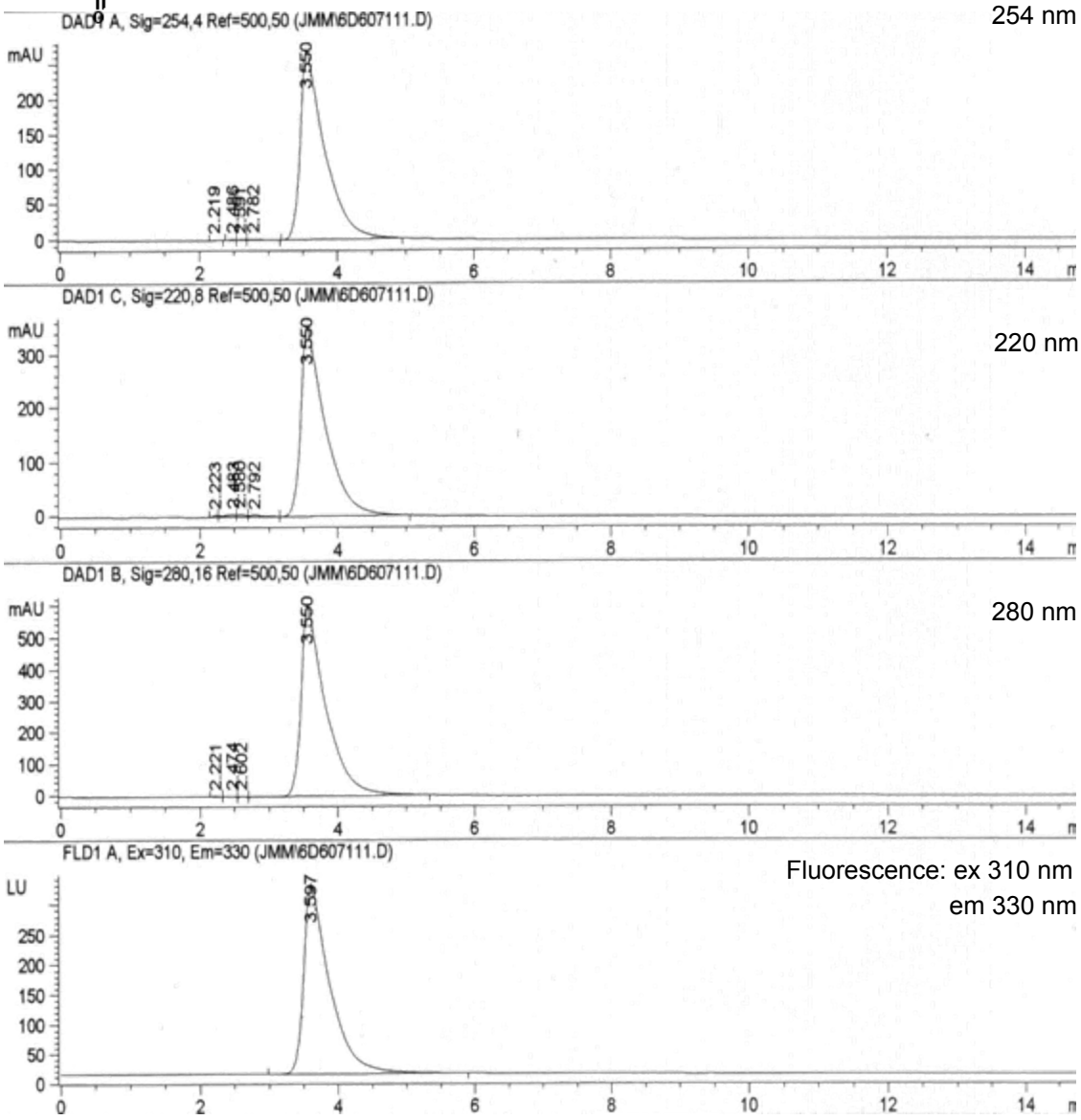

-HPLC trace of purified sample (used for transport and fluorescence studies)

-CONDITIONS: HP series 1100 HPLC

-Macherey-Nagel RP C^{18} "Nucleosil" analytical column (4 mm x 250 mm)

-1:1 CH_3OH: ACN as eluting solvents, flow 1mL/min

HO_2C-**Hex-Dip-Hex-G(12)**-OH

1-7

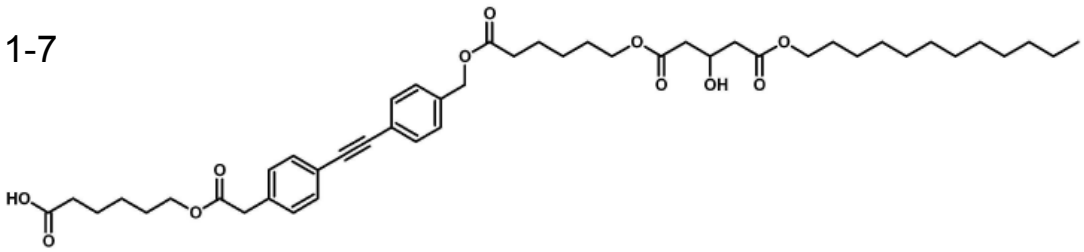

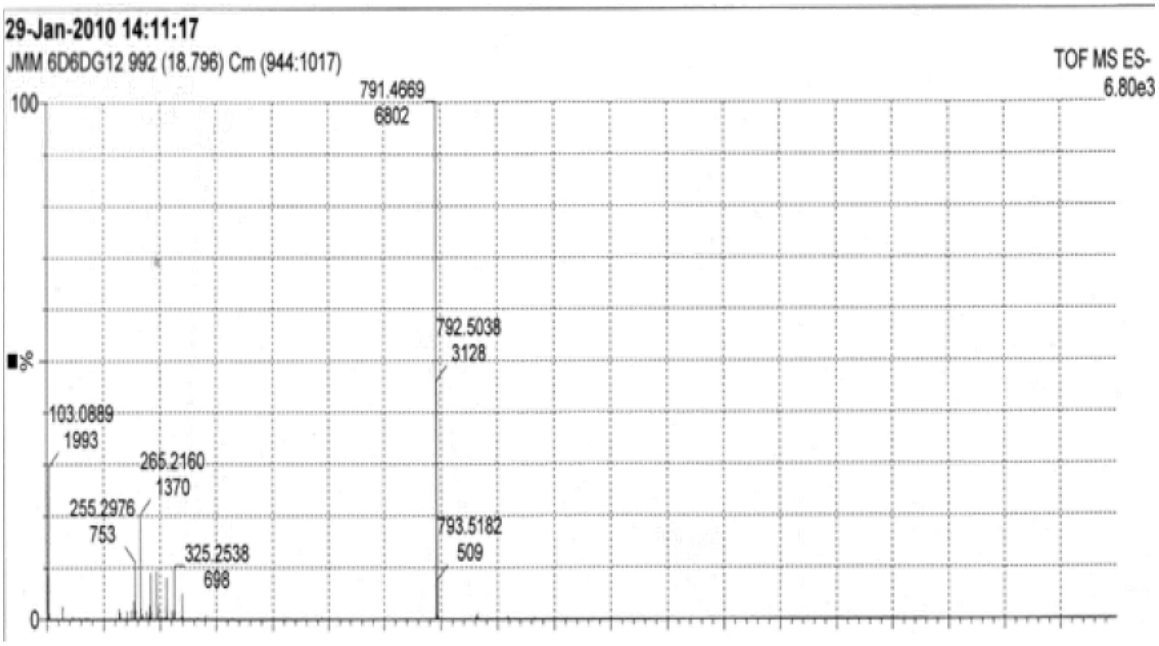

MS: -ve ion ESI, Q-TOF 2 instrument

Calc'd for C46H63O11= 791.4376 amu, obtained = 791.467 amu

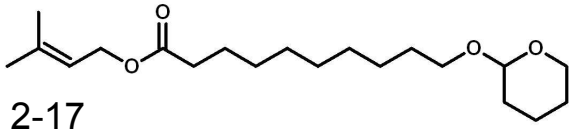

2-17

^{1}H NMR ($CDCl_3$) 300 MHz

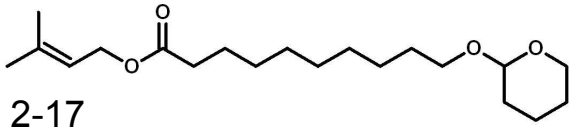

2-17

^{13}C NMR ($CDCl_3$) 75 MHz

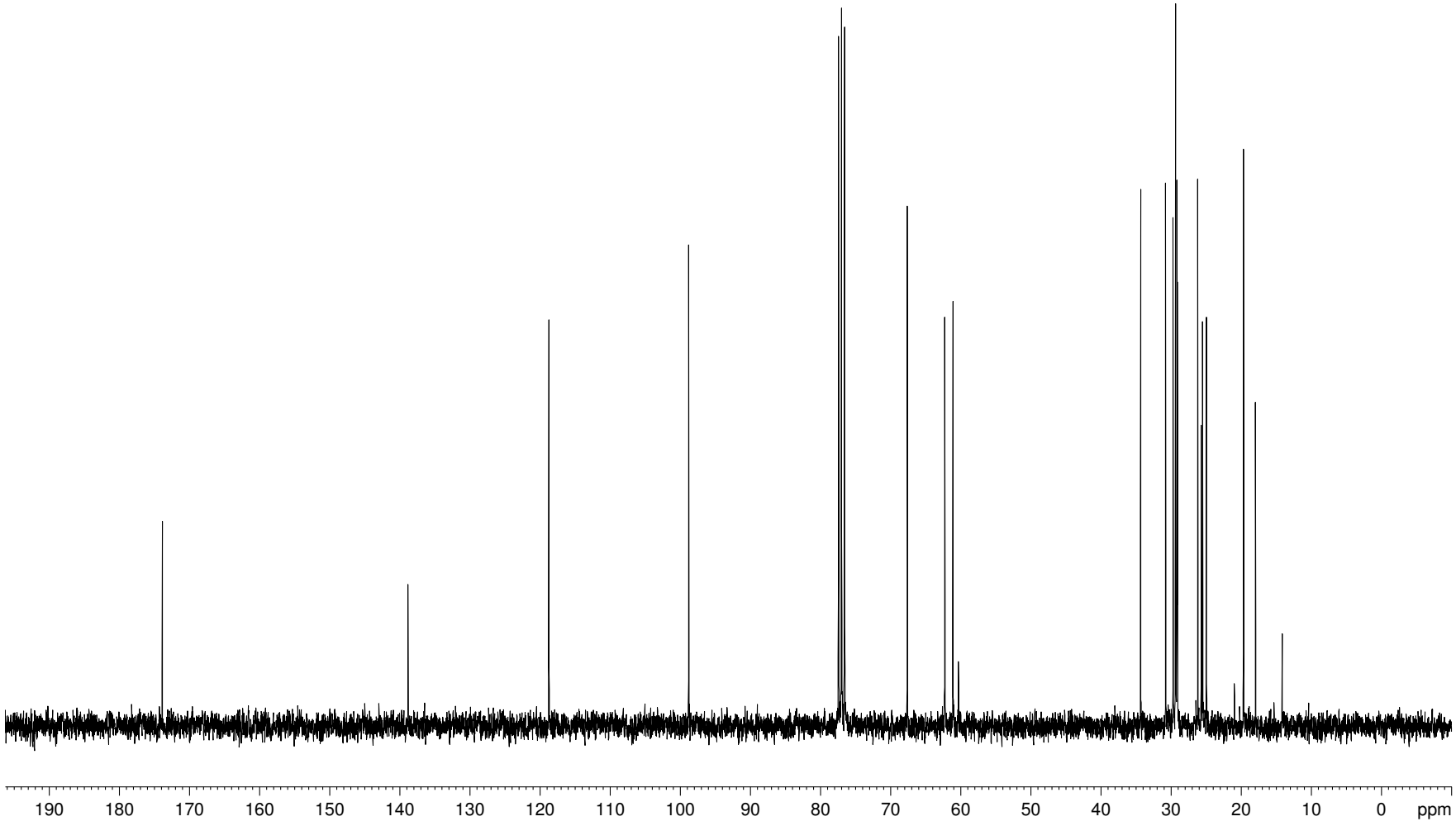

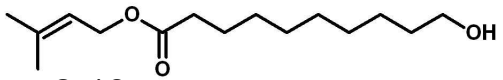

2-18

^{1}H NMR ($CDCl_3$) 300 MHz

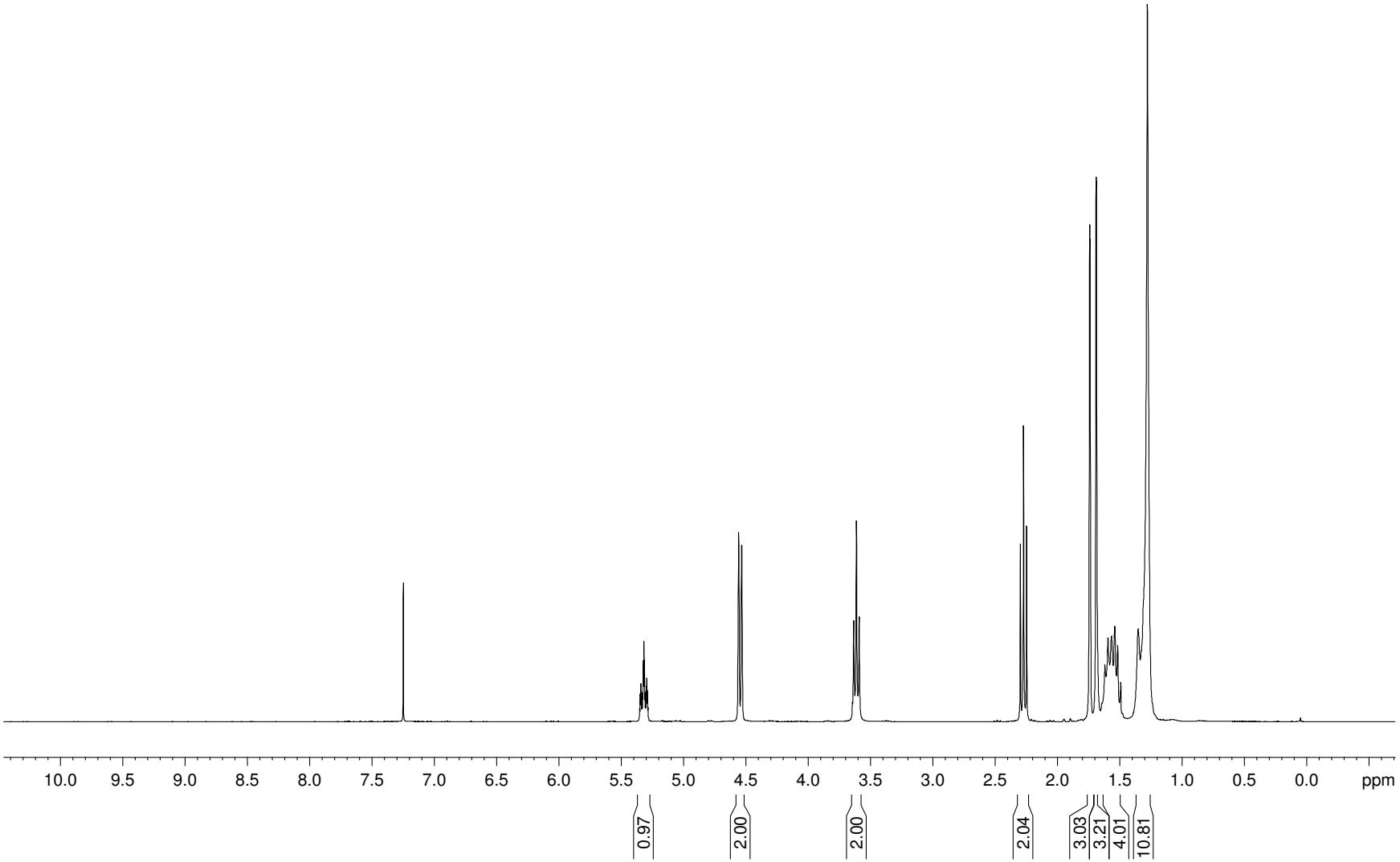

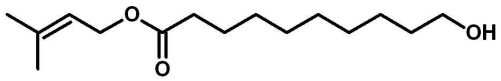

2-18

^{13}C NMR ($CDCl_3$) 75 MHz

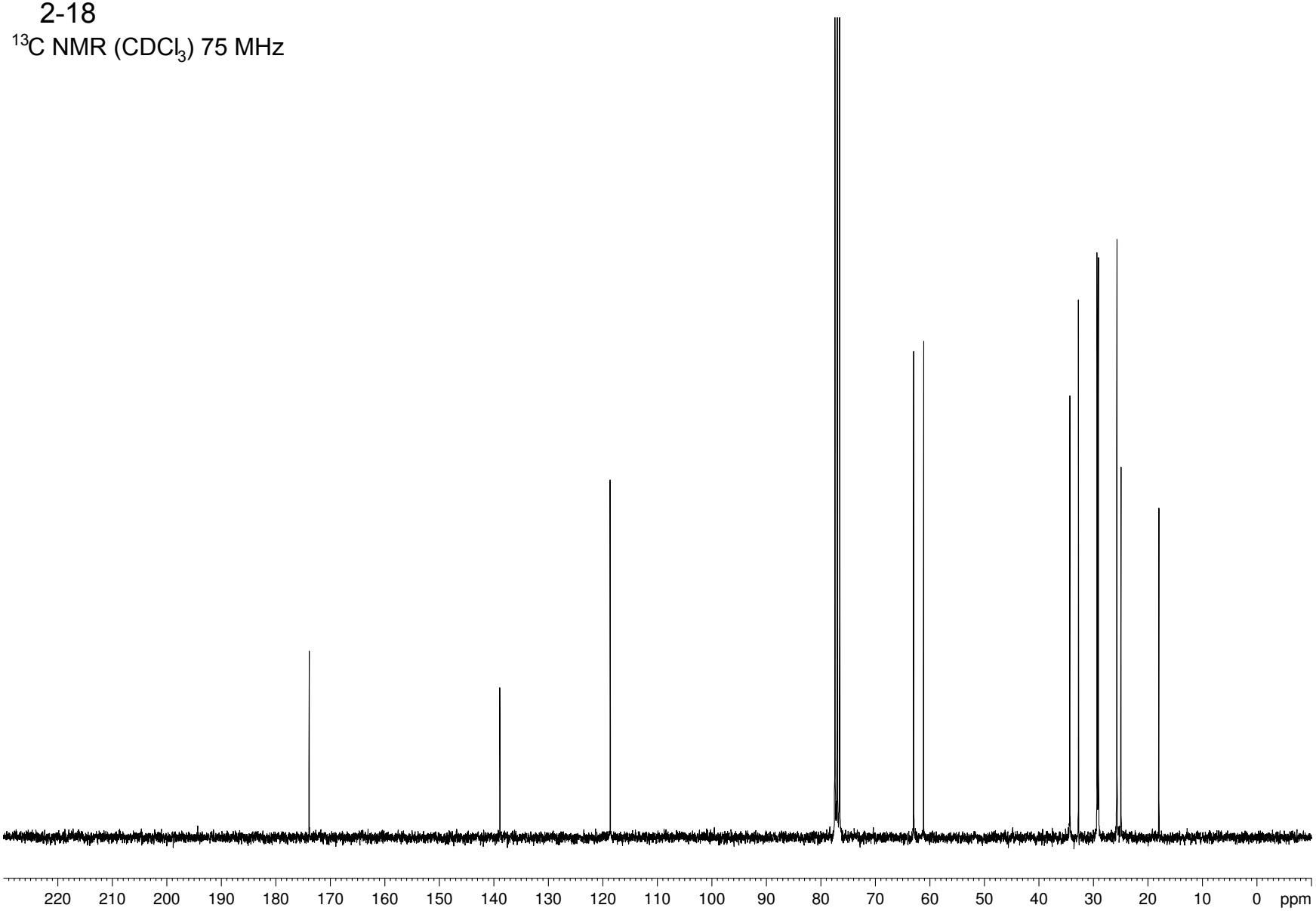

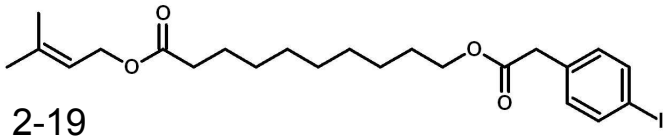

2-19

^{1}H NMR ($CDCl_3$) 300 MHz

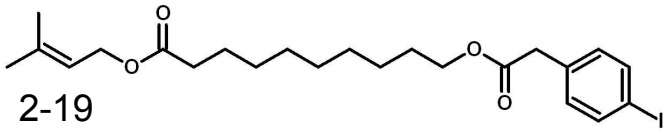

2-19

^{13}C NMR ($CDCl_3$) 75 MHz

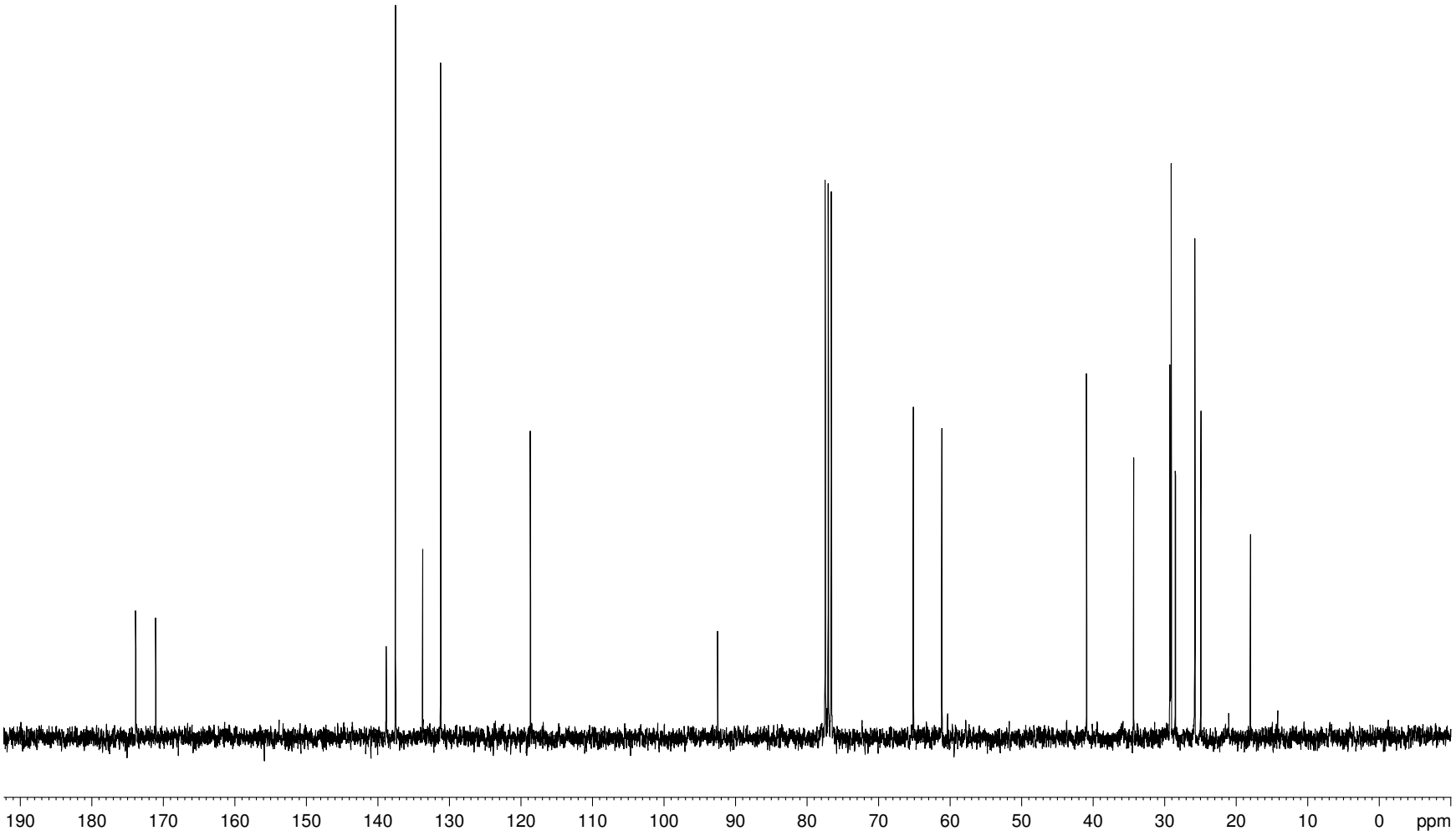

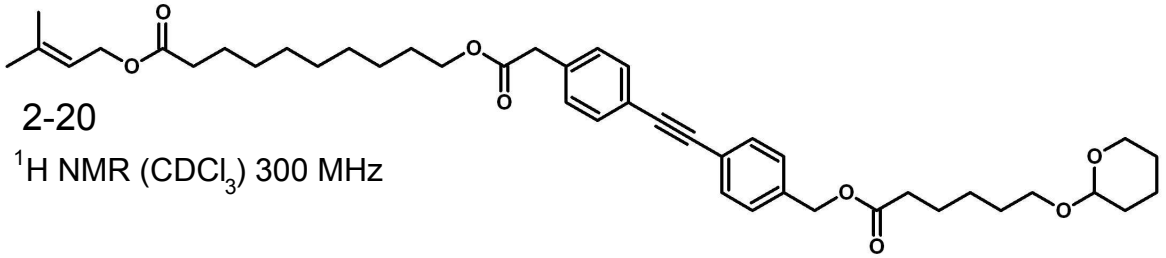

2-20

^{1}H NMR ($CDCl_3$) 300 MHz

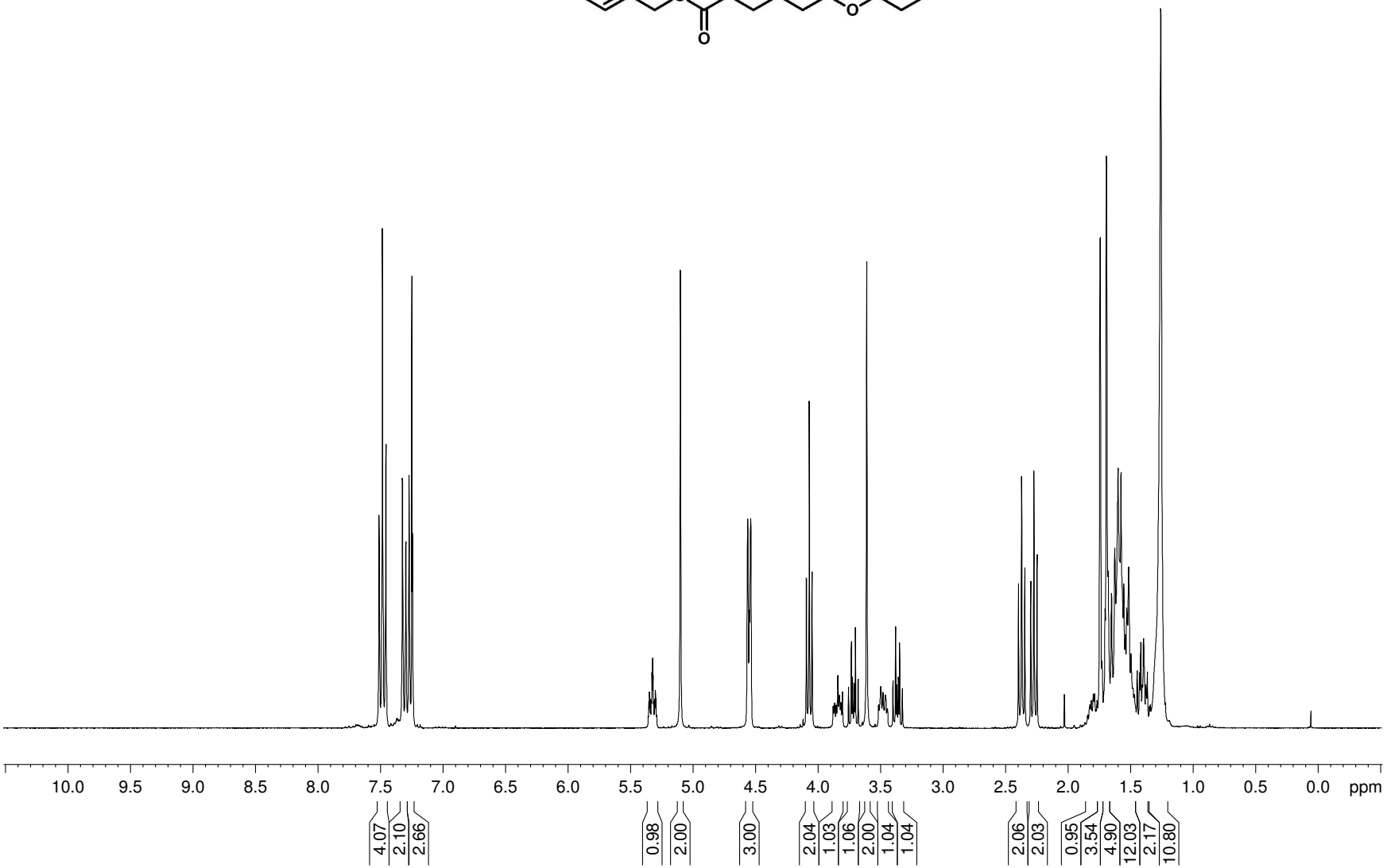

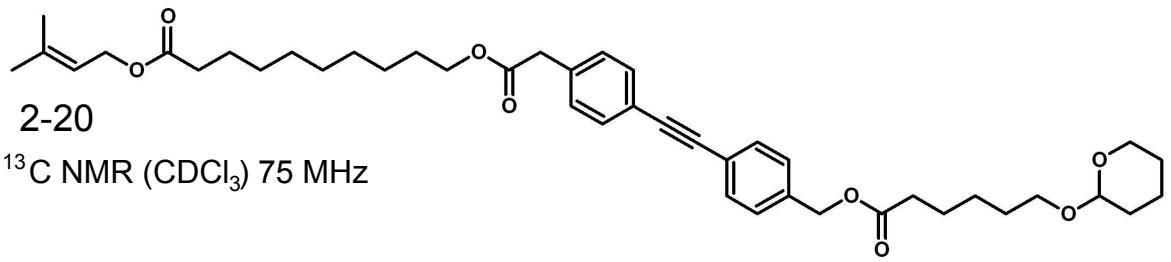

2-20

^{13}C NMR ($CDCl_3$) 75 MHz

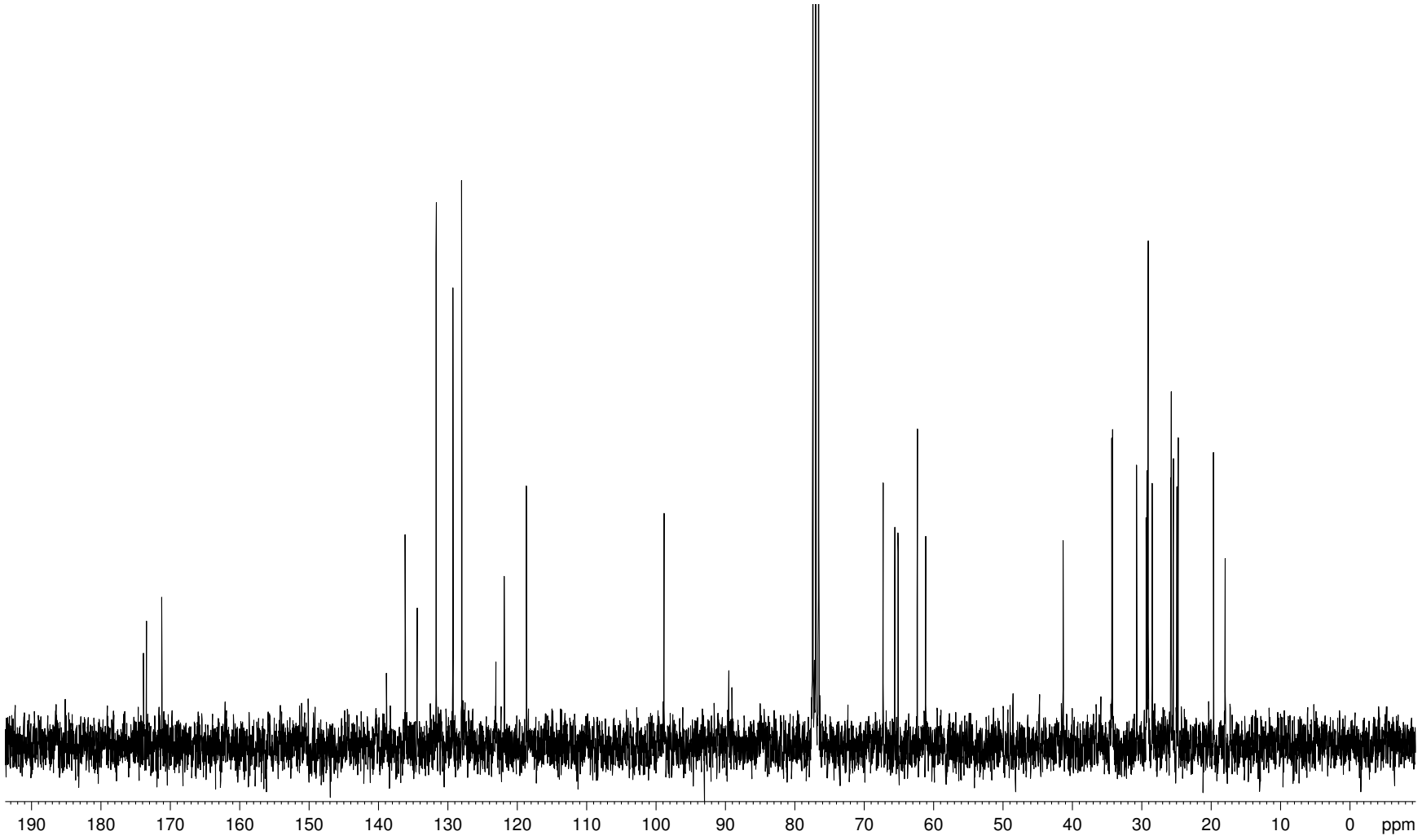

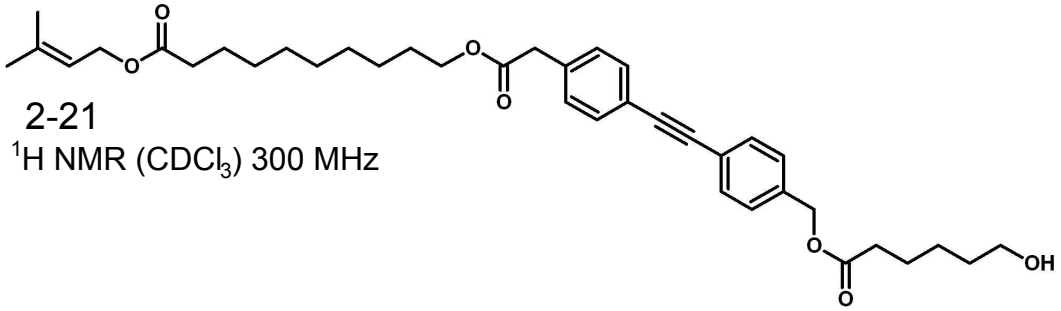

2-21

^{1}H NMR ($CDCl_3$) 300 MHz

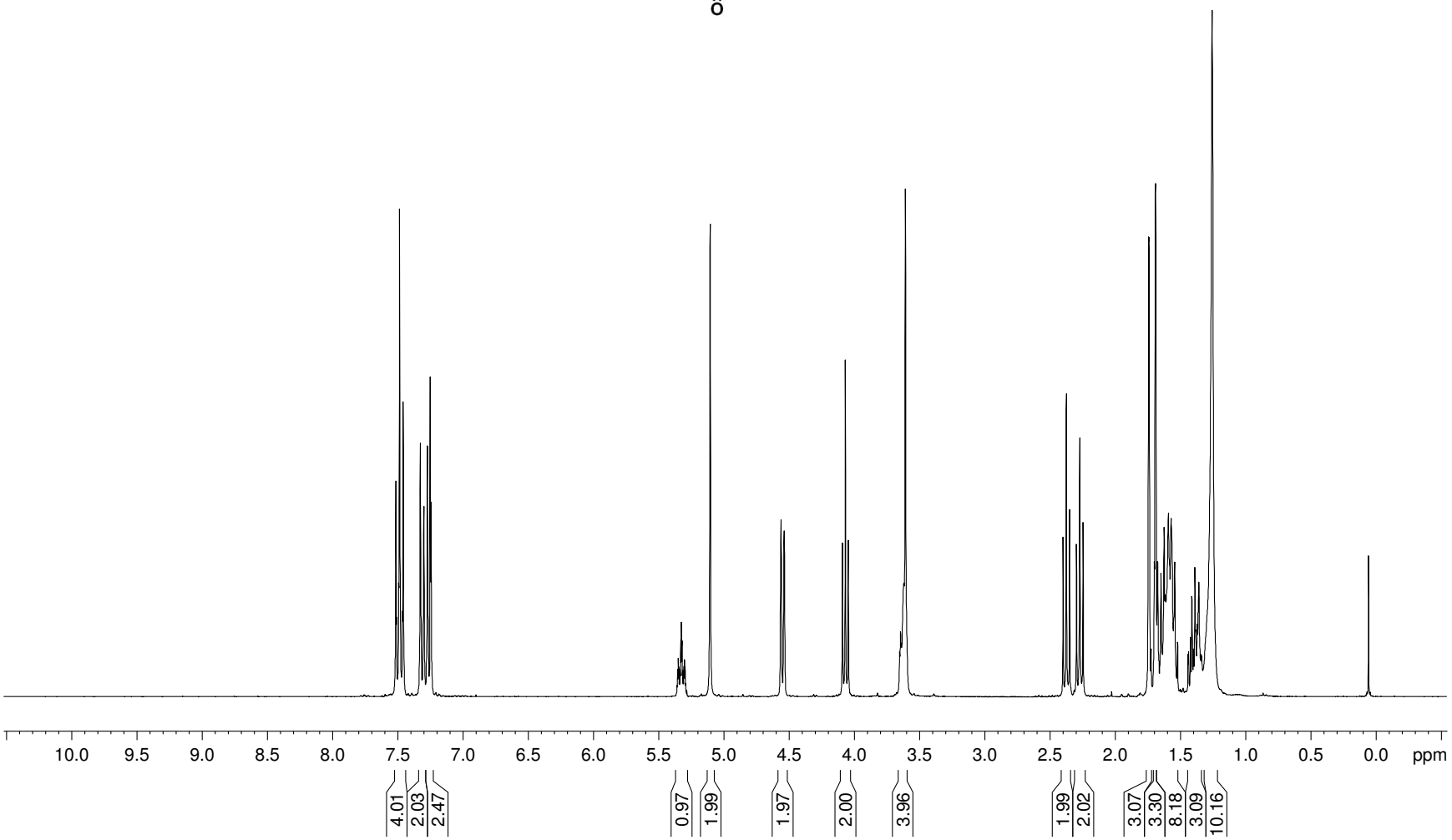

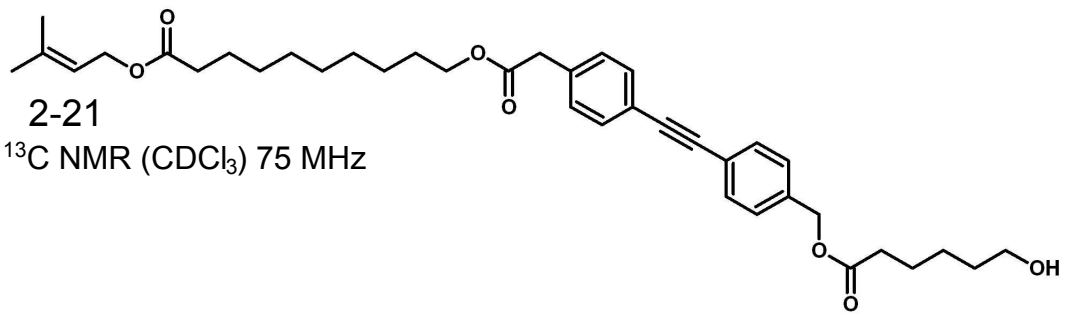

2-21

^{13}C NMR ($CDCl_3$) 75 MHz

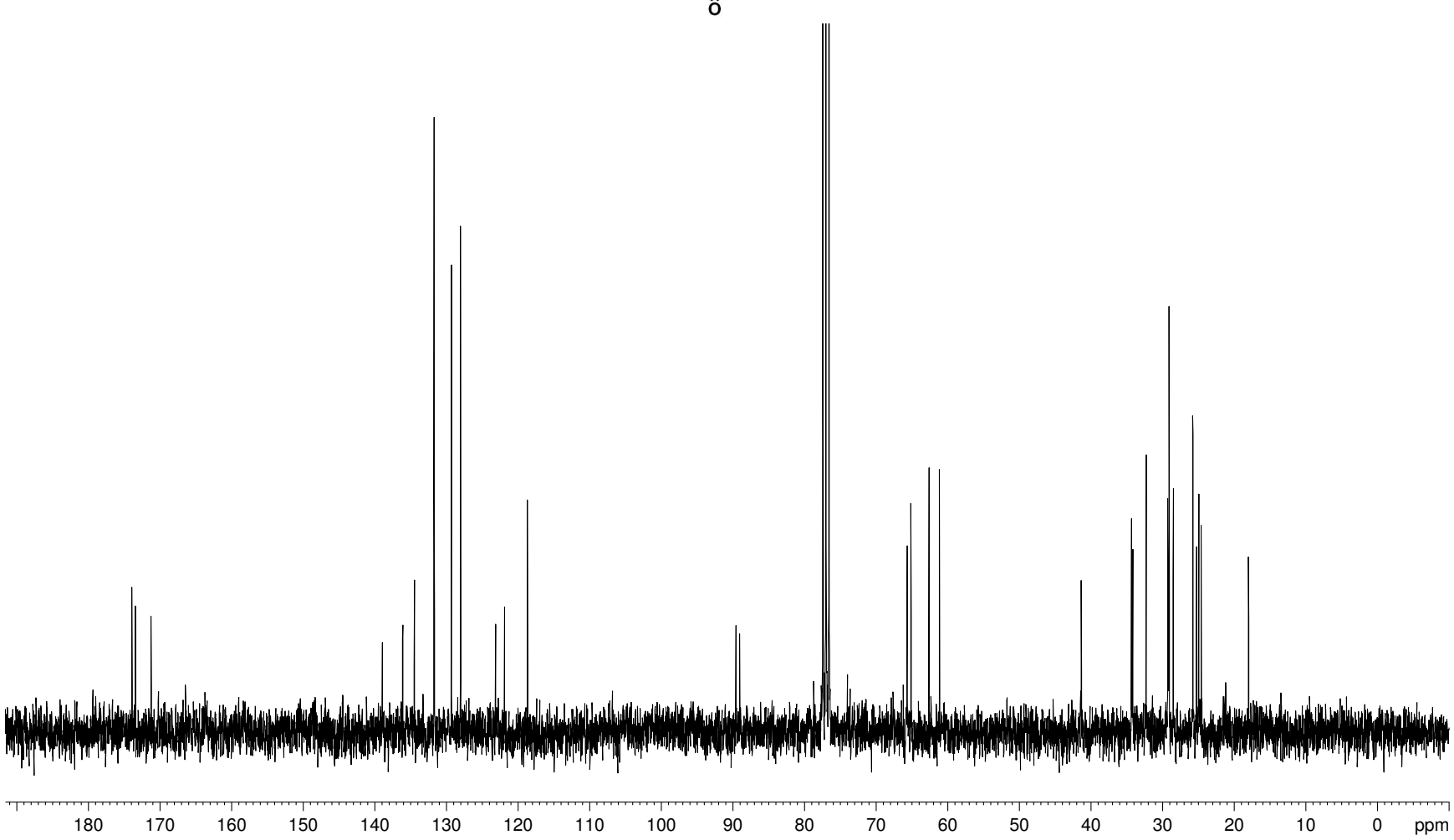

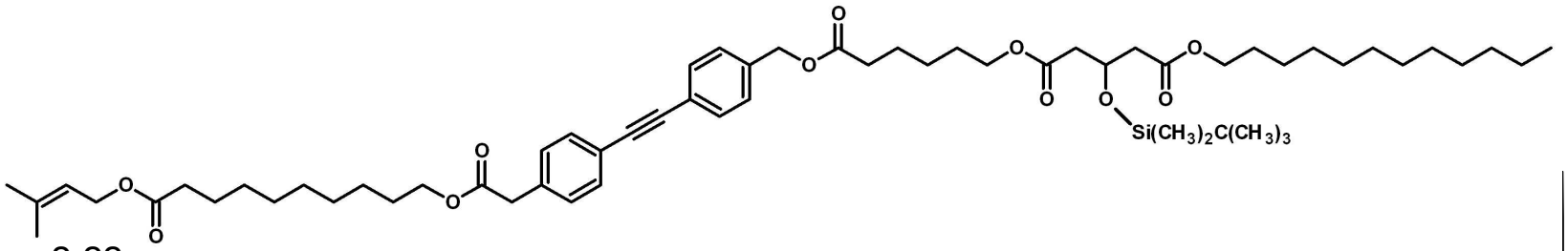

2-22

^{1}H NMR ($CDCl_3$) 300 MHz

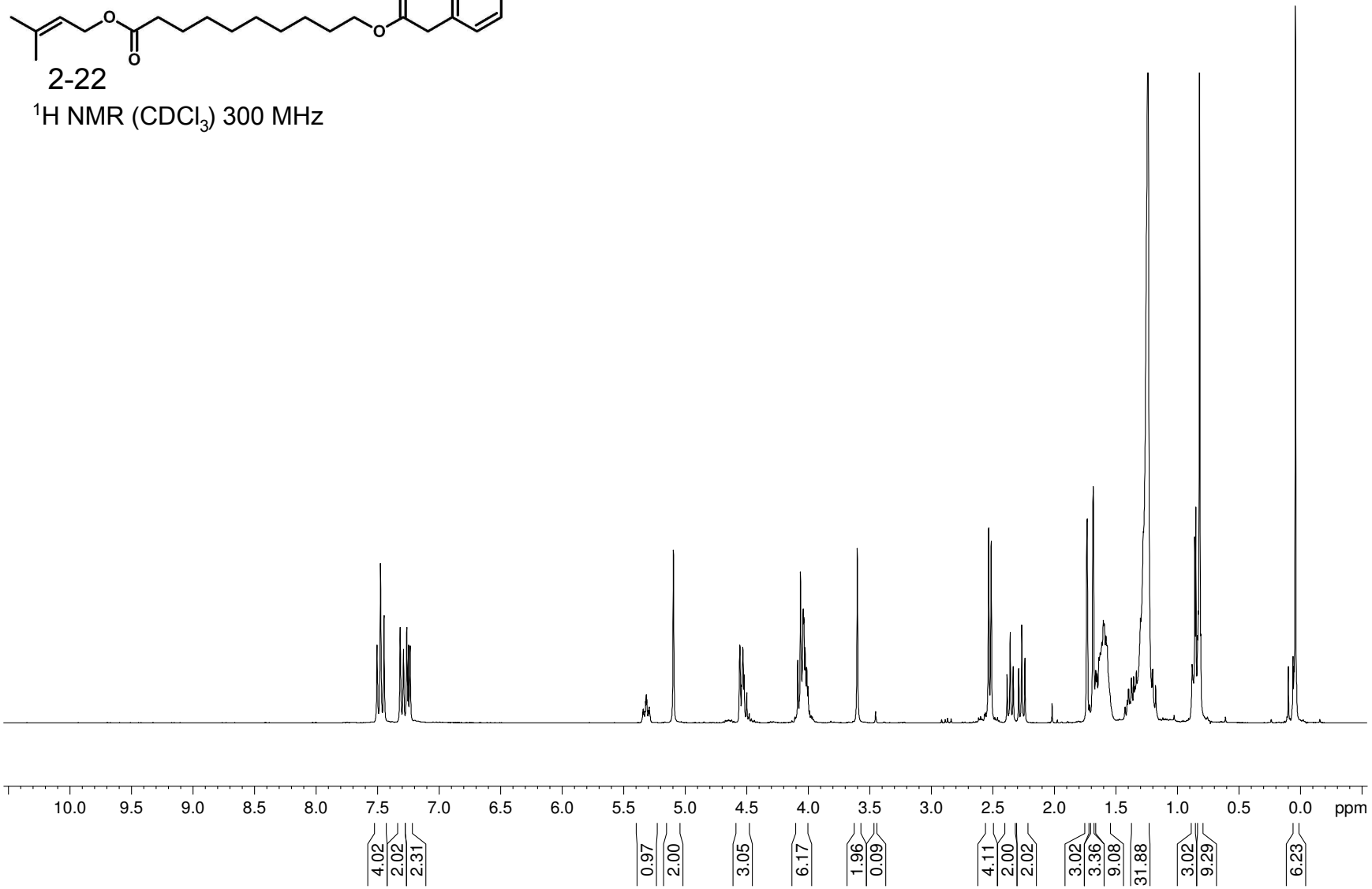

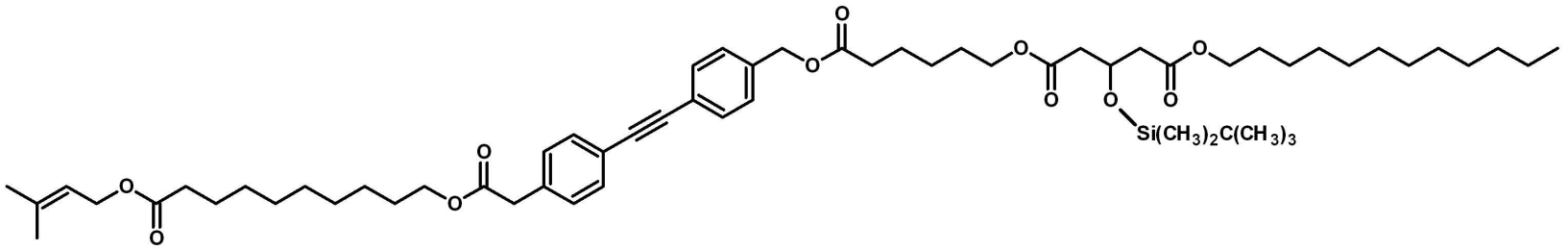

2-22

^{13}C NMR ($CDCl_3$) 75 MHz

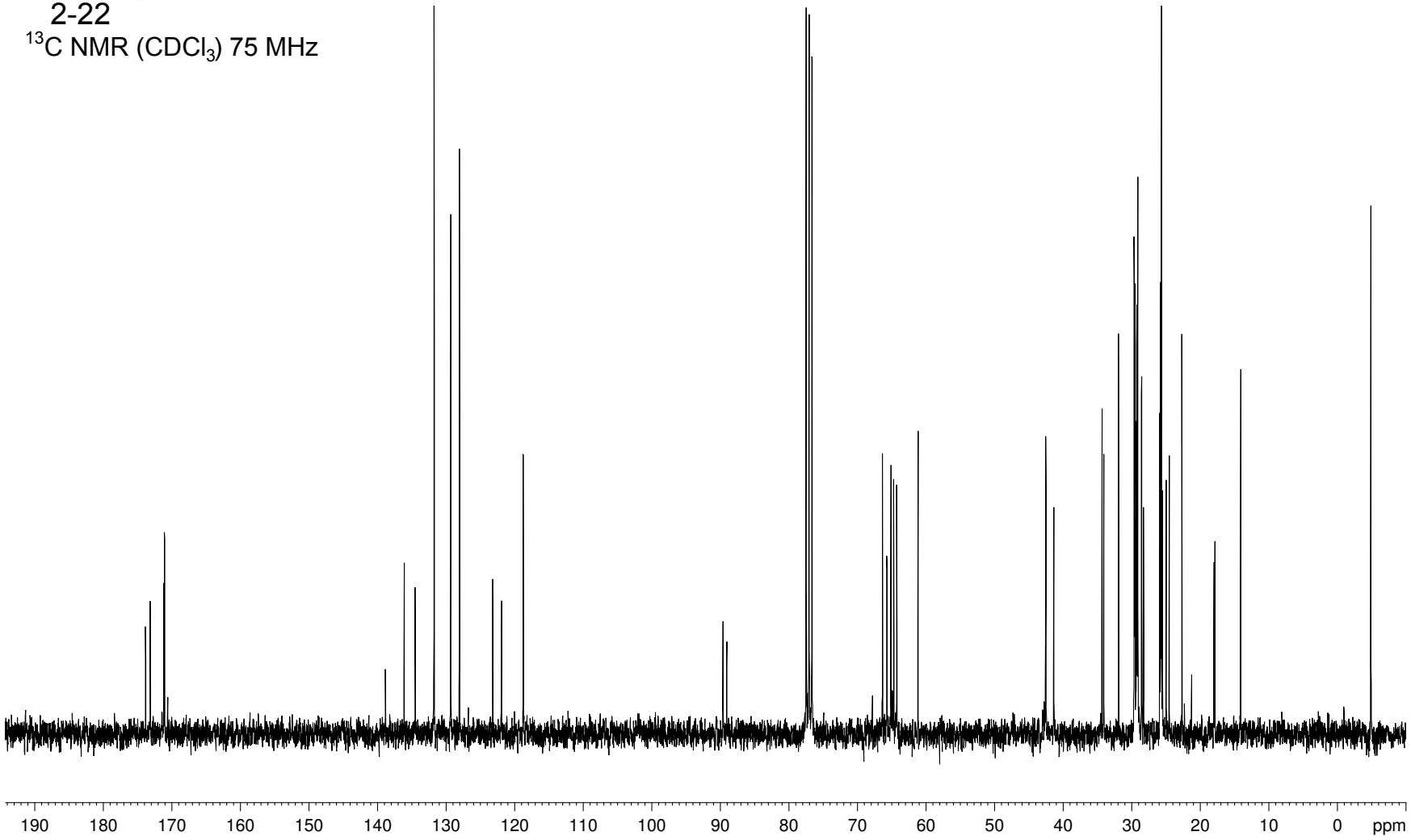

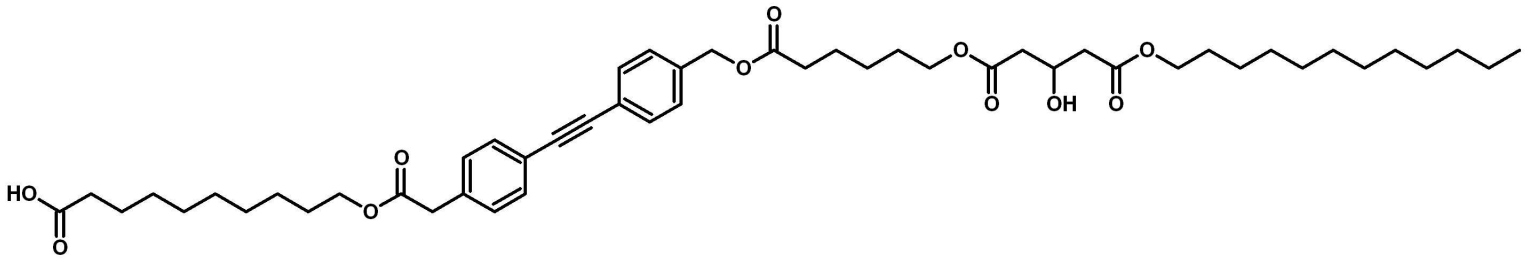

HO_2C-**Dec-Dip-Hex-G(12)**-OH
2-15

^1H NMR ($CDCl_3$) 500 MHz

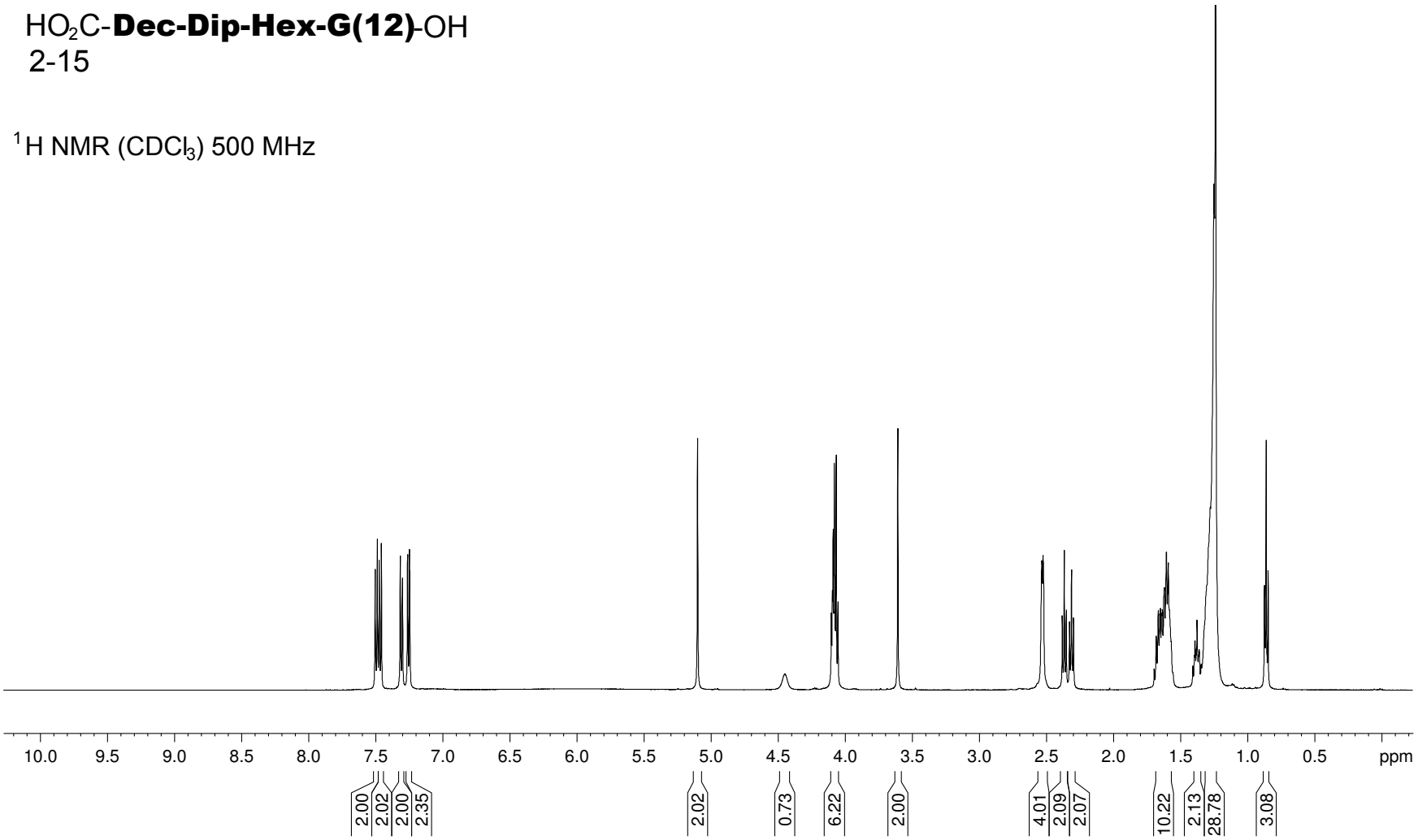

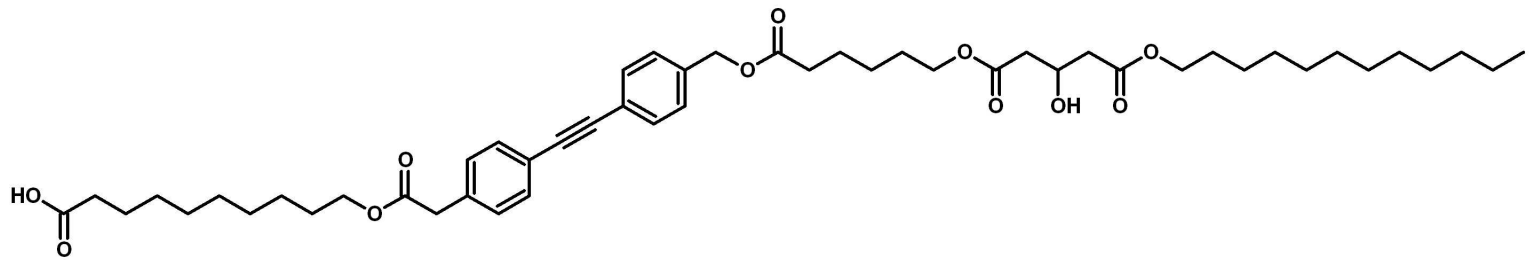

HO_2C-**Dec-Dip-Hex-G(12)**-OH

2-15

^{13}C NMR ($CDCl_3$) 125 MHz

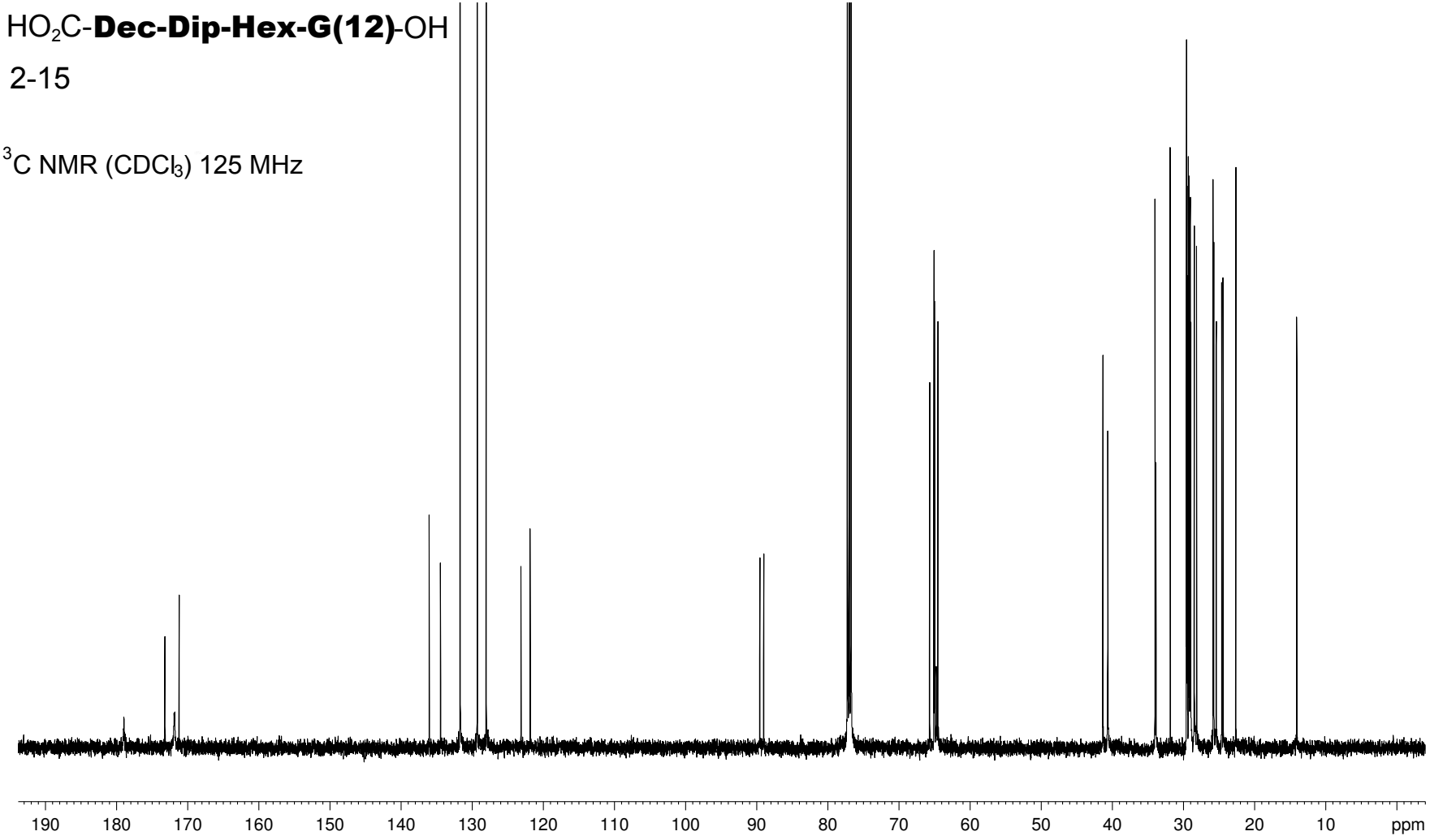

HO_2C-**Dec-Dip-Hex-G(12)**-OH

2-15

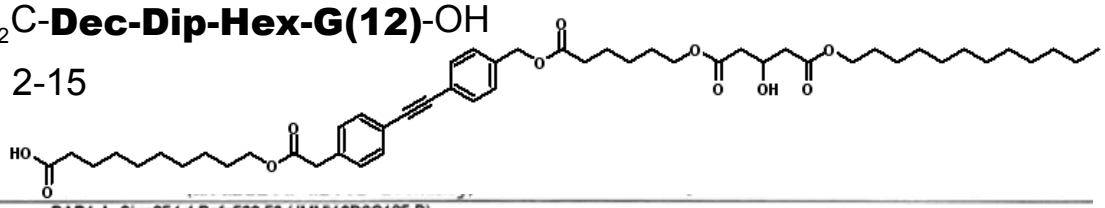

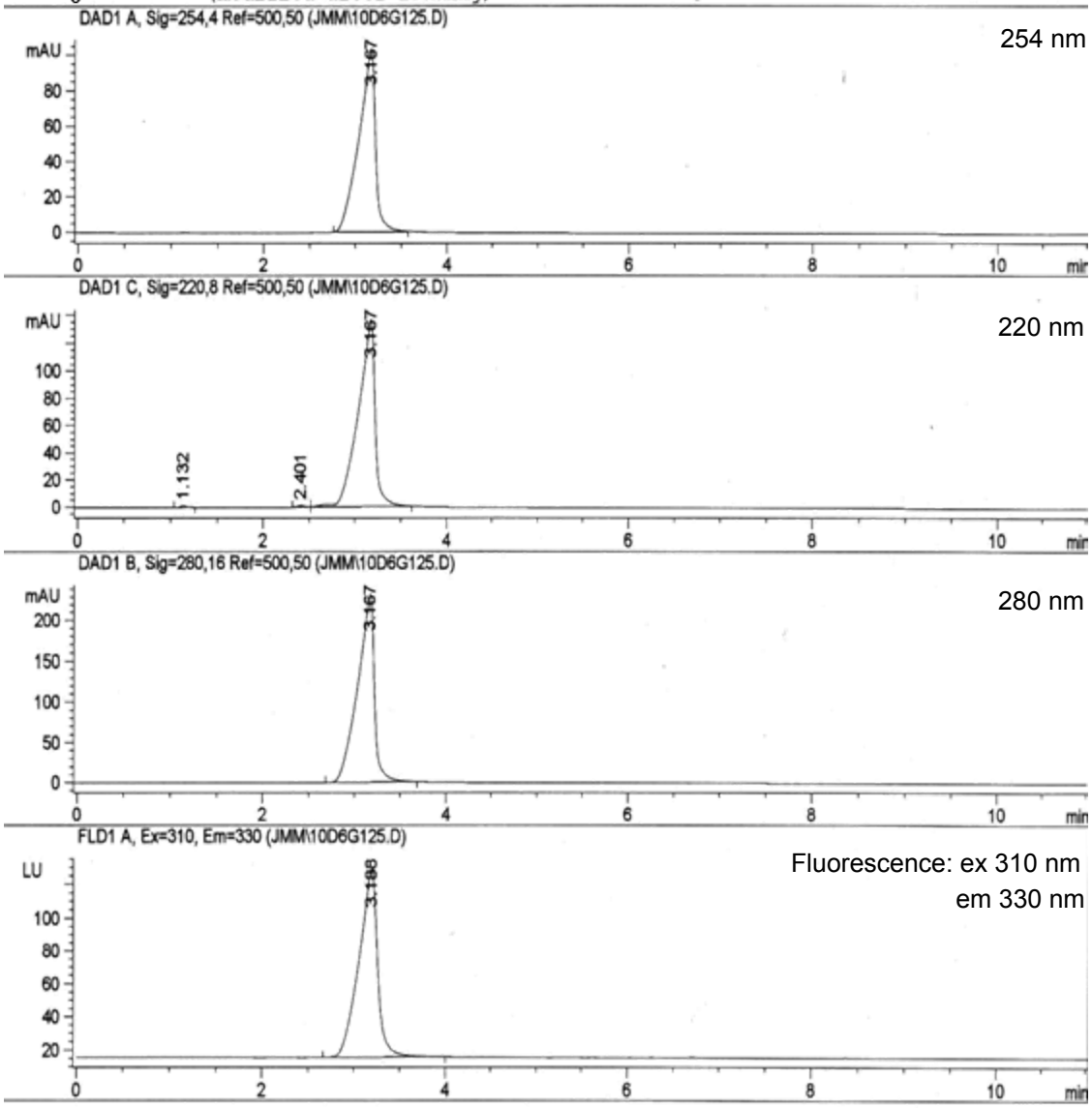

-HPLC trace of purified sample (used for transport and fluorescence studies)
-CONDITIONS: HP series 1100 HPLC
-Macherey-Nagel RP C^{18}"Nucleosil" analytical column (4 mm x 250 mm)
-1:1 CH_3OH: ACN as eluting solvents, flow 1mL/min

HO_2C-**Dec-Dip-Hex-G(12)**-OH

2-15

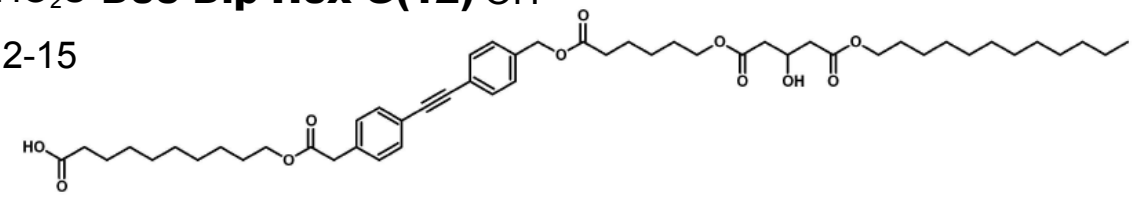

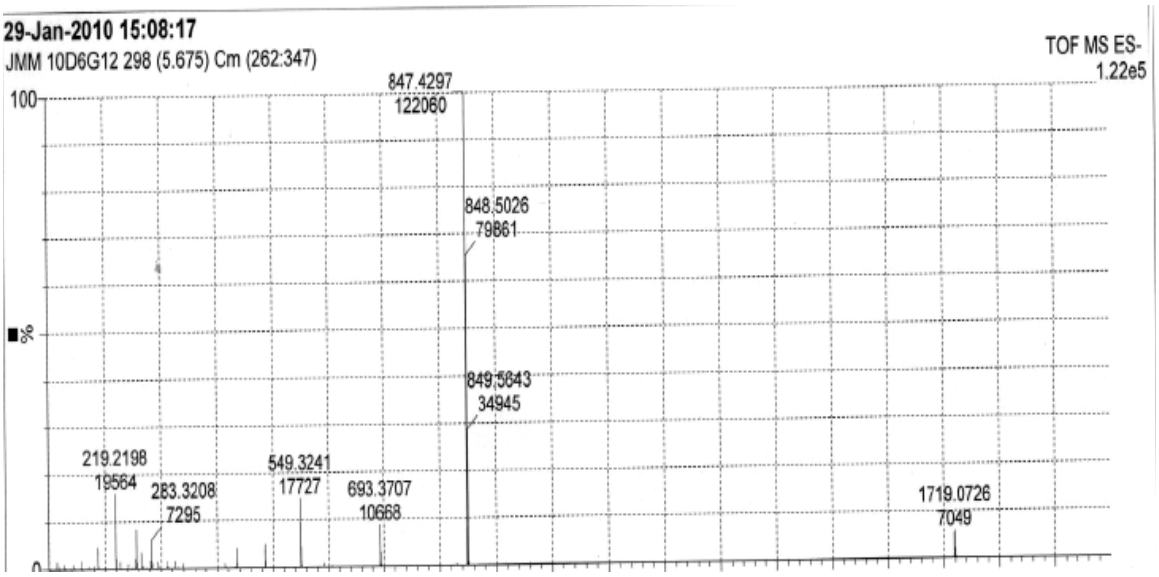

MS: -ve ion ESI, Q-TOF 2 instrument

Calc'd for C50H71O11 = 847.5002 amu, obtained; 847.429amu

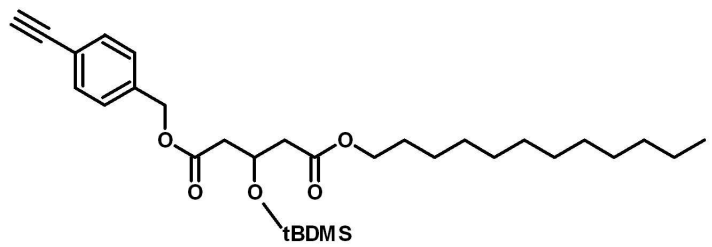

3-8

^{1}H NMR ($CDCl_3$) 300MHz

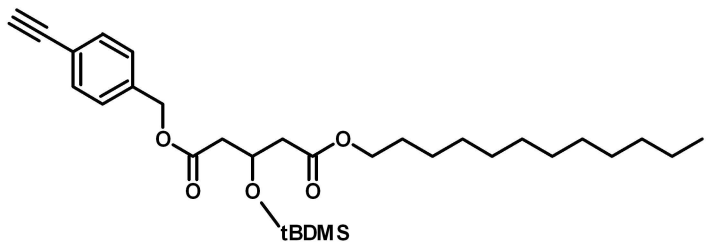

3-8

^{13}C NMR ($CDCl_3$) 75MHz

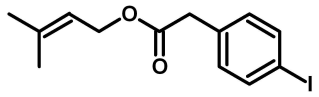

3-16

^{1}H NMR ($CDCl_3$) 300MHz

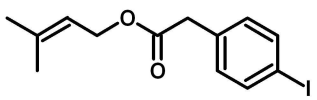

3-16

^{13}C NMR ($CDCl_3$) 75MHz

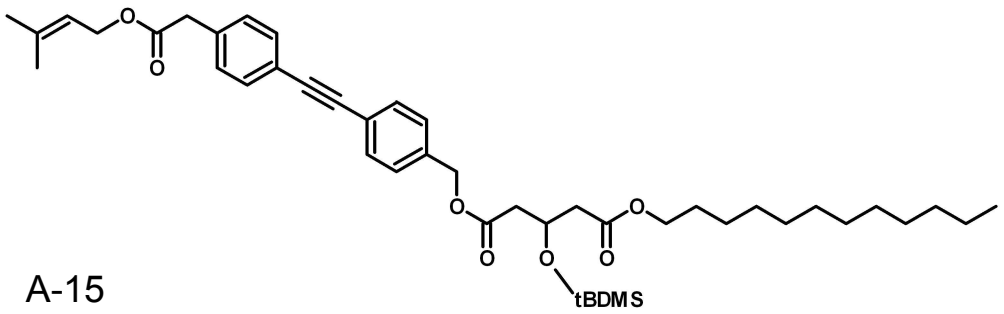

A-15

^{1}H NMR ($CDCl_3$) 300MHz

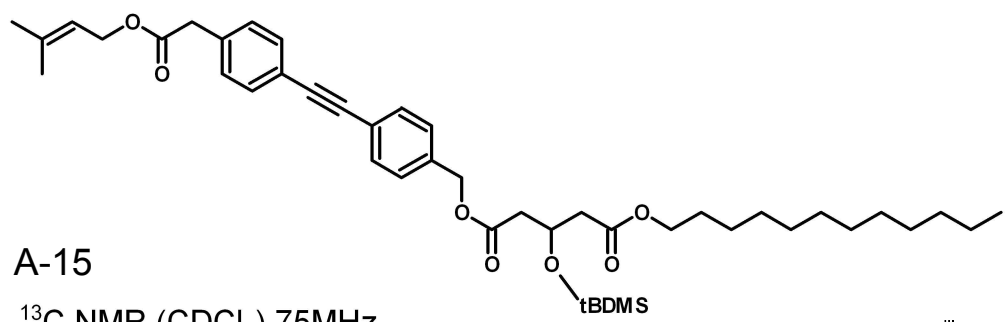

A-15

^{13}C NMR ($CDCl_3$) 75MHz

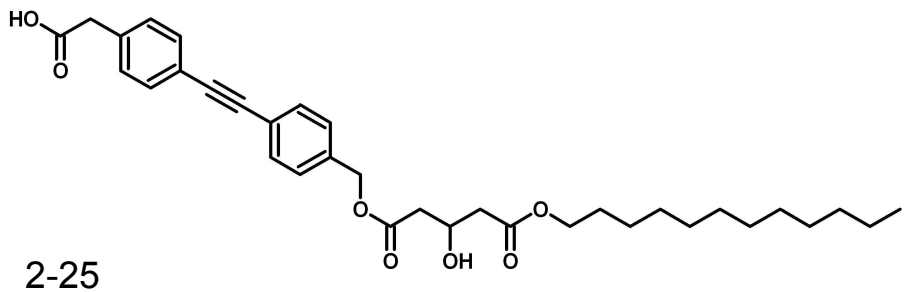

2-25

^{1}H NMR ($CDCl_3$) 300MHz

HO_2C-Dip-G(12)-OH

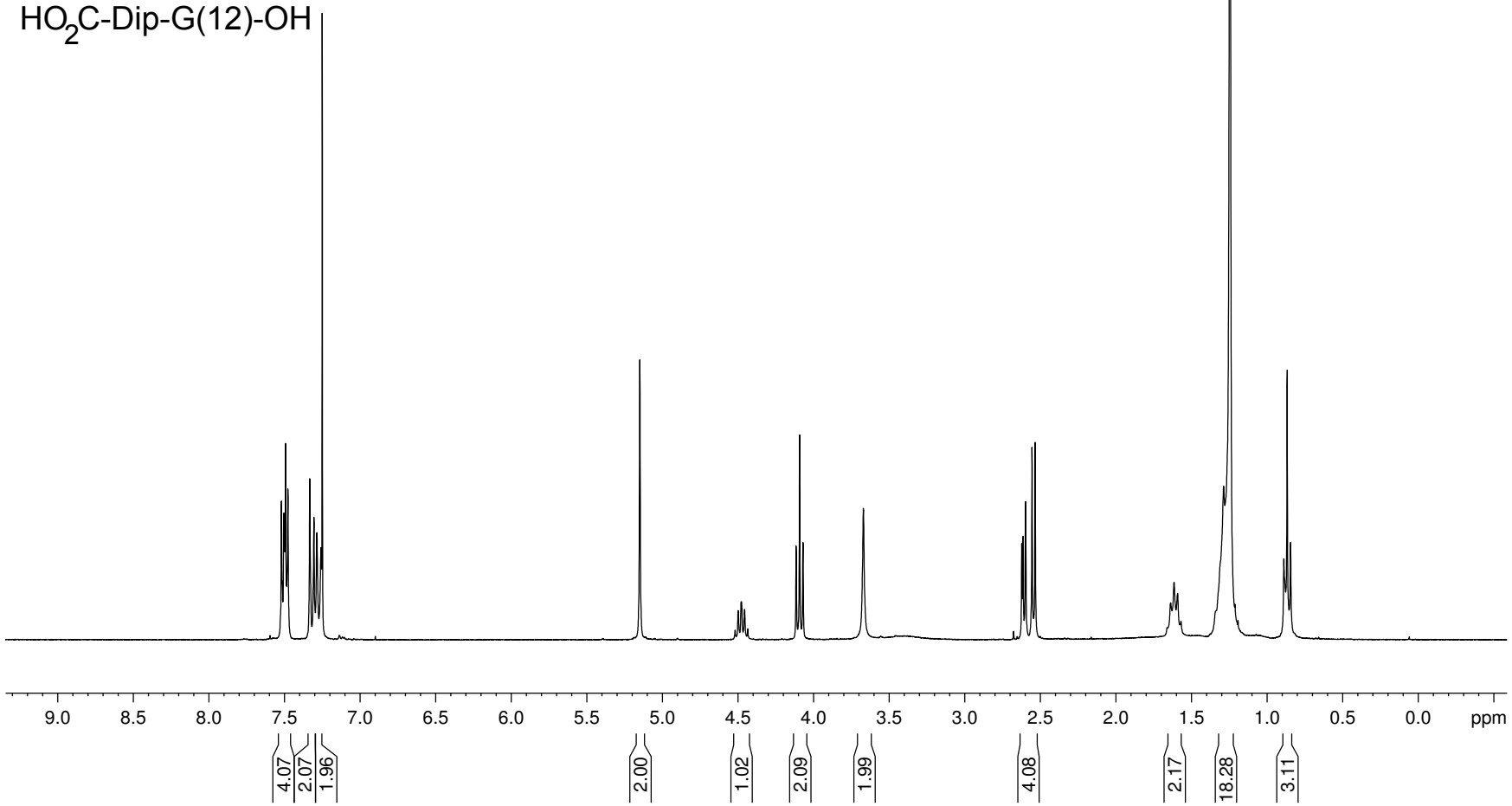

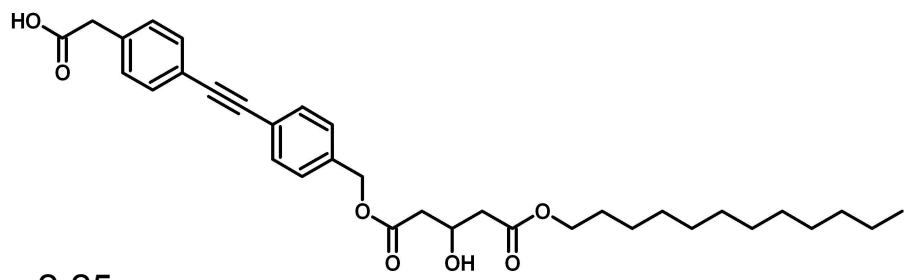

2-25

^{13}C NMR (1:1 $CDCl_3$:CD_3OD) 125MHz

HO_2C-Dip-G(12)-OH

HO_2C-Dip-G(12)-OH

2-25

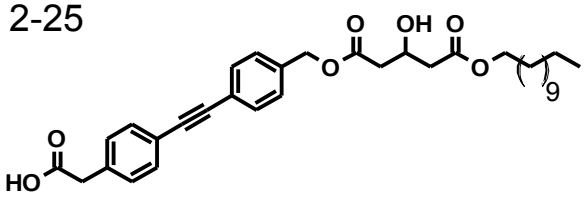

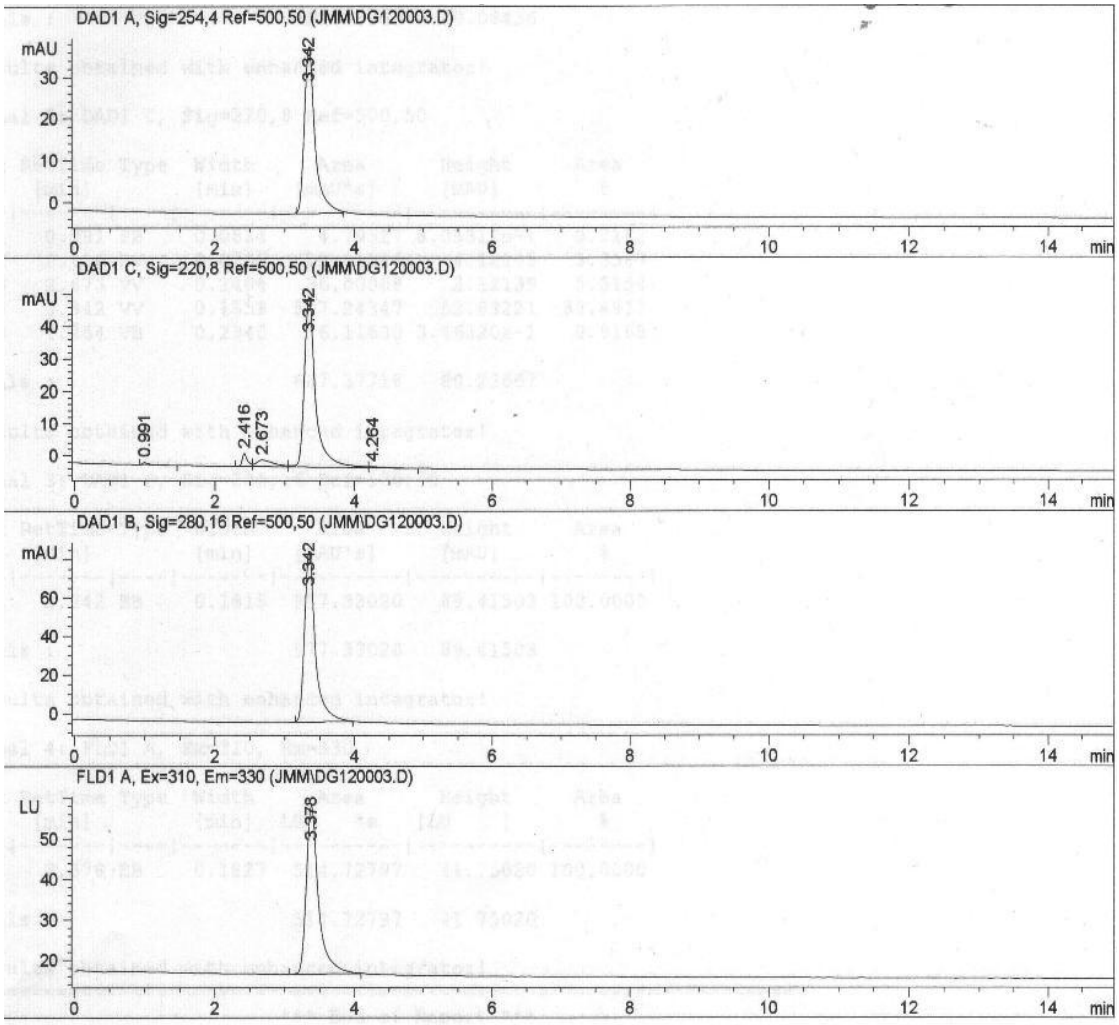

-HPLC trace of sample used for fluorescence and transport studies
-CONDITIONS: HP series 1100 HPLC
-Machery-Nagel RP C18 “Nucleosil” analytical column (4 mm x 250mm)
-3:1 ACN: CH_3OH as eluting solvents, flow 1mL/min

HO_2C-Dip-G(12)-OH

2-25

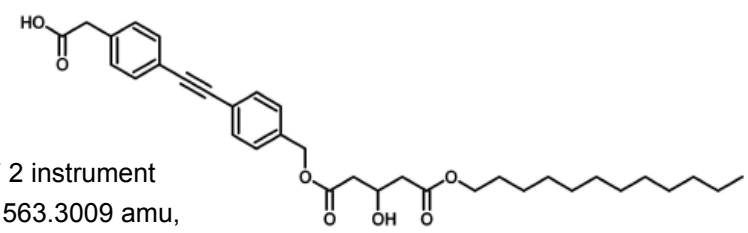

MS: -ve ion ESI, Q-TOF 2 instrument
Calc'd for C34H43O7 = 563.3009 amu,
obtained = 563.3237amu

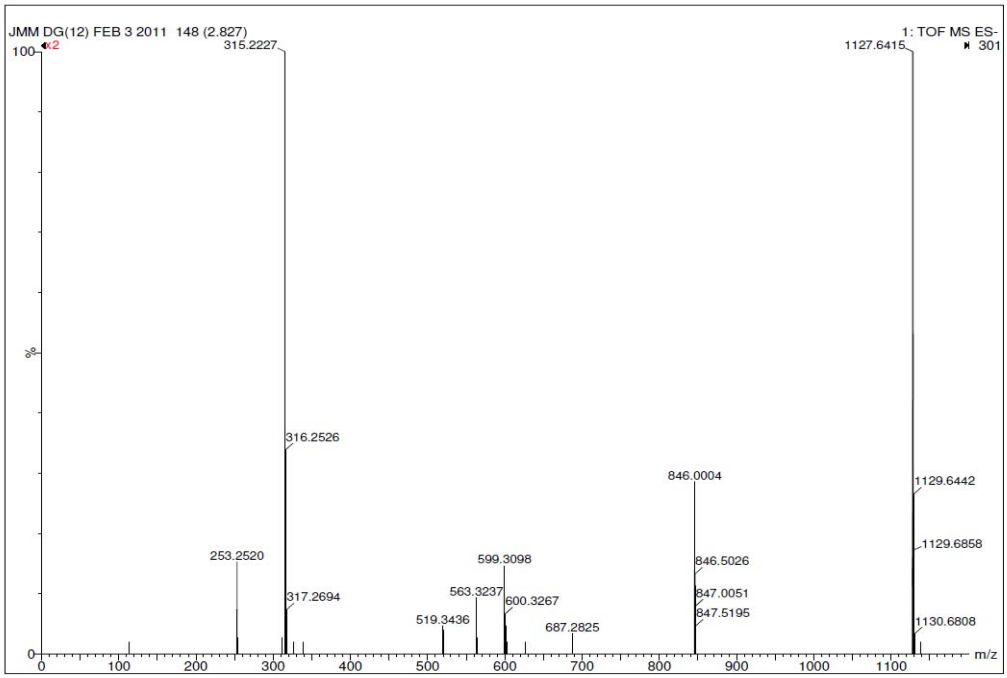

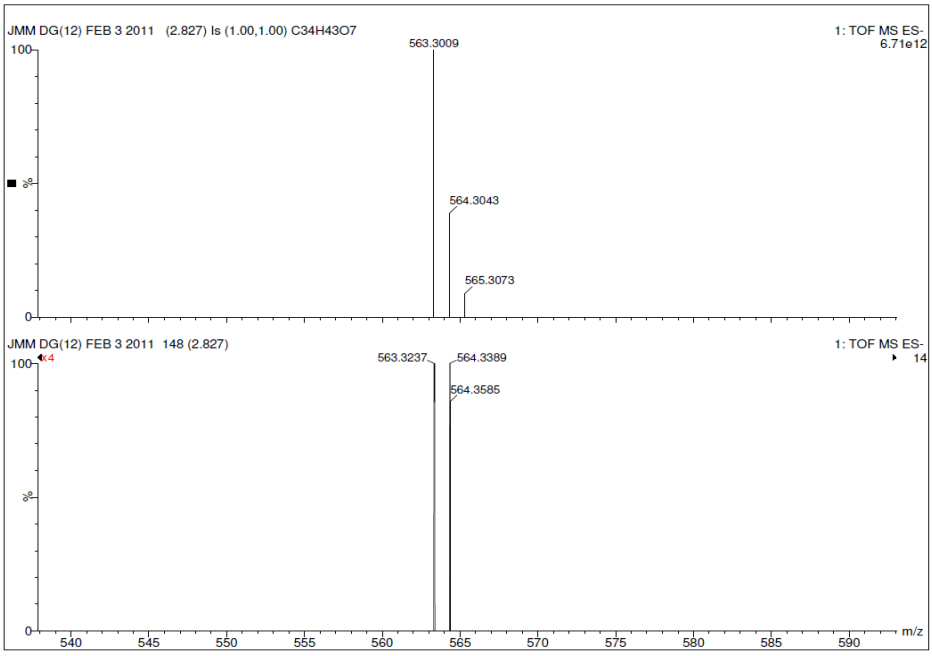

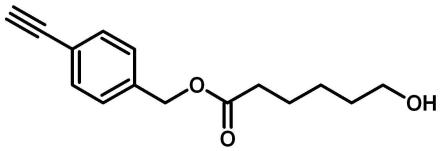

4-1

^{1}H NMR ($CDCl_3$) 300MHz

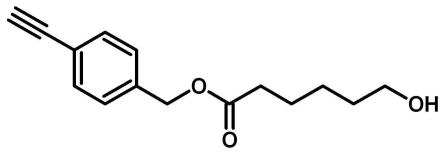

4-1

^{13}C NMR ($CDCl_3$) 75 MHz

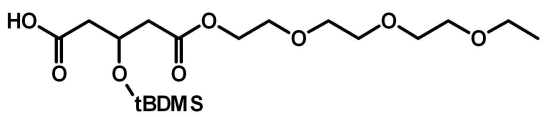

3-20

^{1}H NMR ($CDCl_3$) 300MHz

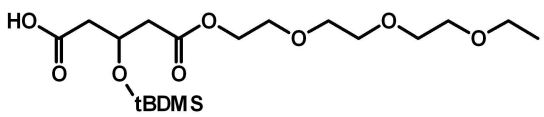

3-20

^{13}C NMR ($CDCl_3$) 75 MHz

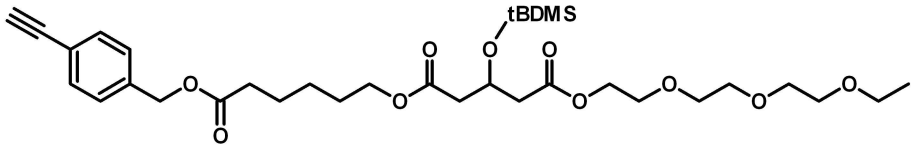

A-16

^{1}H NMR ($CDCl_3$) 300MHz

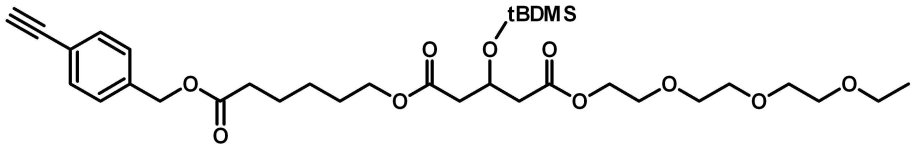

A-16

^{13}C NMR ($CDCl_3$) 75 MHz

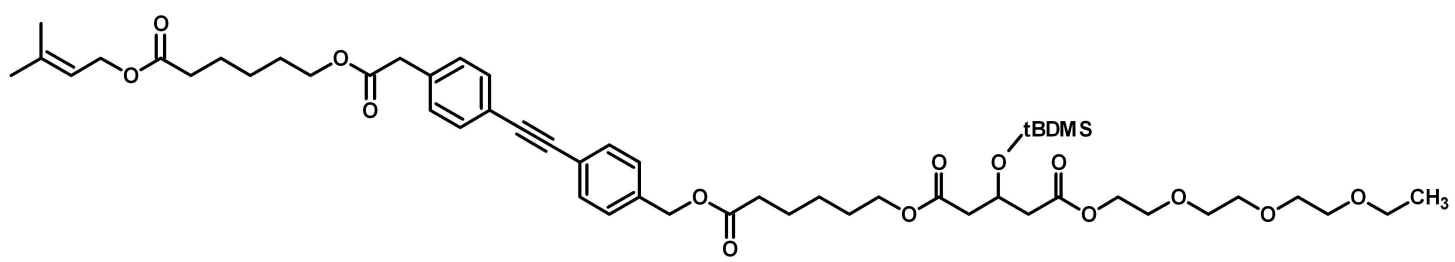

A-17

^{1}H NMR ($CDCl_3$) 300MHz

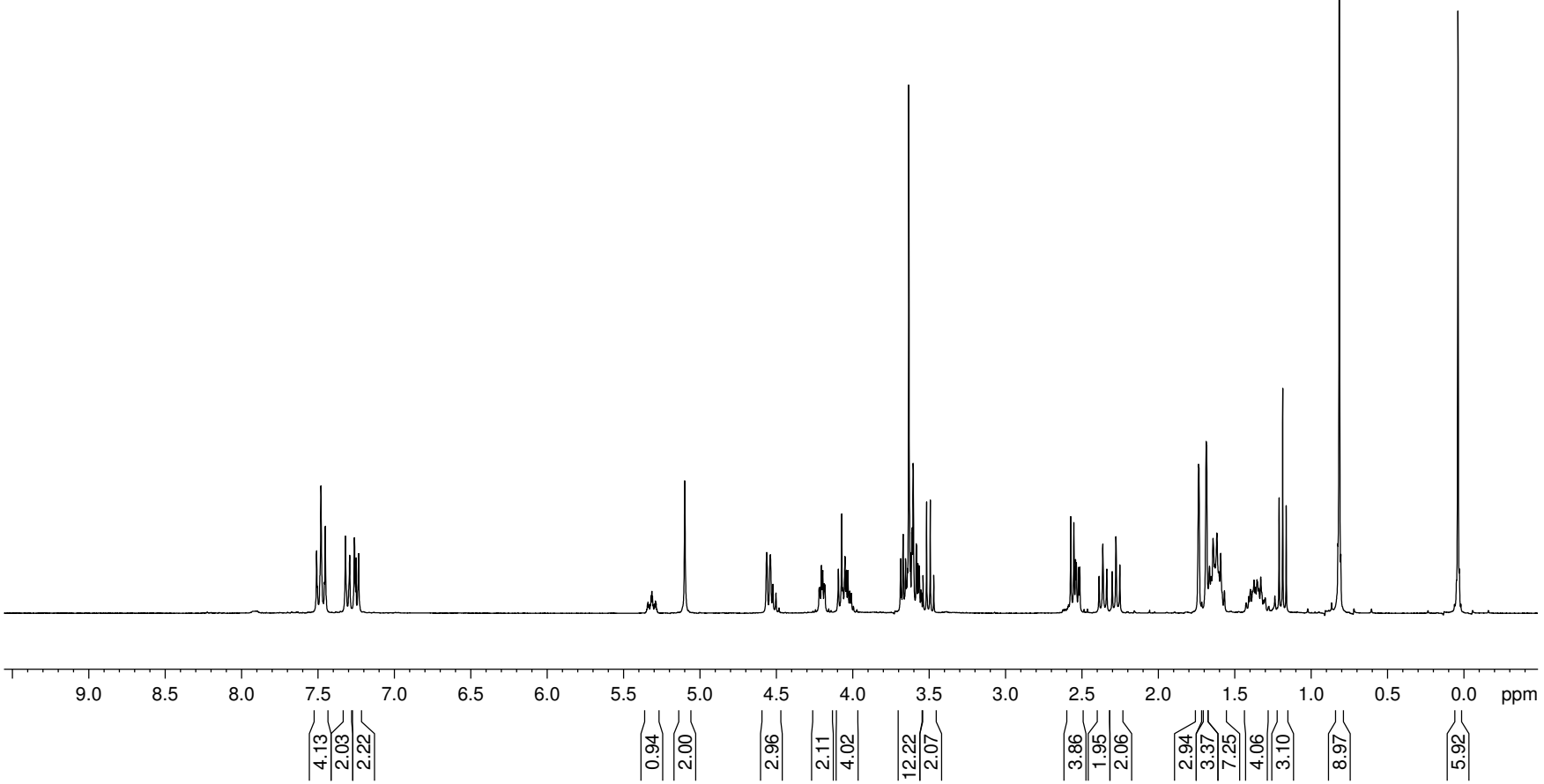

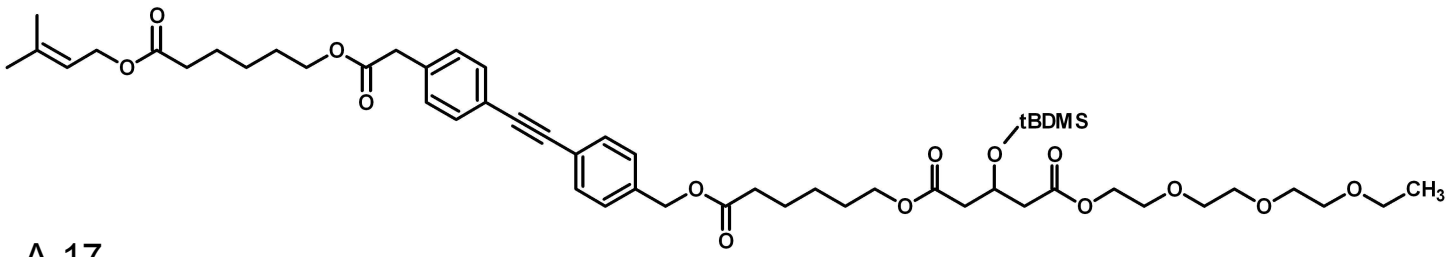

A-17

^{13}C NMR ($CDCl_3$) 75 MHz

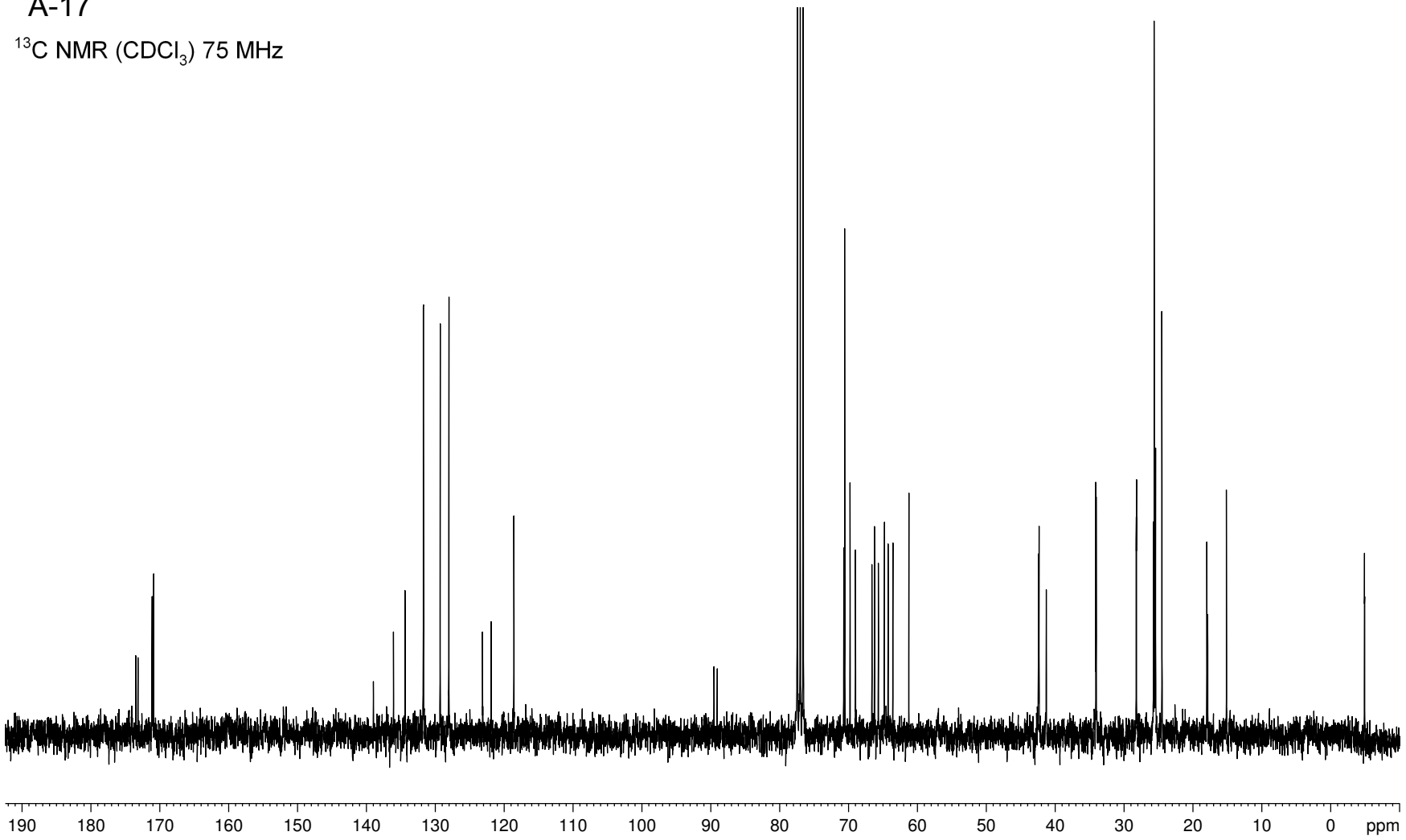

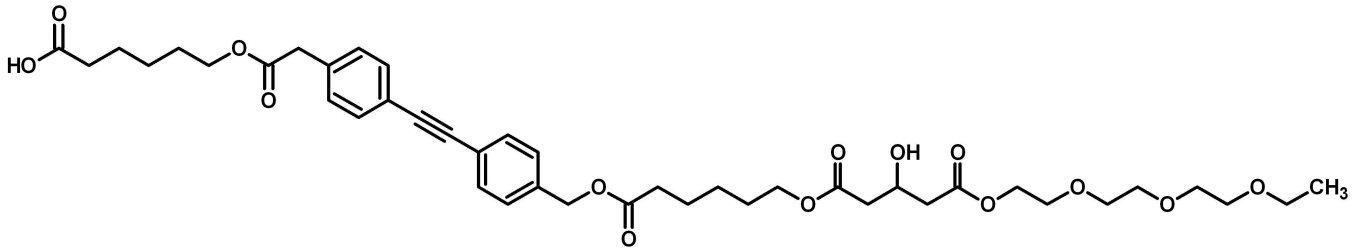

2-26

^{1}H NMR ($CDCl_3$) 300MHz

HO_2C-Hex-Dip-Hex-G(E3)-OH

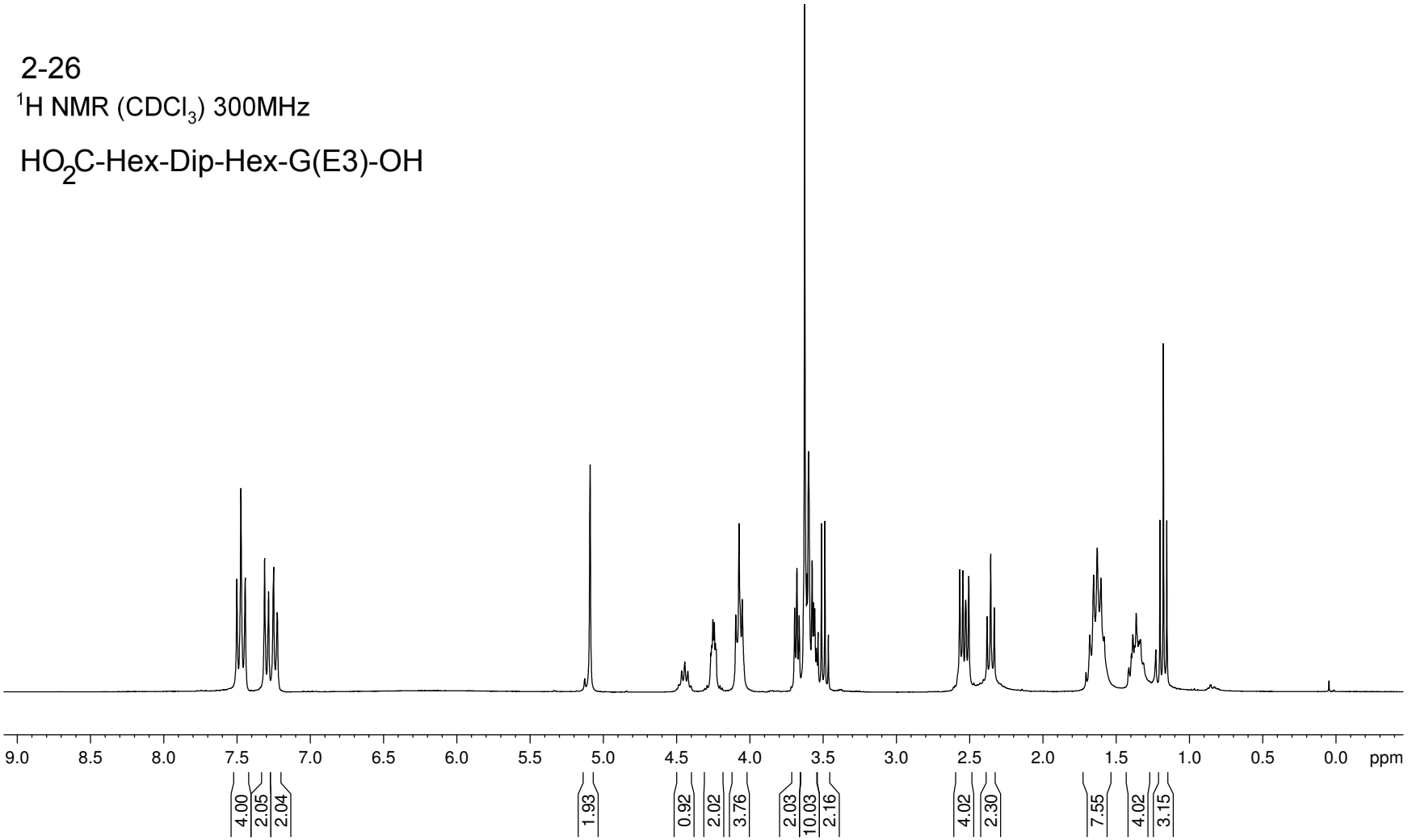

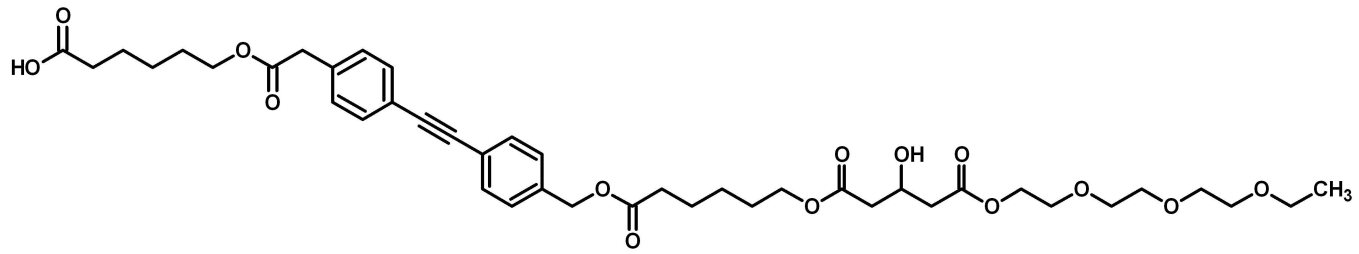

2-26

^{13}C NMR ($CDCl_3$) 75 MHz

HO_2C-Hex-Dip-Hex-G(E3)-OH

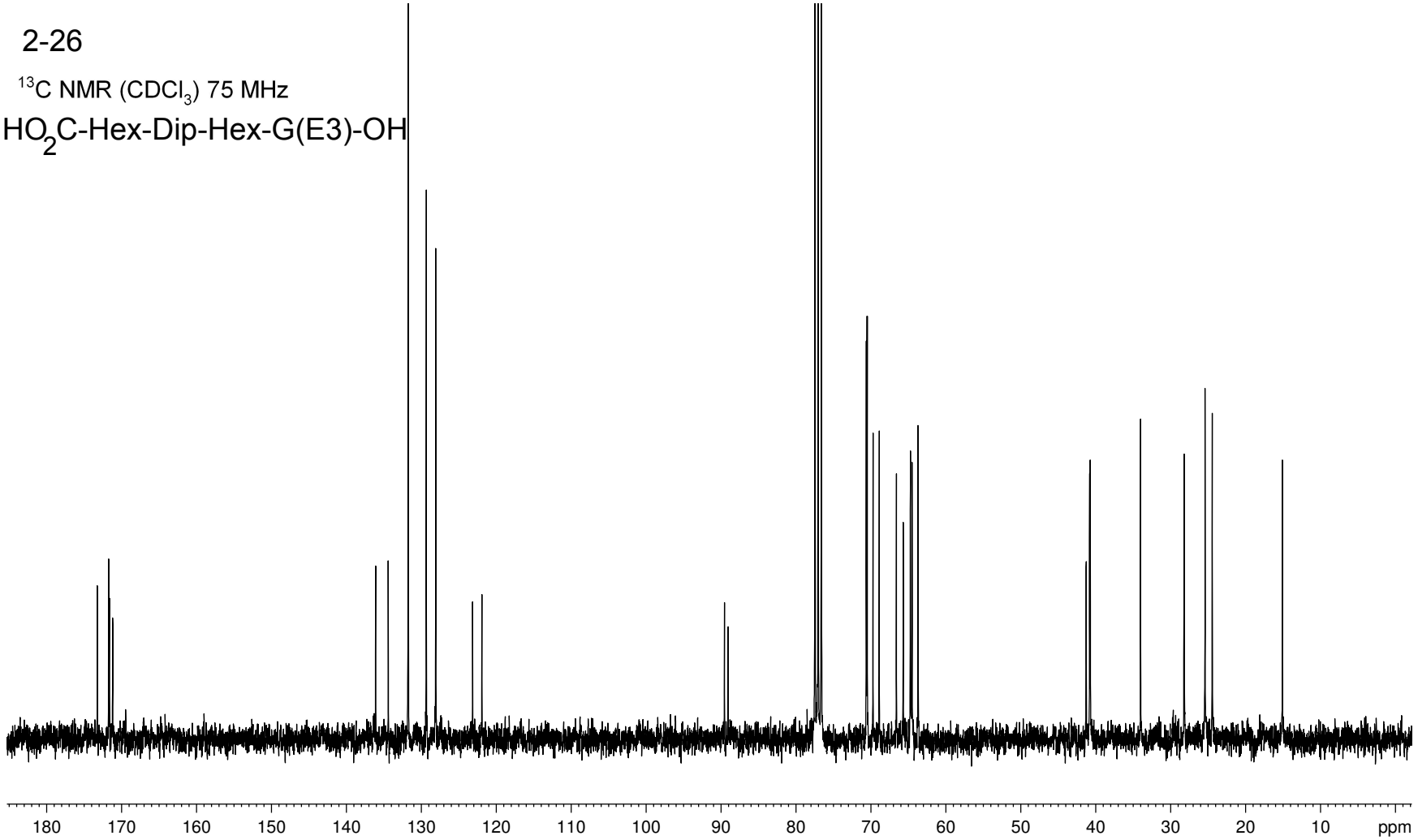

HO_2C-Hex-Dip-Hex-G(E3)-OH

2-26

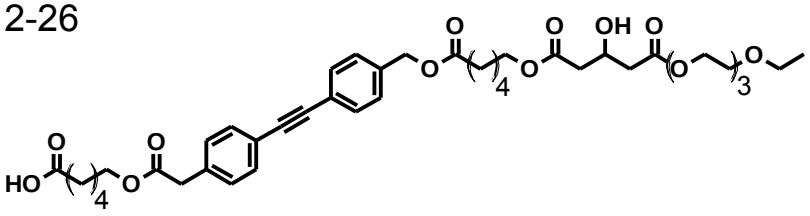

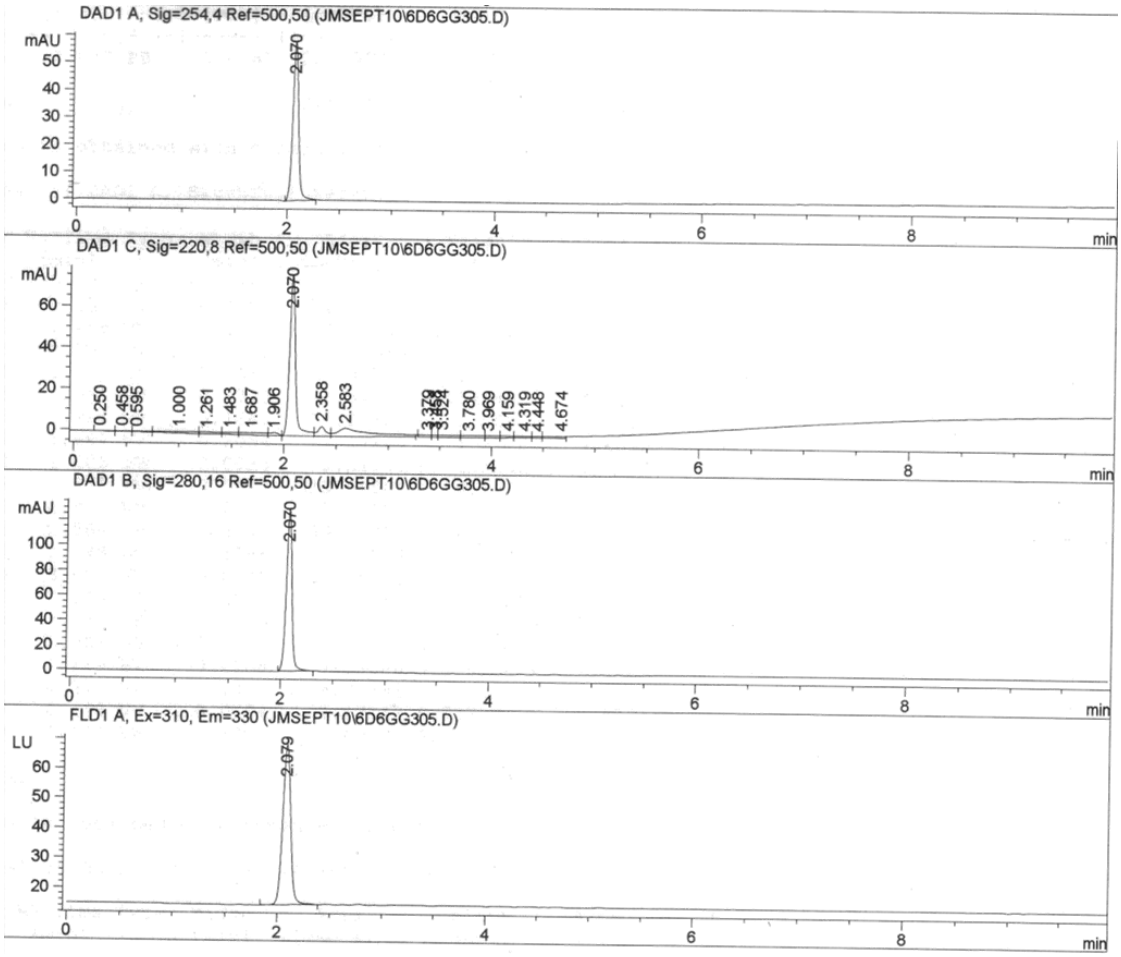

-HPLC trace of sample used for fluorescence and transport studies
-CONDITIONS: HP series 1100 HPLC
-Machery-Nagel RP C18 “Nucleosil” analytical column (4 mm x 250mm)
-1:1 ACN: CH_3OH as eluting solvents, flow 1mL/min

HO_2C-Hex-Dip-Hex-G(E3)-OH

MS: -ve ESI, Q-TOF 2
calc'd for C42H55O14 = 783.3597 amu,
obtained = 783.3397 amu.

2-26

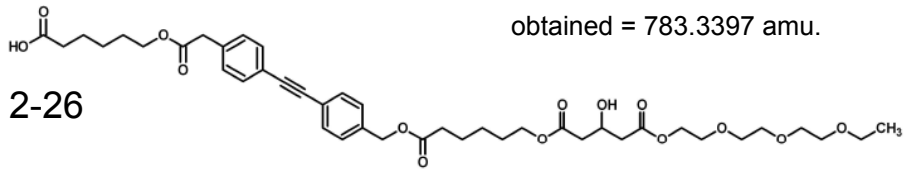

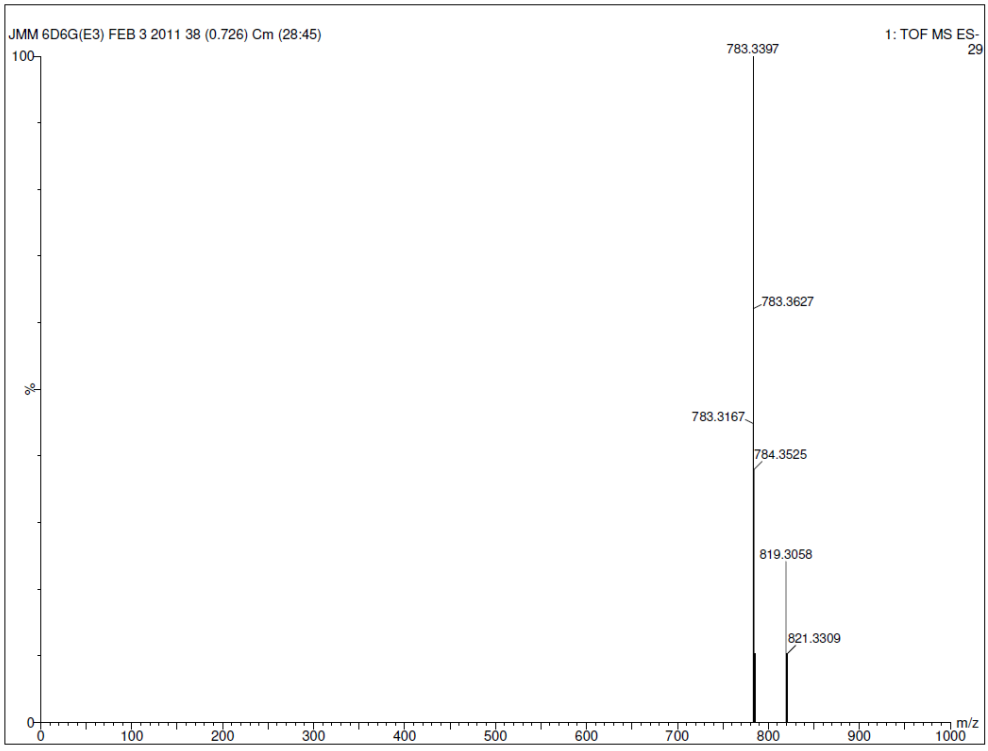

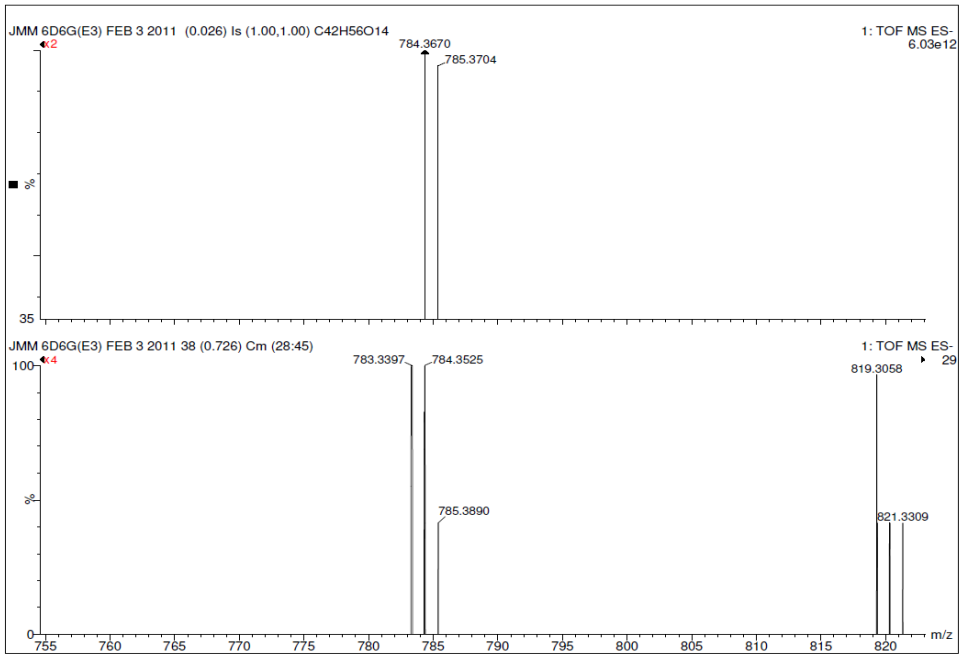

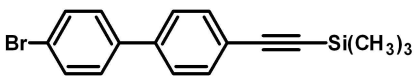

3-4

^{1}H NMR ($CDCl_3$) 300MHz

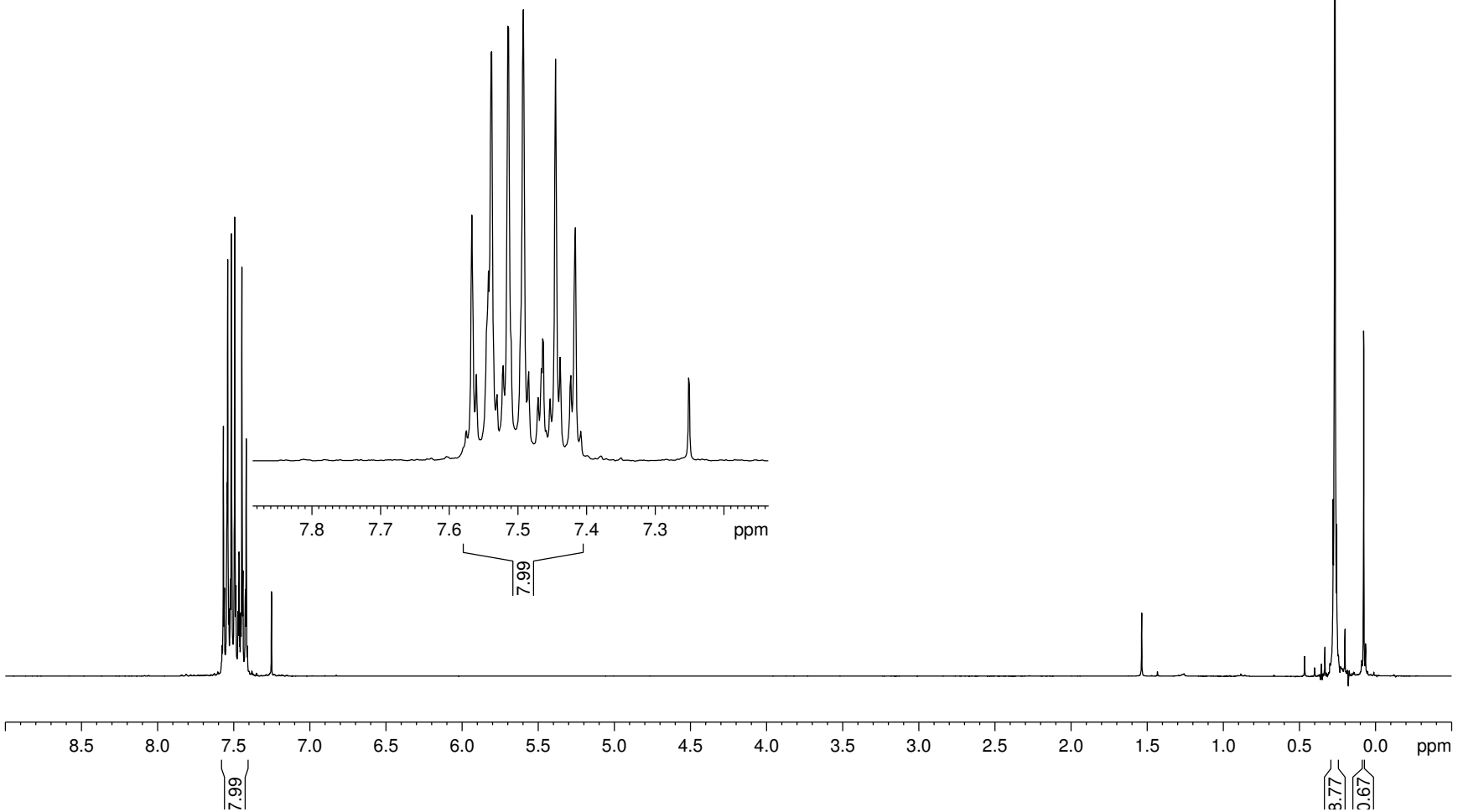

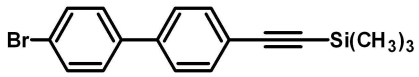

3-4

^{13}C NMR ($CDCl_3$) 75 MHz

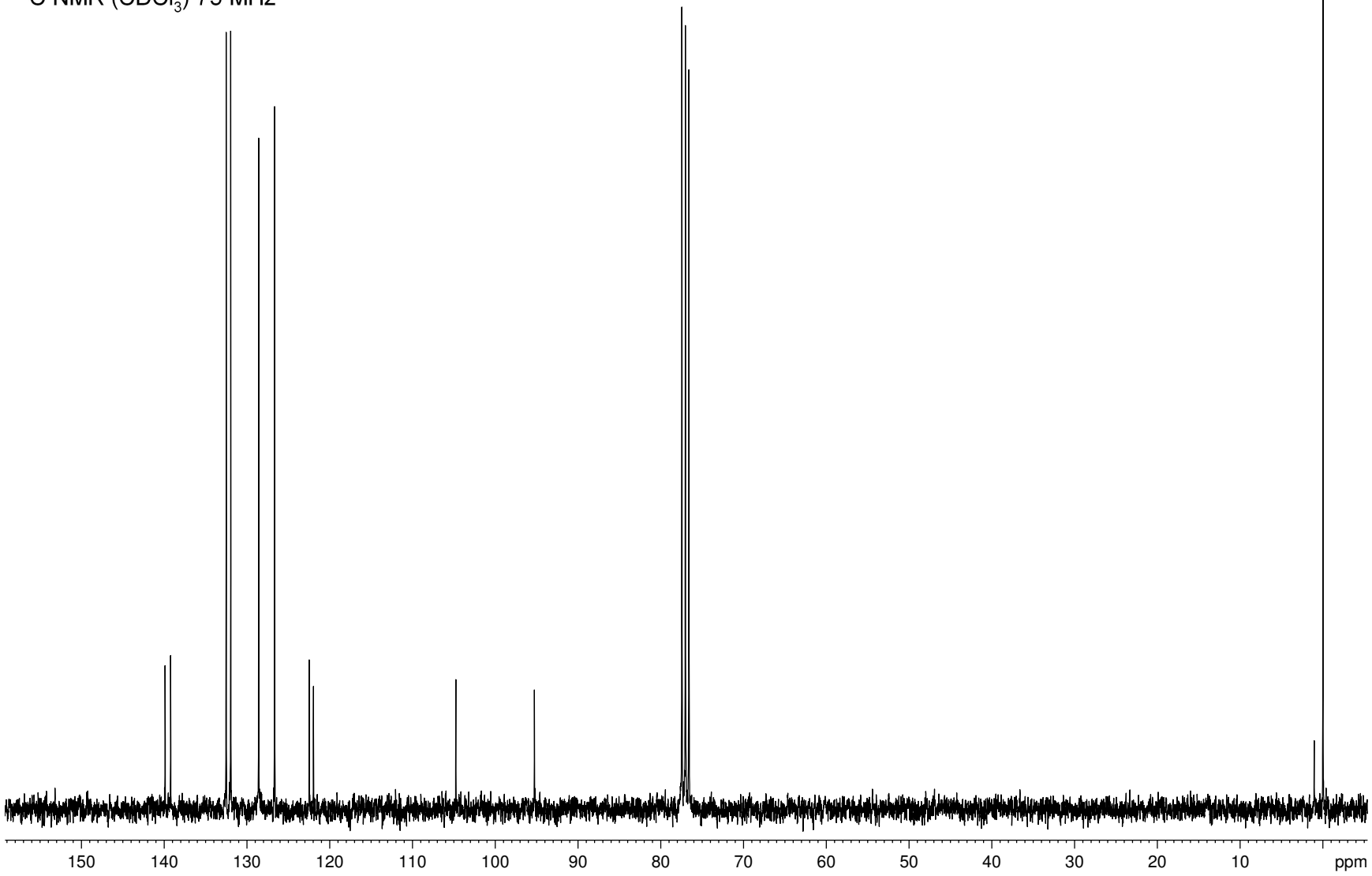

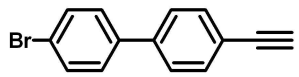

3-5

^{1}H NMR ($CDCl_3$) 300MHz

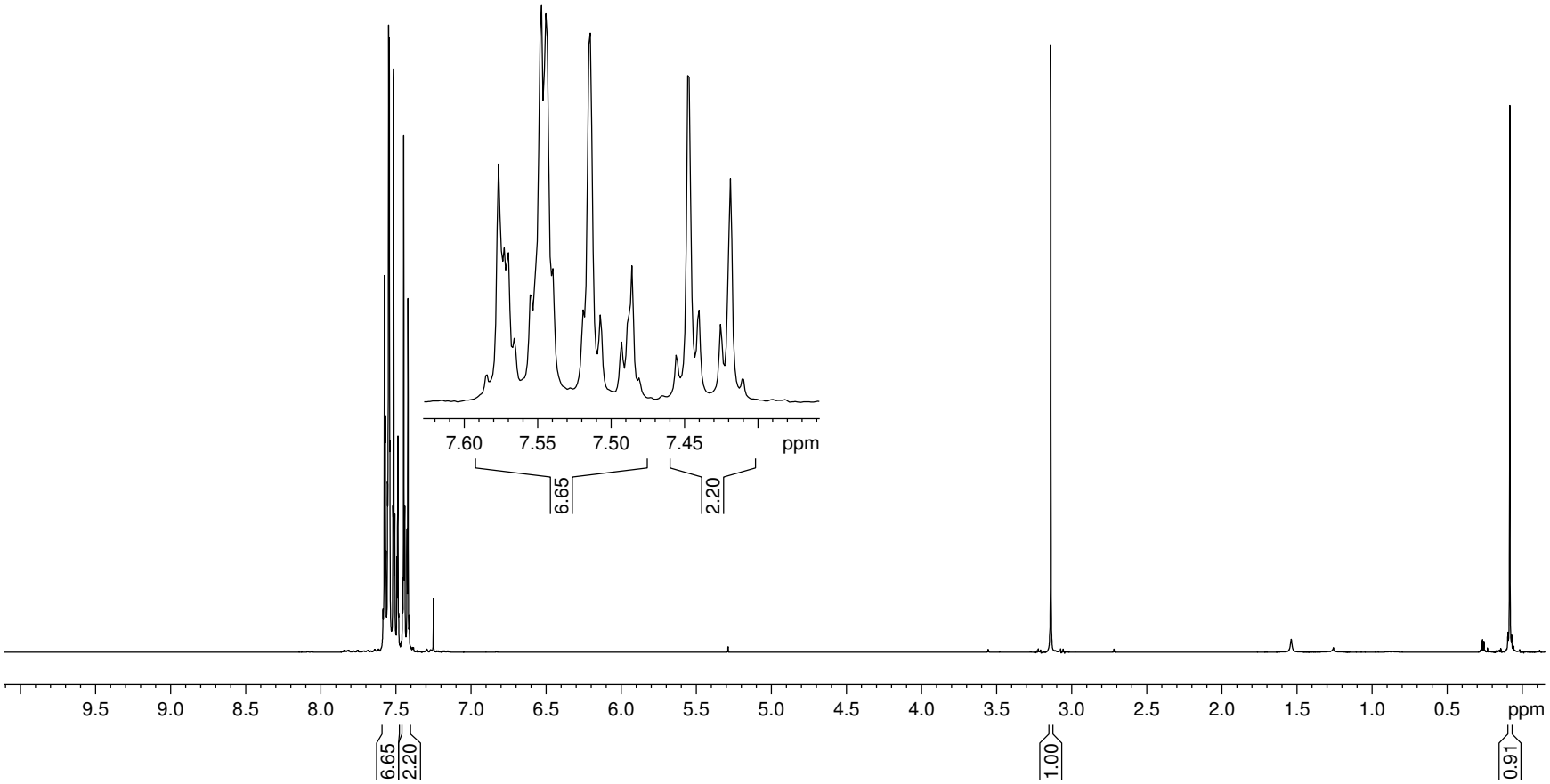

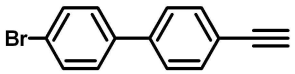

3-5

^{13}C NMR ($CDCl_3$) 75 MHz

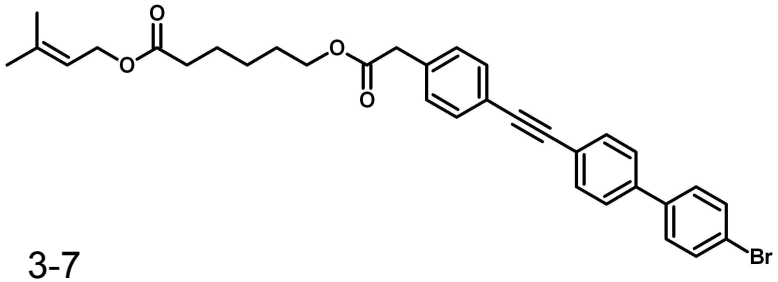

3-7

^{1}H NMR ($CDCl_3$) 300MHz

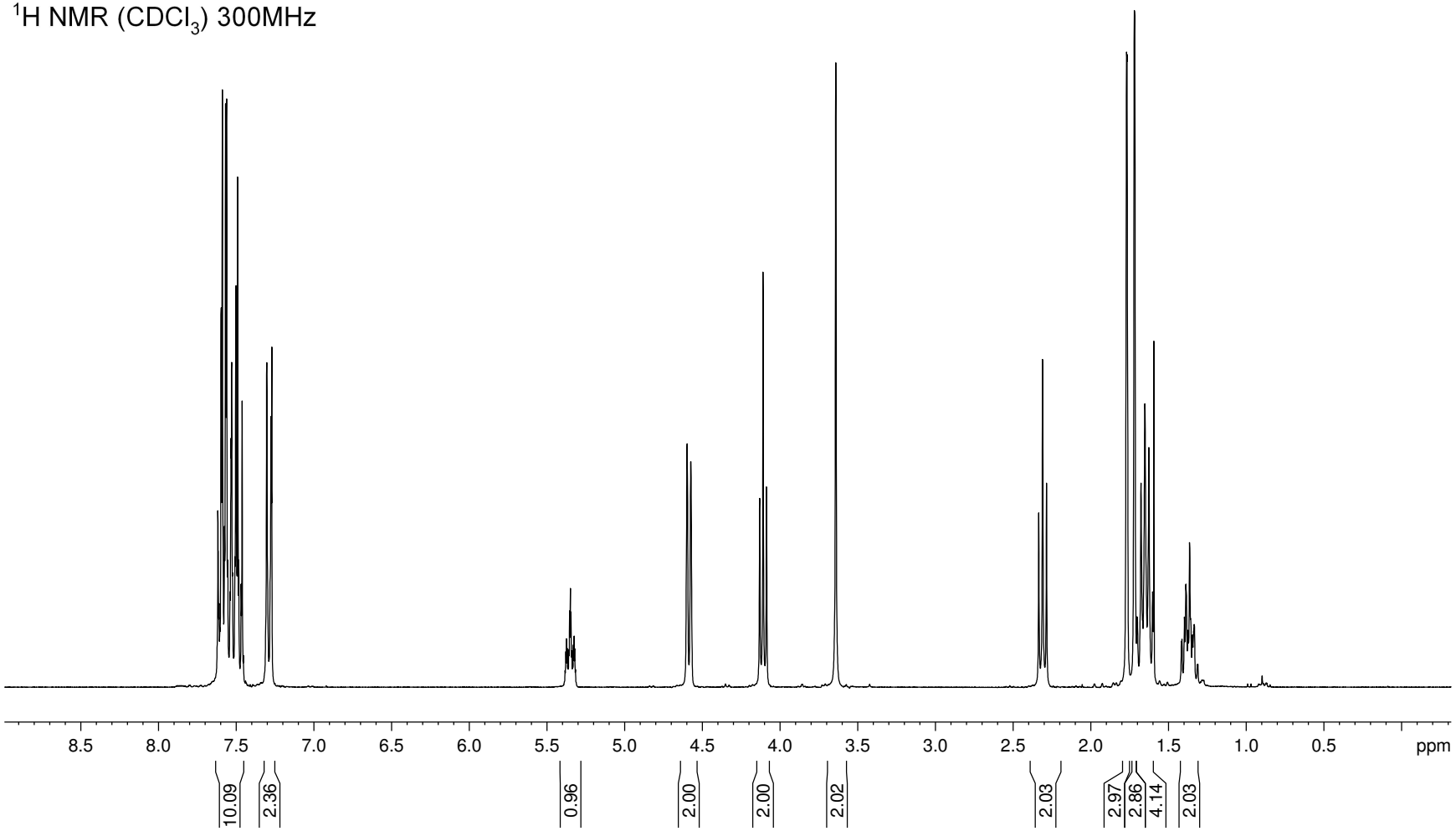

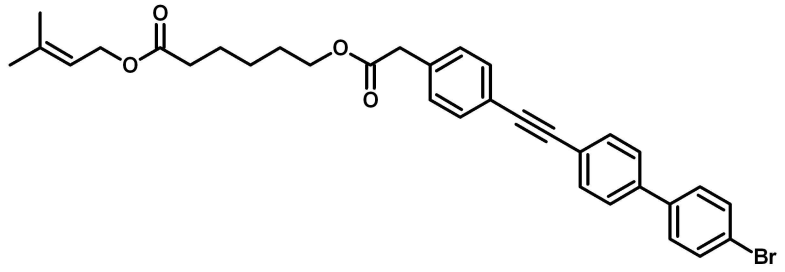

3-7

^{13}C NMR ($CDCl_3$) 75 MHz

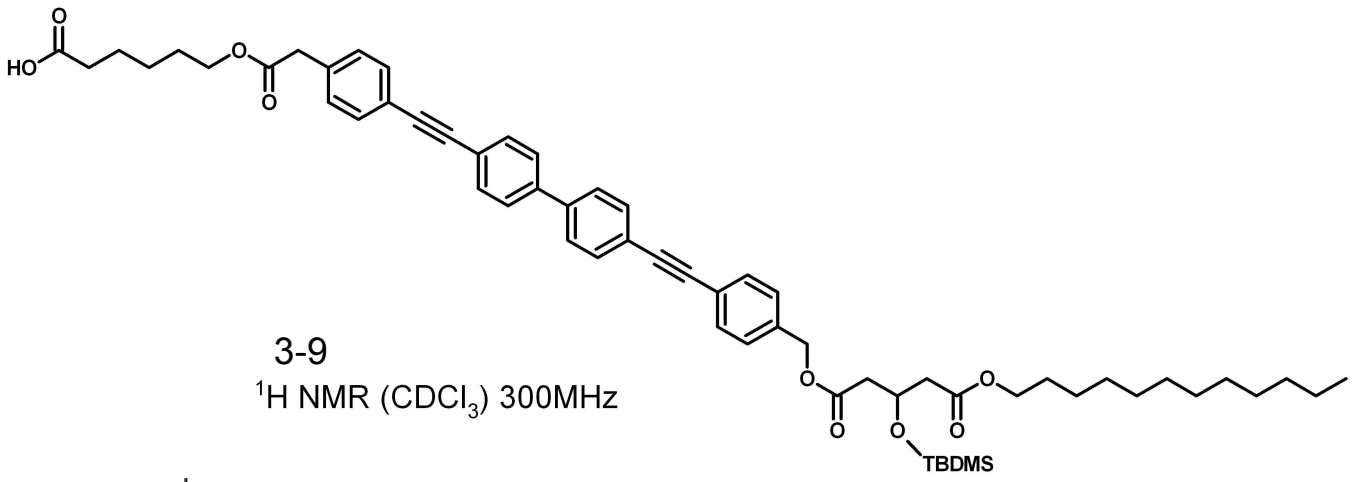

3-9

^{1}H NMR ($CDCl_3$) 300MHz

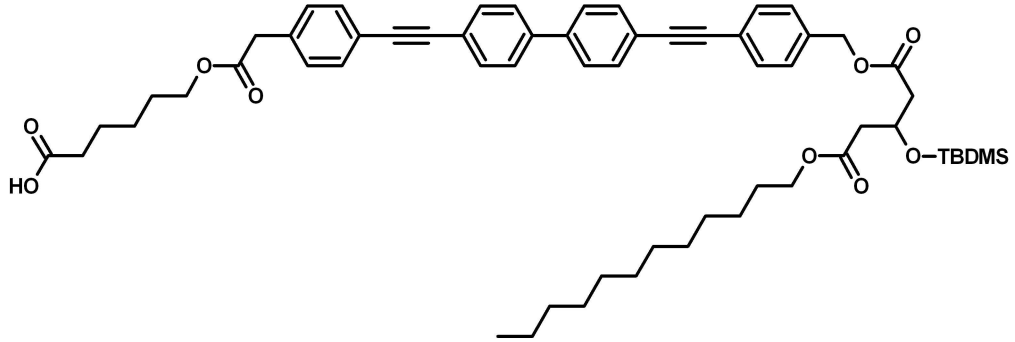

3-9

^{13}C NMR ($CDCl_3$) 75 MHz

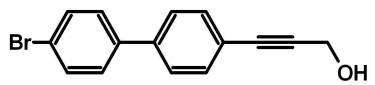

3-13

^{1}H NMR ($CDCl_3$) 300MHz

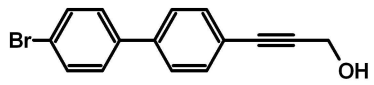

3-13

^{13}C NMR ($CDCl_3$) 75 MHz

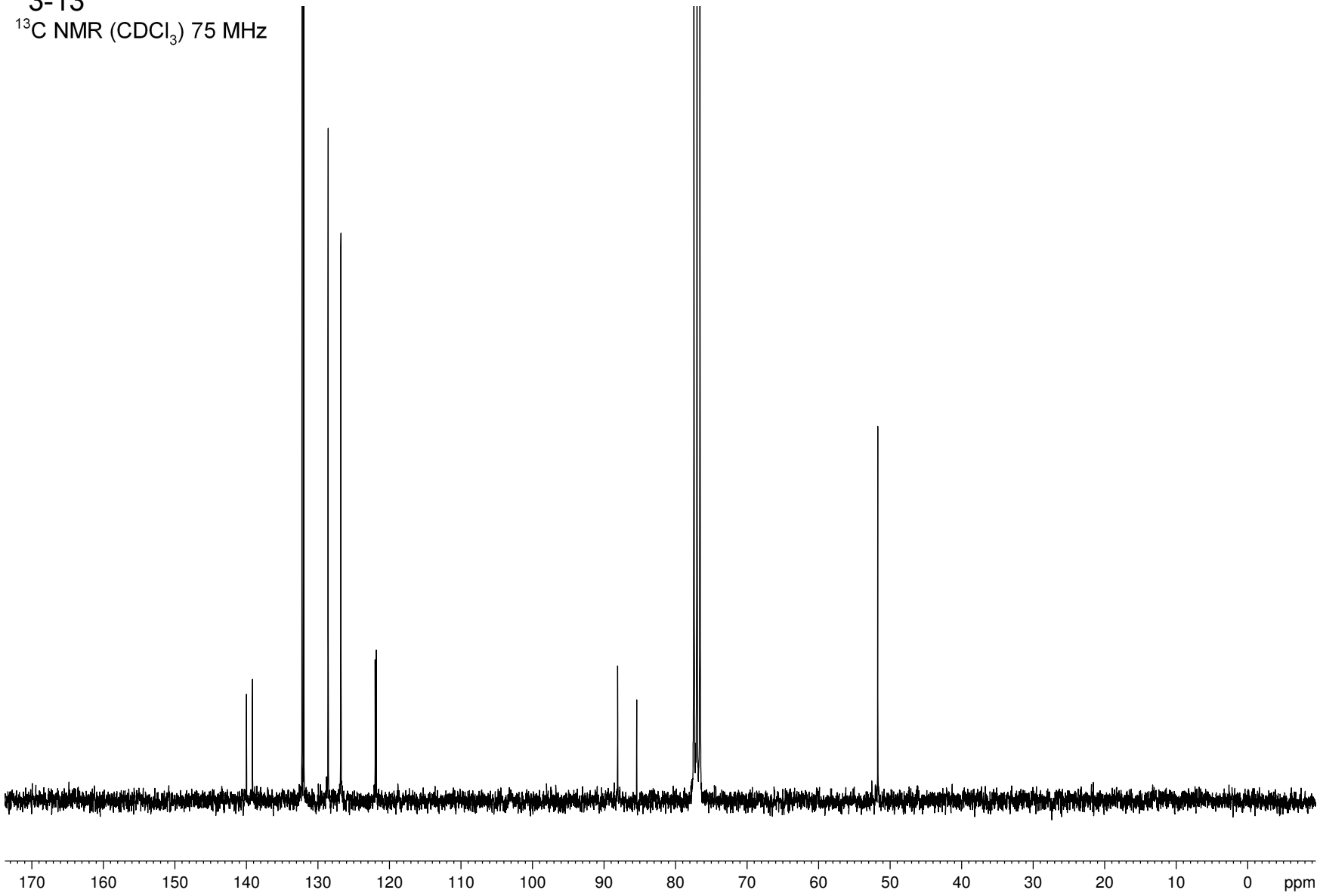

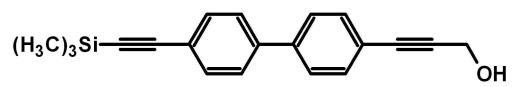

3-14

^{1}H NMR ($CDCl_3$) 300MHz

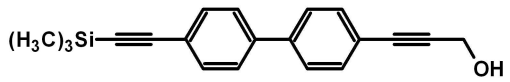

3-14

^{13}C NMR ($CDCl_3$) 75 MHz

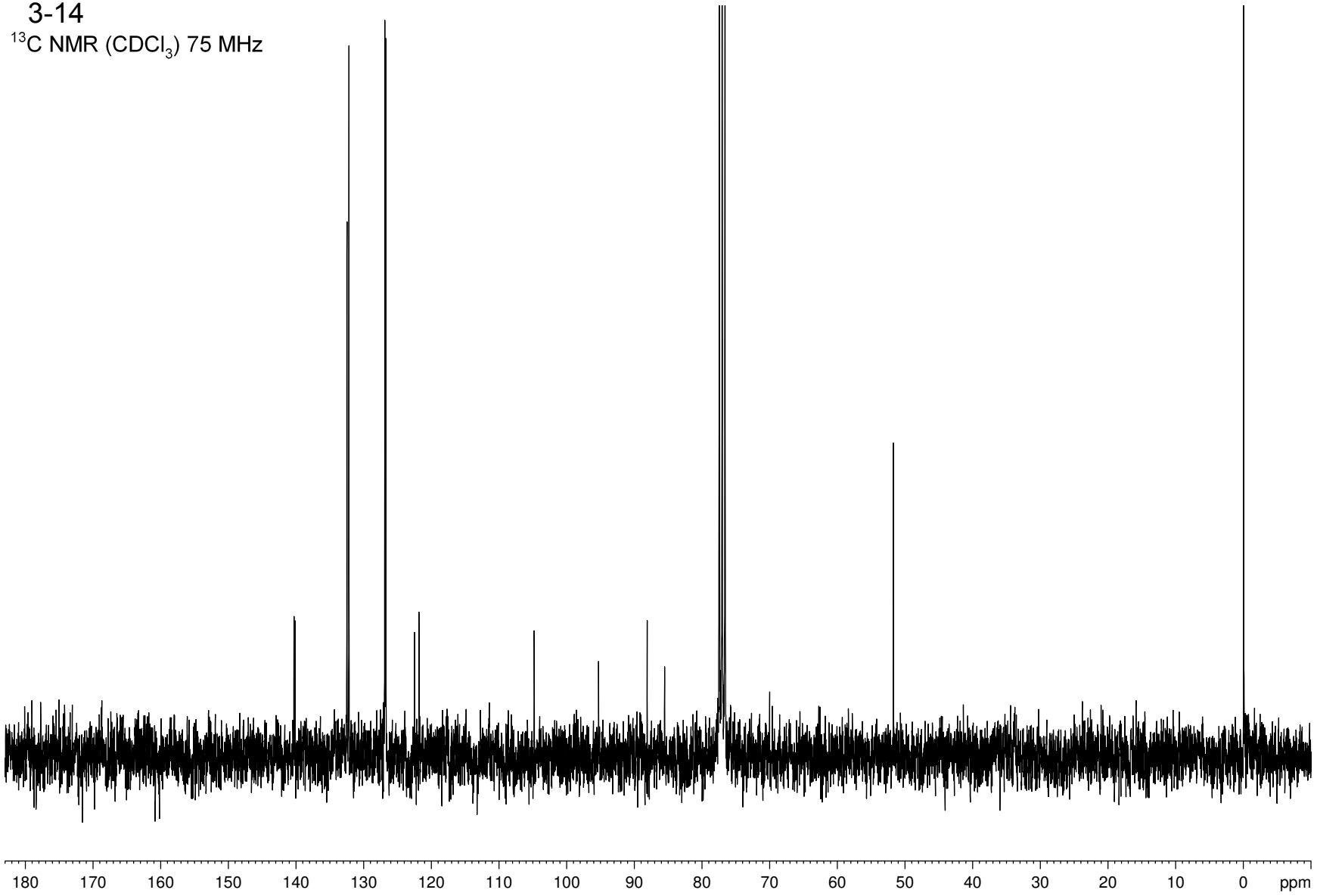

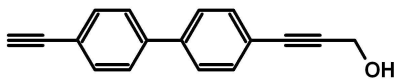

3-15

^{1}H NMR ($CDCl_3$) 300MHz

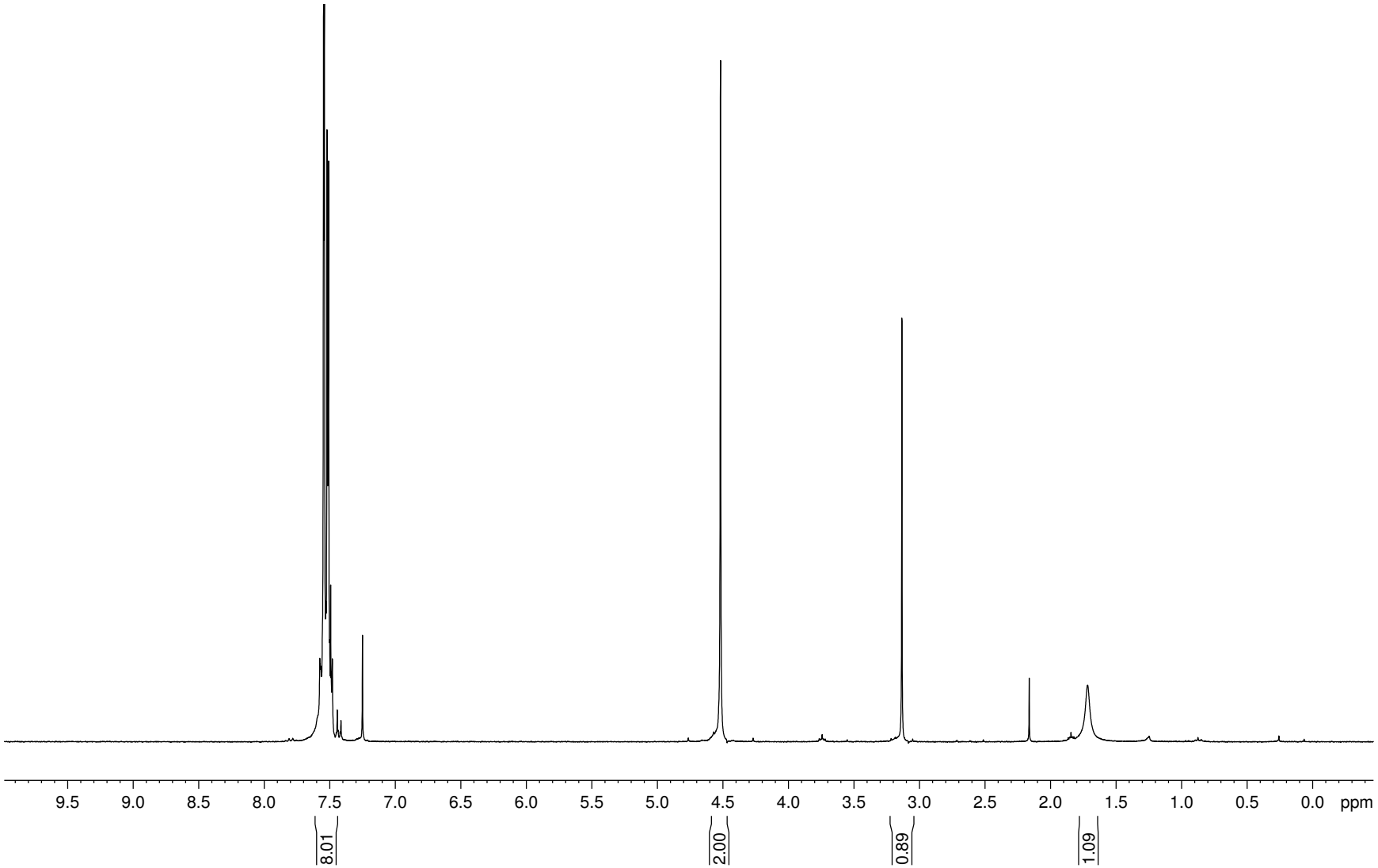

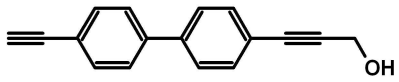

3-15

^{13}C NMR ($CDCl_3$) 75 MHz

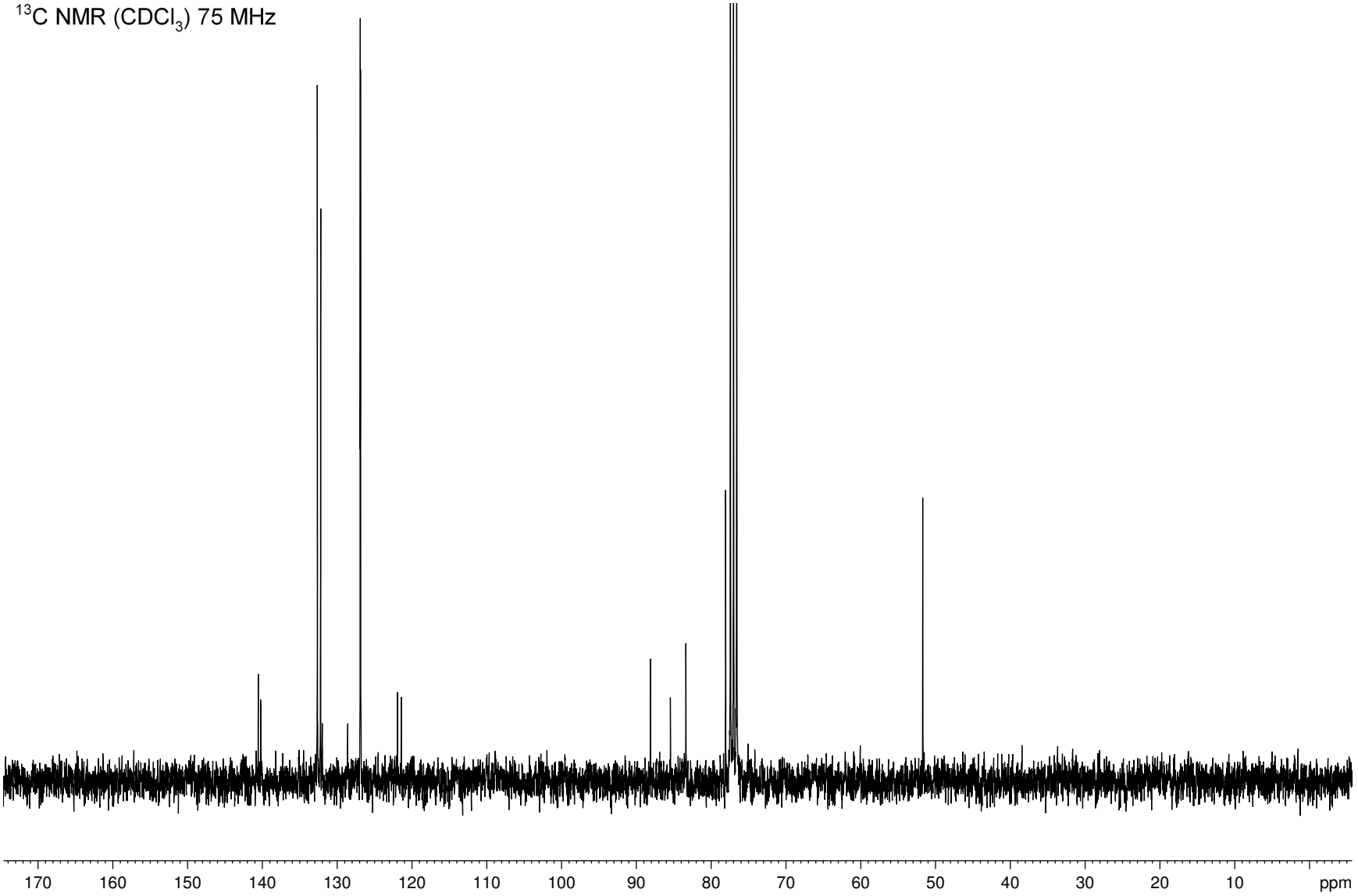

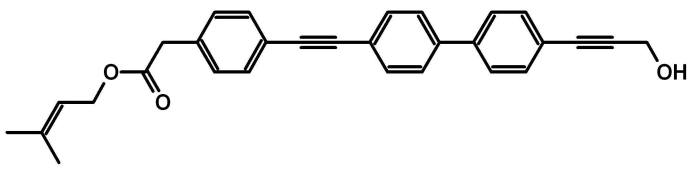

3-17

^{1}H NMR ($CDCl_3$) 300MHz

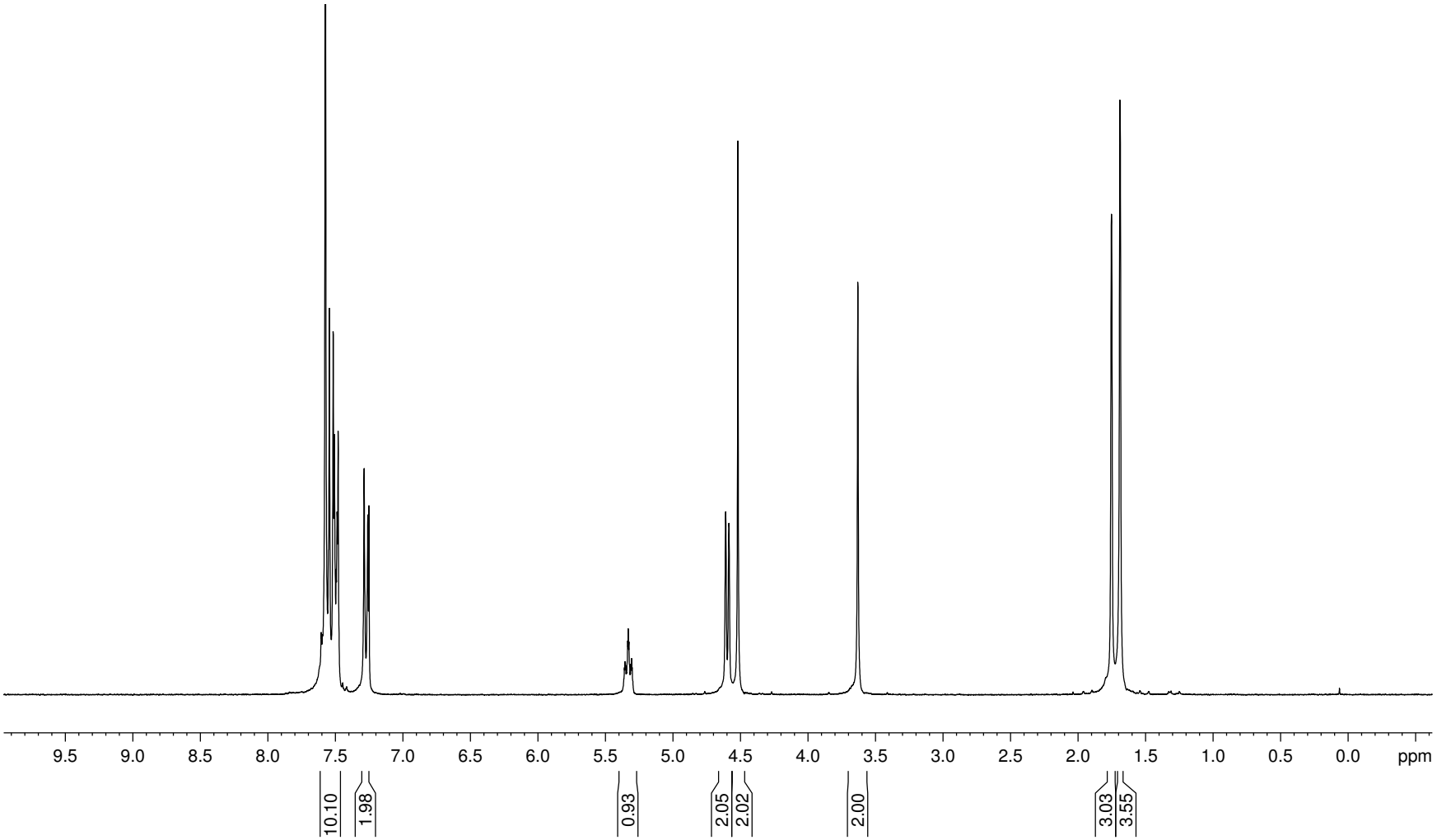

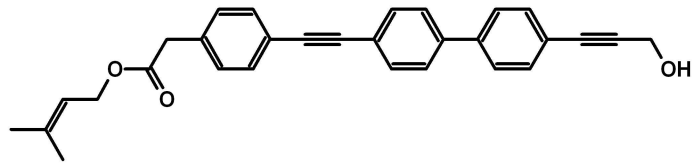

3-17

^{13}C NMR ($CDCl_3$) 75 MHz

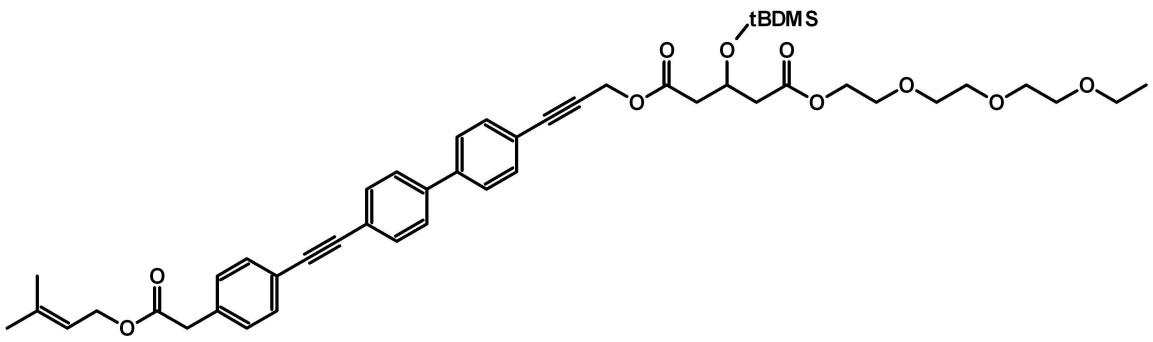

3-21

^{1}H NMR ($CDCl_3$) 300MHz

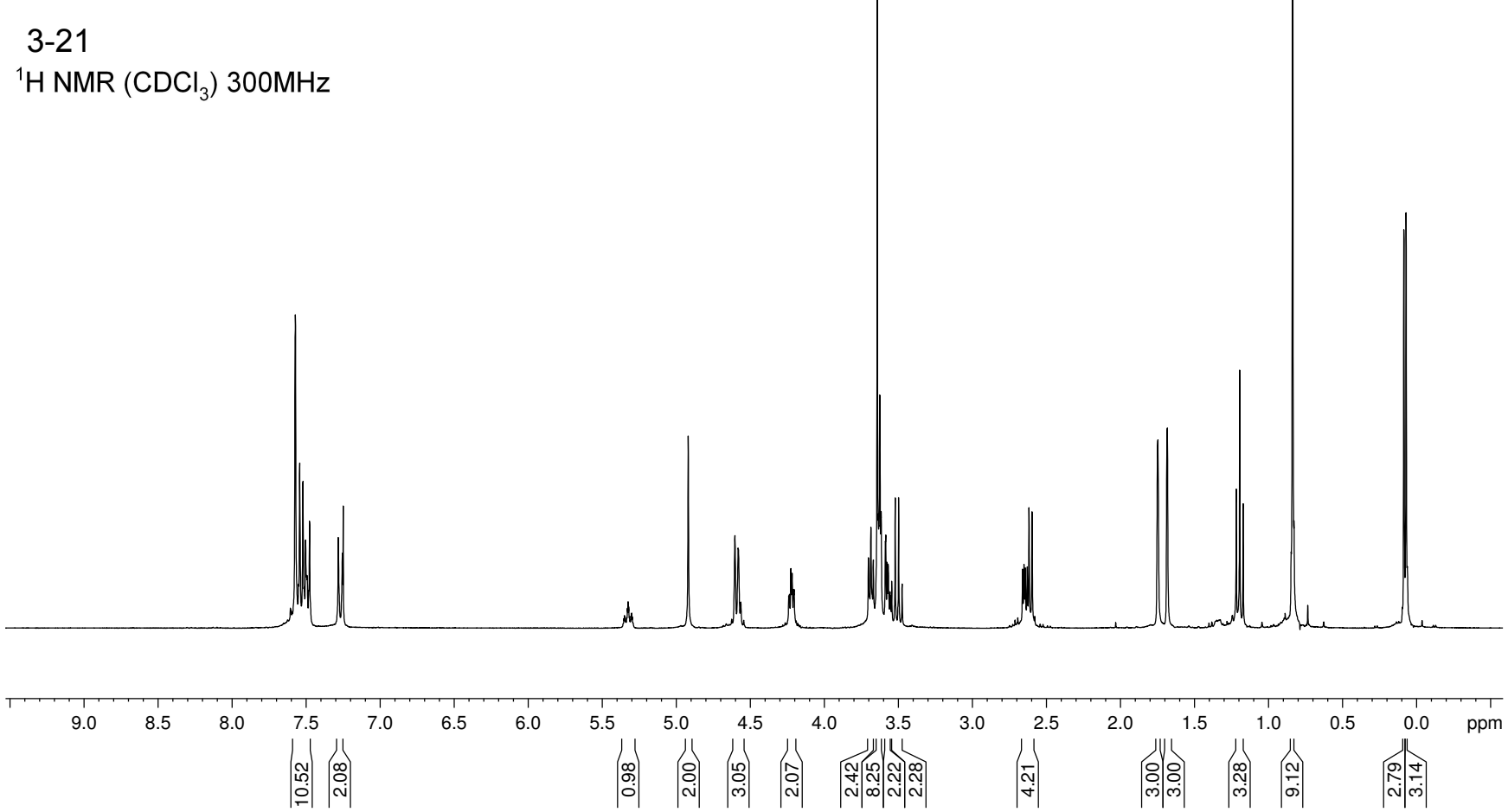

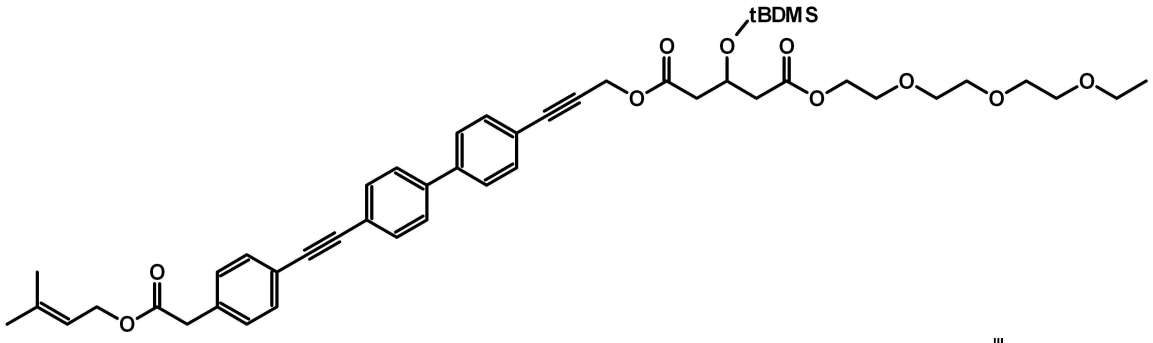

3-21

^{13}C NMR ($CDCl_3$) 75 MHz

^{1}H NMR ($CDCl_3$) 300MHz

HO_2C-Trip-G(E3)-OH

3-22

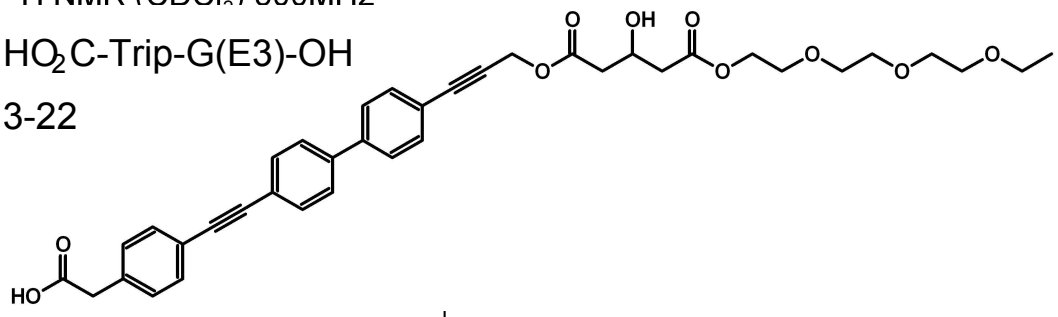

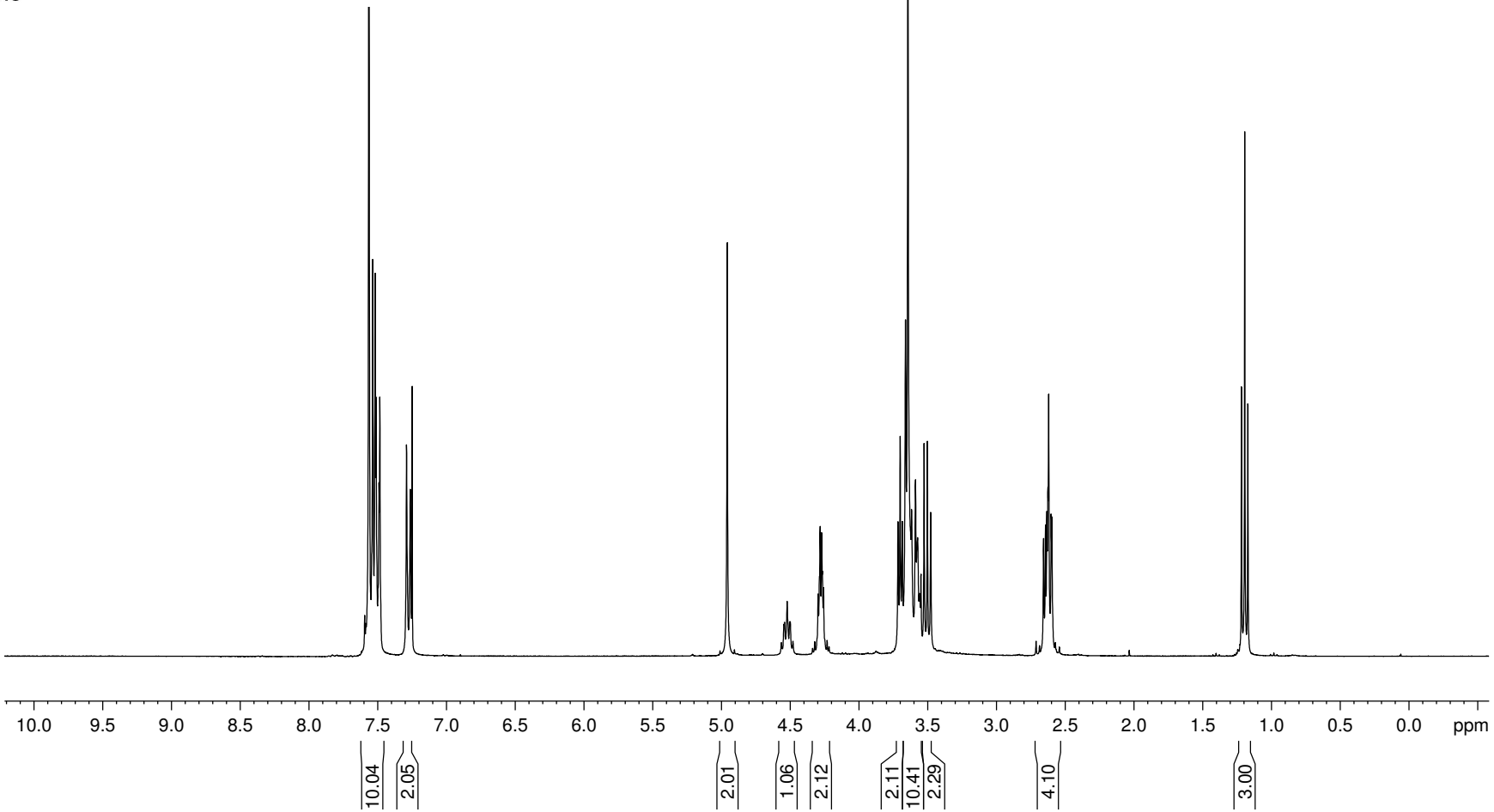

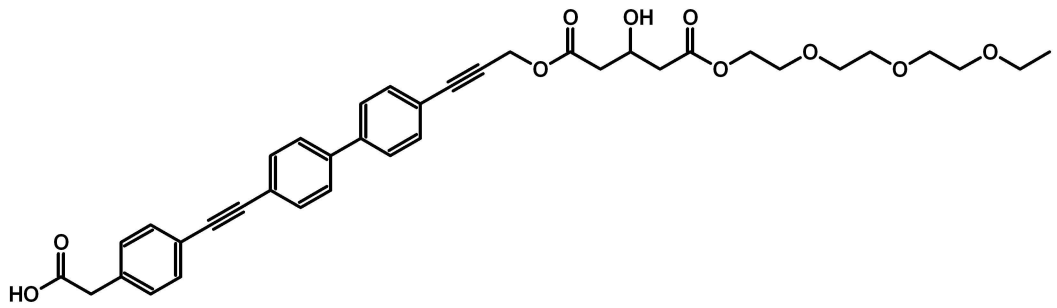

HO_2C-Trip-G(E3)-OH

3-22

^{13}C NMR ($CDCl_3$) 75 MHz

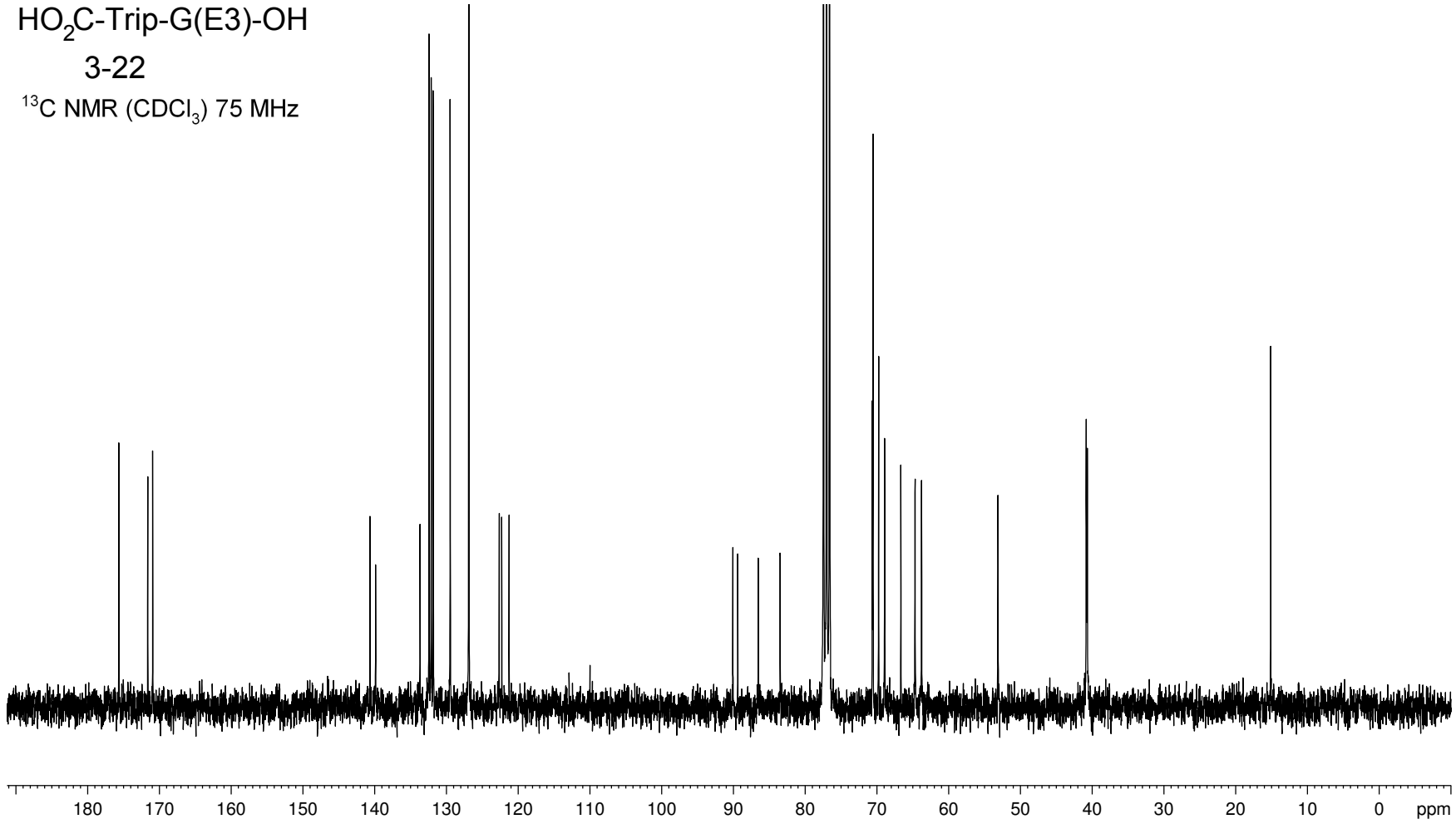

HO_2C-Trip-G(E3)-OH

3-22

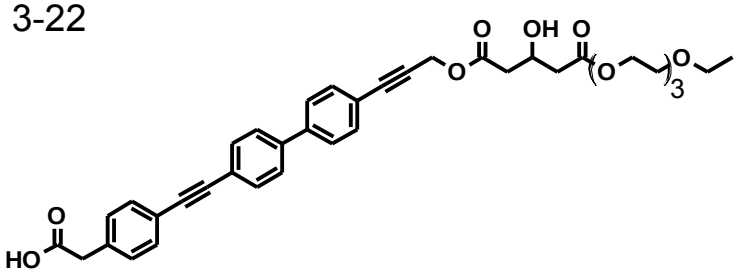

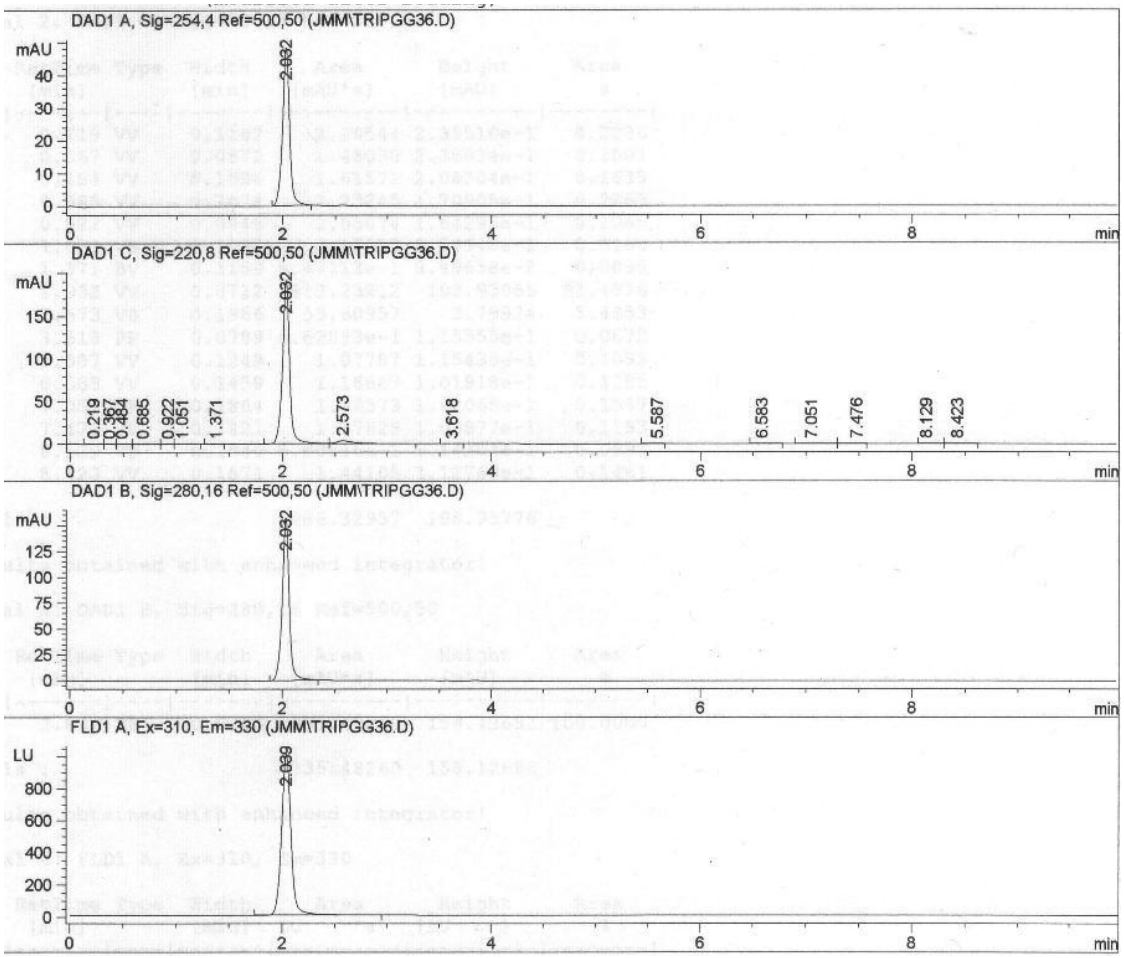

-HPLC trace of sample used for fluorescence and transport studies
-CONDITIONS: HP series 1100 HPLC
-Machery-Nagel RP C18 “Nucleosil” analytical column (4 mm x 250mm)
-3:1 CH_3OH:ACN as eluting solvents, flow 1mL/min

HO_2C-Trip-G(E3)-OH

3-22

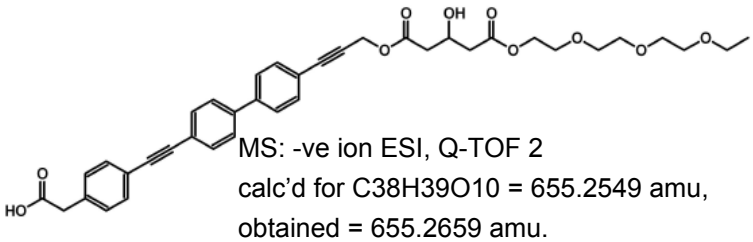

MS: -ve ion ESI, Q-TOF 2
calc'd for C38H39O10 = 655.2549 amu,
obtained = 655.2659 amu.

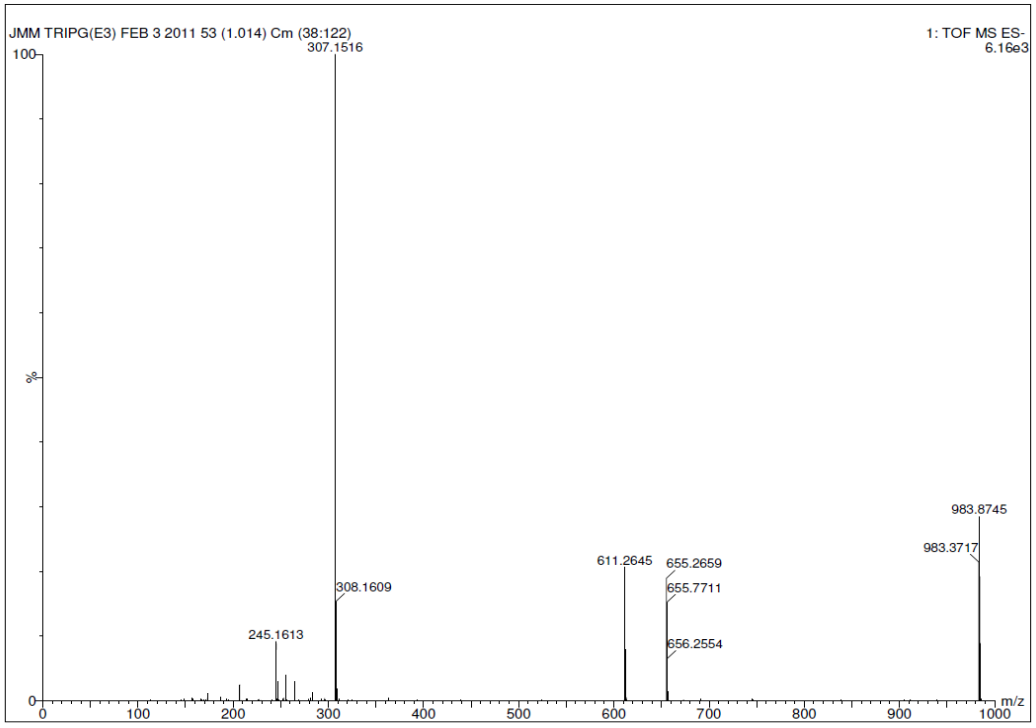

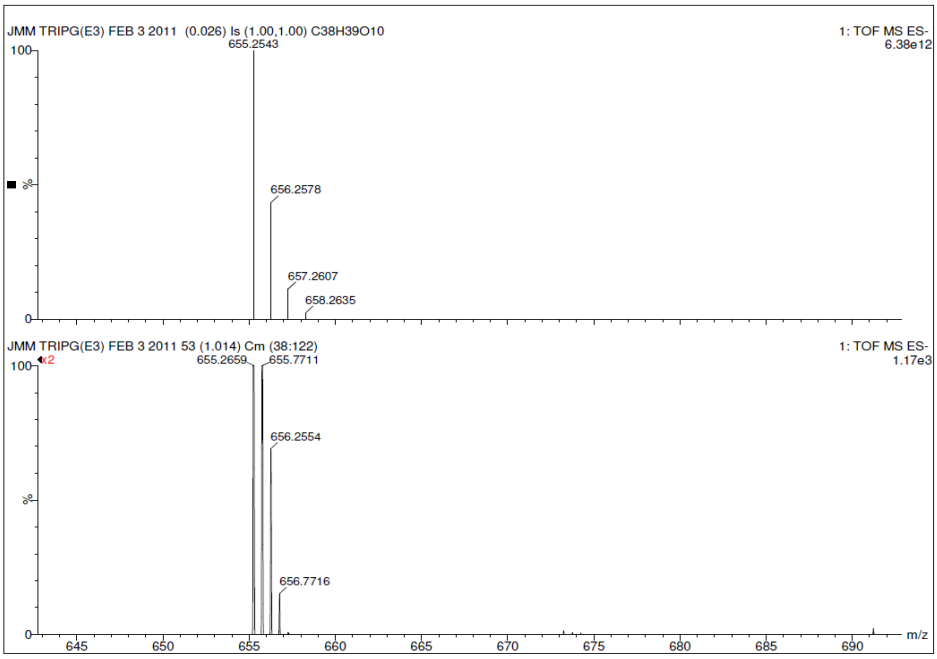

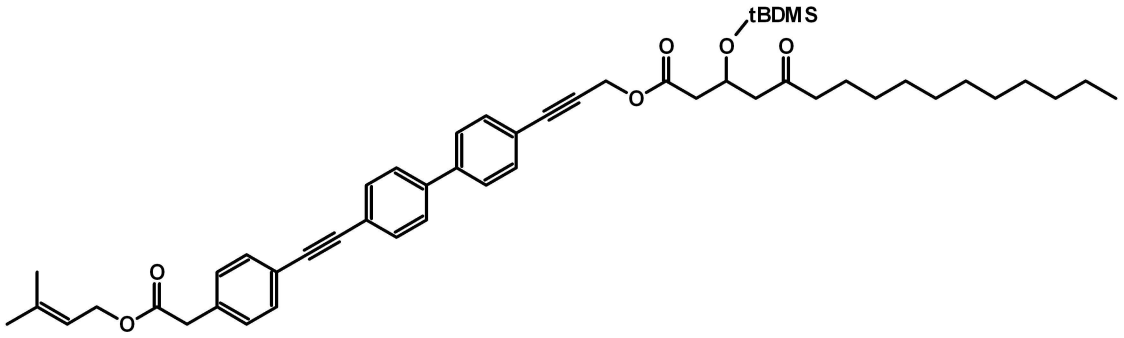

3-18

^{1}H NMR ($CDCl_3$) 300MHz

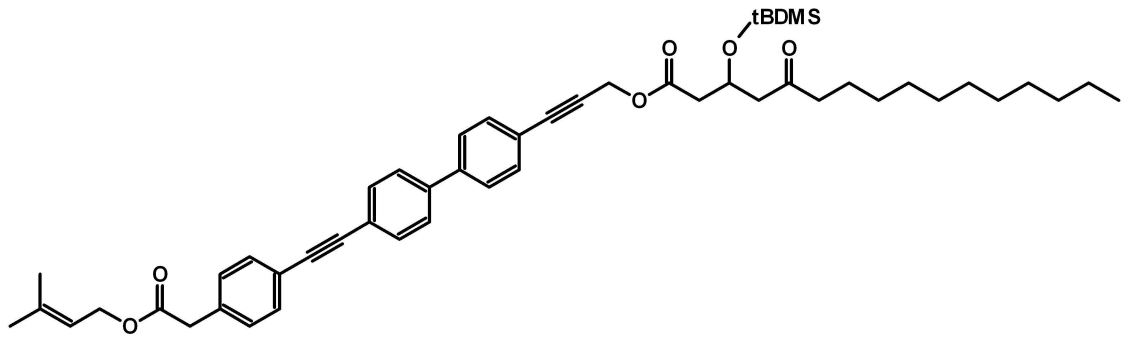

3-18

^{13}C NMR ($CDCl_3$) 75 MHz

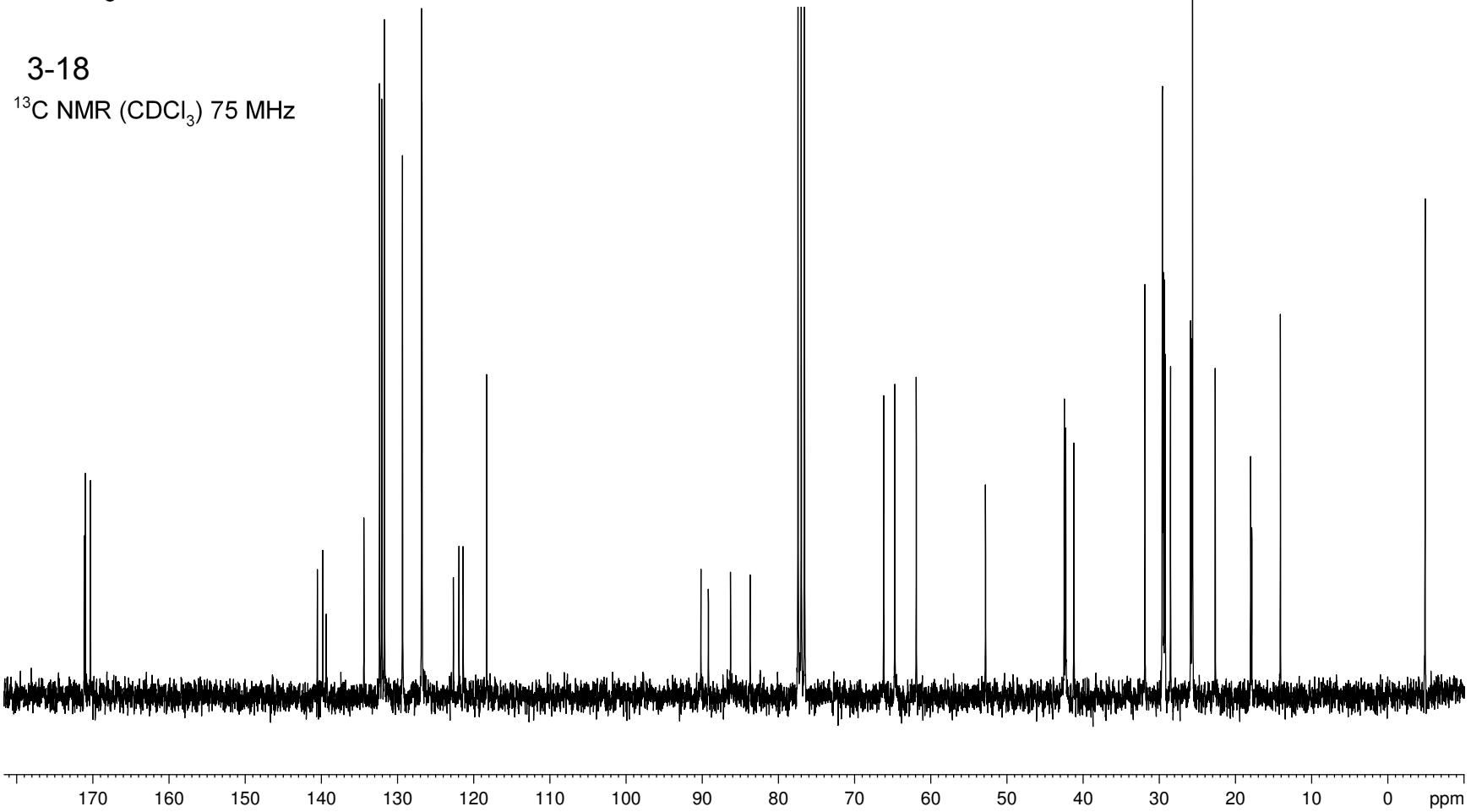

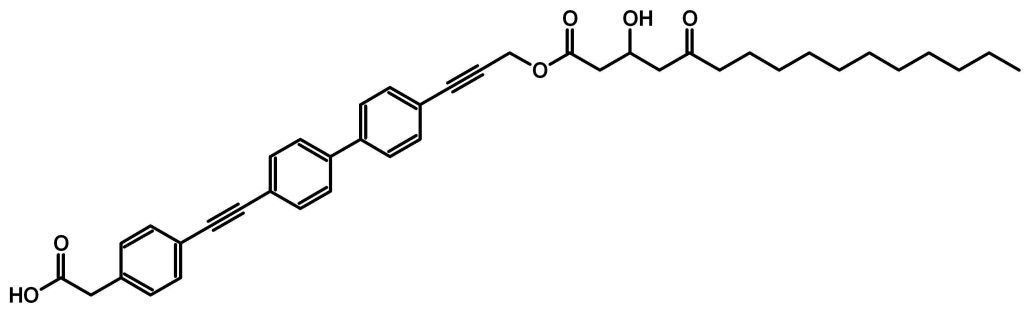

3-19

^{1}H NMR ($CDCl_3$) 500MHz

HO_2C-Trip-G(12)-OH

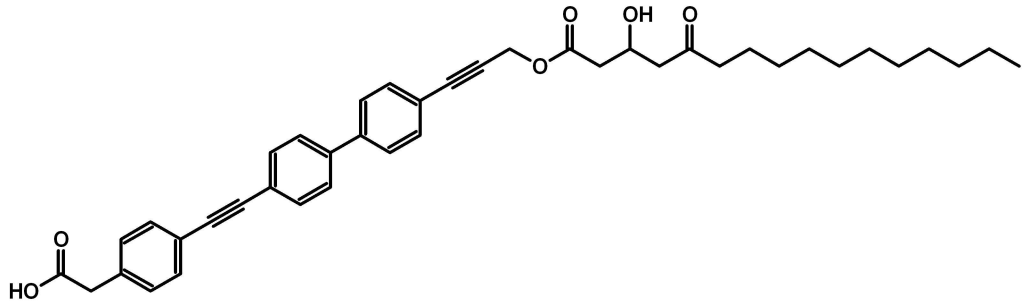

3-19

^{13}C NMR ($CDCl_3$) 125 MHz

HO_2C-Trip-G(12)-OH

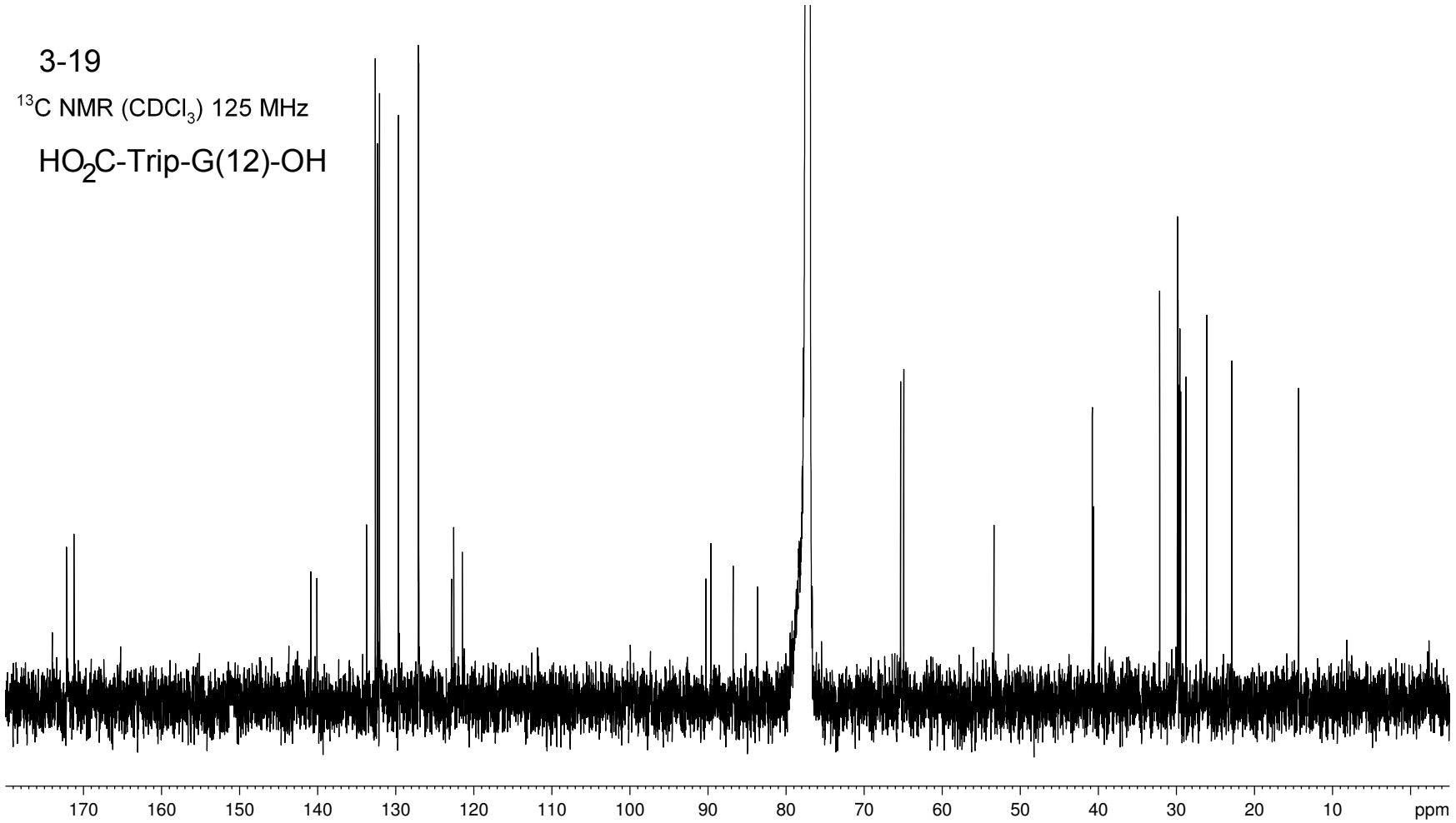

HO_2C-Trip-G(12)-OH

3-19

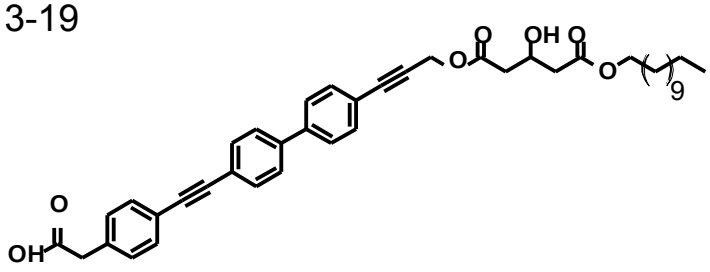

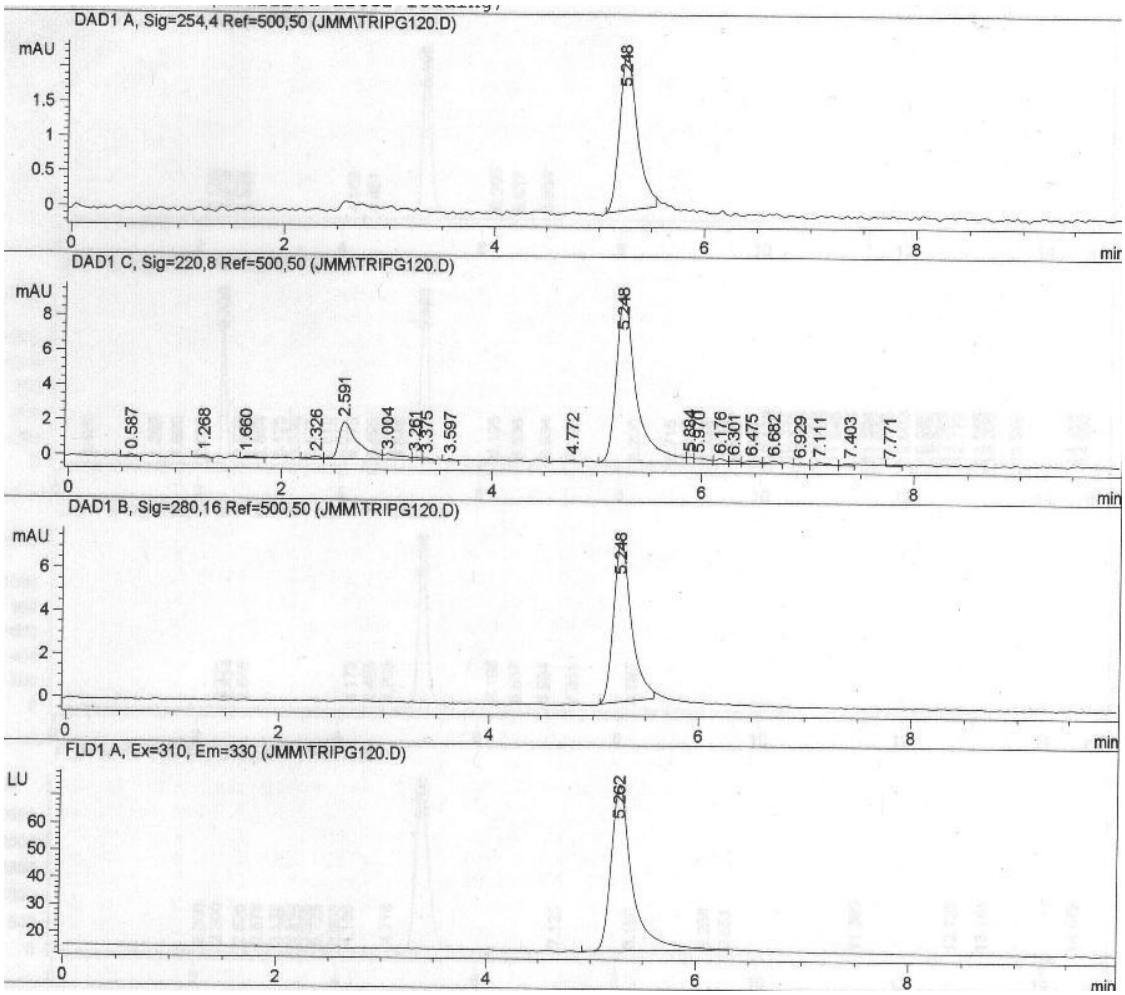

-HPLC trace of sample used for fluorescence and transport studies
-CONDITIONS: HP series 1100 HPLC
-Machery-Nagel RP C18 “Nucleosil” analytical column (4 mm x 250mm)
-1:1 CH_3OH:ACN as eluting solvents, flow 1mL/min

HO_2C-Trip-G(12)-OH

3-19

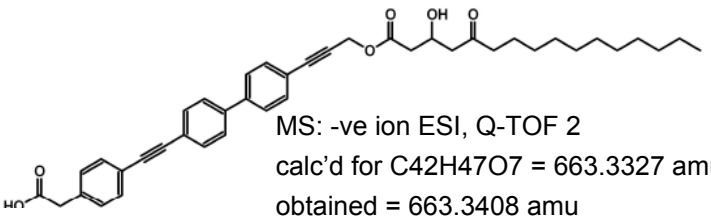

MS: -ve ion ESI, Q-TOF 2
calc'd for C42H47O7 = 663.3327 amu,
obtained = 663.3408 amu

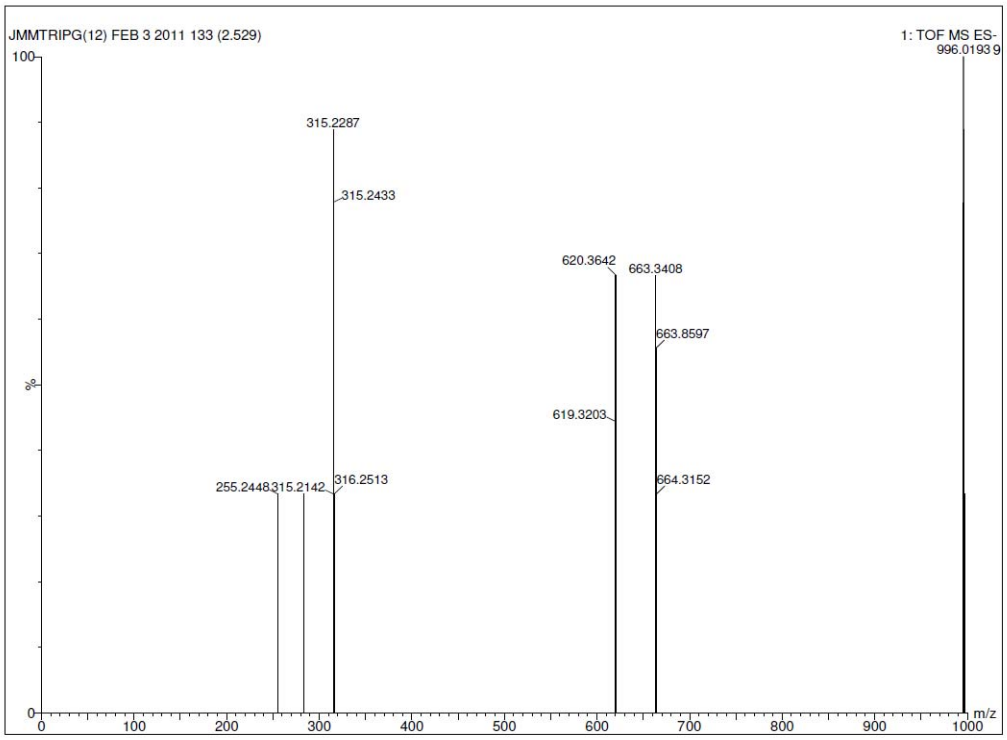

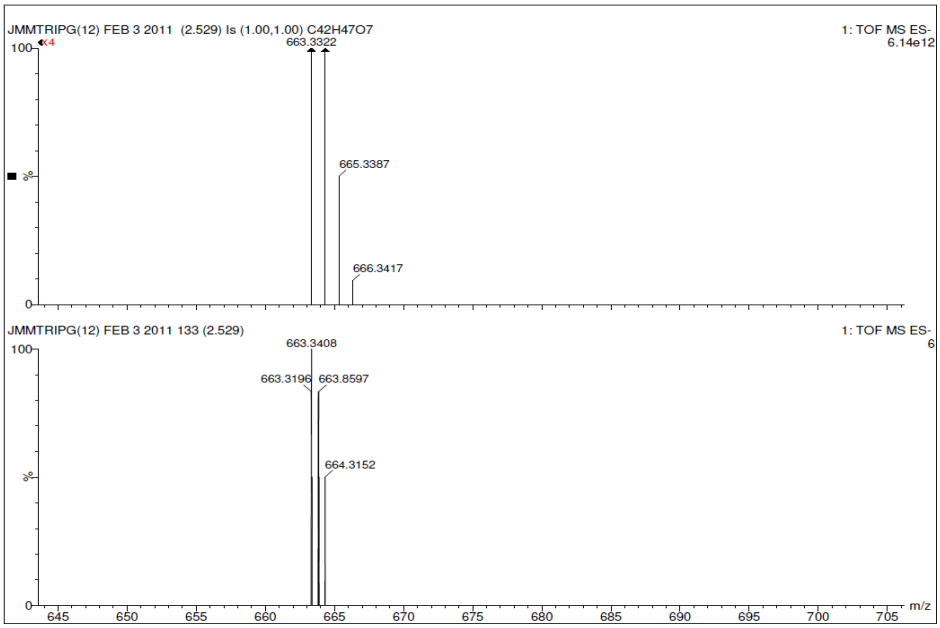

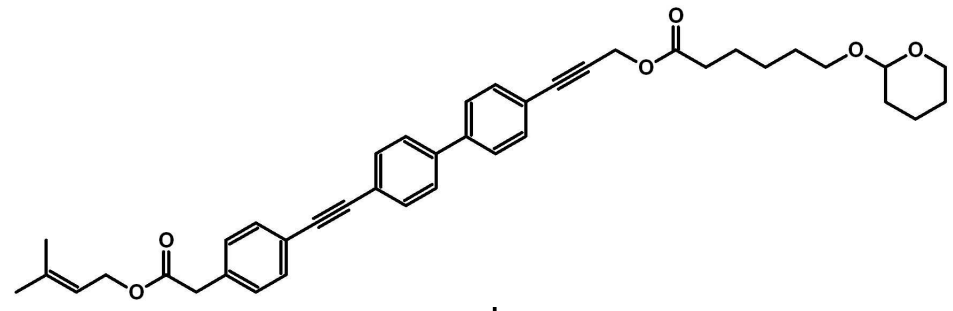

3-23

^{1}H NMR ($CDCl_3$) 300MHz

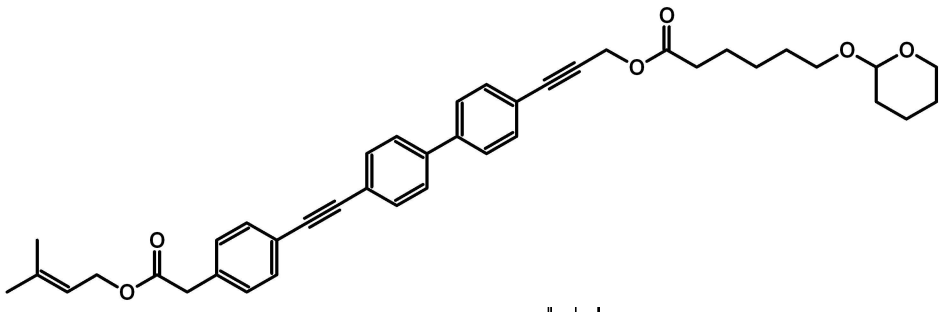

3-23

^{13}C NMR ($CDCl_3$) 75 MHz

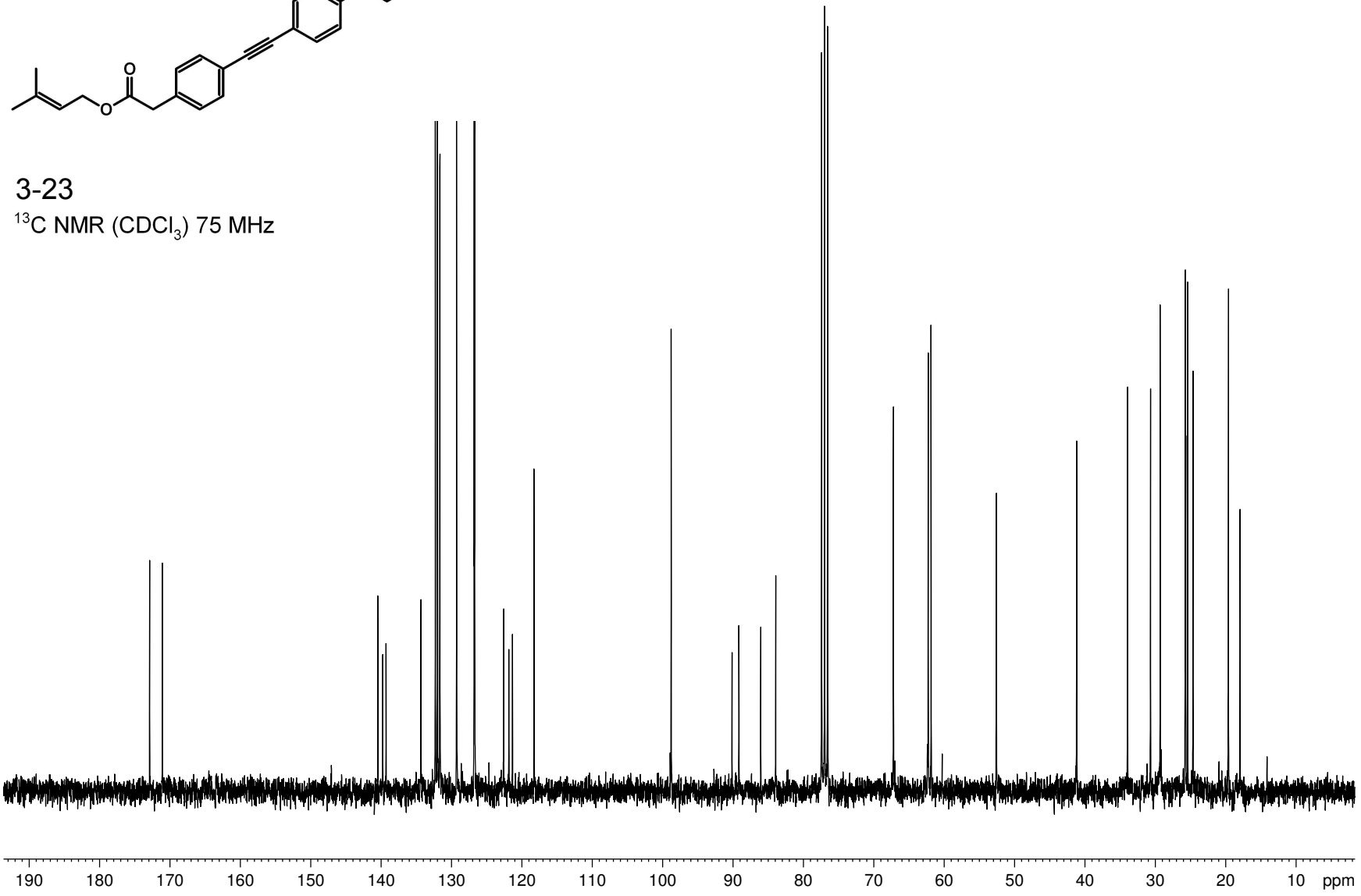

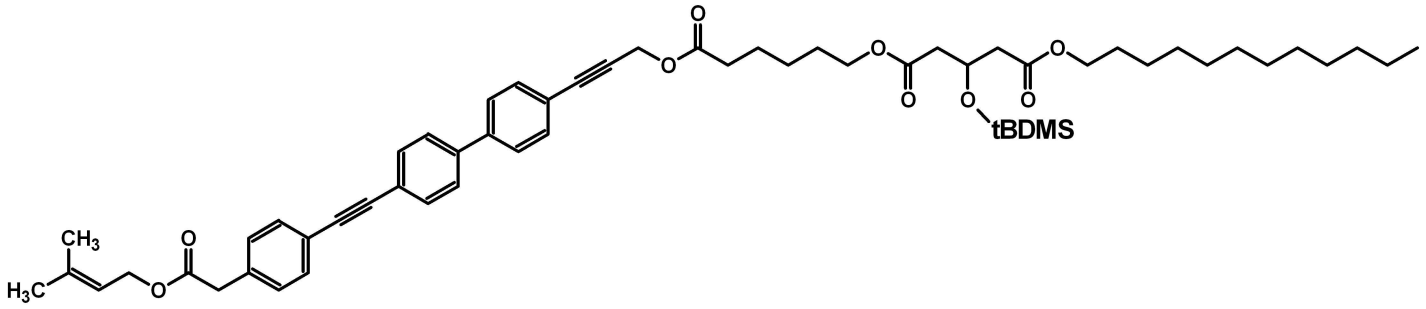

3-25
^{1}H NMR ($CDCl_3$) 300MHz

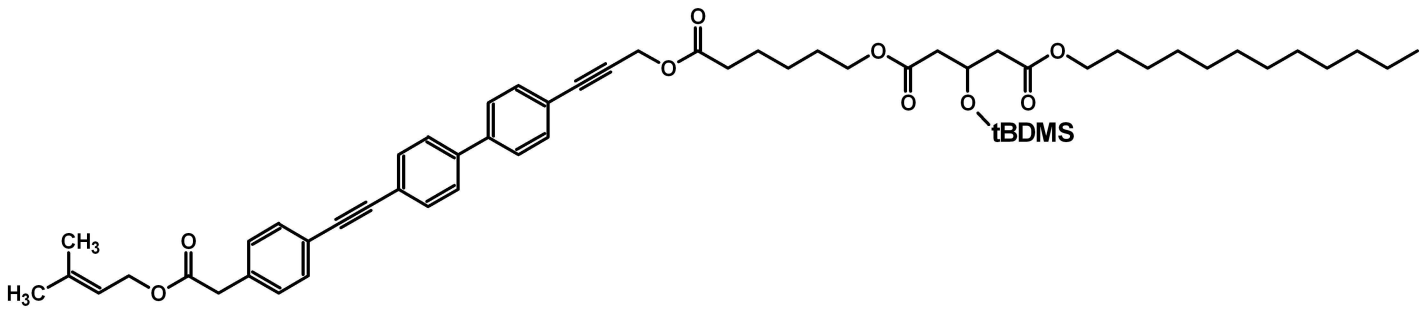

3-25

^{13}C NMR ($CDCl_3$) 75 MHz

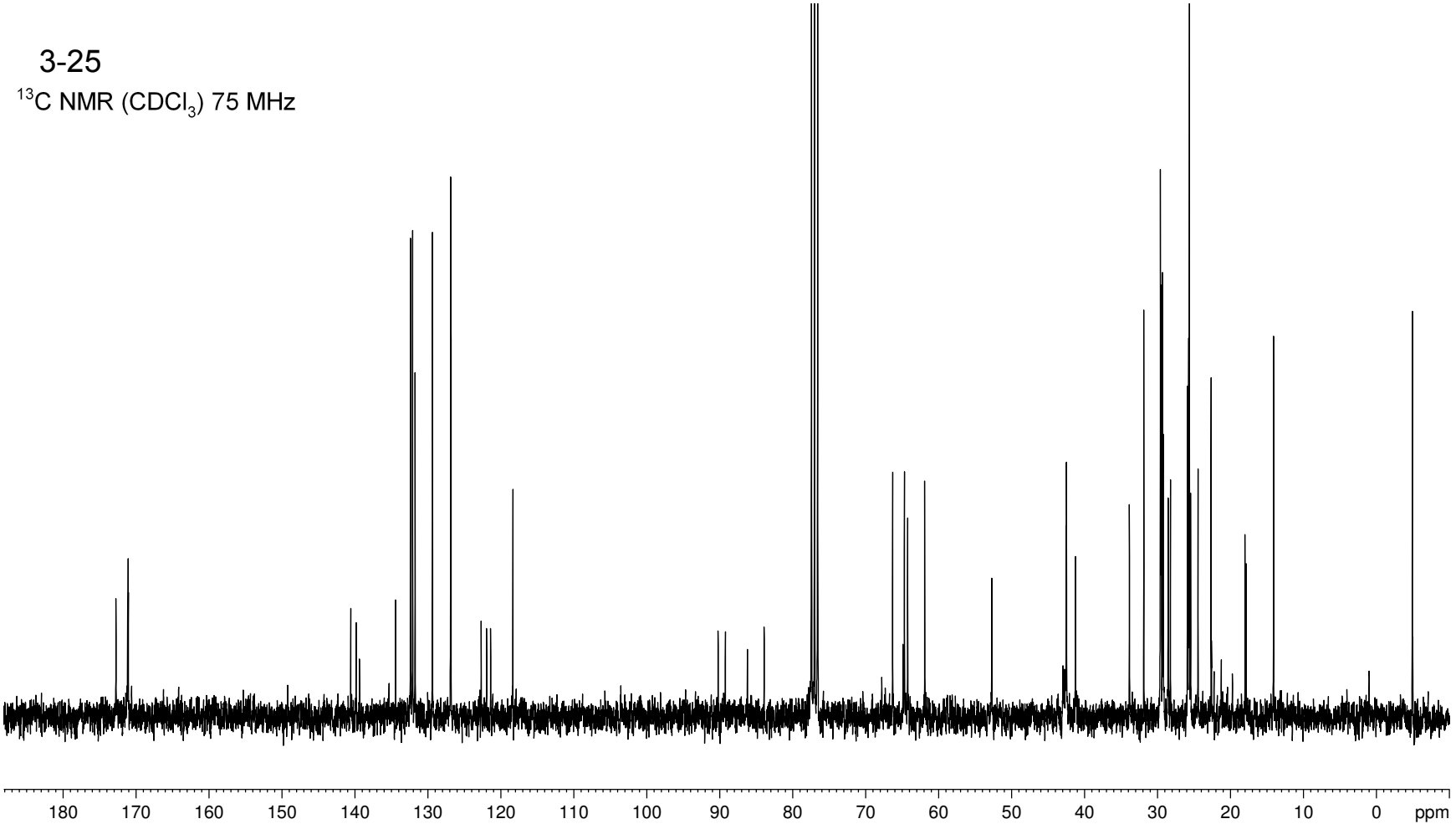

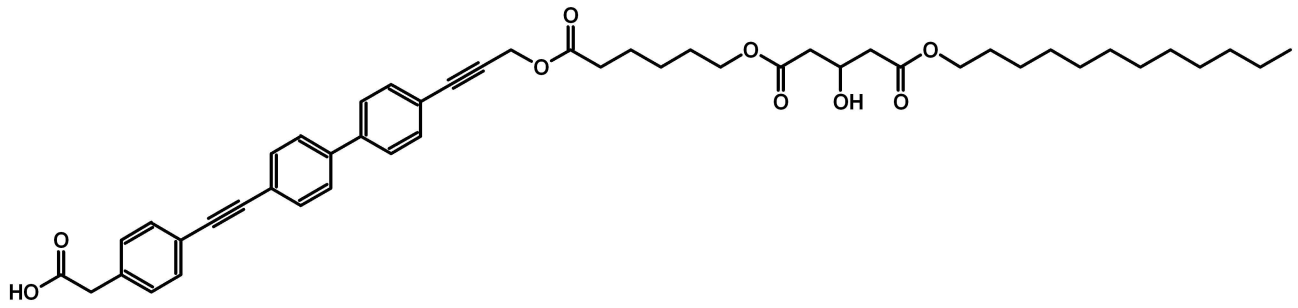

3-26

^{1}H NMR ($CDCl_3$) 300MHz

HO_2C-Trip-Hex-G(12)-OH

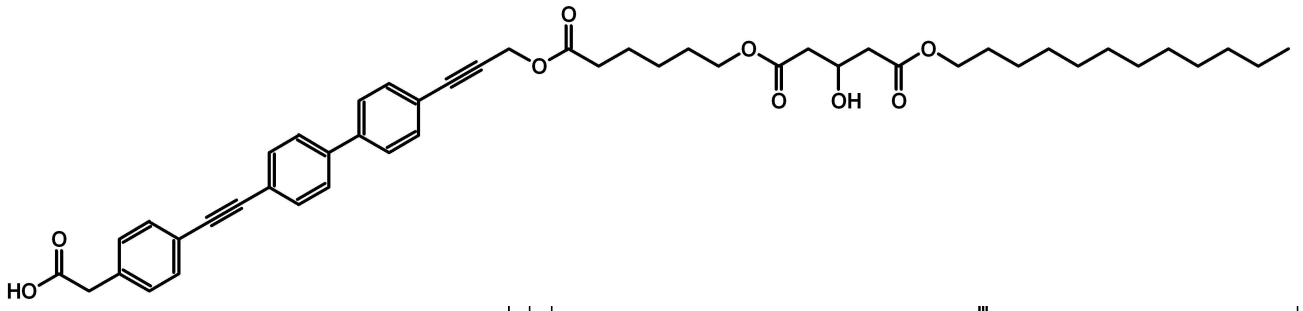

3-26

^{13}C NMR ($CDCl_3$) 75 MHz

HO_2C-Trip-Hex-G(12)-OH

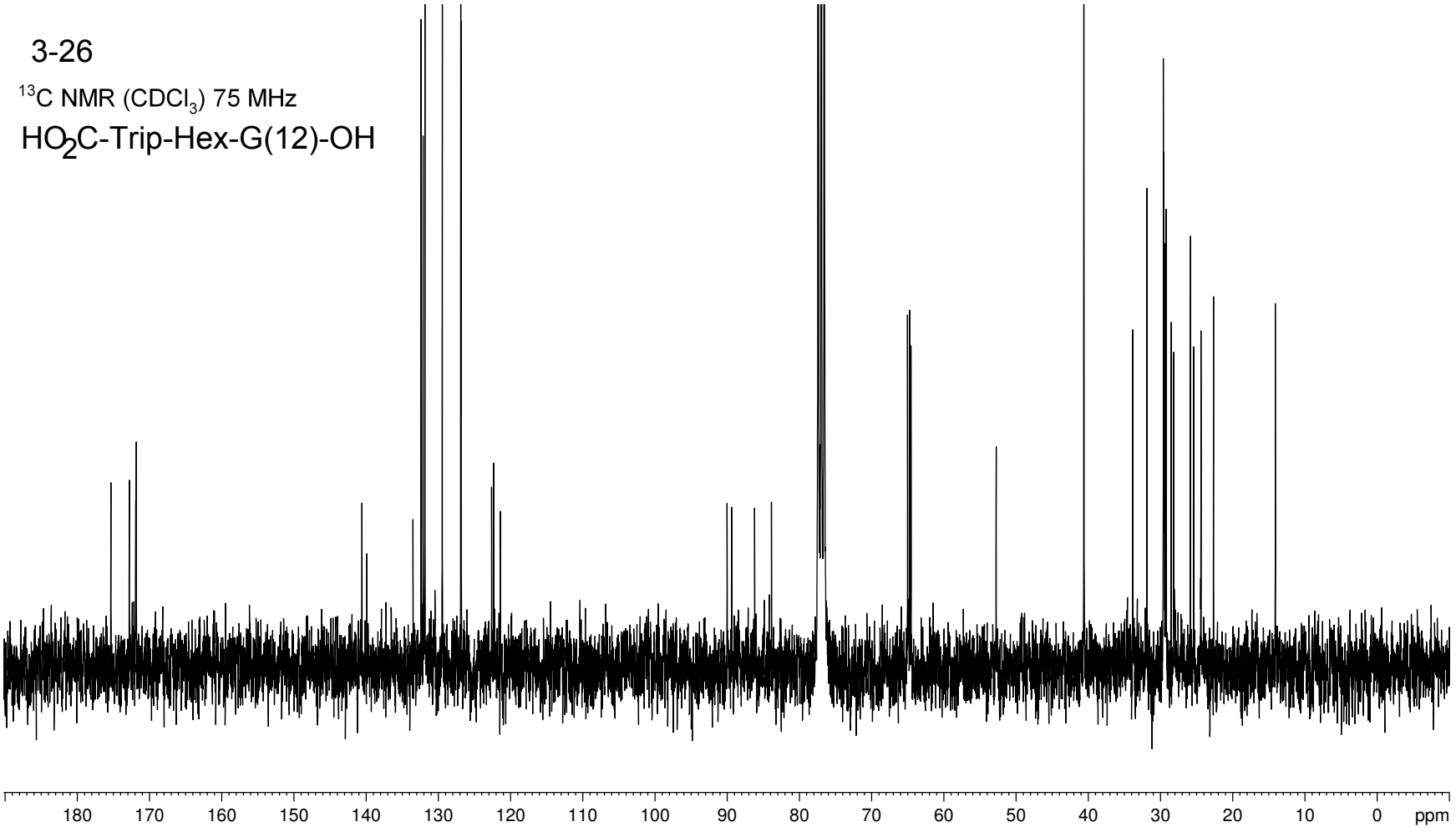

HO_2C-Trip-Hex-G(12)-OH

3-26

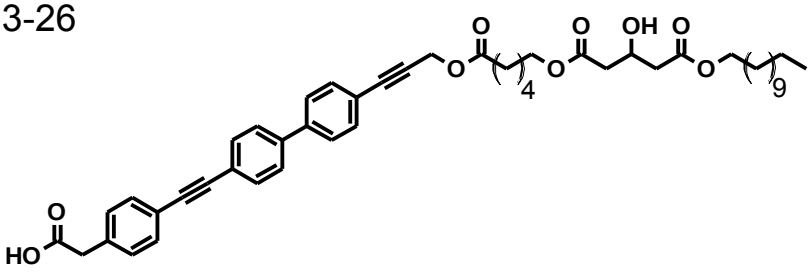

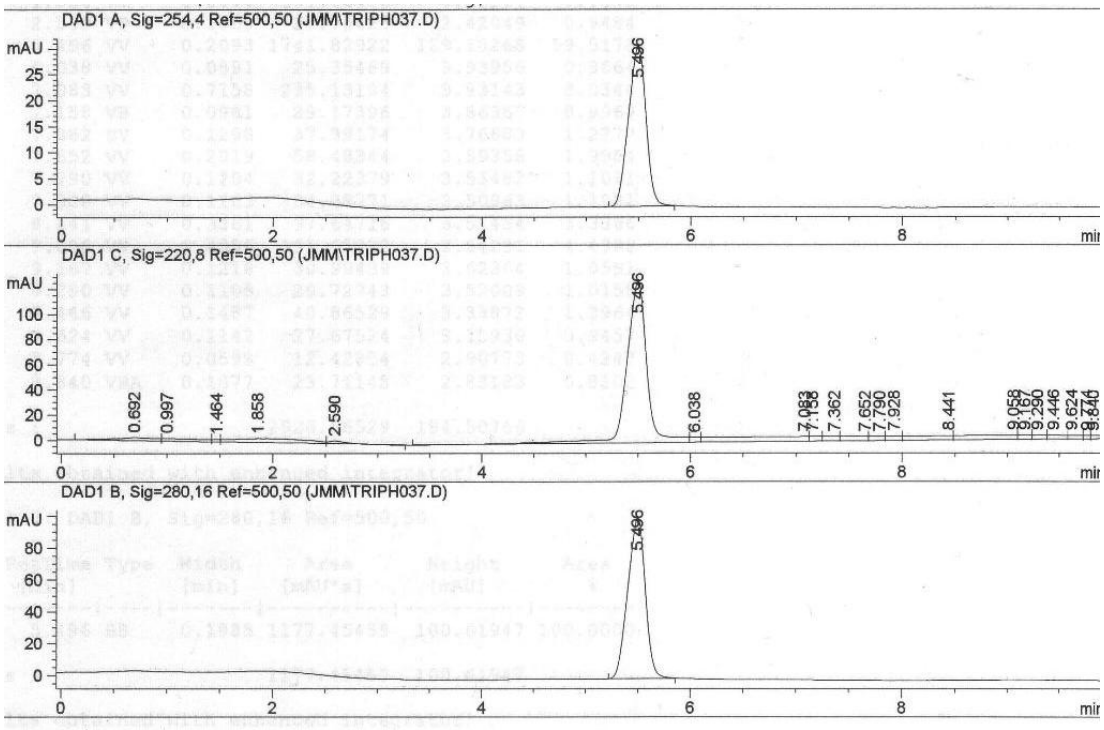

-HPLC trace of sample used for fluorescence and transport studies
-CONDITIONS: HP series 1100 HPLC
-Machery-Nagel RP C18 “Nucleosil” analytical column (4 mm x 250mm)
-3:1 CH_3OH:ACN as eluting solvents, flow 1mL/min

-as the fluorescence response was very high for this compound, the detector was saturated and therefore fluorescence detection was not utilized in this instance.

HO_2C-Trip-Hex-G(12)-OH

3-26

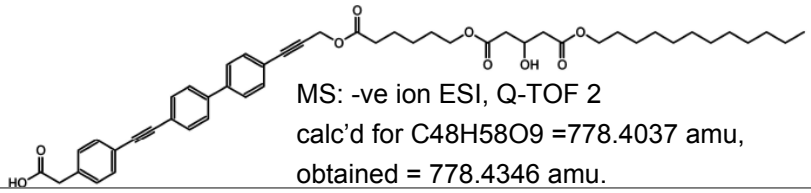

MS: -ve ion ESI, Q-TOF 2
calc'd for C48H58O9 =778.4037 amu,
obtained = 778.4346 amu.

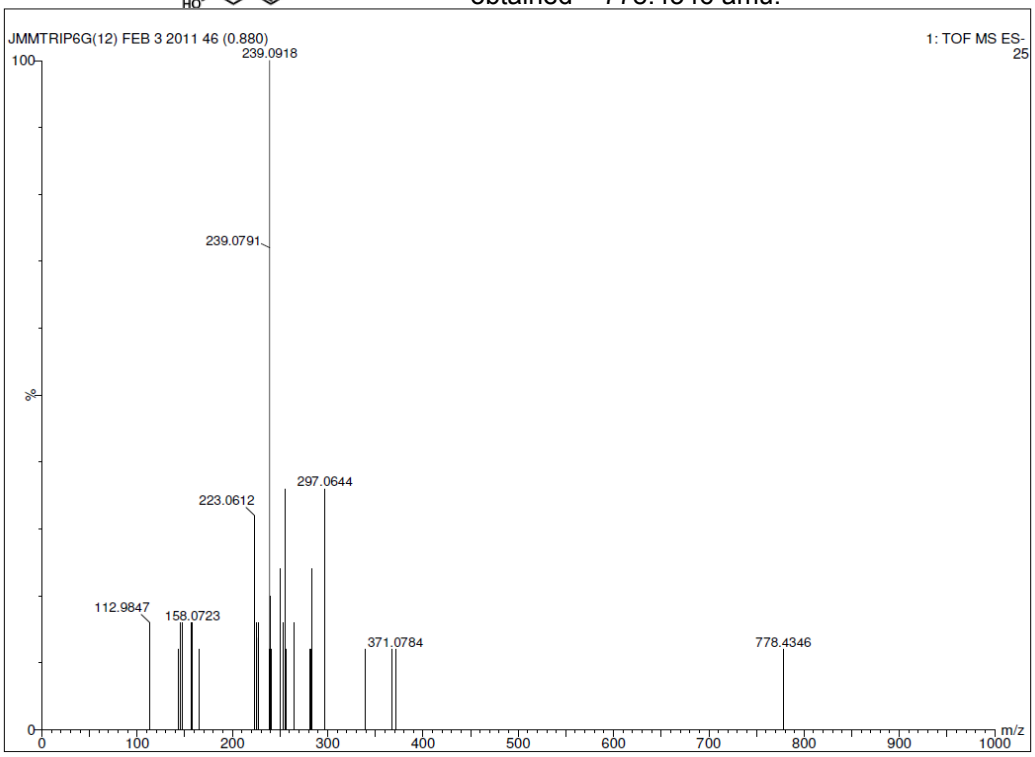

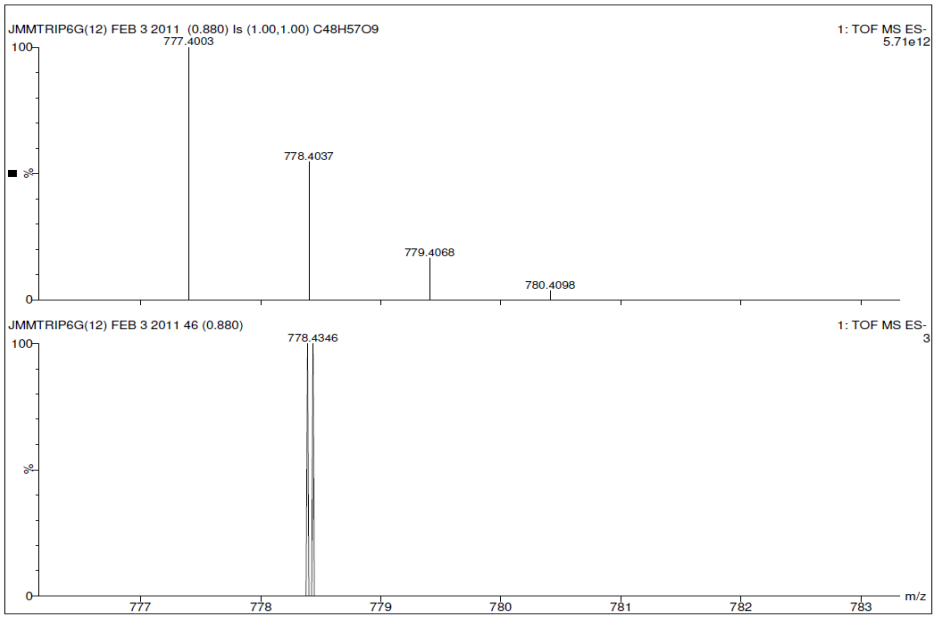

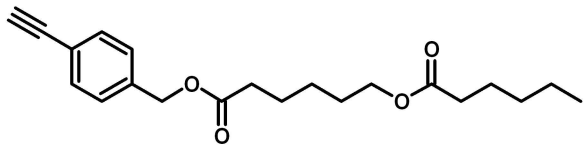

4-7

^{1}H NMR ($CDCl_3$) 300MHz

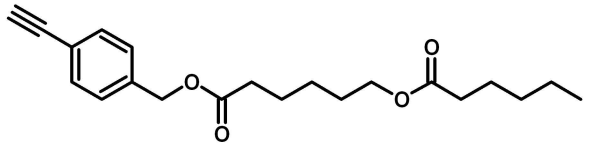

4-7

^{13}C NMR ($CDCl_3$) 75 MHz

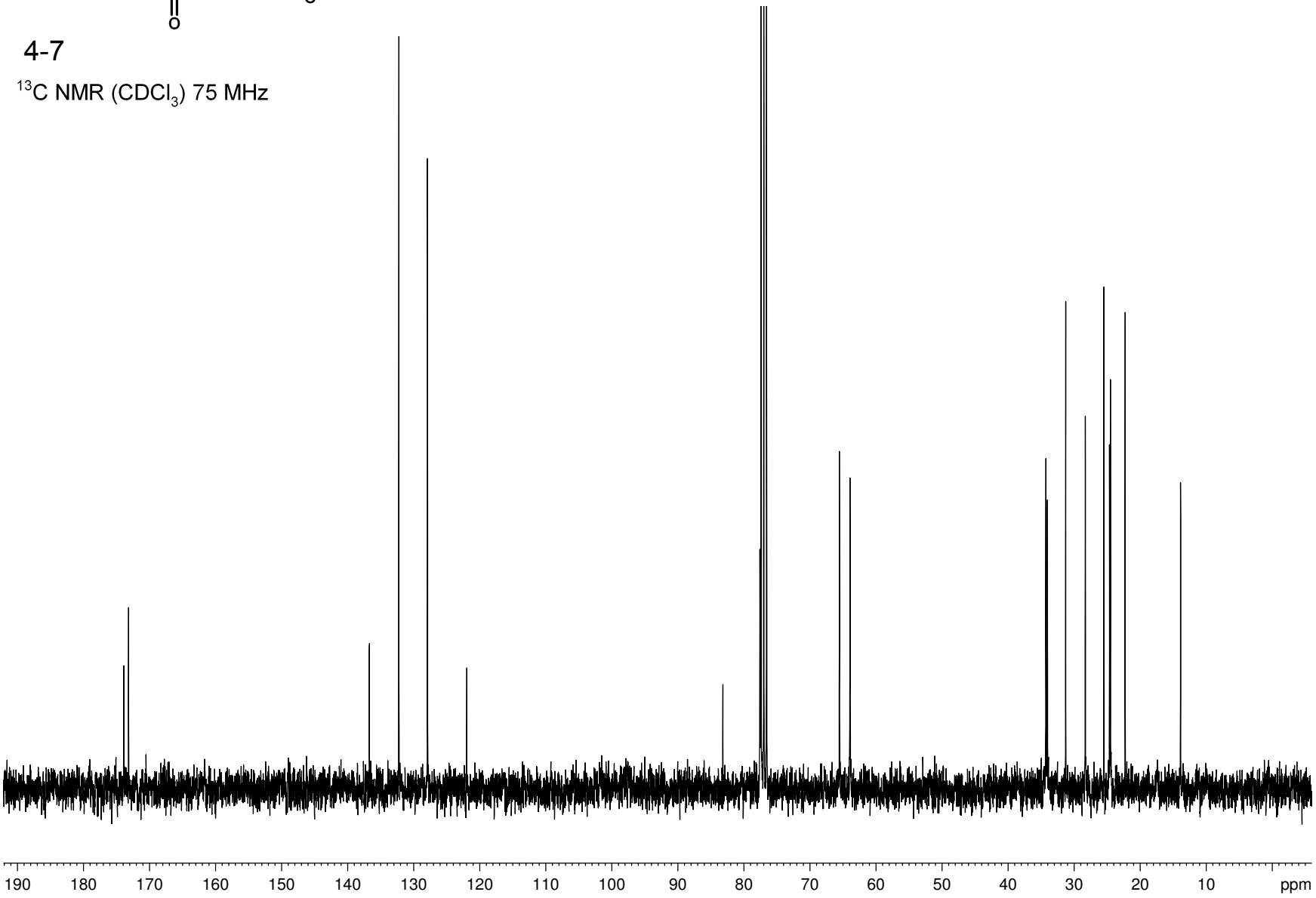

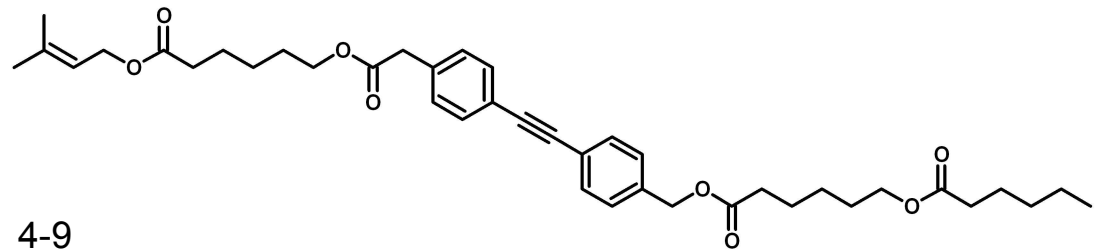

4-9

^{1}H NMR ($CDCl_3$) 300MHz

PREO_2C-Hex-Dip-Hex-C6

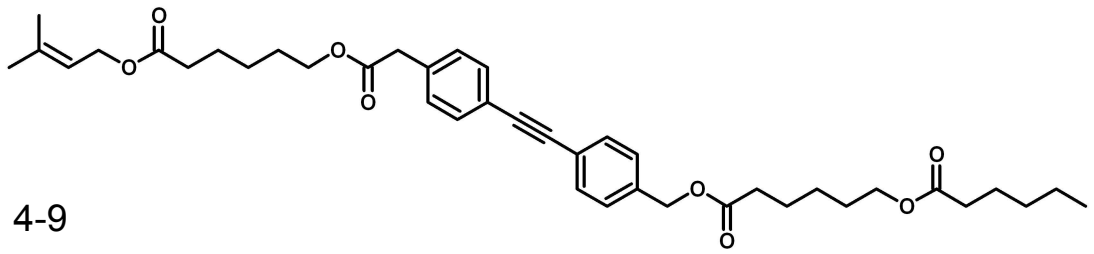

4-9

^{13}C NMR ($CDCl_3$) 75 MHz

PREO$_2$C-Hex-Dip-Hex-C6

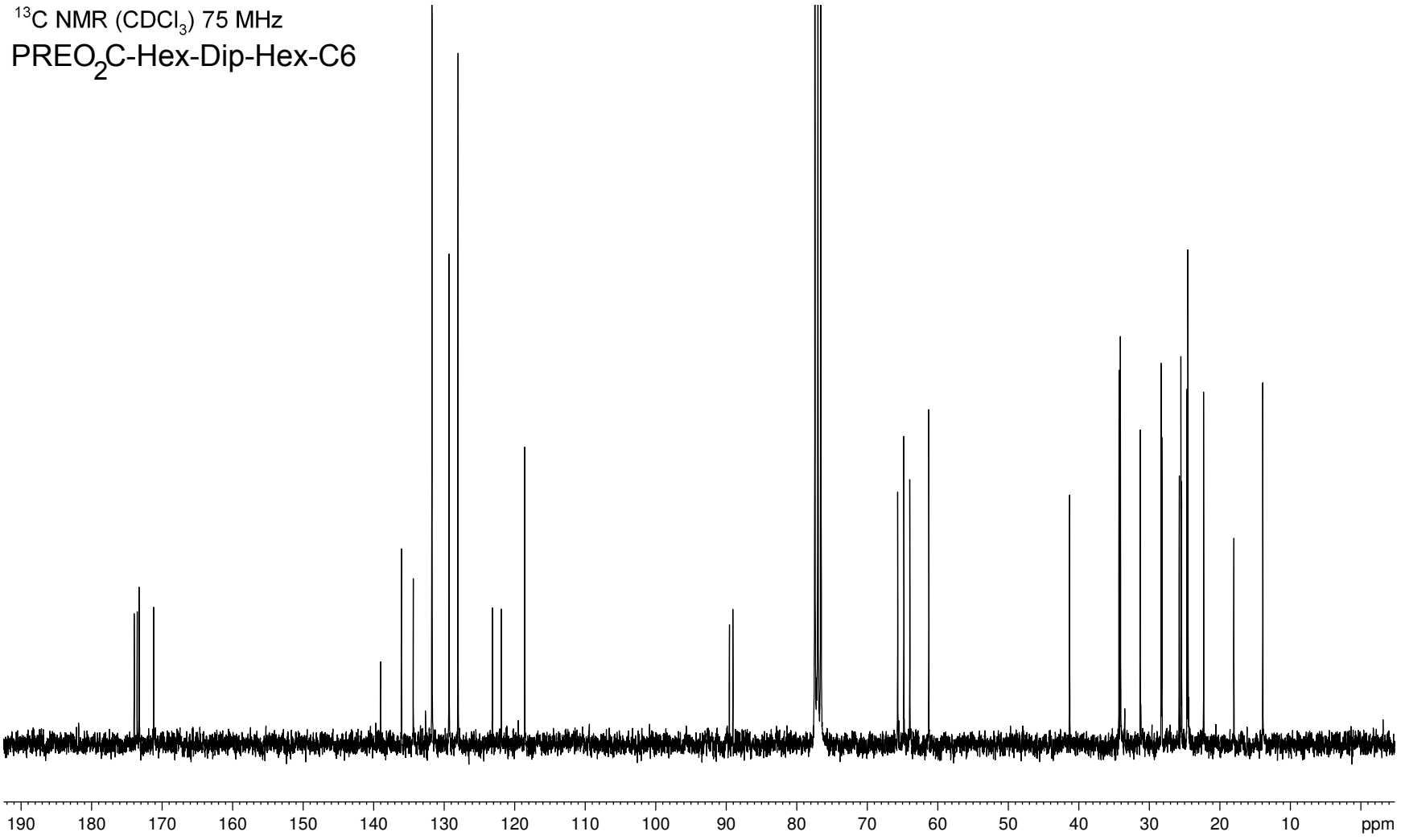

PREO$_2$C-Hex-Dip-Hex-C6

4-9

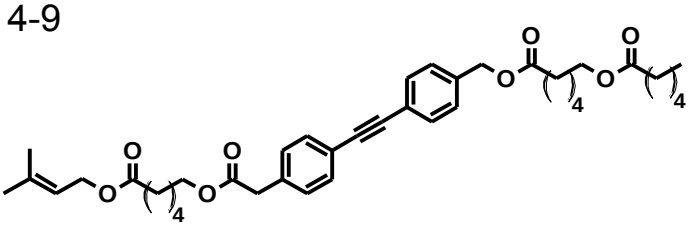

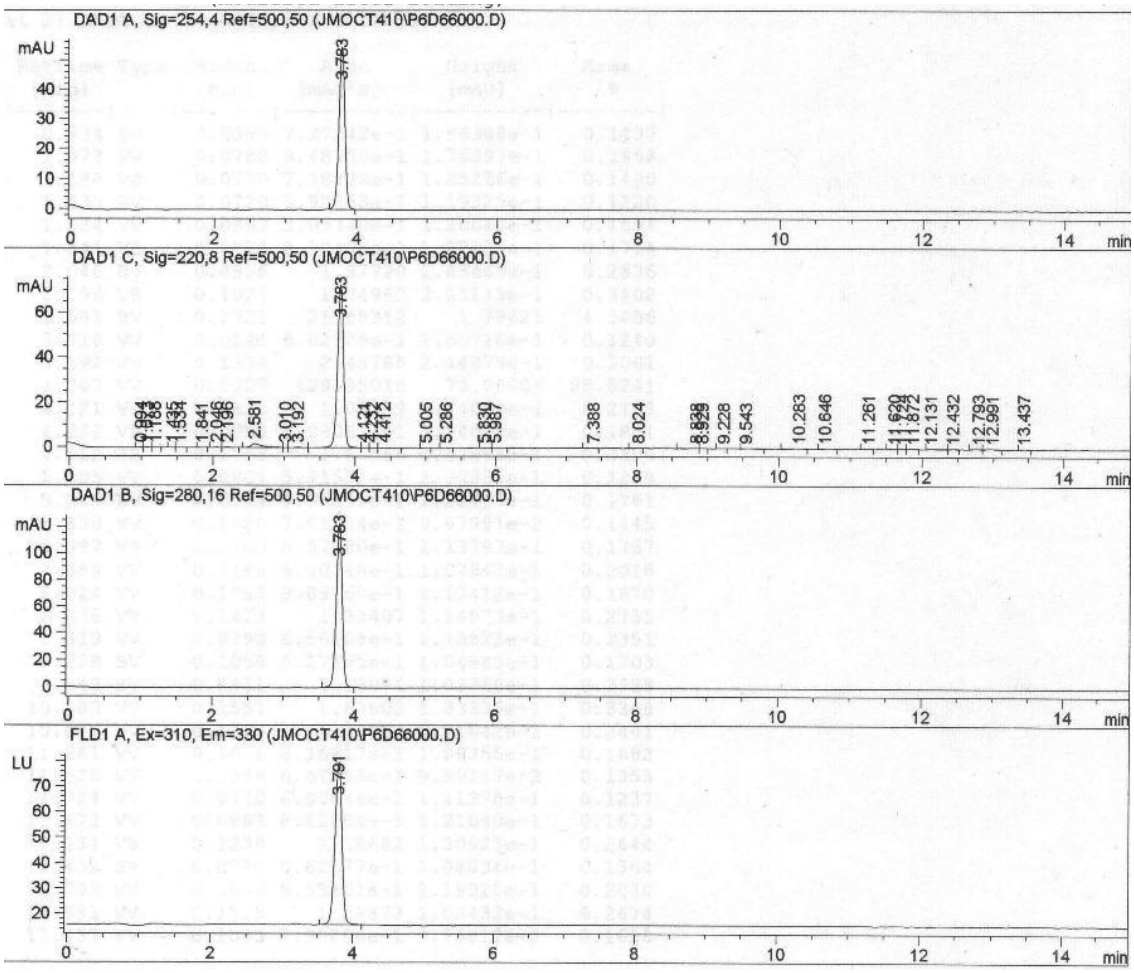

-HPLC trace of sample used for fluorescence and transport studies
-CONDITIONS: HP series 1100 HPLC
-Machery-Nagel RP C18 “Nucleosil” analytical column (4 mm x 250mm)
-1:1 ACN:CH_3OH as eluting solvents, flow 1mL/min

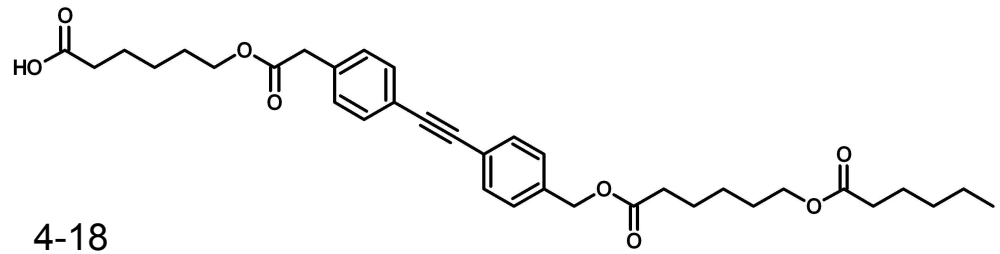

4-18

^{1}H NMR ($CDCl_3$) 300MHz

HO_2C-Hex-Dip-Hex-C6

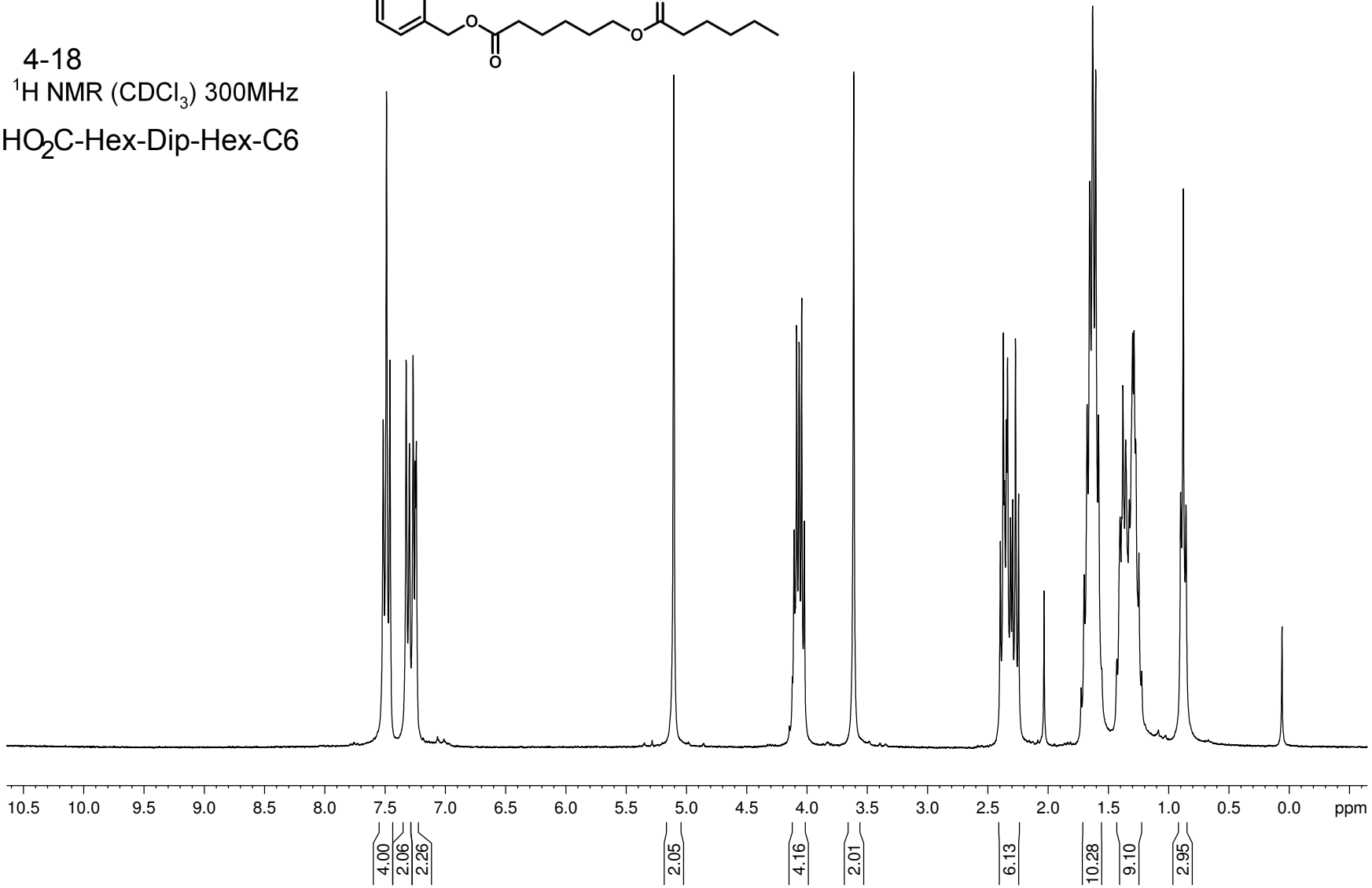

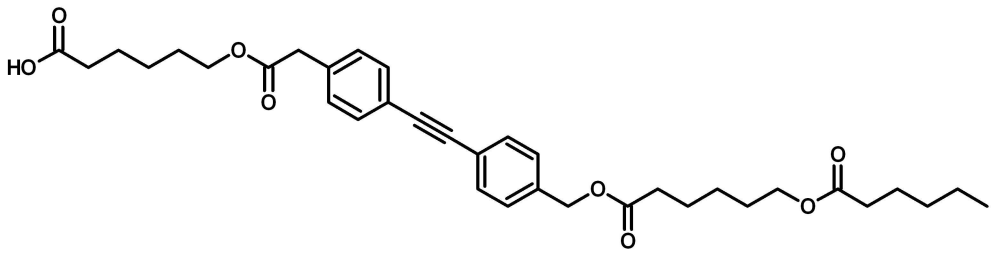

4-18

^{13}C NMR ($CDCl_3$) 75 MHz

HO_2C-Hex-Dip-Hex-C6

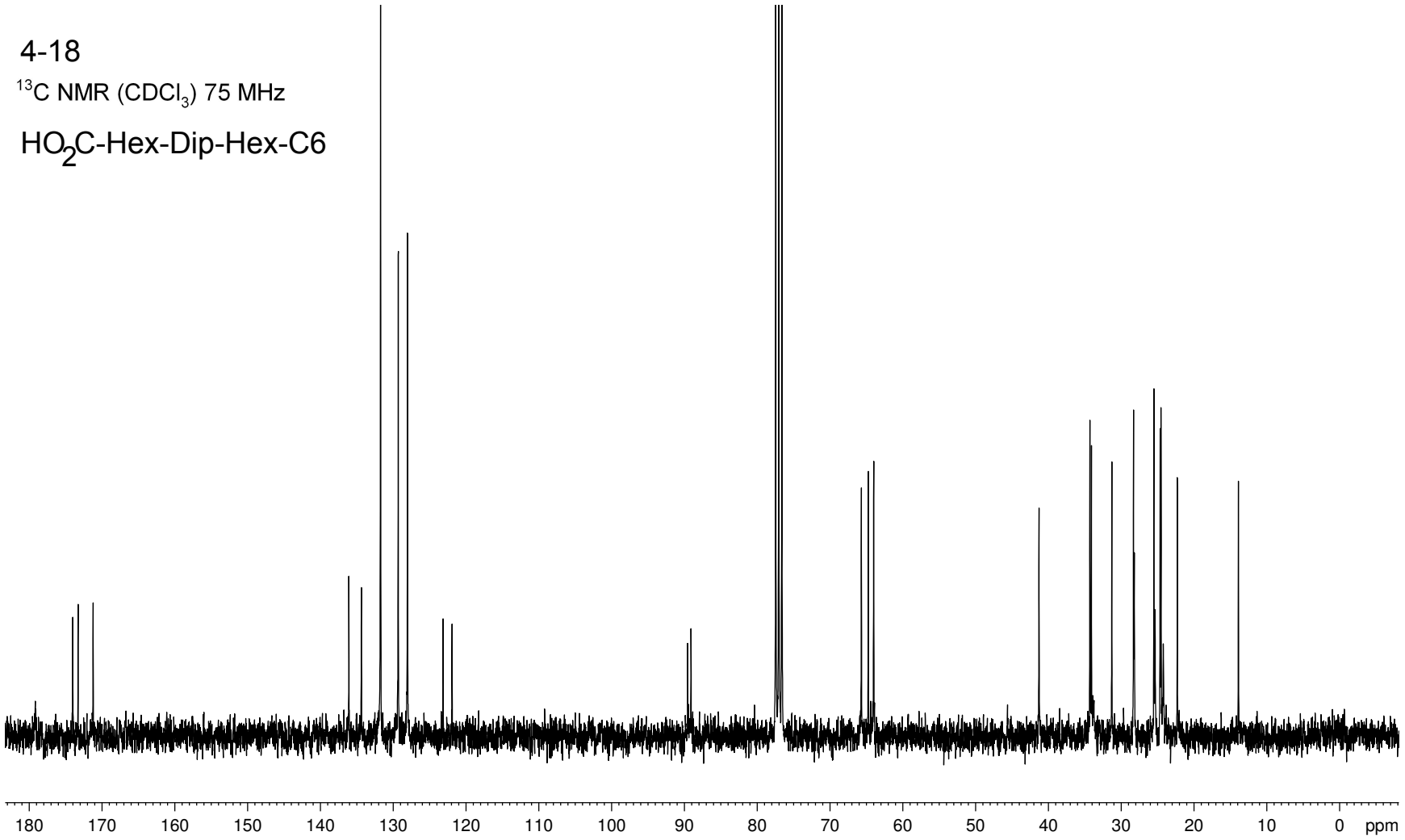

HO_2C-Hex-Dip-Hex-C6

4-18

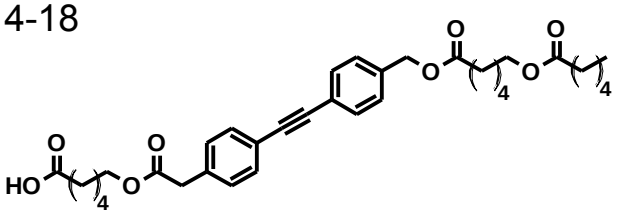

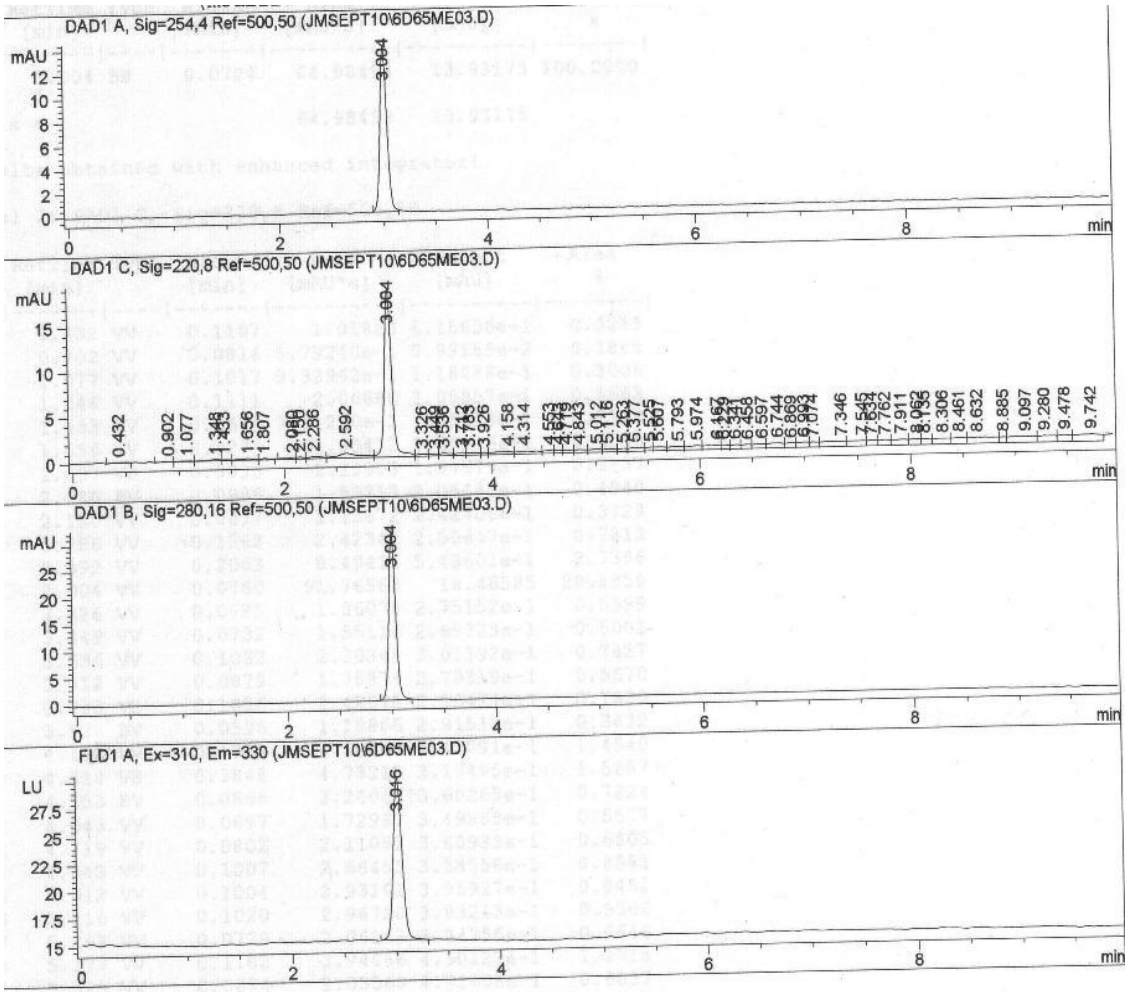

-HPLC trace of sample used for fluorescence and transport studies
-CONDITIONS: HP series 1100 HPLC
-Machery-Nagel RP C18 “Nucleosil” analytical column (4 mm x 250mm)
-3:1 ACN:CH_3OH as eluting solvents, flow 1mL/min

HO_2C-Hex-Dip-Hex-C6

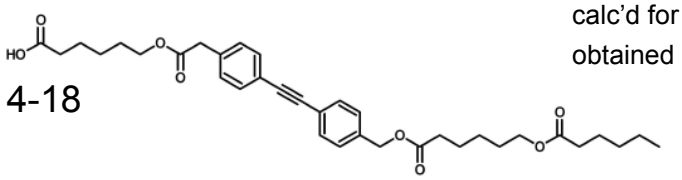

4-18

MS: -ve ion ESI, Q-TOF
calc'd for C35H43O8 = 591.2958 amu,
obtained = 591.2957 amu

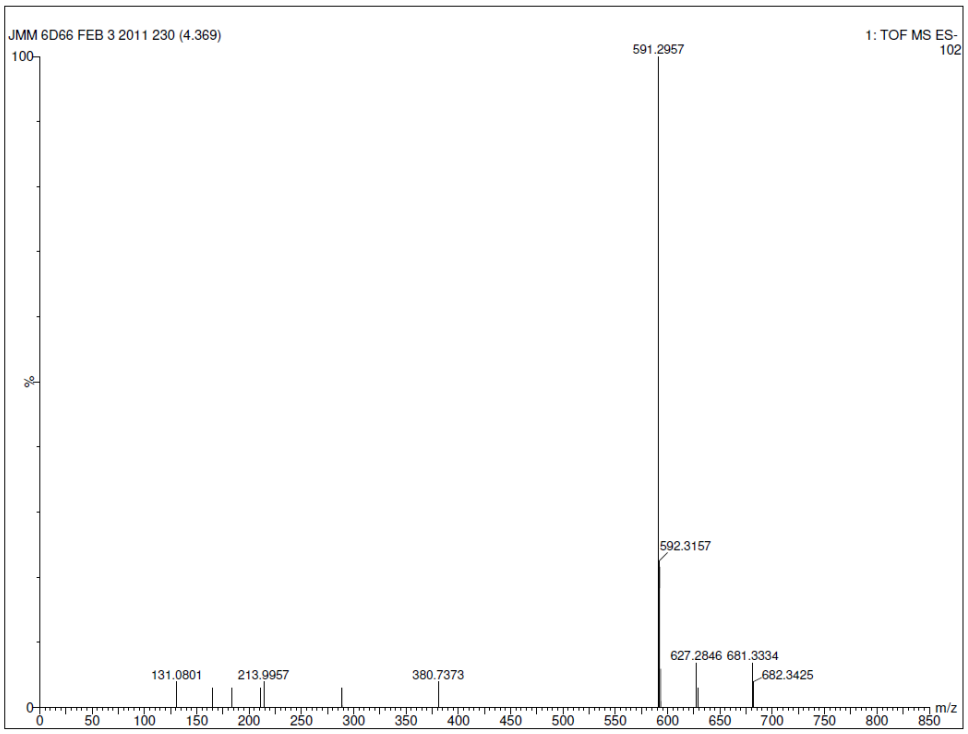

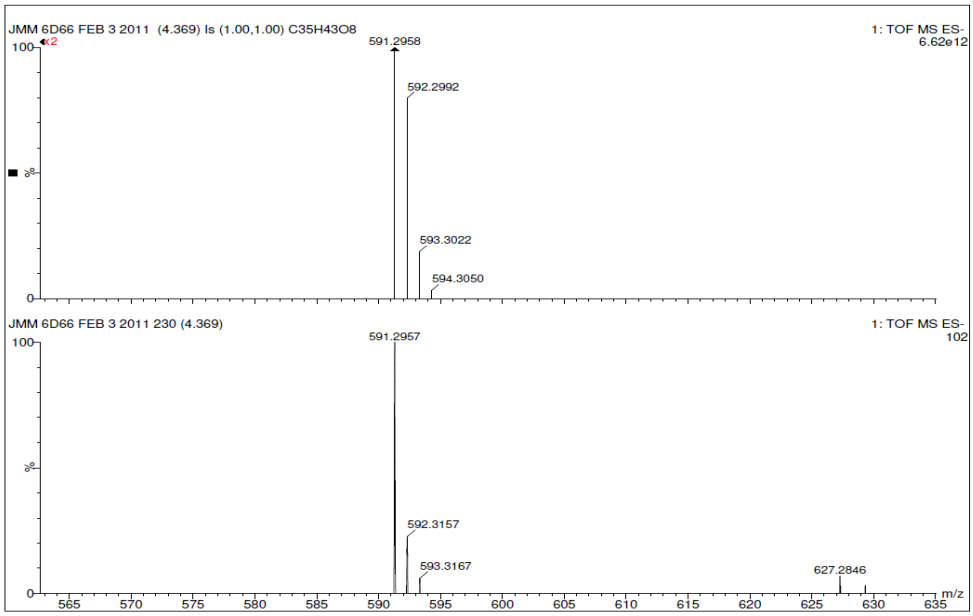

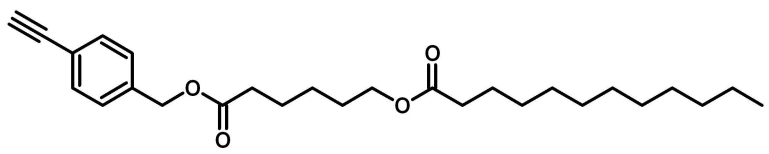

4-8

^{1}H NMR ($CDCl_3$) 300MHz

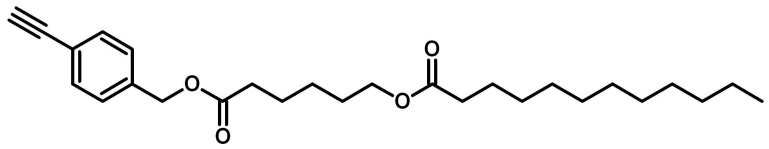

4-8

^{13}C NMR ($CDCl_3$) 75 MHz

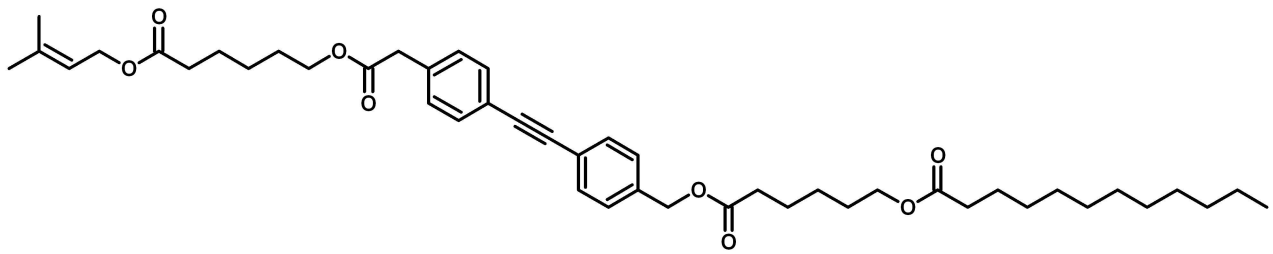

4-12

^{1}H NMR ($CDCl_3$) 300MHz

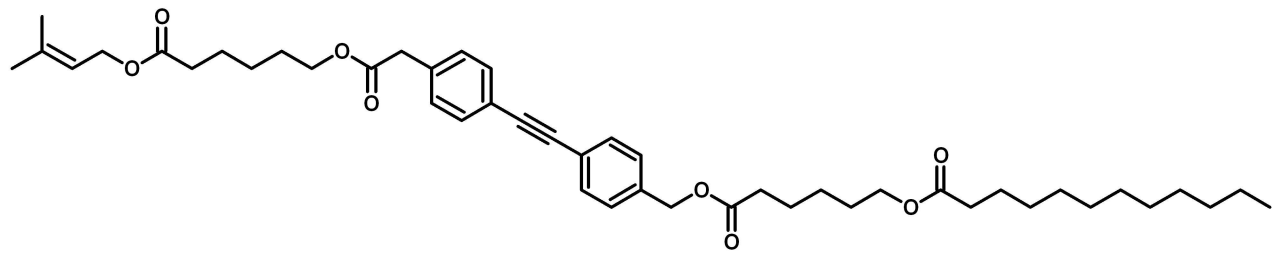

4-12

^{13}C NMR ($CDCl_3$) 75 MHz

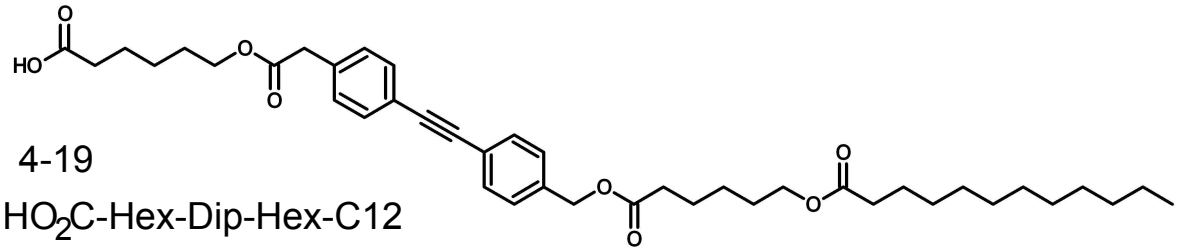

4-19

HO_2C-Hex-Dip-Hex-C12

^1H NMR ($CDCl_3$) 500MHz

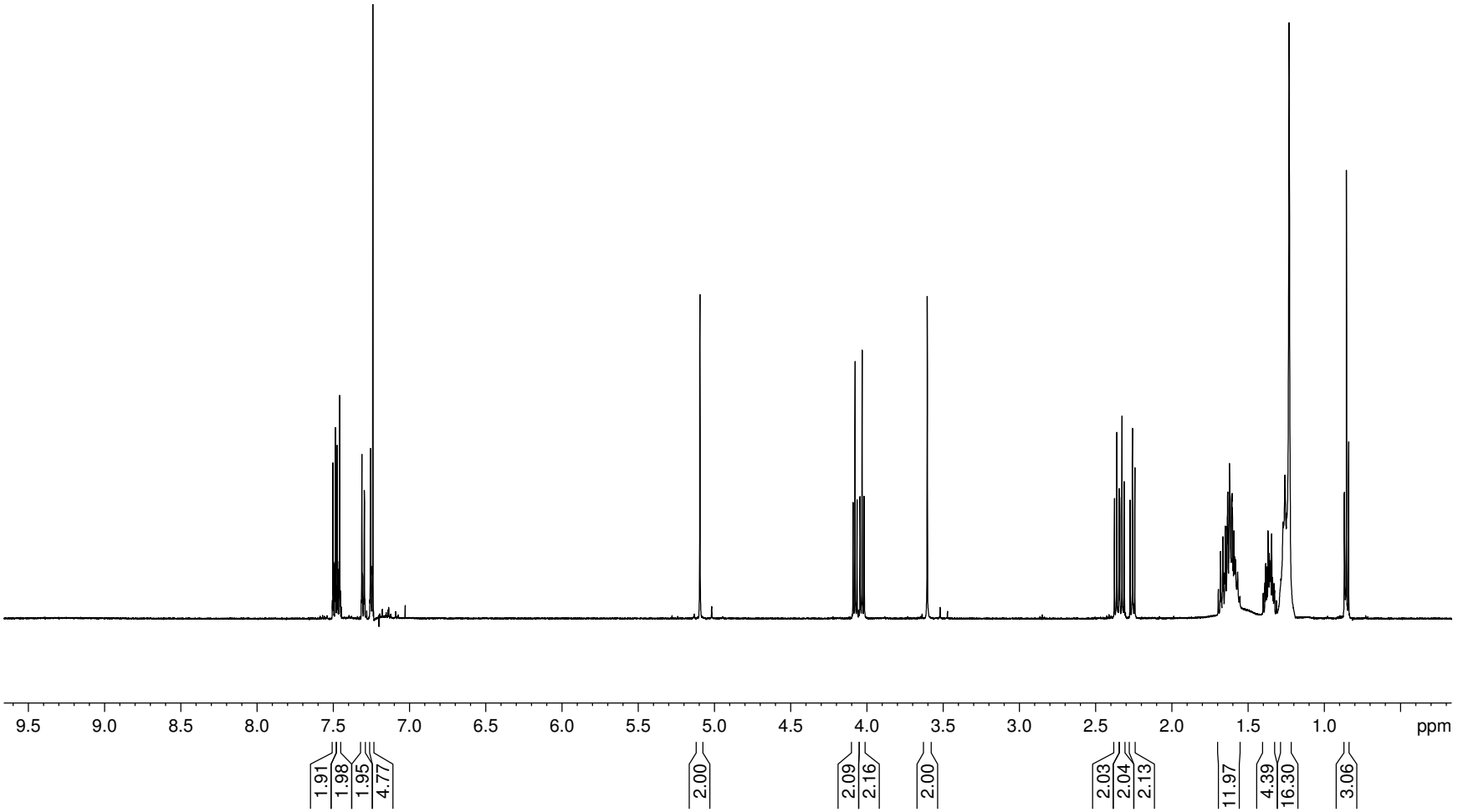

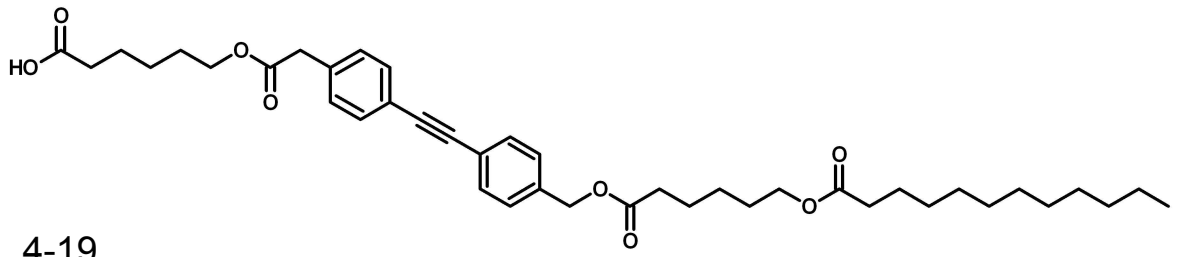

4-19

HO_2C-Hex-Dip-Hex-C12

^{13}C NMR ($CDCl_3$) 125 MHz

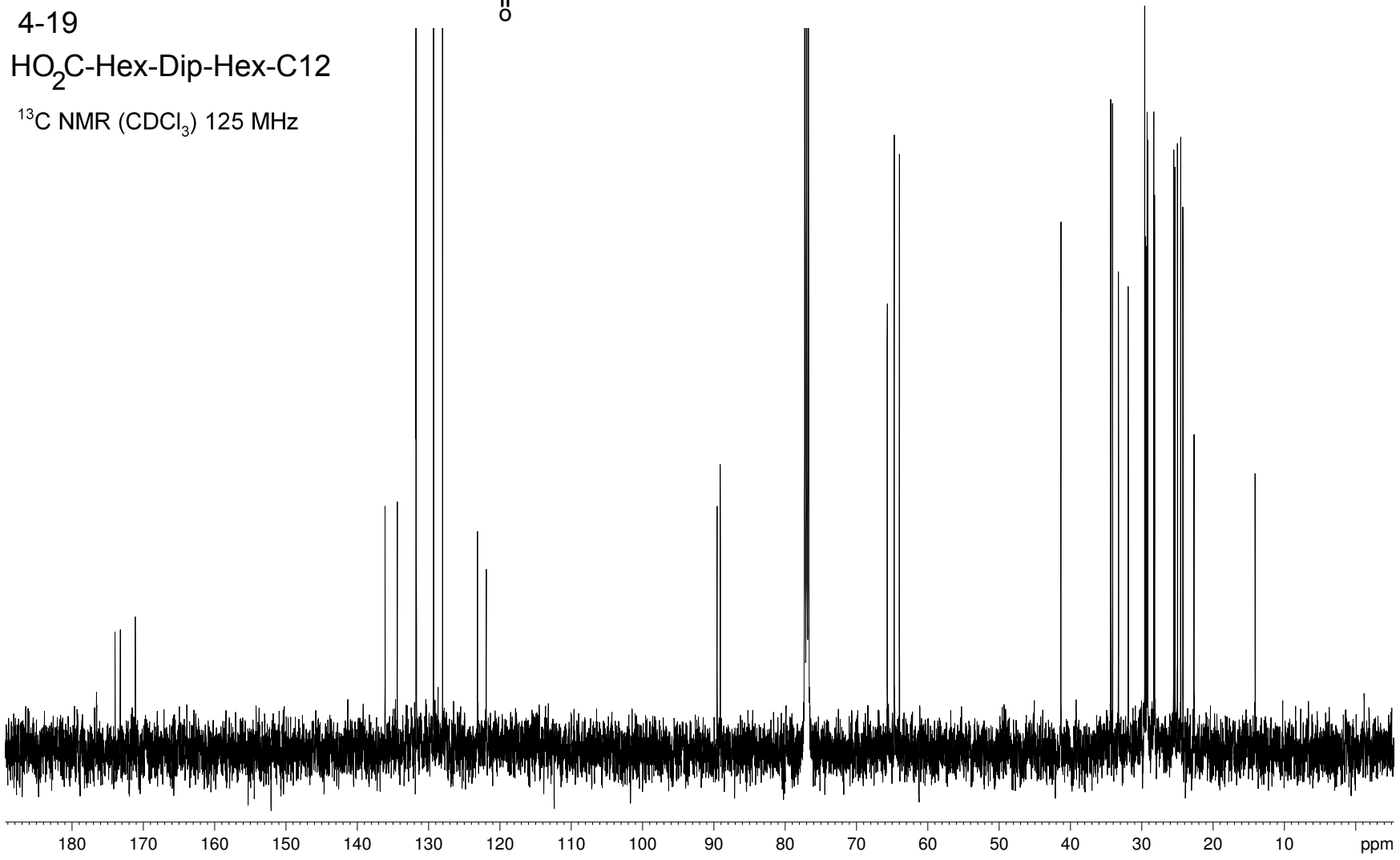

HO_2C-Hex-Dip-Hex-C12

4-19

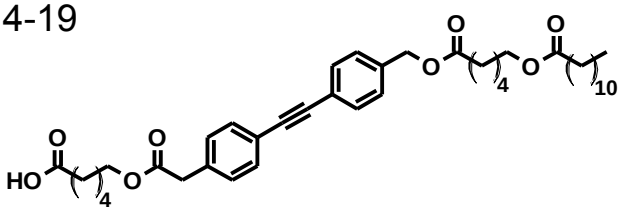

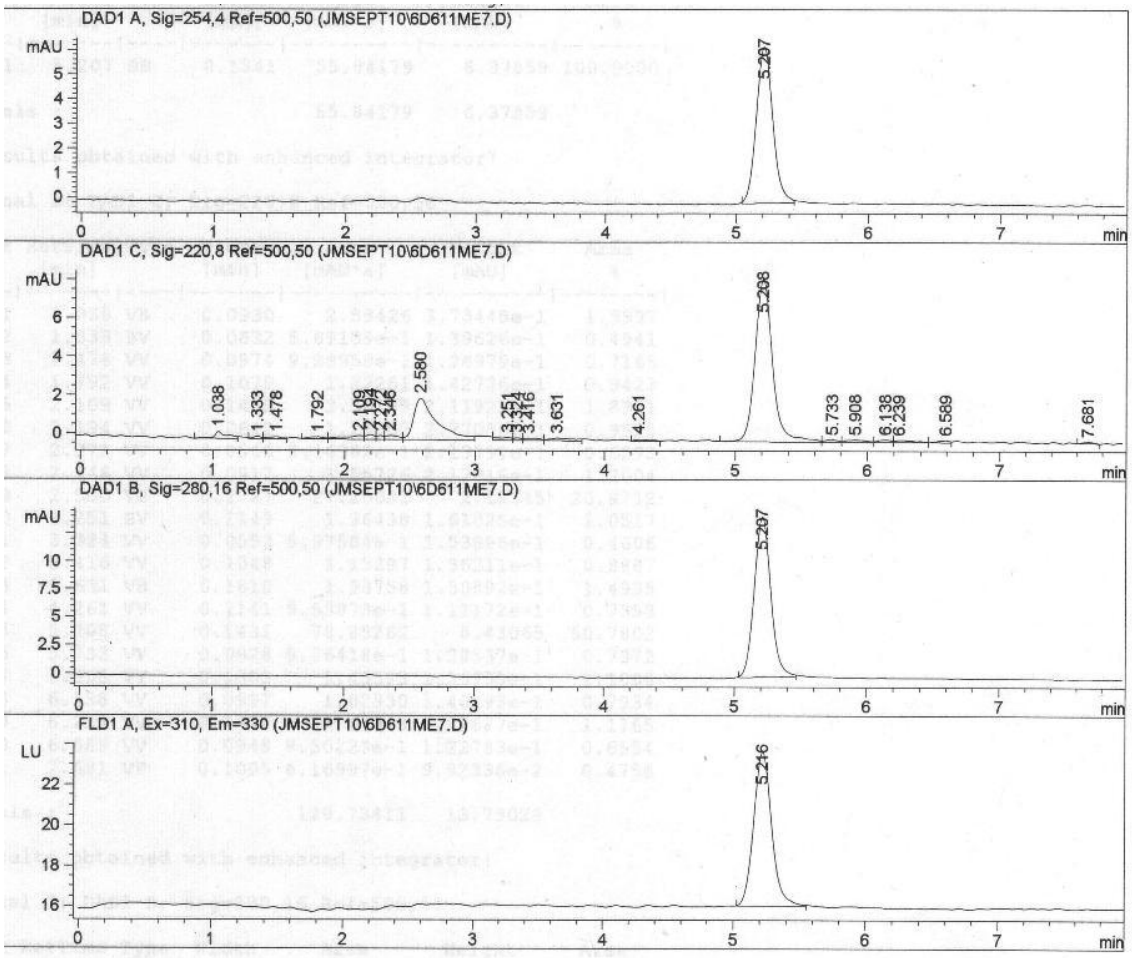

-HPLC trace of sample used for fluorescence and transport studies
-CONDITIONS: HP series 1100 HPLC
-Machery-Nagel RP C18 “Nucleosil” analytical column (4 mm x 250mm)
-3:1 ACN:CH_3OH as eluting solvents, flow 1mL/min

HO_2C-Hex-Dip-Hex-C(12)

MS: -ve ion ESI, Q-TOF
calc'd for C41H55O8 = 675.3897 amu,
obtained = 675.3804 amu

4-19

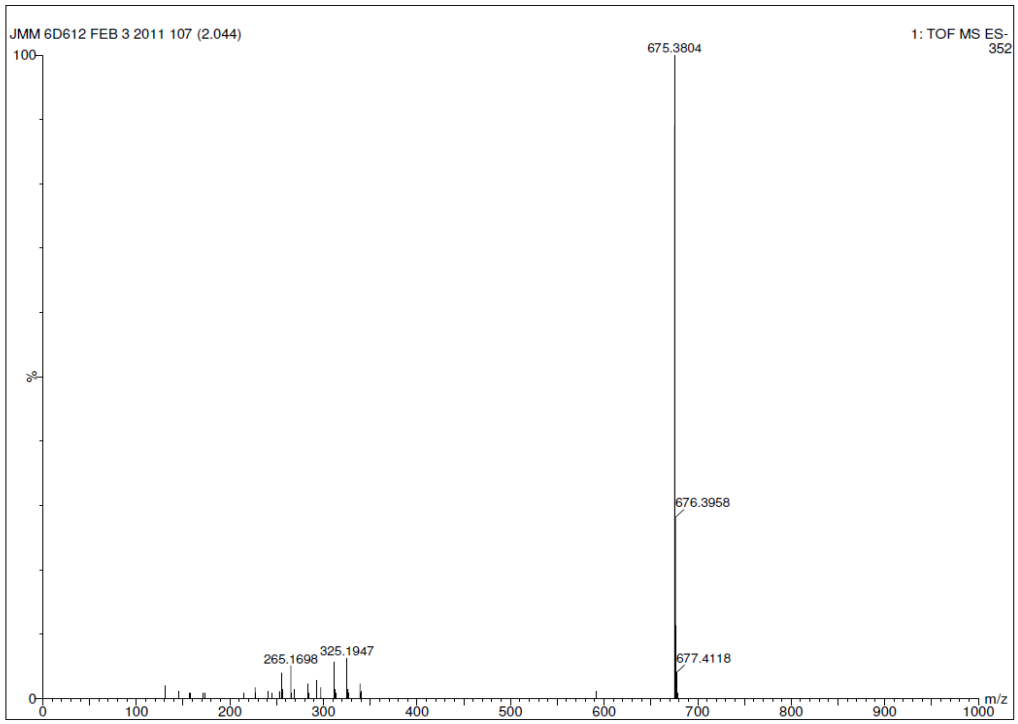

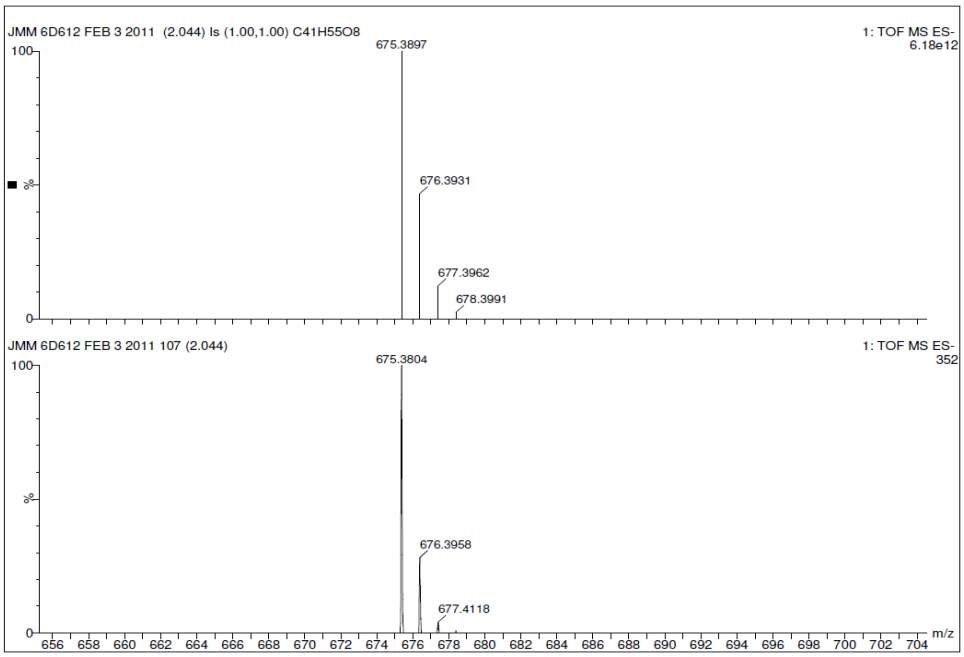

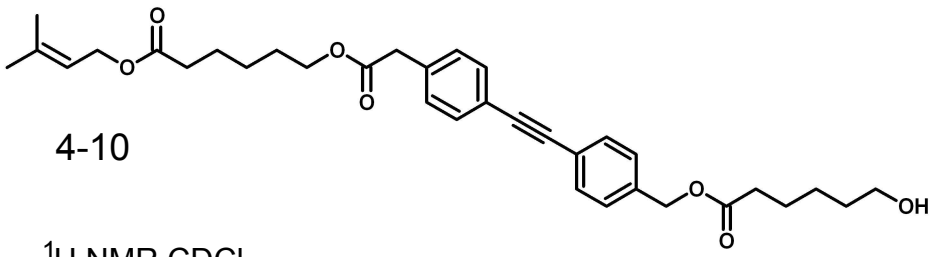

4-10

^{1}H NMR $CDCl_3$

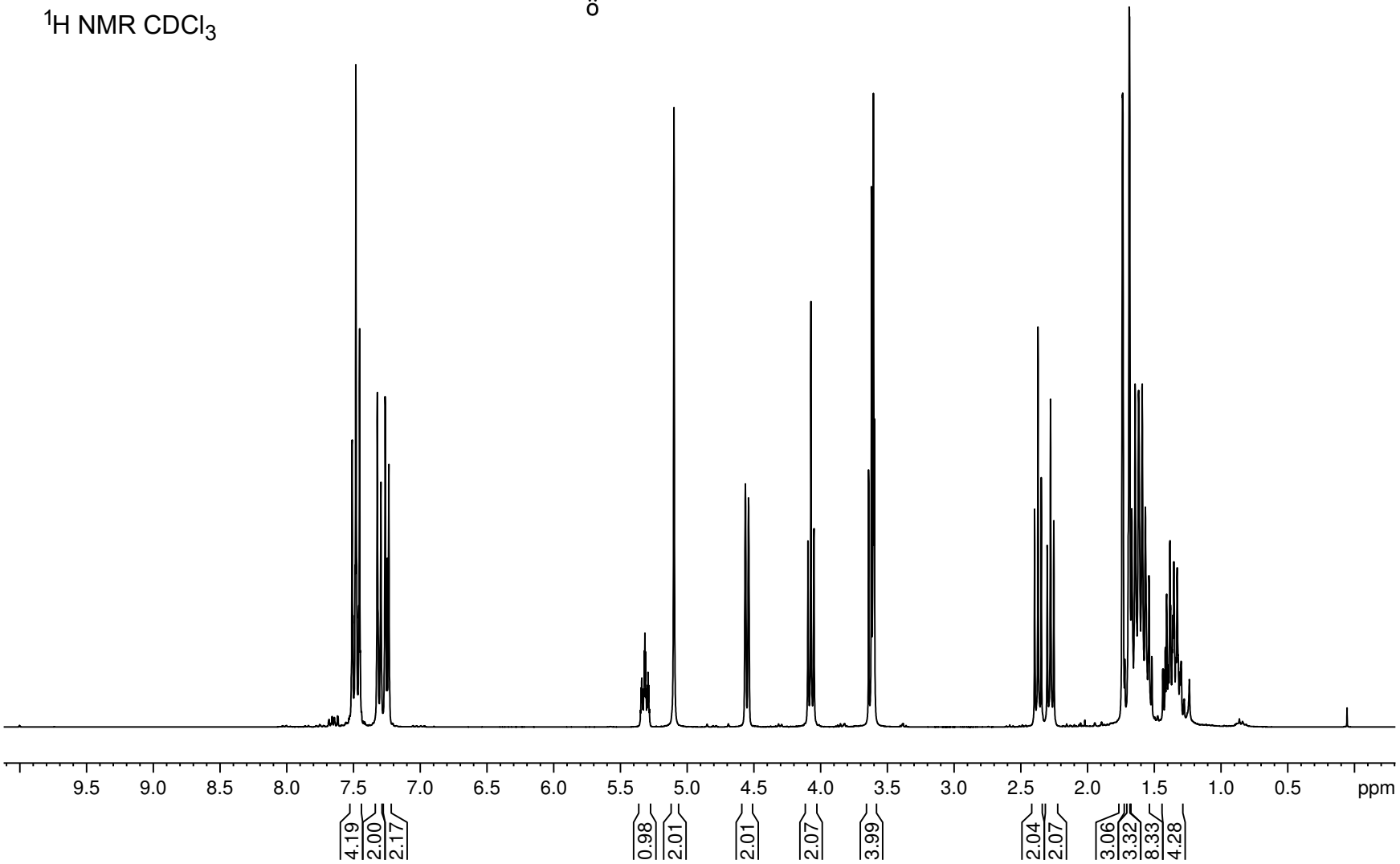

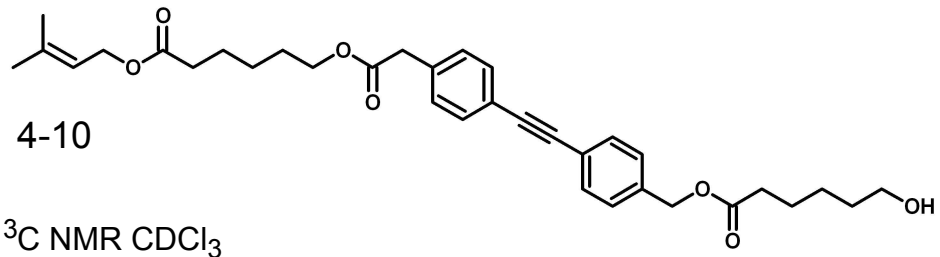

4-10

^{13}C NMR $CDCl_3$

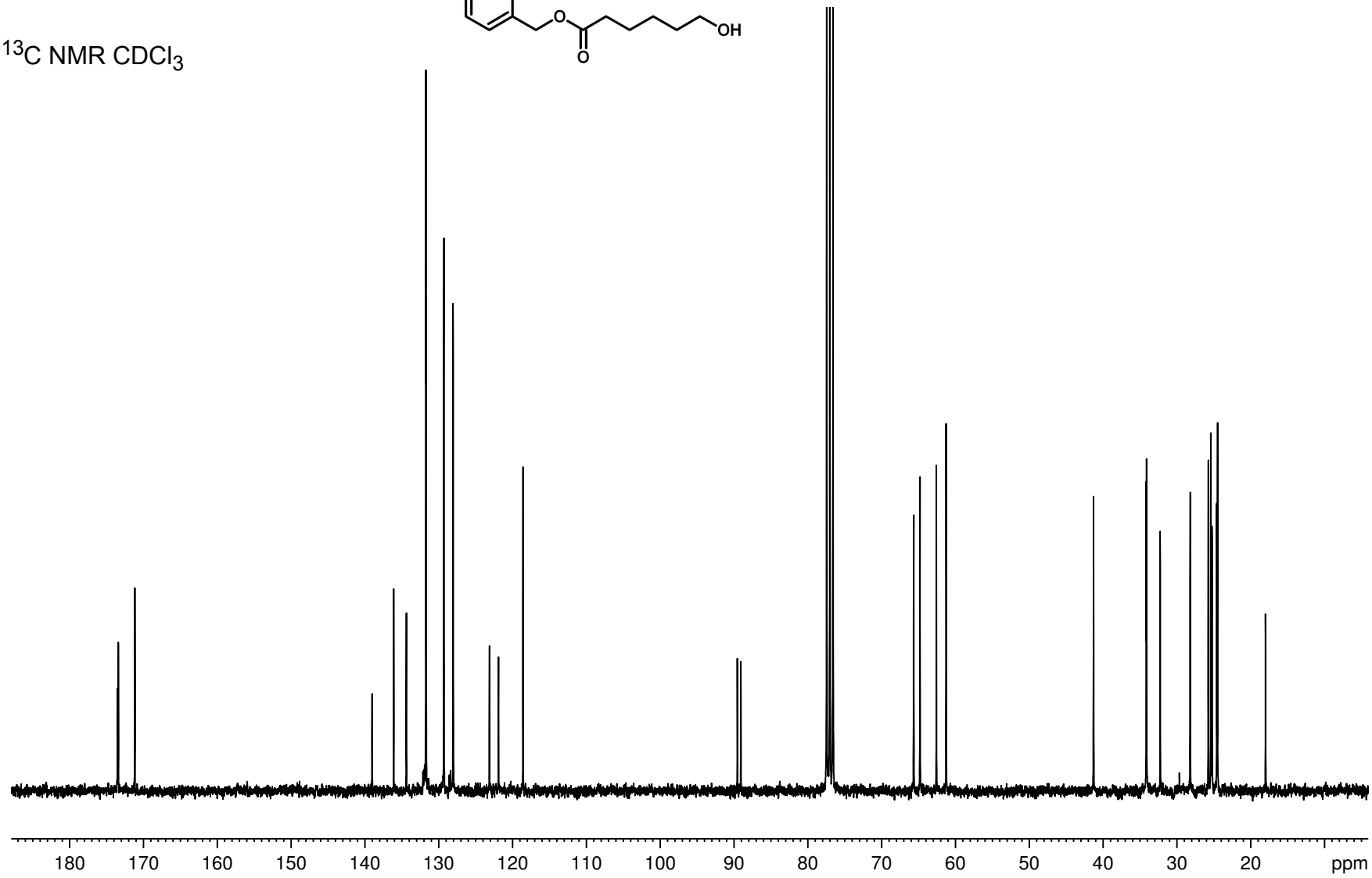

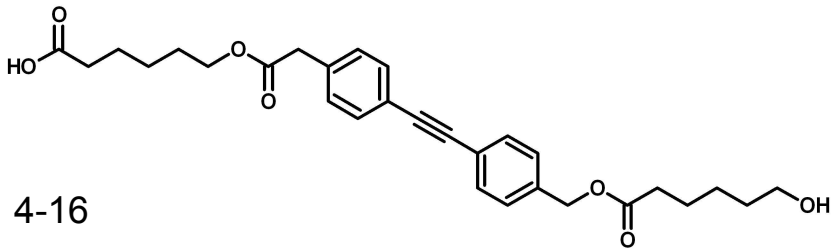

4-16

HO_2C-Hex-Dip-Hex-OH

^1H NMR ($CDCl_3$) 300MHz

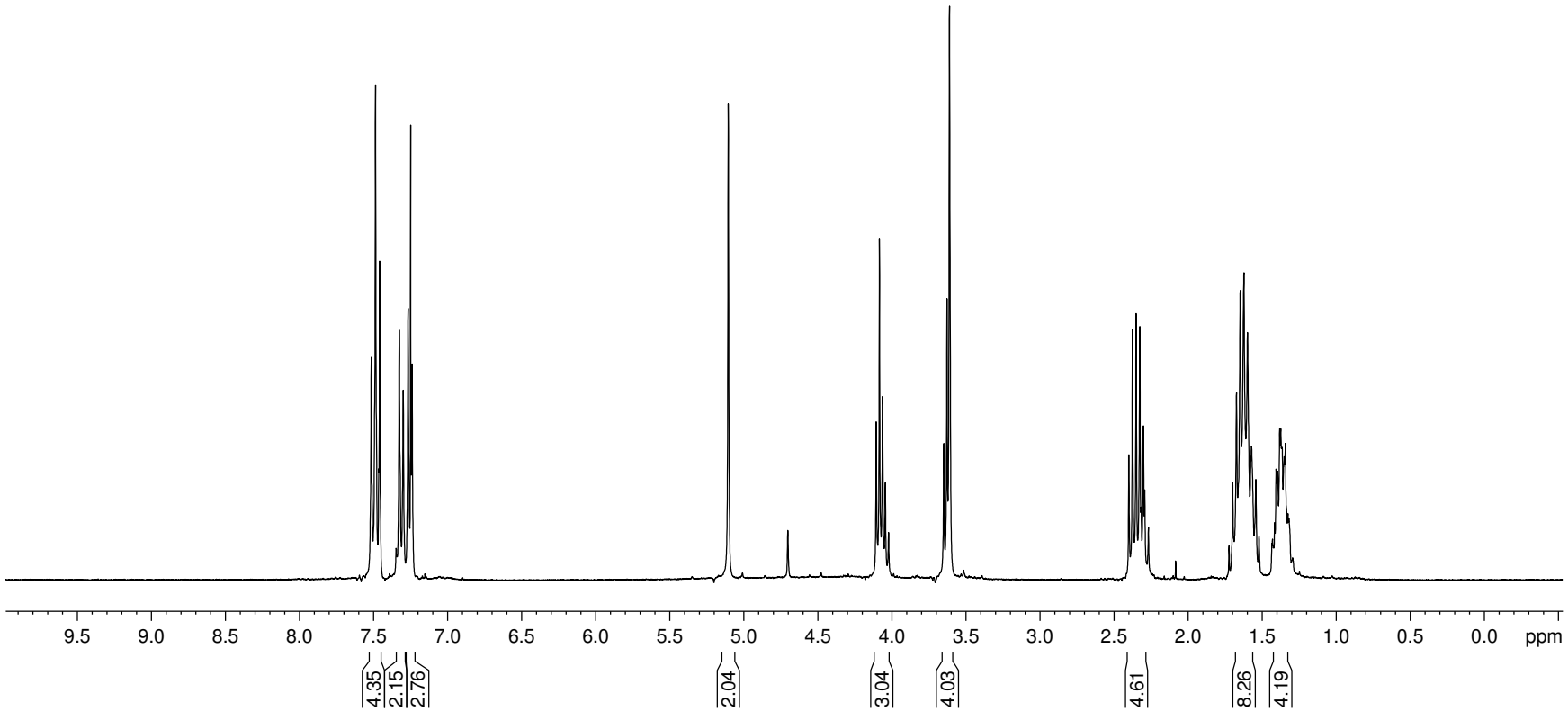

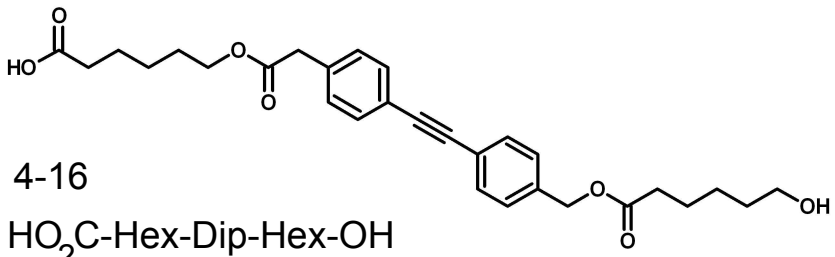

4-16

HO_2C-Hex-Dip-Hex-OH

^{13}C NMR ($CDCl_3$) 75 MHz

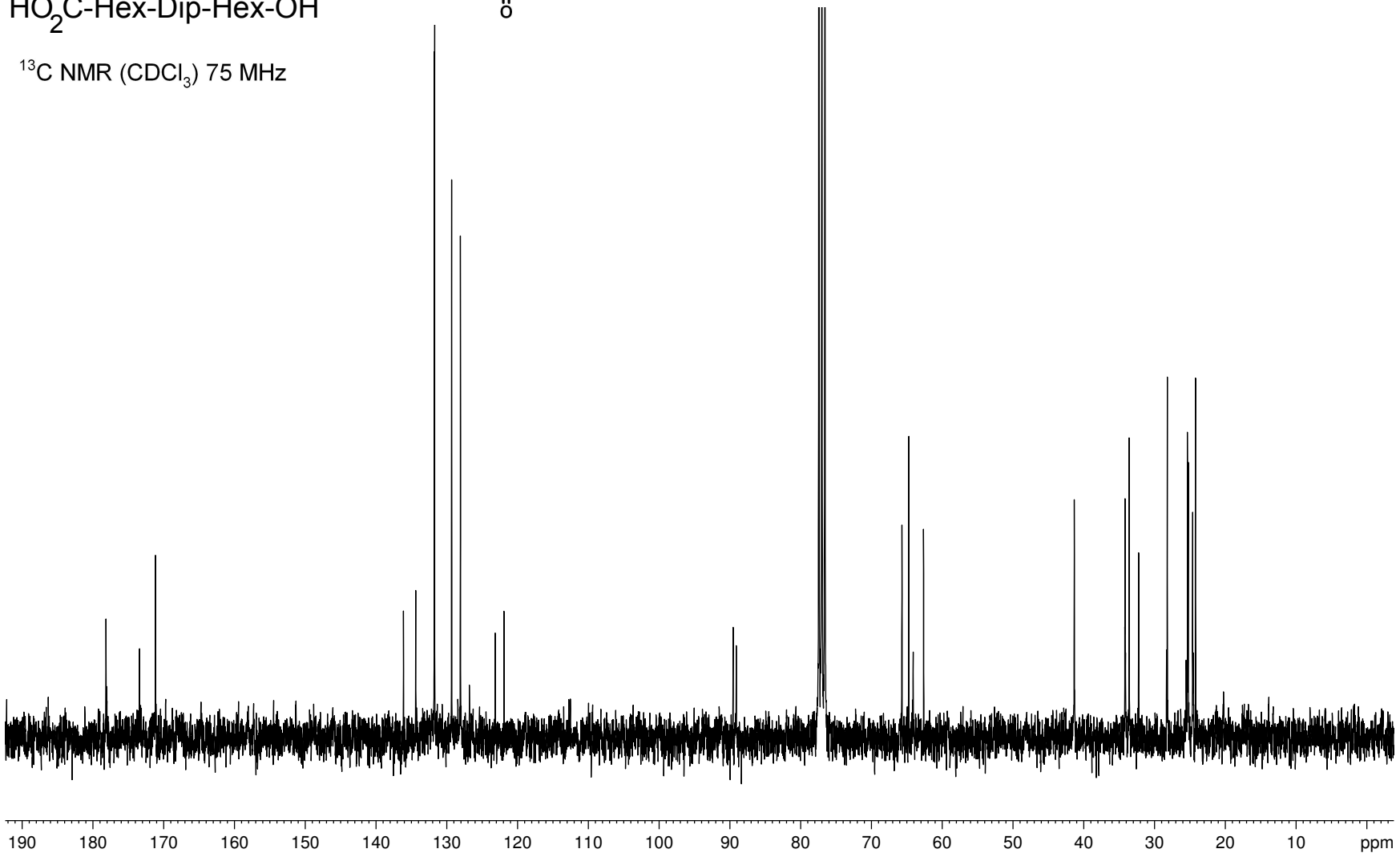

HO_2C-Hex-Dip-Hex-OH

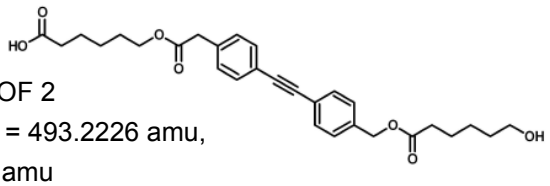

4-16

MS: -ve ion ESI, Q-TOF 2
calc'd for C29H33O7 = 493.2226 amu,
obtained = 493.2171 amu

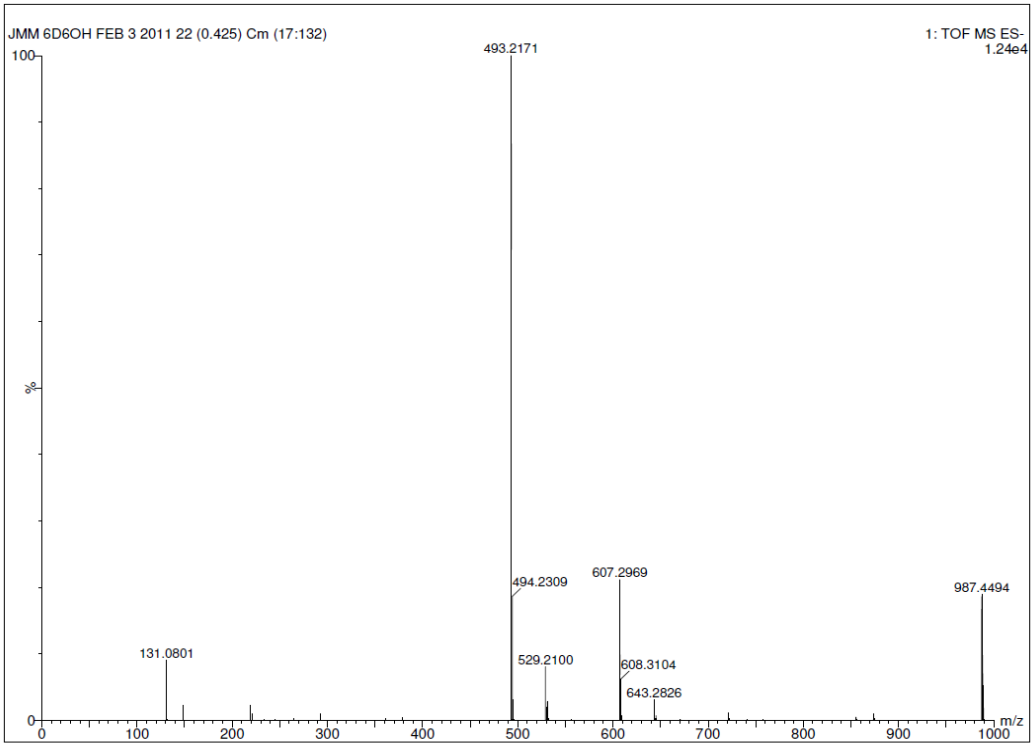

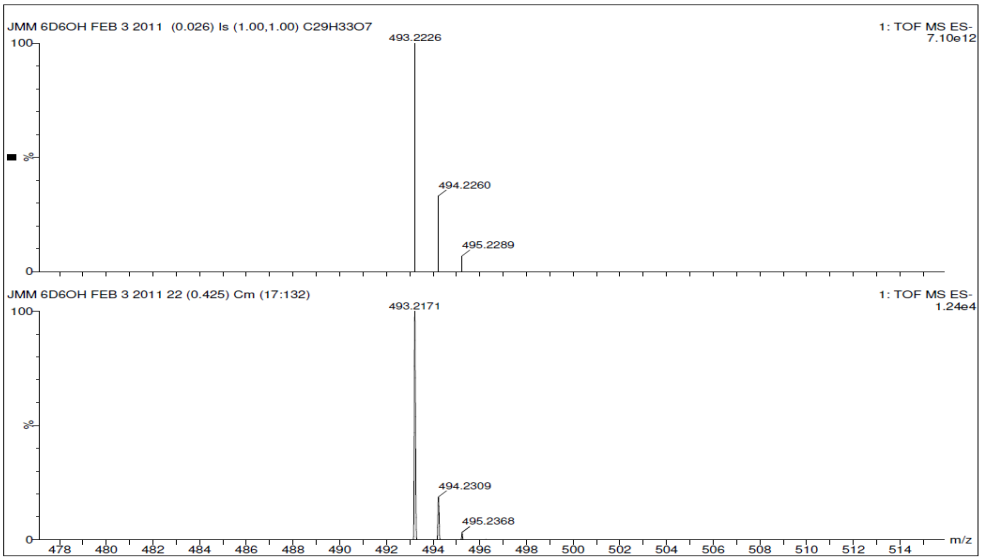

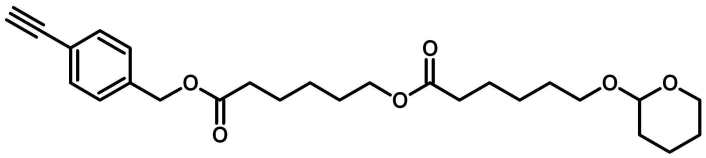

4-2

^{1}H NMR ($CDCl_3$) 300MHz

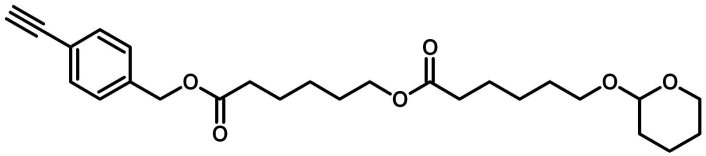

4-2

^{13}C NMR ($CDCl_3$) 75 MHz

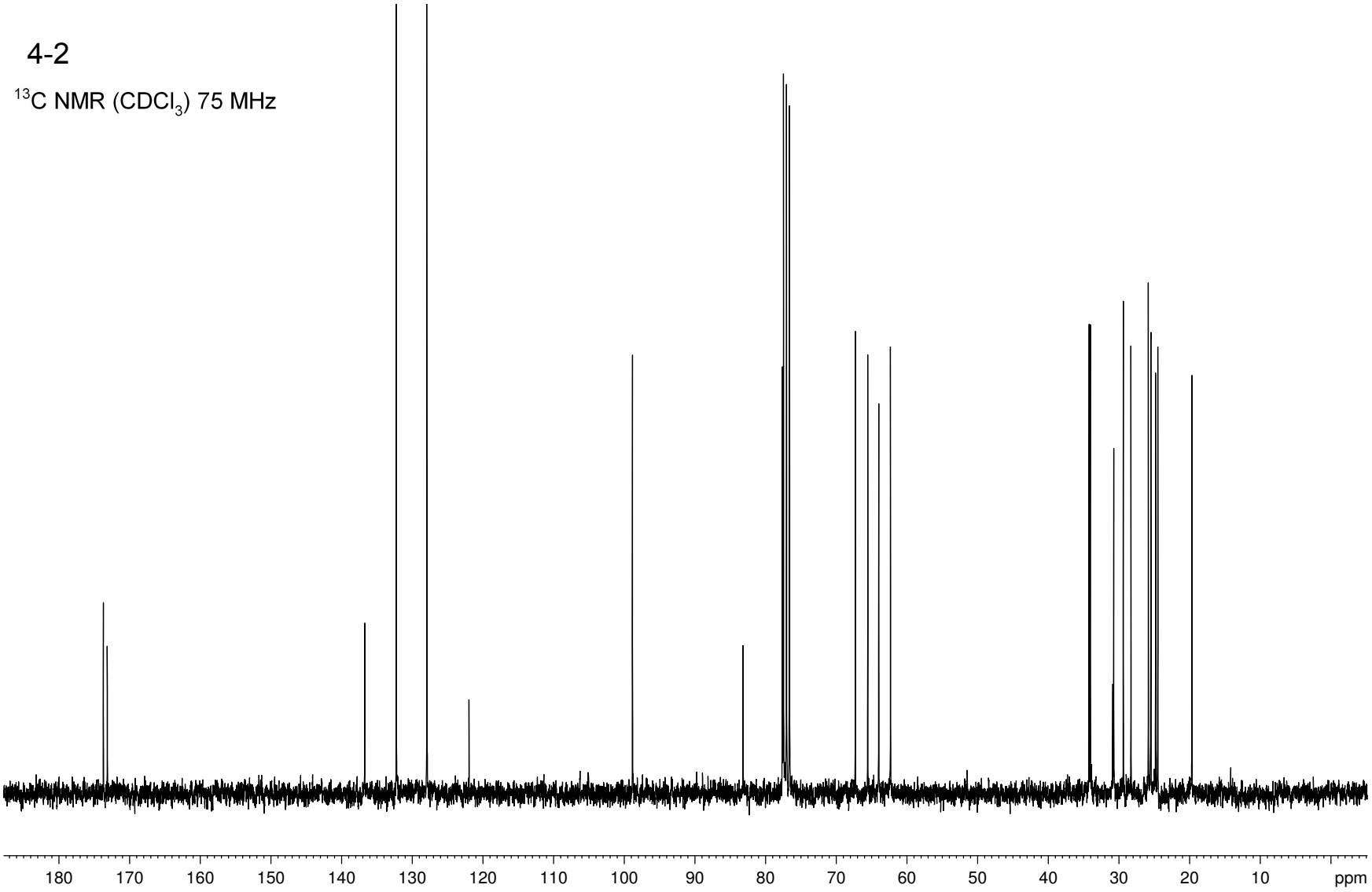

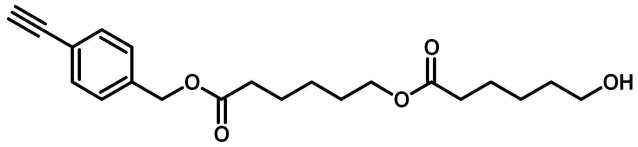

4-3

^{1}H NMR ($CDCl_3$) 300MHz

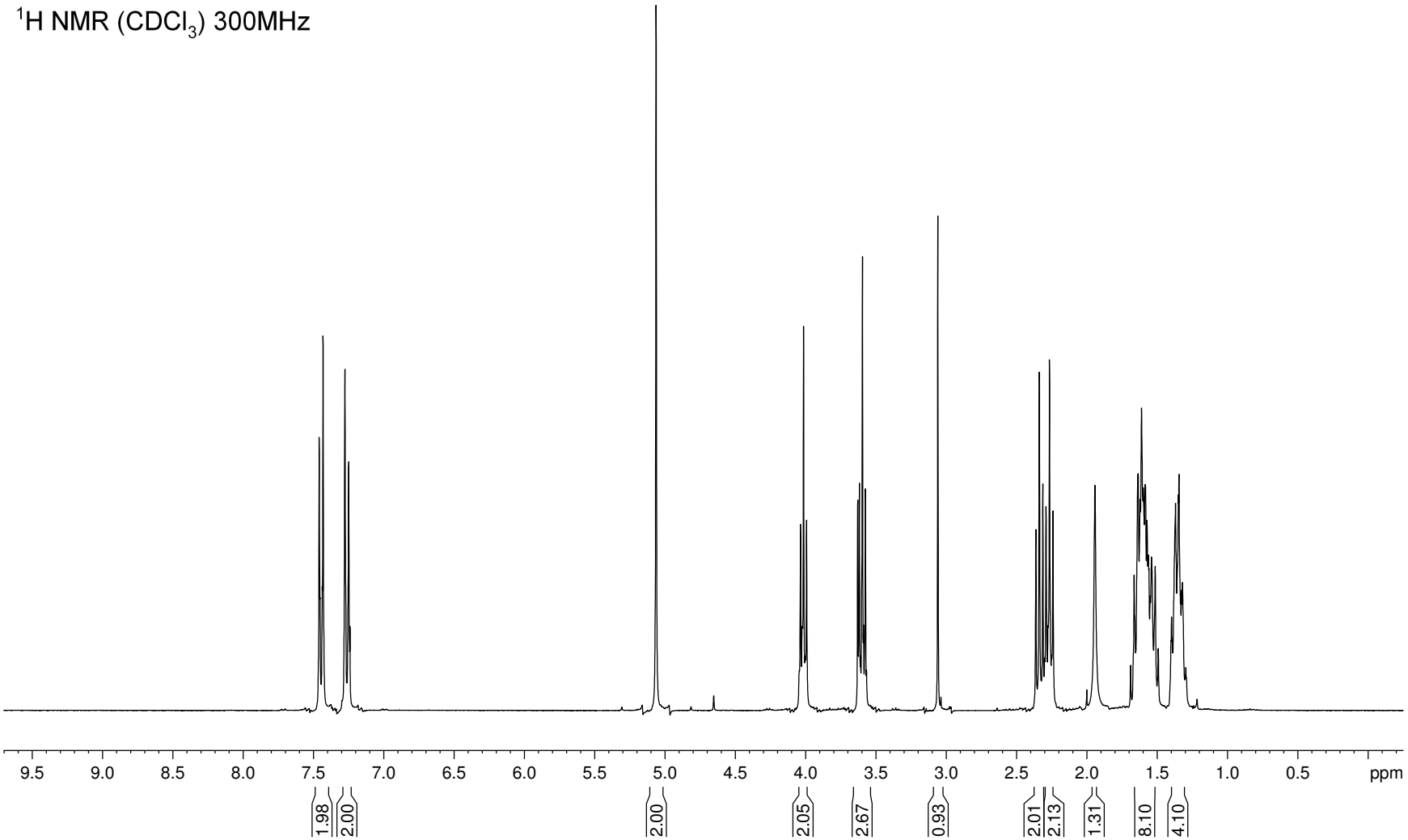

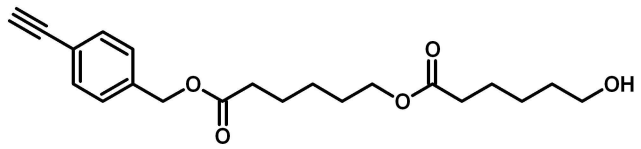

4-3

^{13}C NMR ($CDCl_3$) 75 MHz

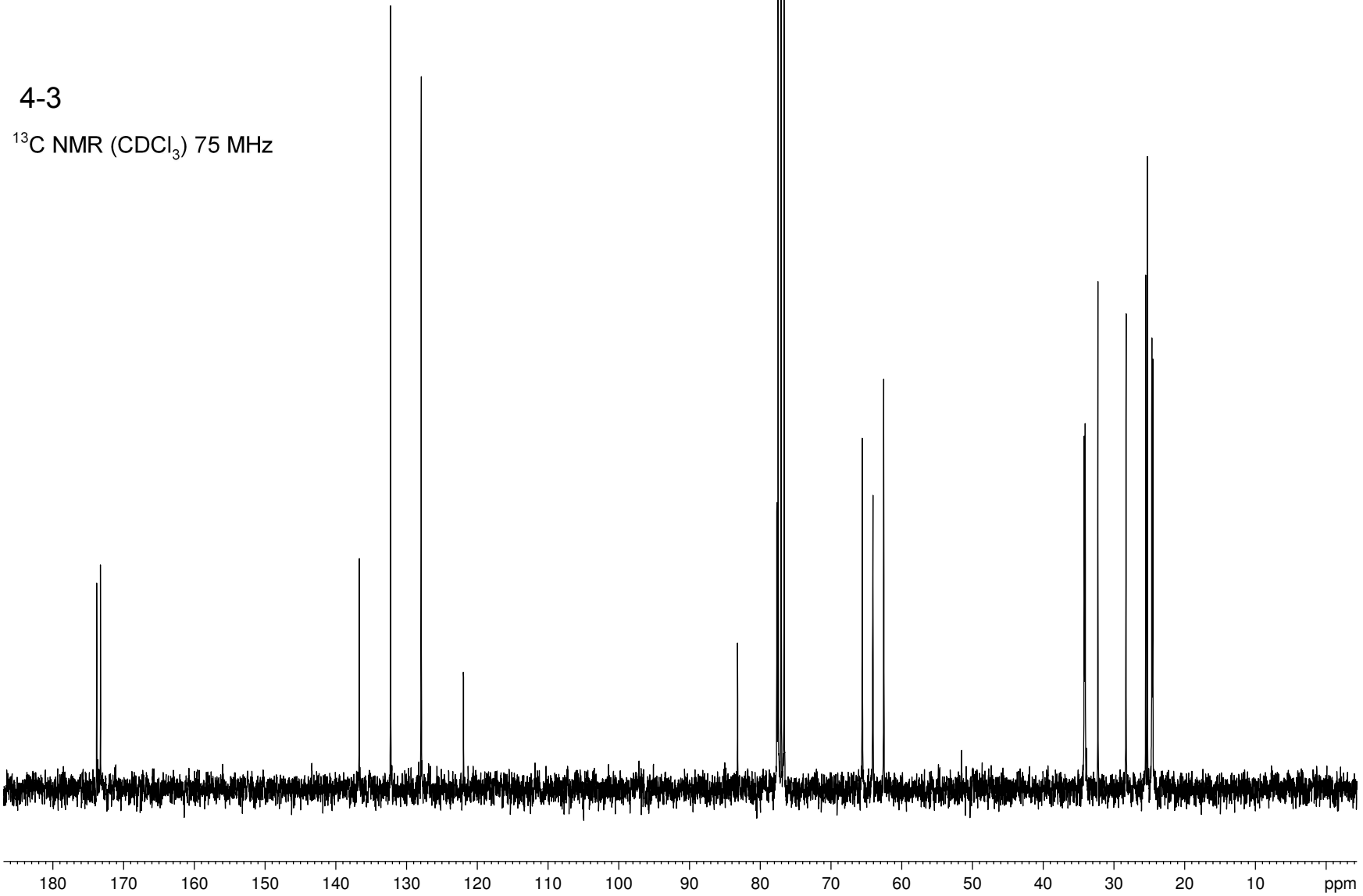

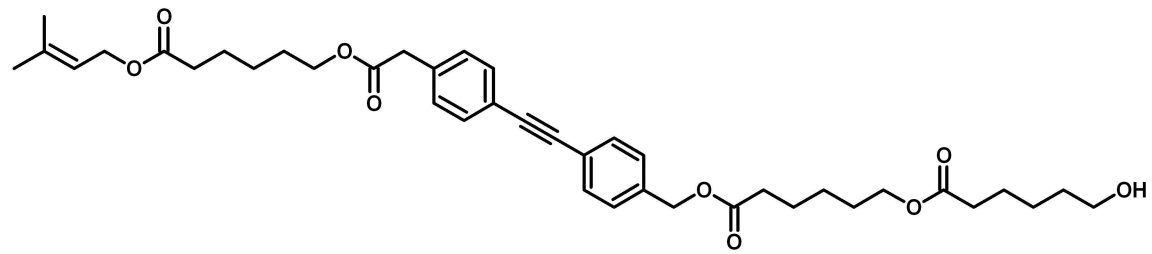

4-11

^{1}H NMR ($CDCl_3$) 300MHz

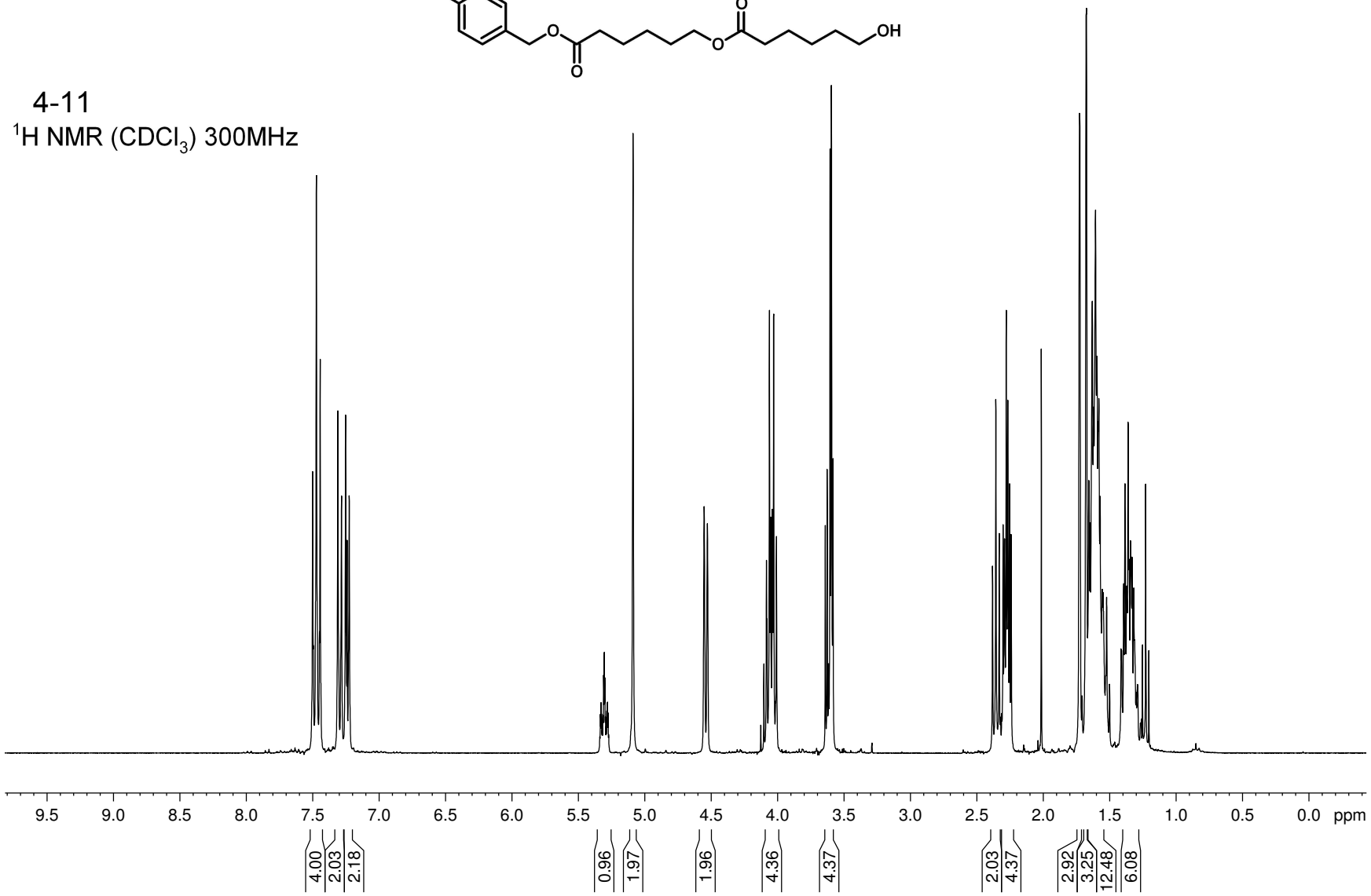

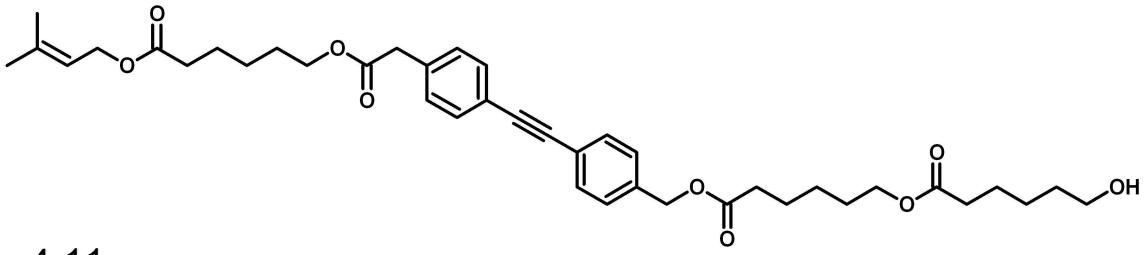

4-11

^{13}C NMR ($CDCl_3$) 75 MHz

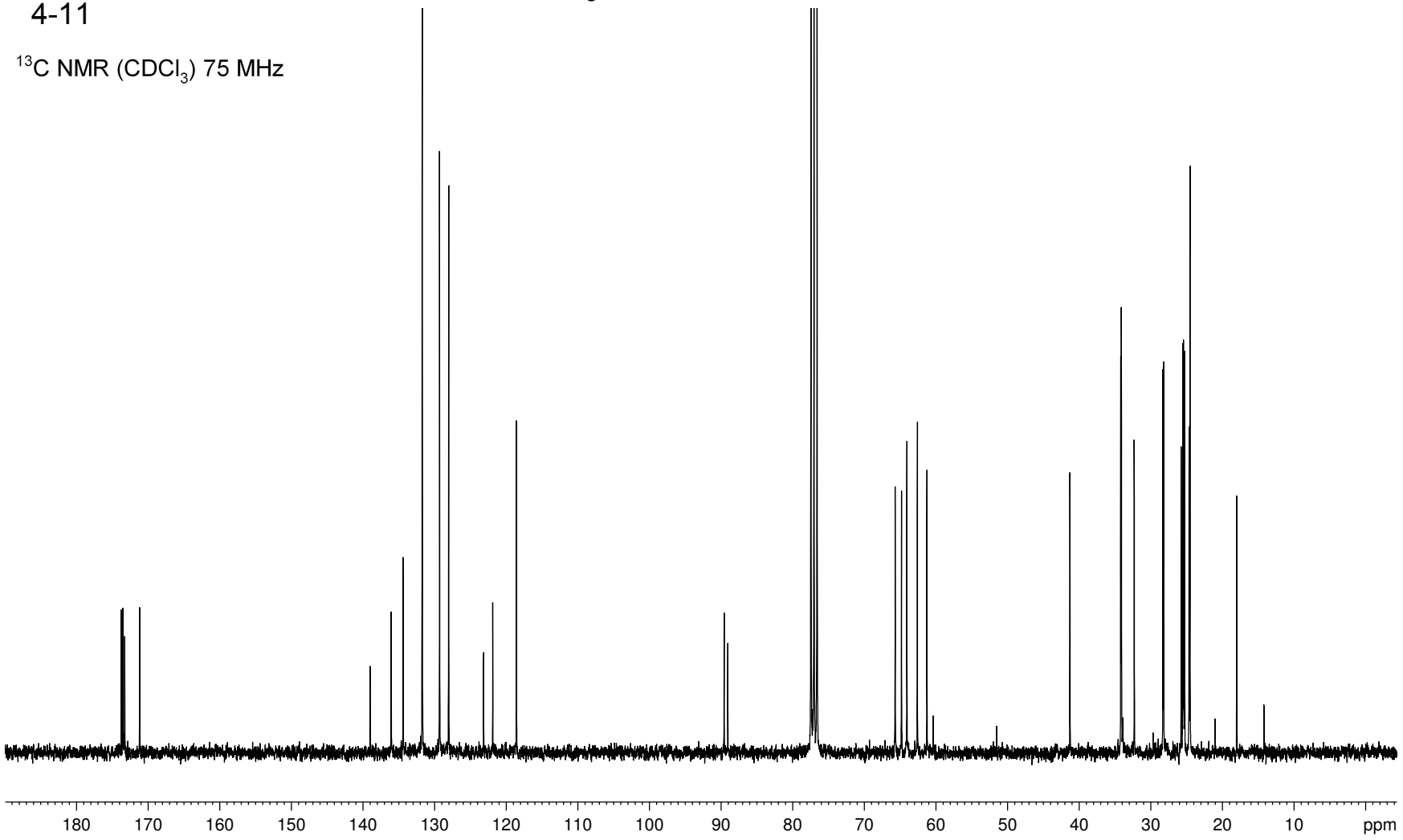

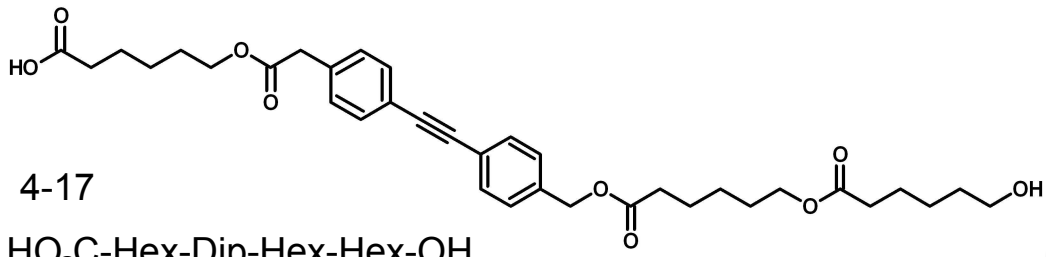

4-17

HO_2C-Hex-Dip-Hex-Hex-OH

^1H NMR ($CDCl_3$) 300MHz

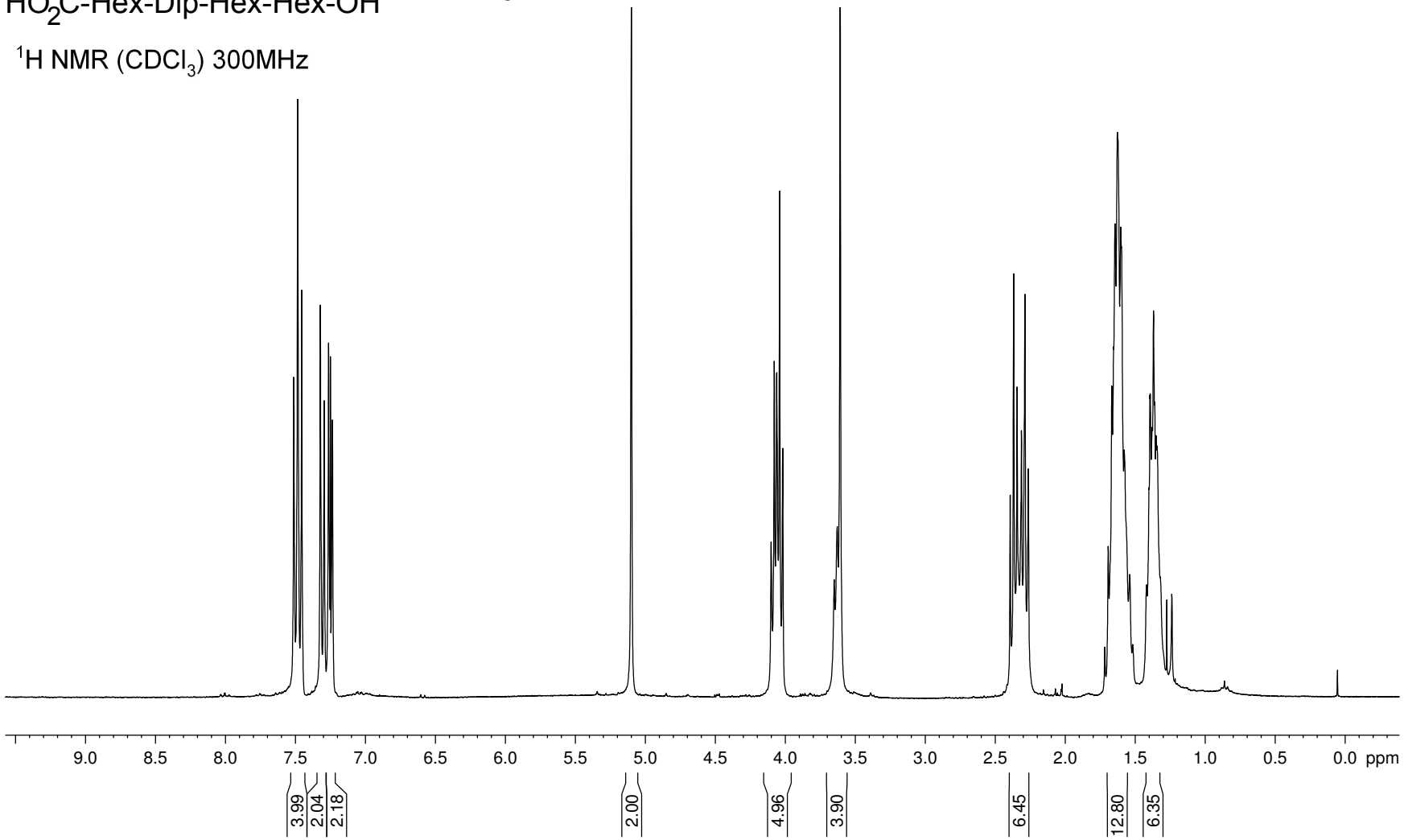

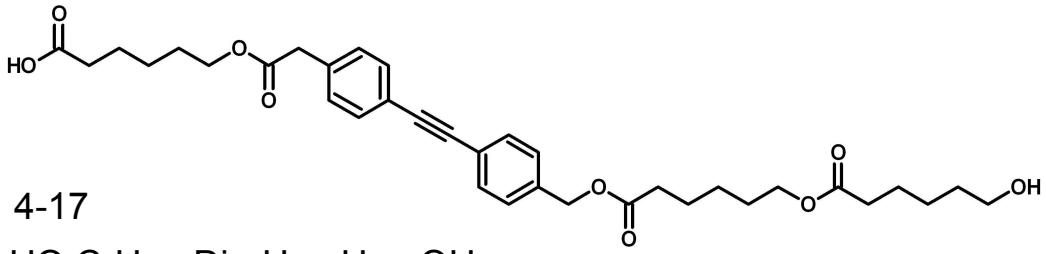

4-17

HO_2C-Hex-Dip-Hex-Hex-OH

^{13}C NMR ($CDCl_3$) 75 MHz

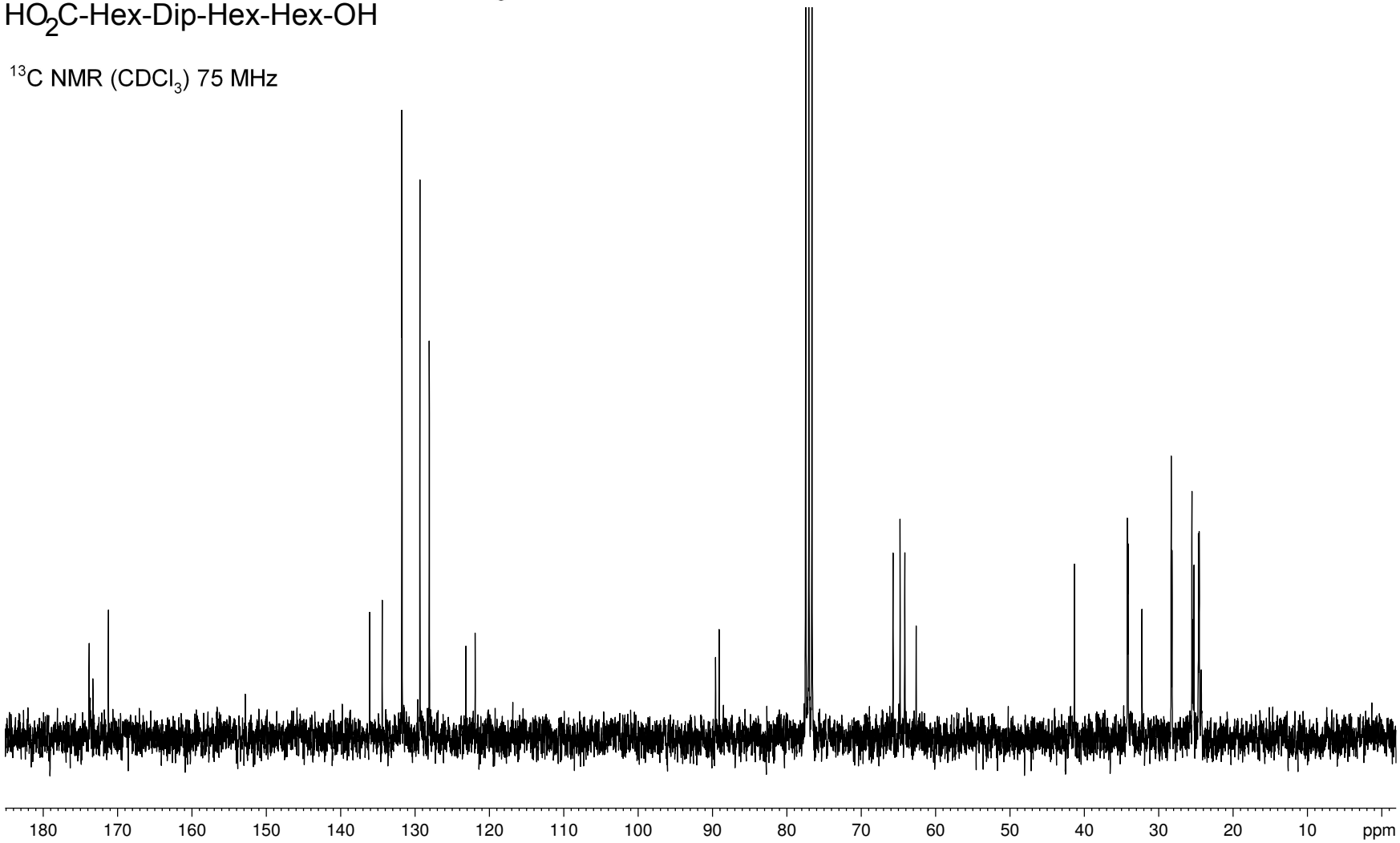

HO_2C-Hex-Dip-Hex-Hex-OH

4-17

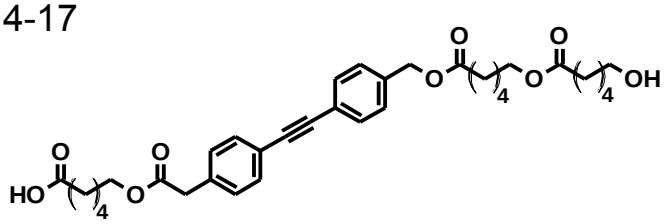

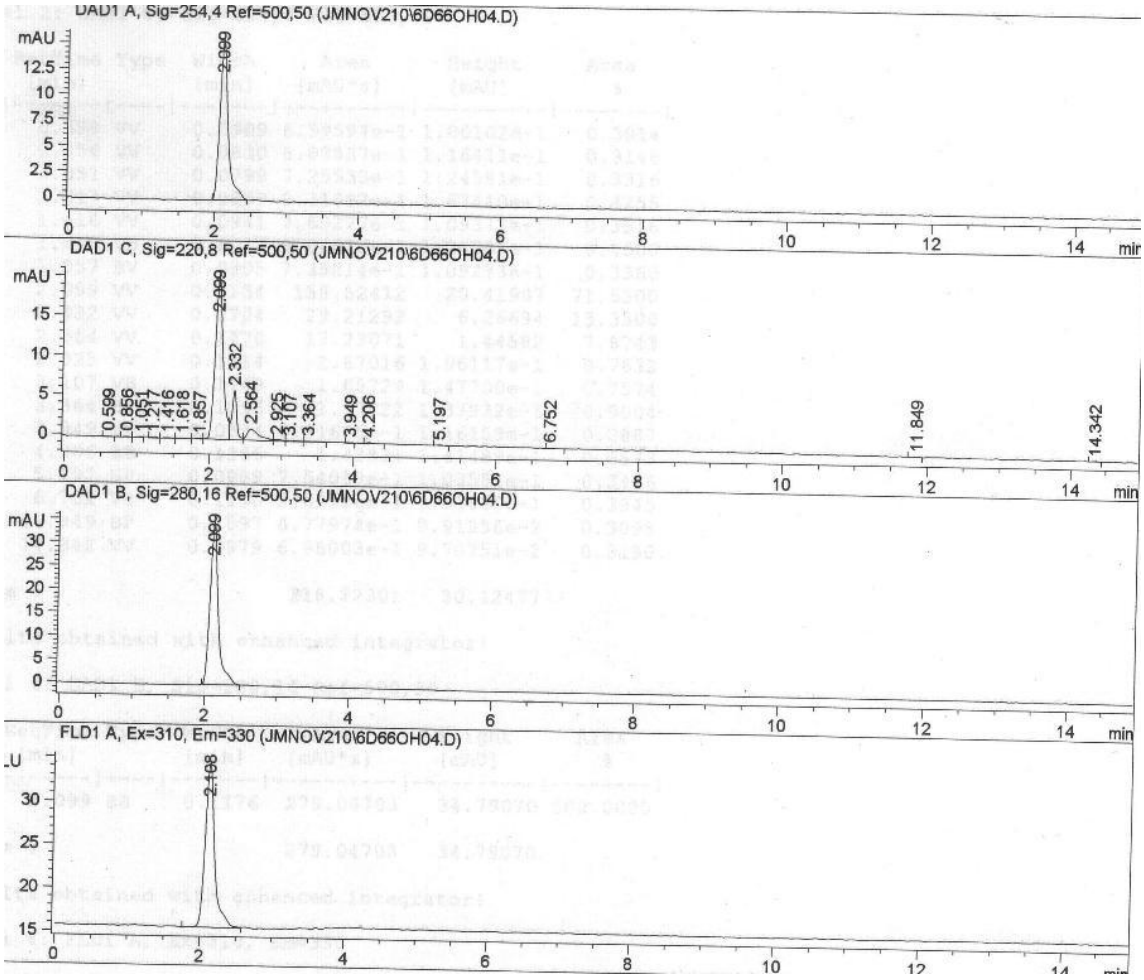

-HPLC trace of sample used for fluorescence and transport studies
-CONDITIONS: HP series 1100 HPLC
-Machery-Nagel RP C18 “Nucleosil” analytical column (4 mm x 250mm)
-3:1 ACN:CH_3OH as eluting solvents, flow 1mL/min

HO_2C-Hex-Dip-Hex-Hex-OH

4-17

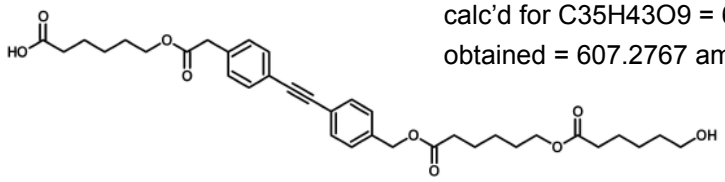

MS: -ve ion ESI, Q-TOF
calc'd for C35H43O9 = 607.2907 amu,
obtained = 607.2767 amu

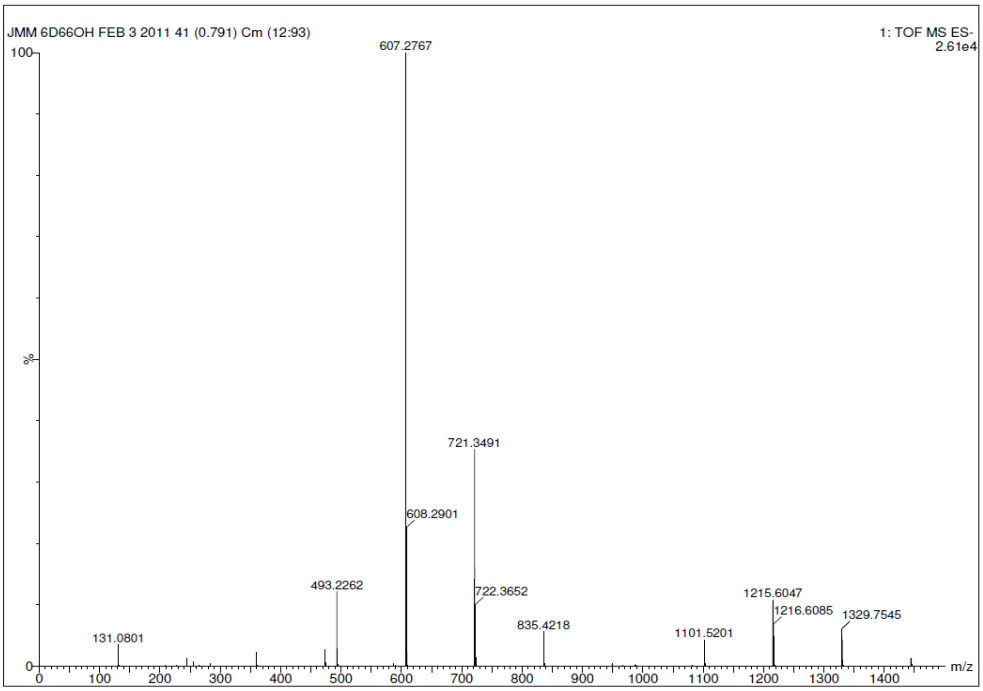

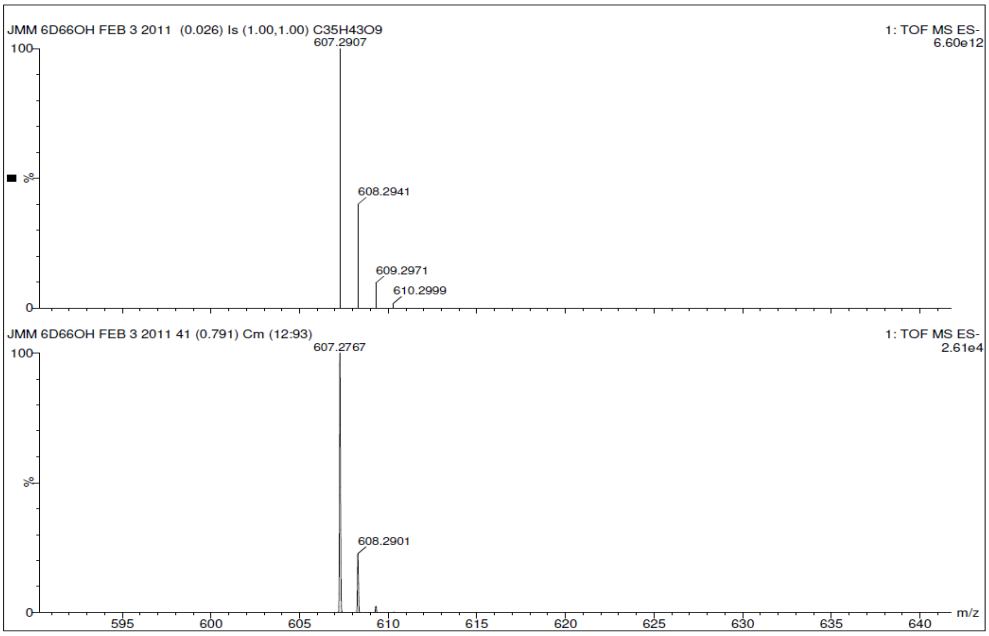

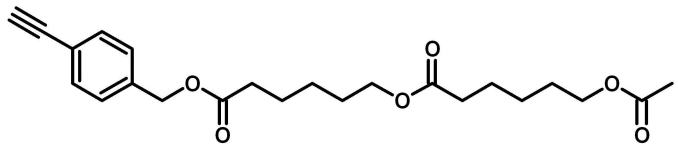

4-4

^{1}H NMR ($CDCl_3$) 300MHz

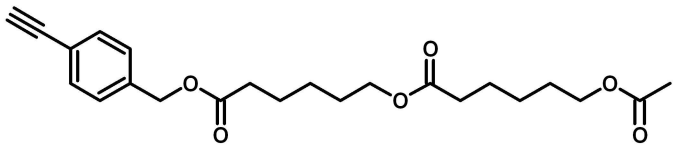

4-4

^{13}C NMR ($CDCl_3$) 75 MHz

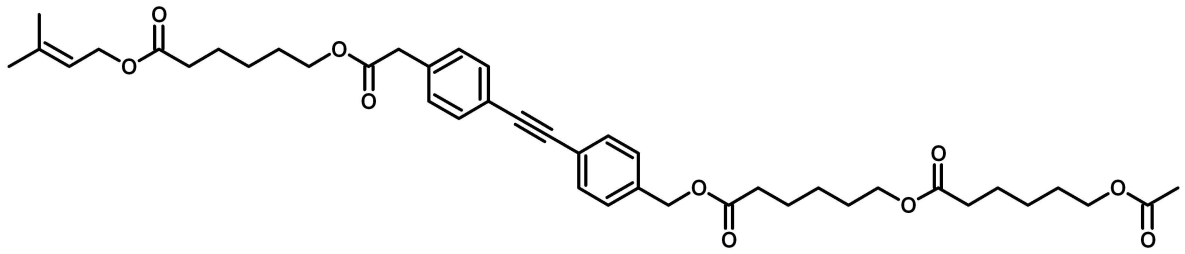

4-13

^{1}H NMR ($CDCl_3$) 300MHz

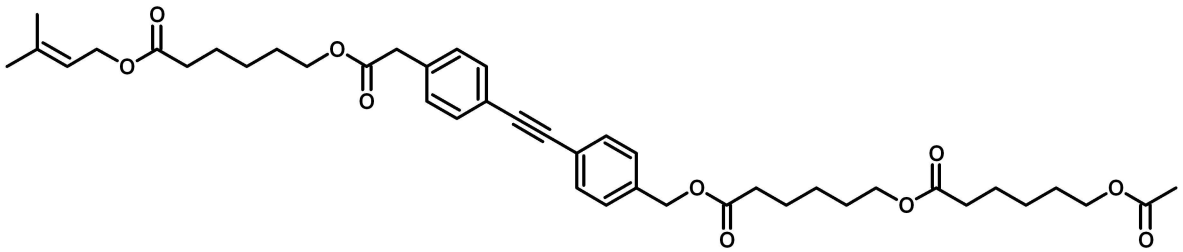

4-13

^{13}C NMR ($CDCl_3$) 75 MHz

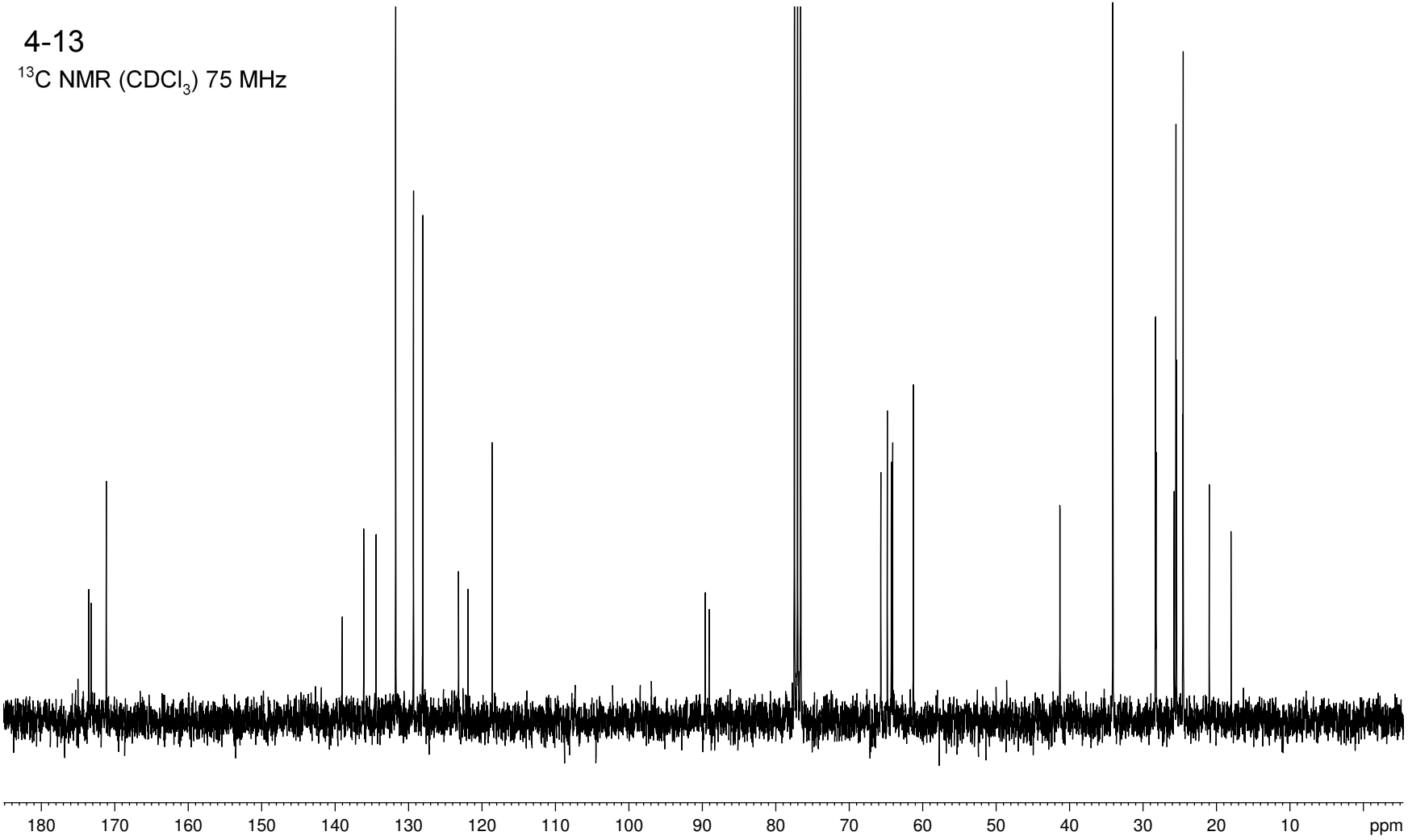

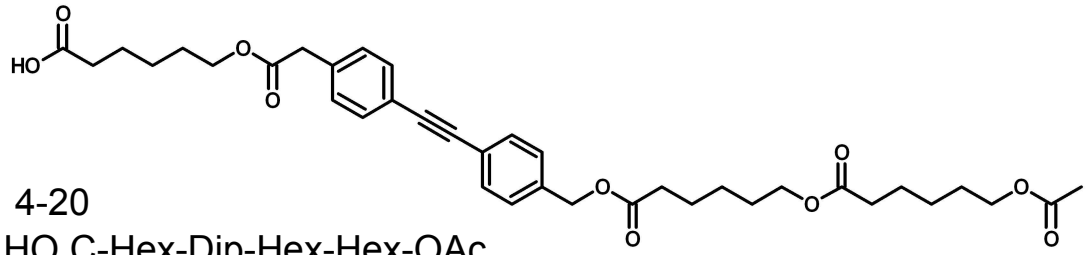

4-20

HO_2C-Hex-Dip-Hex-Hex-OAc

^1H NMR ($CDCl_3$) 500MHz

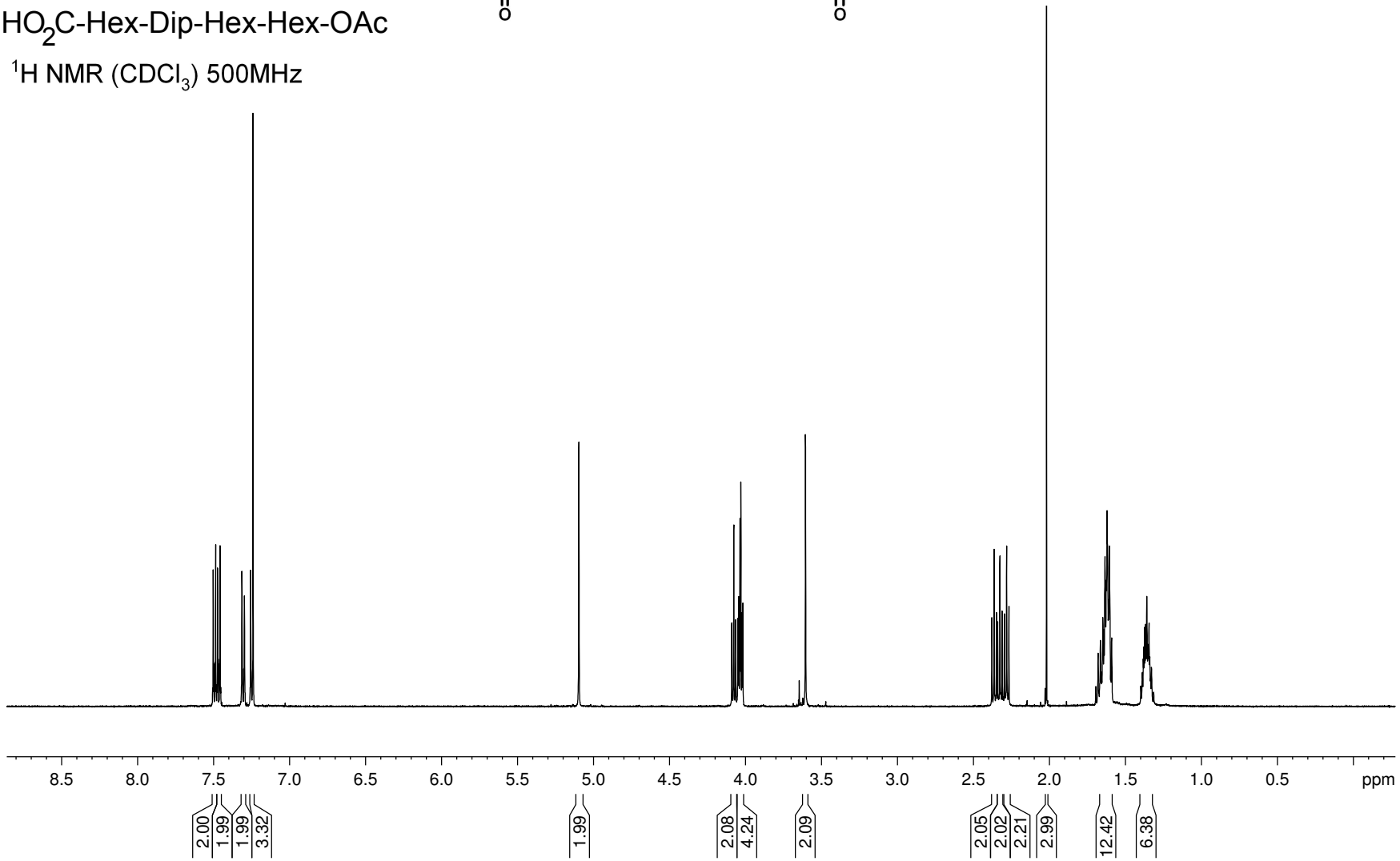

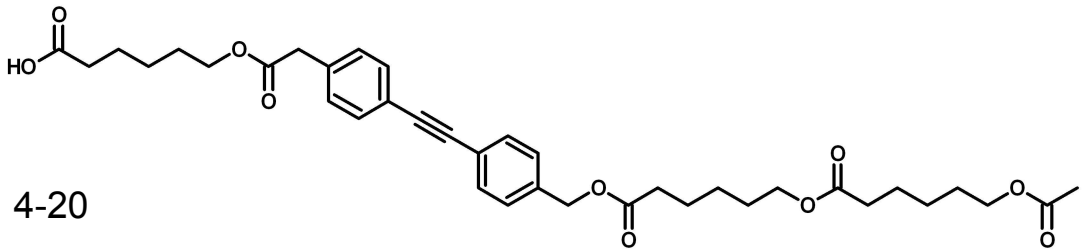

4-20

HO_2C-Hex-Dip-Hex-Hex-OAc

^{13}C NMR ($CDCl_3$) 125 MHz

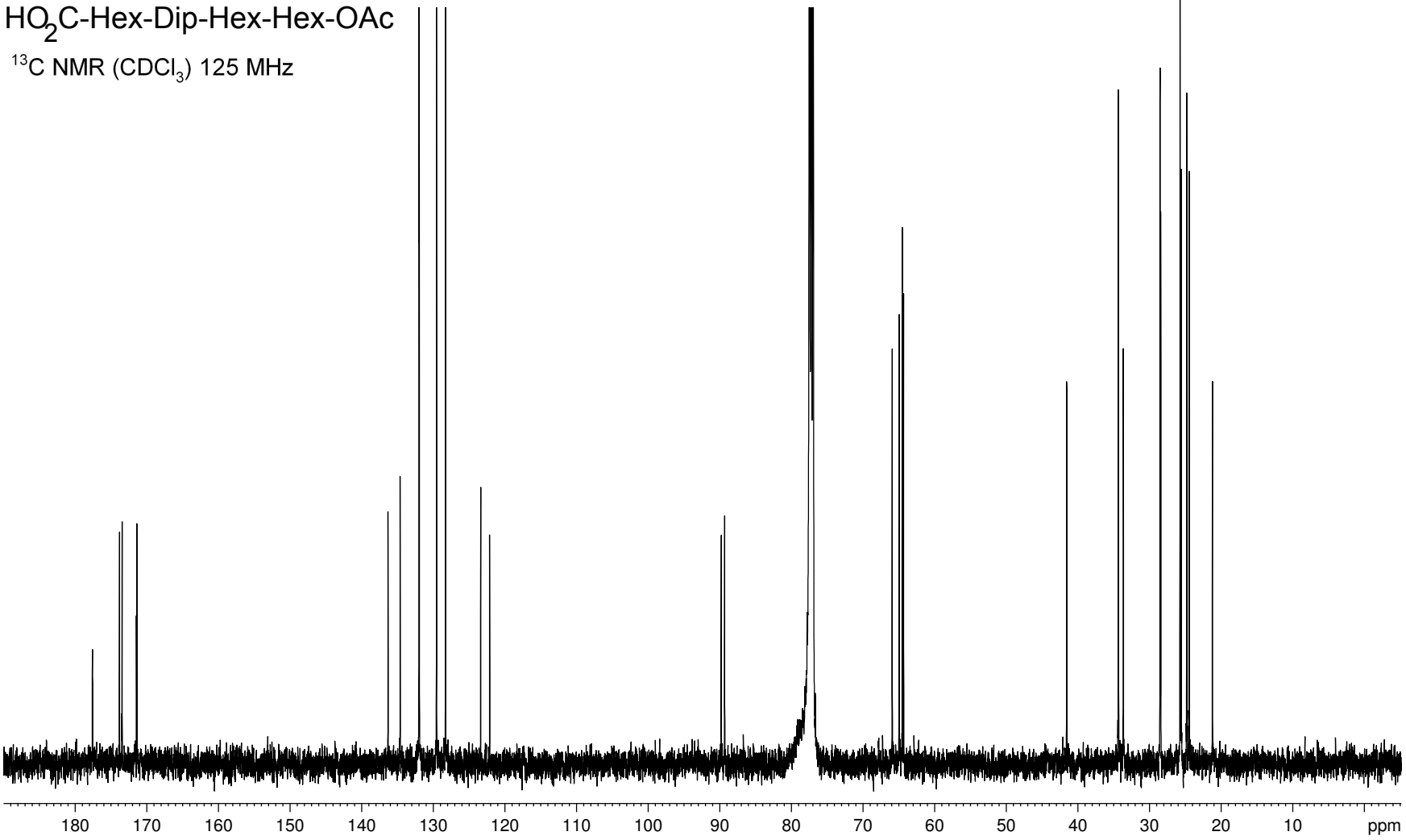

HO_2C-Hex-Dip-Hex-Hex-OAc

4-20

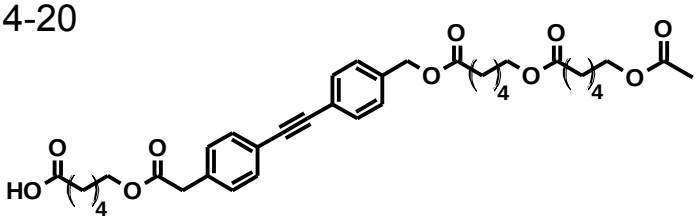

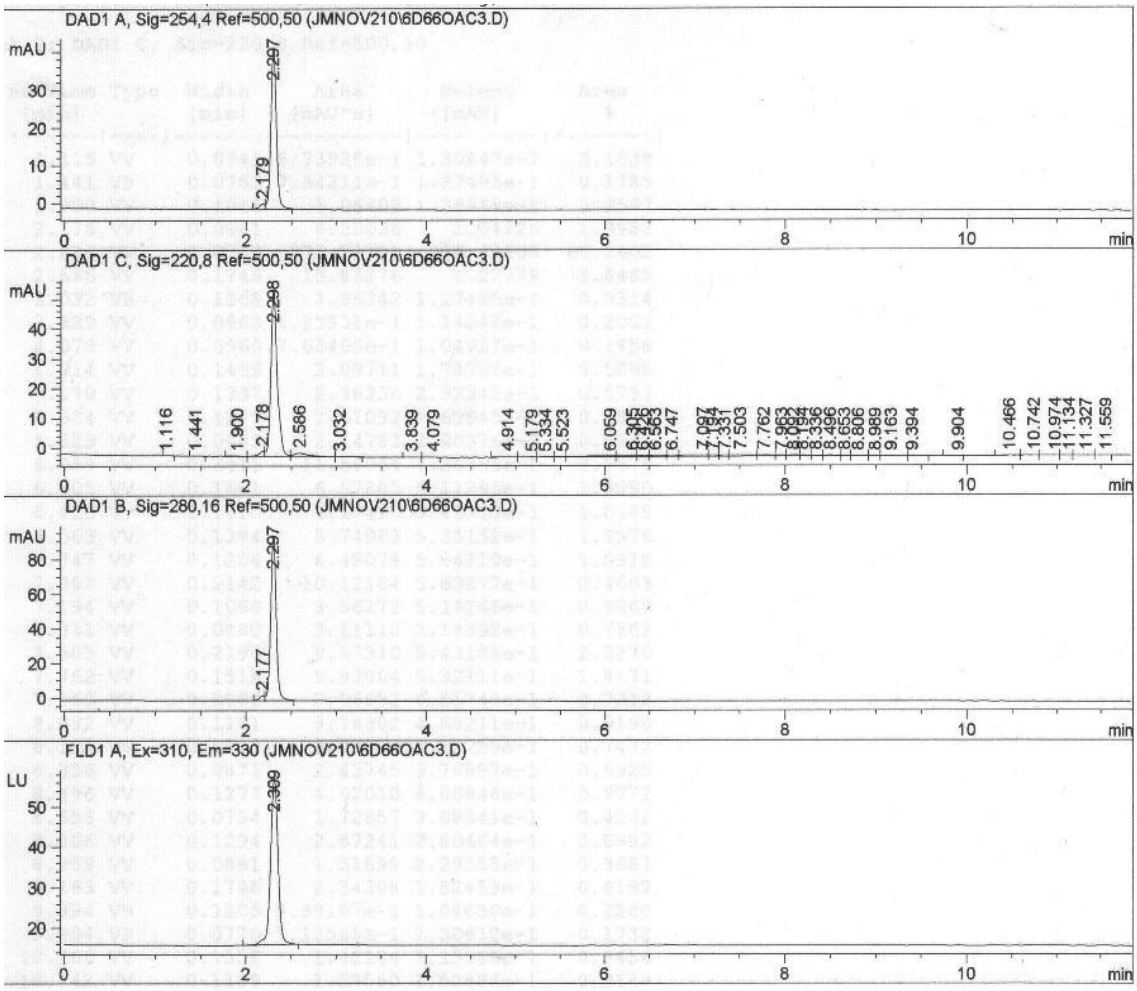

-HPLC trace of sample used for fluorescence and transport studies
-CONDITIONS: HP series 1100 HPLC
-Machery-Nagel RP C18 “Nucleosil” analytical column (4 mm x 250mm)
-1:1 ACN:CH_3OH as eluting solvents, flow 1mL/min

HO_2C-Hex-Dip-Hex-Hex-OAc

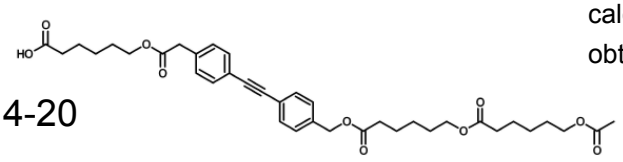

4-20

MS: -ve ion ESI, Q-TOF
calc'd for C37H45O10 = 649.3013 amu,
obtained = 649.3036 amu

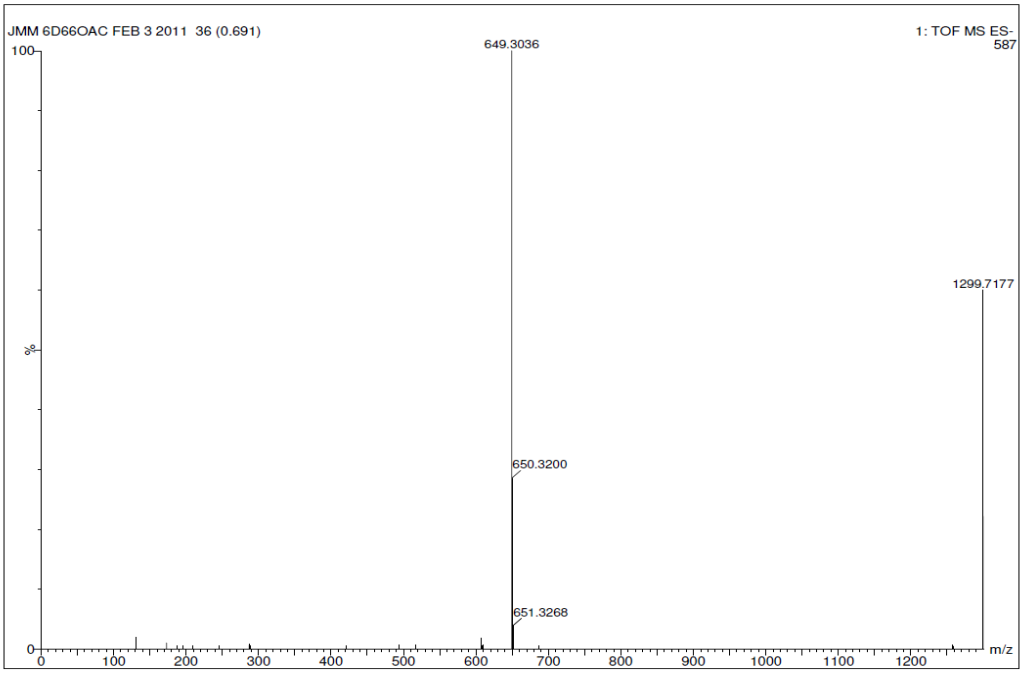

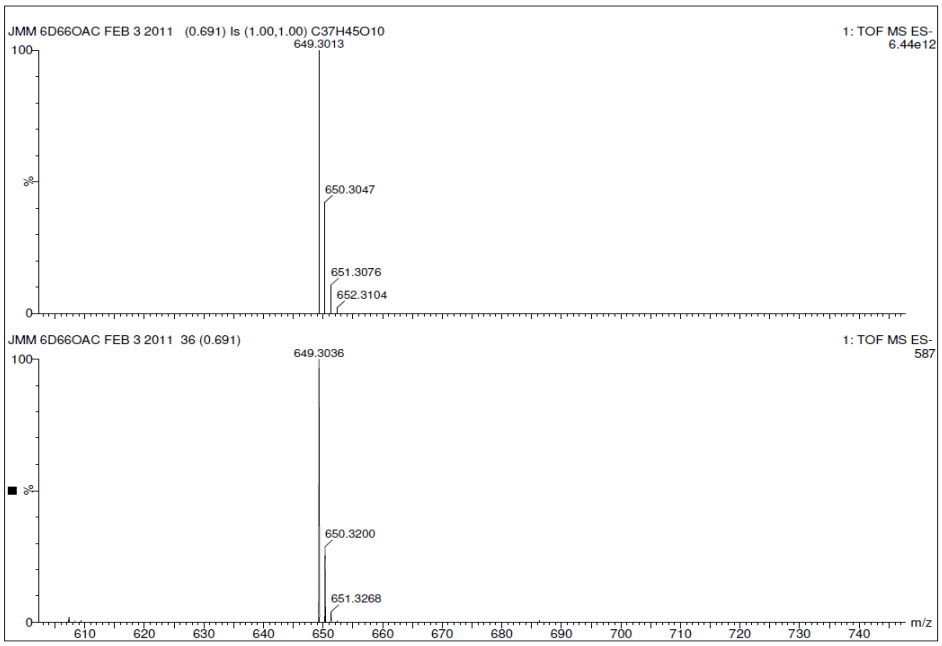

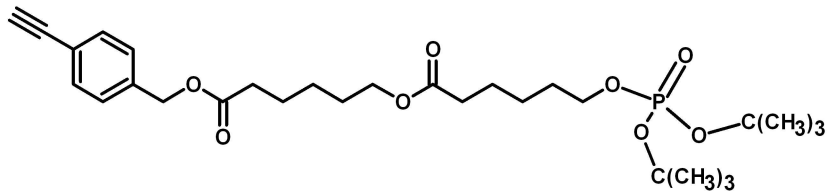

4-6

^{1}H NMR ($CDCl_3$) 300MHz

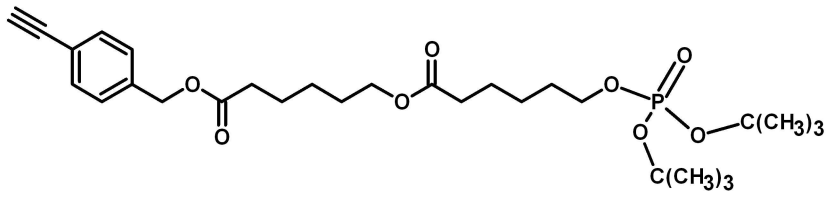

4-6

^{13}C NMR ($CDCl_3$) 75 MHz

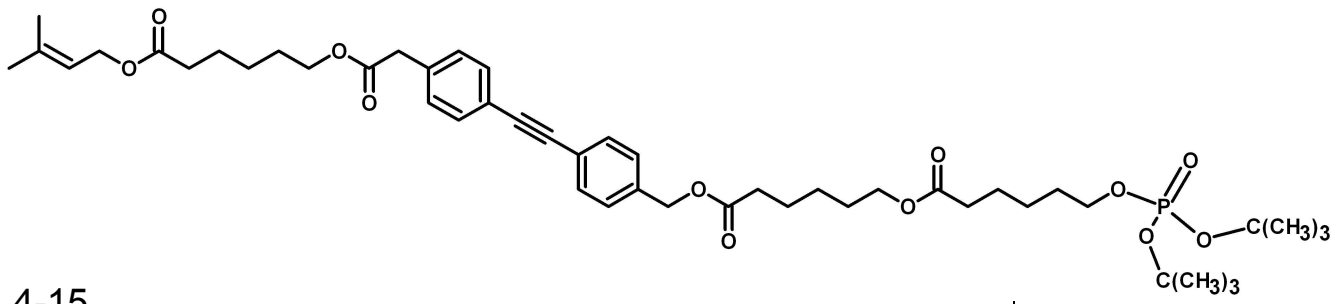

4-15

^{31}P NMR ($CDCl_3$) 200 MHz

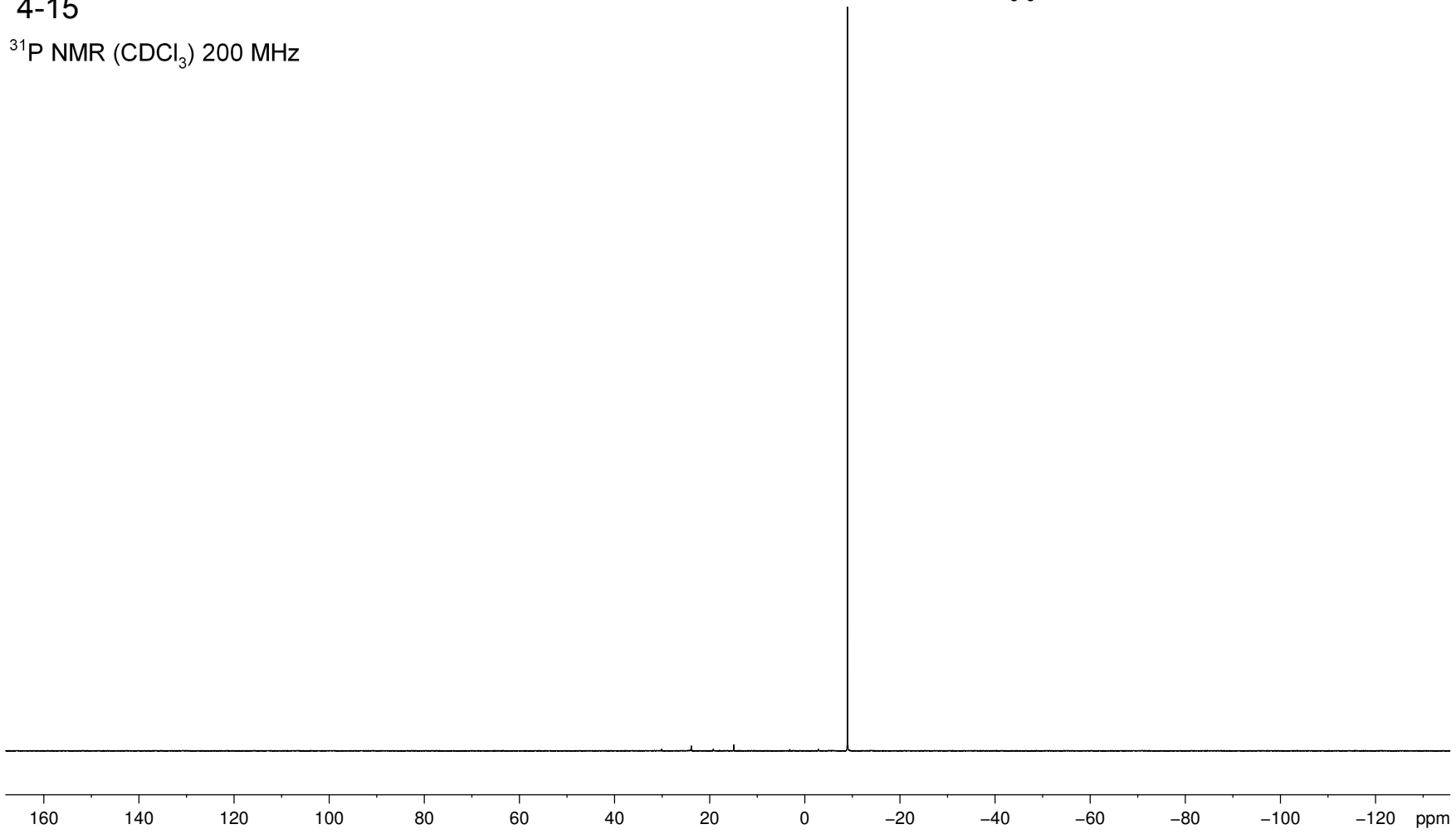

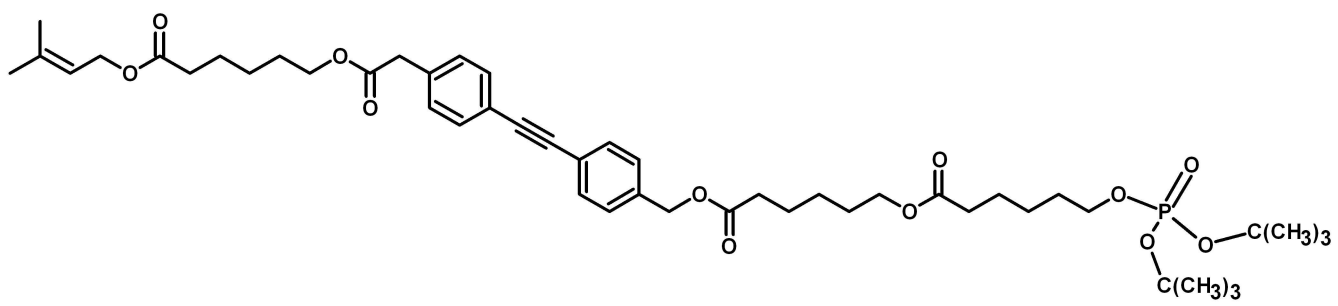

4-15

^{1}H NMR ($CDCl_3$) 300MHz

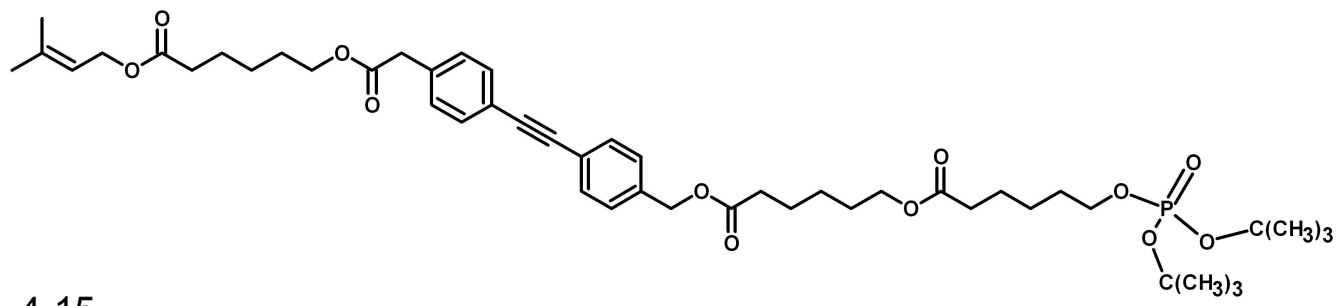

4-15

^{13}C NMR ($CDCl_3$) 75 MHz

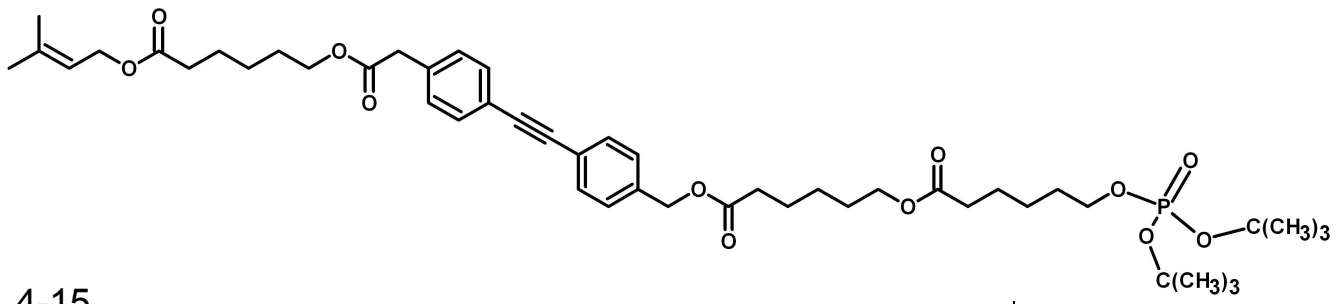

4-15

^{31}P NMR ($CDCl_3$) 200 MHz

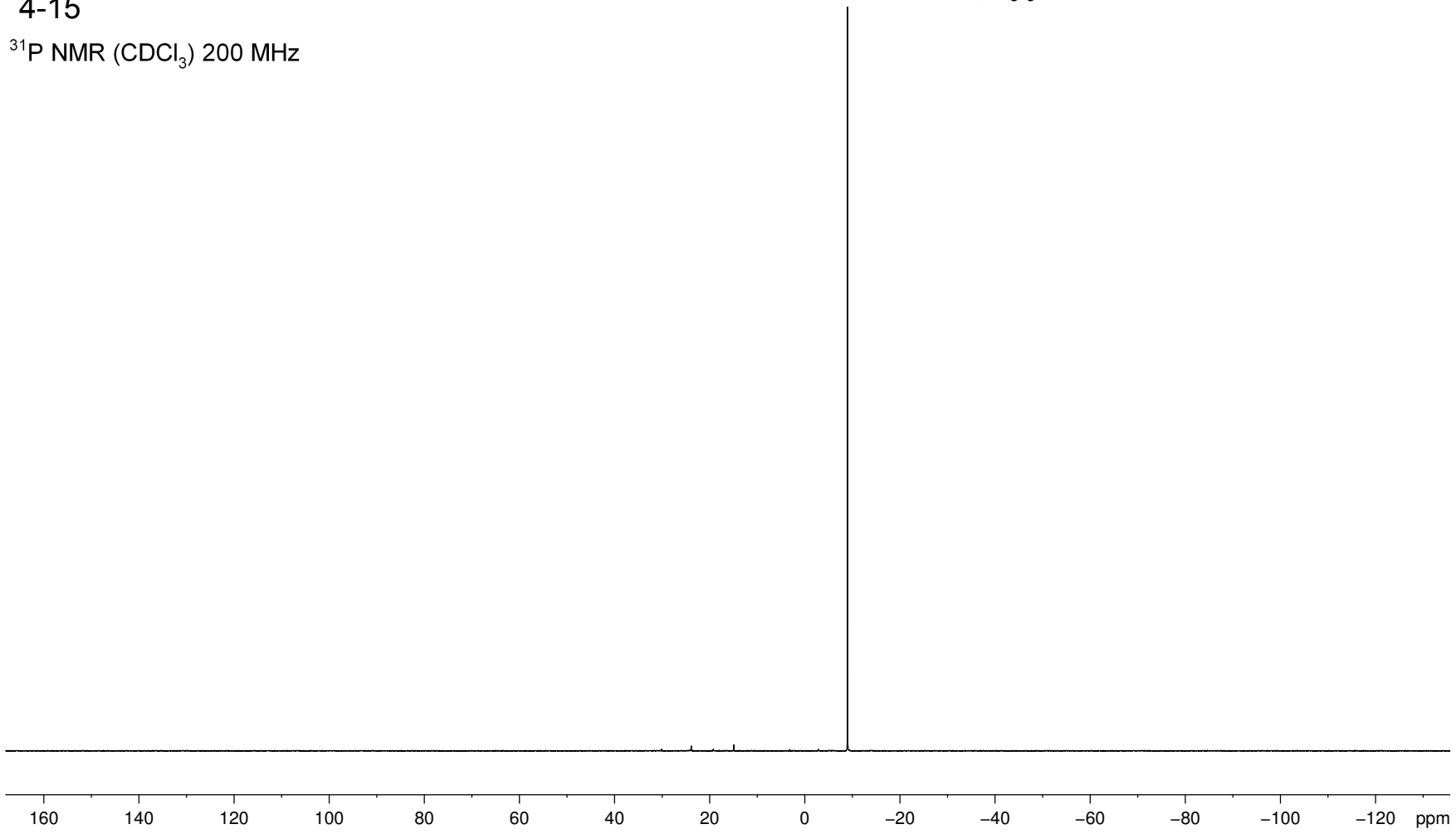

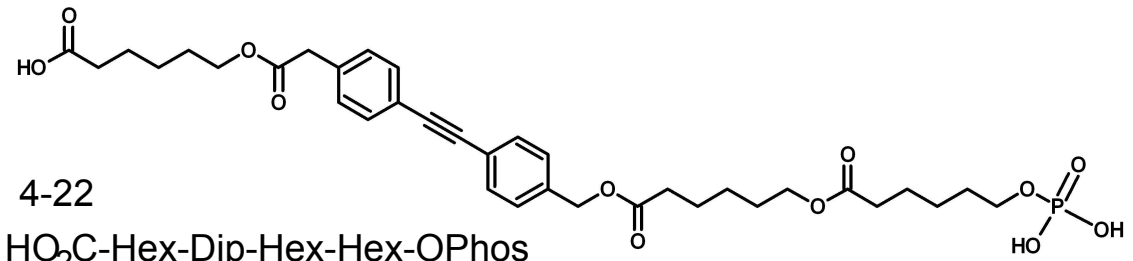

4-22

HO_2C-Hex-Dip-Hex-Hex-OPhos

^1H NMR (CD_3OD) 300MHz

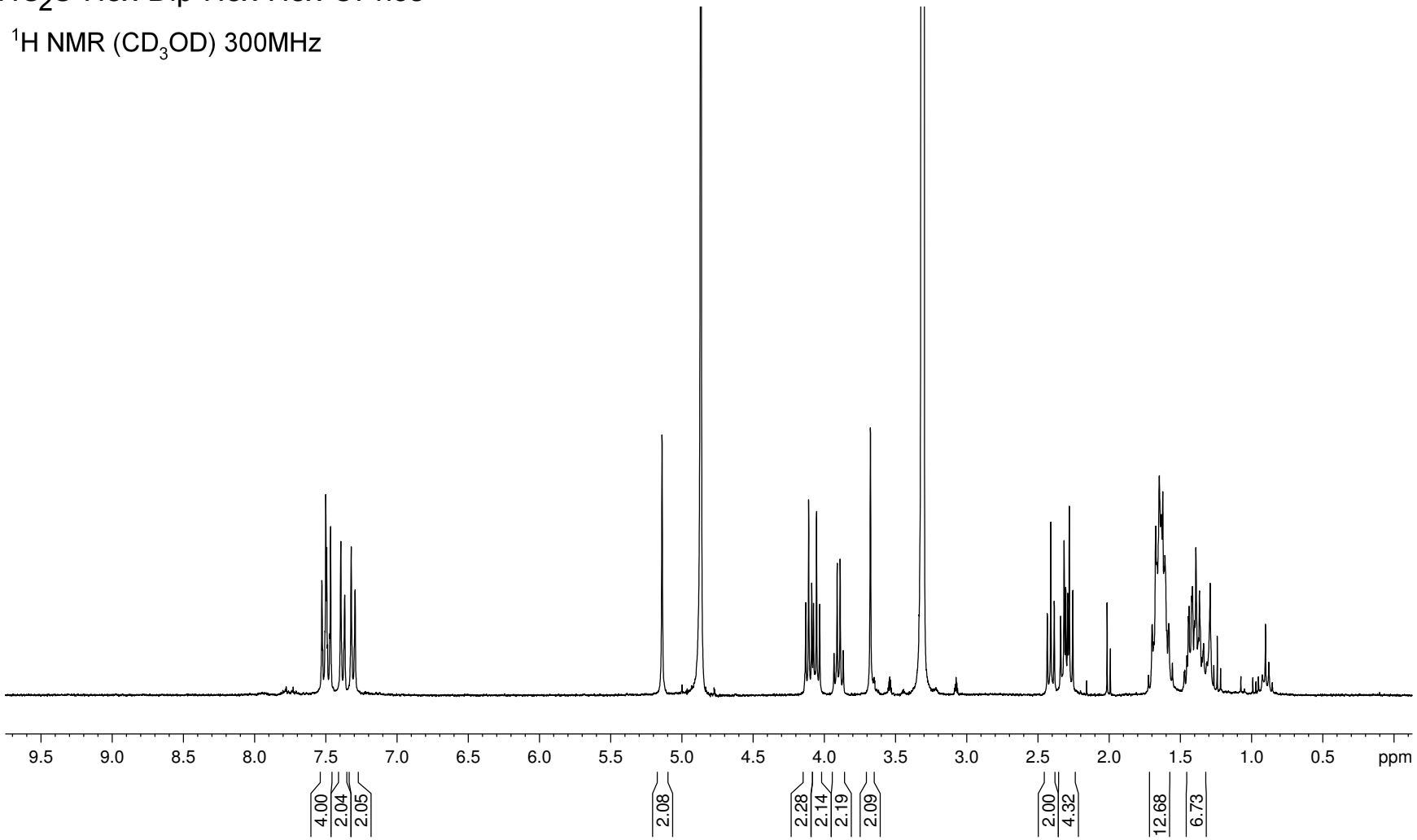

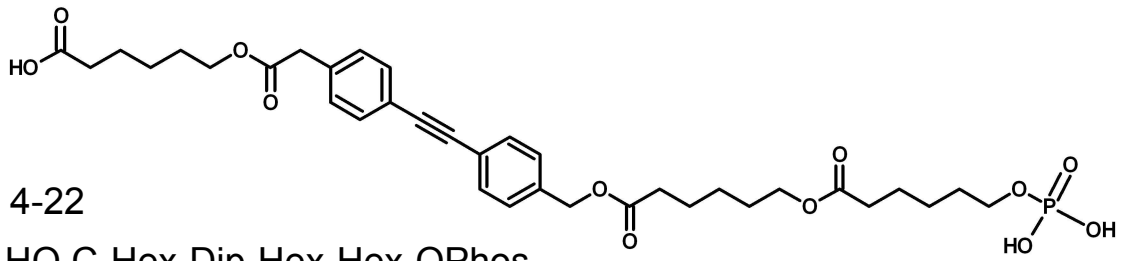

4-22

HO_2C-Hex-Dip-Hex-Hex-OPhos

^{13}C NMR (CD_3OD) 125 MHz

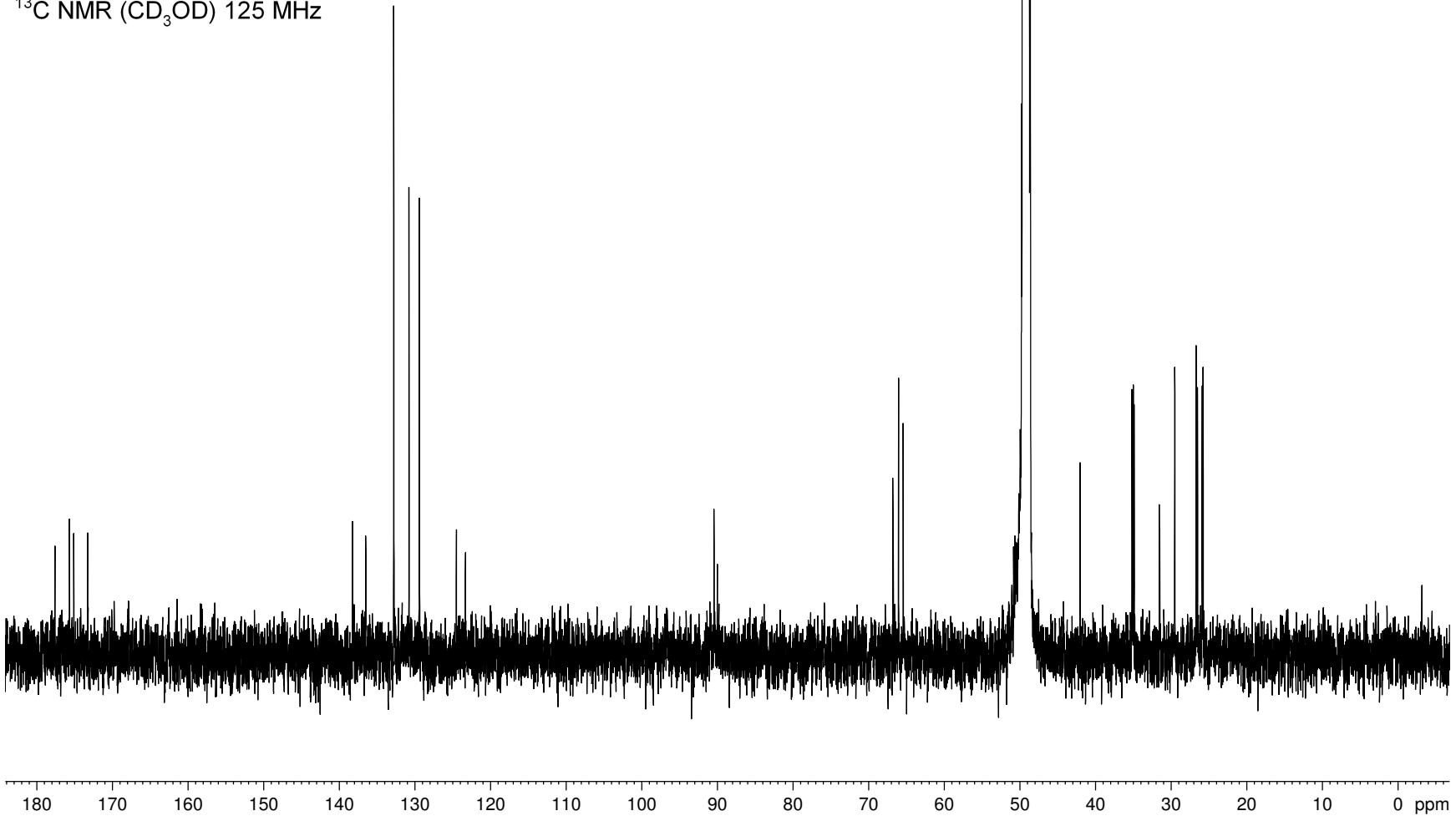

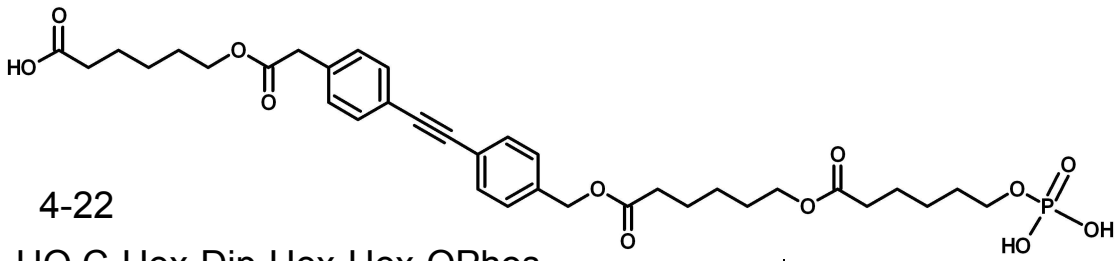

4-22

HO_2C-Hex-Dip-Hex-Hex-OPhos

^{31}P NMR (CD_3OD) 200 MHz

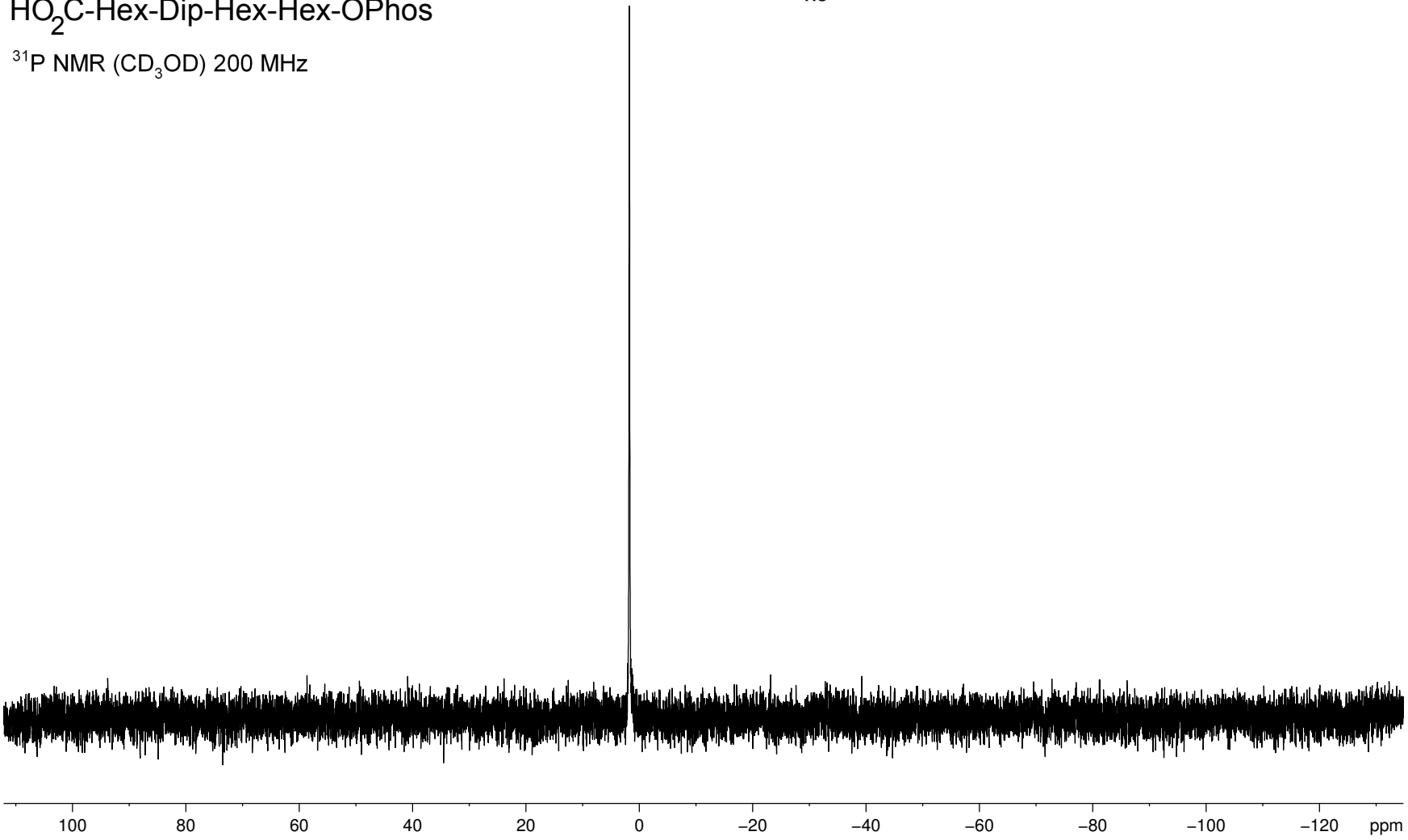

HO_2C-Hex-Dip-Hex-Hex-OPhos

4-22

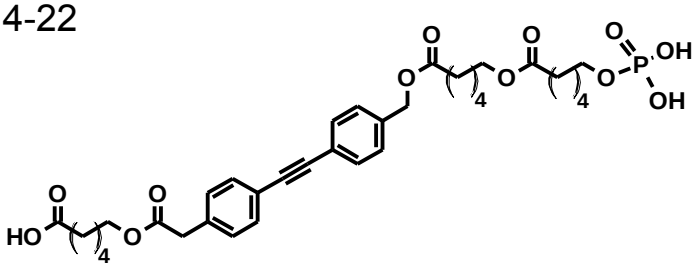

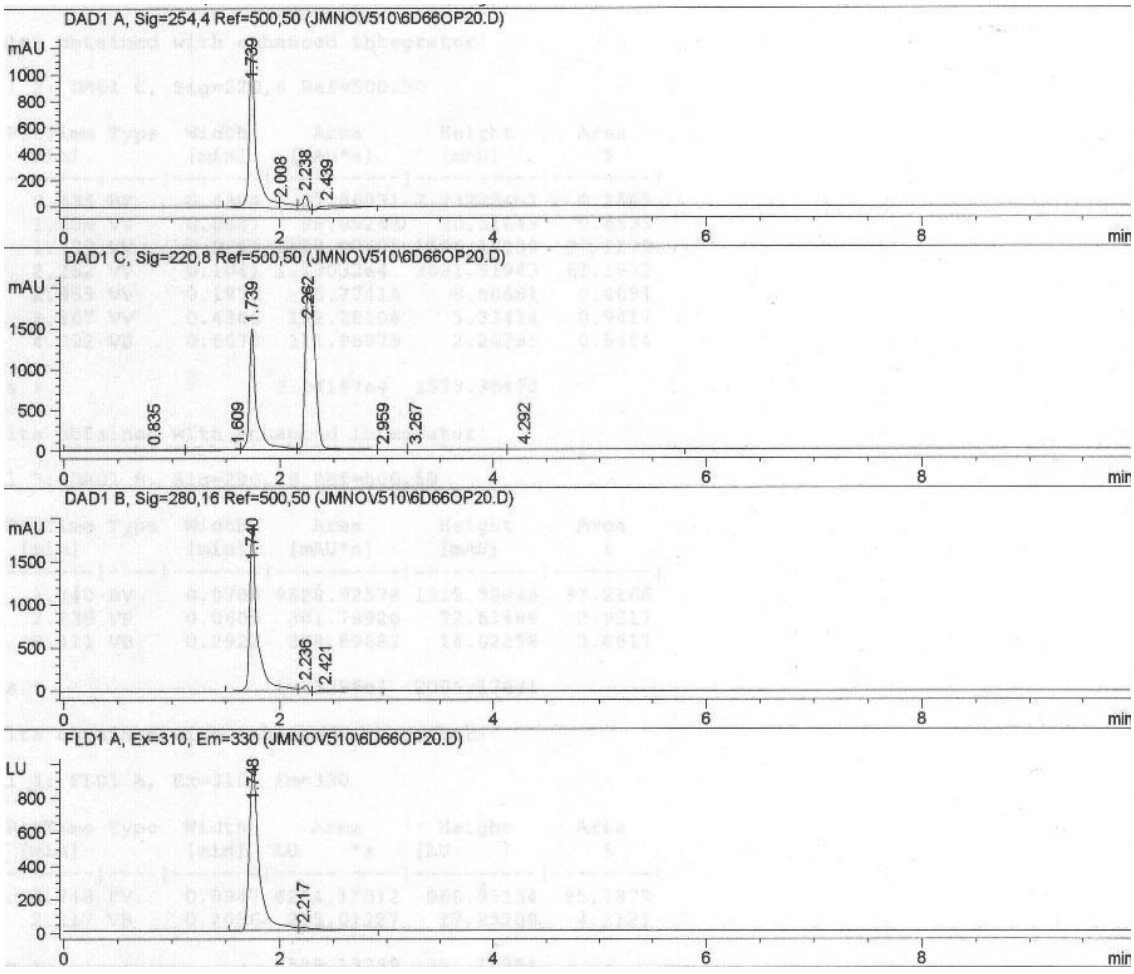

-HPLC trace of sample used for fluorescence and transport studies
-CONDITIONS: HP series 1100 HPLC
-Machery-Nagel RP C18 “Nucleosil” analytical column (4 mm x 250mm)
-CH_3OH as eluting solvent, flow 1mL/min

HO_2C-Hex-Dip-Hex-Hex-OPhos

MS: -ve ion ESI, Q-TOF
calc'd for C35H44O12P = 687.2570 amu,
obtained = 687.2717 amu

4-22

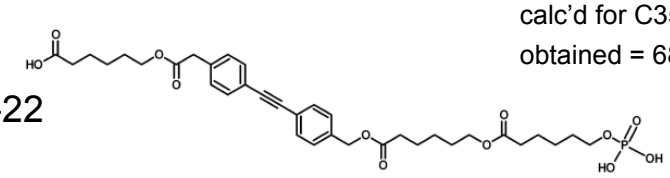

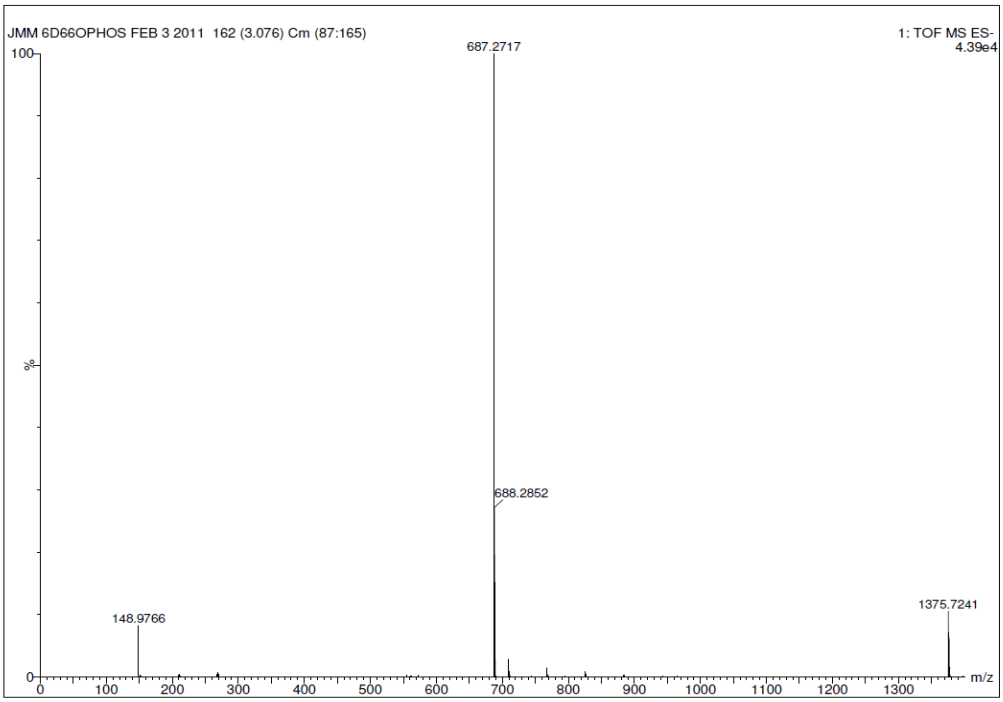

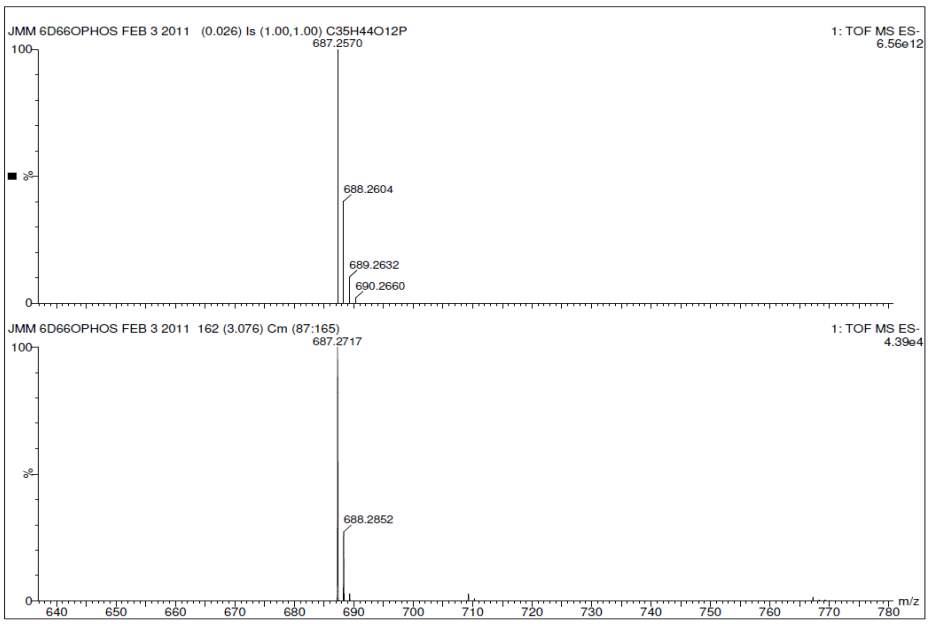

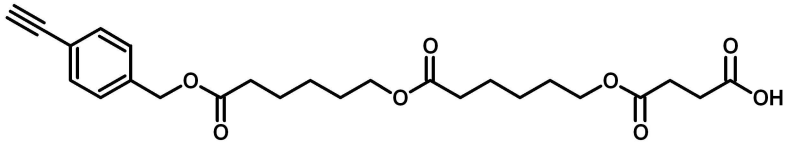

4-5

^{1}H NMR ($CDCl_3$) 300MHz

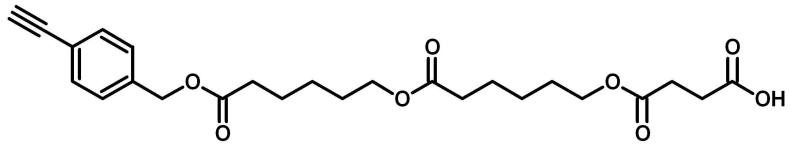

4-5

^{13}C NMR ($CDCl_3$) 125 MHz

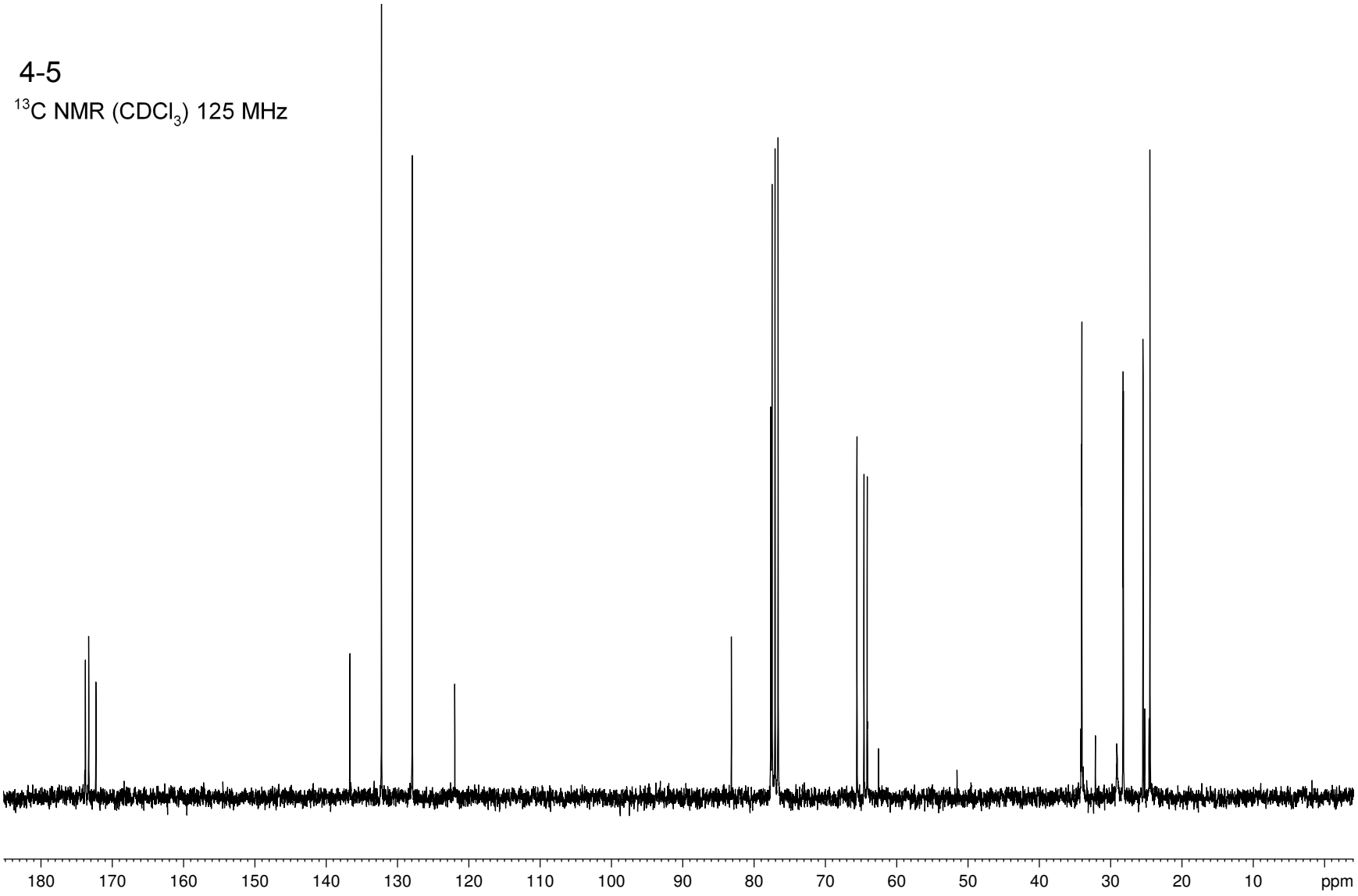

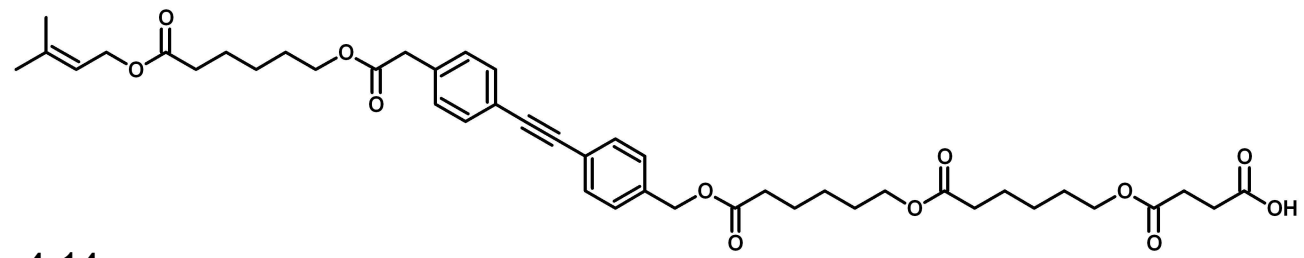

4-14

^{1}H NMR ($CDCl_3$) 300MHz

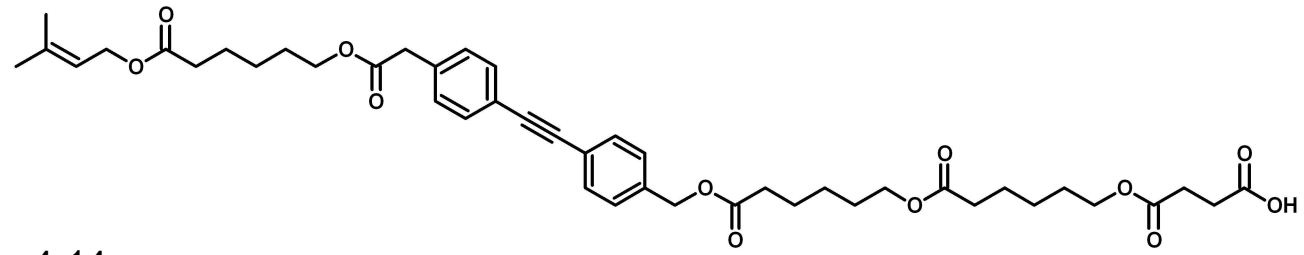

4-14

^{13}C NMR ($CDCl_3$) 75 MHz

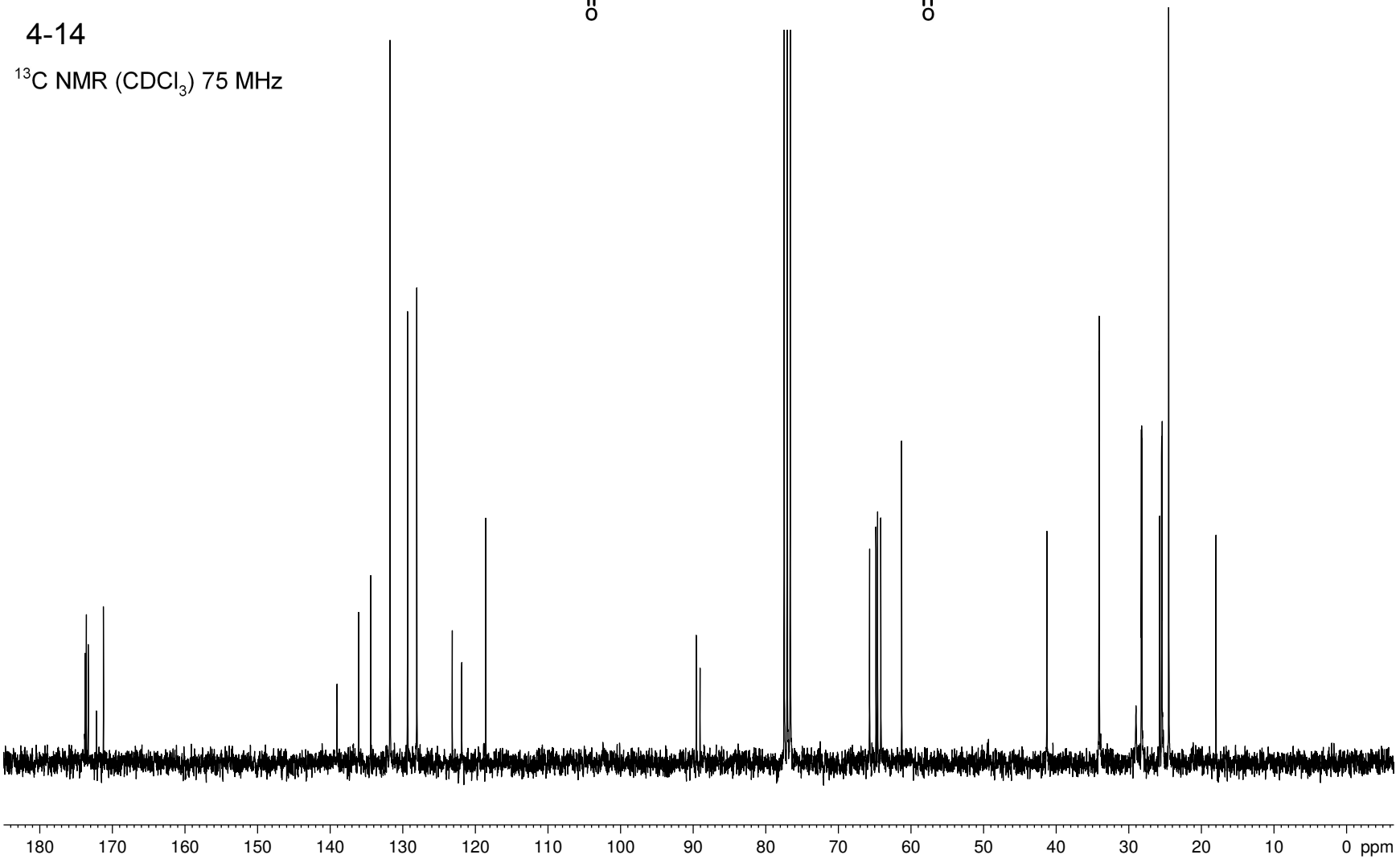

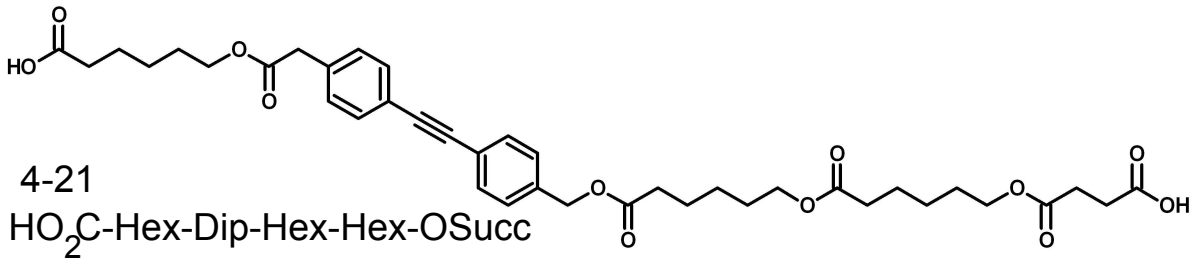

4-21

HO_2C-Hex-Dip-Hex-Hex-OSucc

^1H NMR ($CDCl_3$) 500MHz

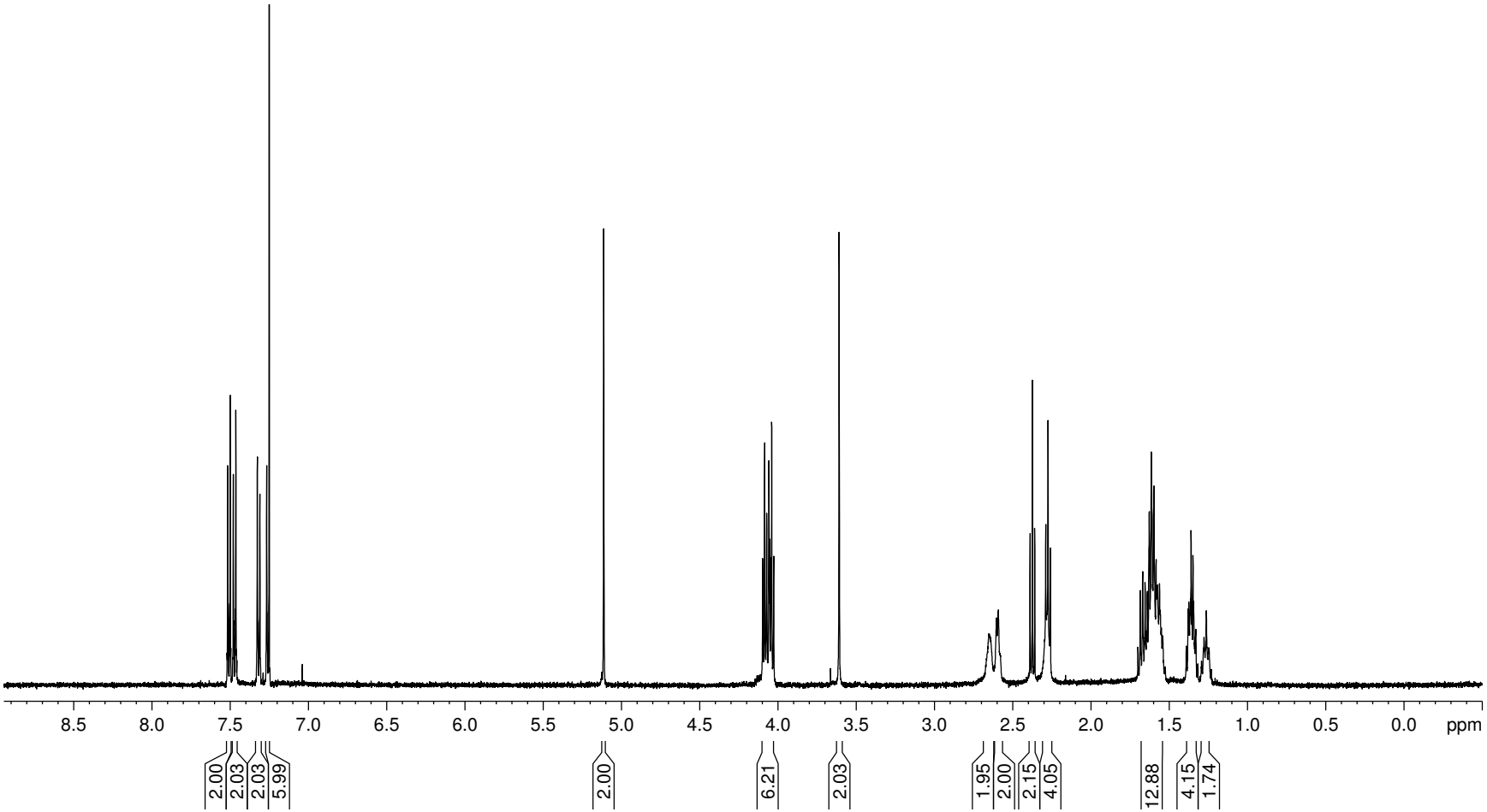

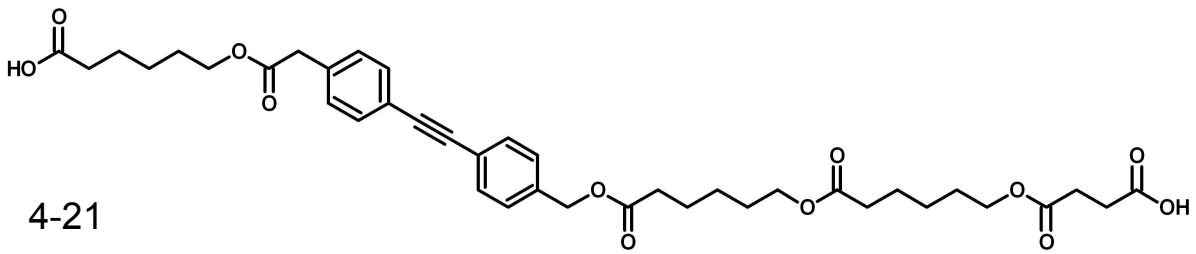

4-21

HO_2C-Hex-Dip-Hex-Hex-OSucc

^{13}C NMR ($CDCl_3$) 125 MHz

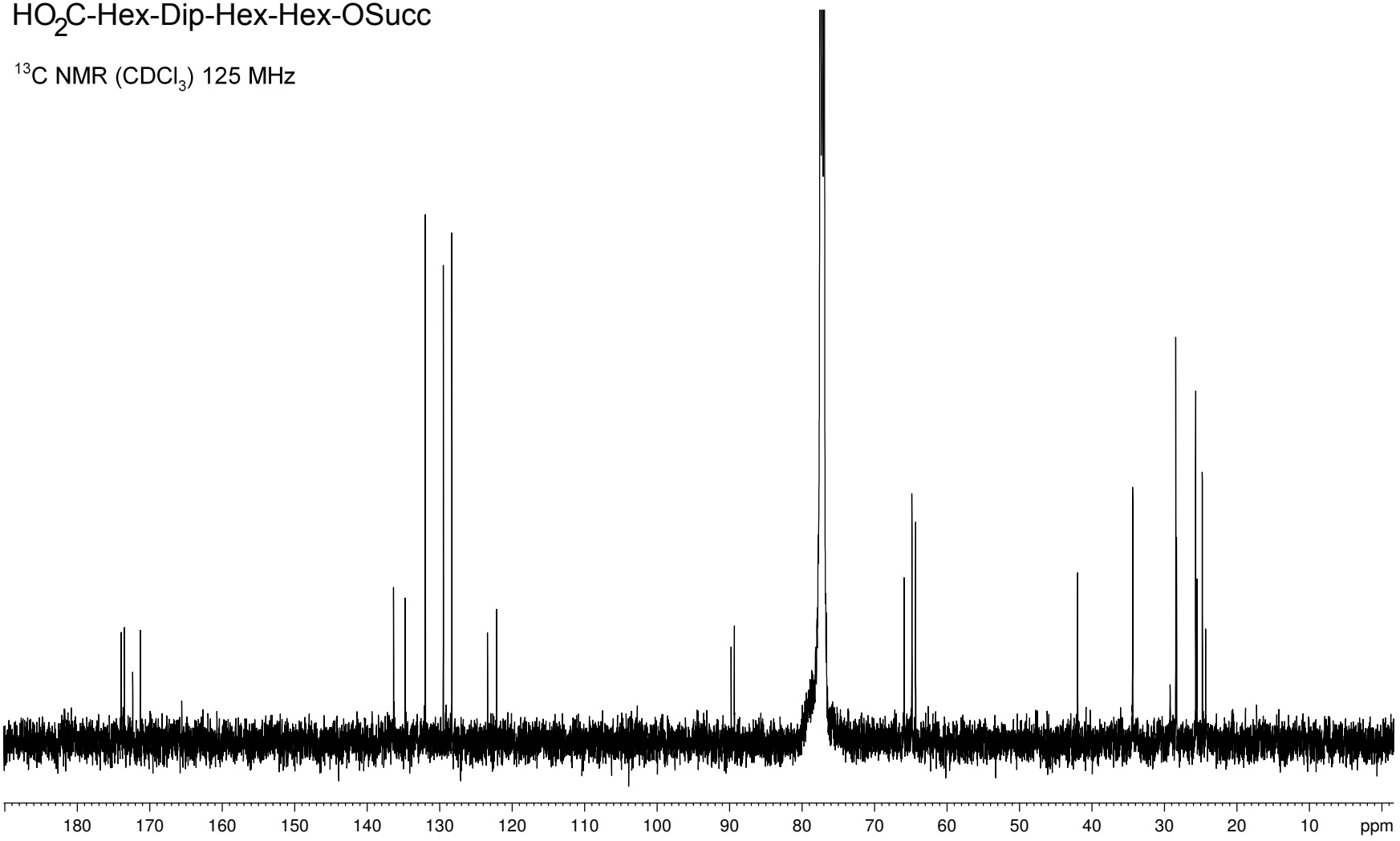

HO_2C-Hex-Dip-Hex-Hex-OSucc

4-21

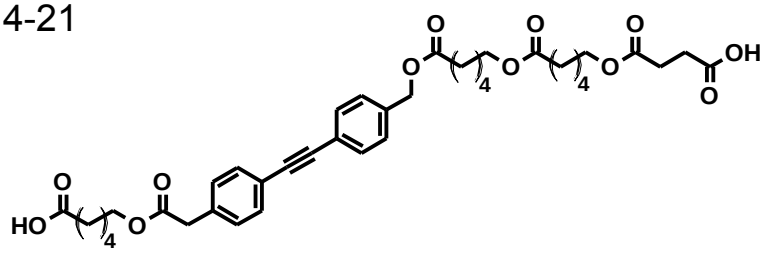

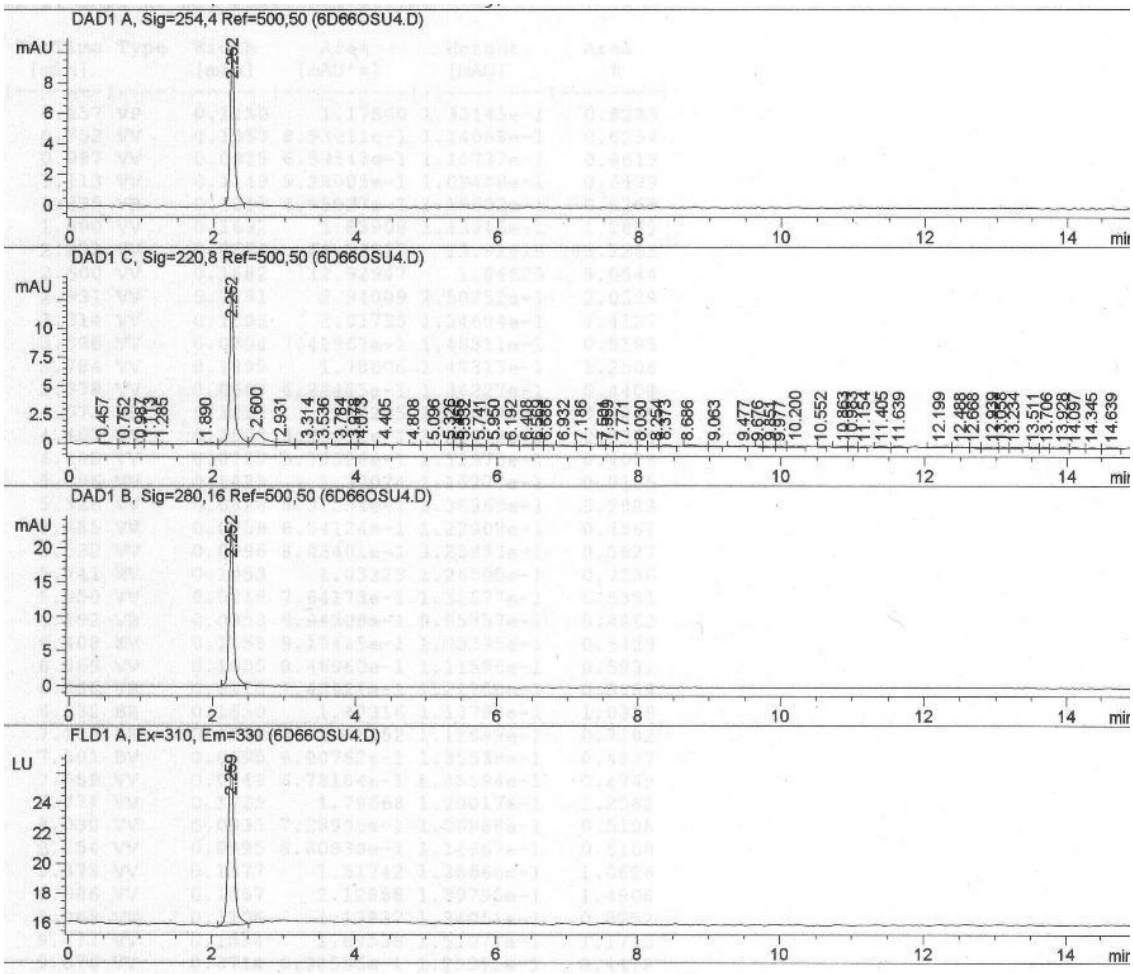

-HPLC trace of sample used for fluorescence and transport studies
-CONDITIONS: HP series 1100 HPLC
-Machery-Nagel RP C18 “Nucleosil” analytical column (4 mm x 250mm)
-15%CH_3OH:ACN as eluting solvents, flow 1mL/min

HO_2C-Hex-Dip-Hex-Hex-OSucc

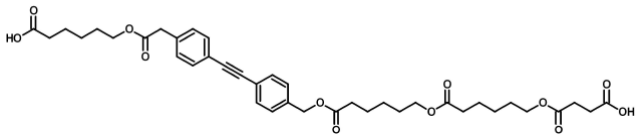

4-21

MS: -ve ion ESI, Q-TOF

calc'd for C39H47O12 = 707.3068 amu, obtained = 707.3105 amu.

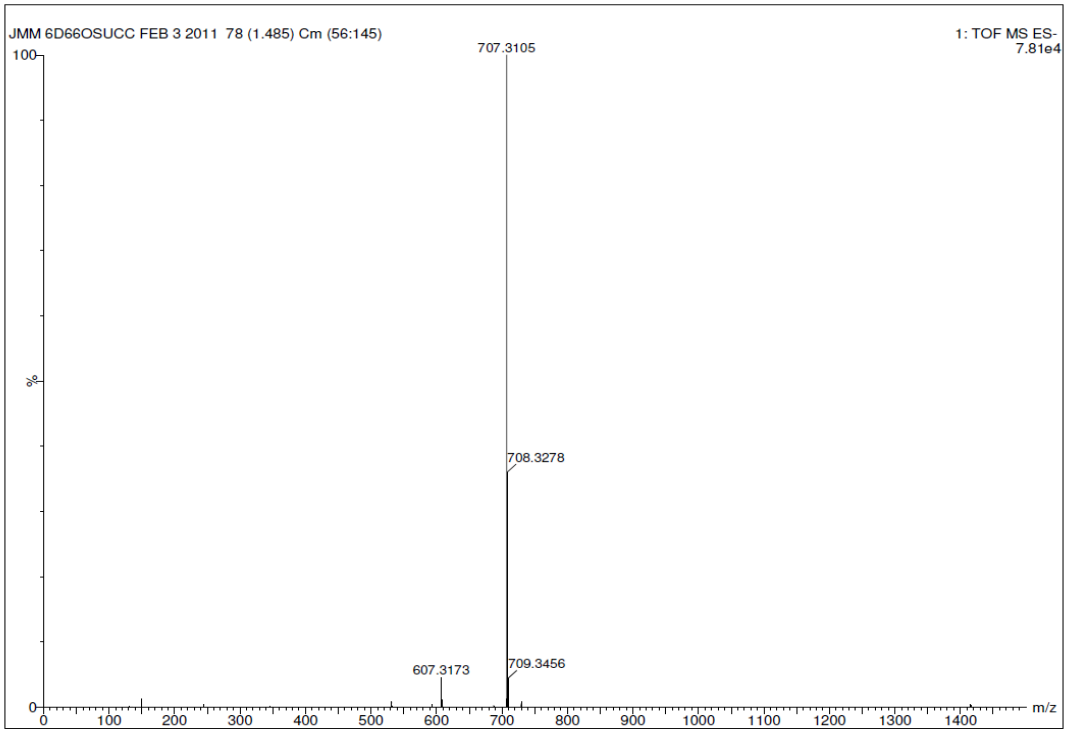

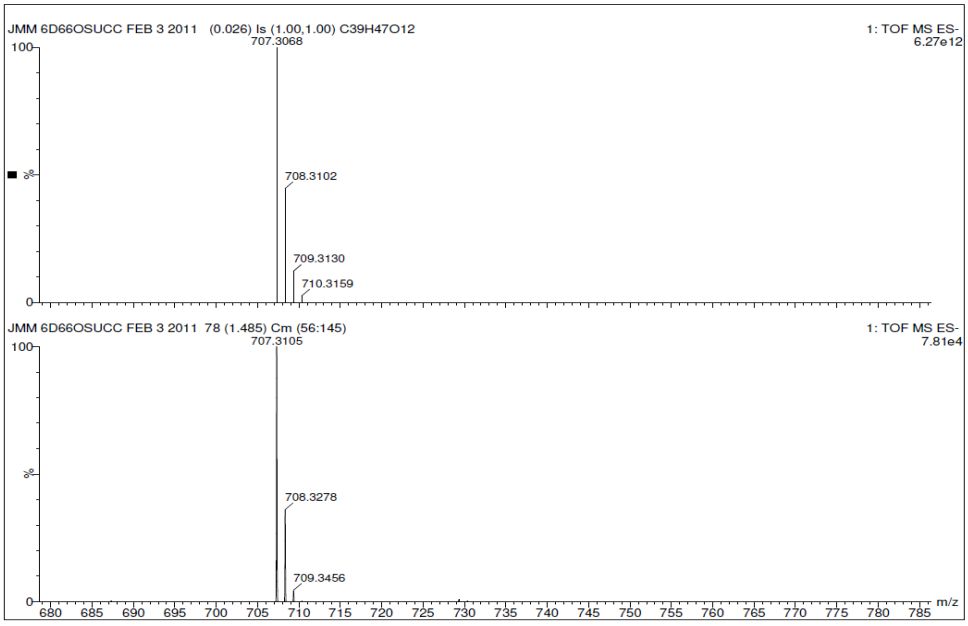

Appendix 3: Transport assay & fluorescence experimental details

All oligomers studied were purified by HPLC prior to use. Stock concentrations of approximately 1 – 6 mM in THF were stored under N_2 in the freezer when not in use, and periodically re-checked by HPLC (HP Agilent series 1100). Steady-state fluorescence spectra were collected on a PTI QM instrument at T= 20^0C (controlled by a circulating water bath, Haake) in 10 x 10 mm quartz cells (Hellma) equipped with a stir rod (volume ~2 mL), or 1 x 10 mm quartz cells (no stir rod, volume ~0.8 mL, Hellma). For general fluorescence experiments with the Dip-containing compounds, the excitation wavelength was ~305 nm, emission wavelength either 320 nm (organic) or 380 nm (aqueous), the bandwidths for the excitation and emission monochromators were both set at 3 nm, integration time= 0.1 s, step size 1 nm. The emission spectra were usually collected from ~320 until 500 nm. For the Trip compounds, λex~320 nm, λEm~ 370 nm, excitation and emission monochromator bandwidths = 1 nm, emission spectra were collected from ~340 until 500 nm. Other parameters for particular experiments are as noted. Time-resolved single photon counting experiments were conducted on an Edinburgh Instruments OB-920 single photon counting system also at T= 20^0C (controlled by a circulating water bath, Lauda) in 10 x 10 mm quartz cells (Hellma) using a 280 nm LED as the excitation source. The bandpass for the excitation and emission monochromators was ~ 16 nm (2 mm slits). The intensity of the laser was set with the use of a neutral density filter so that the collection rate was below 2.5% of the starting pulse rate. Typical counts at the channel with highest intensity were ~1000. The instrument response function (IRF) was determined using a suspension of Ludox (Aldrich) and the scattered light was collected at 280 nm. The IRF was used in the data fitting with the Edinburgh software were it was reconvoluted with the calculated fit and compared to the experimental data. Further information available under the heading "Time-resolved Single-photon counting" further in this Appendix, and Ref 134. For studies in organic solvents, the solvents used were of spectral or higher quality, and

were purged with N_2. For all aqueous studies except those involving $CuSO_4$, the aqueous buffer consisted of 10 mM $Na_3PO_4.12H_2O$, 100 mM NaCl, pH= 6.4. For quenching studies with $CuSO_4$ in aqueous solution, either 100 mM unbuffered NaCl or 10 mM Bis-Tris, 100 mM NaCl, pH= 6.4 were used (as noted). Vesicles were prepared and sized as reported previously[40], however, rather than always containing the HPTS dye, in certain cases, the vesicles were made with the same buffer both internal and external to the vesicle. Alternatively, for certain experiments, the compound was pre-incorporated into the vesicle bilayer by adding a solution of the compound of interest to the lipid mix before continuing the preparation as usual. Regardless of the identity of the vesicles, the volume of vesicle stock solution added to the cell was kept constant at 100 µL for each experiment. An injection port (home-built, UVic) was used to add solutions to the cuvette while the experiment was running.

BILAYER CLAMP ASSAY

As previously described[32,33] . A model BC-525A bilayer clamp (Warner Instrument Corp.) was used for planar bilayer experiments, ClampEx 8 and ClampFit 10 (Axon Instruments) were the software used for acquisition and analysis, respectively. Cups used were made of polystyrene and had 250 µm diameter apertures (Warner Instrument Corp). The lipid used in all cases was diphytanoyl phosphatidylcholine (diPhyPC) (Avanti Polar lipids). A stock solution of 25 mg/mL lipid in $CHCl_3$ was dried under N_2 and then re-suspended in 200 µL decane. For compounds that had to be pre-loaded into the lipid, 0.1 – 1 mol% compound in $CHCl_3$ was added to the lipid mix and then dried down. The electrolytes used were 1 M KCl, NaCl or NMe_4Cl in 10 mM HEPES, 10 mM TRIS, pH 7 (unadjusted). The aperture was primed with 0.5-1 µL of decane/lipid, excess solvent was removed by blowing N_2 over the aperture. The cup was then placed into the electrolyte-filled holding cell, consisting of 5 mL and 3 mL chambers, and salt bridges (KNO_3/Agar) and electrodes (Ag/AgCl) were attached. Bilayers were formed by brushing on 1- 1.5 µL of the decane/lipid mix over the aperture, and were monitored for stability, capacitance and resistance for at least 20 minutes before test compound was added. Test

compounds were added either by injection from an organic solution (typically no more than 1-10 µL of solution) or by breaking the lipid-only bilayer and brushing on the compound-preloaded lipid mix. All data were hardware filtered (8- pole Bessel filter, 1 kHz) and data was collected in a survey mode using the Gap-free protocol. Bilayers were tested repeatedly for capacitance and resistance, and no bilayer was used for more than 2 hrs. Once formed, 'activity' from pristine bilayers was never observed. Each experiment was carried out in each electrolyte at least twice, with two different cups.

HPTS ASSAY

Vesicle preparation: A chloroform solution of 8:1:1 PC:PA:cholesterol (Avanti Polar lipids) was dried *in vacuo* in a pear-shaped flask and then left on the vacuum line overnight. For compounds that were pre-loaded into the vesicle, a solution of the test compound of interest was added to the initial $CHCl_3$ lipid solution at 0.1 – 1 mol%, and then prepared as described. The 50 mg lipid film was hydrated with 1 mL of internal buffer solution (10 µM HPTS, 10 mM $Na_3PO_4 \cdot 12H_2O$, 100 mM NaCl in deionized H_2O, pH 6.4, adjusted with conc. H_3PO_4). The suspension was frozen under liquid nitrogen and subsequently thawed at room temperature over ten minutes (3 times). The mixture was then sonicated in an ice bath for 20 seconds with 2 second pulses (at 50% duty cycle and 20% power output) 3 times, with a 30 s rest between cycles. The unilamellar vesicles were then left to anneal overnight. The vesicle solution was then sized 19 times through a 400 nm polycarbonate Nucleopore filter using a LiposoFast membrane extrusion apparatus (Avestin) (0.5 mL x 2) and purified on a PD-10 Sephadex G-25 column (GE Healthsystems) using an external buffer solution (10 mM $Na_3PO_4 \cdot 12H_2O$, 100 mM NaCl, pH= 6.4). The first three cloudy drops were discarded but thereafter the cloudy fraction was collected and diluted to 5.00 mL using the external buffer solution. A typical preparation of this vesicle stock solution contained 200 ±20 nm diameter vesicles (determined by dynamic light scattering, Brookhaven Instruments, ZetaPALS particle sizing software) and a lipid concentration of typically 7 mg/mL[41]. The vesicle solution was stored at 5^0C and used within 24 hours of preparation.

Typical experiment: in a typical experiment, 100 µL of the vesicle suspension was added to the fluorescence cuvette. 2.00 mL of external buffer (10 mM $Na_3PO_4 \cdot 12H_2O$, 100 mM NaCl, pH= 6.4) and a solution of the test compound in THF or MeOH was then added. The solution was placed in the fluorimeter and left to equilibrate for 3 minutes. An excitation ratio was started (λEx1= 403 nm, λEx2= 460 nm, λEm= 510 nm, excitation and emission monochromator bandwiths = 3 nm, Integration 1s, duration 600 s). At t= 60 s, 50 µL of a 0.5 M aqueous NaOH solution was added through the injection port (continuous monitoring, no pause). At t= 540 s, the experiment was paused and 50 µL of a 0.5% aqueous solution of Triton X-100 was added. The experiment was then re-started after 30 s of stirring time. The data was analysed as reported previously[40], using Equation 1.1 in Chapter 1.

CF ASSAY

Vesicle preparation: Modified[80] from published procedures[42]: 0.45 g 5(6)-Carboxyfluorescein, (CF) was added to ~5 mL deionized water, solvated by titration of 1 M potassium hydroxide to pH 7.5 (to form K^+CF^-), evaporated *in vacuo* and further dried under vacuum for 48 hours. The CF salt was diluted with CF buffer (10 mM Tris·HCl, 0.04 M KCl in deionized H_2O), to KCF solution of 0.1 M (10 mL) (pH 7.5 with 1M HCl). To a 50 mL round bottom flask, 4 mL of lipid stock (8:1:1 PC:PA:Cholesterol in $CHCl_3$) was dried as noted previously. The lipid was re-suspended in diethyl ether (6 mL) and 2 mL of the KCF solution was then added. Sonication was used to disperse the two phases to a cloudy orange dispersion (power = 2.5, probe tip at the interface of the two phases). This dispersion was evaporated slowly under vacuum until bubbling from ether removal stopped. Then, 1 mL external buffer (10 mM Tris·HCl, 0.14 M KCl in deionized H_2O, pH 7.5 with HCl) was added. Slow rotary evaporation of the suspension continued to remove any excess ether for 30 min. The liposomes were sized with the membrane extrusion apparatus 19 times (500 µL vesicle solution x 3) and then size-exclusion filtered as noted. The cloudy fraction, after the first four cloudy drops, was collected, for a total volume of vesicle suspension of ~1.5 mL. The diameter of the resulting vesicles

was ~200 nm (measured by dynamic light scattering). The vesicle solution was stored in the fridge and used within 12 hours.

Typical experiment: 160 µL external buffer (10 mM Tris·HCl, 0.14 M KCl, pH 7.5) and 30 µL test solution (compound in THF or MeOH or 5% aqueous Triton X-100) was added to a 1.5 mL Eppendorf tube and vortexed briefly. To each tube, 20 µL CF vesicle suspension was added, vortexed for 10 seconds, and allowed to incubate at room temperature for 30 min. Each sample was then diluted to 5% in external buffer (1.5 mL total volume, 0.6 mL solution used for each trial). Samples were excited at λ= 475 nm (excitation and emission monochromator bandwidths = 2 nm, integration = 1s) and the fluorescence emission scan was collected from λ= 500-550 nm in a 1 x 10 mm quartz cell at T= 20^0C. The average emission intensity at λ_{max} (~515 nm) was determined for each sample concentration. The percentage of CF released was calculated as $I(\%)=[(I_{sample}-I_{MeOH\ blank})/(I_{triton}-I_{blank})$ and plotted against test compound concentration.

PYRENE ASSAY[74-75]: As reported previously [40]. Pyrene was purified by column chromatography and sublimation, and dissolved in deoxygenated, HPLC grade MeOH at 0.625 mg/mL. This was then diluted to 0.025 mg/mL to make the stock pyrene solution used for the assay. In a typical experiment, 25 µL of test compound in MeOH, 9 µL stock pyrene solution and 0.5 mL aqueous buffer (10 mM Na_3PO_4, 100 mM NaCl in deionized water, pH 6.4) were added to a 1 x 10 mm quartz fluorescence cuvette, and allowed to equilibrate at T= 20^0C for 3 minutes. Scans were taken with an excitation wavelength of 331 nm and the emission collected between 365-400 nm (excitation monochromator bandwidth = 3 nm, emission monochromator bandwidth = 1.5nm, integration = 0.5 s, step size= 0.25 s^{-1}). Spectra were also collected for solutions that contained all components except pyrene (25 µL MeOH blank). A ratio of the emission intensity at λ_{max} ~ 373 nm (I_1) and λ_{max} ~ 383 nm (I_3) was calculated and plotted against test compound concentration.

QUENCHING ASSAYS: For solution quenching studies, experiments were carried out in 10 x 10 mm quartz fluorescence cuvettes, T= 20^0C, excitation and emission monochromator bandwidths = 3 nm for Dip-containing compounds and 1 nm for Trip-containing oligomers. Solvents used were either MeOH or aqueous (10 mM Bis-Tris, 100 mM NaCl, pH= 6.4 or 100 mM NaCl), solutions of quencher ($CuSO_4$) were made in the appropriate solvent. Steady-state scans of compound without copper and with increasing concentrations of copper were taken at time intervals of 1, 5 and 10 minutes, the fluorescence intensity in the absence (I_O) and presence (I_Q) of quencher were then plotted as a ratio (I_O/I_Q) versus copper concentration (Stern-Volmer analysis). The quenching constant was then determined by a linear fit to the data, as per Equation 2.2.

TIME-BASED MEMBRANE INSERTION & QUENCHING ASSAYS: The vesicles used for this assay were prepared as mentioned previously and usually had either 10 mM Bis-Tris, 100 mM NaCl, pH= 6.4 or 100 mM NaCl both internal and external to the vesicle. The $CuSO_4$ solution was also made in either of the two buffers, depending on the experiment. In a typical experiment, 100 µL of the vesicle suspension was added to 2.00 mL of aqueous component, which was left to equilibrate in the fluorimeter at T= 20^0C for 3 minutes. An emission ratio (λEx= 305 nm, λEm1= 320 nm, λEm2= 380 nm) was then started, at t= 60s or 100 s, up to 25 µL of the test compound of interest (dissolved usually in THF or MeOH) was injected into the aqueous vesicle suspension. The fluorescence response was monitored over time (between 10 and 60 minutes, depending on the experiment). The experiment was then repeated with the addition of $CuSO_4$, and then the aqueous-only (no vesicles) experiment was conducted. This gave 4 time-based spectra (aqueous ± copper, vesicles ± copper), from which the extent of quenching could be compared. This experiment was only carried out on the Dip compounds. For the Trip molecules, which exhibited minimal 'excimer' emission, the emission was not followed over time, instead, scans were taken at 5 minute intervals. The emission intensity before and after copper addition in both aqueous solution and in vesicles was then compared.

PARTITIONING COEFFICIENT DETERMINATION: From Ref. [123]. To a 10 x 10 mm fluorescence cuvette a constant concentration of test compound in THF (no more than 20 µL) was added to increasing concentrations of lipid vesicles prepared as noted and containing 10 mM BisTris, 100 mM NaCl, pH= 6.4 both inside and out. The volume of aqueous buffer was modified to maintain a constant volume of 2.00 mL. The solutions were left to equilibrate at T= 20^0C for 3 minutes, and then steady-state spectra at the appropriate excitation and emission wavelengths and slits (depending on the compound) were collected. By generating a double reciprocal plot of the fluorescence intensity ($1/I_i$) as a function of lipid concentration (1/[L]), a line with slope equal to the concentration of water [W] over the partitioning constant (Kp) multiplied by the fluorescence intensity upon maximal partitioning (I_o), is obtained (as per Equation 3.1). Kp is therefore equal to the concentration of water (55 M) multiplied by the x intercept, as reported[123].

$$1/I_i=([W]/K_pI_o) \cdot 1/[L] + 1/I_o \qquad \text{Eqn. 3.1}$$

TIME-RESOLVED SINGLE-PHOTON COUNTING: Experiments were conducted on an Edinburgh Instruments OB-920 single photon counting system also at T= 20^0C (controlled by a circulating water bath, Lauda) in 10 x 10 mm quartz cells using a 280 nm LED as the excitation source. See 'general procedures' for further instrument details. To a 10 x 10 mm quartz fluorescence cell equipped with a stir rod, 100 µL of vesicles containing 10 mM BisTris, 100 mM NaCl, pH= 6.4 both inside and out were suspended in 2.00 mL buffer (10 mM BisTris, 100 mM NaCl, pH= 6.4), to which the compound of interest was added from solution (no more than 25 uL of compound added). The suspension was allowed to equilibrate at T= 20^0C for 3 minutes, after which the TCSPC spectrum was collected. For the experiment shown in Fig. 5.6 and 5.7, this experiment was repeated every 10 minutes for 1.5 hr, with the suspension remaining stirring in the dark between scans. The IRF was also taken every 10 minutes at the same parameters used for the compound scan. The data was collected over a 50 ns time period, and fits

were done over a 25 ns time period. The instrument software was used to fit the data sum of three exponentials in all cases, using the equation: Fit = $A + B_1.\exp(-t/\tau_1) + B_2.\exp(-t/\tau_2) + B_3.\exp(-t/\tau_3)$, where B= proportion of each component. The observed residuals were centred around 0 and chi squared values were between 0.9 and 1.1 for most fits, a visual inspection of the randomness of the residuals was also carried out.

Appendix 4: Supporting information; fluorescence

Chapter 2

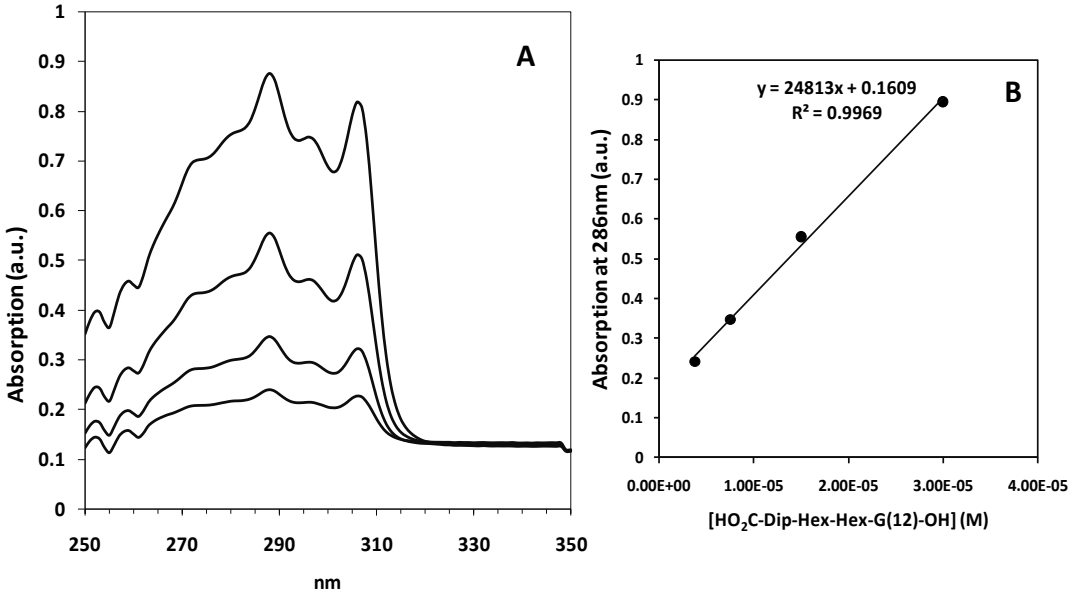

Figure A1: UV absorption spectrum of HO_2C-Dip-Hex-Hex-G(12)-OH in MeOH. **A**: raw spectra, **B**: maximal absorption as a function of concentration; determination of ε. Other first generation Dip isomers had similar spectra and extinction coefficients.

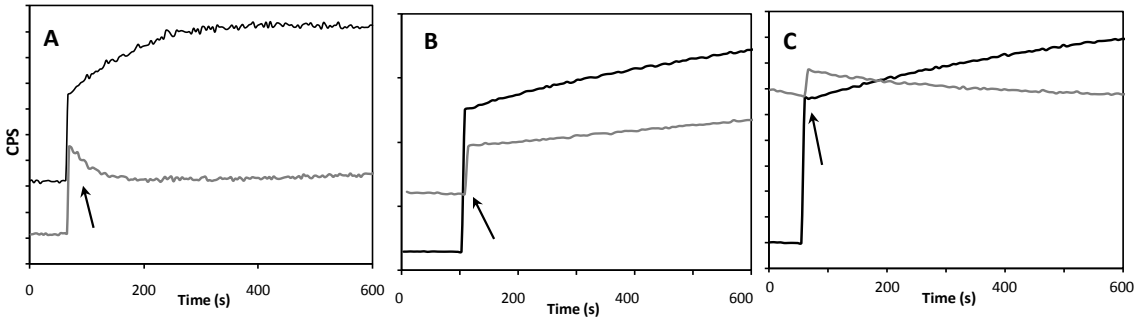

Figure A2: Emission spectra over time for first-generation Dip-containing compounds. Black lines= 320 nm, grey lines = 380 nm. Arrow indicates point at which 100 µL vesicles were injected into a solution of compound of interest in 2 mL 10 mM $Na_3PO_4.12H_2O$, 100 mM NaCl, pH 6.4. **A**: 22 µM HO_2C-Dip-G(12)-OH, **B**: 25 µM HO_2C-Hex-Dip-Hex-G(12)-OH, **C**: 20 µM HO_2C-Hex-Hex-Dip-G(12)-OH

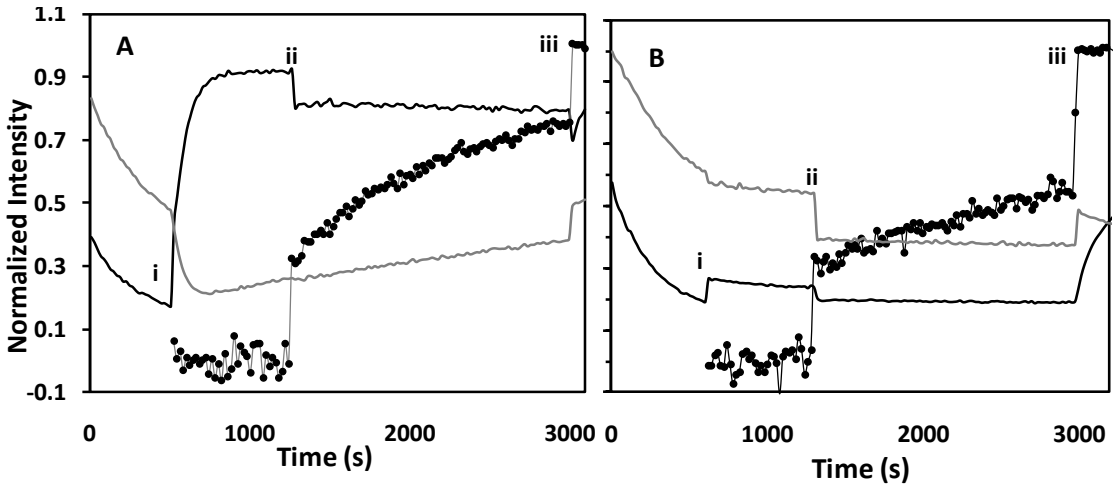

Figure A3: 'Multi-Dye' Experiment: Simultaneous monitoring of HPTS transport activity (black circles) and emission ratio between 320 nm (black line) and 380 nm (grey line) (λ_{ex}= 305 nm) for **A**: 16 µM HO_2C-Dip-Hex-Hex-G(12)-OH, and **B**: 15µM HO_2C-Dec-Dip-Hex-G(12)-OH. The compound is initially in aqueous phosphate buffer. At **i**, 100 µL of lipid vesicles containing the HPTS dye were injected. After an equilibration period, 50 µL of 0.5 M NaOH was injected (**ii**) to initiate the transport assay. After a suitable data collection period, the experiment was concluded by the addition of the surfactant Triton-X 100 (**iii**), which lyses the vesicles. The HPTS data was analyzed as noted in Appendix 3.

Chapter 3

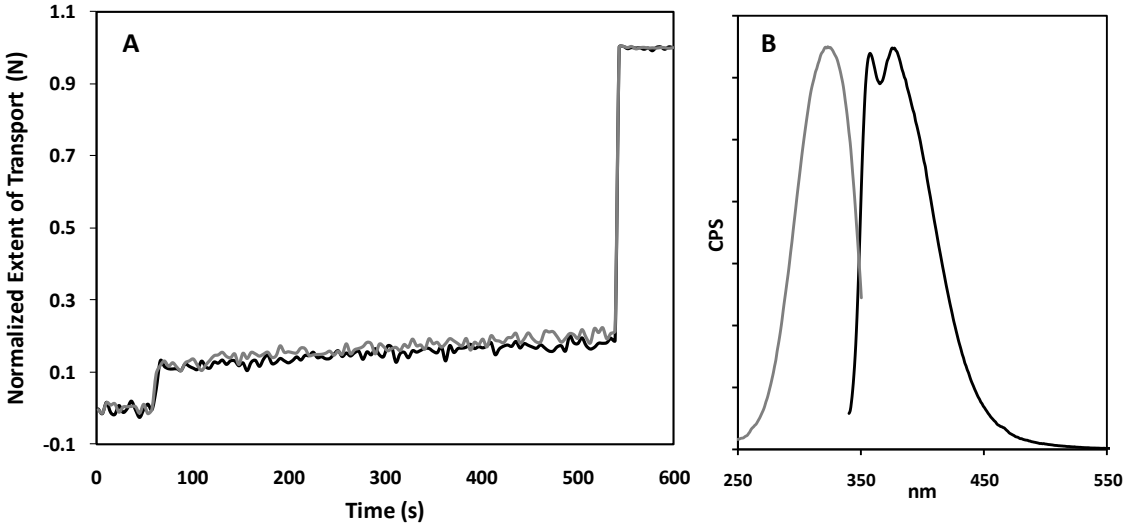

Figure A4: Transport and fluorescence of 0.5% HO_2C-Trip-Hex-G(12)-OH pre-loaded into lipid vesicles. **A**: HPTS scans of 100 µL of compound-containing vesicles (black line) compared with THF blank (grey line) in 2 mL phosphate buffer. **B**: Fluorescence excitation (grey line) and emission (black line) spectra of same solution, vesicles were visibly fluorescent under UV light.

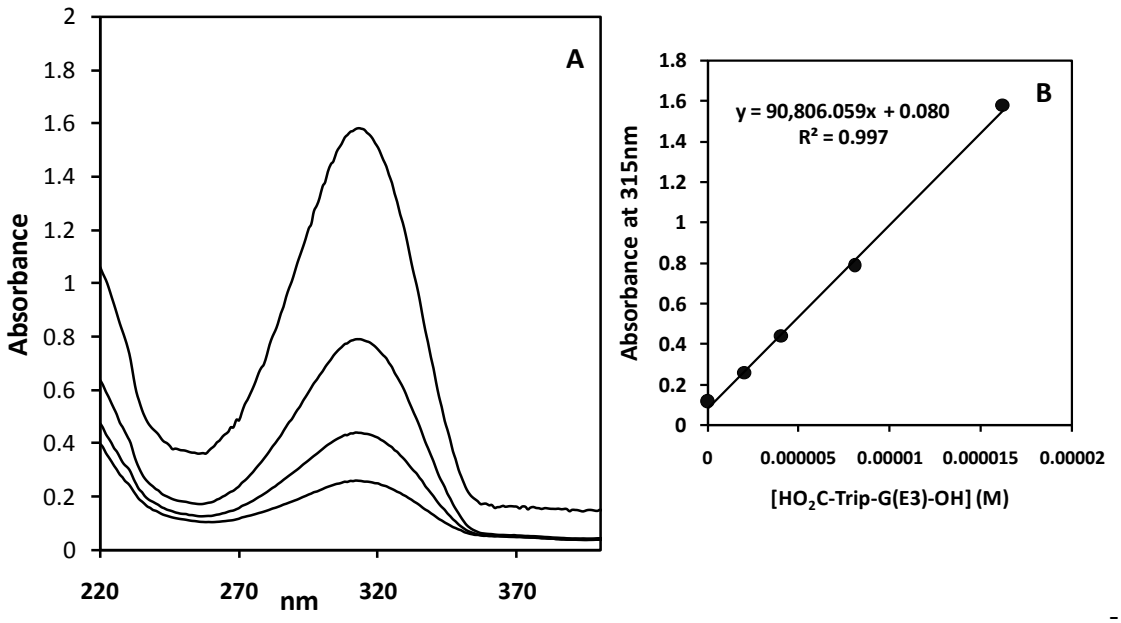

Figure A5: UV absorption data for HO_2C-Trip-G(E3)-OH in MeOH. **A**: raw data, **B**: absorption at maximum wavelength as a function of concentration; determination of ε. Other Trip compounds had very similar extinction coefficients and spectra.

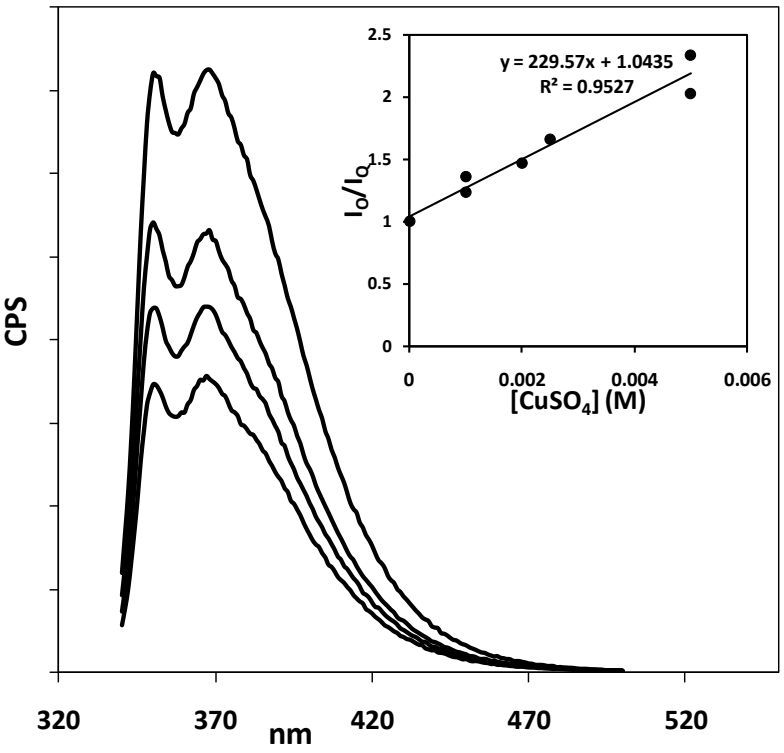

Figure A6: Quenching in MeOH solution by $CuSO_4$ of 10 μM HO_2C-Trip-G(E3)-OH . From top to bottom, $[CuSO_4]$ = 0, 1, 2.5, 5 mM. INSET: Stern-Volmer analysis of data, K_{SV}= 229 M^{-1}.

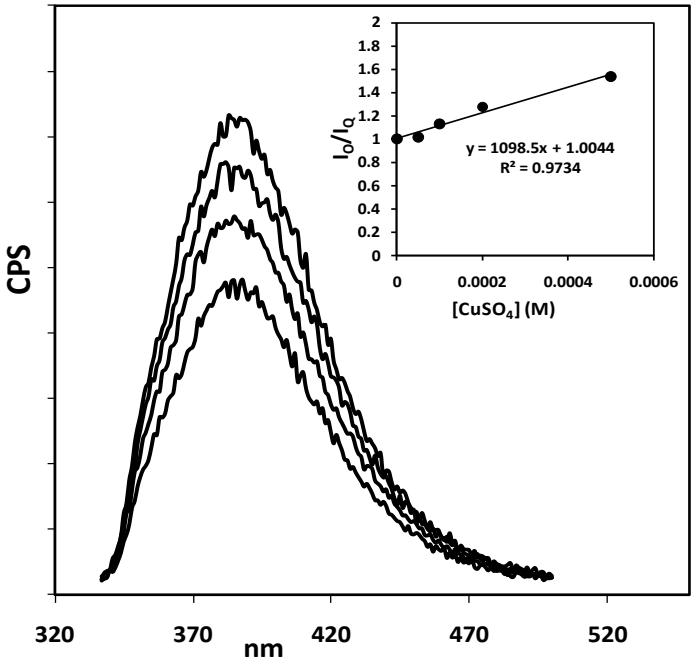

Figure A7: Quenching in aqueous solution by $CuSO_4$ of HO_2C-Trip-G(E3)-OH. 16µM compound in 10 mM BisTris, 100 mM NaCl, pH = 6.4, [$CuSO_4$] from top to bottom = 50, 100, 200, 500 µM in aqueous BisTris buffer. INSET: Stern-Volmer analysis of the data, K_{SV}= 1098 M^{-1}.

Chapter 4

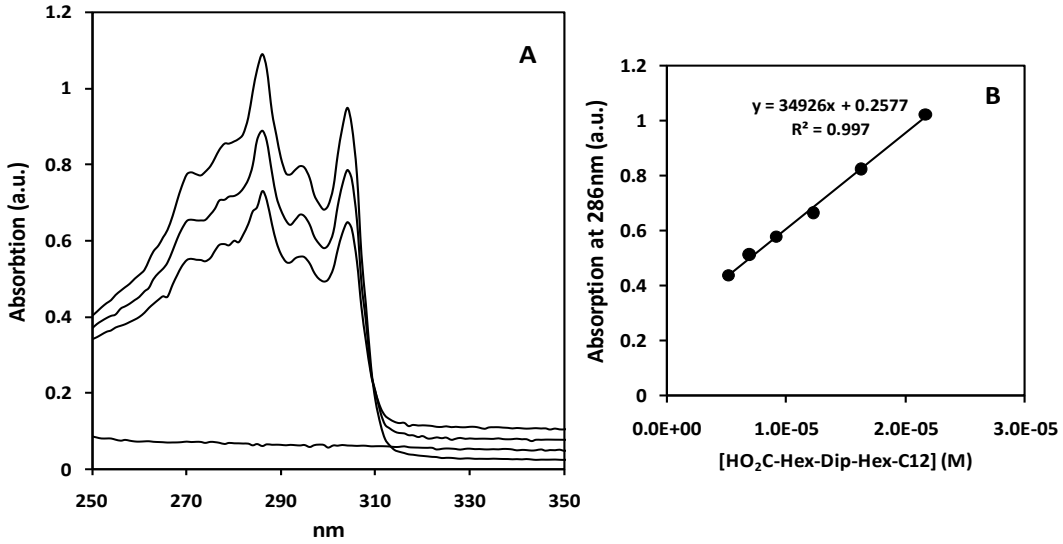

Figure A9: UV absorption data for HO_2C-Hex-Dip-Hex-C6 in MeOH. **A**: raw data, **B**: absorption at maximum wavelength as a function of concentration; determination of ε. Other 2nd-generation Dip compounds had very similar extinction coefficients and spectra.

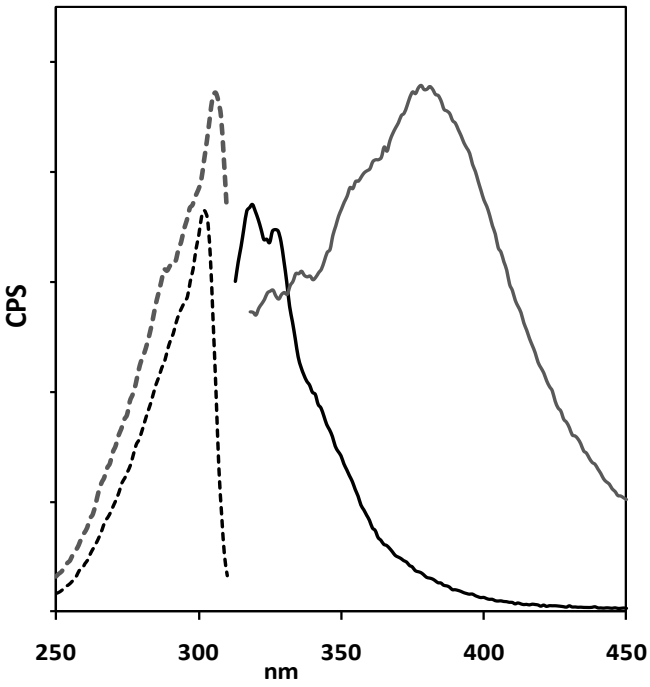

Figure A10: Representative fluorescence spectra of 2nd-generation Dip compounds. Excitation (dashed lines) and emission (solid lines) of 22 µM HO_2C-Hex-Dip-Hex-C6 in MeOH (black) and 10 mM BisTris, 100 mM NaCl, pH 6.4 (grey). Other 2nd-generation Dip compounds had similar excitation spectra in both solvents, and similar emission spectra in MeOH.

Chapter 5

Time (min)	τ_1 (ns)	%	τ_2	%	τ_3	%	χ^2
1	0.19	62	2.35	12	3.91	26	0.941
20	0.18	43	1.79	10	3.74	47	0.995
30	0.20	27	2.33	15	4.02	58	0.922
40	0.09	6	1.39	15	3.86	80	1.048
50	0.15	6	2.50	15	3.95	79	0.989
60	0.18	3	3.46	31	4.30	66	0.937
70	0.11	1	2.54	14	3.87	86	0.947

Table A1: Full TCSPC results for HO_2C-Hex-Dip-Hex-C6. Compare with Table 5.2 in the report. 20 µM of the compound was stirred in an aqueous suspension of vesicles containing 10 mM Na_3PO_4, 100 mM NaCl, pH = 6.4 both inside and out. Lifetimes were recorded every 10minutes for 70 minutes, the solution was left stirring in the dark between scans. Ex= 280 nm, Em = 380 nm. The data was fit using the instrument software, tri-exponential decays were found to fit most satisfactorily in all cases. See Appendix 3 for experimental details.

Time (min)	τ_1 (ns)	%	τ_2	%	τ_3	%	χ^2
1	0.29	26	1.41	41	2.91	33	1.007
10	0.33	33	1.65	45	3.33	22	0.950
20	0.26	32	1.49	42	3.34	25	1.184
30	0.31	38	1.75	46	3.75	16	1.019
70	0.29	42	1.60	39	3.51	19	1.130

Table A2: Full TCSPC results for HO_2C-Hex-Dip-Hex-C12. Compare with Table 5.2 in the report. 20 µM of the compound was stirred in an aqueous suspension of vesicles containing 10mM Na_3PO_4, 100mM NaCl, pH = 6.4 both inside and out. Lifetimes were recorded every 10 minutes for 70 minutes, the solution was left stirring in the dark between scans. Ex= 280 nm, Em = 380 nm. The data was fit using the instrument software, tri-exponential decays were found to fit most satisfactorily in all cases.